

**STUDY OF TITANIUM, TANTALUM AND
CHROMIUM CATALYSTS FOR USE IN
INDUSTRIAL TRANSFORMATIONS**

A thesis submitted in fulfilment of the requirements for the degree of

DOCTOR OF PHILOSOPHY

Of

RHODES UNIVERSITY

By

PRUDENCE LERATO TAU

January 2007

DEDICATION

TO MY MOMMY

ALICE “RAKGADI” NTSEBULANE TAU

AND MY LATE DADDY

JOSEPH “NTATE” N TSAU TAU

ACKNOWLEDGEMENTS

First and foremost, I would like to thank God Almighty, Creator of Heaven and Earth, for without Him, none of this would be possible!

I would like to express my sincere gratitude to my supervisor Prof. Tebello Nyokong for giving me the opportunity to work in her research group. Your constant support, guidance, commitment, encouragement and helpful discussions contributed to every accomplishment presented here. You taught me innumerable lessons and insights on the workings of academic research and thus moulded me into the scientist that I am today! Thank you for opening new avenues and frontiers by sending me to the UK (Norwich) for 2 months. I also appreciate the time you took to read my thesis and providing valuable advice and comments thereof. Your red pen will be solely missed! Once in your presence, it is difficult not to be excited about chemistry. I have learned a tremendous amount from you, and if I manage to retain only a fraction of it, I'll be set for life. A big thank you for believing in me!

Along the same lines I would also like to extend my gratitude to the following:

- The Chemistry department (academic and technical staff), in particular Mr. Andre Adriaan because part of this thesis could have not been done without your help. Buti Dokes, Don, Eric, Harry and Sis' Dambisa, it is true when they say laughter is the best medicine. Enkosini for all the entertainment.
- S22 which is a great group to work in. I am also grateful for the friendship and invaluable insights of all my fellow group members, past and present. Mawezana, may God bless your soul!
- My friends, I cherish all the moments we shared together. To Dudu "Madutsi" Molefe, your invaluable friendship kept me sane. You are truly the best and greatest friend I could ever ask for.
- Andrew Mellon Foundation, SASOL, DAAD and NRF for financial assistance. I am truly honoured to have been selected amongst the many and awarded these prestigious graduate scholarships. I am eternally grateful!

I am especially thankful to my sweetheart, Bolade aka Bo. You have been a wonderful part of my life. You are the bright spot on otherwise dark days, and an even brighter spot to make the good days that much better. You have unselfishly been there when I needed you most. I thank you for everything!

Finally, I would like to express my deepest gratitude and love to my family for their moral support, understanding and patience. To my mom (rakgadi): My deepest thank you and appreciation for being my source of hope, stability and rock throughout my studies. Thank you for providing unconditional love, tolerance, spiritual and inspirational support throughout my life, especially through the tough times. You taught me to balance what I get and what I give and also go for what I want! There were times when I was down and thought that I would never see this through, but you reminded me that life will get better and all that time you knew that I would make it through. I am stronger because your love kept me strong! I am proud and blessed to have a mom like you. God bless you rakgadi. Ke o rata rati rati!

GENERAL STATEMENT

PART A:

Synthesis, photophysicochemical and electrochemical studies of Titanium and Tantalum phthalocyanines, and their use as catalysts for the transformation of 1-hexene

This section of the thesis describes the synthesis of new Titanium and Tantalum phthalocyanines. The first characterisation of the catalysts using spectroscopic methods, photochemistry, photophysics, and electrochemistry was undertaken. The catalysts are further investigated for their photocatalytic and electrocatalytic properties. For photocatalysis, 1-hexene which is useful in industry, is transformed to more useful fine chemicals such as epoxide and allylic alcohol, while electrocatalysis is employed to detect nitrite by oxidation.

PART B:

Synthesis and electrochemical investigation of Chromium and Titanium catalyst systems

This section of the thesis was an industrially funded project with CONFIDENTIALITY agreements, hence is presented separately. An industrially important ethylene trimerisation to 1-hexene using Chromium and Titanium organometallic complexes is discussed. The choice of metals is influenced by the effectiveness of these complexes in the selective trimerisation of ethylene. The aim is to investigate the mechanism of trimerisation by electrochemical methods.

ABSTRACT

PART A

The syntheses, spectroscopic and electrochemical characterisation of a series of titanium and tantalum phthalocyanine complexes are reported. The complexes are unsubstituted and substituted at either the peripheral or non-peripheral positions with sulphonates, aryloxy, arylthio or amino groups. The complexes mostly exhibit Q-bands in the near-infrared region as well as interesting properties in different solvents. The interaction of differently sulphonated titanium and tantalum phthalocyanine complexes with methyl viologen (MV^{2+}), and hence the stoichiometry and association constants are evaluated. Detailed photophysicochemical properties of the complexes were investigated and are for the first time presented with fluorescence lifetimes easily obtained from fluorescence quenching studies. The transformation of 1-hexene photocatalysed by aryloxy- and arylthio-appended complexes is also presented for the first time. The electrochemical properties of the complexes are unknown and are thus presented. Cyclic (CV) and square wave (SWV) voltammetries, chronocoulometry and spectroelectrochemistry are employed in the study of the complexes. Two one-electron reductions and a simultaneous 4-electron reduction are observed for the unsubstituted Cl_3TaPc . Reduction occurs first at the metal followed by ring-based processes. The tetra- and octa-substituted derivatives however exhibit peculiar electrochemical behaviour where a multi-electron transfer process occurs for complexes bearing certain substituents. For all complexes, the first two reductions are metal-based followed by ring-based processes. A comparative study of the electrocatalytic activities of the complexes towards the oxidation of nitrite is also investigated. The complexes are immobilised onto a glassy carbon electrode either by drop-dry or electropolymerisation methods. All the modified electrodes exhibit

improved electrocatalytic oxidation of nitrite than the unmodified electrodes by a two-electron mechanism producing nitrate ions. Catalytic currents are enhanced and nitrite overpotential reduced to ~ 0.60 V. Kinetic parameters are determined for all complexes and a mechanism is proposed.

PART B:

The syntheses and electrochemical characterisation of chromium and titanium complexes for the selective trimerisation of ethylene to 1-hexene are presented. The synthesis of the chromium complex requires simple steps while tedious steps are used for the air-sensitive titanium complex. The spectroscopic interaction of the chromium complex with the co-catalyst methylaluminoxane is investigated. The complexes are characterised by electrochemical methods such as cyclic voltammetry and spectroelectrochemistry.

CONTENTS

Title page	i
Dedication	ii
Acknowledgments	iii
General statement	v
Abstract	vi
Contents	viii
List of abbreviations	xv
List of symbols	xix
List of figures	xxii
List of schemes	xxxiv
List of tables	xxxvii
Publications	124

PART A:

Chapter 1:

Introduction	1
1.1 Discovery and history	2
1.2 Structure and nomenclature of phthalocyanines	4
1.3 Metallophthalocyanines and their general applications	6
1.4 Phthalocyanine syntheses	12
1.4.1 Unsubstituted metal-free and metallophthalocyanines	12
1.4.2 Substituted phthalocyanines	17

1.4.2.1	Tetra-substituted phthalocyanines	18
1.4.2.2	Octa-substituted phthalocyanines	22
1.4.2.3	Water-soluble phthalocyanines	24
1.4.2.4	Survey of the syntheses of TiPcs and TaPcs	27
1.5	UV/Vis spectroscopic properties of phthalocyanines	33
1.5.1	Basic concepts	33
1.5.2	Survey of the UV/Vis properties of TiPcs	40
1.5.3	UV/Vis spectral studies of ionic interactions	42
1.6	Photochemical and photophysical properties	45
1.6.1	Mechanisms of triplet state deactivation	47
1.6.2	Photochemical processes: Singlet oxygen	49
1.6.3	Photochemical processes: Photobleaching	53
1.6.4	Photophysical processes: Fluorescence	56
1.6.4.1	Fluorescence quantum yield	57
1.6.4.2	Fluorescence lifetimes	59
1.6.4.3	Fluorescence quenching	61
1.6.5	Photophysical processes: Triplet state	63
1.6.6	Survey of photochemical and photophysical properties of TiPcs	66
1.7	Photocatalytic oxidation of 1-hexene	69
1.8	Electrochemistry of metallophthalocyanines	72
1.8.1.	Background on the electrochemical techniques used	76
1.8.1.1	Cyclic voltammetry	76
1.8.1.2	Square wave voltammetry	79
1.8.1.3	Chronoamperometry	79

1.8.1.4	Chronocoulometry	80
1.8.1.5	Spectroelectrochemistry	81
1.8.1.6	Survey of the electrochemical properties of TiPcs and TaPcs	82
1.8.2	Electrocatalysis	84
1.8.2.1	Electrocatalytic oxidation of nitrite	89
1.8.2.2	Survey of the electrocatalytic properties of TiPcs	90
1.9	Summary of aims of the thesis	92

Chapter 2:

	Experimental	94
2.1	Materials	95
2.2	Instrumentation	96
2.3	Methods	97
2.3.1	Photochemistry	97
2.3.1.1	Singlet oxygen and photobleaching determinations	97
2.3.1.2	Photocatalytic oxidation of 1-hexene	99
2.3.2	Photophysics	100
2.3.2.1	Fluorescence quantum yield	100
2.3.2.2	Fluorescence quenching	101
2.3.2.3	Triplet quantum yield and lifetime	101
2.3.3	Electrochemistry	102
2.3.3.1	General methods	102
2.3.3.2	Electrode modification and electrocatalysis	103

2.4	Synthesis	103
2.4.1	Unsubstituted metallophthalocyanines	103
2.4.2	Differently sulphonated metallophthalocyanines, MPcS _n	104
2.4.3	Phthalonitriles	105
2.4.3.1	3-Nitrophthalonitrile	105
2.4.3.2	4-Nitrophthalonitrile	106
2.4.3.3	4,5-Dichlorophthalonitrile	107
2.4.3.4	Mono-substituted phthalonitriles	108
2.4.3.5	Disubstituted phthalonitriles	112
2.4.4	Aryloxy and arylthio tetra-substituted phthalocyanines	114
2.4.5	Octa-substituted phthalocyanines	120
2.4.6	Amino substituted titanium phthalocyanine	121

RESULTS AND DISCUSSION

Chapter 3:

	Synthesis and spectroscopic characterisation	126
3.1	Unsubstituted titanium and tantalum phthalocyanines	129
3.2	Differently sulphonated titanium and tantalum phthalocyanines	133
3.3	Tetra- and octa-substituted oxotitanium phthalocyanines	143
3.3.1	Phthalonitriles	143
3.3.2	Synthesis of the OTiPc complexes	145
3.3.3	IR and ¹ H-NMR spectra of the OTiPc complexes	149
3.3.4	Ground state electronic absorption spectra	154
3.4	Conclusion	166

Chapter 4:

Photochemical, photophysical and photocatalytic properties	167
4.1 Photochemical processes	170
4.1.1 Singlet oxygen	170
4.1.2 Photobleaching	173
4.2 Photophysical processes	175
4.2.1 Fluorescence properties	175
4.2.2 Triplet state properties	190
4.3 Photocatalytic oxidation of 1-hexene	194
4.3.1 Photochemical properties	194
4.3.2 Photocatalysis	196
4.4 Conclusion	204

Chapter 5:

Electrochemical characterisation	206
5.1 Tantalum phthalocyanine	209
5.2 Oxotitanium(IV) phthalocyanines	216
5.2.1 Phenoxy- and 4- <i>tert</i> -Butylphenoxy-substituted OTiPcs	216
5.2.2 Benzyloxy- and 4-(benzyloxy)phenoxy tetra- and octa-substituted OTiPcs	227
5.2.3 Phenylthio- and benzylthio-substituted OTiPcs	237
5.2.4 Tetraamino oxotitanium(IV) phthalocyanine	247
5.3 Conclusion	249

Chapter 6:

Electrocatalytic properties	250
6.1 Aryloxy tetra-substituted oxotitanium(IV) phthalocyanines	251
6.2 Arylthio tetra-substituted oxotitanium(IV) phthalocyanines	264
6.3 Amino tetra-substituted oxotitanium(IV) phthalocyanine	279
6.4 Conclusion	292

Chapter 7:

Conclusions and future perspectives	293
7.1 General conclusions	294
7.2 Future perspectives	297
References	298

PART B:

Chapter 1:

Introduction	325
1.1 General introduction	326
1.2 Transition metal catalysis	327
1.3 Ethylene trimerisation	329
1.4 Catalyst activation	331
1.5 Chromium and titanium complexes as catalysts	333

Chapter 2:	
Experimental	336
2.1 Materials	337
2.2 Methods	337
2.2.1 Spectroscopic studies of interaction of MAO with Cr-decylSNS6	337
2.2.2 Electrochemistry	338
2.3 Synthesis	338
2.3.1 Cr(III) - <i>bis</i> [(2-decylsulfanyl)ethyl]amine	338
2.3.2 Ti-Cyclopentadiene-arene complex	340
RESULTS AND DISCUSSION	343
Chapter 3:	
Synthesis and spectroscopic characterisation	344
3.1 Chromium(III)- <i>bis</i> [(2-decylsulfanyl)ethyl]amine	345
3.2 Ti(IV)-cyclopentadienyl-arene	351
Chapter 4:	
Electrochemical characterisation	354
4.1 Chromium(III)- <i>bis</i> [(2-decylsulfanyl)ethyl]amine	355
4.2 Ti(IV)- cyclopentadienyl-arene	358
General conclusion	366
References	367
TOTAL LEAF PAGES (PART A + PART B)	371

LIST OF ABBREVIATIONS

Ac₂O	-	acetic anhydride
ACN	-	acetonitrile
ADMA	-	tetrasodium α,α -(anthracene-9,10-diyl) dimethylmalonate
BHT	-	2,6-di- <i>tert</i> -butyl-4-methylphenol
BQ	-	benzoquinone
1-CNP	-	1-chloronaphthalene
CHCl₃	-	chloroform
CME	-	chemically modified electrode
CT	-	charge-transfer
CA	-	chronoamperometry
CC	-	chronocoulometry
CDCl₃	-	deuterated chloroform
CV	-	cyclic voltammetry
	-	cyclic voltammogram
DABCO	-	1,4-diazabicyclo-octane
DBU	-	1,8-diazabicyclo[5.4.0]undec-7-ene
DCM	-	dichloromethane
DCC	-	dicyclohexylcarbodiimide
DES	-	diethyl sulphate
DMA	-	dimethylacetamide
DMEA	-	<i>N,N</i> -dimethylethanolamine
DMF	-	<i>N,N</i> -dimethylformamide
DMS	-	dimethyl sulphate
DMSO	-	dimethylsulphoxide

DNA	-	deoxyribonucleic acid
DPBF	-	1,3-diphenylisobenzofuran
E(CE)_n	-	electrochemical-chemical-electrochemical
ESR	-	electron spin resonance
GCE	-	glassy carbon electrode
H₂O₂	-	hydrogen peroxide
H₂Pc	-	metal-free phthalocyanine
¹H-NMR	-	proton nuclear magnetic resonance
HOMO	-	highest occupied molecular orbital
HPLC	-	high performance liquid chromatography
HQ	-	hydroquinone
IC	-	internal conversion
IR	-	infrared
ISC	-	intersystem crossing
ITO	-	indium tin oxide
IUPAC	-	International Union of Pure and Applied Chemistry
LMCT	-	ligand-to-metal charge transfer
LUMO	-	lowest unoccupied molecular orbital
MAO	-	methylaluminoxane
MMAO	-	modified methylaluminoxane
MCAA	-	monochloroacetic acid
MLCT	-	metal-to-ligand charge transfer
MPc	-	metallophthalocyanine
MPcS_n	-	differently sulphonated metallophthalocyanine
MV²⁺	-	methyl viologen

NH₂	-	amino
NHE	-	normal hydrogen electrode
NIR	-	near infrared
NLO	-	non-linear optical
ODS	-	optical data storage
OPG	-	ordinary pyrolytic graphite
OSWV	-	Osteryoung square wave voltammetry
	-	Osteryoung square wave voltammogram
OTiPc	-	oxotitanium(IV) phthalocyanine
OTTLE	-	optically transparent thin-layer electrodes
P	-	phosphorescence
PBS	-	phosphate buffer solution
Pc	-	phthalocyanine
PDT	-	photodynamic therapy
TaPcS_n	-	differently sulphonated tantalum(IV) metallophthalocyanine
TBAP	-	tetrabutylammonium perchlorate
TEAP	-	tetraethylammonium perchlorate
THAHPF	-	tetrahexylammonium hexafluorophosphate
THF	-	tetrahydrofuran
TiPc	-	titanium(IV) phthalocyanine
TiPcS_n	-	differently sulphonated titanium(IV) metallophthalocyanine
TTF	-	tetrathiafulvalene
SCE	-	saturated calomel electrode
S_NAr	-	aromatic nucleophilic substitution
SV	-	Stern-Volmer

SWV	-	square wave voltammetry
	-	square wave voltammogram
Sub	-	substrate
Sub_{ox}	-	oxidised substrate
UV/Vis	-	ultraviolet/visible
VCE	-	vitreous carbon electrode
VR	-	vibrational relaxation

LIST OF SYMBOLS

α	-	staggering angle
	-	non-peripheral position
	-	fraction of light absorbed
β	-	peripheral position
e^-	-	electron
ε	-	extinction coefficient
ε_S	-	singlet extinction coefficient
ε_T	-	triplet extinction coefficient
f_a	-	fraction of accessible fluorescence intensity
K_f	-	Stern-Volmer quenching constant of accessible fraction
k	-	photodecomposition rate constant
k_q	-	bimolecular quenching constant
K_{SV}	-	Stern-Volmer constant
Γ	-	surface coverage
η	-	refractive index
n	-	number of electrons transferred
E_{pa}	-	anodic peak potential
E_{pc}	-	cathodic peak potential
Φ_{Δ}	-	singlet oxygen quantum yield
Φ_{DPBF}	-	DPBF quantum yield
Φ_F	-	fluorescence quantum yield
Φ_T	-	triplet state quantum yield

τ_F	-	fluorescence lifetime
τ_N	-	natural lifetime
τ_T	-	triplet state lifetime
ν	-	scan rate
ΔA	-	difference in absorbance following laser pulse
A	-	absorbance
	-	area of electrode
C	-	concentration
D	-	diffusion coefficient
ΔE	-	difference in peak potentials
E^o	-	formal potential
$E_{1/2}$	-	half-wave potential
E_p	-	peak potential
F	-	fluorescence
	-	Faraday's constant
I	-	intensity of light
	-	current
I_{abs}	-	intensity of light absorbed
I_p	-	peak current
I_{pa}	-	anodic current
I_{pc}	-	cathodic current
M	-	molar concentration
$^1O_2 (^1\Delta_g)$	-	excited long-lived singlet state oxygen
$^1O_2 (^1\Sigma_g)$	-	excited short-lived singlet state oxygen

$O_2 (^3\Sigma_g)$	-	ground state molecular oxygen
Q	-	charge
R	-	universal gas constant
S_0	-	ground singlet state
T	-	temperature
T_{filter}	-	transmittance of filter
T_{MPC}	-	transmittance of metallophthalocyanine
T_1	-	first excited triplet state
T_n	-	n th excited triplet state
V	-	volume

LIST OF FIGURES

PART A:

- 1.1 Schematic representation of the phthalocyanine parent compound of chemical formula $C_{32}H_{18}N_8$.
- 1.2 A class of tetrapyrrolic macrocycles.
- 1.3 IUPAC nomenclature for point of fusion in a heterocyclic system (A) and an assignment of external numbering to a macrocyclic system (B).
- 1.4 Periodic table showing metals (in red) that have been used in the metallophthalocyanine synthesis.
- 1.5 MPc structures showing (i) 'shuttlecock-shaped' C_{4v} symmetry and (ii) D_{4h} symmetry.
- 1.6 (i) Various forms of MPc complexes (ii) MPc in which metals in oxidation states greater than +2 are bonded to axial ligands.
- 1.7 Constitutional isomers from (i) 1,(4)- and (ii) 2,(3)-tetrasubstituted MPcs.
- 1.8 Structures of Cl_2TiPc (**33**) and Cl_3TaPc (**34**) studied in this thesis.
- 1.9 Structures of $OTiPcS_n$ (**35**) and Cl_3TaPcS_n (**36**) studied in this thesis.
- 1.10 Synthesised tetra-substituted $OTiPc$ complexes that are substituted at the non-peripheral (**37a – f**) and peripheral (**38a – f**) positions.
- 1.11 Synthesised octa-substituted $OTiPc$ complexes that are substituted at the peripheral (**39a – d**) positions.
- 1.12 Synthesised tetra-substituted nitro (**40**) and amino (**41**) $OTiPc$ complexes.

- 1.13** UV/Vis spectra of typical phthalocyanine complexes that are peripherally (red) and non-peripherally (black) substituted at the periphery.
- 1.14** Phthalocyanine and porphyrin electronic transitions showing the origin of Q and B absorption bands.
- 1.15** Typical ground state absorption spectra of (i) metal-free phthalocyanine and (ii) metallated phthalocyanine.
- 1.16** Two examples of broadened absorption spectra of aggregated MPcs where (i) is less aggregated and (ii) is highly aggregated.
- 1.17** Interaction between molecular orbitals showing the effect of aggregation on the LUMO of Pcs.
- 1.18** (i) Orientation of transition moments for linear H- and J-aggregates and (ii) Exciton model correlating energy levels on dimer formation.
- 1.19** A Jablonski diagram showing the photosensitisation of MPc.
- 1.20** Electronic configuration showing the π -antibonding orbitals of oxygen in the ground state ($^3\Sigma_g$) and electronically excited singlet states, i.e. ($^1\Delta_g$) and ($^1\Sigma_g$).
- 1.21** Normalised absorption (i) and emission (ii) spectra of a typical MPc.
- 1.22** Typical transient spectrum (triplet decay curve) following laser flash photolysis.
- 1.23** A simplified energy-level diagram for a typical MPc where metal orbitals (i) are buried within filled Pc orbitals or (ii) lie between the HOMO-LUMO gap.
- 1.24** A typical cyclic voltammogram (CV).

- 1.25** A double-potential step chronoamperogram.
- 1.26** A double-potential step chronocoulogram.
- 1.27** Electrocatalytic behaviour at (i) unmodified electrode and (ii) modified electrode.
- 2.1** Photochemical set-up where (A) light source, (B) convergence lens, (C) water filter, (D) glass filter, (E) interference filter and (F) UV/Vis cell.
- 2.2** Schematic diagram of a laser flash photolysis set-up for triplet quantum yield and lifetime determinations.
- 3.1** $^1\text{H-NMR}$ spectrum of Cl_3TaPc (**34**) in CDCl_3 .
- 3.2** UV/Vis spectra of (i) Cl_2TiPc (**33**) and (ii) Cl_3TaPc (**34**) in CHCl_3 .
- 3.3** HPLC traces of (i) TiPcS_n and (ii) TaPcS_n .
- 3.4** Ground state absorption spectra of (a) TiPcS_n and (b) TaPcS_n in (i) methanol, (ii) DMSO and (iii) PBS 7.4.
- 3.5** Ground state absorption spectra of TiPcS_n in (i) the absence and (ii) presence of Triton X-100 in PBS 7.4 solution.
- 3.6** UV/Vis spectral changes observed on addition of increasing MV^{2+} concentrations to a solution of TiPcS_n in methanol.
- 3.7** Job diagrams for interaction of (a) TiPcS_n ($\lambda = 687 \text{ nm}$) and (b) TaPcS_n ($\lambda = 688 \text{ nm}$) with MV^{2+} in methanol.

- 3.8** Plots of $A_0/\Delta A$ vs. $1/L_t$ for the association constant (K_a) determination in the interaction of (i) TiPcS_n and (ii) TaPcS_n with MV²⁺.
- 3.9** IR spectra of complexes (i) **38a** and (ii) **37b**.
- 3.10** ¹H-NMR spectrum of complex **38a** in CDCl₃.
- 3.11** ¹H-NMR spectrum of complex **39b** in CDCl₃.
- 3.12** UV/Vis spectra of complexes **37a – d** and **38a – d** in CHCl₃.
- 3.13** UV/Vis spectra of **37e**, **37f**, **38e** and **38f** in (i) DCM, (ii) THF, (iii) CHCl₃ and (iv) DMSO.
- 3.14** UV/Vis spectra of **37f** in DMSO upon decreasing the concentration.
- 3.15** Ground state absorption spectra of complexes **39a – d** in 1-CNP.
- 3.16** UV/Vis spectra of (i) OTiPc(NO₂)₄ (**40**) and (ii) OTiPc(NH₂)₄ (**41**) in DMF.
- 4.1** Spectral changes observed during irradiation of complex **37a** in the presence of DPBF, in DMSO, for singlet oxygen quantum yield determination.
- 4.2** UV/Vis spectral changes of complex **38a** in DMSO, following irradiation in the Q-band region.
- 4.3** Normalised fluorescence emission (i) and excitation (ii) spectra of complex **39a** in 1-CNP
- 4.4** Normalised excitation spectra for **37e**. (i) excitation from the 721 nm band (ii) excitation from the 741 nm band (iii) fluorescence spectrum of **37e** (excitation at 685 nm) in DMSO.

- 4.5** Normalised (i) excitation (652 and 688 nm), (ii) absorbance (687 nm) and (iii) emission (693 nm) spectra of TiPcS_n in methanol.
- 4.6** Normalised (i) excitation (677 nm), (ii) absorbance (690 nm) spectra of TiPcS_n in PBS 7.4.
- 4.7** Normalised (i) excitation (674 nm), (ii) absorbance (688 nm) and (iii) emission (678 nm) spectra of TaPcS_n in methanol.
- 4.8** Normalised (i) excitation (ii) absorbance and (iii) emission spectra of TaPcS_n in PBS 7.4.
- 4.9** Fluorescence emission spectral changes of **39a** on addition of increasing concentrations of BQ.
- 4.10** Stern-Volmer plot for fluorescence quenching of **39a** by increasing concentrations of BQ.
- 4.11** Stern-Volmer plots showing fluorescence quenching of (i) TiPcS_n and (ii) TaPcS_n in methanol as determined by fluorescence intensity as a function of [MV²⁺].
- 4.12** Modified Stern-Volmer plots showing quenching of (i) TiPcS_n and (ii) TaPcS_n in methanol as determined by fluorescence intensity as a function of [MV²⁺].
- 4.13** Triplet state decay curve of **39c** in 1-CNP. Inset shows the first order plot of the complex.
- 4.14** UV/Vis spectra obtained before (i) and after (ii) laser irradiation of **39b** in 1-CNP
- 4.15** GC traces obtained during the photocatalysis of 1-hexene (i) in DCM yielding oxidation products: 1-hexene-3-ol (ii) and 1,2-epoxyhexane (iii).

- 4.16** % Conversion plots of 1-hexene over time for the photocatalytic oxidation of 0.5 mmol 1-hexene in the presence of 1 μ mol aryloxy substituted oxotitanium(IV) phthalocyanines (**37a**, **37c**, **38a** and **38c**) in DCM.
- 4.17** % Conversion plots of 1-hexene over time for the photocatalytic oxidation of 0.5 mmol 1-hexene in the presence of 1 μ mol arylthio substituted oxotitanium(IV) phthalocyanines (**37e**, **37f**, **38e** and **38f**) in DCM.
- 4.18** UV/Vis spectral changes of **38b** observed with variation of light intensities.
- 4.19** % Conversion of the photocatalytic oxidation of 1-hexene in relation to the photobleaching rate constants (k) of oxotitanium (IV) phthalocyanines in DCM.
- 4.20** % Selectivity plots of 1,2-epoxyhexane in (i) absence and (ii) presence of DABCO over time during the photocatalysis of 1-hexene by **38a** (1 μ mol) in DCM.
- 4.21** % Selectivity plots of 1-hexen-3-ol in (i) absence and (ii) presence of BHT over time during the photocatalysis of 1-hexene by **38a** (1 μ mol) in DCM
- 5.1** Cyclic and square wave voltammograms of **34** in DMF containing 0.1M TBABF₄. Scan rate 0.2 V.s⁻¹.
- 5.2** UV/Vis spectral changes observed during controlled potential reduction of **34** in DMF containing 0.1 M TBABF₄ at process **I** (-0.31 V).
- 5.3** UV/Vis spectral changes observed during controlled potential reduction of **34** in DMF containing 0.1 M TBABF₄ at process **II** (-0.48 V).
- 5.4** UV/Vis spectral changes observed during controlled potential reduction of **34** in DMF containing 0.1 M TBABF₄ at process **III** (-0.94 V).

- 5.5** Cyclic and square wave (insert) voltammograms of **37a** in DMF containing 0.1 TBABF₄. Scan rate 0.1 Vs⁻¹
- 5.6** Anson plots for complex **37a** showing process **I – III**.
- 5.7** UV/Vis spectral changes observed during controlled potential reduction of **37a** in DMF containing 0.1 M TBABF₄. Applied potential at: (a) couple **I**, (-0.50 V); (b) couple **II** (-0.80 V); (c) continuation of couple **II** (-0.80 V) and (d) couple **III** (-1.2 V).
- 5.8** UV/Vis spectral changes observed during controlled potential oxidation of **37a** in DMF containing 0.1 M TBABF₄. Applied potential for 1.10V.
- 5.9** CV and SWV (insert) of **38c** in DMF containing 0.1M TBABF₄. Scan rate 0.1 Vs⁻¹.
- 5.10** CV and SWV (insert) of **39b** in DMF containing 0.1M TBABF₄. Scan rate 0.1 Vs⁻¹.
- 5.11** UV/Vis spectral changes observed during controlled potential reduction of (a) **38c** at an applied potential of couple **I** (-0.14 V) and (b) **39b** at an applied potential of couple **I** (-0.08 V) in DMF containing 0.1M TBABF₄.
- 5.12** UV/Vis spectral changes observed during controlled potential reduction of (a) **38c** at an applied potential of couple **II** (-0.6 V) and (b) **39b** at an applied potential of couple **II** (-0.4 V) in DMF containing 0.1M TBABF₄.
- 5.13** UV/Vis spectral changes observed during controlled potential reduction of (a) **38c** at an applied potential of couple **III** (-1.4 V) and (b) **39b** at an applied potential of couple **III** (-1.3 V) in DMF containing 0.1M TBABF₄.
- 5.14** UV/Vis spectral changes observed during controlled potential reduction of **38c** at an applied potential of couple **IV** (-1.71 V) in DMF containing 0.1 M TBABF₄.

- 5.15** Cyclic and square wave (inset) voltammograms of **37e** in DMF containing 0.1 M TBABF₄. Scan rate 0.1 V s⁻¹
- 5.16** UV/Vis spectral changes observed during controlled potential reduction of (a) **37e** (b) **37f** (c) **38e** and (d) **38f** in DMF containing 0.1 M TBABF₄. Applied potential just above couple I (-0.13 V).
- 5.17** UV/Vis spectral changes observed during controlled potential reduction of (a) **37e** (b) **37f** (c) **38e** and (d) **38f** in DMF containing 0.1 M TBABF₄. Applied potential at couple II (-0.60 V).
- 5.18** UV/Vis spectral changes observed during controlled potential reduction of (a) **37e** (b) **37f** (c) **38e** and (d) **38f** in DMF containing 0.1 M TBABF₄. Applied potential at couple III (-1.35 V).
- 5.19** Cyclic and square wave (inset) voltammograms of complex **41** in DMF containing 0.1 M TBABF₄. Scan rate 0.1 Vs⁻¹.
- 6.1** Cyclic voltammograms of **38c** adsorbed on GCE in phosphate buffer solution, pH 7.4. Scan rate 0.1 Vs⁻¹.
- 6.2** Cyclic voltammograms of bare GCE, **38a**, **38c** and **38d** for 1 mM nitrite oxidation in phosphate buffer solution, pH 7.4. Scan rate 0.1 Vs⁻¹.
- 6.3** Cyclic voltammograms of bare GCE, **37a** and **37d** for 1 mM nitrite oxidation in phosphate buffer solution, pH 7.4. Scan rate 0.1 Vs⁻¹.
- 6.4** Plot of E_p vs. $\log v$ for the electrocatalytic oxidation of 1 mM nitrite solution in phosphate buffer, pH 7.4 on: (i) **37a**, (ii) **37d**, and (iv) **38b**.
- 6.5** Plot of $I_p v^{-1/2}$ vs. v for the electrocatalytic oxidation of 1 mM nitrite solution in phosphate buffer, pH 7.4 on **38a**, (ii) **37b**, and (iii) **38b**.

- 6.6** Plot of I_{net} vs. $t^{-1/2}$ for GCE modified with **38a** for the electrocatalytic oxidation of 1 mM nitrite solution in phosphate buffer, pH 7.4. Scan rate 0.1 Vs^{-1} .
- 6.7** UV/Vis spectral changes observed on addition of nitrite to **38b** in DMSO, where (i) is **38b** in absence of nitrite with $\lambda_{\text{max}} = 700$ nm and (ii) in the presence of nitrite
- 6.8** Evolution of cyclic voltammograms of **38f** (1 mM) in DCM containing 0.1 M TBABF₄ during cathodic repetitive cycling on a glassy carbon electrode (GCE). Scan rate = 0.1 Vs^{-1} .
- 6.9** Cyclic voltammograms **38f** (1 mM) at GCE in DCM containing 0.1 M TBABF₄ showing (i) first and (ii) last scans.
- 6.10** Cyclic voltammetry of modified GCE with complex **38f** phosphate buffer solution, pH 7.4. Inset = Plot of current versus scan rate. Scan rate 0.1 Vs^{-1} .
- 6.11** Anodic electrodeposition of **38f** (1 mM) in DCM containing 0.1 M TBABF₄. Scan rate 0.1 Vs^{-1} .
- 6.12** Cyclic voltammograms of unmodified GCE, *poly-37e*, *poly-37f*, *poly-38e* and *poly-38f*, for 1 mM nitrite oxidation in phosphate buffer solution, pH 7.4. Scan rate 0.1 Vs^{-1} .
- 6.13** Repetitive cyclic voltammogram of 1 mM nitrite at a **38f** modified GCE in phosphate buffer, pH 7.4. Scan rate 0.1 Vs^{-1} .
- 6.14** Plots of variation of peak currents with scan number for the voltammetric response of 1 mM nitrite in phosphate buffer solution, pH 7.4 on (a) *poly-38e*, (b) *poly-37e*, (c) *poly-38f* and (d) *poly-37f*.

- 6.15** Plot of I_p vs. $v^{1/2}$ for the electrocatalytic oxidation of 1 mM nitrite solution in phosphate buffer, pH 7.4 on: (i) *poly-38e*, (ii) *poly-37e*, (iii) *poly-38f* and (iv) *poly-37f*.
- 6.16** Plot of $I_p v^{-1/2}$ vs. v for the electrocatalytic oxidation of 1 mM nitrite solution in phosphate buffer, pH 7.4 on: (i) *poly-38e*, (ii) *poly-37e*, (iii) *poly-38f* and (iv) *poly-37f*.
- 6.17** Plot of E_p vs. $\log v$ for the electrocatalytic oxidation of 1 mM nitrite solution in phosphate buffer, pH 7.4 on: (i) *poly-37f*, (ii) *poly-38f*, (iii) *poly-37e* and (iv) *poly-38e*.
- 6.18** Plot of variation of peak current (I_p) vs. nitrite concentration ($[\text{NO}_2^-]$) for *poly-38f* in phosphate buffer, pH 7.4 on. Scan rate 0.1 Vs^{-1} .
- 6.19** UV/Vis spectral changes observed on addition of nitrite to **38e** in DMSO, where spectrum of (a) **38e** ($\text{OTi}^{\text{IV}}\text{Pc}$) in absence of nitrite and (b) in the presence of nitrite.
- 6.20** Schematic diagram illustrating the three limiting coordination modes of the nitrite ligand.
- 6.21** Evolution of CVs during the electropolymerisation of complex **41** on GCE in DMF containing 0.1 M TBABF_4 .
- 6.22** Redox activity of polymer in terms of cathodic current, I_{pc} , as a function of the electropolymerisation scan number of complex **41** in DMF containing 0.1 M TBABF_4 .
- 6.23** Cyclic voltammetry of *poly-41*-modified GCE in phosphate buffer solution (pH 7.4). Scan rate 0.1 Vs^{-1} .

- 6.24** Variation of the cathodic (E_{pc}) and anodic (E_{pa}) peak potentials with the log of scan rate for *poly-41* in phosphate buffer (pH 7.4).
- 6.25** Cyclic voltammograms of electrooxidation of 1 mM nitrite at (i) the bare GCE and (ii) *poly-41*-modified electrode in phosphate buffer (pH 7.4).
- 6.26** Plot of variation of peak currents with scan number for the voltammetric response of 1 mM nitrite in phosphate buffer solution (pH 7.4) on *poly-41*.
- 6.27** Plot of (i) I_p vs. $v^{1/2}$ (ii) $I_p v^{-1/2}$ vs. v (iii) E_p vs. $\log v$ for the electrocatalytic oxidation of 1 mM nitrite solution in phosphate buffer (pH 7.4) on *poly-41*.
- 6.28** Plot of I_{cat}/I_l derived from chronoamperometric data for 1 mM nitrite in phosphate buffer (pH 7.4) solution on *poly-41*.

PART B:

- 1.1** A catalytic cycle.
- 1.2** Proposed structures of MAO.
- 1.3** Complexes used in this study.
- 3.1** $^1\text{H-NMR}$ of decyl-SNS ligand in CDCl_3 .
- 3.2** UV/Vis spectrum of Cr-decylSNS (**12**) in toluene. Inset: d-d transitions.
- 3.3** UV/Vis spectra of (a) 3.6×10^{-4} Cr-decylSNS (**12**) and (b) of the complex formed immediately following addition of 300 equivalents of MAO in toluene.
- 3.4** UV/Vis spectra of (i) complex **12**, (ii) complex **12** + MAO and (iii) complex **17** in toluene

- 3.5** UV/Vis spectra of (i) the ligand and (ii) complex **13** in acetonitrile
- 4.1** Cyclic voltammogram of complex **12** in toluene containing 0.1 M THAHPF as electrolyte. Scan rate 0.1 Vs^{-1}
- 4.2** UV/Vis spectral changes observed during controlled potential reduction of complex **12** in toluene containing 0.1 M THAHPF.
- 4.3** Spectroscopic changes observed on electrolysis of a solution of complex **12** in toluene containing 0.1 M THAHPF.
- 4.4** Spectral changes observed during chemical oxidation of Cr-decylSNS in toluene with nitrosonium tetrafluoroborate
- 4.5** Cyclic voltammogram of the ligand (**24**) in acetonitrile containing 0.1 M THAHPF as electrolyte. Scan rate 0.1 Vs^{-1}
- 4.6** Cyclic voltammogram of the complex **13** in acetonitrile containing 0.1 M THAHPF as electrolyte. Scan rate 0.1 Vs^{-1}
- 4.7** UV/Vis spectral changes observed during controlled potential reduction of complex **13** in acetonitrile containing 0.1 M THAHPF.
- 4.8** Plots of potential applied (E_{applied}) vs. $\log ([O]/[R])$ at 250 nm at (a) first process and (b) second process

LIST OF SCHEMES

PART A:

- 1.1 First synthesis of metal-free phthalocyanine.
- 1.2 Synthesis of metallophthalocyanines (MPc) from typical starting materials.
- 1.3 Nucleophilic attack of $C\equiv N$ of phthalonitrile by an alkoxide leading to formation of H_2Pc .
- 1.4 Preparation of diiminoisoindoline from phthalonitrile.
- 1.5 Synthesis of 3-nitrophthalonitrile (**21**) and 4-nitrophthalonitrile (**22**).
- 1.6 Synthesis of 4,5-dichlorophthalonitrile (**27**).
- 1.7 Synthesis of tetra-sulphonated MPc from 4-sulphonic acid.
- 1.8 Synthesis of a mixture of differently sulphonated MPc, i.e. $MPcS_n$ where $n = 1, 2, 3$ or 4 . $S_n = SO_3^-$
- 1.9 Quaternation of tetrapyrroldiporphyrins (**31**) with AX: monochloroacetic acid (MCAA), diethyl sulphate (DES) or dimethyl sulphate (DMS).
- 1.10 Reactions showing the Type I mechanism.
- 1.11 Reactions showing the Type II mechanism.
- 1.12 The fate of singlet oxygen following the physical and chemical pathways in the presence of sensitiser (MPc) and DPBF.
- 1.13 Possible reactions of MPc with singlet oxygen.

- 3.1 Synthesis of unsubstituted Ti and Ta phthalocyanines.
- 3.2 Synthesis of differently sulphonated TiPcS_n (**35**) and TaPcS_n (**36**).
- 3.3 (A) Synthetic routes to 3-nitrophthalonitrile (**21**) and 4-nitrophthalonitrile (**22**).
(B) Synthetic route to 4,5-dichlorophthalonitrile (**27**).
- 3.4 Synthetic routes to α (**37a – f**) and β (**38a – f**) tetra-substituted oxotitanium(IV) phthalocyanines used in this work.
- 3.5 Synthetic route to octa-substituted oxotitanium(IV) phthalocyanines used in this work.
- 3.6 Synthetic route to tetranitro- and tetraamino-substituted oxotitanium(IV) phthalocyanine used in this work.
- 4.1 Proposed mechanism for the formation of the photooxidation products.
- 6.1 Initial sequence of the electropolymerisation process which is sustained by repeating this initial sequence via the NH_2 groups remaining on the R residue. R represents the rest of the tetraaminophthalocyanine.

PART B:

- 1.1 Proposed catalytic cycle for selective ethylene trimerisation by Chromium based catalysts.
- 1.2 Formation of methylaluminumoxane (MAO) from trimethylaluminum.
- 1.3 Methylation and cationisation of a complex following the methylation step of a halogenated complex with excess MAO.

- 2.1** Synthesis of decyl-SNS ligand leading to the catalyst Cr-decylSNS.
- 2.2** Synthesis of half-sandwich Ti complex with pendant phenyl group.

LIST OF TABLES

PART A:

- 1.1 A list of selected TiPcs and TaPcs that have been synthesised in literature.
- 1.2 UV/Vis data of some selected OTiPc complexes in chloroform (CHCl₃).
- 1.3 Ionic interactions between anionic phthalocyanine and cationic methyl viologen
- 1.4 Photochemical and photophysical parameters of selected MPcs.
- 1.5 Photooxidation of olefins catalysed by porphyrins in the presence of oxygen and visible light.
- 1.6 Potential limits of commonly used solvents with TBAP as electrolyte at platinum electrodes.
- 1.7 Electrochemical data for the electrooxidation of nitrite in pH 7.3 by MPcs.

- 2.1 Calculations for the fraction of light absorbed (α) by a typical MPc.

- 3.1 List of synthesised unsubstituted and sulphonated MPcs, their abbreviations and numbers in this thesis.
- 3.2 List of synthesised α and β tetra-substituted MPcs and their numbers in this thesis.
- 3.3 List of synthesised octa-substituted MPcs and their numbers in this thesis.
- 3.4 List of synthesised nitro- and amino-substituted OTiPcs, their abbreviations and numbers in this thesis.

- 3.5** Structural and calculated association constants (K_a) of TiPcS_n and TaPcS_n with MV^{2+} in methanol.
- 3.6** Properties of solvents used to observe UV/Vis spectra of octa-substituted OTiPc complexes.
- 3.7** Q-band spectral data of all the complexes (**33 – 41**) in various solvents.
- 4.1** DPBF (Φ_{DPBF}), singlet oxygen (Φ_Δ) and photobleaching quantum yields of the complexes under study in DMSO.
- 4.2** Photophysical parameters, i.e. fluorescence (Φ_F) and triplet quantum yields (Φ_T) as well as fluorescence (τ_F) and triplet lifetimes (τ_T) of the complexes under study in DMSO, unless otherwise stated.
- 4.3** Fluorescence quenching data for complexes **39a – d** in 1-CNP.
- 4.4** Quenching parameters of TiPcS_n (**35**) and TaPcS_n (**36**) in methanol in the absence and presence of MV^{2+} .
- 4.5** Singlet oxygen quantum yields, photobleaching quantum yields and the rate constants of **37a, 37c, 38a, 38c, 37e, 37f, 38e** and **38f** in DCM.
- 4.6** Photocatalytic oxidation of 1-hexene by complexes **37a, 37c, 38a, 38c, 37e, 37f, 38e** and **38f** in DCM.
- 5.1** List of redox potentials for MPc complexes studied in this work.

- 6.1** Peak potentials (E_p) obtained during the electrooxidation of nitrite (1 mM) at a modified GCE with **37a – d**, **38 a – d**, *poly-37e*, *poly-37f*, *poly-38e*, *poly-38f* and *poly-41* in phosphate buffer solution (pH 7.4).
- 6.2** Kinetic parameters for 1 mM nitrite detection on **37a – d**, **38 a – d**, *poly-37e*, *poly-37f*, *poly-38e*, *poly-38f* and *poly-41* in phosphate buffer solution (pH 7.4).

PART B:

- 1.1** Catalysts used in the selective ethylene trimerisation to 1-hexene.

Part A:

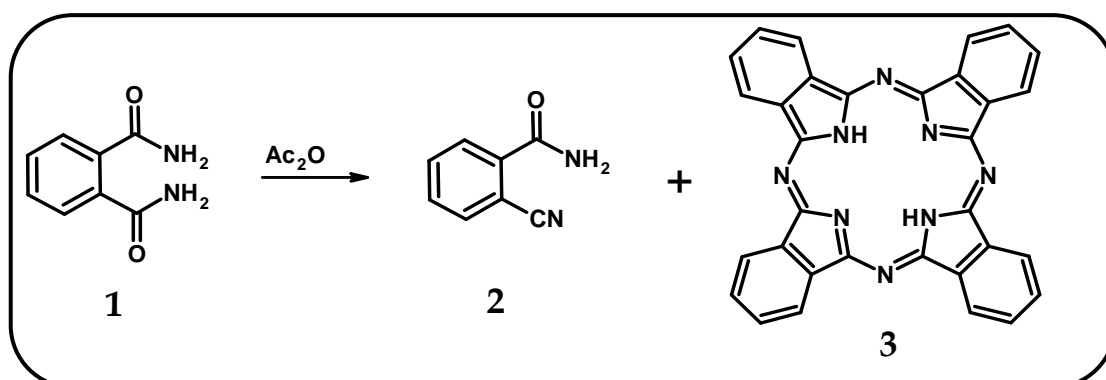
**Synthesis, photophysicochemical and electrochemical studies
of Titanium and Tantalum phthalocyanines, and their use as
catalysts for the transformation of 1-hexene**

CHAPTER 1

Introduction

1.1 Discovery and history of phthalocyanines

In 1907, Braun and Tscherniac accidentally discovered the first sample of a highly coloured phthalocyanine (Pc) [1]. The bright bluish compound, later known as metal-free phthalocyanine (**3**, Scheme 1.1), was obtained as a by-product during an attempted synthesis of *o*-cyanobenzamide (**2**) from phthalamide (**1**). Braun and Tscherniac however failed to appreciate the significance of their discovery and thus never attempted to characterise the compound. It was not until 20 years later that de Diesbach and von der Weid discovered other Pc derivatives by accident, during an attempted synthesis of phthalonitrile from *o*-dibromobenzene and cuprous cyanide [2]. The researchers from Switzerland observed the remarkable stabilities of the copper phthalocyanine derivatives, however, they also failed to fully characterise the blue complexes.



Scheme 1.1: First synthesis of metal-free phthalocyanine, where Ac₂O = acetic anhydride.

The initial investigation of the structure of phthalocyanines began when Scottish Dyes Ltd employees accidentally produced iron phthalocyanine during the transformation of phthalic anhydride to phthalimide. The reaction of phthalic anhydride and urea was carried out in a glass-lined mild steel vessel, which was later found to be lined with a bluish-green impurity instead of an expected white product. They thus concluded that the formation of the blue impurity was as a result of phthalic

anhydride, phthalimide and urea coming into contact with iron found on the mild steel. This thus incited them to successfully synthesise the blue impurity by replicating the vessel reaction conditions in the laboratory, i.e. reacting phthalic anhydride, ammonia and iron filings. In 1929, their discovery led the company to file for a patent which described the preparation of phthalocyanine from phthalic anhydride, ammonia and a metal salt [3].

The discovery was followed on by Linstead and co-workers [4-9] who performed extensive chemical studies to resolve the molecular structure of the unmetallated phthalocyanine. They concluded that the molecular structure of the phthalocyanine derivatives fitted the model in Fig. 1.1.

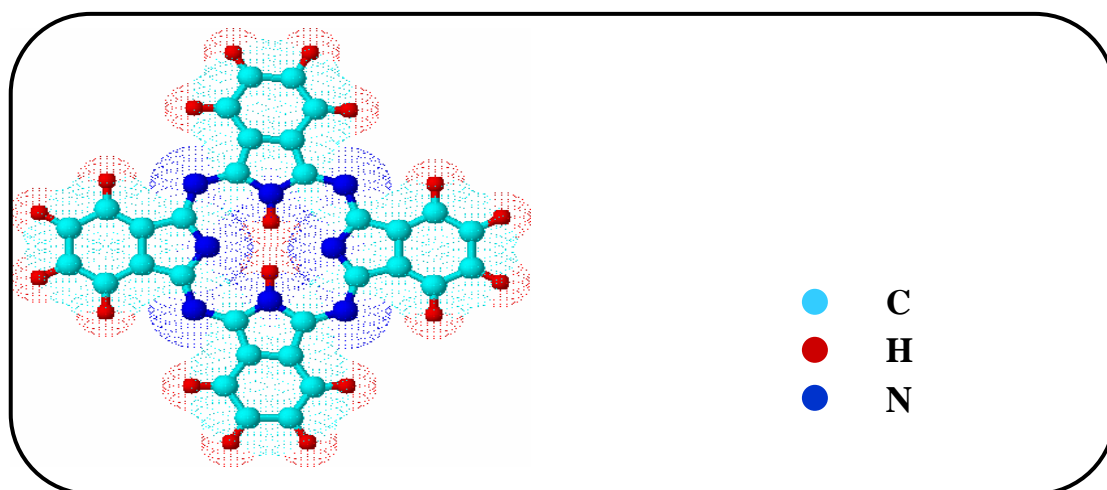


Figure 1.1: Schematic representation of the phthalocyanine parent compound of chemical formula C₃₂H₁₈N₈, i.e. 32 carbon atoms in cyan, 8 nitrogen atoms in blue and 16 surrounding hydrogen atoms and 2 hydrogen atoms in the centre of the ring in red.

The parent compound had the chemical formula C₃₂H₁₈N₈ or (C₈H₄N₂)₄H₂, i.e. it had 16 surrounding hydrogen atoms and 2 hydrogen atoms in the core of the ring. Linstead first used the word phthalocyanine which comes from two Greek terms *naphtha* (rock oil) and *cyanine* (blue). Later on, the crystal structure of these large

organic molecules was confirmed by X-ray diffraction experiments performed by Robertson [10-12].

Despite the serendipitous discovery of phthalocyanines, the interest in their chemistry ceased dismally when Linstead and his group moved on to other synthetic challenges. Most potential researchers were probably discouraged to further continue with phthalocyanine chemistry due to their low solubility in most organic solvents. This limitation thus made it impossible for the properties of these macrocycles to be fully exploited. In the 1960's the preparation of highly soluble phthalocyanine derivatives was revived and nowadays, phthalocyanines are the best studied macromolecules in chemistry.

1.2 Structure and nomenclature of phthalocyanines

Phthalocyanines (**3**), Fig. 1.2, belong to a class of compounds known as tetrapyrrolic macrocycles which includes tetraazaporphyrins also known as porphyrins (**4**), tetrabenzoporphyrins (**5**) and porphyrins (**6**). The macrocycles are structurally similar except **3** and **4** have imino nitrogen atoms at each of the four *meso* positions, commonly known as azamethine bridges, while **5** and **6** have methine bridges. The type of bridges connecting the iminoisindoline units determines the size of the cavity, thus macrocycles with azamethine bridges are known to have smaller inner cavities than macrocycles with methane bridges [13,14]. Macrocycles **3** and **5** additionally have four benzo-subunits which allow for addition of functional groups onto their respective framework. The annulation of the Pcs greatly affects their electronic spectra and therefore they tend to have much stronger absorbances at longer wavelengths than do porphyrins.

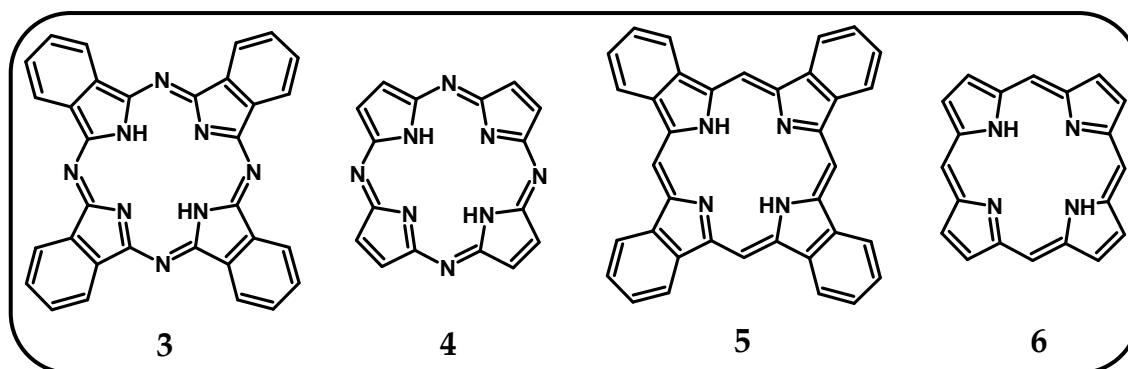


Figure 1.2: A class of tetrapyrrolic macrocycles.

Since four iminoisoindoline units make up the structure of a phthalocyanine, a symmetrical macrocycle with a conjugated system of 18 π electrons that exhibits exceptional stability is formed. The extended conjugation is responsible for the blue-green colour of these macrocycles. Phthalocyanines are considered as fused porphyrin analogs and using the known International Union of Pure and Applied Chemistry (IUPAC) nomenclature of tetrapyrroles [15], they are formally known as tetrabenzo[*b,g,l,q*][5,10,15,20]tetraazaporphyrins, Fig. 1.3.

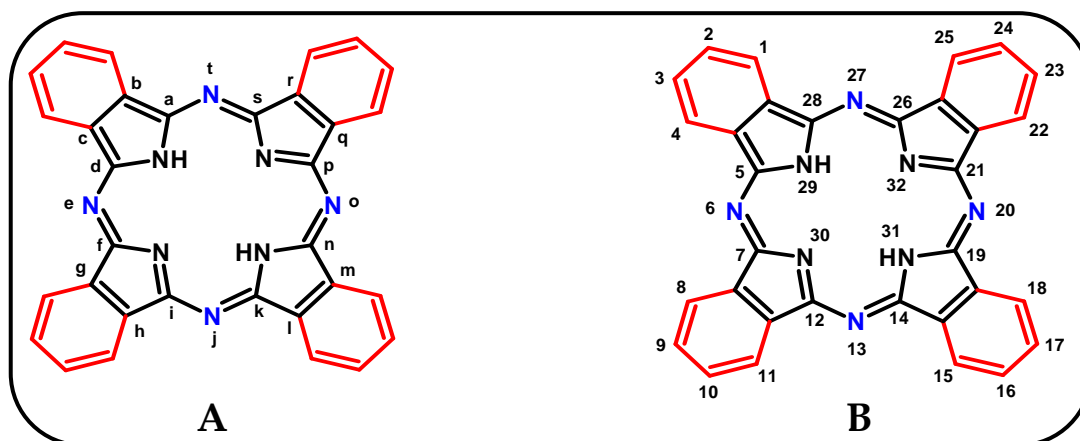


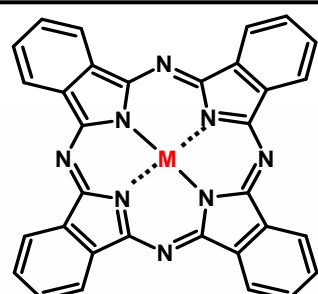
Figure 1.3: IUPAC nomenclature for point of fusion in a heterocyclic system (A) and an assignment of external numbering to a macrocyclic system (B).

There are 16 possible sites of substitution onto the fused benzene rings (red), i.e. peripheral substitution (carbon number 2, 3, 9, 10, 16, 17, 23, 24) and non-peripheral substitution (carbon number 1, 4, 8, 11, 15, 18, 22, 25). Change in the central metal ion or substitution onto the fused benzene rings results in modification

in the properties of the molecule, e.g. colour, crystal structure, solubility, electronic and catalytic properties.

1.3 Metallophthalocyanines and their general applications

Phthalocyanines are versatile systems in that the two central hydrogen atoms can be substituted by metallic atoms - such as those shown in red, Fig.1.4 - to form over 70 different metallophthalocyanines (MPcs), Fig. 1.4 (insert). In MPc, the macrocycle is dianionic, i.e. Pc^{2-} , and thus acts as a ligand which complexes with most metal ions due to its rich coordination chemistry. Two Pc nitrogens (N_{29} and N_{31} , Fig. 1.3) covalently bond with the central atom through loss of the central hydrogens, and two other nitrogens (N_{30} and N_{32}) have a co-ordinate linkage with the metal.



1 H Hydrogen 1.00794																	2 He Helium 4.003	
3 Li Lithium 6.941	4 Be Beryllium 9.012182																	10 Ne Neon 20.1797
11 Na Sodium 22.989770	12 Mg Magnesium 24.3050																	18 Ar Argon 39.948
19 K Potassium 39.0983	20 Ca Calcium 40.078	21 Sc Scandium 44.955910	22 Ti Titanium 47.867	23 V Vanadium 50.9415	24 Cr Chromium 51.9961	25 Mn Manganese 54.938049	26 Fe Iron 55.845	27 Co Cobalt 58.933200	28 Ni Nickel 58.6934	29 Cu Copper 63.546	30 Zn Zinc 65.39	31 Ga Gallium 69.723	32 Ge Germanium 72.61	33 As Arsenic 74.92160	34 Se Selenium 78.96	35 Br Bromine 79.904	36 Kr Krypton 83.80	
37 Rb Rubidium 85.4678	38 Sr Strontium 87.62	39 Y Yttrium 88.90585	40 Zr Zirconium 91.224	41 Nb Niobium 92.90638	42 Mo Molybdenum 95.94	43 Tc Technetium (98)	44 Ru Ruthenium 101.07	45 Rh Rhodium 102.90550	46 Pd Palladium 106.42	47 Ag Silver 107.8682	48 Cd Cadmium 112.411	49 In Indium 114.818	50 Sn Tin 118.710	51 Sb Antimony 121.760	52 Te Tellurium 127.60	53 I Iodine 126.90447	54 Xe Xenon 131.29	
55 Cs Cesium 132.90545	56 Ba Barium 137.327	57 La Lanthanum 138.9055	58 Ce Cerium 140.116	59 Pr Praseodymium 140.90765	60 Nd Neodymium 144.24	61 Pm Promethium (145)	62 Sm Samarium 150.36	63 Eu Europium 151.964	64 Gd Gadolinium 157.25	65 Tb Terbium 158.92534	66 Dy Dysprosium 162.50	67 Ho Holmium 164.93032	68 Er Erbium 167.26	69 Tm Thulium 168.93421	70 Yb Ytterbium 173.04	71 Lu Lutetium 174.967		
87 Fr Francium (223)	88 Ra Radium (226)	89 Ac Actinium (227)	90 Th Thorium 232.0381	91 Pa Protactinium 231.03588	92 U Uranium 238.0289	93 Np Neptunium (237)	94 Pu Plutonium (244)	95 Am Americium (243)	96 Cm Curium (247)	97 Bk Berkelium (247)	98 Cf Californium (251)	99 Es Einsteinium (252)	100 Fm Fermium (257)	101 Md Mendelevium (258)	102 No Nobelium (259)	103 Lr Lawrencium (262)		

Figure 1.4: Periodic table showing metals (in red) that have been used in the metallophthalocyanine synthesis.

A metal-free phthalocyanine (H_2Pc) is generally considered to be of square planar geometry, with a π -electron system of D_{2h} symmetry. Most metal ions in an oxidation state +2, which snugly fit inside the cavity of the ring, complex with the Pc ring to form a stable 1:1 planar metal-ligand complex, thus increasing the symmetry from D_{2h} to D_{4h} . These types of phthalocyanine complexes, e.g. NiPc [16] and CuPc [17], are generally strong such that removal of a metal ion results in the destruction of the Pc ring. They are also not affected by strong acids such as concentrated H_2SO_4 or strong bases; however, they can be broken down to phthalimide or phthalic acid by strong oxidising agents such as dichromate or ceric salts [4,8,18]. Larger metal ions tend to distort the geometry of the macrocycle to some extent as they do not fit into the cavity of the ring. The molecular symmetry is decreased to C_{4v} (i.e. square pyramidal) and thus the metal ions tend to lie above the ring to adopt a ‘shuttlecock-shaped’ configuration [19,20], Fig. 1.5(i). MPcs such as Pb^{2+} [21], Sn^{2+} [22,23] and Ge^{2+} [24], form these non-planar structures of C_{4v} symmetry as a result of the rotation of the rigid isoindole units that reduce the internal stress induced by the large metals. It is worth mentioning that the introduction of two chloride ions to SnPc and GePc leads to both change of valence as well as molecular symmetry from C_{4v} to D_{4h} of Cl_2SnPc and Cl_2GePc as shown in Fig. 1.5(ii).

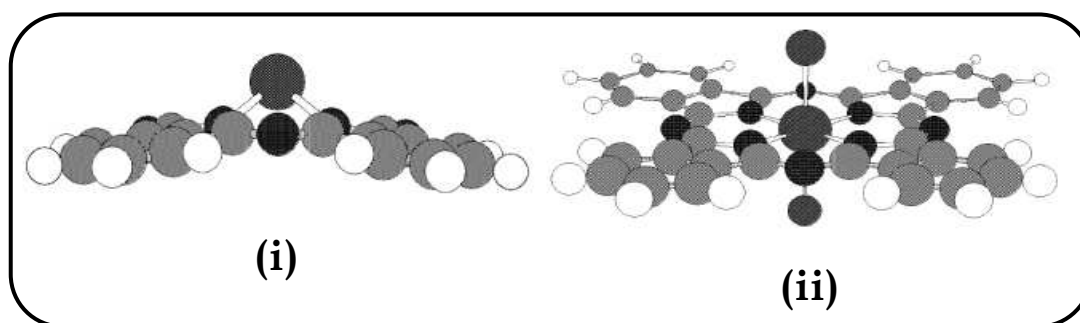


Figure 1.5: MPc structures showing (i) ‘shuttlecock-shaped’ C_{4v} symmetry and (ii) D_{4h} symmetry.

On the contrary, 2:1 metal-ligand derivatives of smaller monovalent ions such as Li^+ , Na^+ , K^+ are formed where both metal ions lie on each face of the Pc plane [25-29], Fig. 1.6(i). The protrusion enhances their solubility in polar organic solvents by disrupting the intermolecular forces between the Pc rings [28,29]. The Li^+ , Na^+ , K^+ ions are also labile such that they are either easily replaced by robust metal ions that have stronger interactions with the ring or are easily removed by dilute acids to produce metal-free phthalocyanines. Hence they are used as precursors for the synthesis of novel MPcs such as tetra-, octa-substituted and sandwich-type MPcs [30-32]. The use of the “dilithium-method” in MPc formation is advantageous over many other routes in that MPc that require low boiling point solvents and stoichiometric amounts of Pc and metal salts can be prepared in large amounts.

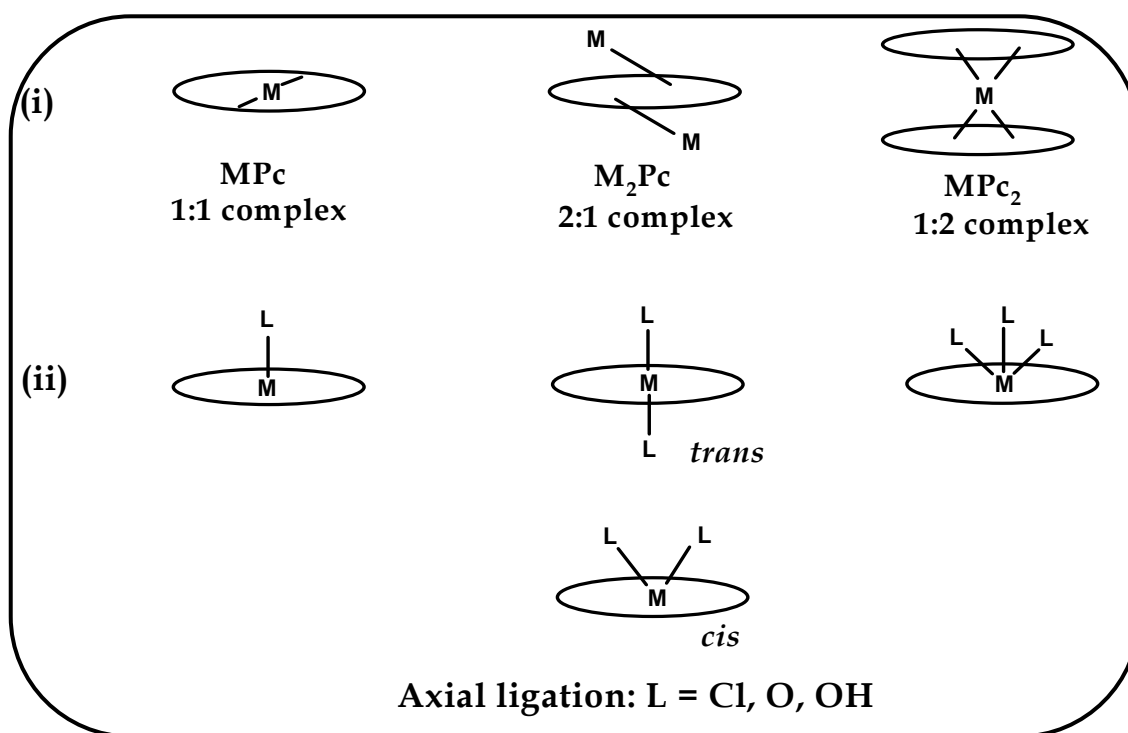


Figure 1.6: (i) Various forms of MPc complexes (ii) MPc in which metals in oxidation states greater than +2 are bonded to axial ligands.

Trivalent, tetravalent or pentavalent metal ions such as Al^{3+} , Sn^{4+} , Ti^{4+} and Ta^{5+} require axial ligands (through a *trans*- or *cis*-coordination) in order to maintain

the neutrality of the metal complex, Fig. 1.6(ii). Some of these metals (e.g. Ti, Nb, Ta) are not fully accommodated into the cavity because of their large size. They are thus displaced from the ring such that they lie above the plane of the Pc [33-35]. Titanium phthalocyanines (TiPcs) may additionally adopt different coordination geometries, depending on whether the axial ligand is 'O' or 'Cl'. OTiPc is square pyramidal with a C_{4v} symmetry [36] while Cl_2TiPc has a trigonal prism geometry of D_{3h} symmetry [33]. MPcs with coordination number 7 such as in the case with Cl_3TaPc [35], have a C_{2v} symmetry and exhibit a capped trigonal prism geometry. In the case of rare-earth metals such as lutetium, a 1:2 metal:ligand complex (known as sandwich complex or bisphthalocyanine) is formed when the large metal ion complexes with two Pc units [37,38]. The formation of bisphthalocyanines is possible through metal coordination to all isoindole nitrogens in each Pc macrocycle. The Pc macrocycles are rotated by a staggering angle (α), with the sandwich complexes either adopting a cubic geometry ($\alpha = 0^\circ$), or square antiprism geometry ($\alpha = 45^\circ$) as in the case with *bis*(phthalocyaninato)M (III) complexes (M = neodymium [39] and lutetium [40]).

Due to their physical and chemical stabilities, the MPcs have been extensively investigated for their potential use in a variety of applications. For example, MPcs are valued for their colour and therefore are important in visible applications such as electrophotography [41,42], ink-jet printing [43,44] and xerography [45]. In electrophotography, light and electricity are used to produce an image, a process familiar in photocopying and laser printing. A type IV polymorph of oxotitanium phthalocyanine (OTiPc) has been found [46] to be the best material to generate the latent image in laser printers through its excellent compatibility with the

semiconductor infrared lasers. In colour photocopiers, the cyan toner used to produce images is based on CuPc pigment, namely CI Pigment Blue 15.

Ink-jet printing produces images by using electromagnetic fields that guide electrically charged ink streams onto a page. Copper phthalocyanines [47] are cyan dyes of choice as they possess all-round properties, namely, high chroma, high strength and high light-fastness. Xerography involves a photocopying process which forms a negative image by a resinous powder on an electrically charged plate, such that the image is transferred to and thermally fixed as positive on paper. Use of Pcs, e.g. OTiPc, NiPc, CuPc [48], as active components is favoured because they are less toxic and many absorb in the infrared (IR) region such that use of infrared lasers is possible.

Pcs have also attracted much attention in oncology as photosensitisers for malignant tumour treatment by photodynamic therapy (PDT). In PDT, O₂, light and a photosensitising drug, e.g. phthalocyanines, are used in combination. Briefly, PDT involves the selective uptake and retention of a photosensitizer in a tumour, followed by irradiation with light of a particular wavelength. Tumour necrosis is then initiated, through the formation of singlet oxygen, the cytotoxic species. Biochemical molecules [49] can suffer significant damage that may lead to death through singlet oxygen ingestion. In vitro/vivo studies utilising diode laser and using axially substituted silicon naphthalocyanine (formed through annulation of further benzene units on MPc) have been found to be effective in cell destruction [50]. Phthalocyanine research activity in the PDT field has expanded tremendously during the past 20 years [51-54]. For example, commercially available Photosens[®], composed of differently sulphonated aluminium phthalocyanines has been

successfully used for both diagnosis and clinical PDT of various cancers including small lung tumors.

Since Pcs strongly absorb light in the red region, introduction of electron donating substituents can shift their main absorption band to the near-IR region. Infrared-absorbing Pcs such as sulphur-substituted Pcs find use in energy conversion and optical applications for laser thermal transfer, solar screens, optical data storage (ODS) as in CD-RW and security, e.g. brand protection. Pcs absorbing at around 780 nm to match the 780 and 830 nm semiconductor lasers are used for ODS whilst for security applications; Pcs are used in lasers to cover the 700-1000 nm range. Near-IR Pcs have also been investigated for their non-linear optical (NLO) applications needed for eye protection against pulsed lasers, photonics and photoelectronics. Lead [55] and indium [56] Pcs have shown to be very good materials for optical limiting as their heavy atom effect reveal enhanced optical limiting behaviours.

MPcs are well known as catalysts for both homogeneous and heterogeneous reactions, which in most cases involve the transfer of electrons. Both the catalyst and analyte are in solution for homogeneous catalysis whereas for heterogeneous catalysis, the catalyst is in solid form. For both homogeneous and heterogeneous systems, reactions are possible through usage of oxidants such as hydrogen peroxide (H_2O_2) or may be light-driven and thus promote reactions photocatalytically. In homogeneous reactions, MPcs exhibit enzyme-like catalytic activities since they are similar in structure to protohemes found in heme-enzymes that are important for many biological reactions [57]. The degree of importance is extended to heterogeneous systems in which MPcs catalyse a number of environmentally toxic pollutants such as chlorophenols by being immobilised or supported onto resins [58] or polymer matrixes [59]. Oxidative decompositions of pollutants such as chlorophenols have

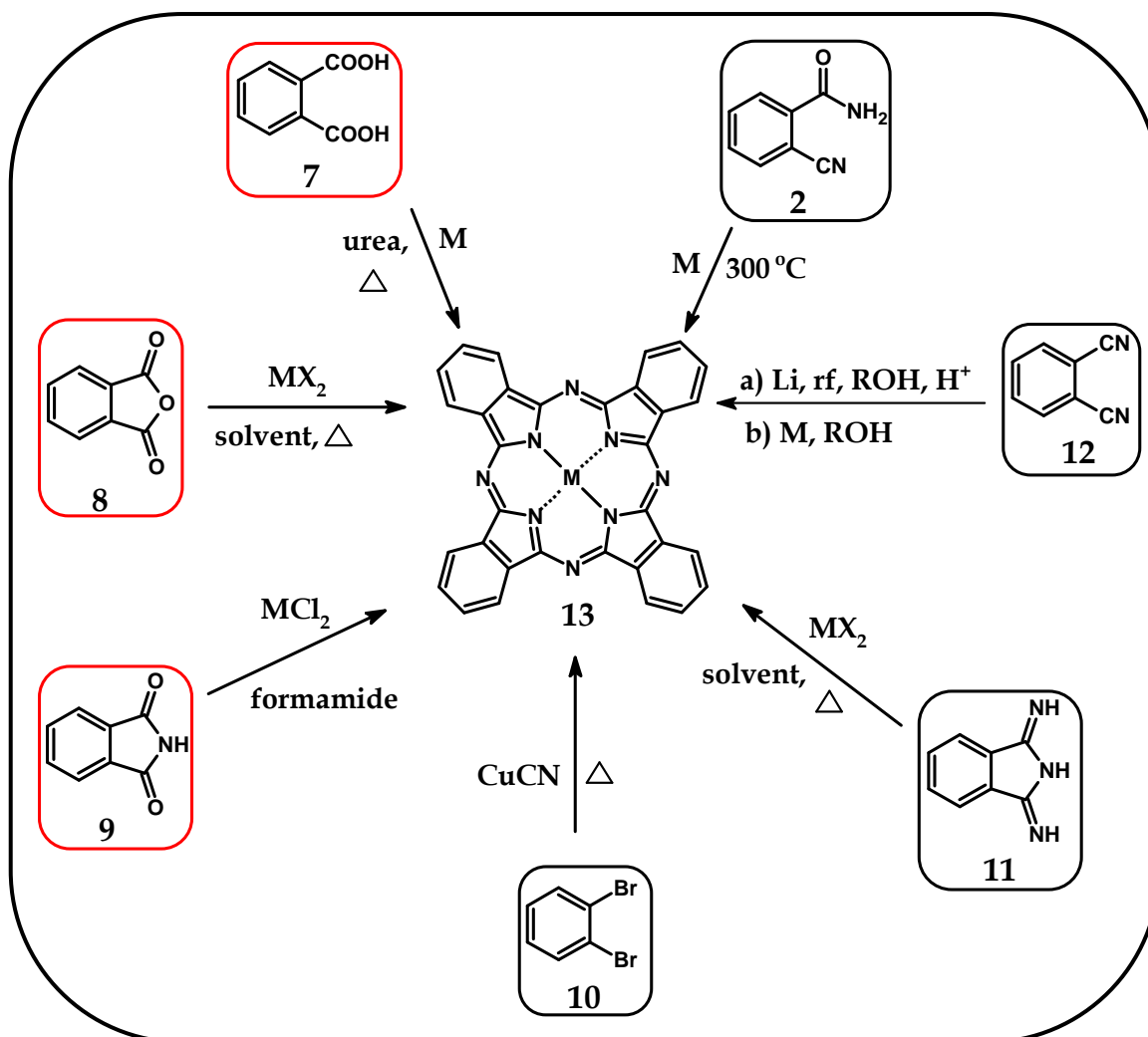
been observed with iron, manganese and cobalt Pcs [59]. Furthermore, MPcs may be insoluble in water-based reactions and thus can be deposited onto electrodes in order to electrochemically catalyse reactions [60]. Here, the surface of the electrode is modified in some way such that reactions are accelerated at the electrode and overpotentials significantly reduced. Modification includes adsorption on the electrode surface thus forming an electroactive film of a chemically modified electrode (CME). Also mixing MPcs with microparticles such that they become part of the electrode constituents, results in the formation of a composite paste electrode, e.g. carbon paste electrode. Oxygen electroreduction to hydrogen peroxide or water [61-63], electrooxidation of mercaptans [64-66], hydrazine [67-69] and nitrite [70-72], are some of the reactions catalysed by MPcs at the electrode surface.

1.4 Phthalocyanine syntheses

As mentioned before, a phthalocyanine macrocycle consists of four iminoisoindoline units. Regardless of the conditions used, Pc macrocycles are formed by the cyclotetramerisation of the precursor units. The synthetic strategy would therefore start from the molecules which make up these units.

1.4.1 Unsubstituted metal-free and metallophthalocyanines

The preparation of unsubstituted phthalocyanines involves a one-step condensation reaction of a precursor which is generally derived from phthalic acid (**7**). Other derivatives include *o*-cyanobenzamide (**2**), phthalic anhydride (**8**), phthalimide (**9**), *o*-dibromobenzene (**10**), diiminoisoindoline (**11**) and phthalonitrile (**12**), Scheme 1.2. Often, one type of precursor is an intermediate in the cyclotetramerisation reaction of another.



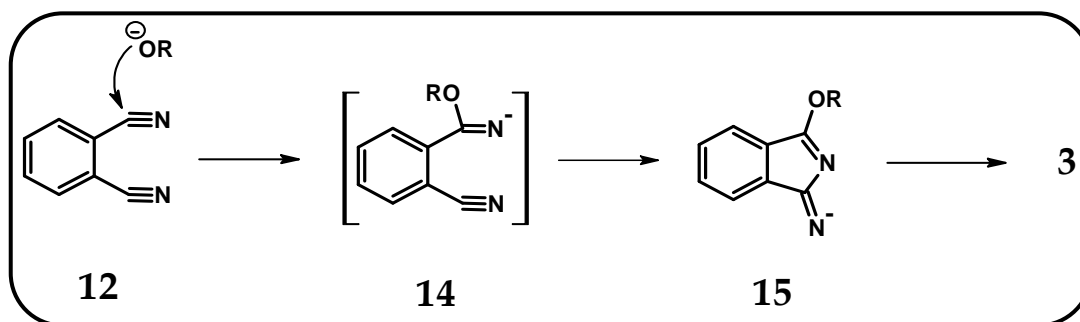
Scheme 1.2: Synthesis of metallophthalocyanines (MPcs) from typical starting materials.

For example:

- i) a stepwise progression from the acid (**7**) through to anhydride (**8**), imide (**9**) and amide (**1**), finally ends in the desired product, i.e. phthalonitrile (**12**) [73,74]
- ii) **12** is an intermediate in the cyclotetramerisation of *o*-dibromobenzene (**10**) in the presence of cuprous cyanide [75,76]
- iii) reaction of **12** with ammonia results in the preparation of diiminoisoindoline (**11**) [77,78]

As phthalic acid derivatives are cheaper, they are normally used for industrial scale syntheses of Pcs, however rigorous conditions such as high temperature, high pressure or use of catalyst are required. For laboratory scale syntheses, phthalonitriles are more commonly used. In the presence of a base, a metal salt and a high boiling point solvent, good yields of MPcs (**13**) are obtained after cyclisation of **12** [79]. Preparations of unsubstituted MPcs and/or H₂Pcs follow basic methods which may have common features and mechanisms.

H₂Pcs are usually prepared by a method derived from the one used by Linstead [4] in the 1930's. The cyclisation of the phthalonitrile is induced by a solution of lithium [80], sodium or magnesium alkoxides often generated *in situ* in an alcohol (e.g. 1-pentanol, 1-octanol). Baumann *et al.* [81] suggested that the phthalonitrile cyano group undergoes a nucleophilic attack by the alkoxide anion (**14**), thus forming a 1-alkoxy-3-iminoisoindolenine intermediate (**15**), which gets reduced and cyclised to **3**, Scheme 1.3.



Scheme 1.3: Nucleophilic attack of C≡N of phthalonitrile by an alkoxide leading to formation of H₂Pc.

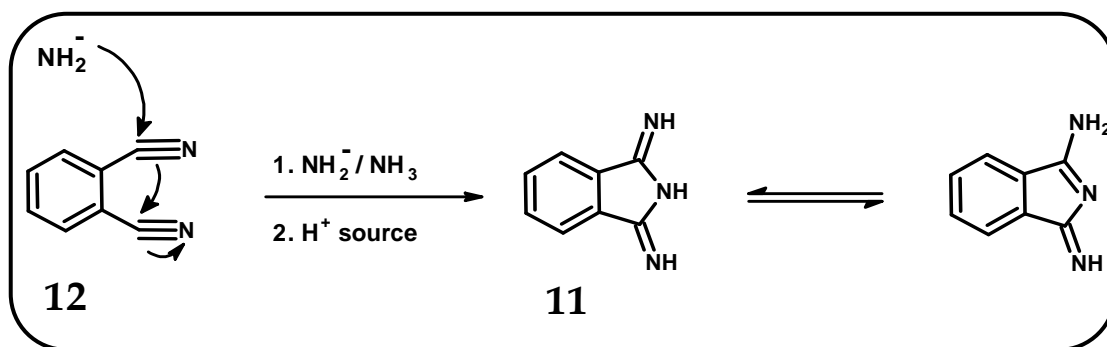
Demetallation of MPc (M = Li₂, Na₂ or K₂) by a solution of dilute acid results in metal-free Pcs [32,82,83]. This method is often preferred over the cyclotetramerisation of phthalonitrile in high-boiling solvents such as 1-chloronaphthalene and quinoline [84,85], which are carried out at elevated

temperatures. Replacement of the “Linstead method” by the commonly used “Tomoda method” [86,87] has proved to be successful in the preparation of H₂Pcs. The “Tomoda method” is an alternative method that involves use of a non-nucleophilic base such as 1,8-diazabicyclo[5.4.0]undec-7-ene (DBU) [88], which avoids side-products usually obtained with other strong bases. Furthermore, the extremely rare preparation of unsubstituted H₂Pcs under non-alkaline conditions is known [89-92]. Organic reducing agents such as hydroquinone are used to enhance the formation of these macrocycles by donating protons in the reaction. A recent report [93] also describes the general approach to the preparation of these macrocycles, with cerium (III) salt as a promoting agent. The new methodology gives moderate yields that are comparable to those obtained by typical base-catalysed cyclisation methods.

Moreover, metal-free analogs serve as precursors for various MPcs, thus addition of a metal salt in a reaction, leads to the formation of MPc in good yields. This method is however limited as the core of the Pc ring is rather small. A pre-existing Pc ligand will thus readily complex with metal ions which fit into the core of the ring. VO²⁺, Co²⁺, Ni²⁺, Pd²⁺, Pt²⁺, Cu²⁺, Zn²⁺, Al³⁺ and Ga³⁺ are examples of such metals. Pcs with metals of larger radii can only be formed via the template reaction, thus causing the resulting Pc to strain in order to accommodate the large metals and hence some planarity is lost.

The most highly used diiminoisoindoline (**11**) has been vital in the preparation of Pcs. Pure **11** can be exclusively obtained from **12** and ammonia, in the presence of sodium methoxide [94-96], Scheme 1.4. The main advantage of **11** is that it readily cyclises such that Pcs are formed under mild conditions, even at room temperature. Therefore, due to its high reactivity, **11** is very useful in cases where phthalonitriles

are resistive towards template formation, hence unnecessary loss of precursors is avoided. Solvents such as trichlorobenzene and *o*-dichlorobenzene are generally used in the synthesis of Pcs. Also, treatment of phthalonitrile with *N,N*-dimethylethanolamine (DMEA) performed under ammonia atmosphere is another common procedure for the preparation of H₂Pcs [97].



Scheme 1.4: Preparation of diiminoisoindoline from phthalonitrile.

MPcs may be prepared by the “Wylar method” which involves the use of phthalic acid (7) [98], phthalic anhydride (8) [99] or phthalimide (9) [100]. The reactions may be carried out as a melt or in a solvent such as nitrobenzene, with urea as a non-volatile source of nitrogen and ammonium molybdate as a catalyst. Most commercial processes are based on 7 – 9 because the substrates are less expensive and are more accessible than the phthalonitrile (12) or diiminoisoindoline (11). Other appropriate precursors although less used are *o*-cyanobenzamide (2) and *o*-dibromobenzene (10). *o*-Cyanobenzamide (2) has been successfully used for the preparation of unsubstituted MPcs such as Cl₂SiPc [101], OsPc [102] and FePc [103] as it is not normally used in the synthesis of substituted derivatives. In reactions of 10, cuprous (I) cyanide is typically a source of cyanine, which generates 12 as an intermediate via an *in situ* Rosenmund-von Braun reaction [75] (converts aryl halides into aryl nitriles by cyano-dehalogenation). The first use of 10 in conjunction with cuprous (I) cyanide in pyridine to form CuPc in 23 % yield was observed in 1927 [2].

MPc complexes are usually obtained in yields higher than that of their metal-free derivatives (3). This is because the template effect which is afforded by the metal ion favours the cyclotetramerisation of the precursor.

Unsubstituted Pcs exhibit poor solubility in common organic solvents due to intermolecular interactions between their π -systems, therefore, a strong crystal lattice is favoured. Nevertheless, these materials have been successfully purified using Soxhlet extraction, repeated sublimation in vacuo or recrystallisation from sulphuric acid and water to yield highly pure unsubstituted Pcs. Introducing substituents at the two different positions on their benzenoid rings, i.e. α (non-peripheral) and β (peripheral) positions greatly improves phthalocyanine solubility. Several synthetic methods for the preparation of substituted Pcs have been developed over the last two decades and they will be described below.

1.4.2 Substituted phthalocyanines

Highly stable crystal structures with high molecular lattice energies are formed by unsubstituted Pcs. They are thus extremely insoluble in most organic solvents and water, due to the high degree of hydrophobicity that is exhibited by the aromatic macrocycle core. Use of sulphuric acid at concentrations greater than 8 M in dissolving unsubstituted Pcs seems to be effective since solubility in universal organic solvents such as dimethylformamide (DMF) and dimethylsulphoxide (DMSO) is negligible. In this instance a major disadvantage of using the acid is the fact that it changes the properties of the Pc by protonating the ring, therefore its usefulness is extremely limited. In order to increase the solubility of these macrocycles, different substituents which include aliphatic chains, aromatics, amines, thiols, halides and acids can be added to the Pc framework.

1.4.2.1 Tetra-substituted phthalocyanines

Two basic methods are used to prepare substituted Pcs, i.e. either by substitution on a preformed Pc ring or by condensation of an appropriately substituted precursor (usually phthalonitrile). The former has been successfully used in for example sulphonation [104] or chlorosulphonation [105] of unsubstituted Pcs with respectively 20 – 30 % oleum and chlorosulphonic acid. With this method, purification and isolation of the desired product is almost impossible, since complex isomeric mixtures with varying degrees of substitution are formed. The use of phthalonitrile is however generally preferred since control of the formation of specifically substituted products is permitted through phthalonitrile substitution at the 3- or 4-position. Although far cleaner than the first method, constitutional isomers of tetrasubstituted Pcs are obtained. Monosubstitution at the 3-position leads to four single isomers of (C_{4h}) 1,8,15,22-, (D_{2h}) 1,11,15,25-, (C_{2v}) 1,11,18,22- and (C_s) 1,8,18,22-tetrasubstituted complexes, Fig. 1.7(i); while at the 4-position, single isomers of (C_{4h}) 2,9,16,23-, (D_{2h}) 2,10,16,24-, (C_{2v}) 2,9,17,24- and (C_s) 2,9,16,24-tetrasubstituted complexes are obtained, Fig. 1.7(ii).

The separation of these regioisomers can be tedious though it has been shown that separation is possible by chromatographic techniques such as high performance liquid chromatography (HPLC) [106,107]. A statistical mixture of 12.5 % (C_{4h}), 12.5 % (D_{2h}), 25.0% (C_{2v}) and 50.0 % (C_s) has always been found in the separation of tetrasubstituted compounds in both α and β positions, i.e. the ratio of 1:1:2:4 is expected [106,107]. Selective formation of the 1,8,15,22-isomer (C_{4h}) has been observed, for example, during the cyclotetramerisation of 3-alkoxyphthalonitriles [106,108]. For both α and β positions, C_{4h} can be isolated due to its generally poor solubility [82].

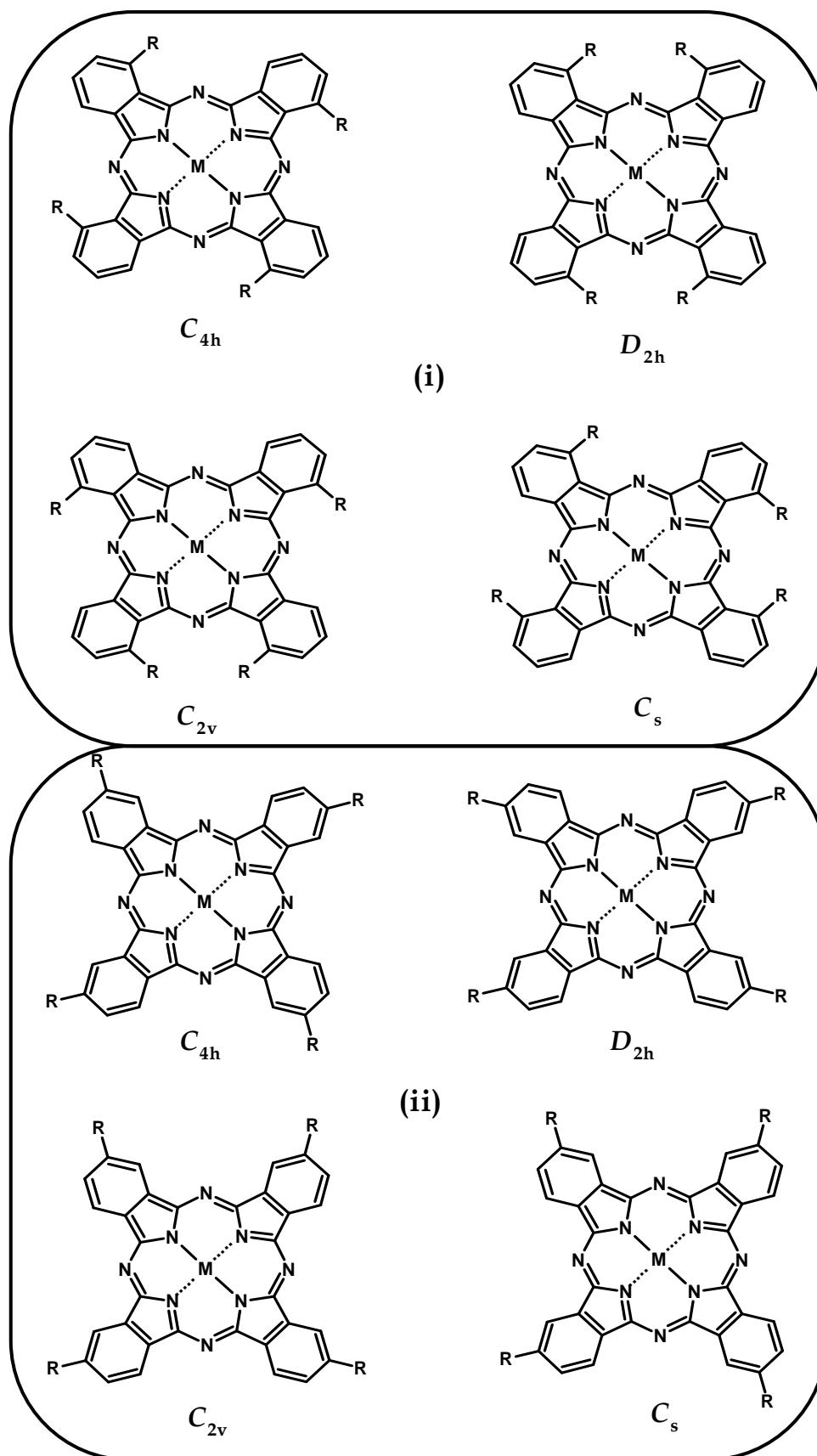
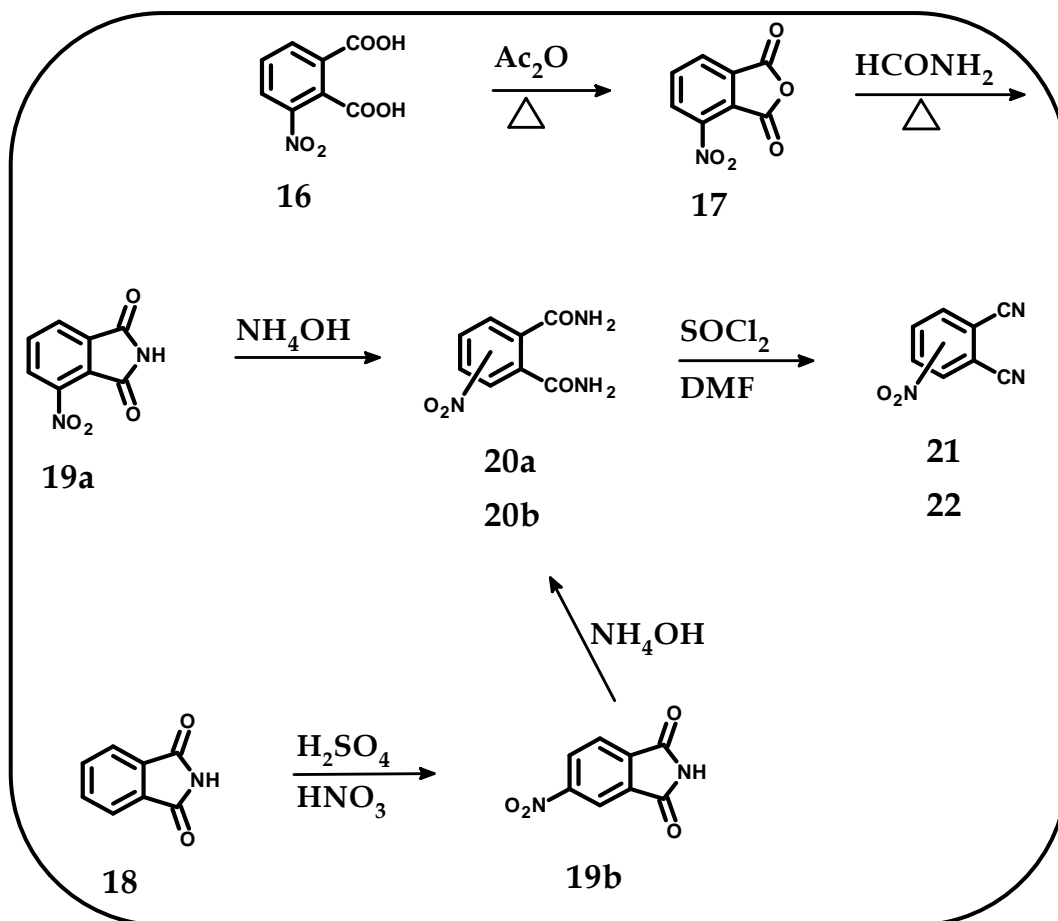


Figure 1.7: Constitutional isomers from (i) 1,(4)- and (ii) 2,(3)-tetrasubstituted MPcs.

Furthermore, Hanack and co-workers [106,107,109] proved that the less symmetrical isomers have a higher dipole moment that is derived from the more unsymmetrical arrangement of the substituents in the periphery of the ring.

The presence of substituents is especially advantageous as they address the problem of insolubility. Substituents confer the complexes soluble in most organic solvents as opposed to unsubstituted Pcs, which have limited applications and thus cannot be fully exploited. Although soluble in most organic solvents, phthalocyanines tend to aggregate. This limitation can be addressed by introducing bulky or long-chain substituents which will render them soluble by causing substantial disruption of the strong interactions of the parent Pc rings. Solubility is more enhanced for tetra-substituted Pc derivatives than the corresponding octa-substituted derivatives due to their lower degree of order in the solid state [110], as well as the formation of constitutional isomers and the high dipole moment that results from the unsymmetrical arrangement of the substituents at the periphery [110-112].

It can also be envisaged that the presence of substituents alters the intrinsic properties of the molecule since they alter the electronic distribution of the Pc ring [113]. In this way, the bulk characteristic of the molecule may be tailored. With substitution, new materials which may show improved or more functional characteristics may also be developed. For example, a large network of conjugated π electrons confers a high electrical polarisability to the ring, thus offering the possibility of several kinds of electronic transitions in the ultraviolet/visible (UV/Vis) spectral range [114].



Scheme 1.5: Synthesis of 3-nitrophthalonitrile (**21**) and 4-nitrophthalonitrile (**22**).

A strategy for the preparation of tetrasubstituted Pcs uses the nucleophilic aromatic substitution of 3- (**21**) or 4-nitrophthalonitrile (**22**) with alcohols or thiols, Scheme 1.5. Although commercially available, the phthalonitrile derivatives can easily be prepared from inexpensive commercially available starting materials in good yields. The synthetic steps for the two phthalonitriles are similar, except for the initial steps. The first step in the synthesis of **21**, is the transformation of 3-nitrophthalic acid (**16**) in acetic anhydride to afford 3-nitrophthalic anhydride (**17**). The dehydration of **16** is rapid and yields are sufficient (95 %). Anhydride formation can also be obtained by refluxing in other dehydrating agents such as methoxyacetylene, dicyclohexylcarbodiimide (DCC) or diphosphorus pentoxide. The anhydride (**17**) can

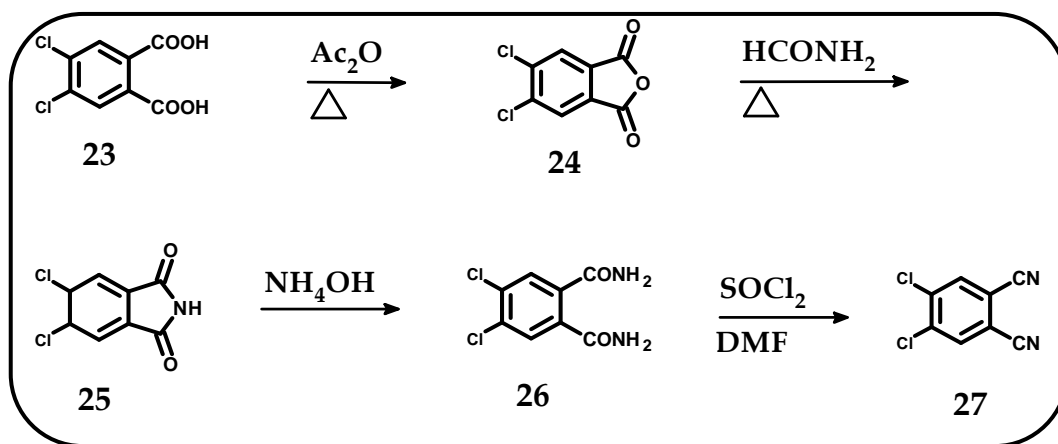
additionally be obtained by direct nitration of phthalic anhydride. However, the isomeric 4-nitro compound is also formed, thus making isolation of the desired compound difficult. 3-Nitrophthalimide (**19a**) is afforded by refluxing the anhydride in formamide, which acts as both solvent and source of ammonia. A feasible reaction for the preparation of 4-nitrophthalimide (**19b**) is achieved by nitration of phthalimide in an acid mixture of concentrated sulphuric and nitric acids at temperatures slightly below room temperature [115,116]. Reacting imides in concentrated aqueous ammonium hydroxide affords the 3- and 4-nitrophthalamides (**20a** and **20b**) respectively, dehydration of which results in the corresponding phthalonitriles.

For the synthesis of substituted phthalonitriles, nucleophilic aromatic substitution reactions, known as S_NAr , are employed. A base catalysed nucleophilic displacement of the nitro group from an activated aromatic substrate has been well investigated [117]. In general, a variety of strong nucleophiles under polar aprotic solvent conditions, effectively displace the nitro group from an activated aromatic substrate. Nucleophiles such as alcoholates [118,119] and thiolates [118,120] effectuate a nitro displacement from cyano activated substrates in dry polar aprotic solvents such as DMF or DMSO at room temperature. Furthermore, nitro groups are comparable to fluoro groups as leaving groups, with the approximate order of leaving group ability as: $F > NO_2 > OTs > OPh > Cl, Br > I$ [117,121].

1.4.2.2 Octa-substituted phthalocyanines

Due to their position, symmetrically disubstituted precursors either form 1,4,8,11,15,18,22,25- or the 2,3,9,10,16,17,23,24-octasubstituted phthalocyanines. The former are formed by substitution at the eight non-peripheral positions, while the latter at the eight peripheral positions. The substituted Pcs studied in detail are the

ones octasubstituted at the peripheral positions, thus in this work, the discussion will be limited to these Pcs. A major advantage in preparing octasubstituted Pc derivatives is that isomerically pure products are produced hence positional isomers formed as in the case of tetrasubstituted Pcs are avoided. Therefore their purification is much easier than with the tetrasubstituted compounds and the molecular geometry is especially fundamental in applications such as non-linear optics. 4,5-Disubstituted phthalonitrile derivatives are prerequisites since their condensation results in the formation of peripherally substituted octasubstituted Pcs. In this work, 4,5-dichlorophthalonitrile (**27**) is employed and it is strategically prepared from the inexpensive commercially available 4,5-dichlorophthalic acid (**23**), which undergoes the reaction steps similar to those of **16**, Scheme 1.6. This affords the 4,5-dichlorophthalic anhydride (**24**) which in turn undergoes nucleophilic addition of ammonia upon heating in formamide to afford 4,5-dichlorophthalimide (**25**).



Scheme 1.6: Synthesis of 4,5-dichlorophthalonitrile (27).

The phthalimide can also be prepared directly from phthalic acid using aqueous ammonia for example, though the formamide route affords overall yields (~80 %) that are higher than the single step ammonolysis. The imide is then transformed to the corresponding 4,5-dichlorophthalamide (**26**) by ammonolysis in

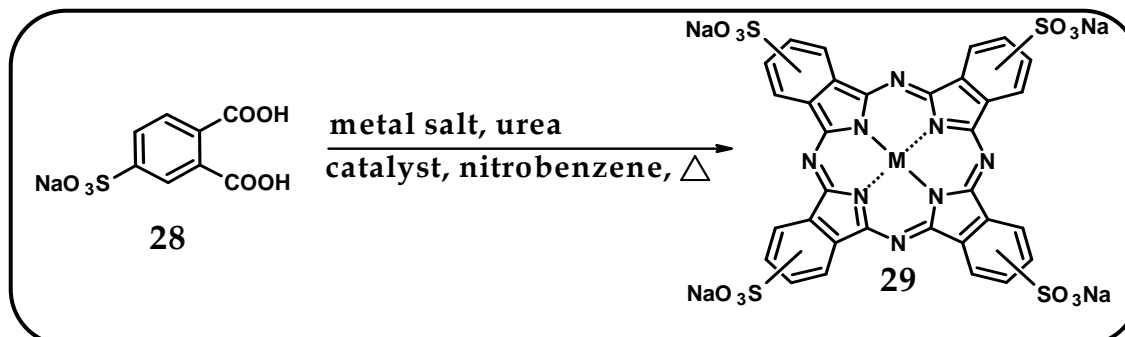
concentrated aqueous solution of ammonia. The reaction times are prolonged since they are carried over 48 hours compared to other 4,5-dihalophthalimides such as 4,5-diiodophthalimide which only takes 1.5 hours to afford 4,5-diiodophthalimide at 50 °C [122]. Eventual dehydration of the diamide **26** affords the dinitrile **27** in undesirable yields of ~ 49 % [123] due to the number of multistep processes, Scheme 1.6. Dehydration of 4,5-dichlorophthalonitrile usually uses the thionyl chloride-DMF mixture while 4,5-diiodophthalonitrile uses trifluoroacetic anhydride-pyridine mixture.

Substitution reactions are quite similar to those used with nitro leaving groups, though the majority involve thiols than alcohols as the former are more reactive nucleophiles than the latter. Substitution with thiols readily takes place at room temperature, while substitution with alcohols requires heat. A variety of 4,5-disubstituted phthalonitriles have also been prepared by Pd-catalysed Heck [124], Stille [125] and Suzuki [126] cross coupling reactions. Thus a large number of octasubstituted phthalocyanines have been synthesised and studied in the context of molecular devices [127], liquid crystalline derivatives [128] and as already mentioned, their non-linear optics applications.

1.4.2.3 Water-soluble phthalocyanines

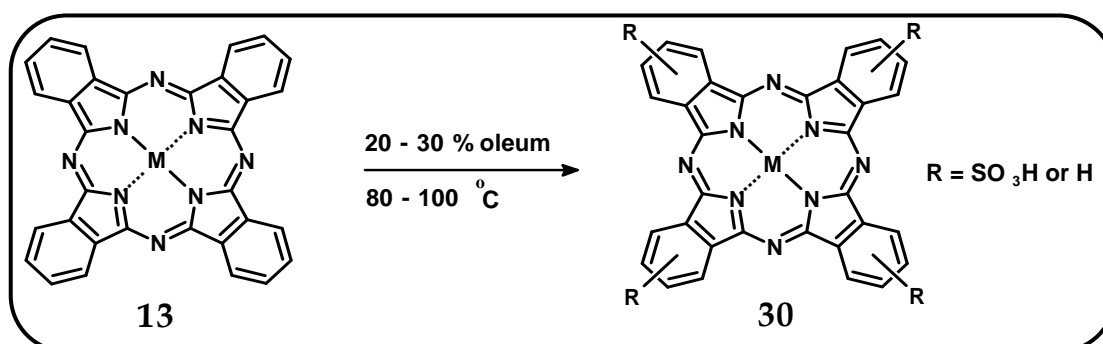
Introduction of hydrophilic groups such as sulpho- [129], carboxy- [130] or phosphono- [131] substituents at the periphery of the ring affords water-soluble Pcs. Sulphonated CuPcs were first reported in 1929 and were the first examples of substituted phthalocyanines [132]. Tetrasulphonated MPc (**29**) are synthesised according to the popular Weber and Busch method [129], wherein the monosodium salt of sulphonic acid (**28**) and metal salt are heated in nitrobenzene in the presence of

urea and ammonium molybdate as catalyst, Scheme 1.7. Ammonium molybdate is found to be most effective [133], compared to other catalysts such as boric acid, molybdenum oxide, zirconium and titanium tetrachloride.



Scheme 1.7: Synthesis of tetra-sulphonated MPC from 4-sulphonic acid.

A preformed unsubstituted MPC represents a different synthetic approach to preparing phthalocyanines. Direct sulphonation results in the formation of complex product mixtures, formally called $\text{MPC}(\text{SO}_3^-)_n$ (**30**), [134] - represented as MPCs_n in this work -, Scheme 1.8. As the degree of sulphonation is uncontrollable during the preparation of the complexes, the MPCs_n may contain a mixture of sulphonates, i.e. mono-, di-, tri- and/or tetra-, which have slightly different polarities and solubilities. In some cases, the reaction can be controlled to some extent by varying the temperature and reaction time and the central ion has been known to play an important role in the product distribution [135].

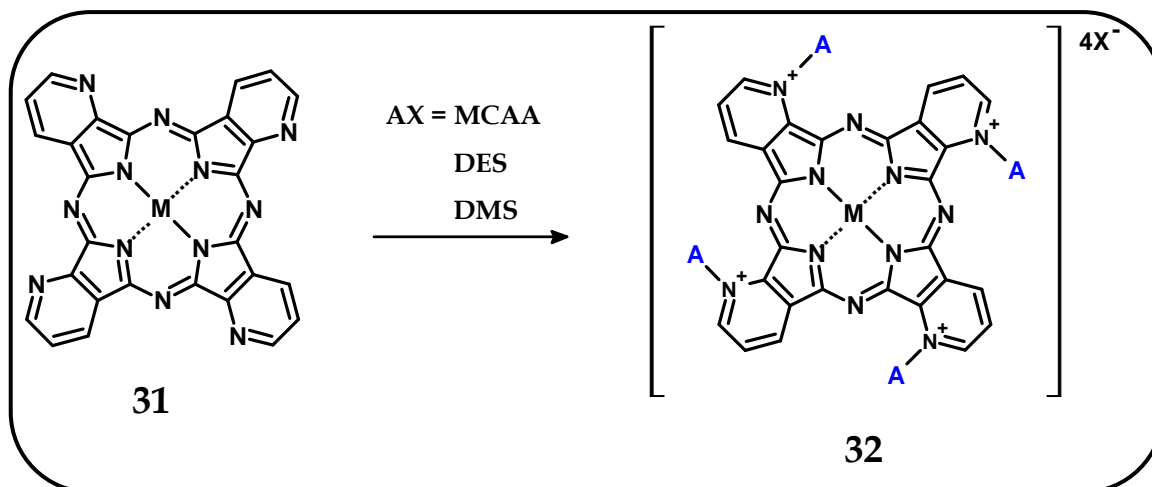


Scheme 1.8: Synthesis of a mixture of differently sulphonated MPC, i.e. MPCs_n where $n = 1, 2, 3$ or 4 . $S_n = \text{SO}_3^-$

The degree of sulphonation will thus vary from batch to batch depending on these factors. For example, varying hydrophobic and hydrophilic properties are exhibited, in especially PDT, depending on the degree of sulphonation [136]. A decrease in photocytotoxicity under both *in vivo* and *in vitro* conditions with increase in the degree of sulphonation of Zn, Ga and Al phthalocyanines [135] was observed and the decrease was directly correlated to the hydrophilicity of the Pc [137,138]. Of all the water-soluble Pcs, derivatives of Al and Zn complexes are the most studied photosensitizers for PDT [54]. Sulphonated Pcs tend to aggregate in aqueous media which leads to photochemical inefficiencies, with aggregation effects increasing in the sequence $S_4 < S_1$. Thus the solubility as well as the extent of aggregation greatly affects the cell uptake and intracellular distribution pattern, depending on the degree of sulphonation, isomeric composition and the nature of the central metal ion [135,139,140]. However, their photoactive monomer forms exhibit photosensitising effects [141]. Grafting phthalocyanines with ionic substituents, e.g. sulphonates can also form stable ion pairs with complexes of opposite charges, e.g. cationic methyl viologen (MV^{2+}). In most cases, the properties of the mixed complexes may notably differ from those of the parent compounds. The ion pairs of differently sulphonated MPc and methyl viologen will be discussed in detail below.

Another form of preparing water-soluble Pcs is through quaternation. Replacement of benzenoid rings by the electron-withdrawing pyridine (**31**) and quaternation of the pyridine nitrogen to obtain tetracationic Pcs (**32**), confers solubility in aqueous media. Linstead *et al.* [142] were the first to synthesise tetrapyrroldiporphyrazines (**31**), which were later quaternised with agents such as monochloroacetic acid (MCAA), diethyl sulphate (DES) and dimethyl sulphate (DMS) [143,144], Scheme 1.9. These compounds have an added advantage over

tetrasulphonated Pcs in that aggregation, which would retard photochemical activities in aqueous solutions, is prevented [145].



Scheme 1.9: Quaternation of tetrapyrrodo porphyrazines (31) with AX: monochloroacetic acid (MCAA), diethyl sulphate (DES) or dimethyl sulphate (DMS).

1.4.2.4 Survey of the synthesis of TiPcs and TaPcs

In this thesis, TiPc and TaPc derivatives are synthesised to be used as catalysts for applications such as photocatalysis and electrocatalysis. Unsubstituted oxotitanium phthalocyanine (OTiPc), a well known near-IR-active photoconductive dye, was first synthesised by Taube in 1963 [146]. Convenient methods were later developed in order to produce ‘pure’ OTiPc [33,147]. Similarly, unsubstituted dichloro(phthalocyaninato)titanium (IV) complex (Cl_2TiPc) was first reported in 1965 [148]. Owing to the poor solubility of OTiPc and Cl_2TiPc in common organic solvents, their spectroscopic data is extremely limited thus introduction of unlimited substituents render them soluble in most organic solvents. Since then, the chemistry of OTiPcs has been growing, Table 1.1. For example, extensive work on the chemistry of axially substituted TiPcs has been done. The Cl_2TiPc complex is extremely sensitive to moisture and is thus hydrolysed to OTiPc. The ancillary

ligands of complexes OTiPc and Cl₂TiPc can however be displaced by strongly chelating oxygen and sulphur bidentate donor ligands of 1,2-arrangement such as oxalic acid, catechol or 1,2-dithiocatechol, Table 1.1. Axially substituted TiPcs exhibit high photoconductivities and excellent nonlinear optical properties.

Table 1.1: A list of selected TiPcs and TaPcs that have been synthesised in literature

Complexes	Reference
Unsubstituted	OTiPc [33,146,147] Cl ₂ TiPc [33,148] Cl ₃ TaPc [35] OTaPcCl [149]
Tetra-substituted	OTiPc - C(CH ₃) ₃ [150] - SC ₂ H ₂ N(CH ₃) ₃ [151] - SC ₆ H ₁₃ [152] - CH ₂ OC ₅ H ₁₁ [153] - OC ₄ H ₉ [153] OTaPc - C(CH ₃) ₃ [149]
Octa-substituted	OTiPc - SC ₂ H ₂ N(CH ₃) ₃ [151] - OC ₅ H ₁₁ [154],[155] - SC ₆ H ₁₃ [152]
Axially substituted	<ul style="list-style-type: none"> • XTiPc X = <i>catechol, dithiocatechol</i> [156] = <i>2,3-dihydroxynaphthalene</i> [157] • XTiPc-[C(CH₃)₃]₄ X = <i>2,2'-biphenol</i> [158] = <i>4-tert-butylcatechol</i> [159] • XTiPc-(C₇H₁₅)₈ X = <i>catechol</i> [154] • XTiPc-[SC₆H₁₃]_{4 or 8} X = <i>catechol</i> [152]

OTiPcs are known to be non-planar with the titanyl group (Ti=O) located perpendicular to the macrocycle [160]. Substitution in the axial position breaks the centrosymmetry of the Pc, thus enhancing the octupolar character of the molecule by adding on a dipole moment. It is these features that yield interesting nonlinear optical properties [161].

The properties of OTiPcs are relatively unexplored compared to other first row transition MPcs. The complexes have however been extensively investigated for their electrical properties especially as thin films [162,163]. There is thus a considerable potential and interest in the full development of the chemistry and applications of these complexes.

Tantalum phthalocyanines (TaPcs) are relatively unknown, except for the unsubstituted Cl_3TaPc [35] complex, the crystal structure of which has been thoroughly investigated [35,164]. The difficulty in obtaining substituted TaPcs stems from the fact that the molecule is highly distorted and hence unstable. A tetra-substituted 4-*tert*-butyl OTaPc has been reported [149] although its synthesis is difficult to reproduce and yields less than 15 % are obtained after purification.

Aims of thesis

The synthesis of TiPcs is somewhat underdeveloped, especially at non-peripheral positions. The syntheses of unsubstituted TiPc and TaPc (Fig. 1.8) will be carried out and sulphonated such that the first differently sulphonated water-soluble derivatives TiPcS_n and TaPcS_n are obtained respectively, Fig. 1.9. Most of the reported TiPcs are substituted with long-chains (alkoxy or alkylthio groups), Table 1.1. To our knowledge there are no reports on OTiPcs with aryloxy, arylthio, nitro and amino substituents. Therefore, the purpose of this thesis is to prepare a number of new and

pure oxotitanium phthalocyanines that are tetra substituted (peripheral and non-peripheral positions) and octa-substituted with either aryloxy or arylthio groups at the periphery, Fig. 1.10 - 1.12. The nature and position of substituents tend to influence the properties of MPcs. Therefore, specific phthalocyanines can be tailored such that they consist of certain properties which are required for various applications since the possibility of combining an unlimited number and type of substituents with a great number of central metals is infinite. Hence the MPcs used in this thesis are investigated for their exceptional and interesting solution photophysicochemical, photocatalytic and electrochemical properties which have never been explored before in contrast to those of other first row transition metals. Also, the choice of Ti and Ta as metals of investigation stems from the fact that both metals bear ligands in the *cis* configuration. The *cis* coordination has a particular significance since it is a prerequisite for many catalytic processes. As earlier mentioned, electrical properties such as photovoltaic, photoconductivity, xerographic and gas sensing to name a few, have been investigated for OTiPcs, especially as thin films, thus there is an avenue to investigate properties that have not been explored before.

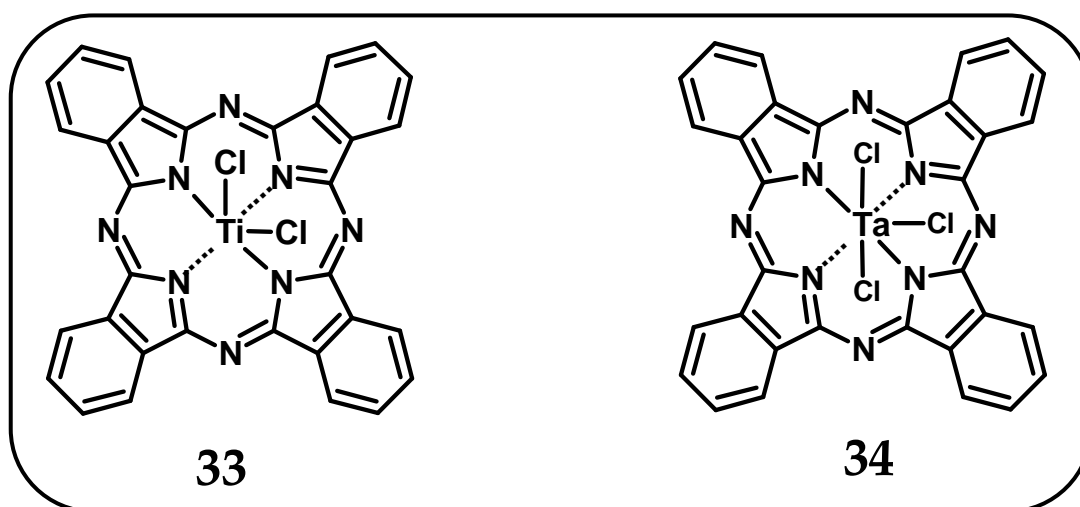


Figure 1.8: Structures of Cl₂TiPc (33) and Cl₃TaPc (34) studied in this thesis.

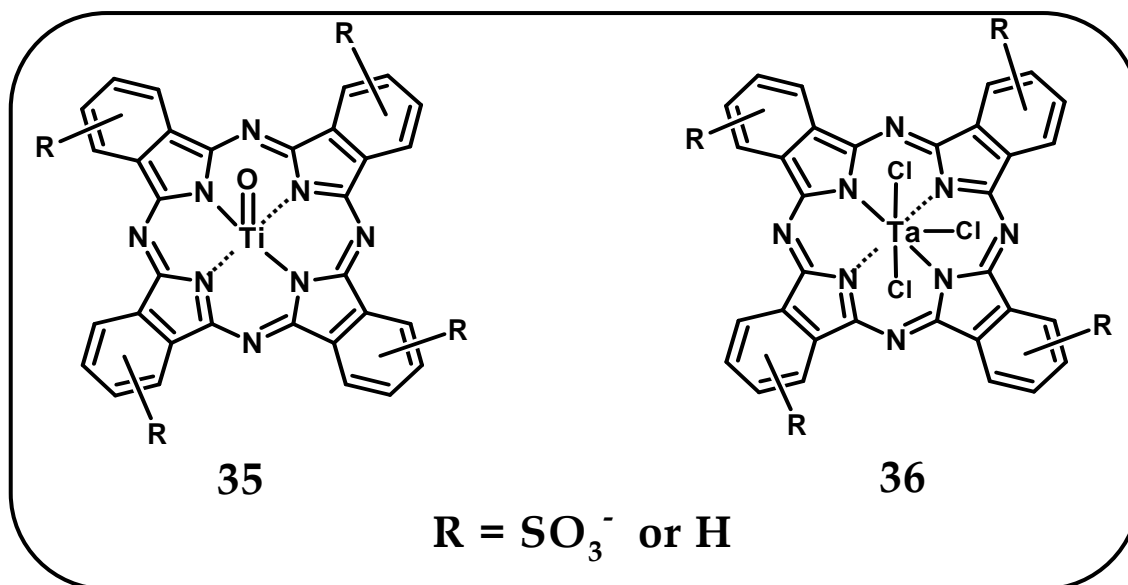


Figure 1.9: Structures of OTiPc_n (35) and Cl₃TaPc_n (36) studied in this thesis.

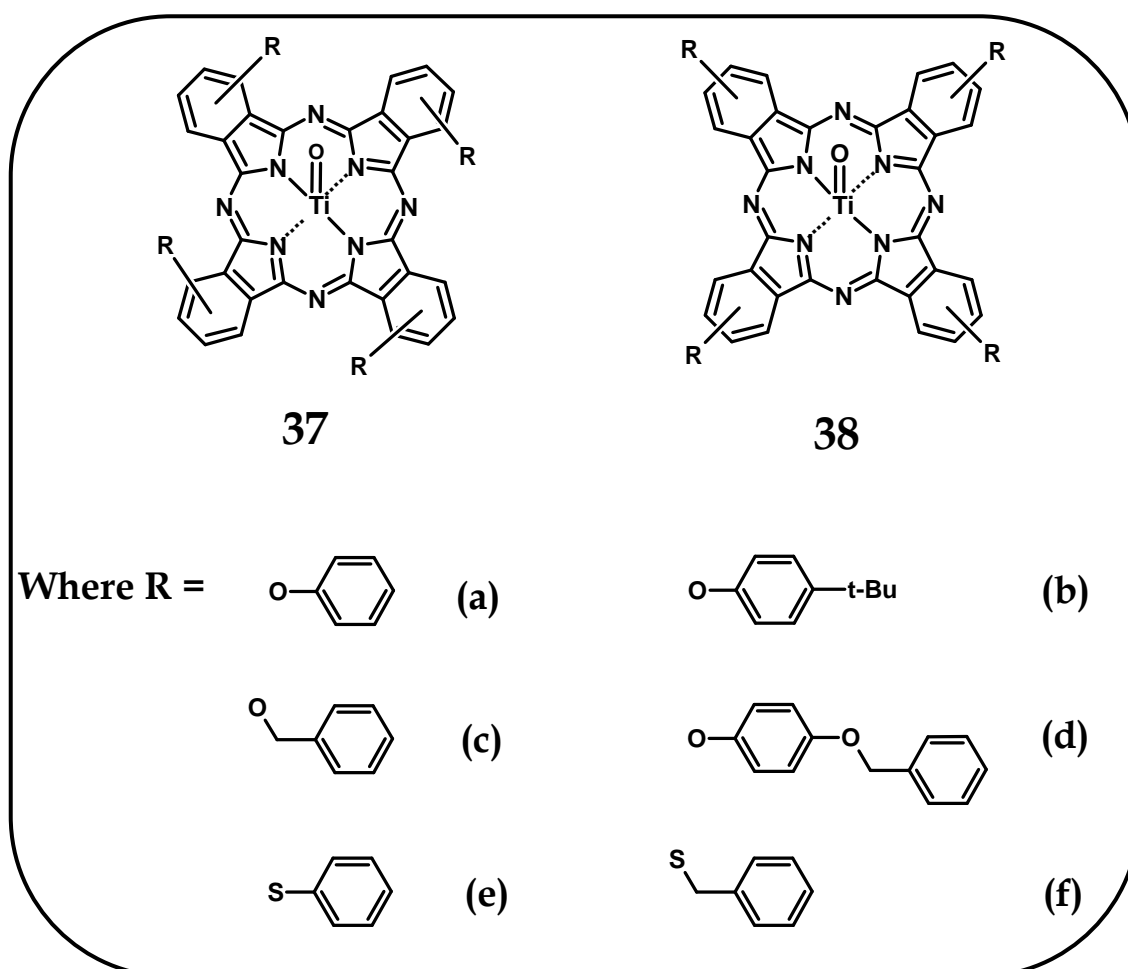


Figure 1.10: Synthesised tetra-substituted OTiPc complexes that are substituted at the non-peripheral (37a – f) and peripheral (38a – f) positions.

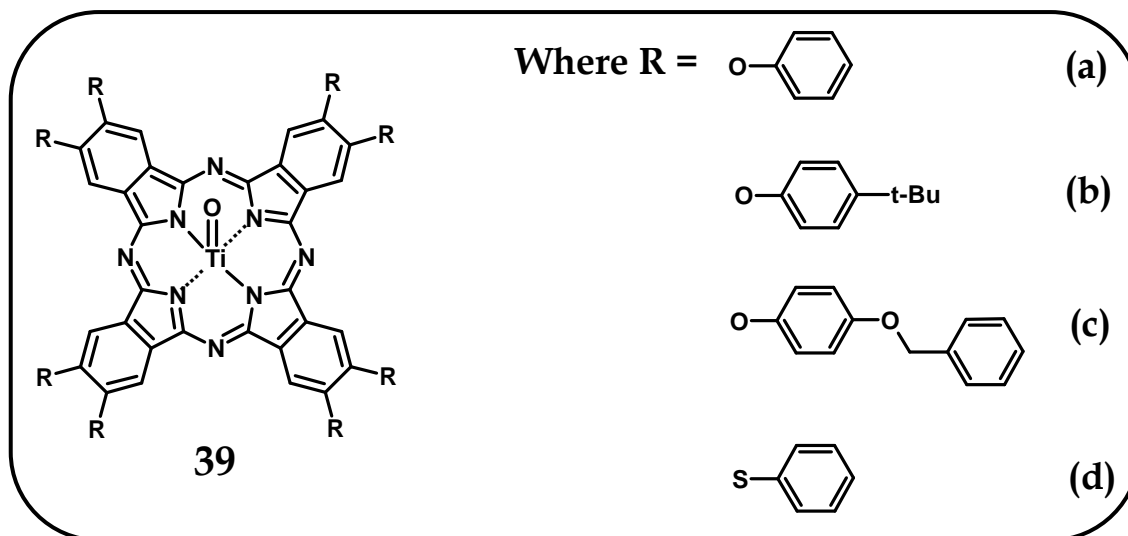


Figure 1.11: Synthesised octa-substituted OTiPc complexes that are substituted at the peripheral (39a – d) positions.

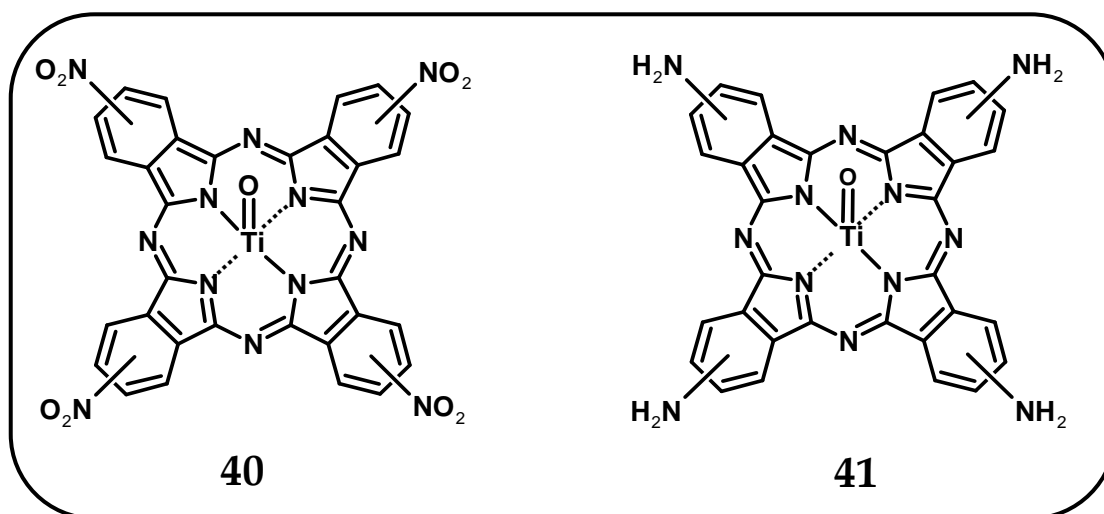


Figure 1.12: Synthesised tetra-substituted nitro (40) and amino (41) OTiPc complexes.

1.5 UV/Vis spectroscopic properties of phthalocyanines

1.5.1 Basic concepts

Fig. 1.13 shows ultraviolet/visible (UV/Vis) spectra that are typical of Pcs. A strong, sharp and isolated absorption found around 700 nm, with a corresponding high molar extinction coefficient ($\epsilon > 10^5 \text{ M}^{-1}\text{cm}^{-1}$) is systematically known as a Q-band, Fig. 1.13. The next absorptions are much less intense and lie at considerably higher energies. Around 340 nm is a band called the B or Soret band. Unique to Pcs, the B-band is broad due to the superimposition of the B_1 and B_2 bands [165]. The next lowest energy bands are called the N, L and C bands which commonly appear around 290 nm, 240 nm and 190 nm respectively. The Q, B_1 , B_2 , N, L and C bands (in order of increasing energy) are primarily due to $\pi\text{-}\pi^*$ electronic transitions in the Pc ligand. Because of interesting spectral properties, several theoretical calculations for the molecular orbitals of Pcs have been obtained [166-168], in order to understand the origin of spectra.

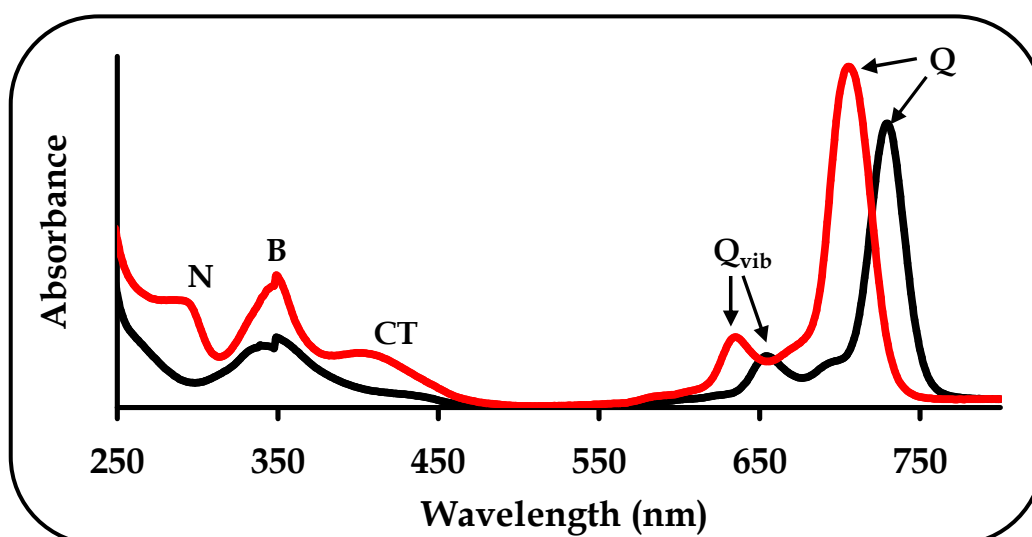


Figure 1.13: UV/Vis spectra of typical phthalocyanine complexes that are peripherally (red) and non-peripherally (black) substituted at the periphery.

To help explain the first two allowed transitions in the UV/Vis region of the spectrum, an easily understood theory involving a four-orbital model is employed. The model considers the top two highest occupied molecular orbitals (HOMO) and the degenerate lowest unoccupied molecular orbital (LUMO) [168]. Fig. 1.14 diagrammatically displays this theory, with symmetry elements on the left of each orbital referring to the symmetry of the orbital involved. For Pcs, a transition from the HOMO with a_{1u} symmetry to the LUMO with e_g symmetry results in the Q-band absorption while a transition from a_{2u} and b_{2u} to the LUMO gives the B-band absorption. The splitting of the B-band into two components, namely B_1 and B_2 is predicted by the model. The components have similar energies and thus appear broad as seen in spectra of phthalocyanines.

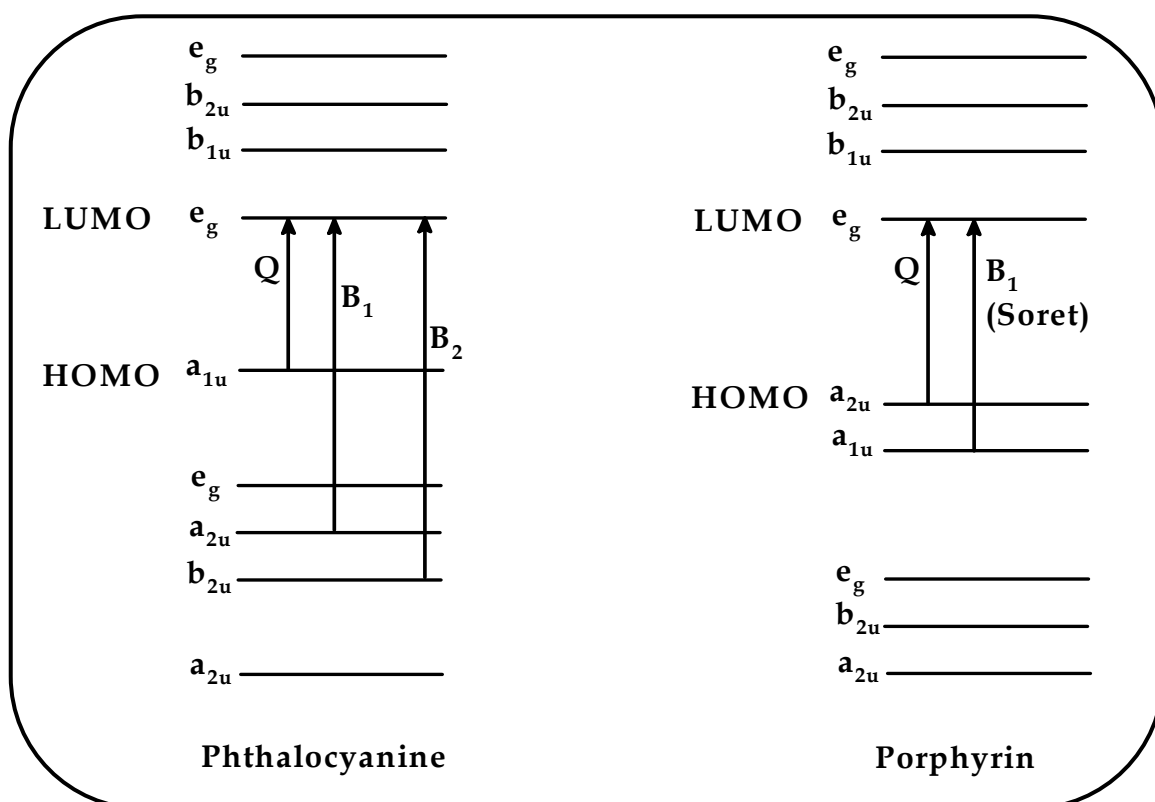


Figure 1.14: Phthalocyanine and porphyrin electronic transitions showing the origin of Q and B absorption bands.

As can be seen in Fig. 1.14, the large energy gap between the a_{1u} and a_{2u} orbitals of the HOMO leads to the isolation of the Q-band in the UV/Vis spectra of Pcs. This is brought about by either the benzo annulation or aza groups significantly breaking the accidental degeneracy of these top filled orbitals. The result is the significant red shift and intensification of the Q-band relative to the B-band. In contrast, according to Gouterman's four-orbital theory [169,170], the a_{1u} and a_{2u} orbitals of porphyrins (Fig. 1.14) are accidentally degenerate as they are close together. This leads to the extensive configuration interaction of the Q and B-bands, giving rise to an intense B (Soret) band, and a lower energy state giving rise to a weak Q-band.

In addition, for every electronic state there are vibrational levels. A feature that is characteristic of Pcs is vibrational overtones of the Q-band in the blue, namely Q_{vib} with absorbance that is less than 10 % of the main band, Fig. 1.13. Other absorption bands usually occurring in the 400 – 500 nm region with moderate absorptions, as well as weak absorptions in the near infrared (NIR) are assigned to charge-transfer (CT) transitions, Fig. 1.13. CT transitions usually occur when metal d-orbitals lie within the HOMO-LUMO gap of the Pc ring [168,171]. A charge transfer from an electron rich ligand to an electron poor metal is known as a ligand-to-metal charge transfer (LMCT) while charge transfer from metal to ligand is termed a metal-to-ligand charge transfer (MLCT).

The UV/Vis spectrum of the less symmetric H_2Pc – due to the two core protons – is slightly different from that of MPc. Fig. 1.15 shows a typical H_2Pc spectrum with a split Q-band, with one of the components found at slightly longer wavelengths than is the case with MPcs. The presence of the core protons causes the

LUMO to become non-degenerate, thus giving rise to two allowed transitions (x or y polarised) of varying energy such that a split in the Q-band is observed.

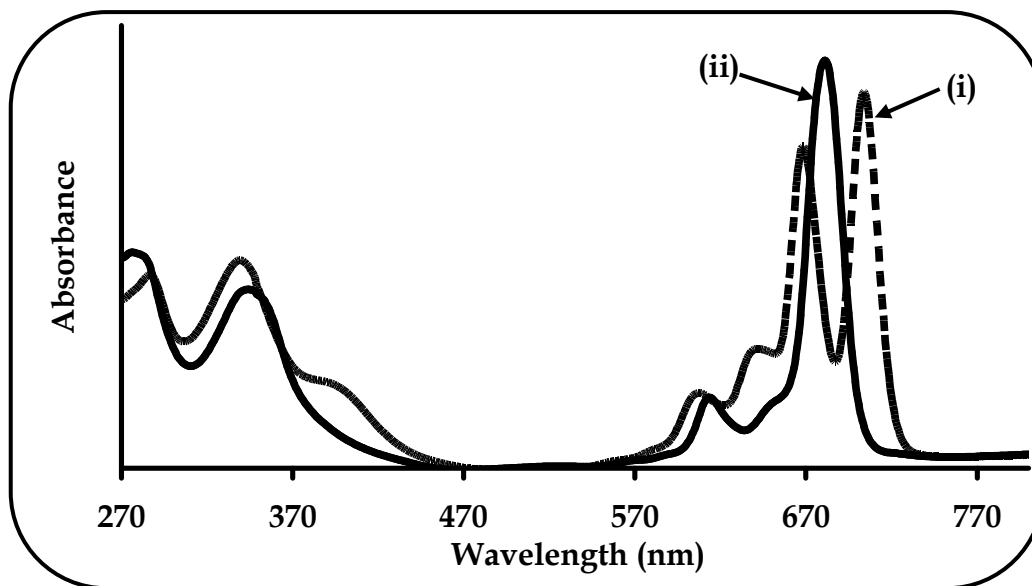


Figure 1.15: Typical ground state absorption spectra of (i) metal-free phthalocyanine and (ii) metallated phthalocyanine.

Furthermore, the position of the Q-band varies according to the position, type and number of substituents at the periphery. The effect of substituents at the α position is much larger than at the β position. Electron donating substituents such as alkoxy or alkyl(phenyl)thio groups at the α positions tend to significantly shift the spectrum to the red exemplified in Fig. 1.13 [172]. Electron-withdrawing groups such as nitro or sulphonyl groups shift the Q-band to shorter or longer wavelengths with substitution at α or β positions respectively [173].

The above model explains UV/Vis spectra that are typical of monomeric Pcs however effects of aggregation on the spectra of Pcs can further be explained by the model. The propensity of phthalocyanines to form aggregates due to the strong interactions between planar macrocycles in solution, is well-known [174-179]. The relative geometry of the macrocycles determines the spectroscopic behaviour of aggregates, i.e. co-facial arrangement (common in most Pc aggregates) yields a blue-

shifted Q-band absorption called H-aggregates, whereas an edge-to-edge arrangement (rare in Pc aggregates) yields a red-shifted absorption, called J-aggregates. The former arrangement is primarily due to the hydrophobic nature of the benzene rings which readily allows Pc macrocycles to stack on top of each other, thus leading to a stabilised overlap of their π electron cloud. The effect is the broadening of the Q-band with a corresponding blue-shift in their λ values, typically to around 630 nm,

Fig. 1.16.

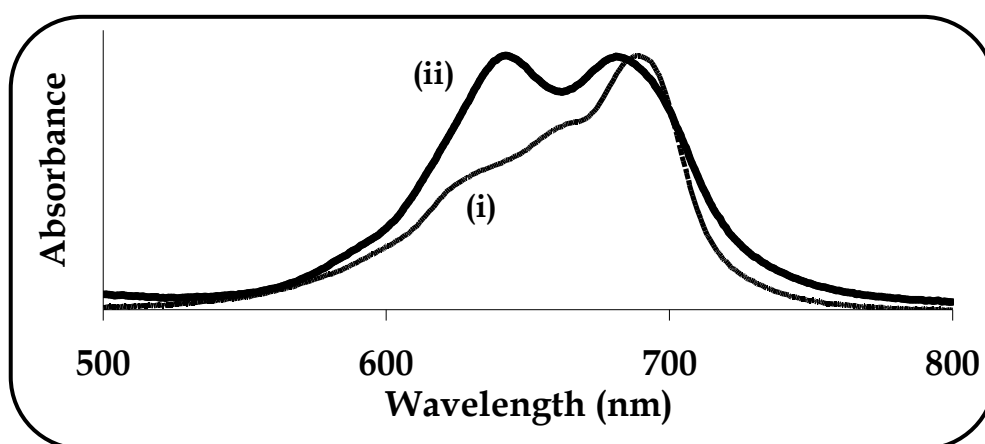


Figure 1.16: Two examples of broadened absorption spectra of aggregated MPcs where (i) is less aggregated and (ii) is highly aggregated

The overlap of π -electron clouds of dimers results in the degeneracy of the two LUMO orbitals to be lifted, causing them to split into different energies. According to the exciton coupling theory [180,181] only transitions to the higher energy state (1E_u) are allowed, therefore a blue-shifted absorption results, whereas transitions to the lower energy state are forbidden (1E_g), Fig. 1.17. A few factors govern the broadening of the bands. A transition to the lower energy LUMO can still occur to a small extent even though it is forbidden, thus resulting in a broad absorption, Fig. 1.16. The overlap position, tilt angle, extinction coefficient of the absorption bands

involved, the closeness of the rings, are other factors which determine how well the π -electron clouds overlap and will thus vary for each aggregate in solution.

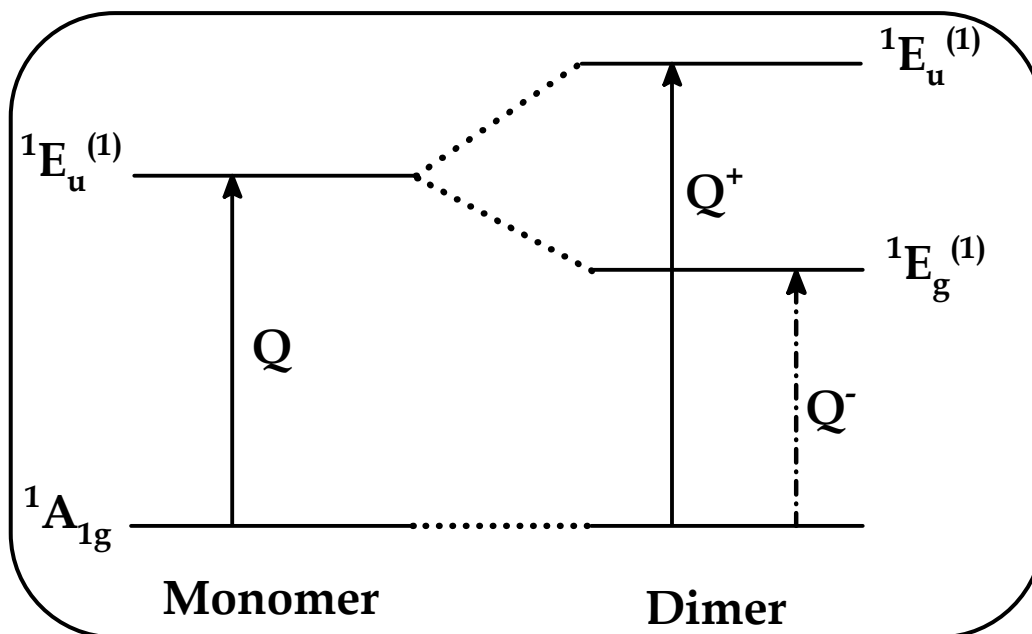


Figure 1.17: Interaction between molecular orbitals showing the effect of aggregation on the LUMO of Pcs. The solid and dashed arrows indicate allowed and forbidden transitions respectively.

For J-aggregates, the tilt angle approaches 0° and the transition intensity of the exciton accumulates in the red-shifted direction, Fig. 1.18(i) [182]. The exciton coupling model was employed to explain the occurrences of the blue and red spectral shifts from the formation of H- and J-aggregates respectively, Fig. 1.18(ii) [183]. Since dimers have two possible excited energy states, one state corresponds to parallel transition moments as in a co-facial arrangement, while the other to transition moments that are anti-parallel as in an edge-to-edge arrangement. The former results in a strongly allowed blue-shifted transition to a higher energy state while the latter results in a red-shifted low energy transition.

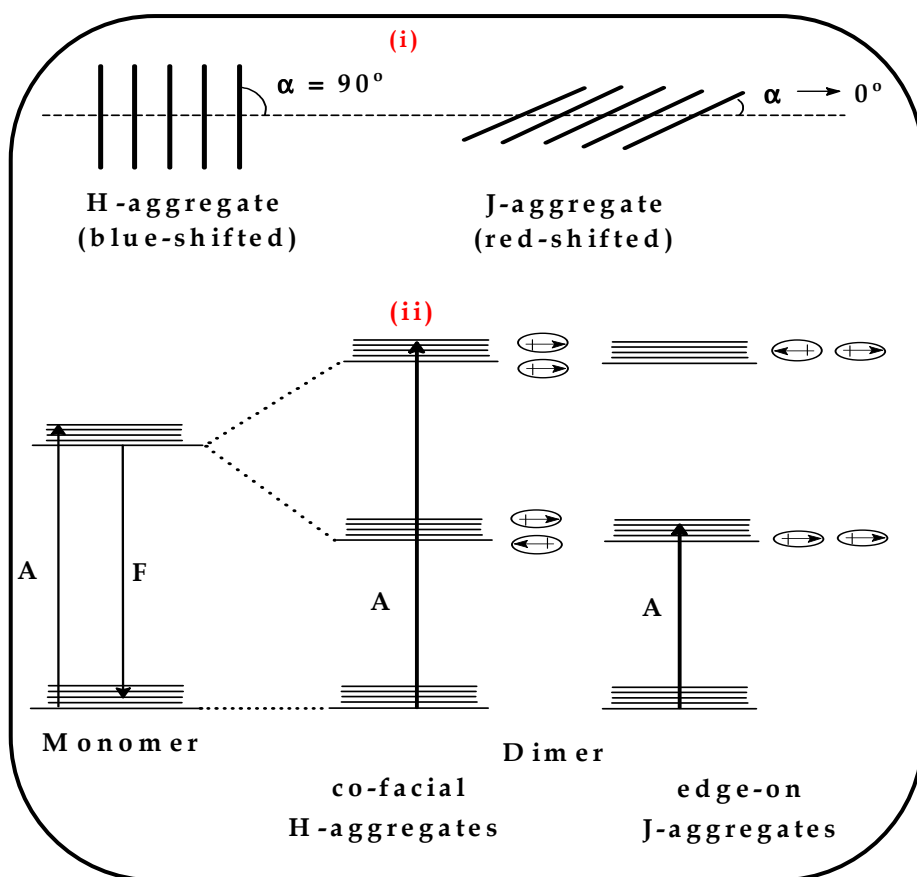


Figure 1.18: (i) Orientation of transition moments for linear H- and J-aggregates [182] and (ii) Exciton model correlating energy levels on dimer formation with co-facial and edge-on orientations of the H- and J-aggregates [183]. A = Absorbance.

Photophysical properties are extensively affected by aggregation. For example, significant quenching of the usually strong Pc fluorescence is induced by the modification of the absorption or emission bands. Axial substitution such as in the case with SiPcs [184], and bulky substituents [185,186] at the periphery of MPcs are able to prevent aggregation, thereby giving rise to sharply defined UV/Vis absorption peaks.

1.5.2 Survey of the UV/Vis properties of TiPcs

OTiPcs are well-known near-IR active materials because their light sensitivity in the IR region makes them useful for various photosensitive applications. These features are stronger when compared to other MPcs. Their absorption spectra are typical of MPcs with Q-bands in the 700 nm region and B-bands in the 350 nm region. Ways of shifting Q-bands of OTiPcs into the near-IR involve substitution at the periphery with electron donating groups such as $-OR$, $-SR$ and $-NH_2$. The presence of TiO^{2+} in the core of the ring also causes a Q-band shift, notably so when compared to other transition metals. For example a ZnPc that is tetra- or octa-substituted with dimethylaminoethylsulfanyl groups has Q-band absorptions at 685 nm and 715 nm respectively. Q-band absorptions for OTiPc that is tetra- or octa-substituted with dimethylaminoethylsulfanyl groups are however observed at 723 nm and 739 nm respectively, Table 1.2 [151]. Also, in comparison to substitution at the 2,(3) positions, the 1,(4) analogues show a significant bathochromic shift, thus substitution offers a useful way of regulating the wavelength of the Q band [187,188].

Long chain substituted OTiPcs tend to aggregate in less polar solvents such as hexanes. Axially-substituted TiPcs however prevent aggregation in solution, and do not significantly shift in spectra, i.e. 1 – 3 nm shifts to red/blue are observed. Moreover, exciton interactions between the Pc and axial ligand tend to cause broadening of Q-bands, which tend to split in cases where large axial dipole moments are exhibited [158].

Table 1.2: UV/Vis data of some selected OTiPc complexes in chloroform (CHCl₃)

Complex	Substituent / position	λ_{\max} (nm) [Ref]
OTiPc	-	686 [147]
OTiPc(SC ₆ H ₁₃) ₄	hexylthio / β	720 [152]
OTiPc[SCH ₂ N(CH ₃) ₃] ₄	dimethylaminoethylsulfanyl / β	723 [151]
OTiPc(OC ₄ H ₉) ₄	butyloxy / α	791 [153]
OTiPc(SC ₆ H ₁₃) ₈	hexylthio / β	739 [152]
OTiPc[SCH ₂ N(CH ₃) ₃] ₈	dimethylaminoethylsulfanyl / β	739 [151]
OTiPc	2,3-dihydroxynaphthalene / axial	703 [156]
OTiPc	2,2'-biphenol / axial	699, 722 [158]
OTiPc[SCH ₂ N(CH ₃) ₃] ₄	dimethylaminoethylsulfanyl / axial	720 [151]

Although MPc complexes have been extensively studied, their properties cannot be fully exploited as they have low solubility in most organic solvents and they tend to aggregate. In the thesis, the OTiPc complexes have been substituted with bulky groups at α and β positions to render them soluble as well as prevent aggregation. Substitution at the more sterically crowded α position also reduces aggregation tendencies more than substitution at the β position [189-191]. Furthermore, the choice of substituents for the OTiPcs in this thesis is to shift the complexes into the red since they have interesting properties in that region.

1.5.3 UV/Vis spectral studies of ionic interactions

Interactions of water-soluble TiPc and TaPc with methyl viologen (MV^{2+}) will be studied in this thesis and hence the following review.

Tetrapyrrole macrocycles such as porphyrins and phthalocyanines can be grafted with ionic substituents of opposite charges in order to form stable ion pairs. These individually charged components are held together by coulombic attractions. Often, the properties of the mixed complexes formed differ from those of the individual components. The mixed complexes may display different and complementary absorption spectra, thus spectroscopic methods can be used to study their properties. Complexation plays an important role in catalysis, genetic information, enzyme-substrate interactions and many other important processes. Biological processes such as photosynthesis for example and oxidative processes that involve the degradation of biological material in living cells, show an important role that the ion-pairs, and hence electron-transfer reactions, play in such systems [192].

Pcs are in fact extensively used in PDT where electron-transfer reactions occurring in living cells take place. Electronically charged phthalocyanines such as sulphonated phthalocyanines, are commonly used as water-soluble electron-transfer photosensitisers, often used in conjunction with electron-acceptor molecules such as dicationic methyl viologen, Table 1.3 [193,194]. Numerous photochemical investigations have been performed on the reduction of MV^{2+} , which is a typical one-electron transfer acceptor. Following reduction, a MV radical is produced which then cleaves water to produce hydrogen for energy storage in the presence of a catalyst in these donor-acceptor systems [195-197].

Table 1.3: Ionic interactions between anionic phthalocyanines and cationic methyl viologen

Complex	Association constant, K (M^{-1})	Reference
$ZnPc(SO_3^-)_4$	1.40×10^5	[198]
$Si(OH)_2Pc(SO_3^-)_4$	6.60×10^5	[198]
$H_2Pc(SO_3^-)_4$	1.30×10^5	[198]

Formation of supramolecular assemblies can be readily detected by spectroscopic techniques, more specifically UV/Vis spectroscopy. It is obvious that UV/Vis spectroscopy is important in the characterisation of ground state interactions or charge transfer reactions within the ion pairs. Complexation of the ions can be monitored by UV/Vis spectrophotometric titration. Spectrophotometric titration involves keeping an ion (e.g. MPc) constant and adding a variable amount of complexing agent (e.g. MV^{2+}). A simple and effective approach which has been successfully used for tetrapyrrole systems [199-201], namely Job's method, is commonly employed to determine the stoichiometry of the mixed complexes.

Analysis of ionic interactions

Job's method works on the assumption that the absorbance of the mixture of the solutes which do not interact is the sum of the absorbance of each solute separately. As the composition of the solution is continuously varied, the departures from additivity (i.e. the presence of interactions between the solutes) can thus be interpreted as evidence of the formation of the complex. Therefore the composition at which the deviation from additivity is a maximum determines the stoichiometry of the complex that is responsible for such effects.

At a given wavelength for mixtures with various ratios of cationic MV^{2+} and anionic MPC, the measured absorptions are used to calculate the function $F(x)$ in Eq. 1.1 [202].

$$F(x) = d(x) - (\varepsilon_{MV^{2+}} - \varepsilon_{MPC})x - \varepsilon_{MPC} \quad (1.1)$$

where $d(x) = \frac{Abs}{[MV^{2+}] + [MPC]}$ and Abs is the absorbance of the sample, $\varepsilon_{MV^{2+}}$ and

ε_{MPC} are the molar extinction coefficients of MV^{2+} ($\varepsilon_{MV^{2+}} = 1.84 \times 10^4 \text{ M}^{-1} \cdot \text{cm}^{-1}$) and

MPC, respectively, and $x = [MV^{2+}] / ([MV^{2+}] + [MPC])$ is the mole fraction of MV^{2+} .

Deviation from additivity of the absorption of a mixture of $x \text{ M}$ (MV^{2+}) and $(1-x) \text{ M}$ (where M is the concentration) of MPC is thus represented by $F(x)$ in molar absorption units. Job plots, $F(x)$ vs. mole fraction of MV^{2+} for titration of MPC with varying concentrations of MV^{2+} show the stoichiometry of the mixed complexes. Furthermore, association constants which are a measure of strength of interaction of MV^{2+} with the MPC can be calculated from these UV/Vis spectrophotometric titrations. The data obtained are analysed by Eq. 1.2 [203],

$$\frac{A_0}{\Delta A} = \frac{A_0}{\Delta A_{max}} + \frac{A_0}{\Delta A_{max}} \frac{1}{K_a} \frac{1}{L_t} \quad (1.2)$$

where $\Delta A = A_0 - A$, A_0 and A are the absorbances of the MPC in the absence and presence of total MV^{2+} concentration (L_t) respectively, and ΔA_{max} is the maximum

change in absorbance. The association constant K_a is obtained from the ratio of

$A_0 / \Delta A_{max}$ and the slope obtained from a plot of $A_0 / \Delta A$ vs. $1/L_t$.

Aims of thesis

Water-soluble MPcs have been used for the photoproduction of hydrogen from reduction of water in a donor-acceptor system. In this work, the interactions of ion pairs of new anionic TiPcS_n and TaPcS_n with the cationic methyl viologen are investigated spectroscopically. The ion pairs may involve charge transfer that is crucial in designing devices where photoinduced electron transfer is achieved. Such donor-acceptor systems are important in performing light induced functions such as the photocatalytic reduction of water. The quenching of the singlet excited state of the photoexcited MPcS_n complexes by methyl viologen is also investigated since the excited state deactivation is of importance in photocatalytic processes. The choice of Ta is based on the fact that the central metal is large (and a d⁰) and will enhance intersystem crossing to the triplet state, hence increase the yield of the triplet state. TiPc containing a d⁰ metal will also have enhanced triplet yields. Both of these MPcs have potential as photocatalysts but their properties have not been explored compared to other closed shell MPcs such as Zn and Al phthalocyanines.

1.6 Photochemical and photophysical properties

The photochemical and photophysical properties of TiPcs and TaPcs are studied, more so for the former complexes as they are used as photocatalysts for the transformation of 1-hexene.

Photochemistry is that branch of chemistry that is concerned with interactions between molecules and light. The effect is a gain in activation energy from light by molecules such that they undergo a chemical or physical change [204]. Photochemical reactions such as oxidative decomposition or transformation of organic substrates (e.g. alkenes) by oxygen using photocatalysts such as MPcs are known.

MPCs - which have excellent light-absorption properties - absorb irradiated light and may transfer the energy to another molecule, e.g. O₂, by the process called photosensitisation. A highly reactive oxygen, known as singlet oxygen (¹O₂), is thus generated and reacts with a substrate to form a product that may be useful in industry.

Photophysics is defined as the field that deals with relaxation processes such as radiative and non-radiative pathways. Following irradiation of MPC with light at an appropriate wavelength, energy (hν) is absorbed and subsequently excitation from the singlet ground state (S₀) to the vibronic level of the singlet excited state (S₁) occurs. Loss of excitation energy of the excited MPC (now ¹MPC*) by physical deactivation, via radiative (energy loss in the form of light) and radiationless (energy loss in the form of heat) processes takes place. Fluorescence (F), phosphorescence (P), internal conversion (IC) and intersystem crossing (ISC) are some of the physical deactivation processes that take place. A molecule is said to fluoresce (strong intensity) if photon emission occurs between states of the same multiplicities, i.e. S₁ to S₀, Fig. 1.19. Furthermore, a molecule is said to phosphoresce (weak intensity) if energy loss occurs between states of different multiplicities, i.e. T₁ to S₀. Statistically, fluorescence which is of short lifetimes (~ ns), is more likely to occur than phosphorescence while the probability of the latter is low, with lifetimes typically in ms due to the spin-forbidden transition [205].

The number of routes that the MPC can take following photoexcitation can be conveniently represented by the Jablonski diagram, Fig. 1.19.

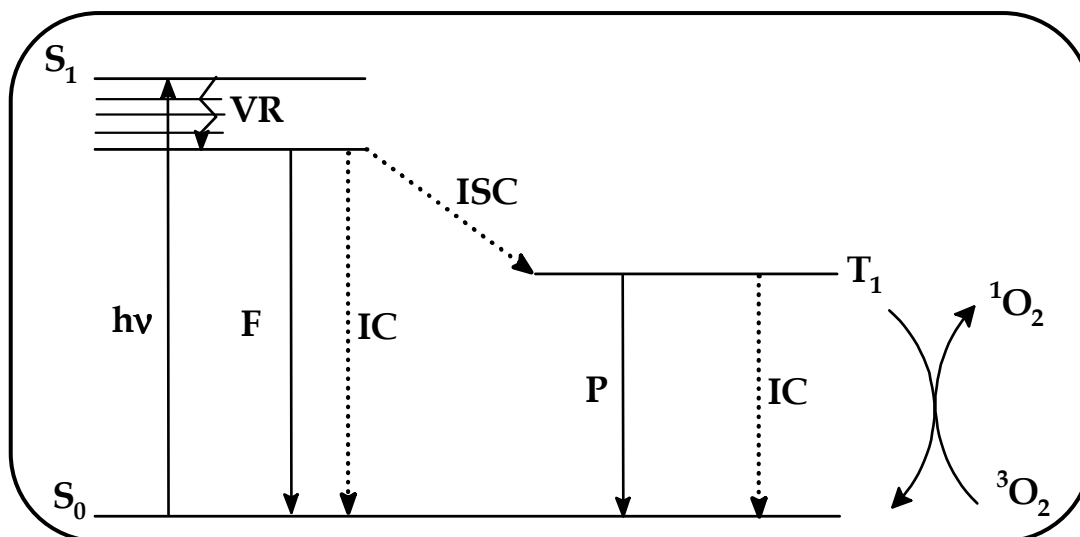


Figure 1.19: A Jablonski diagram showing the photosensitisation of MPC, where $h\nu$ = absorption energy, F = fluorescence, IC = internal conversion, ISC = intersystem crossing, P = phosphorescence, S_0 = singlet ground state, S_1 = singlet excited state, T_1 = triplet excited state and VR = vibrational relaxation.

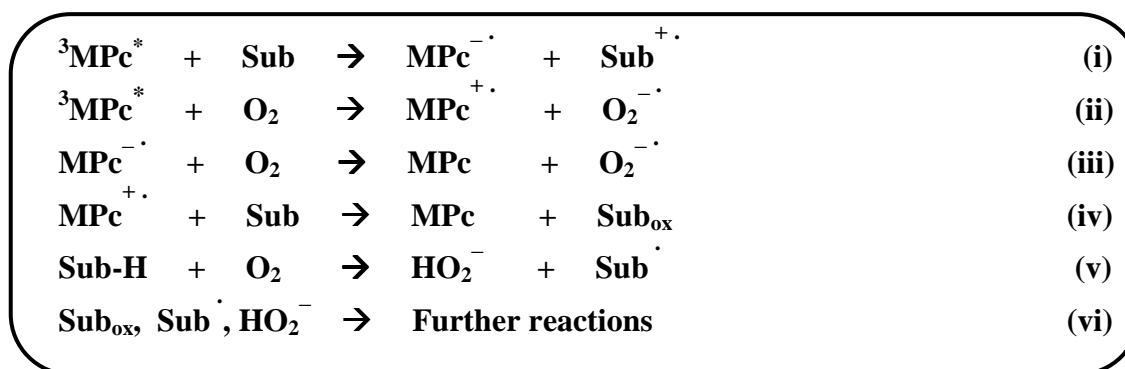
IC, ISC and vibrational relaxation (VR) are three non-radiative deactivation processes that are also significant, Fig. 1.19. IC is a rapid radiationless transition between states of the same multiplicity. On the other hand, ISC requires a spin-flip as the transition is between different spin states. Heavy atoms in the molecular structure or medium usually promote the ISC such that population of the lowest energy triplet state is enhanced.

1.6.1 Mechanisms of triplet state deactivation

Since the lifetime of the triplet state (μs) is much longer than that of the singlet state (ns), this allows the photosensitiser triplet state to follow two pathways, namely Type I or Type II.

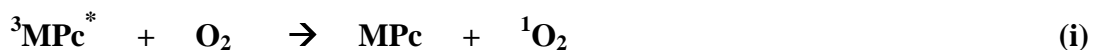
Type I pathway involves the direct reaction of $^3\text{MPC}^*$, through electron transfer, with a substrate that is in close proximity therefore producing a reduced sensitiser and an oxidised substrate, Scheme 1.10. Furthermore, the sensitiser may

react with ground state oxygen with subsequent formation of superoxide anion radical. Radical species are also formed by hydrogen atom abstraction from the substrate. This pathway usually takes place in oxygen poor environments and may be suitable for radical initiated reactions such as lipid peroxidation or photooxidation of tyrosine [206].



Scheme 1.10: Reactions showing the Type I mechanism.

The Type II pathway involves the triplet-triplet energy transfer from ${}^3\text{MPc}^*$ to triplet oxygen with the formation of the energetically rich and chemically more reactive singlet oxygen (${}^1\text{O}_2$), followed by oxidation of the substrate, Scheme 1.11 [196,207]. Typically about $10^3 - 10^5$ molecules of ${}^1\text{O}_2$ can be produced by a sensitizer molecule [54]. Provided that the sensitizer is of appropriate energy, i.e. triplet energy (E_T) $\geq 94 \text{ kJ.mol}^{-1}$, efficient energy transfer to ground state oxygen to afford the highly toxic singlet oxygen occurs. This pathway is especially prevalent in oxygen-rich or air saturated environments where the oxygen concentration is in the range of 10^{-2} to 10^{-3} M [208]. A variety of alkenes undergo photo-oxygenation reactions via this pathway [209,210]. Biomolecules such as unsaturated lipids, cholesterol, amino acid derivatives and purine bases, are among others that readily react with the singlet oxygen, due to the presence of the double bonds.



Scheme 1.11: Reactions showing the Type II mechanism.

Both Type I and Type II processes may operate simultaneously as in the case with tryptophan oxidation [211], since they take place independently of each other. The pathways are constantly in competition with each other and thus to distinguish between the two processes, several tests have been employed. For example, an anti-oxidant 2,6-di-*tert*-butyl-4-methylphenol (BHT) and electron spin resonance (ESR) spectroscopy are employed to confirm radical Type I processes. Singlet oxygen quenchers such as 1,4-diazabicyclo-octane (DABCO) and sodium azide, as well as singlet oxygen traps such as 1,3-diphenylisobenzofuran (DPBF) and tetrasodium α,α -(anthracene-9,10-diyl) dimethylmalonate (ADMA) are used in the detection of singlet oxygen in the Type II pathway. Since Type II mechanism is dominant in most alkene photooxidations, it is essential to discuss the singlet oxygen in detail.

1.6.2 Photochemical processes: Singlet oxygen

Almost all molecules are in singlet ground states, though oxygen constitutes a rare case in that its ground state is a triplet, i.e. ${}^3\Sigma_g$. The triplet oxygen is somewhat inactive to biological material due to spin conservation rules however; a more reactive type of oxygen, namely, singlet oxygen (${}^1\text{O}_2$) reacts rapidly with the material such as amino acids, lipids and deoxyribonucleic acid (DNA). There are various ways of generating singlet oxygen, but the simplest way is through energy transfer, facilitated by a photosensitiser such as MPc.

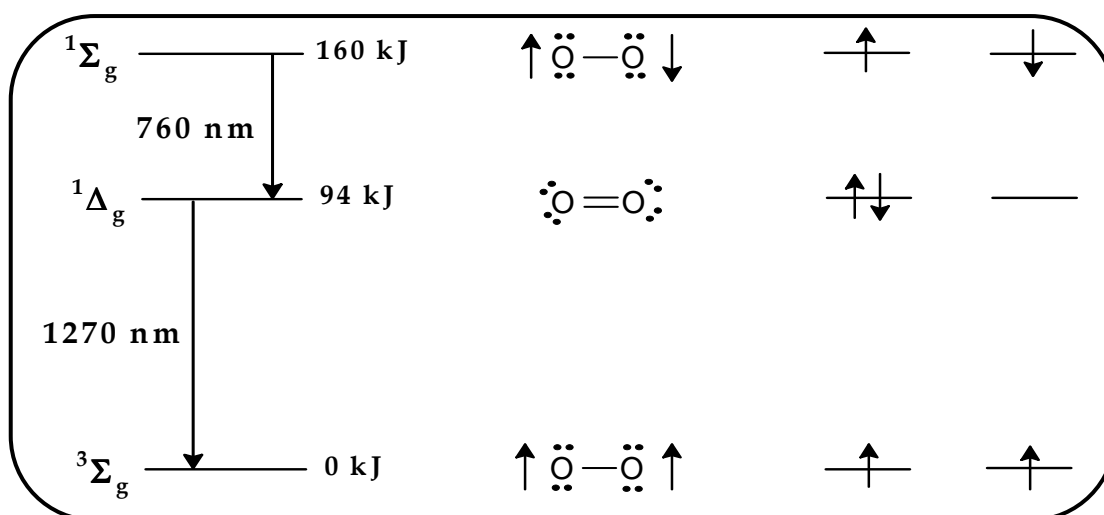


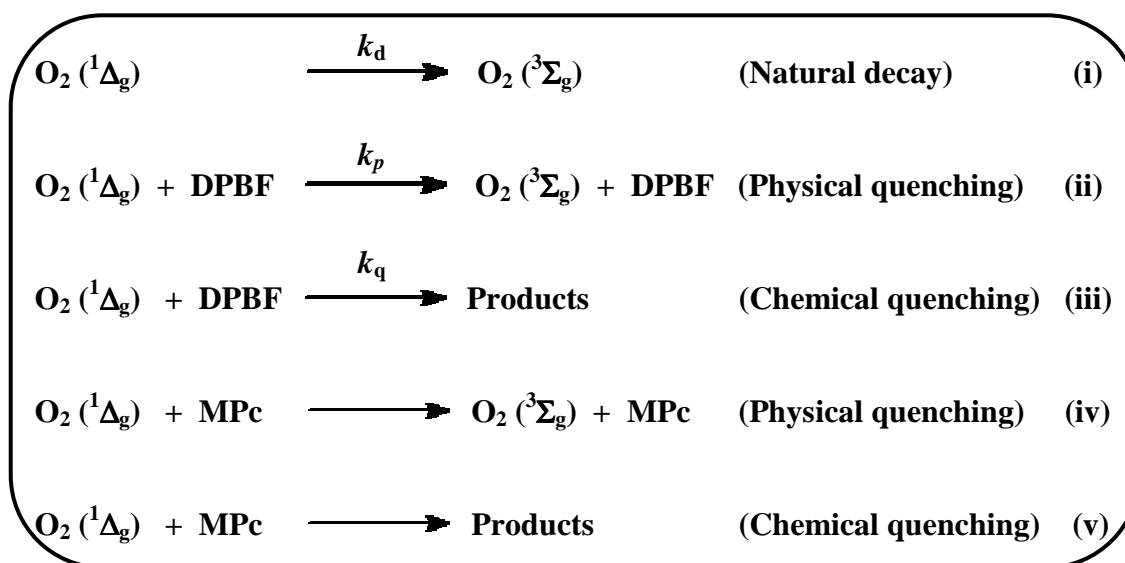
Figure 1.20: Electronic configuration showing the π -antibonding orbitals of oxygen in the ground state ($^3\Sigma_g$) and electronically excited singlet states, i.e. ($^1\Delta_g$) and ($^1\Sigma_g$)

As earlier proposed by Mulliken [212,213], two forms of singlet oxygen, namely, 1O_2 ($^1\Delta_g$) and 1O_2 ($^1\Sigma_g$) are generated through a spin allowed energy transfer from $^3MPC^*$, coupled with spin inversion of triplet oxygen. The electronic configurations of the two singlet states differ only by structure of their π -antibonding orbitals, Figure 1.20. The 1O_2 ($^1\Delta_g$) is relatively long-lived surviving $\sim 10^8$ collisions due to the spin-forbidden transition, $^1\Delta_g \rightarrow ^3\Sigma_g$; while 1O_2 ($^1\Sigma_g$) is short-lived due to a spin-allowed transition, $^1\Sigma_g \rightarrow ^1\Delta_g$ only surviving up to 10 collisions [214,215]. Singlet oxygen is thus conventionally rendered as $^1\Delta_g$.

Upon relaxation, O_2 ($^1\Delta_g$) can be detected at 1270 nm by luminescence [216] or photochemical methods using DPBF as singlet oxygen quencher [217,218]. The quencher quickly reacts with the singlet oxygen in a 1:1 ratio without side reactions or decomposition products that may interfere with the detection of singlet oxygen [219]. DPBF was employed in this work because of its ease of availability. The quencher is also suitable in that it allows quantitative evaluation of the efficiency of singlet

oxygen generation. The decay of the quencher absorption maximum around 416 nm is easily monitored. The efficiency of a sensitizer to generate singlet oxygen is referred to as singlet oxygen quantum yield, Φ_{Δ} . The yield is defined as the number of singlet oxygen molecules generated per photon absorbed by the sensitizer.

Singlet oxygen can be deactivated via several competing pathways depicted in Scheme 1.12. DPBF is known to act exclusively as a chemical quencher in organic solvents [220,221], thus reaction (ii) is insignificant and can be ignored. Additionally, Φ_{Δ} is independent of the sensitizer (MPc) concentration therefore reaction (iv) is ignored. Moreover, reaction (v) is ignored since the rate of reaction of sensitizer with singlet oxygen is negligible compared to that with DPBF. Thus the rate of disappearance of singlet oxygen is dependent on reactions (i) and (iii).



Scheme 1.12: The fate of singlet oxygen following the physical and chemical pathways in the presence of sensitizer (MPc) and DPBF.

The quantum yield is mathematically represented by Eq. 1.3:

$$\Phi_x = \frac{\text{number of molecules (x) disappearing/formed}}{\text{number of quanta absorbed}} \quad (1.3)$$

therefore for disappearing molecules, Eq. 1.4 applies

$$\Phi_x = \frac{-d[x]/dt}{I_{abs}} \quad (1.4)$$

where I_{abs} is the light absorbed by the sensitiser and t is the photolysis time. The

DPBF quantum yield can thus be expressed as Eq. 1.5, [222]:

$$\Phi_{DPBF} = \frac{(C_0 - C_t)V}{t.I_{abs}} \quad (1.5)$$

where C_0 and C_t are the DPBF concentrations before and after irradiation at each cycle respectively and V is the volume of the sample in the cell. I_{abs} is determined

by Eq. 1.6:

$$I_{abs} = \frac{\alpha SI}{N_A} \quad (1.6)$$

where α is the fraction of light absorbed, S is the irradiated cell area, I is the light intensity and N_A is Avogadro's constant. Ultimately, the singlet oxygen quantum yields, Φ_{Δ} can then be calculated according to Eq. 1.7 [223]:

$$\frac{1}{\Phi_{DPBF}} = \frac{1}{\Phi_{\Delta}} + \frac{1}{\Phi_{\Delta}} \cdot \frac{k_d}{k_q} \cdot \frac{1}{[DPBF]} \quad (1.7)$$

where k_d and k_q are respectively, the singlet oxygen decay rate constant and reaction rate constant of chemical reaction of DPBF with singlet oxygen. From the plot of $1/\Phi_{DPBF}$ vs. $1/[DPBF]$, the value of $1/\Phi_{\Delta}$ is obtained from the intercept.

The efficiency of singlet oxygen generation is a key property of a sensitising agent that is governed by various factors. For example, it is essential for energy transfer to take place and thus MPC with Mg^{2+} , Al^{3+} , Zn^{2+} or Si^{4+} as central metal ions,

i.e. those with closed shell or d orbital configuration, manifest long lifetimes in the excited state. Also aggregation should be avoided as dissipation of energy of the excited state occurs, thus resulting in lower Φ_{Δ} values [196]. Also, the presence of heavy atoms promotes ISC - such that the probability of singlet oxygen formation is high - due to increased spin-orbit coupling in the molecule. For most MPcs, quantum yields of singlet oxygen range between 0.30 and 0.80 which are good enough to drive cycloaddition reactions of alkenes and aromatic hydrocarbons.

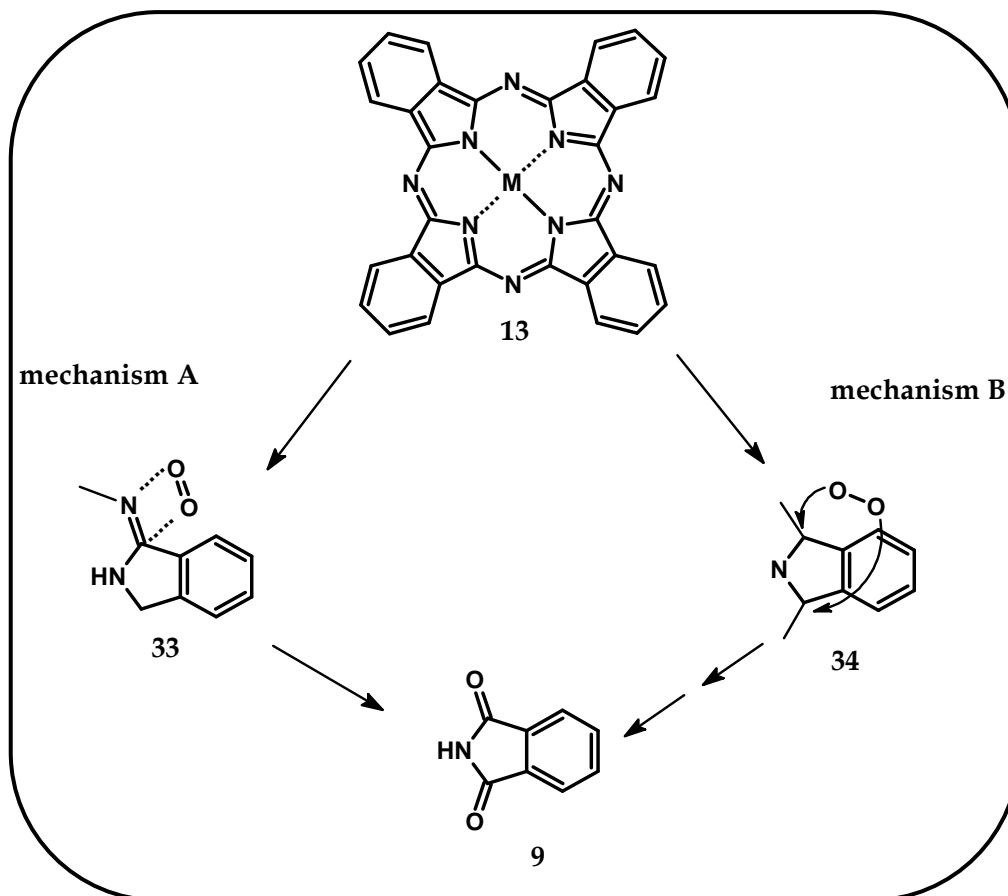
1.6.3 Photochemical processes: Photobleaching

Photobleaching is a process by which Pc macrocycles oxidatively decompose or degrade with time in the presence of singlet oxygen upon irradiation with visible light [223]. Decomposition of MPcs is expected if no other species that may otherwise react with the singlet oxygen is found in the system. In practice, two photobleaching processes predominate [224], i.e.

- (i) *photomodification* where a chromophore is retained in a modified form during absorbance loss, e.g. a main absorption peak diminishes at a particular wavelength and a corresponding new absorption peak is observed at another wavelength
- (ii) *true photobleaching* where a chromophore undergoes a chemical change such that smaller fragments with no absorption in the visible part of the spectrum result, i.e. the chromophore essentially becomes colourless

Phthalimide is most likely to be the product following degradation of MPcs as reported by Cook *et al.* [225] who isolated and identified 3,6-*bis*-decylphthalimide. The singlet oxygen may add across the C=N bond of the interior ligand followed by

cleavage at the *meso* position (Scheme 1.13, mechanism A) [226] or add across the carbons of the pyrrole by a [4 + 2] cycloaddition (Scheme 1.13, mechanism B) [227].



Scheme 1.13: Possible reactions of MPc with singlet oxygen.

Initial rates of photobleaching are often observed to be 1st order in the sensitiser [228], as such quantum yields of photobleaching (Φ_P), which are a measure of the stability of the macrocycle, can be determined. MPC degradation can easily be followed by UV/Vis spectroscopy. To determine how many molecules were degraded per photon of light, Φ_P values are calculated from Eq. 1.8, similar to Eq. 1.5:

$$\Phi_P = \frac{(C_0 - C_t)V}{t \cdot I_{abs}} \quad (1.8)$$

Various factors affect the photobleaching rate. Aggregated MPcs are much more resistant to photobleaching than monomeric MPcs [229,230] and at times they

tend to phototransform into monomers [217]. Wöhrle and co-workers [231] examined the effects of substituents on several MPCs. Electron-withdrawing substituents tend to slow down the photobleaching process as they stabilise the ring by increasing the redox potential. The opposite is true for electron-donating substituents which accelerate the photobleaching process by lowering the redox potential. Also, MPCs with low valent central metals such as Zn^{2+} and Mg^{2+} lower the redox potential of the Pc, thus photobleaching rates are expected to increase. MPCs will additionally display different photobleaching rates in different solvents. For example, photobleaching is faster in chlorinated solvents such as chloroform ($CHCl_3$) and dichloromethane (DCM) because radicals formed from C-Cl bond cleavage aid in the photodecomposition. In deuterated solvents, the singlet oxygen lifetime is longer, thus the photodegradation rate is enhanced [232,233]. MPC stability is essential in applications such as PDT. Therefore, the rate of photobleaching should be within acceptable limits, e.g. rapid sensitiser bleaching will result in incomplete tumour destruction, though damage to surrounding normal tissue is minimal [234]. In photocatalytic reactions, catalyst decomposition may result, leading to termination of photocatalytic cycles. Photooxidation reactions are also governed by MPC stabilities which are determined from the decay of the Q-band in the visible region either in air or oxygen-saturated solutions, i.e. photobleaching. From the absorbance decay, the photodecomposition rate constant, k , can be determined [227] using Eq. 1.10 which is obtained from the rearrangement of Eq. 1.9, i.e.

$$E_t = E_0 \exp(-kt) \quad (1.9)$$

$$\ln \frac{E_0}{E_t} = kt \quad (1.10)$$

where E_0 and E_t are the extinctions measured at time $t = 0$ and t respectively.

1.6.4 Photophysical processes: Fluorescence

Fluorescence is governed by three processes, i.e. excitation of molecules, vibrational relaxation to the lowest excited state energy level, followed by the emission to the ground state. The emission spectrum is normally located on the long wavelength side of the absorption spectrum, Fig. 1.21. Also when the same transitions are involved in both absorption and emission, the fluorescence may appear as an approximate mirror image of the absorption. Depending on the MPc, emission spectra are observed at 660 – 710 nm [235,236]. For MPcs, Stokes shifts of less than 10 nm mean that the excited state has a geometry that is similar to that of the ground state, i.e. the electronic energy levels are unaltered. The Stokes shift is obtained by measuring the difference between the maximum wavelengths in the absorption and emission spectra.

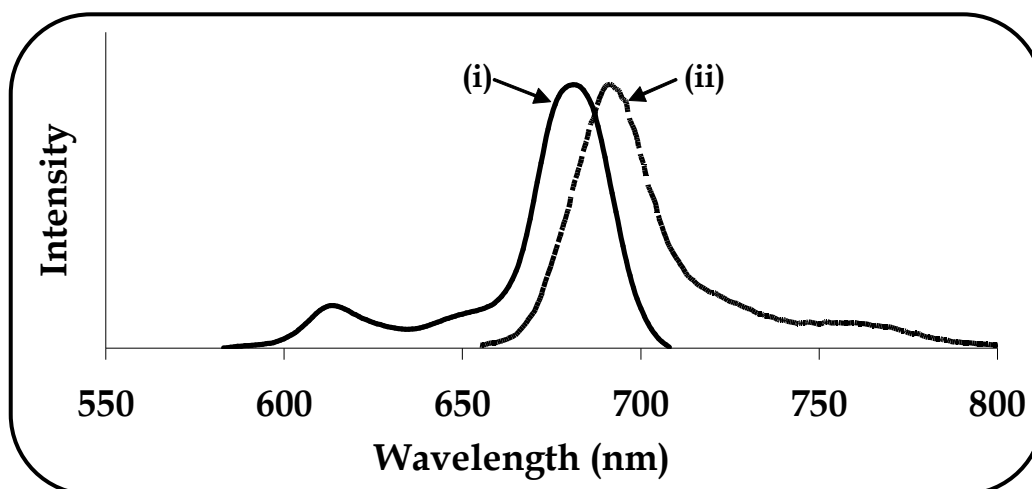


Figure 1.21: Normalised absorption (i) and emission (ii) spectra of a typical MPc.

The emission spectrum may be excited to give an excitation spectrum which provides information about the absorption spectrum of the fluorescent molecules. An excitation spectrum is usually compared to the corresponding absorption spectrum and should ideally closely resemble the latter for a one-component solution, e.g. ZnPc

in DMSO. However, in a case where one component is fluorescent in a mixture, the excitation spectrum will be that of the fluorescing component although the absorption spectrum will contain additional bands. Thus dissimilar excitation and absorption spectra will be obtained. Differently sulphonated MPc or monomers fluorescing in aggregated solutions of MPc are such examples.

Phthalocyanine fluorescence properties are strongly influenced by the presence and nature of the central metal. Spectral shifts, quantum yields and lifetimes are some of the fluorescence properties that have found a niche in scientific and analytical applications [237,238]. Although sufficient fluorescence that enables detection and visualisation of MPc sensitiser distribution in tumour cells is a prerequisite [51,54, 239], little or none is desirable for photocatalytic reactions. Thus parameters such as fluorescence quantum yield (Φ_F) and fluorescence lifetimes (τ_F) are determined since they are in competition with other processes.

1.6.4.1 Fluorescence quantum yields

The efficiency of the fluorescence process is, i.e. fluorescence quantum yield (Φ_F) is defined as the ratio of the number of photons emitted and number of photons absorbed. The Φ_F values are usually determined by a comparative method - similar to that of Williams *et al.* [240] – which involves known Φ_F values of well characterised standard samples, e.g. unsubstituted ZnPc in DMSO with $\Phi_F = 0.18$ [241] or chlorophyll *a* in ether with $\Phi_F = 0.32$ [242]. The comparative method is defined by Eq. 1.11, i.e.:

$$\Phi_F = \Phi_{F(std)} \frac{F \cdot A_{std} \cdot \eta^2}{F_{std} \cdot A \cdot \eta_{std}^2} \quad (1.11)$$

where F and F_{std} are the areas under the fluorescence curves of the sample and standard respectively, A and A_{std} are the respective absorbances of the sample and standard at the excitation wavelengths while η^2 and η_{std}^2 are the refractive indices of the solvents used for the sample and standard, respectively. By definition, A and F account for the number of photons absorbed and emitted respectively.

A number of considerations must be taken into account when determining values of Φ_F , for example the presence of concentration effects which result in self-quenching or use of different solvents for the sample and standard. At the excitation wavelength, absorbance readings should be taken at 0.05 in order to minimise re-absorption effects [243] due to inner filter effects that result in perturbed quantum yield values. When the exciting or emitting light penetration through a spectrophotometric cell is hindered by strongly absorbing solutions, an apparent decrease in Φ_F values results. This phenomenon is known as an *inner filter effect*. Solvent refractive indices [244] are also used as a correction measure within the ratio calculation (Eq. 1.9) when different solvents for the standard and sample are used. Relative fluorescence quantum yields for most monomeric MPcs are similar, ranging from 0.10 – 0.30 [245].

Aggregation extensively affects MPc fluorescence properties [140]. For example, selection rules, explained by exciton coupling, predict non-fluorescent spectra and reduced quantum yields for aggregated MPcs [246]. However recently, aggregates in cooled solutions of MPcs have been shown to fluoresce [247,248]. The fluorescence efficiency may also be reduced by structural features such as double-bond torsion, low-energy n to π^* levels, “heavy” atoms, weak bonds and photo-induced electron transfer [249].

1.6.4.2 Fluorescence lifetimes

The time it takes for a molecule to stay in its excited state before emitting a photon is referred to as fluorescence lifetime. The lifetimes, τ , are defined by the exponential function

$$F_t = F_0 \cdot e^{-t/\tau} \quad (1.12)$$

where F_t is the fluorescence at time t and F_0 is the initial fluorescence observed immediately after excitation. Therefore the fluorescence lifetime, τ_F , is formally defined as the time taken for the fluorophore to decay to $1/e$ or $\sim 37\%$ of the initial fluorescence intensity. Sophisticated techniques such as the steady-state and time-correlated single-photon counting with laser excitation are usually employed to determine fluorescence lifetime measurements [250,251]. The former measures fluorescence intensity as a function of wavelength while the latter as a function of time.

The fluorescence quantum yield and lifetime are often related to what is called the natural radiative lifetime, τ_N , in the absence of competing quenching processes by,

$$\Phi_F = \frac{\tau_F}{\tau_N} \quad (1.13)$$

The radiative lifetime is not in a true sense the lifetime of the excited state; it is rather that lifetime if radiationless transitions were absent. The values of τ_N can be calculated from the absorption spectrum of the molecule using Eq. 1.14 [252,253]:

$$\tau_N = \frac{3.417 \times 10^8}{\nu_{max}^2 \cdot \eta^2 \cdot A} \quad (1.14)$$

where ν_{max}^2 is the wavenumber of maximum absorption band in cm^{-1} , and A is the absorption band area. Theoretically, τ_N is related to the absorption band area, thus using the absorbance and fluorescence spectra, τ_N values can also be estimated by the modified Strickler-Berg equation, i.e. Eq. 1.15, [254-256]:

$$\frac{1}{\tau_N} = 2.88 \times 10^{-9} \cdot \eta^2 \frac{\int \frac{F(\lambda)}{\lambda^2} \cdot d(\lambda)}{\int F(\lambda) \lambda \cdot d(\lambda)} \int \frac{\varepsilon(\lambda)}{\lambda} \cdot d(\lambda) \quad (1.15)$$

where $F(\lambda)$ and $\varepsilon(\lambda)$ are the areas under the fluorescence and absorption spectra respectively. The actual fluorescence lifetimes can then be evaluated using Eq. 1.11, using experimental Φ_F values.

Another method of determining the lifetime is by using a software package, PhotochemCAD, by Du *et al.* [257] which also utilises the Strickler-Berg equation [258]. The program allows for rapid calculations of fluorescence lifetimes of complexes using their absorbance and emission spectra. Accurate predictions of fluorescence lifetimes of various MPc complexes of Si, Ge and Sn within the error of 10 % have been obtained with the program [259, 260]. Fluorescence lifetimes which may otherwise be impossible to obtain due to equipment limitations, can thus be obtained from simple routes.

Decay times of most MPcs are of the order of nanoseconds, usually shorter than 10 ns [261]. MPcs with lighter atoms such as Si lead to lower rates of ISC and hence longer fluorescence lifetimes than those observed with MPcs with heavier atoms such as Zn. Axially substituted SiPcs are more suited to fluorescence studies as they are known to have longer lifetimes than ZnPcs [262]. Also, ring expansion as a result of benzoannulation results in shorter lifetimes [263,264].

1.6.4.3 Fluorescence quenching

The decrease of the fluorescence quantum yield from a fluorophore induced by a variety of molecular interactions with a quencher molecule is known as fluorescence quenching. There are several quenching mechanisms which are also competing with the fluorescence process, namely, dynamic (collisional) quenching, static quenching, quenching by energy transfer and charge transfer reactions [237]. Environmental factors such as ionic strength, pH, solvent effects, aggregation, heavy atom effect and high concentration reduce the emission efficiency.

Photoredox reactions involving the MPc singlet excited state and quenchers such as methyl viologen [265,266], benzoquinone [267,268], hydroquinone [269,270] and azaferrocene [271,272] are known. During photosynthesis, these photosensitised electron transfer reactions are the primary processes and are vital for the conversion and storage of solar energy. Reductive/oxidative quenching of the MPc singlet state depends on the redox potentials of both the MPc and quencher. For example reductive quenching of ZnPc S₁ state (0.49 vs. SCE) with the amine donor, azaferrocene (0.65 vs. SCE) is only possible due to the close redox potentials [272]. Other MPc mediated processes include the photoreduction of methyl viologen [194] and photoreduction/photooxidation of water [196,273]. Phthalocyanine fluorescence can also be effectively quenched by substituents such as tetrathiafulvalene (TTF) units at the periphery due to intramolecular transfer between the Pc and the TTF units [274].

In dynamic quenching, a collisional encounter between the fluorophore in the excited state and the quencher occurs. Subsequently, energy or electron transfer takes place with a decrease in the lifetime and emission intensity. Diffusion measurements can be obtained only if the fluorophore and the quencher diffuse fast enough during

the excited state of the fluorophore. Thus for purely collisional quenching, the reduction in fluorescence intensity is proportional to the quencher concentration, summarised by the Stern-Volmer (SV) equation 1.16 [269]:

$$\frac{F_0}{F} = 1 + K_{SV}[Q] \quad (1.16)$$

where F_0 and F are the fluorescence intensities of the complexes in the absence and presence of the quencher respectively, $[Q]$ is the quencher concentration and K_{SV} is the SV constant obtained from the slope of F_0/F vs. $[Q]$. K_{SV} is also the product of the bimolecular quenching constant, k_q , and the fluorescence lifetime, τ_F , in the absence of the quencher, Eq. 1.17.:

$$K_{SV} = k_q \cdot \tau_F \quad (1.17)$$

For simplest dynamic quenching processes, the plot of SV should give a straight line starting from 1. The bimolecular quenching constant, k_q , reflects the efficiency of quenching with values near $1 \times 10^{10} \text{ M}^{-1} \cdot \text{s}^{-1}$. Smaller k_q values result from steric shielding, while larger values are an indication of some binding interaction/association. A SV plot with an upward curvature indicates a combined dynamic and static quenching contribution usually influenced by charge effects in the quenching, while a downward SV curvature is an indication that there are two or more fluorophore populations, some of which are less efficiently quenched. To determine the fractional accessibility of the fluorescing compound to the quencher, the SV equation is thus modified to Eq. 1.18 [237,275]:

$$\frac{F_0}{\Delta F} = \frac{1}{f_a K_f [Q]} + \frac{1}{f_a} \quad (1.18)$$

where $\Delta F = F_0 - F$, f_a is the fraction of fluorescence intensity accessible to the quencher $[Q]$ and K_f is the SV quenching constant of the accessible fraction. Plots of $F_0/\Delta F$ vs. $1/[Q]$ should be linear with intercept f_a^{-1} and $(f_a K_f)^{-1}$ as slope. Well-known collisional quenchers include oxygen, halogens, amines and many other electron deficient organic molecules. Oxygen is especially an effective fluorescence quencher thus leading to singlet oxygen, due to its unusual triplet ground state. Fluorescence quenching of differently sulphonated MPcs of titanium and tantalum with methyl viologen in methanol will be discussed in this thesis.

1.6.5 Photophysical processes: Triplet state

As mentioned earlier, the singlet excited state can be deactivated in various ways, i.e. emission of a photon to give fluorescence, radiationless deactivation to the ground state or intersystem crossing (ISC). ISC requires a forbidden spin flip such that the lowest energy triplet state is populated. Illumination with red light causes phthalocyanines to transform into the singlet excited state and then reaching the excited triplet state by ISC. The triplet state generation in these macrocycles is essential for PDT processes as well as photooxidation reactions by imparting the excitation energy to molecular oxygen thus yielding the essential singlet oxygen. Phthalocyanines are capable of generating singlet oxygen since their triplet energy is between $110 - 126 \text{ kJ.mol}^{-1}$ which is more than the required 94 kJ.mol^{-1} to allow for efficient energy transfer to ground state oxygen [276].

A technique that is used to generate and study excited states, e.g. the triplet excited state is known as flash photolysis. Transient chemical species at the excited states are generated by a short and intense light pulse from a pulsed laser source.

Incorporation of the laser results in an extremely powerful tool for the study of very short-lived species, called laser flash photolysis. A plot of the difference between the absorbance before and after a laser pulse (ΔA) results in a transient spectrum, Fig. 1.22. The lifetimes of the transients are easily determined from a software program such as OriginPro 7.5 via first order kinetics.

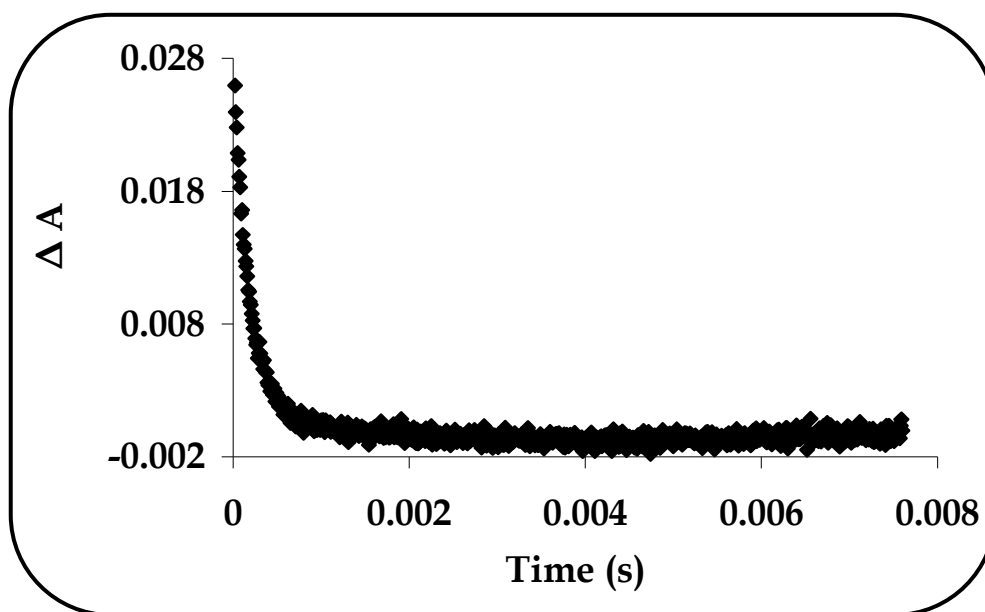


Figure 1.22: Typical transient spectrum (triplet decay curve) following laser flash photolysis

Triplet state quantum yields and lifetimes

The determination of photophysical parameters of the triplet state, i.e. triplet quantum yield (Φ_T) and triplet lifetime (τ_T) is based on the maximum absorption of the triplet state, which occurs at ~ 500 nm for most phthalocyanines. The resulting triplet-triplet absorption is due to the transition from the lowest triplet state of a molecule to higher triplet states, i.e. T_1 to T_n .

The triplet quantum yield, which is the probability of a sensitiser to convert absorbed quanta of light to the T_1 state, is determined by a comparative method [277]. The method involves a reference of known Φ_T and triplet extinction coefficient ε_T at a given wavelength, e.g. unsubstituted ZnPc in DMSO with $\Phi_T = 0.65$ and $\varepsilon_T = 3000 \text{ M}^{-1} \cdot \text{cm}^{-1}$ [278]. The triplet quantum yield of a sample is given by Eq. 1.19,

$$\Phi_T = \Phi_T^{Std} \frac{\Delta A_T^{Sample} \cdot \varepsilon_T^{Std}}{\Delta A_T^{Std} \cdot \varepsilon_T^{Sample}} \quad (1.19)$$

where ΔA_T^{Sample} and ΔA_T^{Std} are the changes in the triplet state absorbances of the sample and standard respectively, ε_T^{Sample} and ε_T^{Std} are the triplet state extinction coefficients of the sample and standard respectively.

Before the evaluation of Φ_T for the sample, the ε_T value has to be precisely known. The values of ε_T are determined by the singlet depletion method. With this method, the difference in absorbance (ΔA_S) is measured where the ground state absorbs [279], i.e. in the region where $\varepsilon_T \ll \varepsilon_S$. The molar extinction coefficient of the ground singlet state ε_S , is normally determined by the Beer-Lambert law. The measurement of ΔA_T is simpler in phthalocyanines as the triplet state absorption does not absorb in the Q-band region ($\sim 700 \text{ nm}$). For phthalocyanines, ΔA will thus be negative corresponding to the depletion in the singlet absorptions at that particular Q-band absorption. The triplet state extinction coefficient ε_T of a sample is given by Eq. 1.20,

$$\varepsilon_T = \frac{(\Delta A)_T \cdot \varepsilon_S}{(\Delta A)_S} \quad (1.20)$$

As earlier mentioned, the triplet lifetimes can easily be determined from a software program via first order kinetics. Alternatively, a linear plot of $\ln A$ vs. time gives k as a gradient, the reciprocal of which gives the triplet lifetime, i.e. $\tau_T = 1/k$.

The efficiency of the MPcs as photosensitisers depends on their high triplet quantum yield ($\Phi_T > 0.40$) and long triplet state lifetimes ($\tau_T > 1\mu\text{s}$). Introduction of heavy atoms such as halogens on the periphery of the Pc promotes ISC due to enhanced spin-orbit coupling to the triplet state. Additionally, care should be taken in designing appropriate phthalocyanines. Structural distortion caused by heavy atom substitution enhances the T_1 to S_0 relaxation pathway and thus tends to reduce the efficiency of energy transfer to the singlet oxygen. MPcs with diamagnetic or metals with closed shells such as Zn or Al phthalocyanine derivatives tend to have long τ_T values [194] than paramagnetic Cr [280] or Cu [281] phthalocyanine derivatives. Interestingly, the exciton coupling theory predicts a high triplet yield for MPc dimers though they reduce the photosensitising ability. It is believed that vibronic coupling rapidly deactivates the triplet excited state, such that the triplet state population is diminished and triplet lifetimes shortened and hence lower Φ_Δ production [282].

1.6.6 Survey of photochemical and photophysical properties of TiPcs

OTiPcs have been investigated for their photoconductivities as thin films [155,283,284]. This requires determining their photostabilities in the presence and absence of oxygen. Only a few examples of OTiPcs have been studied with reference to their photostability in solution [155,284]. These complexes have been found to be sensitive to photooxidation, especially for alkyl and alkoxy substituted derivatives. Singlet oxygen quantum yield determinations however, have not been reported.

The photophysical properties of TiPcs are very useful in applications involving non-linear optics, optical limiters and photoelectric devices as these macrocycles exhibit remarkable properties [159,285]. At most, TiPcs are axially substituted with substituents that allow light-induced transfer processes - which are essential in the fabrication of photoelectric devices - to take place [286]. Photophysical properties of TaPcs are unknown due to their extremely limited synthesis.

A perpendicular dipole moment with respect to the macrocycle plane is induced by the presence of the oxygen axial ligand on the titanium atom. This introduces new steric effects, thus altering the electronic structure of the macrocycle as well as the spatial relationships between the neighbouring molecules [36, 157]. There is thus an intrinsic curiosity about how TiPcs can be made and in understanding the properties of their low-lying electronic states. In addition, the potential which some of the TiPcs have for use as near-infrared light absorbers in optical data storage is immense.

Due to an electron transfer, phthalocyanine fluorescence can be strongly quenched by an electron acceptor. Quenching by quinones, *e.g.* benzoquinone (BQ) and hydroquinone (HQ), is of utmost interest due to the important role of the quinone moiety as an electron acceptor in photobiological processes [287]. Moreover, titanium based phthalocyanines have been scarcely reported [152-154] and their photochemistry and photophysics are unknown compared to the consistent investigations of other non-transition metal phthalocyanines, Table 1.4.

Table 1.4: Photochemical and photophysical parameters of selected MPcs.

MPc	Φ_{Δ}	$\Phi_P (10^{-5})$	Φ_F	Φ_T	$\tau_T (\mu s)$	Ref
ZnPcS _n	0.72	13.65	0.14	0.86	530	[269]
SiPcS _n	0.52	7.35	0.21	0.58	439	[269]
Si(Cl ₂)PcPhenoxy ₈	0.14	1.00	0.21	0.31	194	[232,260]
SnPcPhenoxy ₈	0.22		0.04	0.19	30	[259]
GePcPhenoxy ₈	0.18		0.12	0.30	340	[259]
ZnPcOTbutPhenoxy ₄	0.60	3.33	0.14	0.85	160	[217,288]
ZnPcOPhenoxy ₈	0.60	2.53				[233]
ZnPcOTbutPhenoxy ₈	0.52	3.30				[289]

Aims of thesis

The newly substituted complexes are investigated for their photochemical properties, i.e. singlet oxygen and photostability, used in areas such as photocatalysis where they play a major role in terms of product distribution. Sufficient singlet oxygen is required for oxidation of substrates in photocatalytic reactions, thus the efficiency of the complexes to generate singlet oxygen will be investigated. The stability of a catalyst is of utmost importance in photocatalytic reactions since the more stable the complexes are, the more effective the catalysis is and hence the better the yields. Thus the complexes will be investigated for their photostability.

There has been no reference to the photophysical properties of TiPcs and TaPcs. Sufficient triplet quantum yields as well as lifetimes are also important in photocatalytic reactions in that interaction with ground state triplet oxygen is facilitated and prolonged for generation of singlet oxygen. The effect of substitution

pattern, i.e. peripheral vs. non-peripheral and tetra- vs. octa-, as well as the nature of the substituents, i.e. aryloxy vs. arylthio on the photochemical and photophysical properties are investigated since substituents affect the electronic nature of the macrocycle and tend to strongly influence excited state properties of these macrocycles. Furthermore, fluorescence quenching efficiencies of OTiPcs by benzoquinone (BQ) and methyl viologen (MV) are investigated. The ease of quenching is important since deactivation of excited states greatly affects the catalytic behaviour of the complexes. Also fluorescence lifetimes which may otherwise be impossible to obtain due to equipment limitations, can be obtained from quenching experiments.

1.7 Photocatalytic oxidation of 1-hexene

Oxidation of olefins into useful products is of immense interest. For example, epoxides are useful intermediates obtained on catalytic oxidation of alkenes that are widely used for petrochemicals, fine chemicals and polymers such as oxygen-containing natural products or production of epoxy resins. Use of molecular oxygen as an oxidant for the transformation of alkenes is preferred as it is cheap, environmentally clean and is readily available [290,291]. The economical and environmental impact of chemical productions is severely scrutinised, such that restrictions are placed on chemical companies in order to reduce environmental pollution, hence the use of molecular oxygen.

Phthalocyanines are employed as sensitisers for the oxidation of chemicals via singlet oxygen since they are able to generate singlet oxygen through their intense absorption in the visible region and excited triplet-state energies capable of transferring energy to molecular oxygen. Excited state oxidation reactions of alkenes

using phthalocyanines and molecular oxygen are rare compared to those catalysed by porphyrins [292-295]. This is surprising since MPCs are known to be most active and stable than porphyrins in photocatalytic reactions. Also catalytic photooxidation for the synthesis of organic compounds is scarce [296]. In fact photocatalysis by MPCs has been exclusively limited to the degradation of pollutants [297]. Photodegradation of toxic sulphur compounds, phenols and chlorinated phenols are known to be catalysed by MPCs [298-300]. Photocatalytic oxidation reactions usually selectively proceed at room temperature using light, oxygen and a sensitiser, e.g. metallophthalocyanine (MPC). The active species is often singlet oxygen such that a variety of useful compounds can be obtained from starting compounds, e.g. olefins. Furthermore, oxidative degradation of the sensitiser may result depending on the nature of the substituents.

Many photocatalytic olefin oxidations are affected by the highly energetic and oxidative singlet oxygen through the so-called Type II mechanism, Scheme 1.11. Alternatively, radicals such as superoxides may be generated through the Type I mechanism (Scheme 1.10), however their participation is generally limited. Interestingly, porphyrins with iron [301,302], manganese [303,304], osmium [305], niobium [306,307] or molybdenum [308,309] as central atoms tend to yield products of oxidation via a radical mechanism. However, singlet oxygen sensitisers such as oxovanadium porphyrins and oxotitanium porphyrins have been reported [293,310].

Much effort has been shifted to heterogeneous catalysts which tend to have a longer shelf-life and better catalytic efficiency [311]. The use of such catalysts is especially advantageous since they can be reused. Other catalysts include semiconductors such as TiO which have been mostly used in the treatment of wastes and pollutants [312]. As earlier mentioned, titanyl porphyrins are a few examples that

catalyse photooxidation reactions of cyclic olefins such as cyclohexene using oxygen and visible light, Table 1.5.

Table 1.5: Photooxidation of olefins catalysed by porphyrins in the presence of oxygen and visible light.

Complex	Substrate	Solvent	Epoxide yield	Ref
OTiTPP	Cyclohexene	DCM	10	[293]
OTiTPPCl ₄	Cyclohexene	DCM	10	[294]
(O ₂)TiTPP	Cyclohexene	DCM	5	[310]
NbTTP	1-Hexene	Benzene	22	[306]
OMo(OEt)(TTP)	2-Hexene	Benzene	24	[307]
Fe(TFPF)	Cyclooctene	DCM	20	[313]

TPP = tetraphenylporphyrin, TPPCl₄ = tetrachloro-tetraphenylporphyrin, TTP = tetrakis(p-tolyl)porphyrin, OEt = oxoethoxy, TFPF = tetrakis(pentafluorophenyl) porphyrin

Aims of thesis

The oxidation of 1-hexene by molecular oxygen with aldehydes as reductants to selectively yield 1,2-epoxyhexane, is well-known [314-316]. However catalysis of 1-hexene by MPc in oxygen and visible light is unknown. A comparative study on the catalytic efficiency of selected aryloxy and arylthio oxotitanium complexes for the photooxidation of 1-hexene will be performed. The titanium metal is of closed shell configuration and hence has a potential to generate sufficient amounts of singlet oxygen required for the transformation of 1-hexene. Although electron-withdrawing groups stabilise catalysts, a systematic investigation of the effect of electron donating

substituents such as aryloxy and arylthio on the photocatalytic properties of OTiPcs is investigated. Use of molecular oxygen as oxidant overrides the use of harsh and harmful oxidants such as hydrogen peroxide. Another aim of this study is to identify products in order to propose a photocatalytic oxidation pathway.

1.8 Electrochemistry of metallophthalocyanines

The electrochemical characterisations of the MPcs as well as their ability to electrocatalyse analytes are studied, hence a review of electrochemical techniques follows.

Over the past 40 years the electrochemistry of MPcs has been an area of intense research [317]. From rather primitive beginnings, the electrochemistry of the macrocycles was not investigated sooner (unlike porphyrins) due to their poor solubility and hence relative purity. Phthalocyanines have the capacity to gain or lose electrons and it is these interesting electronic properties that make them useful in many areas including solar cells and electricity production.

The Pc exists as a dianion, i.e. Pc^{2-} , which may be oxidised or reduced in successive steps to give positive or negative ions respectively. The Pc ring redox activity is directly related to the frontier orbitals in the molecule where oxidation is the removal of electron(s) from the HOMO (a_{1u}) while reduction is the addition of electron(s) to the LUMO (e_g), Fig. 1.23. Thus up to four electrons can be successively added to the doubly degenerate e_g orbitals of the LUMO to form Pc^{-3} , Pc^{-4} , Pc^{-5} and Pc^{-6} , and two electrons can be removed from the HOMO to form Pc^{-1} and Pc^0 [318]. This redox activity is typical of H_2Pcs and phthalocyanines with redox inactive metals, i.e. complexes with closed-shell central ions such as Mg^{2+} and Zn^{2+} .

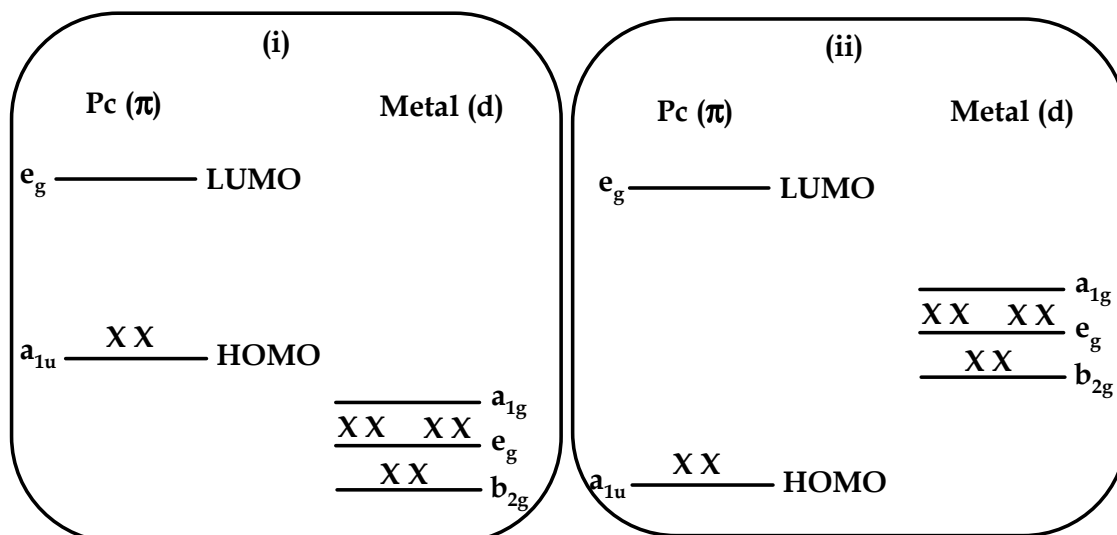


Figure 1.23 A simplified energy-level diagram for a typical MPc where metal orbitals (i) are buried within filled Pc orbitals, e.g. ZnPc or (ii) lie between the HOMO-LUMO gap, e.g. FePc

Oxidation or reduction of MPcs with redox active metals (i.e. with vacant or partially occupied orbitals) may occur both at the metal and/or the ring depending on the relative energies and proximity of metal d and pc ring π orbitals. In light of this, the metal orbitals (b_{2g} , e_g , a_{1g} and b_{1g}) of redox inactive metals are buried inside filled Pc orbitals while those of redox active metals lie between the HOMO and LUMO of the Pc ligand, Fig. 1.23 [319,320]. For metals in MPcs the most important orbitals are the five 3d-orbitals which when placed on the xy plane transform to b_{2g} (d_{xy}), e_g (d_{xz} and d_{yz}), a_{1g} (d_{z^2}) and b_{1g} ($d_{x^2-y^2}$). Additionally, the oxidation and reduction of an electroactive metal invariably occurs at potentials between the first oxidation and first reduction of the Pc ligand [321-323].

Phthalocyanine redox properties can be altered by two aspects, namely the interaction of the 18 electron aromatic core of the Pc ring with substituents as well as the central metal atom. Thus the nature and oxidation state of the central metal, the nature of axial ligands and solvents as well as the nature of substituents on the ring

periphery determine the redox properties of a given complex [324]. Significant alteration of phthalocyanine electrochemical properties occurs with substituents at the non-peripheral positions. Electron-donating substituents, e.g. alkoxy or alkylthio groups, increase the electron density of the central metal atom, thereby making it easier to oxidise and harder to reduce MPc complexes [325]. In contrast, electron-withdrawing substituents, e.g. CN groups, decrease the electron density thereby lowering the LUMO energy levels of the conjugated system. As a result, the electron affinity of the macrocycle is increased and hence MPcs are easier to reduce. In general, central metal ion redox energies are a function of their polarising power, expressed as charge/radius (z_e/r). Thus in most redox reactions, there is an apparent well-defined pattern, i.e. oxidation of MPcs with more positive central metal ions is difficult [326].

MPc electrochemical reactions are often performed at platinum or a carbon [327] working electrode, the latter being popular as it is cheaper and is a suitable alternative to platinum. Examples of carbon electrode materials – depending on percentages of crystalline graphite - include glassy carbon, pyrolytic graphite, carbon paste, carbon fiber and many more. The most common reference electrode whose potential does not change with time is silver-silver chloride (Ag|AgCl). Other reference electrodes employed include normal hydrogen electrode (NHE) and saturated calomel electrode (SCE). Platinum wire is usually used as the counter electrode as it is inert and therefore is resistant to corrosion.

As in all electrochemical reactions, inert electrolytes which carry the task of ion transportation between electrodes are required. Tetraalkylammonium salts are employed in organic media, e.g. tetraethylammonium perchlorate (TEAP), tetrabutylammonium perchlorate (TBAP) and tetrabutylammonium tetrafluoroborate

(TBABF₄). Sodium hydroxide and potassium chloride or nitrate are utilised in aqueous media whereas buffer salts are employed for pH controlled experiments. In addition, solvents influence Pc electrochemical properties due to protic or aprotic and electrophilic or nucleophilic properties. For example oxidation is easier in DMF than in pyridine for a divalent FePc [320] due to stabilisation in the latter solvent. The strongly donating pyridine enhances the back-donation of charge from metal to the ring, by acting as an axial ligand and hence stabilising the ferrous state. It is important that an optimal combination of solvent and electrolyte is found within a usable potential window range such that they do not react at the electrodes. A list of potential limits for commonly used solvents is shown in Table 1.6.

To gain valuable information on the electrochemical properties, a combination of electrochemical techniques, namely, cyclic voltammetry (CV), osteryoung square-wave voltammetry (OSWV), chronocoulometry (CC), chronoamperometry (CA) and spectroelectrochemistry; have been used in this work and will be discussed below. Information on electrode reaction mechanism, identification of intermediates or products as well as elucidation of complete electrochemical mechanisms can be obtained from these techniques.

Table 1.6: Potential limits of commonly used solvents with TBAP as electrolyte at platinum electrodes [328].

Solvent	ϵ^a	Potential limit (V)	
		Cathodic	Anodic
Acetonitrile (ACN)	36.2	-2.6	+2.7
Dichloromethane (DCM)	9.10	-1.7	+1.8
Dimethylacetamide (DMA)	38.0	-2.6	+1.3
Dimethylformamide (DMF)	36.7	-2.7	+1.5
Dimethylsulphoxide (DMSO)	46.6	-2.7	+1.3
Water	80.0	-2.9 ^b	+1.4

^a ϵ = dielectric constant, ^b mercury electrode

1.8.1 Background on the electrochemical techniques used

1.8.1.1 Cyclic voltammetry

Cyclic voltammetry (CV) is a versatile and effective electroanalytical technique commonly used to study electrochemical reactions. The technique provides a rapid and simple way of acquiring information about the rate of electron transfer, stability of electrolysed (oxidised or reduced) analyte, adsorption processes as well as electrode kinetics and mechanisms. In an electrochemical study, CV is generally the first experiment to be performed. The basic theory behind CV experiments is that the electrode potential is cyclically scanned between the initial potential (E_i) and the final potential (E_f) such that a current response is measured at the electrode surface.

Figure 1.24 shows a typical current-potential plot, known as a cyclic voltammogram which is characterised by peak potentials (E_p) and peak currents (I_p).

As the electrode potential is swept to a negative potential, i.e. reduction, current increases with increase in potential until the potential of the analyte is reached. Close to the electrode surface, the analyte is depleted, resulting in the reduction of the current. Reversal of the applied potential results in the reoxidation of the analyte with a current of reverse polarity from that of the forward scan. Analyte mass transport towards the electrode is facilitated in three ways; namely migration, convection and diffusion. Diffusion, which is a movement of species due to a concentration difference, is often favoured for electroanalytical purposes [329].

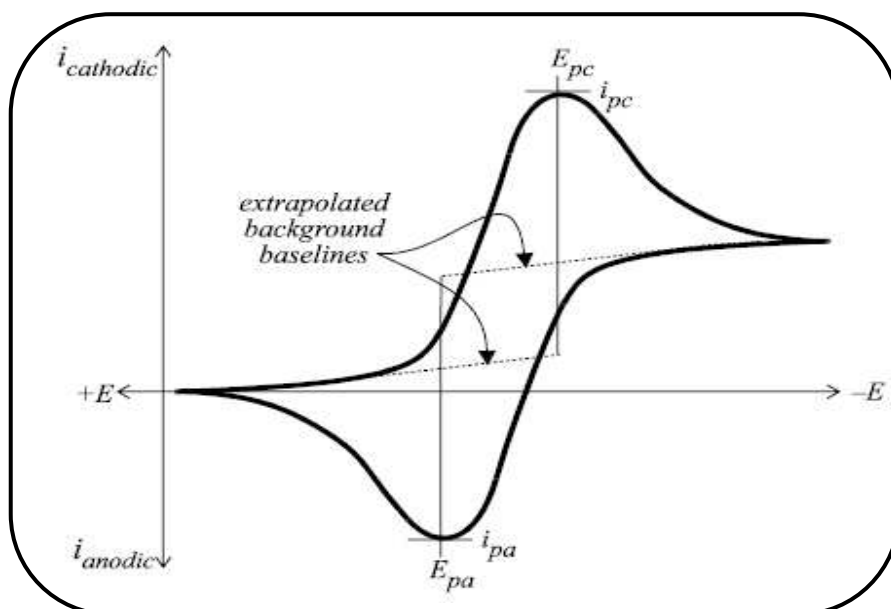


Figure 1.24: A typical cyclic voltammogram (CV).

From a cyclic voltammogram, a system may be classified as reversible, quasi-reversible or irreversible. A *reversible* system involves the reduction (or oxidation) of an electroactive species in the forward scan which is then oxidised (reduced) in the reverse scan, i.e. both the reduced and oxidised species are in equilibrium as required by the Nernst equation.

For these conditions, the peak potential difference, ΔE ($E_{pa} - E_{pc}$) does not change with scan rate ($v^{1/2}$), ΔE is ~ 59 mV and the ratio of the reverse to forward

peak currents is equal to unity for all scan rates, i.e. $I_{pa} / I_{pc} = 1$. For a reversible couple, the number of electrons transferred, n , can be determined from the difference in peak potentials given by Eq. 1.21 at 25 °C, i.e.:

$$\Delta E = E_{pa} - E_{pc} = \frac{RT}{nF} = \frac{59}{n} \text{ mV} \quad (1.21)$$

where R is the universal gas constant, T is the temperature in Kelvin and F is Faraday's constant (96485 C.mol⁻¹). The formal potential, E^o , which is related to the half-wave potential, $E_{1/2}$, is determined by Eq. 1.22.:

$$E^o = E_{1/2} = \frac{E_{pa} + E_{pc}}{2} \quad (1.22)$$

If concentrations of the reduced and oxidised species are not maintained, then the process is said to be *quasi-reversible*. The process is characterised by $I_{pa} < I_{pc}$ or $I_{pa} > I_{pc}$ and $\Delta E > 59/n$ mV, with the value increasing with increasing scan rate. Therefore, slow electron transfer kinetics including lack of equilibrium between the reduced and oxidised species occur, since charge transfer and mass transport control the current. In contrast, for an *irreversible* system, a peak in the reverse direction is weak or is not observed, an indication that the starting reactant is not regenerated. A shift in the peak potential with scan rate characterises an irreversible system due to a slow electron exchange or chemical reaction at the electrode surface. In light of this, the cyclic voltammograms of MPCs are easily obtained and studied in order to estimate their electron transfer abilities as well as mechanisms.

1.8.1.2 Square wave voltammetry

Square wave voltammetry (SWV) is a sensitive electroanalytical technique used to investigate redox reactions that may otherwise be impossible with CV. The more popular technique is known as Osteryoung square wave voltammetry (OSWV) after its inventors in the 1950s [330]. Current signals are sampled at two points, the difference of which is plotted as a function of applied potential, such that peaks rather than voltammetric waves are observed. SWV eliminates the charging current caused by the electrode double layer, thus an increased signal-to-noise ratio results. Therefore shortcomings observed with CV, e.g. overlapping or closely spaced peaks with poor resolution are overcome by SWV. Optimal peak separation, greater analysis speed, lower electroactive species consumption and lower detection limits of up to 10^{-8} M, are advantages that can be obtained with this technique.

1.8.1.3 Chronoamperometry

Chronoamperometry (CA) is a transient technique in which the applied potential is instantaneously stepped from an initial potential (E_i) where no electrolysis occurs to a potential that leads to the electrolysis of the analyte (E_1). At this potential, a current flow begins and is maintained for a time period (T_1). At this stage the experiment is termed a single-potential step CA. When the potential is further stepped to a second step potential (E_f) where the analyte is re-electrolysed and held for a time period (T_2), the experiment is termed as a double-potential step CA, Fig. 1.25. This experiment is particularly useful in investigating kinetics of chemical reactions followed by an electron transfer.

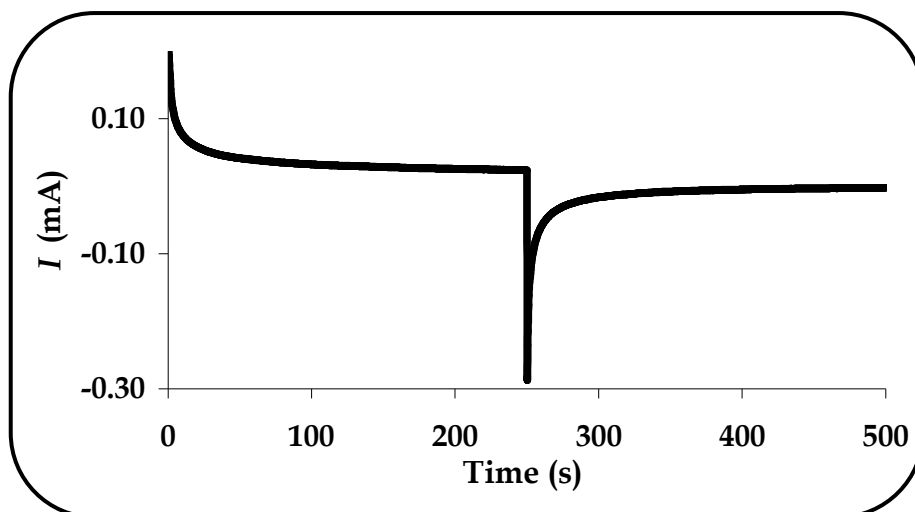


Figure 1.25: A double-potential step chronoamperogram.

In both experiments, a transient signal is observed as the large current rapidly decays due to the depletion of the analyte near the electrode, Fig. 1.25. In CA experiments, the current is monitored as a function of time. The data is analysed according to the Cottrell equation (Eq. 1.23), which defines the current-time dependence for a linear diffusion control [331], i.e.:

$$I = \frac{nFACD^{1/2}}{\pi^{1/2}t^{1/2}} \quad (1.23)$$

where A is the area of the electrode (cm^2), C is the analyte concentration ($\text{mol}\cdot\text{cm}^{-3}$), D is the diffusion coefficient ($\text{cm}^2\cdot\text{s}^{-1}$) and the others are as described above. A plot of I vs. the $t^{-1/2}$ results in a linear relationship known as the Cottrell plot. A , D , n and C can be determined based on this plot, if any of the three parameters are known.

1.8.1.4 Chronocoulometry

Chronocoulometry (CC) is simply chronoamperometry in which the current is integrated, such that the monitored response is charge, Q . Thus by integrating the

Cottrell equation (Eq. 1.23), the Anson equation (Eq. 1.24) which defines the charge-time dependence from linear diffusion control is obtained [331]:

$$Q = \frac{2nFACD^{1/2}t^{1/2}}{\pi^{1/2}} \quad (1.24)$$

In CC experiments, the charge is monitored as a function of time, thus yielding a chronocoulogram, Fig. 1.26. Typically a plot of Q vs. $t^{1/2}$ gives an Anson plot from which A , D , n and C are determined, although concentration determination is rare due to poor detection limits. Adsorption processes as well as modified electrodes that involve surface-constrained reactions can be studied by this method. An advantage of using CC is that slow electron transfer kinetics are eliminated.

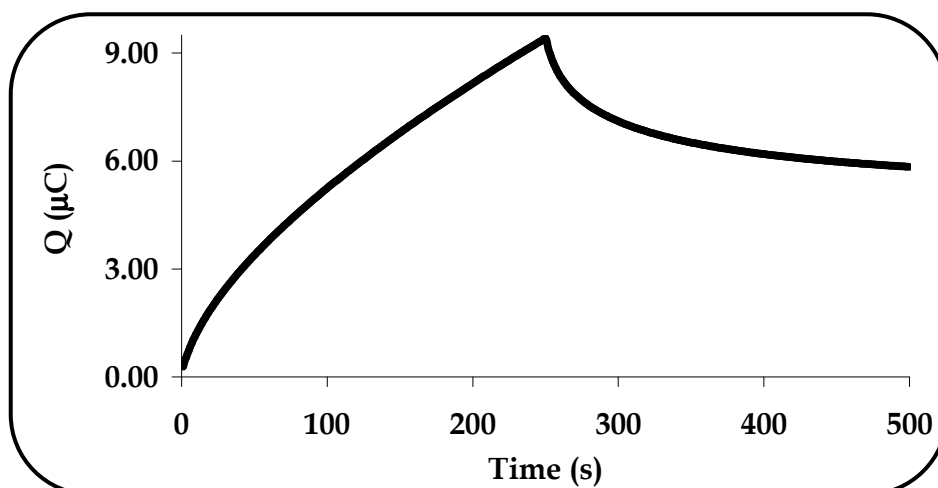


Figure 1.26: A double-potential step chronocoulogram.

1.8.1.5 Spectroelectrochemistry

The redox chemistry of organic, inorganic and biological molecules can be studied by spectroelectrochemistry [332-334]. Spectroelectrochemistry is the combination of electrochemistry and spectroscopy that allows simultaneous acquisition of both techniques. Reaction mechanisms, reaction kinetics and electrode surface phenomena can be studied by this widely used technique [335]. Optically

transparent thin-layer electrodes (OTTLE) enable observation of the electrogenerated species spectroscopically via a light beam that passes through the thin layer of solution and electrode [336]. Typically, OTTLE cell volumes range between 30 – 50 μl [331,337] such that electrolysis takes place in seconds. The number of electrons transferred may be determined by Faraday's equation (Eq. 1.25):

$$Q = nFVC \quad (\text{Eq. 1.25})$$

where V is the volume of the cell and other constants are as previously defined. The nature of MPc redox processes which cannot be distinguished by CV alone, may take place at the central metal atom or the ring. Depending on the applied potential, MPc spectroelectrochemical studies facilitate understanding for MPc properties. Ring based redox processes often result in colour changes, while metal based redox processes exhibit less dramatic colour changes [319]. Monitoring spectral changes of MPc ring gives information on the nature of the redox process, for example a shift in the Q-band is due to oxidation/reduction of the central metal [168] whereas a decrease in the Q-band intensity, accompanied with an increase in intensity at the 500 – 600 nm region is due to oxidation/reduction of the ring [338]. In this work, UV/Vis spectroelectrochemistry is used to characterise and determine sites of redox activity in OTiPcs.

1.8.1.6 Survey of the electrochemical properties of TiPcs and TaPcs

Film voltammetric behaviour of OTiPc on ITO (indium tin oxide) was found to exhibit two ring reduction processes although decomposition resulted during oxidation [339]. At the start of this work, the solution electrochemistry of titanium phthalocyanines has been unknown. Recently, a study on the electrochemistry of TiPcs, where two metal-based and one ring-based reductions were observed, was

reported [340]. More detailed electrochemical studies are known for MPcs such as ZnPc, MnPc and CoPc [341]. Understanding the electrochemical behaviour of TiPc and TaPc complexes is important for their possible applications in for example, catalysis. It is thus important to study the electrochemical behaviour of these complexes for such applications more so because of their rare or unknown solution electrochemistry.

Introduction of different kinds of substituents onto the periphery and changing the central metal can alter spectroscopic and electrochemical properties. In fact, the choice of substituents and metal strongly influence the electrochemical properties of these macrocycles. For example, multi-electron redox processes are common in biological systems and are needed for reduction of species such as carbon dioxide and oxygen. Hence, the study of the electrochemistry of MPc complexes, which show potential as catalysts for multi-electron processes such as those of TiPc and TaPc is essential.

Aims of thesis

As earlier mentioned, the solution electrochemistry of OTiPcs and TaPcs has not been exploited in comparison to other first row transition metals. In this thesis the electrochemical characterisation of the newly synthesised complexes by CV, OSWV, CC and spectroelectrochemistry is described for the first time. The influence of the nature, number and position of the substituents on the redox properties of these MPcs is investigated. The data obtained is essential in understanding electrocatalytic properties of the MPcs. The solution electrochemistry of TaPc is also investigated for the first time.

1.8.2 Electrocatalysis

One electrochemical application of MPcs is in electrocatalysis hence OTiPc complexes were employed for the electrocatalytic oxidation of nitrite. However, the background on MPc electrocatalysis is presented.

Electrocatalysis in a wide sense is the study of electrochemical reactions at electrode surfaces such that rates of reaction are increased and a decrease in overpotential results. Equations 1.26 and 1.27 may represent an electrocatalytic reaction, i.e.:



where O is the oxidised species, R is the reduced species, A is the analyte and P is the product. Equation 1.26 generates the active catalyst which then reacts with an analyte (Eq. 1.27), resulting in the regeneration of the catalyst and formation of product. A return peak may not be observed due to a fast chemical reaction taking place [342].

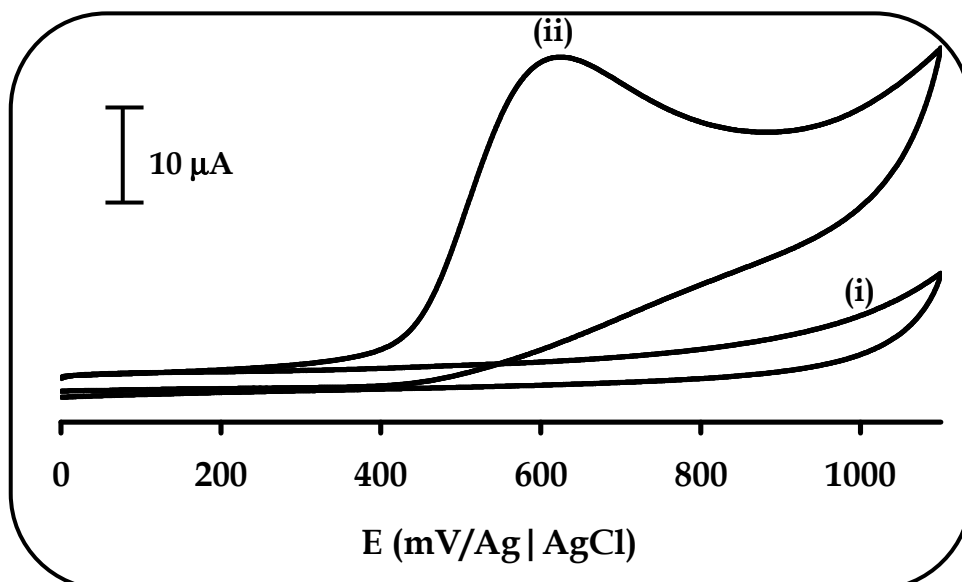


Figure 1.27: Electrocatalytic behaviour at (i) unmodified electrode and (ii) modified electrode.

A mediating molecule known as an electrocatalyst is often used to modify the electrode surface in some way. Modified electrodes tend to lower overpotentials because electrochemical reactions are accelerated by molecules at the surface. Unmodified electrode surfaces however, often exhibit large overpotentials for electrochemical reactions that take place at very low rates or that do not occur at all, Fig. 1.27(i). Electrocatalysis is thus characterised by current enhancement, lowered overpotentials and absence of a reverse peak, Fig. 1.27(ii).

MPcs are electrocatalysts since they serve as mediators in many electron transfer reactions, due to their rich and reversible redox chemistry. Their high thermal and chemical stabilities as well as their catalytic efficiency for a variety of analytes, makes them the best electrocatalysts used thus far. As MPcs have been used for a great variety of electrochemical reactions, their catalytic activity can be fine-tuned by the nature of the substituents at the periphery as well as the central metal. Generally, electrocatalytic activities are observed at potentials close to those of the central metal or ring [343], therefore electrocatalytic reactions tend to be mediated by the central metal or the ring [344,345]. Electrocatalysis by MPc usually starts with the oxidation/reduction of the metal or ring. Thereafter, a chemical reaction with an analyte follows to form product and regeneration of the catalyst. For example, electroreduction by MPc at both metal (Eq. 1.28 and 1.29) as well as ring (Eq. 1.30 and 1.31) based redox process is illustrated below:



OR



The electrocatalytic activity of MPcs for oxidation/reduction of various analytes is far from complete as their applicability for this field is diverse, therefore a variety of reactions are still to be investigated with catalysts of this type.

As earlier mentioned, the surface of the electrode is modified with a mediator. There are various methods of attaching the mediator to the electrode surface. The simplicity of most MPcs to adsorb onto electrode surfaces leads to what is known as chemically modified electrodes (CME), which exhibit electrocatalytic activity for a variety of electrochemical reactions. In this way, the selectivity of the CME is increased since some chemical specificity is imparted onto the electrode surface which may not be available at an unmodified electrode surface.

It is important to note that mediation of electron transfer is only possible if the mediator is itself electroactive. Also MPc film formation (monomer, polymer, aggregates) is largely influenced by the method of deposition; hence the electrocatalytic activity at the electrode surface will be affected. Methods of modification include adsorption by dip-dry [346], vapour deposition [347], carbon paste [348], self-assembled monolayer [349,350], drop-dry [351-353] and electropolymerisation [354-356] onto conventional electrodes such as gold, platinum or glassy carbon. In this work, modification was performed on a glassy carbon electrode (GCE) using drop-dry and electropolymerisation methods since MPcs tend to strongly adsorb on graphite through π - π interactions. For the purpose of this thesis the methods discussed are:

Drop-dry method - the catalyst is dissolved in a solvent where maximum solubility is achieved and preferably one that easily evaporates off. A drop of catalyst solution is applied onto the electrode surface and the solvent is allowed to dry.

Substantial electrocatalytic activity occurs even though this method forms films that are irreproducible and unstable over long periods of time, due to loss of catalyst and possible passivation. From a linear relationship of I_p vs. v , the surface coverage ($\text{mol}\cdot\text{cm}^{-2}$), Γ , can be estimated using Eq. 1.32 [357]:

$$I_p = \frac{n^2 F^2 \Gamma A v}{4RT} \quad (1.32)$$

where all the symbols have their usual meanings or are described above. The surface coverage can also be determined by integration of the peak area of the MPc by Eq. 1.33,

$$\Gamma_{MPc} = \frac{Q}{nFA} \quad (1.33)$$

where Q is the charge under the reduction or oxidation peak and all the other symbols are as described above.

Electropolymerisation - There are a number of ways to polymerise phthalocyanines on conducting supports, one of which is electropolymerisation. In analytical chemistry, considerable attention has been generated by MPc attachment to electrode surfaces via electropolymerisation. In this regard, MPcs immobilised on the electrode surfaces have been extensively exploited in electrocatalysis since electronic conductivity is exhibited by the polymeric coatings produced on the electrode surface. Hence, a catalytically active electrode is employed. This method is mostly favoured as uniform and stable electro-conducting polymers thus formed; ensure reproducible control over their thicknesses. Also, the thick polymeric phthalocyanine networks formed are attractive in that chemical and thermal stabilities are enhanced without compromising the catalytic activity. An additional advantage is that a three-

dimensional reaction zone is formed at the electrode surface. Hence rates of reaction occurring at the electrode surface are increased and the response sensitivity improved.

The electrode is immersed in ~ 1 mM solution of catalyst containing supporting electrolyte and this is followed by repetitive cycling between two predetermined potentials. The fact that the first scan differs from the successive scans, an increase in both anodic and cathodic currents as well as formation of new peaks, is an indication that polymer formation is taking place [358]. The main advantage of using this method is that polymer formation is reproducible and film thickness can be carefully controlled.

Electropolymerisation which is generally accepted to be complex, is believed to proceed via a general electrochemical-chemical-electrochemical, $E(CE)_n$, mechanism [359] of substituents containing 'N' or 'S'. The most frequently electropolymerised MPcs are the amino-, pyrrole- or thiophene-appended complexes; employed as catalysts for detection of various analytes [360-362]. MPcs with such substituents are suitable in that coupling of their strong and well-defined electronic π -systems produce polymers of high stability and rigidity. Briefly, the initial electrochemical step (E) involves the oxidation/reduction of the monomer to its radical. The rate of electron transfer exceeds that of the monomer diffusion to the electrode surface, thus a high concentration of the radical species results. In the chemical step (C), two radicals dimerise with subsequent loss of protons, thus forming a neutral dimer. The dimer so formed is easily oxidised/reduced than the monomer to form radicals and further couples with other radicals in solution. The $E(CE)_n$ mechanism forms an oligomer and continues until the polymer becomes insoluble in the medium and precipitates onto the electrode surface [363,364]. Various factors such as the nature and solubility of the monomer, the nature of the counter ion, the

nature and size of the electrode surface, determine the mechanism of polymer growth [365,366].

1.8.2.1 Electrocatalytic oxidation of nitrite

Electrooxidation of nitrite by OTiPcs was chosen with the aim of lowering the overpotential occurring at ~ 0.80 V [367].

Nitrites play an important role in the inhibition of corrosion in industrial waters and are a source of nitrogen which is essential for environmental processes in green plants. Despite the wide use of nitrites, there is much concern about their level in for example foods and beverages, since they are known to have carcinogenic effects [368-370]. Degradation of some fertilizers forms nitrite and therefore the determination of nitrites is of environmental importance, since its presence is an indication of the extent of pollution and eutrophication in natural waters [371].

Nitrites can be determined by the time-consuming spectrophotometric [372,373], chromatographic [374,375] as well as the faster electrochemical [376-378] methods. The first method uses sulphanilamide and *N*-(1-naphthyl)ethylenediamine, however acidity needs to be carefully controlled otherwise interferences may occur [379,380], while the latter method is attractive in that it allows rapid and precise analysis of the ion. The electrochemical methods often involve the catalytic oxidation of nitrite since this is a more convenient approach in contrast to reduction. The choice of nitrite oxidation in this study is that it does not suffer from poor sensitivity due to the interference from nitrate and molecular oxygen, which are major limitations for the cathodic determination of nitrite [381]. An additional advantage is that electrooxidation of nitrite tends to give nitrate as the final product, in contrast to its electroreduction in which several products are produced.

Nitrite oxidation on conventional solid electrodes such as platinum [382], glassy carbon [383], gold [384] and diamond [385] is known. Although nitrite is electroactive, it exhibits poor electrochemical behaviour at these bare electrodes. The oxidation occurs at undesirable high potentials [383,386] and the result is the generation of species that tend to poison the electrode surface and hence decrease the sensitivity and accuracy [387].

As earlier mentioned, modification of the electrode surface with a suitable electrocatalyst is a very good way of improving the electrode sensitivity, as well as efficiently lowering the potentials [378]. For example, electrode modification by haemoglobin, myoglobin, enzymes, porphyrins and MPcs used in catalysis of various analytes are known [388-397]. MPcs are well known catalysts for the electrooxidation of nitrite [70-72,398,399]. Both ring and central metal have shown to mediate the electrocatalysis of nitrite. These modified electrodes offer an effective route in the fabrication of nitrite electrochemical sensors.

1.8.2.2 Survey of the electrocatalytic properties of TiPcs

The electrochemistry of titanium phthalocyanines is rare and their electrocatalytic properties are unknown. MPc complexes have been employed for the electrocatalytic oxidation of nitrites in neutral, basic and acidic media [70-72,367,399]. Generally, nitrite electrooxidation occurs at ~ 0.80 V on porphyrin and phthalocyanine modified electrodes [367] regardless of the media, Table 1.7. There is thus -a need to lower this potential. The activities of MPcs for the oxidation of nitrite are influenced minimally by the nature of the central metal (when comparing CoPc, MnPc, FePc and CrPc) and more substantially by the nature of the substituents [367]. A study of MPc complexes containing other transition metals and a wider variety of

substituents is useful in that new trends in what is required to lower overpotentials for nitrite may be determined.

Table 1.7: Electrochemical data for the electrooxidation of nitrite in pH 7.3 by MPcs.

Complex	Electrode	Method of modification	E (V) vs. Ag AgCl	Ref
CoPc	VCE	Drop-dry	0.92	[70]
FePc	OPG	Drop-dry	0.80	[72]
CrTAPc	GCE	Electropolymerisation	0.80	[355]
NiTAPc	GCE	Electropolymerisation	0.92	[398]
CoTSPc/ FeTMPyP	GCE	Electrodeposition	0.85	[399]

TA = tetraamino, TS = tetrasulpho, TMPyP = tetra-(methyl-4-pyridyl)-porphyrin, VCE = vitreous carbon electrode, OPG = ordinary pyrolytic graphite, GCE = glassy carbon electrode

Aims of thesis

The electrochemical study of the OTiPcs synthesised in this work is extended in order to determine their potential as electrocatalysts for the oxidation of nitrite for the first time. Modification of GCE by two convenient methods, namely adsorption and electropolymerisation is probed since passivation by adsorption effects from products of oxidation in solution readily occurs on a bare electrode. The main aims are to electrocatalyse the oxidation of nitrite at lower potential, i.e. lowering of overpotential, as well as increase or enhance catalytic currents. The comparative catalytic activity based on the titanium metal and the nature of the substituents is also investigated. The electrode kinetics for the electrooxidation process are also explored.

1.9 Summary of Aims of the thesis

The aims of the thesis discussed are summarized as follows:

- (a) Synthesise and spectroscopically characterise oxotitanium(IV) phthalocyanine complexes that are tetra-substituted at the peripheral and non-peripheral positions with aryloxy, arylthio, nitro and amino groups (see Fig. 1.10 and Fig. 1.12). Additionally, octa-substituted OTiPcs are synthesised, Fig. 1.11. Furthermore, unsubstituted Cl_2TiPc and Cl_3TaPc (Fig. 1.8) are synthesised together with their water-soluble derivatives, Fig. 1.9.
- (b) Determine the electrochemical characteristics of the synthesised complexes by CV, OSWV, CC, CC and spectroelectrochemistry which are important for electrocatalytic reactions.
- (c) Determine the photochemical (singlet oxygen quantum yields, photobleaching quantum yields) and photophysical (fluorescence quantum yields and lifetimes, triplet quantum yields and lifetimes) properties of some selected complexes, the information which is essential for photocatalysis. Moreover, the fluorescence quenching experiments in the presence of quenchers are studied.
- (d) Photocatalyse 1-hexene with selected aryloxy and arylthio OTiPcs which are tetra-substituted at the peripheral and non-peripheral positions. A comparative study of their photochemical and photocatalytic properties - which are important for product distribution - is done. Also a mechanism for the product distribution is proposed.
- (e) Investigate the effect of charge transferability of anionic TiPcS_n and TaPcS_n complexes on interaction with a cationic acceptor compound, methyl viologen, by spectroscopic methods. Fluorescence quenching of the complexes is investigated and parameters are determined.

- (f) Investigate the catalytic efficiencies as well as kinetics of tetra-substituted OTiPcs modified onto glassy carbon electrode by drop-dry or electropolymerisation, towards the electrooxidation of nitrite.

The MPc complexes studied are:

- Unsubstituted Cl_2TiPc and Cl_3TaPc (Fig. 1.8), as well as their differently sulphonated derivatives, i.e. OTiPcS_n and $\text{Cl}_3\text{TaPcS}_n$ (Fig. 1.9)
- Peripherally and non-peripherally substituted OTiPc complexes that are substituted with phenoxy, *tert*-butylphenoxy, benzyloxy, 4-(benzyloxy)phenoxy, phenylthio and benzylthio groups (Fig. 1.10)
- Peripherally substituted octa-substituted OTiPc complexes that are substituted with phenoxy, *tert*-butylphenoxy, 4-(benzyloxy)phenoxy and phenylthio groups (Fig. 1.11)
- Peripherally substituted OTiPc complexes that are substituted with nitro and amino groups (Fig. 1.12)

CHAPTER 2

Experimental

2.1 Materials

Acetone, benzene, chloroform (CHCl_3), 1-chloronaphthalene (1-CNP), dichloromethane (DCM), dimethylformamide (DMF), dimethylsulphoxide (DMSO), ethanol, hexane, methanol, 1-octanol and tetrahydrofuran (THF) were purchased from either SAARCHEM or Aldrich and were dried and distilled over calcium hydride or sodium/benzophenone before use. Water collected from a nanopure Milli-Q water purification system of Millipore was used for all aqueous solutions. Deuterated chloroform (CDCl_3), deuterated dimethylsulphoxide (d_6 -DMSO), acetic anhydride, ammonia (25 % or 32 %), benzoquinone (BQ), benzyl alcohol, benzyl mercaptan, 4-(benzyloxy)phenol, bromine, 2,6-di-*tert*-butyl-4-methylphenol (BHT), 4-*tert*-butylphenol, 1,4-diazabicyclo-octane (DABCO), 4,5-dichlorophthalic acid, 1,3-diphenylisobenzofuran (DPBF), 1,2-epoxyhexane, formamide, 1-hexene, 1-hexen-3-ol, hydrochloric acid (32 % HCl), magnesium sulphate (MgSO_4), methyl viologen dichloride hydrate, nitric acid (55 % HNO_3), 3-nitrophthalic acid, oleum (30 %), phenol, phthalimide, phthalonitrile (recrystallised from ethanol), potassium bromide (KBr), potassium carbonate (K_2CO_3), sodium carbonate (Na_2CO_3), sodium dihydrogen phosphate (NaH_2PO_4), sodium hydrogen phosphate (Na_2HPO_4), sodium hydroxide (NaOH), sodium nitrite, sodium sulphide nonahydrate ($\text{Na}_2\text{S}\cdot 9\text{H}_2\text{O}$), sulphuric acid (98 % H_2SO_4), tantalum pentachloride (TaCl_5), tetrabutylammonium tetrafluoroborate (TBABF_4), thionyl chloride, thiophenol, titanium butoxide, titanium tetrachloride (TiCl_4 , distilled from calcium hydride), Triton X-100, urea, were purchased from Sigma-Aldrich, SAARChem or Merck. All other reagents were of analytical grade and were used as received from the suppliers. Chromatography was performed on silica gel 60 (0.04 – 0.063 mm).

2.2 Instrumentation

UV/Vis spectra were recorded on a Cary 500 UV-Vis/NIR spectrophotometer. IR spectra (KBr pellets/Nujol) were recorded on a Perkin-Elmer spectrum 2000 FTIR spectrometer. ^1H -NMR and ^{13}C -NMR spectra were recorded using a Bruker EMX 400 MHz NMR spectrometer. MALDI TOF spectra were recorded with Perseptive Biosystems Voyager DE-PRO Biospectrometry Workstation and Processing Delayed Extraction Technology at the University of Cape Town. Elemental Analyses were also performed at the University of Cape Town. Fluorescence excitation and emission spectra were recorded on a Varian Eclipse spectrofluorometer. Triplet absorption and decay kinetics were recorded on a laser-flash photolysis system. The excitation pulses were produced by a Nd:YAG laser (Quanta-Ray providing 400 mJ, 90 ns pulses of laser light at 10 Hz) pumping a tunable dye laser (Lambda Physic FL 3002, Pyridine 1 dye in methanol). The single pulse energy was 7 mJ. The analyzing beam source was from a Thermo Oriel xenon arc lamp, and a photomultiplier tube was used as a detector. Signals were recorded with a two-channel, digital real-time oscilloscope (Tektronix TDS 360); the kinetic curves were averaged over 256 laser pulses. Photocatalytic product analyses were performed on a Hewlett-Packard HP 5890 Gas Chromatograph (GC) fitted with an FID detector, using a PONA (crosslinked methyl siloxane) capillary column (50 m length, 0.2 mm internal diameter, 0.5 μm film thickness and 100 phase ratio). Mass spectra were recorded with Finnigan GC-MS using the same column as above. The light intensity was measured with a power meter (POWER MAX51100 – with incorporated Molelectron detector) for photocatalytic experiments. Electrochemical data were obtained under purified nitrogen gas with BioAnalytical Systems (BAS) model 100B/W Electrochemical Workstation and spectroelectrochemical data from BAS CV 27 voltammograph.

2.3 Methods

2.3.1 Photochemistry

2.3.1.1 Singlet oxygen and photobleaching determinations

Experimental methods for the determination of quantum yields of singlet oxygen and photobleaching were performed with a home-made photochemical set-up shown in Fig. 2.1. Solutions of the complexes were placed in a 1 cm pathlength spectrophotometric quartz cell that is fitted with a tight-fitting stopper. Typically, 2.0 ml of air-saturated DMSO solution of MPc ($\sim 10^{-6}$ – 10^{-5} M) with DPBF ($\sim 3 \times 10^{-5}$ M) for singlet oxygen or without DPBF for photobleaching, were placed in the cell and then photolysed at the Q-band region with a 300 W General Electric Quartz line lamp (A). The UV and far infrared radiations were filtered off by a 600 nm Schott glass (D) and water (C) filters. An interference filter (E) [Intor 670, 700 or 750 nm with bandwidths of 20 nm (670 nm filter) or 40 nm (700 and 750 nm filters)] was placed in the light path before sample cell (F). The wavelength of the interference filter was chosen such that it was close to the Q band absorption of the MPc. Light intensities were measured with a power meter which gives values in $\text{Js}^{-1} \cdot \text{cm}^{-2}$ and converted to appropriate values in $\text{photons} \cdot \text{s}^{-1} \cdot \text{cm}^{-2}$ using Eq. 2.1.

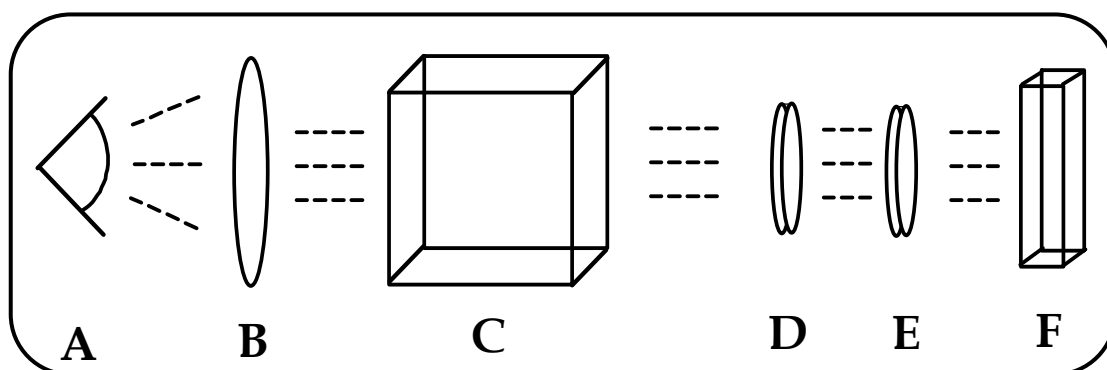


Figure 2.1: Photochemical set-up where (A) light source, (B) convergence lens, (C) water filter, (D) glass filter, (E) interference filter and (F) UV/Vis cell.

$$E_{at\lambda} = \frac{hc}{\lambda} \tag{2.1}$$

where E is the energy of light, h is Planck's constant, c is the speed of light and λ is the wavelength of the interference filter. The fraction of light that passes through the filter and is actually absorbed by the MPc in Eq. 1.6 was determined by Eq. 2.2:

$$\alpha = \frac{\sum T_{filter}(1 - T_{MPc})}{\sum T_{filter}} \tag{2.2}$$

where α is the fraction of the overlap integral of the light absorbed by the MPc, T_{filter} is the light transmitted through the interference filter and T_{MPc} is light transmitted through the MPc solution. The transmittances were obtained by converting the absorbances of the filter and the MPc. The interference filter so chosen must have a transmittance that has maximum overlap with the respective MPc. Table 2.1 shows a sample computation of $\alpha = 0.46$, using Eq. 2.2.

Table 2.1: Calculations for the fraction of light absorbed (α) by a typical MPc

λ (nm)	T_{filter}	T_{MPc}	$1 - T_{MPc}$	$T_{filter}(1 - T_{MPc})$
685	0.526	0.528	0.472	0.248
690	0.618	0.495	0.505	0.312
695	0.648	0.458	0.542	0.351
700	0.640	0.432	0.568	0.364
705	0.619	0.418	0.582	0.360
710	0.604	0.421	0.579	0.350
715	0.609	0.460	0.540	0.328
720	0.519	0.526	0.474	0.246
	$\sum T_{filter} = 4.783$			$\sum T_{filter}(1 - T_{MPc}) = 4.783$

The singlet oxygen quantum yields (Φ_{Δ}) of the complexes were determined by monitoring the absorbance decay of DPBF at 416 nm. The concentration of DPBF is kept at $\sim 3 \times 10^{-5}$ M to avoid chain reactions. The DPBF quantum yields (Φ_{DPBF}) were firstly calculated using Eq. 1.5 for each irradiation cycle. Ultimately, the singlet oxygen quantum yields can then be calculated according to Eq. 1.7. The photostabilities of the MPc complexes were determined by monitoring the decay of the Q-band intensity in the visible region of light. To determine the number of molecules degraded per photon of light, photodegradation quantum yields Φ_P were calculated from Eq. 1.8. Additionally, the time decay of the Q-band maxima for MPc tend to obey first-order kinetics, thus the photobleaching rate constant k , which is a measure of phthalocyanine stability, is calculated from Eq. 1.20.

2.3.1.2 Photocatalytic oxidation of 1-hexene

The photocatalytic experiments were carried out with the set-up (Fig. 2.1) described for the determination of singlet oxygen and photobleaching quantum yields. In a typical experiment, a 5 ml glass vial was charged with a phthalocyanine complex (1 μ mol) and 1-hexene (molar ratio of photosensitiser to substrate was 1:500) in oxygen saturated DCM. The reaction vessel was irradiated under intensive magnetic stirring with a General Electric Quartz lamp (300 W), with a 600 nm glass (Schott) and water filters used to filter off the UV and far infrared radiations respectively. An interference filter of appropriate wavelength was placed in the light path before the reaction vessel. The light intensity was measured with a power meter and was found to be $\sim 4.0 \times 10^{16}$ photons.s⁻¹.cm⁻². At appropriate intervals, aliquots were removed and immediately analysed by GC. The identification of the reaction products was verified by co-injection with authentic samples and GC-MS analyses. The total

reaction time was 8 hours at room temperature. The GC conversions (%) and oxidation product selectivities (%) were measured relative to the starting substrate, 1-hexene. Equations used to determine % conversion and selectivity are shown below in Eq. 2.3 and 2.4 respectively. The amounts were calculated relative to the GC % peak area

$$\% \text{ Conversion} = \frac{\text{initial substrate} - \text{substrate remaining}}{\text{initial substrate}} \times 100 \quad (2.3)$$

$$\% \text{ Selectivity} = \frac{\text{product obtained}}{\text{initial substrate} - \text{final substrate}} \times 100 \quad (2.4)$$

2.3.2 Photophysics

2.3.2.1 Fluorescence quantum yield

Fluorescence quantum yield determination begins with the choice of the right standard when using the comparative method. The solutions of the MPc investigated as well as the standard were prepared such that the absorbance of each is ~ 0.05 at the wavelength of excitation. Since excitation is assumed to be monochromatic, the excitation bandwidth was kept small [400]. Emission spectra were recorded and the areas under the curves were measured. Corrections for refractive indices were done where different solvents for MPc and standard were used. Quantum yields were determined using Eq. 1.9, with unsubstituted ZnPc in DMSO ($\Phi_F = 0.18$ [241]) or Chlorophyll *a* in ether ($\Phi_F = 0.32$ [242]) as standards.

2.3.2.2 Fluorescence quenching

Fluorescence quenching experiments were carried out by addition of increasing concentrations of the quencher, BQ, i.e., 0, 0.005, 0.010, 0.015, 0.020 and 0.025 M or MV^{2+} i.e. $0, 0.5 \times 10^{-5}, 1.0 \times 10^{-5}, 1.5 \times 10^{-5}, 2.0 \times 10^{-5}, 2.5 \times 10^{-5}, 3.0 \times 10^{-5}$ M to a fixed MPc complex concentration, i.e. 1.0×10^{-6} M. MPc fluorescence spectra were recorded at each BQ or MV^{2+} concentration and the dependence of the emission intensity on quencher concentration were given by the Stern-Volmer (SV) equation, Eq. 1.14. The ratio F_0/F was plotted against quencher concentration $[Q]$.

2.3.2.3 Triplet quantum yield and lifetime

Triplet quantum yields and lifetimes were determined by recording the triplet absorption and decay kinetics from a laser flash photolysis system shown in Fig. 2.2.

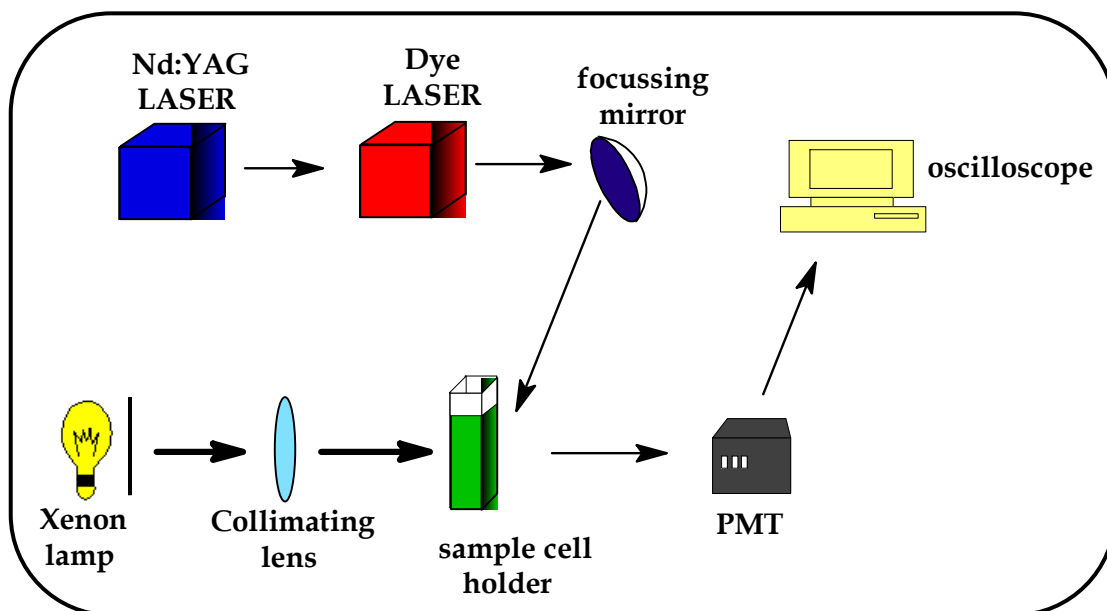


Figure 2.2: Schematic diagram of a laser flash photolysis set-up for triplet quantum yield and lifetime determinations.

A de-aerated (nitrogen bubbled for 20 min) MPc solution was placed in a 1 cm pathlength spectrophotometric cell. The solution with absorbance of ~ 1.5 was irradiated at the Q-band maximum with laser light from a Nd:YAG laser. Triplet quantum yields (Φ_T) were determined by the comparative triplet absorption method, Eq. 1.17 with unsubstituted ZnPc in DMSO ($\Phi_T = 0.65$) or 1-CNP ($\Phi_T = 0.65$) [278] employed as standards. Triplet lifetimes were obtained by fitting the transient curves exponentially using OriginPro 7.5 software.

2.3.3 Electrochemistry

2.3.3.1 General methods

Cyclic voltammetry (CV), Osteryoung square wave voltammetry (OSWV), chronoamperometry (CA) and chronocoulometry (CC) data were collected using a conventional three-electrode set-up with glassy carbon electrode (GCE, 3 mm diameter) as a working electrode, platinum wire as counter electrode and Ag|AgCl wire as pseudo-reference electrode. Electrochemical experiments were performed in dry DMF containing ~ 0.1 M tetrabutylammonium tetrafluoroborate (TBABF₄) as a supporting electrolyte. Prior to scans, the working electrode was polished with alumina paste on a Buehler felt pad, followed by washing with deionised water and rinsing with methanol and DMF or DCM (depending on the solvent in which the MPc was dissolved). The concentration of the MPc complexes was maintained at 1×10^{-4} M in DMF. A nitrogen atmosphere was maintained throughout the electrochemical experiments. Spectroelectrochemical data were recorded using a home-made optically transparent thin-layer electrochemical (OTTLE) cell with a design similar to that previously reported [401]. The OTTLE cell consisted of a platinum wire mesh as working and counter electrodes and silver wire as pseudo-reference electrode. The

OTTLE cell was connected to a BAS CV 27 voltammograph and UV/Vis spectra were recorded with Cary 500 UV/Vis/NIR.

2.3.3.2 Electrode modification and electrocatalysis

Electrode modification was achieved by employing either the drop-dry or electropolymerisation methods. For the drop-dry method, a drop of 1 mM OTiPc complex solution in DCM was placed on the surface of GCE and allowed to adsorb for 15 min. Excess complex was removed by rinsing in DCM, followed by methanol before use for electrocatalytic studies. Electropolymerisation was achieved by repetitive scanning (via cyclic voltammetry) of the solutions of the MPc complexes (1 mM) in DMF at a scan rate of 100 mVs^{-1} , in the presence of TBABF₄ as electrolyte. During electropolymerisation, the number of cycles swept was considered as an indication of film thickness. Once the desired number of cycles was completed, the GCE modified with the film was removed from the electrolytic cell and rinsed with DMF and finally with water. Distilled deionised Millipore water was employed for electrocatalytic studies in aqueous solutions. Electrocatalysis was performed in solutions of nitrite in phosphate buffer (pH 7.4) prepared from sodium hydrogen phosphate (Na₂HPO₄) and sodium dihydrogen phosphate (NaH₂PO₄).

2.4 Synthesis

2.4.1 Unsubstituted metallophthalocyanines (Scheme 3.1)

Dichloro(phthalocyaninato)titanium(IV) [33]: The preparation of Cl₂Ti^{IV}Pc (**33**) was achieved by following a method reported in literature [33] with slight modification on the purification of the complex. Briefly, the complex was prepared by refluxing under a blanket of nitrogen at 220 °C for 10 hours, anhydrous TiCl₄ (1.0

g, 5.27 mmol) and phthalonitrile (2.0 g, 15.6 mmol) dissolved in hot 1-CNP (20 ml). The resulting product was cooled, filtered and Soxhlet extracted with acetone, then methanol, and finally benzene, and dried in vacuo. Yield: 2.16 g (65 %). UV/Vis (CHCl_3): λ_{max} nm (log ϵ) 349 (4.04), 620 (3.52), 692 (4.38). IR [(Nujol) $\nu_{\text{max}}/\text{cm}^{-1}$]: 390 and 356 (Ti-Cl). ^1H NMR (CDCl_3): δ ppm 9.71 (8-H, s, Pc), 8.55 (4-H, s, Pc),

Trichloro(phthalocyaninato)tantalum (V) [35]: $\text{Cl}_3\text{Ta}^{\text{V}}\text{Pc}$ (**34**) was prepared by using a method adopted in literature [35]. Phthalonitrile (0.81 g, 6.28 mmol) was heated together with anhydrous TaCl_5 (0.75 g, 2.09 mmol) at 240 °C for 24 hours, under a blanket of nitrogen. The resulting product was Soxhlet extracted with acetone, then methanol, and finally benzene, and dried in vacuo. Yield: 1.15 g (68%). UV/Vis (CHCl_3): λ_{max} nm (log ϵ) 342 (4.02), 625 (3.58), 697 (4.22). IR [(Nujol) $\nu_{\text{max}}/\text{cm}^{-1}$]: 366 (Ta-Cl). ^1H NMR (CDCl_3): δ ppm 9.17 (4-H, d, Pc), 7.93 (4-H, d, Pc), 7.86 (4-H, t, Pc), 7.71 (4-H, t, Pc). ^{13}C NMR ($\text{DMSO-}d_6$): δ ppm (Pc- C_a): 136.31, 136.27, 135.93, 135.89; (Pc- C_b): 134.25, 133.29, 133.25, 132.52; (Pc- C_c): 132.52, 132.50, 131.53, 131.52; (Pc- C_d): 122.85, 122.81, 118.61, 111.19. Anal. calc. C 48.08, H 2.02, N 14.01. Found: C 48.13, H 2.15, N 14.06. MS (MALDI-TOF): m/z calc. 799.8, Found 764.6 for $(M - \text{Cl})^+$, 729.9 for $(M - 2\text{Cl})^+$.

2.4.2 Differently sulphonated metallophthalocyanines, MPcS_n

(Scheme 3.2)

General sulphonation procedure [134]: The differently sulphonated MPcs were synthesised from Cl_2TiPc (**33**) and Cl_3TaPc (**34**), using oleum (30% SO_3) according to a literature method described for AlPcS_n [134]. The required unsubstituted MPC complex ($M = \text{Ti}$ or Ta , 8 mmol) was placed in a round-bottomed flask and heated to

100 °C. Oleum (25 ml, 30% SO₃) was slowly added and the mixture vigorously stirred at 100 °C. After 25 minutes, the reaction mixture was quenched by pouring onto crushed ice (~ 200 g). The resulting mixture was adjusted to pH 7.0 – 7.5 by careful addition of 1.0 M NaOH, evaporated to dryness and the residue Soxhlet extracted into methanol for 12 hours. The solvent was evaporated and the solid product air-dried to yield green and deep green products of TiPcS_n (**35**) and TaPcS_n (**36**) respectively.

2.4.3 Phthalonitriles

2.4.3.1 3-Nitrophthalonitrile (Scheme 3.3 A) [402]

3-Nitrophthalic anhydride (17) [403]: 3-Nitrophthalic acid (**16**) (180 g, 0.85 mol) in acetic anhydride (162 ml) was refluxed in a round-bottomed flask with gentle boiling until the acid completely dissolved. The reaction mixture was refluxed for a further 10 minutes, poured into a porcelain dish and allowed to cool. The resulting yellow solid mass was thoroughly ground and filtered. The crystals were then washed with diethyl ether until the unreacted acid could not be detected. The resulting yellow crystals were allowed to dry in air. Yield: 156 g (95 %). IR [(KBr) $\nu_{\max}/\text{cm}^{-1}$]: 1720 and 1697 (-O-CO-O-), 1530 (NO₂ asym), 1338 (NO₂ sym).

3-Nitrophthalimide (19a): 3-Nitrophthalic anhydride (**17**) (140 g, 0.73 mol) in formamide (180 ml) was heated under reflux for 3 hours. The reaction mixture was cooled, filtered, thoroughly washed with water and dried at 60 °C, thus yielding the title compound. Yield: 126 g (92 %). IR [(KBr) $\nu_{\max}/\text{cm}^{-1}$]: 3435 (N-H), 1535 (NO₂ asym), 1343 (NO₂ sym).

3-Nitrophthalimide (20a): 3-Nitrophthalimide (**19a**) (120 g, 0.62 mol) was stirred in 32 % ammonia solution (660 ml) for 24 hours. The resulting deep yellow product was filtered and washed with cold water until the excess ammonia could not be detected. The title compound was dried at 110 °C. Yield: 126 g (92 %). IR [(KBr) $\nu_{\max}/\text{cm}^{-1}$]: 3435 (N-H), 1540 (NO₂ asym), 1346 (NO₂ sym).

3-Nitrophthalonitrile (21): DMF (417 ml) was placed in a three-necked flask under nitrogen and cooled to 0 °C with an ice bath. Thionyl chloride (42 ml) was slowly added to DMF (while the temperature was maintained at 0 °C), thereafter, the mixture was allowed to reach room temperature and stirred for 30 minutes. The mixture was cooled to 0 °C and 3-nitrophthalimide (**20a**) (50.0 g, 0.24 mol) was slowly added to the mixture while stirring. The slurry was then stirred at room temperature for 3 hours, slowly poured onto crushed ice (~ 1.3 kg), filtered under reduced pressure and thoroughly washed with cold water. The pale yellow title compound was then dried at 110 °C. Yield: 32.4 g (78 %). IR [(KBr) $\nu_{\max}/\text{cm}^{-1}$]: 2232 (C≡N), 1529 (NO₂ asym), 1339 (NO₂ sym). ¹H-NMR (DMSO-*d*₆): δ ppm 8.68 (1-H, d, Ar-H), 8.52 (1-H, d, Ar-H), 8.16 (1-H, t, Ar-H).

2.4.3.2 4-Nitrophthalonitrile (Scheme 3.3 A) [116]

4-Nitrophthalimide (19b): To concentrated H₂SO₄ (400 ml) was slowly added 55 % HNO₃ (80 ml). The mixture was then allowed to cool to 15 °C, in an ice bath. Thereafter, phthalimide (**18**) (80.0 g, 0.54 mol) was added portion-wise to the acid mixture while stirring and maintaining the temperature between 10 and 15 °C. The temperature was then taken up to 35 °C and the slurry stirred at that temperature for 1 hour. After cooling to 0 °C, the yellow reaction mixture was poured onto crushed ice

(~ 2 kg) while stirring to yield a beige suspension. After filtration, the solid was thoroughly washed with cold water and the title compound was dried at 110 °C. Yield: 62.2 g (60 %). IR [(KBr) $\nu_{\max}/\text{cm}^{-1}$]: 2232 (C≡N), 1536 (NO₂ asym), 1340 (NO₂ sym). ¹H-NMR (DMSO-*d*₆): δ ppm 8.66 (1-H, s, Ar-H), 8.58 (1-H, d, Ar-H), 8.08 (1-H, d, Ar-H).

4-Nitrophthalamide (20b) and *4-nitrophthalonitrile (22)* were synthesised by following methods similar to *3-nitrophthalamide (20a)* and *3-nitrophthalonitrile (21)*.

4-Nitrophthalamide (20b): Yield: 54 g (90 %). IR [(KBr) $\nu_{\max}/\text{cm}^{-1}$]: 3430 (N-H), 1538 (NO₂ asym), 1342 (NO₂ sym).

4-Nitrophthalonitrile (22): Yield: 36.5 g (73 %). IR [(KBr) $\nu_{\max}/\text{cm}^{-1}$]: 2229 (C≡N), 1531 (NO₂ asym), 1334 (NO₂ sym). ¹H-NMR (DMSO-*d*₆): δ ppm 9.23 (1-H, s, Ar-H), 8.68 (1-H, d, Ar-H), 8.42 (1-H, d, Ar-H).

2.4.3.3 4,5-Dichlorophthalonitrile (Scheme 3.3 B) [123]

4,5-Dichlorophthalic anhydride (24): A mixture of 4,5-dichlorophthalic acid (**23**) (90.0 g, 0.38 mol) and acetic anhydride (150 ml) was heated under weak reflux for 5 hours. After cooling, a greyish white product was filtered, thoroughly washed with petroleum ether (40 – 60 °C) and air-dried to yield 4,5-dichlorophthalic anhydride. Yield: 76.7 g (93 %). IR [(KBr) $\nu_{\max}/\text{cm}^{-1}$]: 1826, 1783 (-O-CO-O).

4,5-Dichlorophthalimide (25): 4,5-dichlorophthalic anhydride (**24**) (75.0 g, 0.35 mol) in formamide (102 ml) was refluxed for 3 hours. After cooling the greyish

white product was filtered, thoroughly washed with water and dried at 110 °C for 3 hours, thus yielding the title compound. Yield: 73.3 g (97 %). IR [(KBr) $\nu_{\max}/\text{cm}^{-1}$]: 1770, 1714 (imide).

4,5-Dichlorophthalamide (26): A solution of 4,5-dichlorophthalimide (**25**) (70.0 g, 0.32 mol) in 25 % ammonia (955 ml) was stirred for 24 hours and then stirred for a further 24 hours after addition of 33 % ammonia (318 ml). The product was filtered, thoroughly washed with water and dried at 60 °C. Yield: 52.2 g (70 %). IR [(KBr) $\nu_{\max}/\text{cm}^{-1}$]: 1641, 1622 (amide)

4,5-Dichlorophthalonitrile (27): At 0 °C was added thionyl chloride (175 ml) under nitrogen and stirring to dry DMF (250 ml). After two hours, dry 4,5-dichlorophthalamide (**26**) (50.0 g, 0.21 mol) was added and the mixture stirred at 0 - 5 °C for 5 hours and then at room temperature for 24 hours. The product was slowly added to ice water, filtered, thoroughly washed with water and recrystallised from methanol to yield a pale white title compound. Yield: 30.0 g (70 %). IR [(KBr) $\nu_{\max}/\text{cm}^{-1}$]: 2230 (C \equiv N). ¹H-NMR (DMSO-*d*₆): δ ppm 8.58 (2-H, s, Ar-H).

2.4.3.4 Mono-substituted phthalonitriles (Scheme 3.4)

3 - Phenoxyphthalonitrile (42a): Under a blanket of nitrogen, phenol (3.50 g, 37 mmol) and 3-nitrophthalonitrile (**21**) (4.50 g, 26 mmol) were dissolved in dry DMSO (52 ml). To this suspension was added anhydrous K₂CO₃ (7.19 g, 51 mmol) and the mixture stirred at room temperature. Further K₂CO₃ (0.33 g, 2.4 mmol) was added portion-wise after 4 hours and 24 hours of stirring. After 48 hours total reaction time, the mixture was poured into 1 M HCl (260 ml), thus forming a precipitate that was

recrystallised from methanol/water (1:1) to yield a brownish yellow product. Yield: 2.08 g (85 %). IR [(KBr) $\nu_{\max}/\text{cm}^{-1}$]: 2235 (C \equiv N), 1245 (C-O-C). $^1\text{H-NMR}$ (DMSO): δ , ppm 7.80-7.84 (2-H, m, Ar-H), 7.48-7.54 (2-H, t, Ar-H, Ar'-H), 7.21-7.35 (4-H, m, Ar'-H).

3 – (4 – *tert*-Butylphenoxy) phthalonitrile (42b): Synthesis and purification was as described for complex **42a**, using 4-*tert*-butylphenol (5.90 g, 39 mmol) and **21** (4.50 g, 26 mmol). Yield: 3.43 g (88 %). IR [(KBr) $\nu_{\max}/\text{cm}^{-1}$]: 2965 (Bu^t), 2230 (s) (C \equiv N), 1240 (C-O-C). $^1\text{H-NMR}$ (CDCl₃): δ , ppm 7.78-7.84 (2-H, m, Ar-H), 7.50 (2-H, d, Ar-H, Ar'-H), 7.21-7.26 (1-H, m, Ar'-H), 7.14 (2-H, d, Ar'-H), 1.30 (9-H, s, Bu^t).

3-Benzoyloxyphthalonitrile (42c): In a stream of nitrogen, benzyl alcohol (4.54 g, 42.0 mmol) and **21** (6.00 g, 35.0 mmol) were dissolved in dry DMSO (30 ml). To this suspension was added anhydrous K₂CO₃ (9.70 g, 70.0 mmol) and the mixture stirred at room temperature. Further K₂CO₃ (2.43 g, 18.0 mmol) was added after 4 hours and again after 24 hours of stirring. After 48 hours total reaction time, the mixture was poured into water (100 ml), thus forming a precipitate that was thoroughly washed with water and recrystallised from methanol to yield a brownish yellow title compound. Yield: 7.38 g (90 %). IR [(KBr) $\nu_{\max}/\text{cm}^{-1}$]: 2226 (C \equiv N), 1250 (C-O-C). $^1\text{H-NMR}$ (DMSO-*d*₆): δ , ppm 7.82 (1-H, t, Ar-H), 7.71 (1-H, d, Ar-H), 7.62 (1-H, d, Ar-H), 7.49 (2-H, d, Ar'-H), 7.41 (2-H, t, Ar'-H), 7.33 (1-H, t, Ar'-H), 5.36 (2-H, s, CH₂).

3-[4-(Benzyloxy)phenoxy]phthalonitrile (42d): Synthesis and purification of **42d** was as described for compound **42c**, using 4-(benzyloxy)phenol (8.41 g, 42.0 mmol), **21** (6.00 g, 35.0 mmol) and DMSO (30 ml). Yield: 10.28 g (90 %). IR [(KBr) $\nu_{\max}/\text{cm}^{-1}$]: 2240 (C \equiv N), 1260 (C-O-C). $^1\text{H-NMR}$ (DMSO- d_6): δ , ppm 7.53 (1-H, s, Ar-H), 7.47-7.32 (6-H, m, Ar-H, Ar'-H), 7.05 (5-H, m, Ar''-H), 5.10 (2-H, s, CH $_2$).

For the synthesis of phthalonitriles (**42e** and **42f**), a procedure similar to that reported [404] for the synthesis of 4,5-di(alkylthio)phthalonitriles was employed.

3-(Phenylthio)phthalonitrile (42e): Under a stream of nitrogen, thiophenol (4.63 g, 42.0 mmol) and **21** (6.00 g, 35.0 mmol) were dissolved in DMSO (30 ml) and the mixture stirred at room temperature for 15 min. Thereafter, finely ground K $_2$ CO $_3$ (15.0 g, 0.105 mol) was added portion-wise over a period of 2 hours and the reaction mixture left to stir for a further 12 hours. The mixture was added to water (100 ml) and stirred for 30 min. The resulting precipitate was filtered off, thoroughly washed with water, dried and recrystallised from ethanol. Yield: 6.78 g (82 %). IR [(KBr) $\nu_{\max}/\text{cm}^{-1}$]: 2229 (C \equiv N), 689 (C-S-C). $^1\text{H-NMR}$ (DMSO- d_6): δ , ppm 7.94 (1-H, d, Ar-H), 7.75 (1-H, t, Ar-H), 7.58-7.48 (5-H, m, Ar'-H), 7.36 (1-H, d, Ar-H).

3-(Benzylthio)phthalonitrile (42f): Synthesis and purification of **42f** was as described for **42e**, using benzyl mercaptan (3.73 g, 30.0 mmol), **21** (4.00 g, 23.0 mmol) and DMSO (20 ml). Yield: 5.18 g (90 %). IR [(KBr) $\nu_{\max}/\text{cm}^{-1}$]: 3067, 3030 (CH $_2$), 2227 (C \equiv N), 696 (C-S-C). $^1\text{H-NMR}$ (DMSO- d_6): δ , ppm 7.95 (1-H, d, Ar-H), 7.88 (1-H, d, Ar-H), 7.80 (1-H, t, Ar-H), 7.43 (5-H, m, Ar'-H), 4.50 (2-H, s, -CH $_2$).

4 – Phenoxyphthalonitrile (43a): Synthesis and purification was as described for complex **42a**, using phenol (5.64 g, 60 mmol) and 4-nitrophthalonitrile (**22**) (6.00 g, 35 mmol). Yield: 2.63 g (80 %). IR [(KBr) $\nu_{\max}/\text{cm}^{-1}$]: 2230 (C≡N), 1233 (C-O-C). $^1\text{H-NMR}$ (CDCl_3): δ , ppm 7.70 (1-H, d, Ar-H), 7.43 (2-H, t, Ar-H), 7.20-7.31 (3-H, m, Ar'-H), 7.06 (2-H, d, Ar'-H).

4 – (4-*tert*-Butylphenoxy) phthalonitrile (43b): Synthesis and purification was as described for complex **42a**, using 4-*tert*-butylphenol (7.81 g, 52 mmol) and **22** (6.00 g, 35 mmol). Yield: 3.68 g (70 %). IR [(KBr) $\nu_{\max}/\text{cm}^{-1}$]: 2960 (Bu^t), 2233 (s) (C≡N), 1245 (C-O-C). $^1\text{H-NMR}$ (CDCl_3): δ , ppm 7.35 (1-H, d, Ar-H), 7.21 (2-H, d, Ar-H), 7.15 (2-H, d, Ar'-H), 7.00 (2-H, d, Ar'-H), 1.30 (9-H, s, Bu^t).

4-Benzoyloxyphthalonitrile (43c): Synthesis and purification of **43c** was as described for compound **42c**, using benzyl alcohol (4.54 g, 42.0 mmol), **22** (6.00 g, 35.0 mmol) and DMSO (30 ml). Yield: 6.97 g (85 %). IR [(KBr) $\nu_{\max}/\text{cm}^{-1}$]: 2224 (C≡N), 1252 (C-O-C). $^1\text{H-NMR}$ ($\text{DMSO-}d_6$): δ , ppm 8.01 (2-H, d, Ar-H), 7.60-7.32 (6-H, m, Ar-H, Ar'-H), 5.30 (2-H, s, CH_2).

4-[4-(Benzoyloxy)phenoxy]phthalonitrile (43d): Synthesis and purification of **43d** was as described for compound **42c**, using 4-(benzyloxy)phenol (8.41 g, 42.0 mmol), **22** (6.00 g, 35.0 mmol) and DMSO (30 ml). Yield: 9.36 g (82 %). IR [(KBr) $\nu_{\max}/\text{cm}^{-1}$]: 2235 (C≡N), 1253 (C-O-C). $^1\text{H-NMR}$ ($\text{DMSO-}d_6$): δ , ppm 7.52 (1-H, d, Ar-H), 7.49-7.32 (5-H, m, Ar''-H), 7.21 (2-H, m, Ar-H), 7.00 (4-H, q, Ar'-H), 5.10 (2-H, s, CH_2).

4-(Phenylthio)phthalonitrile (43e): Synthesis and purification of **43e** was as described for **42e**, using thiophenol (4.63 g, 42.0 mmol), **22** (6.00 g, 35.0 mmol) and DMSO (30 ml). Yield: 7.02 (85 %). IR [(KBr) $\nu_{\max}/\text{cm}^{-1}$]: 2232 (C \equiv N), 699 (C-S-C). $^1\text{H-NMR}$ (DMSO- d_6): δ , ppm 7.92 (1-H, d, Ar-H), 7.75 (1-H, s, Ar-H), 7.60-7.48 (5-H, m, Ar'-H), 7.41 (1-H, d, Ar-H).

4-(Benzylthio)phthalonitrile (43f): Synthesis and purification of **43f** was as described for **42e**, using benzyl mercaptan (5.22 g, 42.0 mmol), **22** (6.00 g, 35.0 mmol) and DMSO (30 ml). Yield: 8.06 g (92 %). IR [(KBr) $\nu_{\max}/\text{cm}^{-1}$]: 3060, 3026 (CH $_2$), 2230 (C \equiv N), 698 (C-S-C). $^1\text{H-NMR}$ (DMSO- d_6): δ , ppm 8.17 (1-H, s, Ar-H), 7.93 (1-H, d, Ar-H), 7.73 (1-H, d, Ar-H), 7.38-7.23 (5-H, m, Ar'-H), 4.45 (2-H, s, -CH $_2$).

2.4.3.5 Disubstituted phthalonitriles (Scheme 3.5)

4,5-Diphenoxyphthalonitrile (44a): A mixture of 4,5-dichlorophthalonitrile (**27**) (6.00g, 30.5 mmol), phenol (8.60 g, 91.4 mmol) and dry DMSO (61 ml) was stirred at 90 °C, while anhydrous K $_2$ CO $_3$ (8 \times 8.43 g, 8 \times 61.0 mmol) was added every 5 minutes until eight portions have been added. The reaction mixture was stirred at 90 °C for an additional 45 minutes and allowed to cool. Thereafter the mixture was added to ice water (100 ml) and the aqueous phase extracted with CHCl $_3$ (3 \times 50 ml). The combined extracts were first washed with Na $_2$ CO $_3$ (5%), then with water and dried over MgSO $_4$. The solvent was evaporated and the product recrystallised from ethanol and dried at room temperature. Yield: 7.81 g (82 %). IR [(KBr) $\nu_{\max}/\text{cm}^{-1}$]: 2227 (s) (C \equiv N), 1245 (C-O-C). $^1\text{H-NMR}$ (DMSO- d_6): δ , ppm 7.68 (2-H, s, Ar-H), 7.42 (4-H, d, Ar'-H), 7.30 (4-H, d, Ar'-H), 7.22 (2-H, s, Ar'-H).

4,5-bis(4-tert-Butylphenoxy)phthalonitrile (44b): Synthesis and purification of **44b** was as described for compound **44a**, using 4-tert-butylphenol (10.36 g, 69 mmol), **27** (4.50 g, 23 mmol) and K₂CO₃ (8×6.63 g, 8×43.0 mmol), DMSO (46 ml). Yield: 7.03 g (72 %). IR [(KBr) $\nu_{\max}/\text{cm}^{-1}$]: 2900 (Bu¹), 2233 (s) (C≡N), 1242 (C-O-C). ¹H-NMR (DMSO-*d*₆): δ , ppm 7.70 (2-H, s, Ar-H), 7.20 (4-H, d, Ar'-H), 6.76 (4-H, d, Ar'-H), 1.32 (18-H, s, But).

4,5-bis[4-(Benzyloxy)phenoxy]phthalonitrile (44c): Synthesis and purification of **44c** was as described for compound **44a**, using 4-(benzyloxy)phenol (18.32 g, 91.4 mmol), **27** (6.00g, 30.5 mmol) and K₂CO₃ (8×8.43 g, 8×61.0 mmol), DMSO (46 ml). Yield: 11.20 g (70 %). IR [(KBr) $\nu_{\max}/\text{cm}^{-1}$]: 2229 (s) (C≡N), 1244 (C-O-C). ¹H-NMR (DMSO-*d*₆): δ , ppm 8.50 (2-H, s, Ar-H), 7.45 (8-H, br d, Ar'-H), 7.10 (10-H, d, Ar'-H), 5.21 (4-H, s, CH₂).

4,5-bis(Phenylthio)phthalonitrile (44d): Under a stream of nitrogen, thiophenol (4.63 g, 42.0 mmol) and **27** (6.00 g, 30.5 mmol) were dissolved in DMSO (30 ml) and the mixture stirred at room temperature for 15 min. Thereafter, finely ground K₂CO₃ (15.0 g, 0.105 mol) was added portion-wise over a period of 2 hours and the reaction mixture left to stir for a further 12 hours. The mixture was added to water (100 ml) and stirred for 30 min. The resulting precipitate was filtered off, thoroughly washed with water, dried and recrystallised from ethanol. Yield: 8.62 g (82 %). IR [(KBr) $\nu_{\max}/\text{cm}^{-1}$]: 2230 (C≡N), 692 (C-S-C). ¹H-NMR (DMSO-*d*₆): δ , ppm 7.72 (2-H, s, Ar-H), 7.51 (4-H, d, Ar'-H), 7.43-7.38 (6-H, m, Ar'-H).

2.4.4 Aryloxy and arylthio tetra-substituted phthalocyanines

(Scheme 3.4)

1,(4)-(Tetraphenoxyphthalocyaninato)oxotitanium(IV) (37a, Scheme 1): Under a blanket of nitrogen, **42a** (1.60 g, 7.3 mmol) was dissolved in 1-CNP (8 ml). TiCl_4 (0.26 ml, 2.4 mmol) was then added to the solution via a syringe and the reaction mixture refluxed at 180°C for 14 hours under nitrogen. After cooling, the solution was chromatographed with hexane as eluent to remove 1-CNP. The column was then eluted with THF which was evaporated off, thus affording **37a** as a crude product. The crude product was washed with ethanol in a Soxhlet apparatus, thus affording a dark-green solid which was oven dried at 80°C . Yield: 1.27 g (56 %). UV/VIS (CDCl_3): λ_{max} nm (log ϵ) 348 (4.88), 651 (4.71), 728 (5.41). IR [(KBr) $\nu_{\text{max}}/\text{cm}^{-1}$]: 1251 (C-O-C), 973 (Ti=O). $^1\text{H-NMR}$ (CDCl_3): δ , ppm 7.53-9.03 (12-H, m, Pc-H), 7.15-7.50 (20-H, m, Phenyl-H). $\text{C}_{56}\text{H}_{32}\text{N}_8\text{O}_5\text{Ti} \cdot 2\text{H}_2\text{O}$: Calc. C 68.52, H 3.67, N 11.42; Found C 68.83, H 3.16 N 11.32. MALDI-TOF-MS m/z : Calc. 944.8; Found (M^+) 945.6.

1,(4)-(Tetra-tert-butylphenoxyphthalocyaninato)oxotitanium(IV) (37b): Synthesis and purification was as outlined for **37a** except **42b** instead of **42a** was employed. The amounts of the reagents employed were as follows: **42b** (2.50 g, 9.1 mmol), TiCl_4 (0.33 ml, 3.3 mmol) and 1-CNP (9 ml). Yield: 2.32 g (60 %). UV/VIS (CDCl_3): λ_{max} nm (log ϵ) 348 (4.66), 653 (4.53), 730 (5.29). IR [(KBr) $\nu_{\text{max}}/\text{cm}^{-1}$]: 2957 (C-H), 1255 (C-O-C), 975 (Ti=O). $^1\text{H-NMR}$ (CDCl_3): δ , ppm 7.62-9.52 (12-H, m, Pc-H), 7.18-7.57 (16-H, m, Phenyl-H), 1.42 (36-H, s, Bu^t). $\text{C}_{72}\text{H}_{64}\text{N}_8\text{O}_5\text{Ti}$: Calc. C 73.96, H 5.52, N 9.58; Found C 73.07, H 5.42, N 9.33. MALDI-TOF-MS m/z : Calc. 1169.2; Found (M^+) 1170.1.

1,(4)-(Tetrabenzoyloxyphthalocyaninato) oxotitanium(IV) (37c): In 1-octanol (32 ml), compound **42c** (4.00 g, 17.0 mmol), titanium butoxide (1.45 g, 4.25 mmol) and urea (1.02 g, 17.0 mmol) were stirred under a blanket of nitrogen at 150 °C for 14 hours. The reaction mixture was allowed to cool, thereafter, methanol (80 ml) was added and the mixture was refluxed for 2 hours. After cooling, the mixture was filtered, and the resulting solid sequentially washed with methanol and water and then dried. The crude product was purified by column chromatography, using THF as the eluting solvent. After evaporation of solvent, the product was further purified by washing with acetone and then with ethanol in a Soxhlet apparatus to afford the title compound as a dark-green solid. Yield: 1.19 g (28 %). UV/VIS (CHCl₃): λ_{\max} nm (log ϵ) 350 (4.78), 648 (4.67), 728 (5.38). IR [(KBr) $\nu_{\max}/\text{cm}^{-1}$]: 1248 (C-O-C), 970 (Ti=O). ¹H-NMR (CDCl₃): δ , ppm 8.90-8.1 (4-H, m, Pc-H), 8.0-6.9 (28-H, m, Pc-H, Phenyl-H), 5.2 (8-H, m, CH₂). C₆₀H₄₀N₈O₅Ti: Calc. C 72.00, H 4.03, N 11.20; Found C 71.67, H 3.97, N 11.01. MALDI-TOF-MS m/z : Calc. 1000.9; Found (M⁺) 1001.1

1,(4)-{Tetrakis[4-(benzyloxy)phenoxy]phthalocyaninato}oxotitanium(IV) (37d): Synthesis and purification was as outlined for **37c** except **42d** instead of **42c** was employed. The amounts of the reagents employed were: **42d** (2.50 g, 7.70 mmol), titanium butoxide (0.66 g, 1.93 mmol) and urea (0.46 g, 7.70 mmol) in 1-octanol (15 ml). Yield: 0.79 g (30 %). UV/VIS (CHCl₃): λ_{\max} nm (log ϵ) 346 (4.87), 656 (4.74), 730 (5.41). IR [(KBr) $\nu_{\max}/\text{cm}^{-1}$]: 1257 (C-O-C), 972 (Ti=O). ¹H-NMR (CDCl₃): δ , ppm 8.85-8.40 (3-H, m, Pc-H), 8.00-7.60 (3-H, m, Pc-H), 7.59-6.92 (42-H, m, Pc-H, Phenyl-H), 5.11 (8-H, m, CH₂). C₈₄H₅₆N₈O₉Ti: Calc. C 73.68, H 4.12, N 8.18;

Found C 73.76, H 4.16, N 8.14. MALDI-TOF-MS m/z : Calc. 1369.3; Found (M^+) 1368.3

1,(4)-(Tetraphenylthiophthalocyaninato)oxotitanium(IV) (37e): In 1-octanol (32 ml), **42e** (4.00 g, 17.0 mmol), titanium butoxide (1.45 g, 4.25 mmol) and urea (1.02 g, 17.0 mmol) were stirred under a blanket of nitrogen at 150 °C for 14 hours. The reaction mixture was allowed to cool, thereafter, methanol (80 ml) was added and the mixture was refluxed for 2 hours. After cooling, the mixture was filtered, and the resulting solid sequentially washed with methanol and water and then dried. The crude product was purified by column chromatography, using THF as the eluting solvent. After evaporation of the solvent, the product was further purified by washing with acetone and then with ethanol in a Soxhlet apparatus to afford the title compound as a black-green solid. Yield: 1.72 g (40 %). UV/VIS (DCM): λ_{\max} nm (log ϵ) 265 (4.87), 344 (4.94), 669 (4.68), 747 (5.36). IR [(KBr) $\nu_{\max}/\text{cm}^{-1}$]: 968 (Ti=O), 687 (C-S-C). $^1\text{H-NMR}$ (CDCl_3): δ , ppm 9.15 (1-H, d, Pc-H), 9.05 (1-H, d, Pc-H), 8.92-8.75 (2-H, m, Pc-H), 8.50 (1-H, t, Pc-H), 8.08-7.90 (9-H, m, Phenyl-H, Pc-H), 7.75 (2-H, m, Pc-H), 7.70-7.50 (13-H, m, Phenyl-H), 7.45 (1-H, t, Pc-H), 7.31 (1-H, d, Pc-H), 7.05 (1-H, dd, Pc-H). Calc. for $\text{C}_{56}\text{H}_{32}\text{N}_8\text{OS}_4\text{Ti}$: C 66.66, H 3.20, N 11.11; Found: C 66.33, H 3.16 N 10.83. MALDI-TOF-MS m/z : Calc. 1009.0; Found (M^+) 1010.2

1,(4)-(Tetrabenzylthiophthalocyaninato)oxotitanium(IV) (37f). Synthesis and purification was as outlined for **37e** except **42f** instead of **42e** was employed. The amounts of the reagents employed were: **42f** (4.00 g, 16 mmol), titanium butoxide (1.36 g, 4.00 mmol) and urea (0.96 g, 16.0 mmol) in 1-octanol (30 ml). Yield:

1.83 g (43 %). UV/VIS (DCM): λ_{\max} nm (log ϵ) 264 (4.88), 342 (4.84), 675 (4.66), 746 (510). IR [(KBr) $\nu_{\max}/\text{cm}^{-1}$]: 3020 (CH₂), 967 (Ti=O), 695 (C-S-C). ¹H-NMR (CDCl₃): δ , ppm 8.95-8.80 (4-H, m, Pc-H), 7.80-7.00 (26-H, m, Pc-H, Phenyl-H), 6.82 (2-H, broad s, Pc-H), 4.63 (8-H, m, -CH₂). Calc. for C₆₀H₄₀N₈OS₄Ti: C 67.66, H 3.79, N 10.52; Found: C 65.96, H 3.70, N 10.14. MALDI-TOF-MS m/z : Calc. 1065.1; Found (M⁺) 1065.5

2,(3)-(Tetraphenoxyphthalocyaninato) oxotitanium(IV) (38a): Synthesis and purification was as outlined for **37a** except **43a** instead of **42a** was employed. The amounts of the reagents employed were as follows: **43a** (2.50 g, 11 mmol), TiCl₄ (0.40 ml, 3.7 mmol) and 1-CNP (12 ml). Yield: 2.35 g (67 %). UV/VIS (CDCl₃): λ_{\max} nm (log ϵ) 290 (4.57), 347 (4.77), 400 (4.43) 630 (4.50), 702 (5.21). IR [(KBr) $\nu_{\max}/\text{cm}^{-1}$]: 1232 (C-O-C), 946 (Ti=O). ¹H-NMR (CDCl₃): δ , ppm 8.66-8.92 (4-H; t,q,t; Pc-H), 8.37-8.56 (4-H; s,s,d; Pc-H), 7.69-7.82 (4-H, m, Pc-H), 7.59-7.66 (8-H, m, Phenyl-2,6-H), 7.47-7.54 (8-H, m, Phenyl-3,5-H), 7.34-7.42 (4-H, m, Phenyl-4-H). C₅₆H₃₂N₈O₅Ti: Calc. C 71.19, H 3.41, N 11.86; Found C 70.54, H 3.37, N 11.73. MALDI-TOF-MS m/z : Calc. 944.8; Found (M⁺) 944.7.

2,(3)-(Tetra-tert-butylphenoxyphthalocyaninato) oxotitanium(IV) (38b): Synthesis and purification was as outlined for **37a** except **43b** instead of **42a** was employed. The amounts of the reagents employed were as follows: **43b** (2.10 g, 7.6 mmol), TiCl₄ (0.30 ml, 2.5 mmol) and 1-CNP (8 ml). Yield: 2.05 g (70 %). UV/VIS (CDCl₃): λ_{\max} nm (log ϵ) 290 (4.59), 348 (4.96), 410 (4.82), 632 (4.71), 704 (5.40). IR [(KBr) $\nu_{\max}/\text{cm}^{-1}$]: 2959 (C-H), 1232 (C-O-C), 948 (Ti=O). ¹H-NMR (CDCl₃): δ , ppm 8.34-8.96 (12-H, m, Pc-H), 7.32-7.84 (16-H, m, Phenyl-H), 1.52 (36-H, s, Bu^t).

$C_{72}H_{64}N_8O_5Ti$: Calc. C 73.96, H 5.52, N 9.58; Found C 72.50, H 5.37, N 9.33.

MALDI-TOF-MS m/z : Calc. 1169.2; Found (M^+) 1169.9.

2,(3)-(Tetrabenzoyloxyphthalocyaninato)oxotitanium(IV) (38c): Synthesis and purification was as outlined for **37c** except **43c** instead of **42c** was employed. The amounts of the reagents employed were: **43c** (4.00 g, 17.0 mmol), titanium butoxide (1.45 g, 4.25 mmol) and urea (1.02 g, 17.0 mmol) in 1-octanol (32 ml). Yield: 1.36 g (32 %). UV/VIS ($CHCl_3$): λ_{max} nm (log ϵ) 294 (4.71), 347 (4.88), 633 (4.61), 703 (5.21). IR [(KBr) ν_{max}/cm^{-1}]: 1241 (C-O-C), 965 (Ti=O). 1H -NMR ($CDCl_3$): δ , ppm 8.81-6.82 (32-H, m, Pc-H, Phenyl-H), 5.10 (8-H, m, CH_2). $C_{60}H_{40}N_8O_5Ti$: Calc. C 72.00, H 4.03, N 11.20; Found C 71.33, H 3.93, N 11.45. MALDI-TOF-MS m/z : Calc. 1000.9; Found (M^+) 1001.6

2,(3)-{Tetrakis[4-(benzyloxy)phenoxy]phthalocyaninato}oxotitanium(IV) (38d): Synthesis and purification was as outlined for **37c** except **43d** instead of **42c** was employed. The amounts of the reagents employed were: **43d** (2.50 g, 7.70 mmol), titanium butoxide (0.66 g, 1.93 mmol) and urea (0.46 g, 7.70 mmol) in 1-octanol (15 ml). Yield: 0.92 g (35 %). UV/VIS ($CHCl_3$): λ_{max} nm (log ϵ) 293 (4.73), 347 (4.86), 635 (4.57), 705 (5.24). IR [(KBr) ν_{max}/cm^{-1}]: 1252 (C-O-C), 966 (Ti=O). 1H -NMR ($CDCl_3$): δ , ppm 8.88-8.18 (7-H, m, Pc-H), 7.82-7.18 (41-H, m, Pc-H, Phenyl-H), 5.19 (8-H, m, CH_2). $C_{84}H_{56}N_8O_9Ti$: Calc. C 73.68, H 4.12, N 8.18; Found C 73.81, H 4.03, N 8.13. MALDI-TOF-MS m/z : Calc. 1369.3; Found (M^+) 1368.4

2,(3)-(Tetraphenylthiophthalocyaninato)oxotitanium(IV) (38e): Synthesis and purification was as outlined for **37e** except **43e** instead of **42e** was employed. The amounts of the reagents employed were: **43e** (4.00 g, 17.0 mmol), titanium butoxide (1.45 g, 4.25 mmol) and urea (1.02 g, 17.0 mmol) in 1-octanol (32 ml). Yield: 2.23 g (52 %). UV/VIS (DCM): λ_{max} nm (log ϵ) 256 (4.62), 305 (4.57), 351 (4.68), 645 (3.47), 714 (5.06). IR [(KBr) ν_{max} /cm⁻¹]: 968 (Ti=O), 690 (C-S-C). ¹H-NMR (CDCl₃): δ , ppm 8.70-8.18 (6-H, m, Pc-H), 7.95 (2-H, q, Pc-H), 7.88-7.72 (9-H, m, Phenyl-H), 7.68 (3-H, t, Pc-H), 7.61-7.48 (11-H, m, Phenyl-H), 7.40 (1-H, bs, Pc-H). Calc. for C₅₆H₃₂N₈OS₄Ti: C 66.66, H 3.20, N 11.11; Found: C 66.88, H 3.20 N 11.03. MALDI-TOF-MS m/z : Calc. 1009.0; Found (M⁺) 1008.7

2,(3)-(Tetrabenzylthiophthalocyaninato)oxotitanium(IV) (38f): Synthesis and purification was as outlined for **37e** except **43f** instead of **42e** was employed. The amounts of the reagents employed were: **43f** (4.00 g, 16 mmol), titanium butoxide (1.36 g, 4.00 mmol) and urea (0.96 g, 16.0 mmol) in 1-octanol (30 ml). Yield: 2.04 g (48 %). UV/VIS (DCM): λ_{max} nm (log ϵ) 264 (4.68), 306 (4.79), 349 (4.88), 645 (4.69), 714 (5.19). IR [(KBr) ν_{max} /cm⁻¹]: 3022 (CH₂), 965 (Ti=O), 693 (C-S-C). ¹H-NMR (CDCl₃): δ , ppm 8.42-8.12 (4-H, m, Pc-H), 7.90 (2-H, broad s, Pc-H), 7.70-7.22 (26-H, m, Pc-H, Phenyl-H), 4.40 (8-H, m, -CH₂). Calc. for C₆₀H₄₀N₈OS₄Ti: Calc. C 67.66, H 3.79, N 10.52; Found: C 67.35, H 3.73, N 10.62. MALDI-TOF-MS m/z : Calc. 1065.1; Found (M⁺) 1064.5

2.4.5 Octa-substituted phthalocyanines (Scheme 3.5)

2,3,9,10,16,17,23,24-(Octaphenoxyphthalocyaninato)oxotitanium(IV) (39a):

Synthesis and purification was as outlined for **37e** except **44a** instead of **42e** was employed. The amounts of the reagents employed were: **44a** (4.00 g, 12.8 mmol), titanium butoxide (1.45 g, 4.25 mmol) and urea (1.02 g, 17.0 mmol) in 1-octanol (32 ml). Yield: 1.95 g (35 %). UV/VIS (1-CNP): λ_{\max} nm (log ϵ) 356 (4.58), 636 (4.34), 709 (5.08). IR [(KBr) $\nu_{\max}/\text{cm}^{-1}$]: 1268 (C-O-C), 965 (Ti=O). $^1\text{H-NMR}$ (CDCl_3): δ , ppm 8.70 (8-H, s, Pc-H) 7.45 – 7.10 (40-H, m, Phenyl-H). Calc. $\text{C}_{80}\text{H}_{48}\text{N}_8\text{O}_9\text{Ti}$: C 73.17, H 3.68, N 8.53; Found: C 72.97, H 3.57, N 8.49. MALDI-TOF-MS m/z : Calc. 1313.2; Found (M^+) 1314.00.

2,3,9,10,16,17,23,24-[Octakis(4-t-butylphenoxyphthalocyaninato)]oxotitanium(IV)

(39b): Synthesis and purification was as outlined for **37e** except **44b** instead of **42e** was employed. The amounts of the reagents employed were: **44b** (8.00 g, 19.0 mmol), titanium butoxide (1.62 g, 4.75 mmol) and urea (1.14 g, 19.0 mmol) in 1-octanol (35 ml). Yield: 2.09 g (20 %). UV/VIS (1-CNP): λ_{\max} nm (log ϵ) 354 (4.80), 638 (4.59), 710 (5.35). IR [(KBr) $\nu_{\max}/\text{cm}^{-1}$]: 2916 (C-H), 1269 (C-O-C), 962 (Ti=O). $^1\text{H-NMR}$ (CDCl_3): δ , ppm 8.90 (8-H, s, Pc-H), 7.43 (16-H, d, Phenyl-H), 7.22 (16-H, d, Phenyl-H), 1.40 (72-H, s, But). $\text{C}_{112}\text{H}_{112}\text{N}_8\text{O}_9\text{Ti}$: Calc. C 76.34, H 6.41, N 6.36; Found C 75.51, H 6.26, N 6.25. MALDI-TOF-MS m/z : Calc. 1762.0; Found (M^+) 1763.3.

2,3,9,10,16,17,23,24-{Octakis[(4-benzyloxy)phenoxy]phthalocyaninato}

oxotitanium(IV) (39c): Synthesis and purification was as outlined for **37e** except **44c** instead of **42e** was employed. The amounts of the reagents employed were: **44c** (5.00 g, 11.4 mmol), titanium butoxide (0.97 g, 2.85 mmol) and urea (0.68 g, 11.4 mmol) in 1-octanol (21 ml). Yield: 2.34 g (38 %). UV/VIS (1-CNP): λ_{\max} nm (log ϵ) 354 (4.97), 639 (4.71), 712 (5.38). IR [(KBr) $\nu_{\max}/\text{cm}^{-1}$]: 1299 (C-O-C), 963 (Ti=O). $^1\text{H-NMR}$ (CDCl_3): δ , ppm 8.80 (8-H, s, Pc-H), 7.80-7.00 (72-H, m, Phenyl-H, 'Phenyl-H), 5.20 (16-H, s, CH_2). $\text{C}_{136}\text{H}_{96}\text{N}_8\text{O}_{17}\text{Ti}$: Calc. C 75.55, H 4.48, N 5.18; Found C 74.90, H 4.22, N 5.02. MALDI-TOF-MS m/z : Calc. 2162.1; Found (M^+) 2161.9

2,3,9,10,16,17,23,24-(Octaphenylthiophthalocyaninato)oxotitanium(IV) (39d):

Synthesis and purification was as outlined for **37e** except **44d** instead of **42e** was employed. The amounts of the reagents employed were: **44d** (5.00 g, 15.0 mmol), titanium butoxide (1.28 g, 3.75 mmol) and urea (0.90 g, 15.0 mmol) in 1-octanol (28 ml). Yield: 2.16 g (40 %). UV/VIS (1-CNP): λ_{\max} nm (log ϵ) 354 (4.83), 639 (4.56), 742 (5.29). IR [(KBr) $\nu_{\max}/\text{cm}^{-1}$]: 689 (C-S-C), 961 (Ti=O). $^1\text{H-NMR}$ (CDCl_3): δ , ppm 8.82 (8-H, s, Pc-H) 7.60 – 7.35 (40-H, m, Phenyl-H). $\text{C}_{80}\text{H}_{48}\text{N}_8\text{OS}_8\text{Ti}$: Calc. C 66.65, H 3.36, N 7.77; Found C 66.52, H 3.27, N 7.62. MALDI-TOF-MS m/z : Calc. 1441.7; Found (M^+) 1442.3

2.4.6 Amino substituted titanium phthalocyanine (Scheme 3.7)

2,(3)-(Tetranitrophthalocyaninato)oxotitanium(IV) (40): A mixture of 4-nitrophthalonitrile (**22**) (5.0 g, 28.9 mmol), titanium butoxide (2.72 g, 7.98 mmol), urea (0.87 g, 14.5 mmol) in 1-octanol (7.3 ml) was heated under an atmosphere of nitrogen at 150 °C for 6 hours. Thereafter, the reaction mixture was cooled, followed

by refluxing in methanol (30 ml) for 30 minutes. The fine green-black product was collected by filtration, washed with distilled water and methanol and then dried at 70 °C to give the title compound. Yield: 4.23 g (70 %). UV/VIS (DMF): λ_{max} nm (log ϵ) 343 (4.87), 705 (5.09). IR [(KBr) $\nu_{\text{max}}/\text{cm}^{-1}$]: 1520 (NO₂ asym), 1328 (NO₂ sym), 962 (Ti=O).

2,(3)-(Tetraaminophthalocyaninato)oxotitanium(IV) (41): To a slurry of distilled water (75 ml) and complex **40** (2.50 g, 3.31 mmol) was added sodium sulphide nonahydrate (12.5 g, 52 mmol) and the reaction mixture stirred at 50 °C for 5 hours. After separation by centrifuge, purification of the solid product was effectuated by treatment with 1 M HCl (200 ml), followed by treatment with 1 M NaOH (200 ml) and finally washed to neutrality with distilled water. Yield: 4.23 g (70 %). UV/VIS (DMF): λ_{max} nm (log ϵ) 335 (4.91), 455 (4.02), 755 (5.24). IR [(KBr) $\nu_{\text{max}}/\text{cm}^{-1}$]: 3358 (NH₂), 964 (Ti=O).

RESULTS AND DISCUSSION

- **Publications**

- **Chapter 3:**

Synthesis and spectroscopic characterisation

- **Chapter 4:**

*Photochemical, photophysical and
photocatalytic properties*

- **Chapter 5**

Electrochemical characterisation

- **Chapter 6**

Electrocatalytic properties

PUBLICATIONS

The results recapitulated in this thesis have been published in recognised and accredited journals listed below, and are not referenced further:

1. Synthesis and electrochemical characterization of α - and β - tetrasubstituted oxo(phthalocyaninato) titanium(IV) complexes. **Prudence Tau** and Tebello Nyokong, *Polyhedron*, **25** (2006) 1802
2. Unique electrochemical behaviour of tantalum(V) phthalocyanine. **Prudence Tau** and Tebello Nyokong, *J. Porphyrins Phthalocyanines*, **10** (2006) 69
3. Synthesis, electrochemical and photophysical properties of phthalocyaninato oxotitanium(IV) complexes tetra-substituted at the α and β position with arylthio groups. **Prudence Tau** and Tebello Nyokong, *Dalton Transactions*, (2006) 4482
4. Synthesis and photophysical properties of octa-substituted phthalocyaninato oxotitanium(IV) derivatives. **Prudence Tau** and Tebello Nyokong, *J. Porphyrins Phthalocyanines*, **10** (2006) 1040
5. Electrochemical characterization of tetra- and octa-substituted oxo(phthalocyaninato) titanium(IV) complexes. **Prudence Tau** and Tebello Nyokong, *Electrochim. Acta*, **52** (2007) 3641

6. Electrocatalytic activity of arylthio tetra-substituted oxotitanium(IV) phthalocyanines towards the oxidation of nitrite. **Prudence Tau** and Tebello Nyokong, *Electrochim. Acta*, **52** (2007) 4547
7. Spectroscopic characterization and interactions of sulphonated titanium and tantalum phthalocyanines with methyl viologen. **Prudence Tau** and Tebello Nyokong, *Inorg. Chim. Acta*, (2007) **in press**
8. Comparative photocatalytic efficiency of oxotitanium(IV) phthalocyanines for the oxidation of 1-hexene. **Prudence Tau** and Tebello Nyokong, *J. Mol. Cat. A: Chem.*, (2007) **in press**
9. Electrocatalytic oxidation of nitrite by tetra-substituted oxotitanium(IV) phthalocyanines adsorbed or polymerised on glassy carbon electrode. **Prudence Tau** and Tebello Nyokong, *J. Electroanal. Chem.*, (2007) **in press**

CHAPTER 3

Synthesis

and

**Spectroscopic
characterisation**

This chapter deals with the synthesis and spectroscopic characterisation of metallophthalocyanines synthesised in this work. A compiled list of the MPcs is collated in Table 3.1 – 3.4.

Table 3.1: List of synthesised unsubstituted and sulphonated MPcs, their abbreviations and numbers in this thesis

MPc complex	Abb.	No.
Dichloro(phthalocyaninato)titanium(IV)	Cl ₂ TiPc	33
Trichloro(phthalocyaninato)tantalum(V)	Cl ₃ TaPc	34
Differently sulphonated titanium phthalocyanine	TiPcS _n	35
Differently sulphonated tantalum phthalocyanine	TaPcS _n	36

Table 3.2: List of synthesised α and β tetra-substituted MPcs and their numbers in this thesis

MPc complex	No.
1,(4)-(Tetraphenoxyphthalocyaninato) oxotitanium(IV)	37a
1,(4)-(Tetra- <i>tert</i> -butylphenoxyphthalocyaninato) oxotitanium(IV)	37b
1,(4)-(Tetrabenzoyloxyphthalocyaninato) oxotitanium(IV)	37c
1,(4)-{Tetrakis[4-(benzyloxy)phenoxy]phthalocyaninato} oxotitanium(IV)	37d
1,(4)-(Tetraphenylthiophthalocyaninato)oxotitanium(IV)	37e
1,(4)-(Tetrabenzylthiophthalocyaninato)oxotitanium(IV)	37f
2,(3)-(Tetraphenoxyphthalocyaninato) oxotitanium(IV)	38a
2,(3)-(Tetra- <i>tert</i> -butylphenoxyphthalocyaninato) oxotitanium(IV)	38b

2,(3)-(Tetrabenzyloxyphthalocyaninato)oxotitanium(IV)	38c
2,(3)-{Tetrakis[4-(benzyloxy)phenoxy]phthalocyaninato}oxotitanium(IV)	38d
2,(3)-(Tetraphenylthiophthalocyaninato)oxotitanium(IV)	38e
2,(3)-(Tetrabenzylthiophthalocyaninato)oxotitanium(IV)	38f

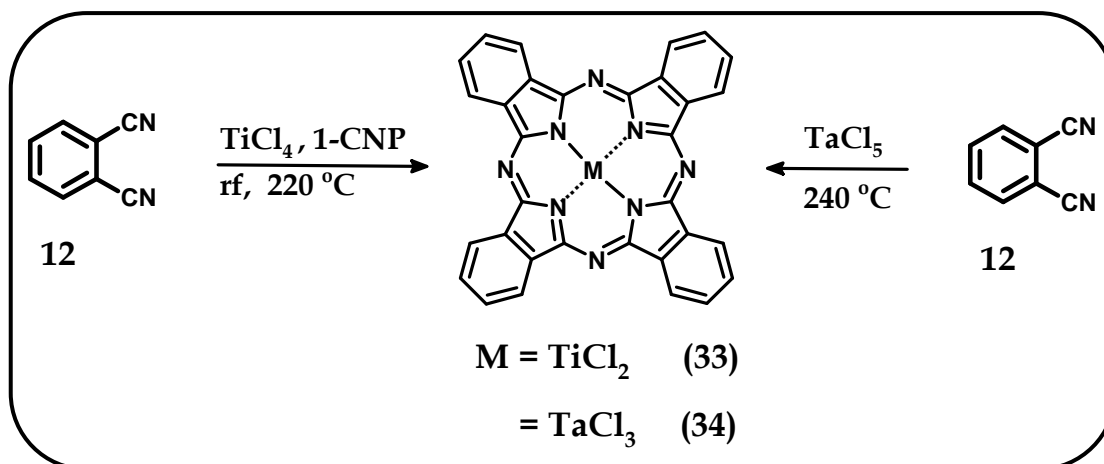
Table 3.3: List of synthesised octa-substituted MPcs and their numbers in this thesis

MPc complex	No.
2,3,9,10,16,17,23,24-(Octaphenoxyphthalocyaninato)oxotitanium(IV)	39a
2,3,9,10,16,17,23,24-[Octakis(4- <i>tert</i> -butylphenoxyphthalocyaninato)] oxotitanium(IV)	39b
2,3,9,10,16,17,23,24-{Octakis[(4-benzyloxy)phenoxy]phthalocyaninato} oxotitanium(IV)	39c
2,3,9,10,16,17,23,24-(Octaphenylthiophthalocyaninato)oxotitanium(IV)	39d

Table 3.4: List of synthesised nitro- and amino-substituted OTiPcs, their abbreviations and numbers in this thesis

MPc complex	Abb.	No.
2,(3)-Tetranitrophthalocyaninato oxotitanium(IV)	OTiPc(NO ₂) ₄	40
2,(3)-Tetraaminophthalocyaninato oxotitanium(IV)	OTiPc(NH ₂) ₄	41

3.1 Unsubstituted titanium and tantalum phthalocyanines (Scheme 3.1)



Scheme 3.1: Synthesis of unsubstituted Ti and Ta phthalocyanines.

The syntheses and characterisation of dichloro(phthalocyaninato)titanium(IV) and trichloro(phthalocyaninato)tantalum(V) complexes, i.e. Cl_2TiPc (**33**) and Cl_3TaPc (**34**) respectively, have been reported before [33, 35]. The Cl_2TiPc (**33**) and Cl_3TaPc (**34**) complexes in this work were respectively obtained by facile ‘wet’ and ‘dry’ syntheses, Scheme 3.1. The former complex was obtained by refluxing at $\sim 220\text{ }^\circ\text{C}$ the metal chloride (TiCl_4) and phthalonitrile in dry chloronaphthalene (1-CNP) while the latter complex was obtained through heating phthalonitrile and anhydrous TaCl_5 at relatively high temperatures ($240\text{ }^\circ\text{C}$), Scheme 3.1. The experiments were performed under a blanket of nitrogen as the respective metal chlorides are moisture-sensitive. In these reactions however, formation of ring-chlorinated Pcs as by-products or decomposition of the ring as a result of HCl cannot be avoided. The complexes were purified by Soxhlet extraction of impurities to afford satisfactory yields of dark-blue crystals with a violet gloss.

The IR spectra showed moderately strong vibrations of Ti-Cl at 390 cm^{-1} and 356 cm^{-1} which were assigned to the chloride ions in a *cis*-arrangement [33]. The

vibrations of Ta-Cl were observed at 366 cm^{-1} . Elemental analyses gave expected results, further confirming the presence of three chloride ions in complex **34**. Mass spectral data also showed loss of the chloride ligands (see experimental section), thus the purity of the complex was confirmed. The purity of **34** was determined by these methods of analyses since the complex is less well-known compared to complex **33**. Although the syntheses of Cl_2TiPc and Cl_3TaPc are known, the NMR data of the complexes are relatively unknown. The proton NMR spectrum of complex **33** was typical of unsubstituted MPcs, exhibiting two singlets at 8.55 ppm and 9.71 ppm due to equivalent peripheral and equivalent non-peripheral protons respectively.

The proton NMR of complex **34**, shown in Fig. 3.1 was different from the norm, such as was observed for complex **33**. The predicted singlets for unsubstituted MPcs were not observed. Instead, it was interesting to note that for the Cl_3TaPc complex, four signals, i.e. two doublets due to non-peripheral protons (at 9.17 ppm and 7.93 ppm) and two triplets due to peripheral protons (at 7.86 ppm and 7.71 ppm) were observed. Each signal integrated for four protons indicating that four sets of protons (labelled **a** and **b** in Fig. 3.1) were in different environments altogether. The X-ray data for Cl_3TaPc has been reported [35] and the noticeable features are that tantalum is displaced from the core of the ring (C_8N_8), thus resulting in the three chlorine atoms assuming a *cis*-arrangement. The isoindole moieties have been found to be planar and bent a little with respect to the core of the ring. Thus a compromise between a staggered and an eclipsed conformation results, hence the four sets of protons display the observed four signals. Titanium complexes are also displaced from the core of the ring though to a lesser extent.

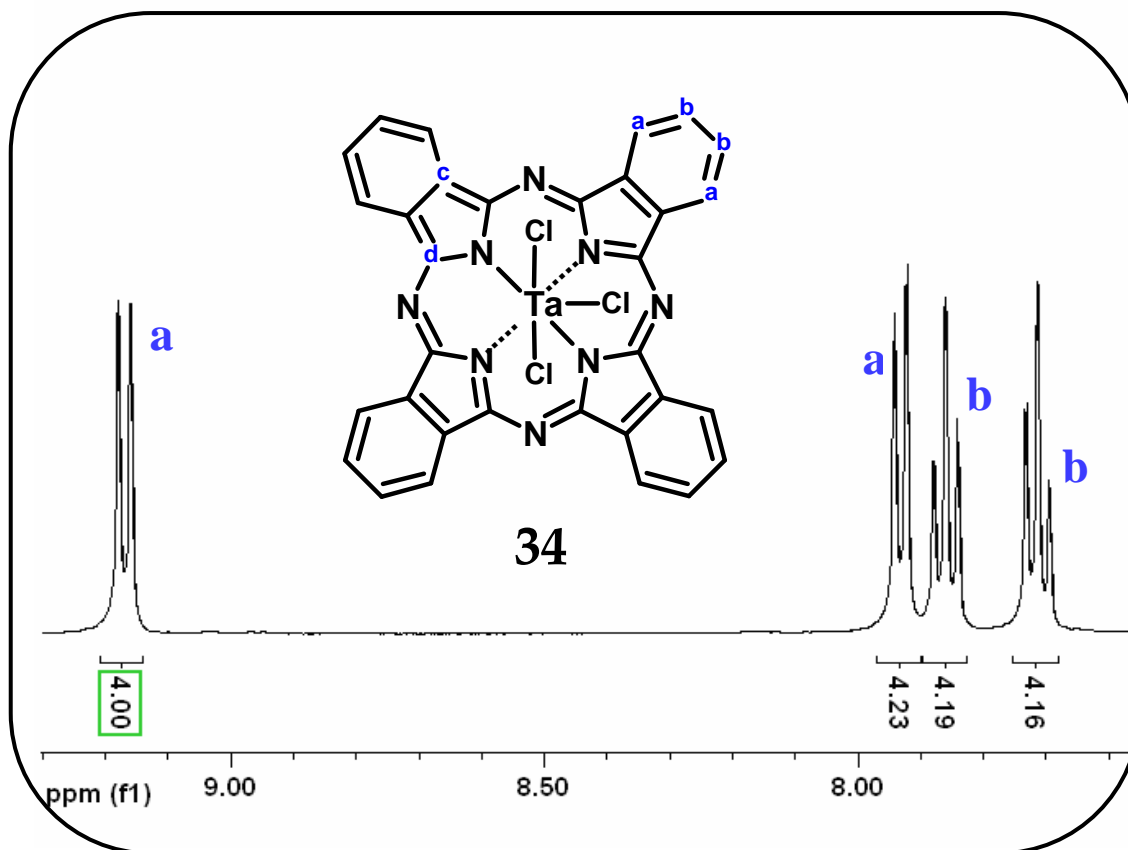


Figure 3.1: ^1H -NMR spectrum of Cl_3TaPc (**34**) in CDCl_3 .

Four signals, corresponding to carbons **a**, **b**, **c** and **d** in Fig. 3.1 (insert), are expected in the ^{13}C -NMR spectra of unsubstituted MPC complexes. If the nuclei are non-equivalent, then the signals or resonances will be split. Four unequivalent nuclei have been observed before in which the carbon signals in phthalocyanines were split into four signals each [405]. Sixteen ^{13}C signals (four for each carbon atom) of Cl_3TaPc were observed (see experimental section), showing that the carbon atoms were non-equivalent and hence confirming the proton signals observed above.

Figure 3.2 shows the electronic absorption spectra of complexes **33** and **34** recorded in chloroform (CHCl_3). The solubility of the complexes were limited to solvents such as dimethylformamide (DMF), dichloromethane (DCM) and CHCl_3 due

to the fact that the complexes lacked substituents that would render them soluble in many organic solvents, as is typical of unsubstituted phthalocyanines.

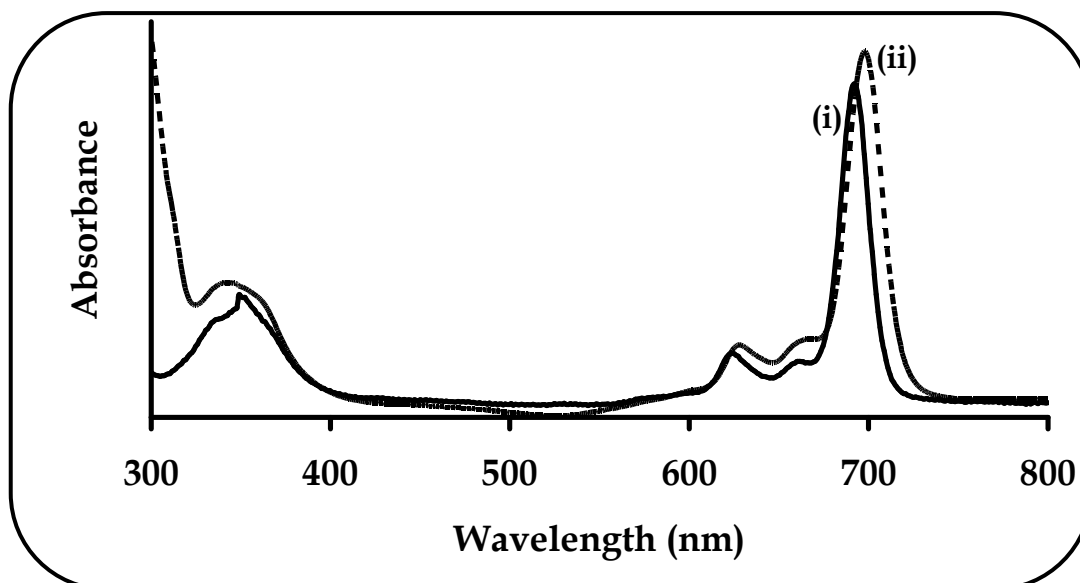
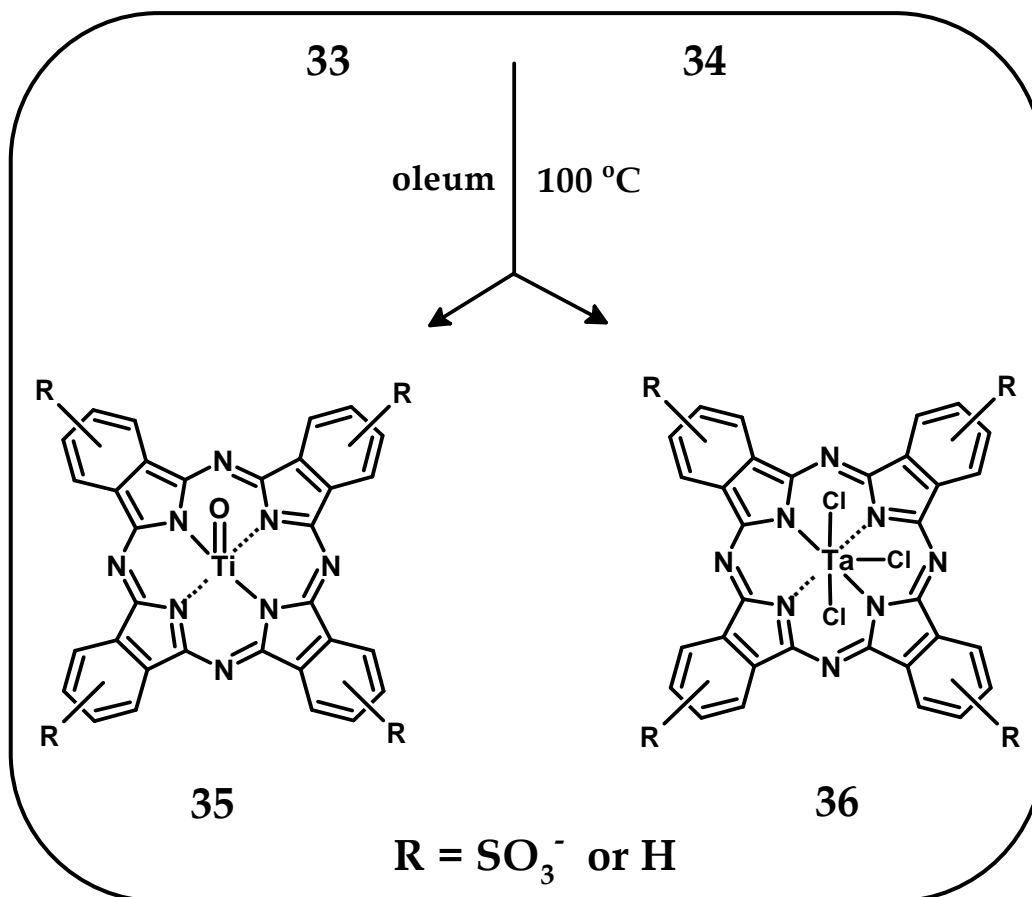


Figure 3.2: UV/Vis spectra of (i) Cl_2TiPc (**33**) and (ii) Cl_3TaPc (**34**) in CHCl_3 . Concentration $\sim 10^{-6}$ M.

In CHCl_3 , the complexes displayed typical monomeric Q-bands at 692 nm (complex **33**) and 697 nm (complex **34**) with B-bands observed at 349 nm (complex **33**) and 342 nm (complex **34**). The presence of Ta in complex **34** caused a 5 nm red-shift relative to complex **33**. Low extinction coefficients for both complexes were obtained, which was surprising since this may suggest that the complexes were aggregated. Low extinction coefficients have been reported for MPc complexes such as $\text{Fe}^{\text{I}}\text{Pc}$ and $\text{Co}^{\text{I}}\text{Pc}$ [168]. Beer's law did not however show aggregation for concentrations as high as 1×10^{-4} M. Also, the presence of the axial chloride ligands in both complexes is expected to prevent aggregation.

3.2 Differently sulphonated titanium and tantalum phthalocyanines (Scheme 3.2)



Scheme 3.2: Synthesis of differently sulphonated TiPcS_n (35) and TaPcS_n (36).
S_n = SO₃⁻.

Sulphonated MPCs are the most common water-soluble macrocycles although those of TiPc and TaPc are relatively unknown and hence their spectroscopic characteristics in organic and aqueous solvents are not well-established. The differently sulphonated complexes, TiPcS_n (35) and TaPcS_n (36) were obtained by treating the respective ring unsubstituted MPC derivatives, i.e. 33 and 34, with fuming sulphuric acid (oleum 30%), Scheme 3.2. Oleum is known to directly sulphonate pre-existing MPCs as the acid is not strong enough to destroy the macrocycles [134]. MPCs which have been sulphonated by oleum are known and

their spectroscopic properties have been characterised, e.g. AlPcS_n, ZnPcS_n, SiPcS_n, SnPcS_n, GePcS_n and GaPcS_n [134,267,269]. The presence of the axial oxygen ($\nu_{\text{Ti-O}} = 968 \text{ cm}^{-1}$) for TiPcS_n and axial chlorides ($\nu_{\text{Ta-Cl}} = 365 \text{ cm}^{-1}$) for TaPcS_n were confirmed using IR spectroscopy as these appeared as typical medium bands. For TiPcS_n, the disappearance of the axial chloro ligands was due to the fact that the complex easily hydrolysed during purification, such that the vibration band of Ti = O was observed instead.

As the degree of sulphonation is uncontrollable during the preparation of the complexes, the MPcS_n complexes may contain a mixture of sulphonates, i.e. mono-, di-, tri- and/or tetra-. In some cases, the reaction can be controlled to some extent by varying the temperature and reaction time and the central ion has been known to play an important role in the product distribution [135]. The degree of sulphonation will thus vary from batch to batch depending on these factors. Although it is very difficult to separate the mixtures of isomers, in this work, the same batch of each differently sulphonated complex was employed throughout the study. To determine the extent of sulphonation, reverse-phase HPLC was employed. Fig. 3.3 shows the HPLC traces obtained for the MPcS_n complexes used in the study. It is expected that the most highly sulphonated fraction – which is the most soluble – would be eluted first from the column, thus giving the shortest retention time [134,406]. The monosulphonated fractions are however expected to be eluted last, thus giving longer retention times. Both MPcS_n showed strong peaks at ~ 15 min and these were assigned to the disulphonated components, which were expected to be eluted third. Tetrasulphonated MPcS₄ derivatives were employed to confirm a peak at low retention times. The presence of one strong HPLC peak confirms that there is one dominant component in each MPcS_n, which was associated with mainly the disubstituted derivative.

Therefore the amount of other substituted derivatives such as tetrasulphonates was insignificant. In this work, it was assumed that there was mainly one component involved in the studies, i.e. the disubstituted derivative.

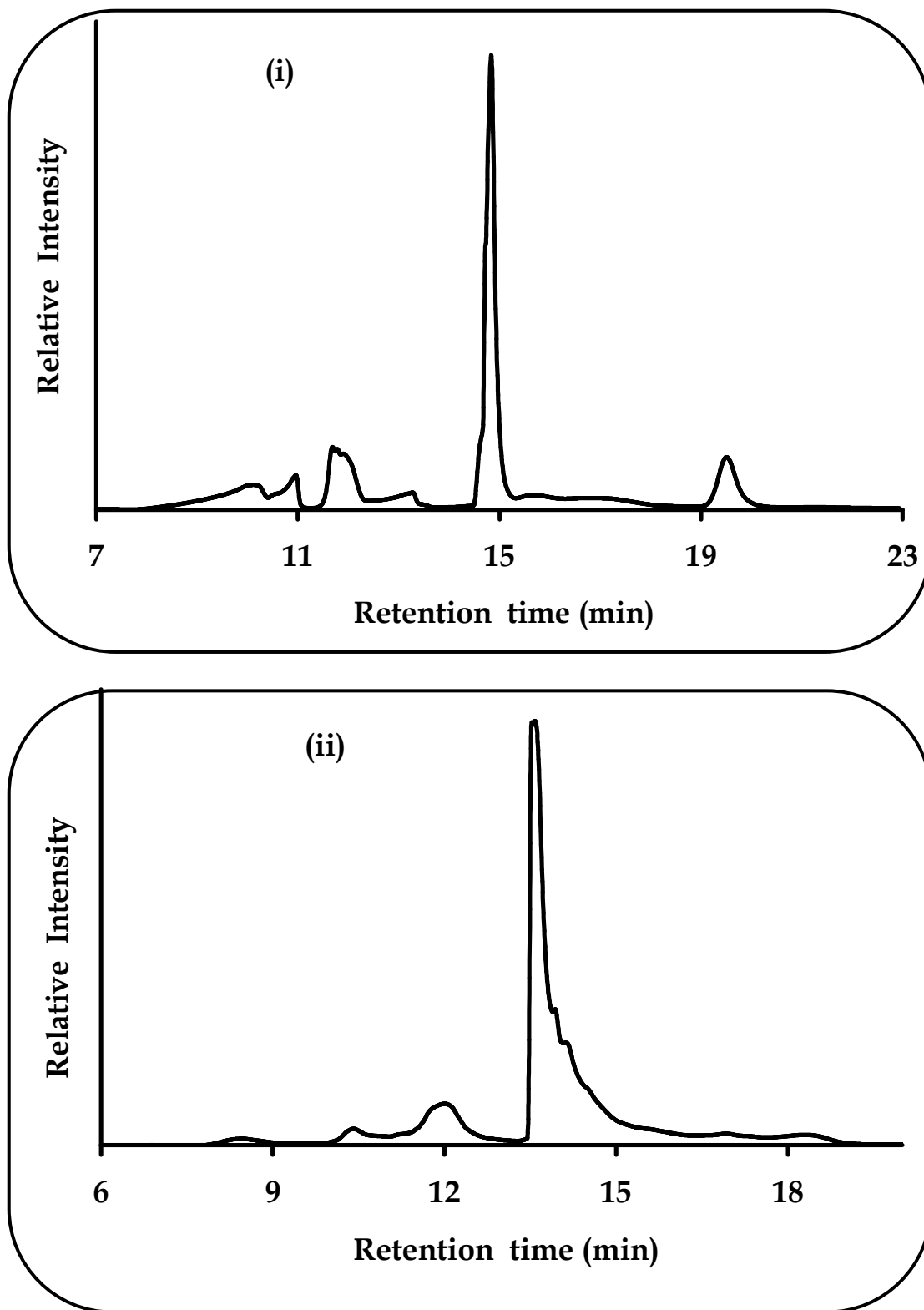
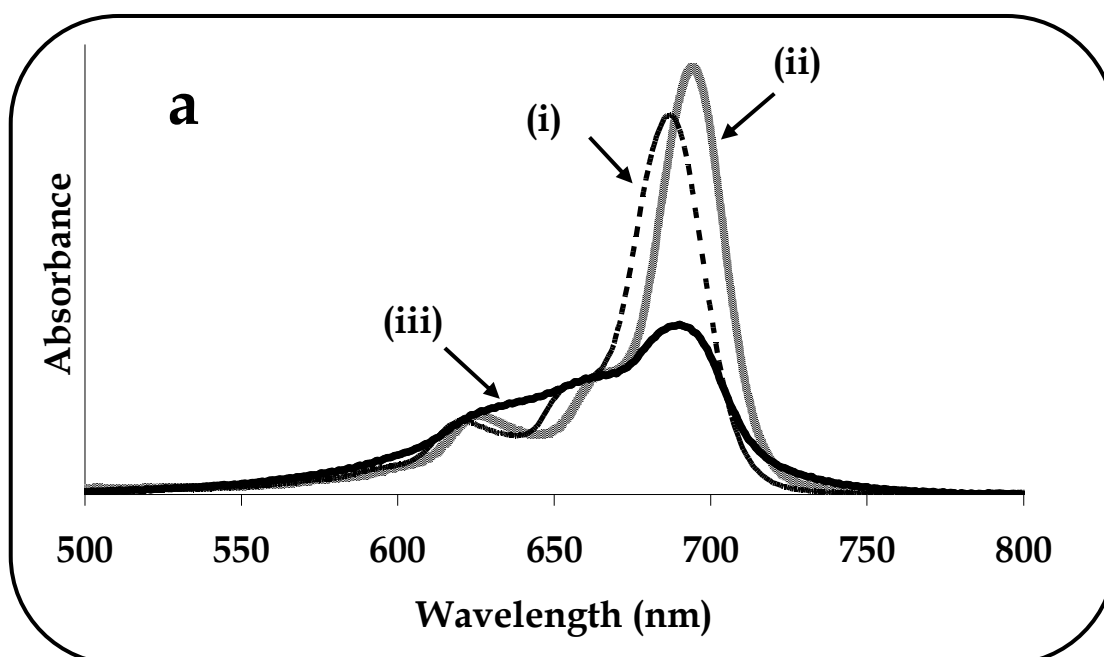


Figure 3.3: HPLC traces of (i) TiPcS_n and (ii) TaPcS_n .

The ground state electronic absorption spectra of the complexes in methanol, DMSO and phosphate buffer solution (PBS) of pH 7.4 are shown in Fig. 3.4. TiPcS_n exhibited monomeric behaviour in methanol and DMSO since it is known that organic solvents tend to favour the monomeric nature of the complexes compared to aqueous solutions [269,407,408], Fig. 3.4a. The Q-band of TaPcS_n was however broadened in methanol and DMSO, probably due to loss in symmetry of the complex as a result of the displacement of the large metal from the core of the ring, Fig. 3.4b. The broadness was observed even on dilution, showing that it was not due to aggregation.

Both complexes were water-soluble due to their negative charge. Complex **35** (TiPcS_n) exhibited a broad spectrum in PBS, suggesting that the complex is aggregated in aqueous solutions, Fig. 3.4a(iii). Formation of aggregates is normally accompanied by an absorption band near 630 nm as was observed in Fig. 3.4a(iii). The spectrum of complex **36** (TaPcS_n) however was less broadened in PBS, further suggesting a more pronounced tendency of **35** to aggregate in PBS, apparent even at concentrations as low as 10^{-6} M.



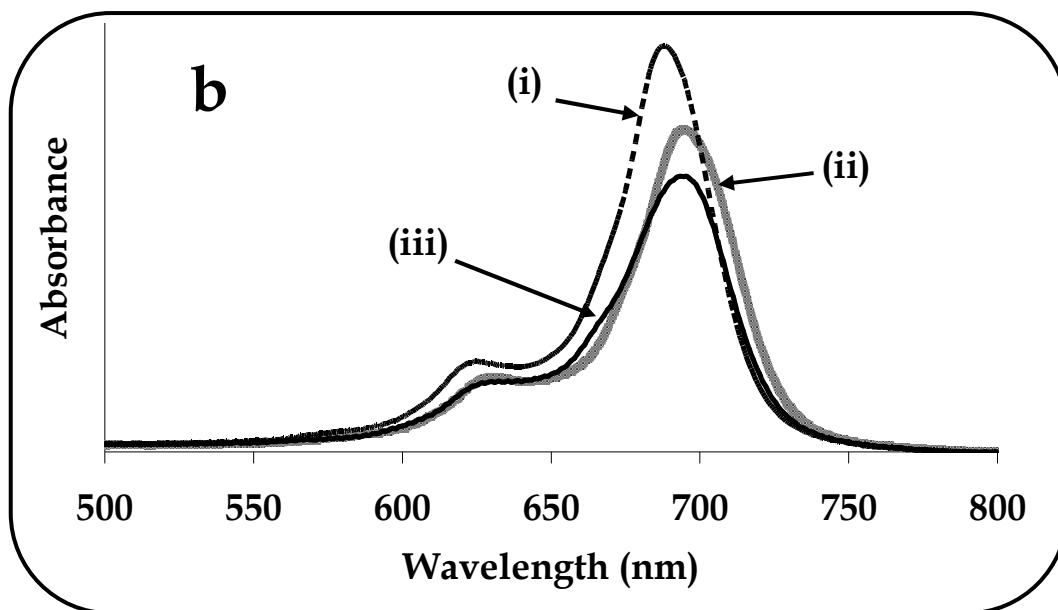


Figure 3.4: Ground state absorption spectra of (a) TiPcS_n and (b) TaPcS_n in (i) methanol, (ii) DMSO and (iii) PBS 7.4. Concentration $\sim 1 \times 10^{-5}$ M.

Partial monomerisation of **35** on addition of a surfactant, Triton X-100, to PBS was observed since the Q-band narrowed and increased in intensity due to monomeric species absorbing, Fig. 3.5. Adding the surfactant to PBS of complex **36** did not however bring about an observable change in the Q-band intensity as well as position. Since the prepared complexes contained less sulphonated components, the complexes were expected to be more aggregated in aqueous solutions than if they were highly sulphonated. As earlier mentioned, the spectrum of **36** in PBS did not change on addition of Triton X-100. This suggested that either the forces responsible for aggregation (as expected for less sulphonated MPcs) were too strong to be broken by surfactants or that the observed broadness was due to the distortion of the ring and not aggregation, since the Q-band was broad even in organic solvents (unlike **35**). Confirmation of the oxidation states of the complexes, i.e. +4 for Ti and +5 for Ta, was brought about by addition of an oxidant such as bromine. The Q-bands were not affected by the oxidant.

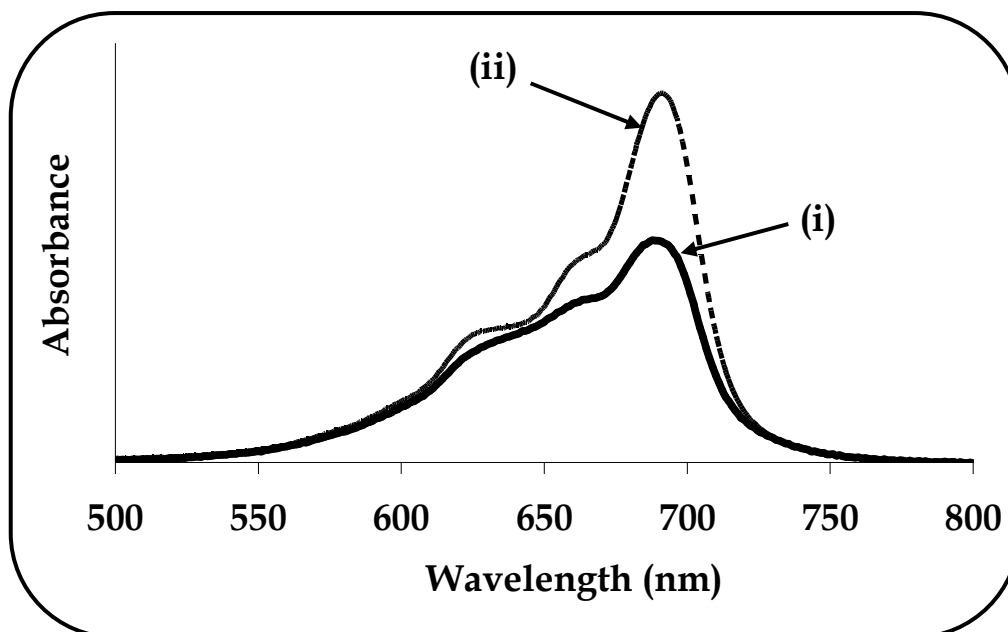


Figure 3.5: Ground state absorption spectra of TiPcS_n ($1 \times 10^{-5} \text{ M}$) in (i) the absence and (ii) presence of Triton X-100 ($1 \times 10^{-5} \text{ M}$) in PBS 7.4 solution.

Since the MPcS_n complexes are negatively charged and thus are electron donors, their interaction with a cationic molecule or an electron acceptor, methyl viologen (MV^{2+}) was investigated by UV/Vis spectroscopy in methanol. Methyl viologen does not dissolve in DMSO and thus methanol was the solvent of choice since both the MPcS_n complexes and MV^{2+} were soluble in it. Also, studies in aqueous solutions were not performed because the complexation of ion-pairs is known not to occur in solvents of high polarity [265]. Figure 3.6 shows spectral changes observed on addition of increasing concentrations of MV^{2+} to fixed concentrations of TiPcS_n (as an example). Addition of MV^{2+} resulted in the gradual reduction in intensity and shift in the Q-band of the MPcS_n complexes. The Q-band maximum shifted from 687 to 692 nm for TiPcS_n (Fig. 3.6) and for TaPcS_n , the Q-band shifted from 688 to 694 nm. The shifts were an indication of the interaction between MPcS_n and MV^{2+} .

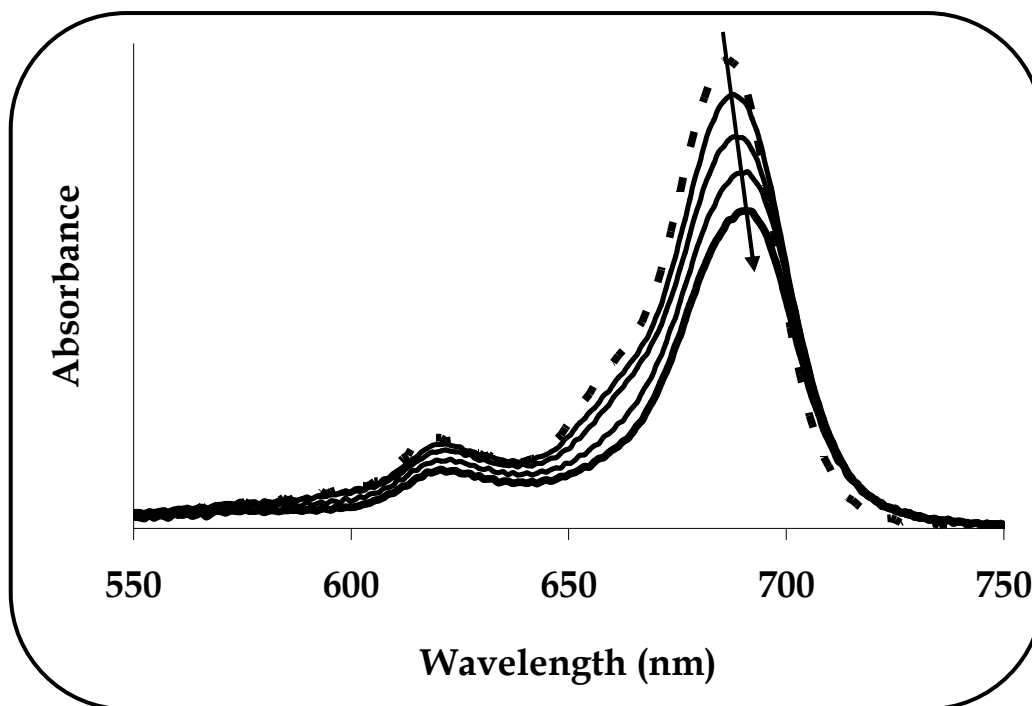


Figure 3.6: UV/Vis spectral changes observed on addition of increasing MV^{2+} concentrations to a solution of $TiPcS_n$ (1.5×10^{-6} M) in methanol. $[MV^{2+}] =$ (i) 0, (ii) 2.2×10^{-5} , (iii) 4.1×10^{-5} , (iv) 5.4×10^{-5} , (v) 8.9×10^{-5} M.

The spectrophotometric studies which were analysed by Job's method were performed as described in the Experimental section. Job plots of $F(x)$ vs. mole fraction of MV^{2+} , Eq. 3.1 (which is the same as Eq. 1.1), i.e.

$$F(x) = d(x) - (\varepsilon_{MV^{2+}} - \varepsilon_{MPc})x - \varepsilon_{MPc} \quad (3.1)$$

for titration of $TiPcS_n$ and $TaPcS_n$ with varying concentrations of MV^{2+} are shown in Fig. 3.7, taken at $\lambda = 687$ nm for **35** and $\lambda = 688$ nm for **36**. Fig. 3.7a shows that a stoichiometry of approximately 1:2 and 2:1 for $MV^{2+}/TiPcS_n$ complexation is obtained, an indication that two different species for this couple, i.e. $(MV^{2+})-(TiPcS_n)_2$ and $(MV^{2+})_2-(TiPcS_n)$, were formed. The $MV^{2+}/TaPcS_n$ complexation however indicated that a 1:2 complex due to $(MV^{2+})-(TaPcS_n)_2$ was formed. Thus $TiPcS_n$ showed two different complexation species with MV^{2+} , while $TaPcS_n$ showed one

complex formation. The difference in the interactions with the electron acceptor was due to the fact that MV^{2+} had a higher affinity for $TiPcS_n$ than $TaPcS_n$. There was also a possibility that different components of the $TiPcS_n$ complex coordinate with MV^{2+} , while only one component coordinates in the case of $TaPcS_n$.

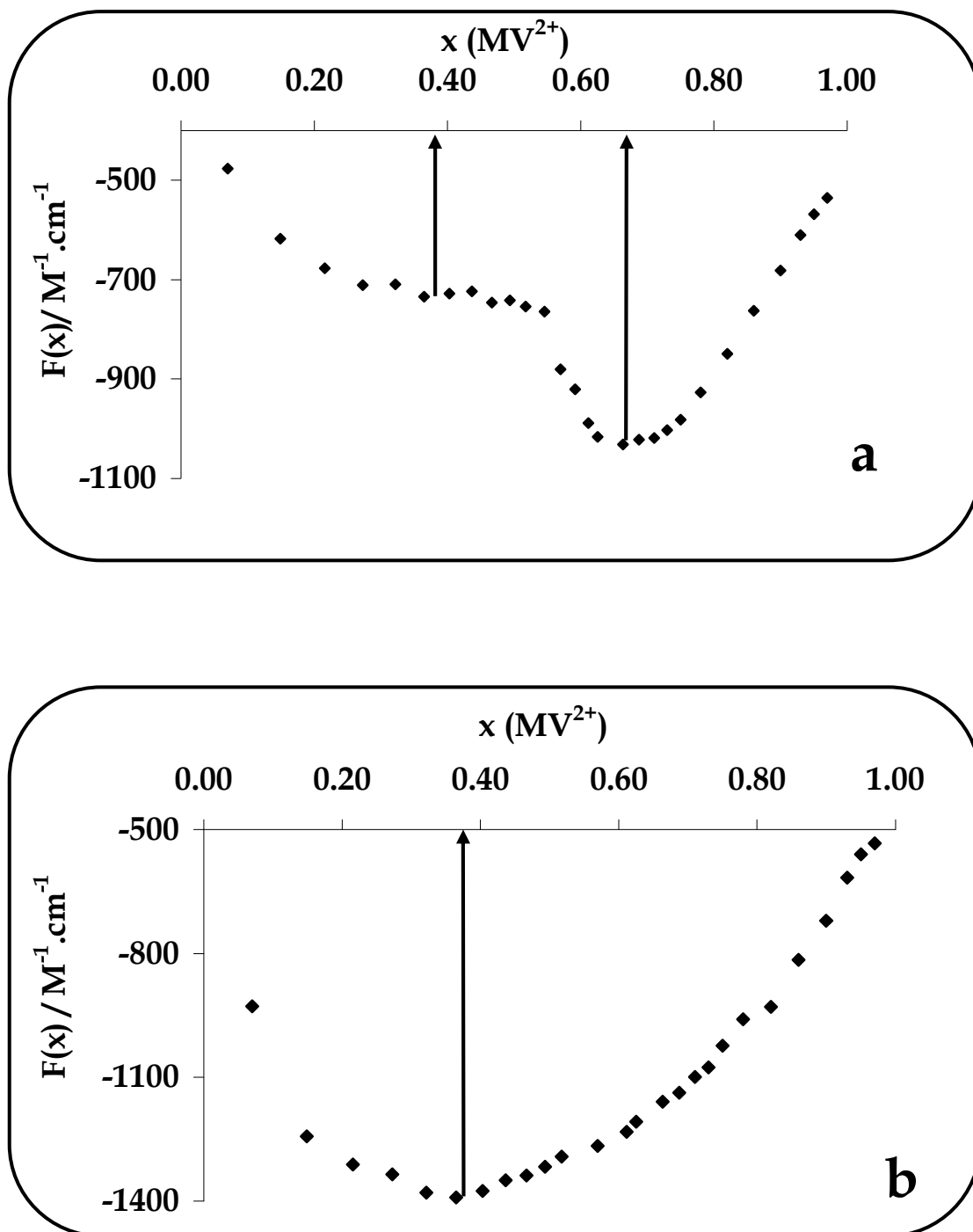


Figure 3.7: Job diagrams for interaction of (a) $TiPcS_n$ ($\lambda = 687$ nm) and (b) $TaPcS_n$ ($\lambda = 688$ nm) with MV^{2+} in methanol.

The strength of interactions, i.e. association constants, K_a , were determined from Eq. 1.2, shown here as Eq. 3.2, i.e.

$$\frac{A_0}{\Delta A} = \frac{A_0}{\Delta A_{max}} + \frac{A_0}{\Delta A_{max}} \frac{1}{K_a} \frac{1}{L_t} \quad (3.2)$$

Plots of $A_0/\Delta A$ vs. $1/L_t$ yielded straight lines (Fig. 3.8) and from the ratio of $A_0/\Delta A_{max}$ and the slope, K_a was obtained. For both complexes, the association constants thus obtained were within ranges of supramolecular complexes or assemblies, i.e. 10^2 to 10^6 M^{-1} . The association constant was found to be largest for TaPcS_n (10^5 M^{-1}) than for both the 1:2 (10^3 M^{-1}) and 2:1 (10^4 M^{-1}) trimers of TiPcS_n , Table 3.5. This thus suggested that the interaction between the former complex and methyl viologen was stronger than in the case with the latter complex.

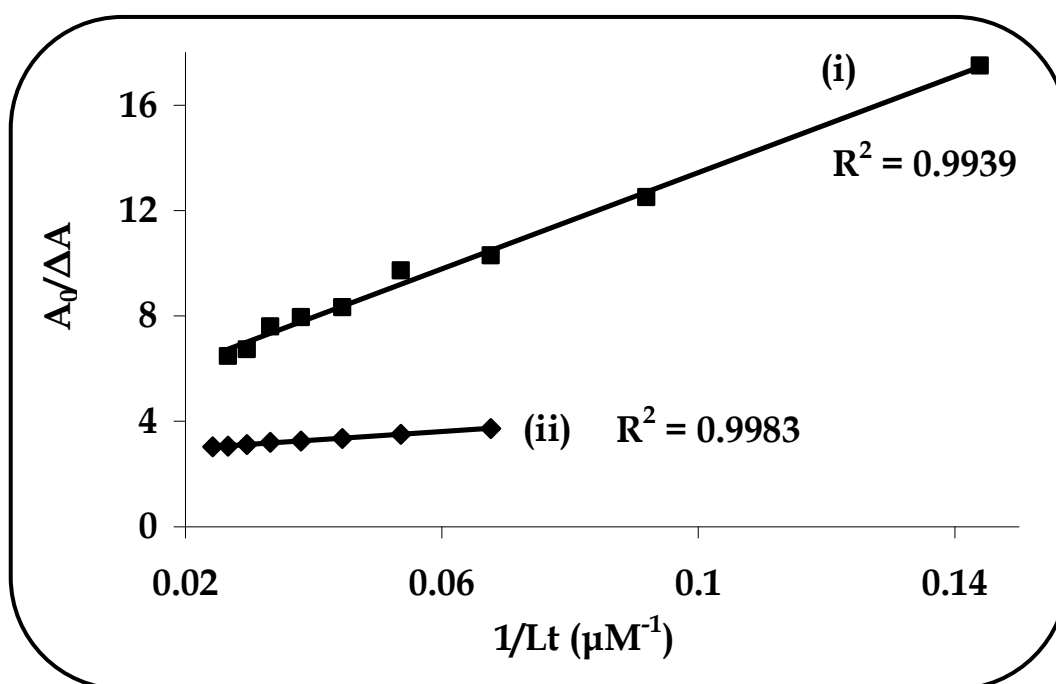


Figure 3.8: Plots of $A_0/\Delta A$ vs. $1/L_t$ for the association constant (K_a) determination in the interaction of (i) TiPcS_n and (ii) TaPcS_n with MV^{2+} .

Furthermore, it was evident that the interaction was stronger for the 2:1 (10^4 M^{-1}) trimer than it was for the 1:2 (10^3 M^{-1}) trimer in the case of TiPcS_n , Table 3.5. The observed interactions confirmed the formation of ground state complex of TiPcS_n and TaPcS_n with MV^{2+} . The association constant of complex **36** (TaPcS_n) was found to be comparable to those reported [198] for Zn and Sn tetrasulphonated complexes where either complexation ratios of 1:1 or 1:2 ($\text{MPC}:\text{MV}^{2+}$) were observed. That of complex **35** (TiPcS_n) was much lower, probably due to the two competing complexation reactions affecting the degree of ion-interaction between the complex and MV^{2+} .

Table 3.5: Structural and calculated association constants (K_a) of TiPcS_n and TaPcS_n with MV^{2+} in methanol.

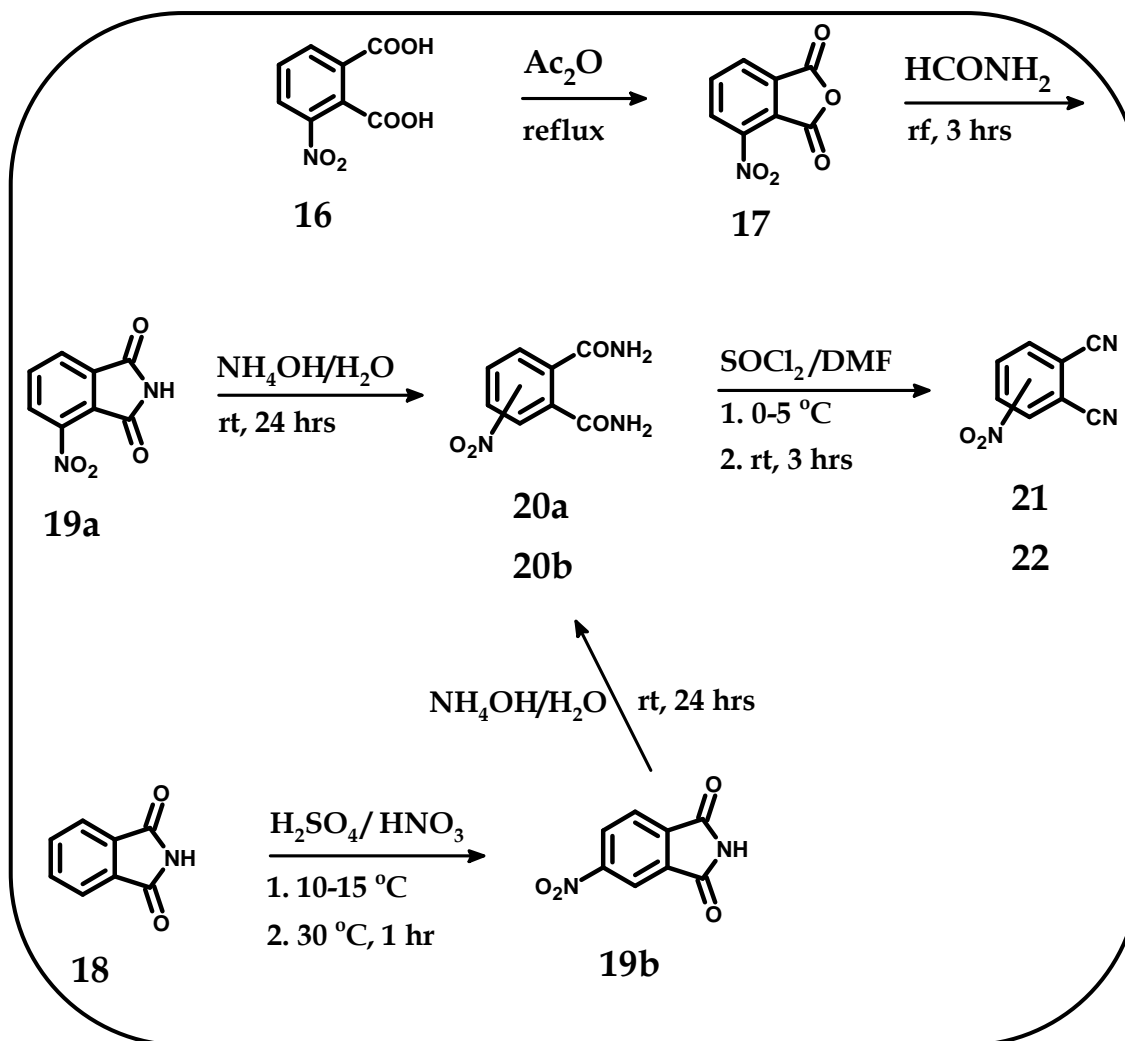
	Complexation	Ratio	K_a (M^{-1})	References
TiPcS_n	$(\text{MV}^{2+})-(\text{TiPcS}_n)_2$	1:2	4.79×10^3	tw
	$(\text{MV}^{2+})_2-(\text{TiPcS}_n)$	2:1	4.73×10^4	tw
TaPcS_n	$(\text{MV}^{2+})-(\text{TaPcS}_n)_2$	1:2	1.65×10^5	tw
$\text{ZnPc}(\text{SO}_3^-)_4$		1:x ^a	1.40×10^5	[198]
$\text{Si}(\text{OH})_2\text{Pc}(\text{SO}_3^-)_4$		1:x ^a	6.60×10^5	[198]
$\text{H}_2\text{Pc}(\text{SO}_3^-)_4$		1:x ^a	1.30×10^6	[198]

^a x = 1 or 2, tw = this work

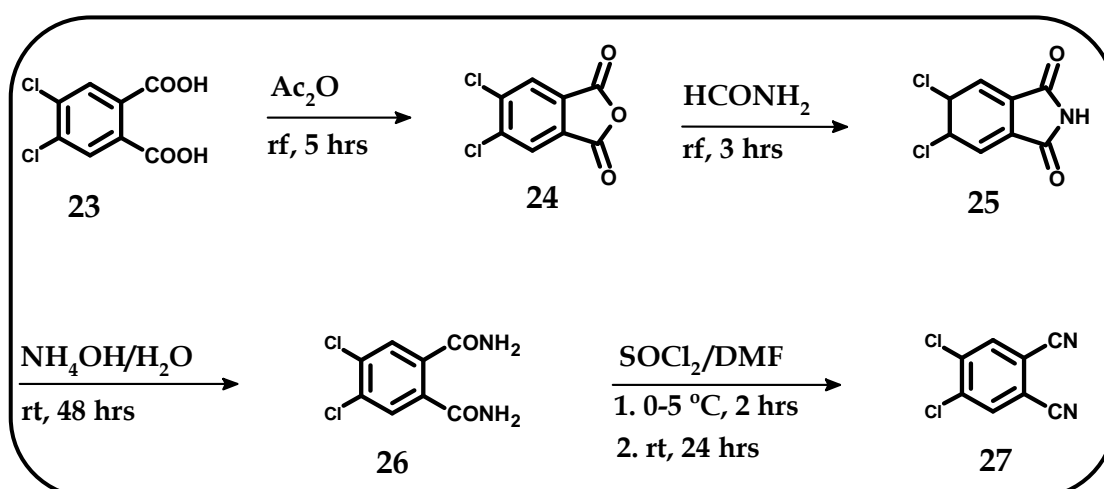
3.3 Tetra- and octa-substituted oxotitanium phthalocyanines

3.3.1 Phthalonitriles (Scheme 3.3)

The complexes in this study were obtained by condensation of 3-, 4- or 4,5-substituted phthalonitriles, the syntheses of which are discussed in Scheme 3.3A and 3.3B. A strategy for the preparation of the substituted phthalonitriles started from the inexpensive 3-nitrophthalic acid (**16**), phthalimide (**18**) and 4,5-dichlorophthalic acid (**23**). Dehydration of phthalic acids **16** and **23** in acetic anhydride afforded - in relatively good yields - 3-nitrophthalic anhydride (**17**) and 4,5-dichlorophthalic anhydride (**24**) respectively. Dehydration of **16** occurred in less than an hour whereas it took 3 hours for complete dehydration of **23** to occur. Acetic acid is produced as a by-product and its presence lowers the product yield. The nucleophilic addition of ammonia (from formamide) to compounds **17** and **24** respectively resulted in the formation of 3-nitrophthalimide (**19a**) and 4,5-dichlorophthalimide (**25**). 4-Nitrophthalimide (**19b**) may similarly be synthesised, however in this work, the compound was obtained via direct nitration of phthalimide (**18**), Scheme 3.3A. Ammonolysis of the imides was achieved to afford the respective amides **20a**, **20b** and **26**, dehydration of which resulted in the corresponding phthalonitriles **21**, **22** and **27** with satisfactory yields. The phthalonitriles were pure by ¹H-NMR as shown in the experimental section. The substituted phthalonitriles (**42** – **44**) depicted in Schemes 3.4 and 3.5 were obtained by a base-catalysed (K₂CO₃) nucleophilic aromatic nitro and chloro displacement of 3-nitrophthalonitrile (**21**), 4-nitrophthalonitrile (**22**) and 4,5-dichlorophthalonitrile (**27**) respectively [409-411]. The characteristic C≡N stretches were observed at ~ 2300 cm⁻¹ and their proton NMR correctly corresponded to the number of expected protons.



Scheme 3.3A: Synthetic routes to 3-nitrophthalonitrile (21) and 4-nitrophthalonitrile (22).

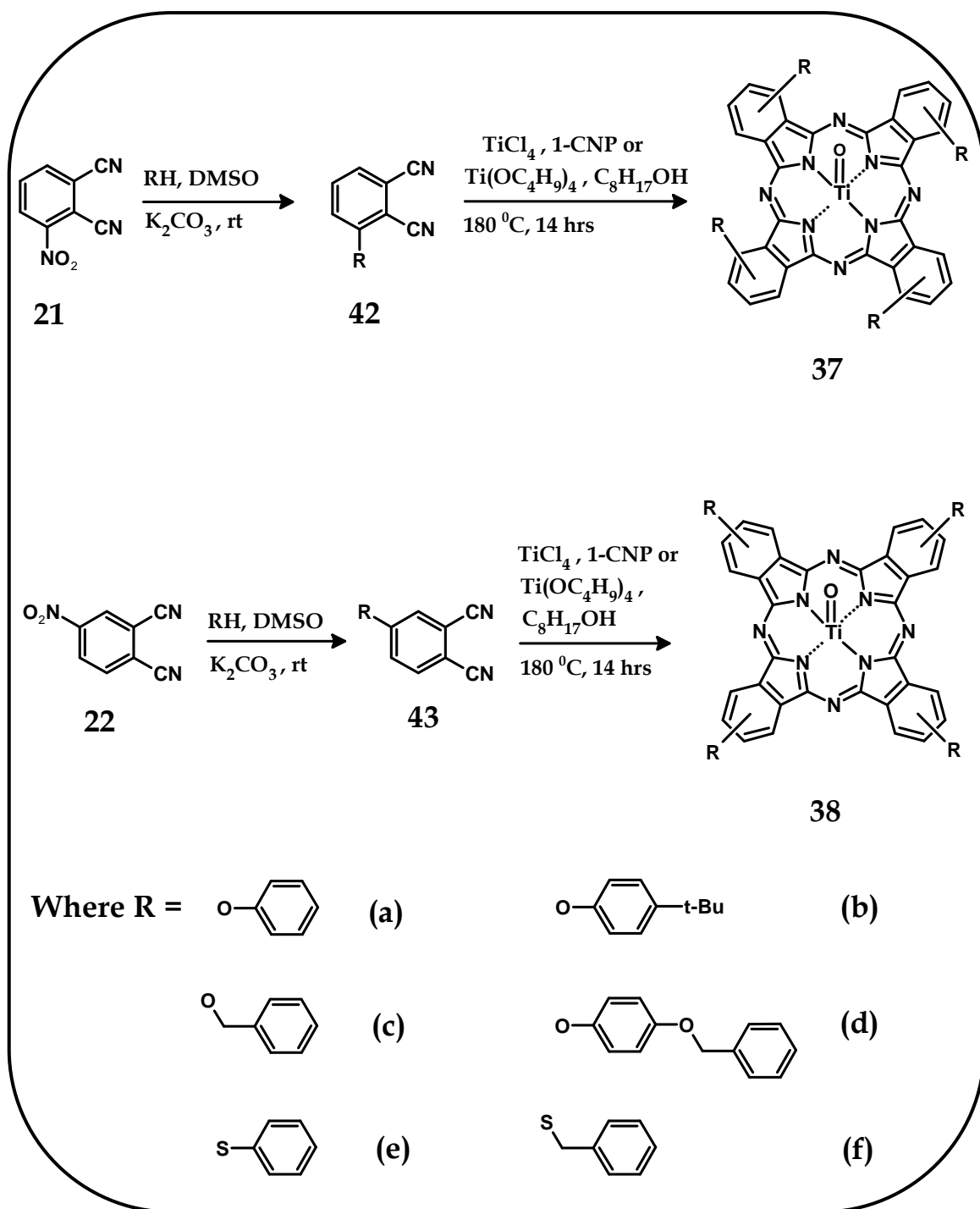


Scheme 3.3B: Synthetic route to 4,5-dichlorophthalonitrile (27).

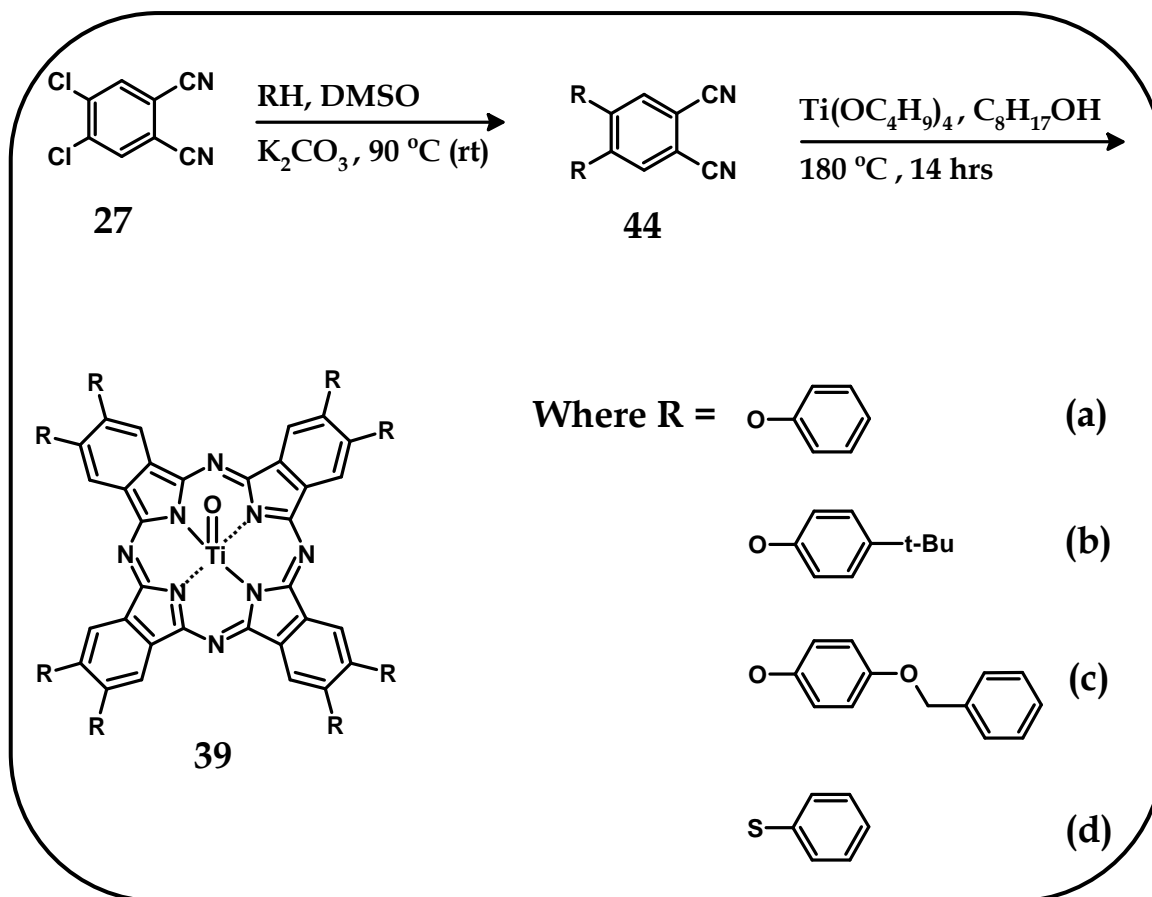
3.3.2 Synthesis of the OTiPc complexes

Treatment of phthalonitriles **21**, **22** and **27** with phenol, 4-*tert*-butylphenol, benzyl alcohol, 4-(benzyloxy)phenol, thiophenol and benzyl mercaptan afforded the corresponding disubstituted dinitriles **42a – f** (Scheme 3.4), **43a – f** (Scheme 3.4) and **44a – d** (Scheme 3.5). The oxotitanium complexes were then prepared by the typical cyclotetramerisation of stoichiometric amounts of the substituted phthalonitriles. The tetra-substituted complexes **37** and **38** were respectively non-peripherally (α) and peripherally (β) substituted, while complexes **39** were octa-substituted at the peripheral positions.

The template reaction to afford complexes **37a**, **37b**, **38a** and **38b** was achieved by treatment of the corresponding dinitriles with TiCl_4 in 1-CNP. Because Ti is a large atom and thus does not fit into the cavity of the ring, high energy is required in order to form the TiPcs. A high-boiling point solvent such as 1-CNP was therefore employed to achieve this purpose. The method used was similar to that reported [154] by Law *et al.* in the synthesis of octa-substituted oxotitanium(IV) phthalocyanines. Also the ratio of the metal to phthalonitrile derivative employed was 1:4. A lower ratio, e.g. 1:3 or 1:2, resulted in the decomposition of the reaction mixture, presumably due to excess HCl produced in solution which could have cleaved the ring, thus generating decomposition products. 1-CNP proved to be difficult to remove, however Soxhlet extraction with hexane was effective.



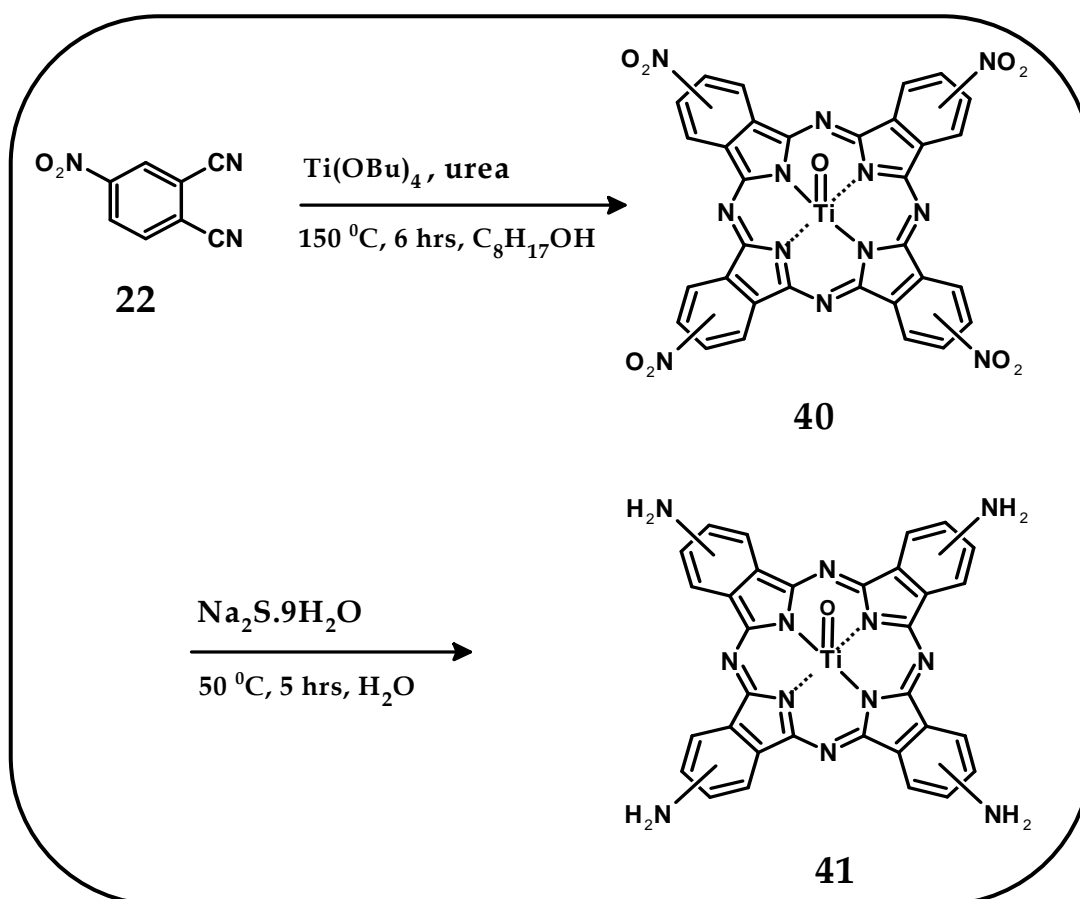
Scheme 3.4: Synthetic routes to α (37a – f) and β (38a – f) tetra-substituted oxotitanium(IV) phthalocyanines used in this work.



Scheme 3.5: Synthetic route to octa-substituted oxotitanium(IV) phthalocyanines used in this work.

The other oxotitanium complexes were however prepared by the cyclisation of the corresponding dinitriles with titanium butoxide in the presence of urea in 1-octanol. The advantage of using titanium butoxide over TiCl_4 is due to the fact that the former avoids the formation of HCl which tends to cleave MPcs and thus higher yields tend to be obtained with this method. Urea was used to prevent possible formation of metal-free phthalocyanines such that a facile MPc formation was achieved. Purification by chromatography and Soxhlet-extraction of impurities resulted in the green to dark-green MPcs with yields ranging from 20 % to 70 %. A major advantage of preparing octa-substituted MPc derivatives is that their chromatographic purification is greatly simplified since a single isomer is expected.

The syntheses of oxotitanium tetranitrophthalocyanine (**40**) and oxotitanium tetraaminophthalocyanine (**41**) have not been reported thus far. A simple procedure was employed to synthesise the nitro-derivatised titanium phthalocyanine (**40**). Generally, 4-nitrophthalic acid is employed in the synthesis of complex **40**, however simple nitro-substituted derivatives of phthalic acids, 1,3-diiminoisoindolines or phthalodinitriles may be employed. Nitration of the phthalocyanine macrocycle may result in its destruction, thus nitro-substituted phthalocyanine complexes are usually obtained from starting compounds containing nitro groups in the molecule. The amino-derivatised complex (**41**) was synthesised in good yields by a facile reduction of complex **40** using sodium sulphide, similar to earlier reports [412], Scheme 3.6.



Scheme 3.6: Synthetic route to tetranitro- and tetraamino-substituted oxotitanium(IV) phthalocyanine used in this work.

3.3.3 IR and $^1\text{H-NMR}$ spectra of the OTiPc complexes

The new complexes were characterised by IR, NMR, MALDI-TOF, elemental analysis and UV/Vis spectra, and were found to be consistent with the predicted structures as shown in the experimental section. The disappearance of the sharp $\text{C}\equiv\text{N}$ stretches confirmed the cyclotetramerisation of the phthalonitriles and the presence of typical $\text{Ti}=\text{O}$ stretches at $\sim 960\text{ cm}^{-1}$ further confirmed the formation of the MPcs, Fig. 3.9.

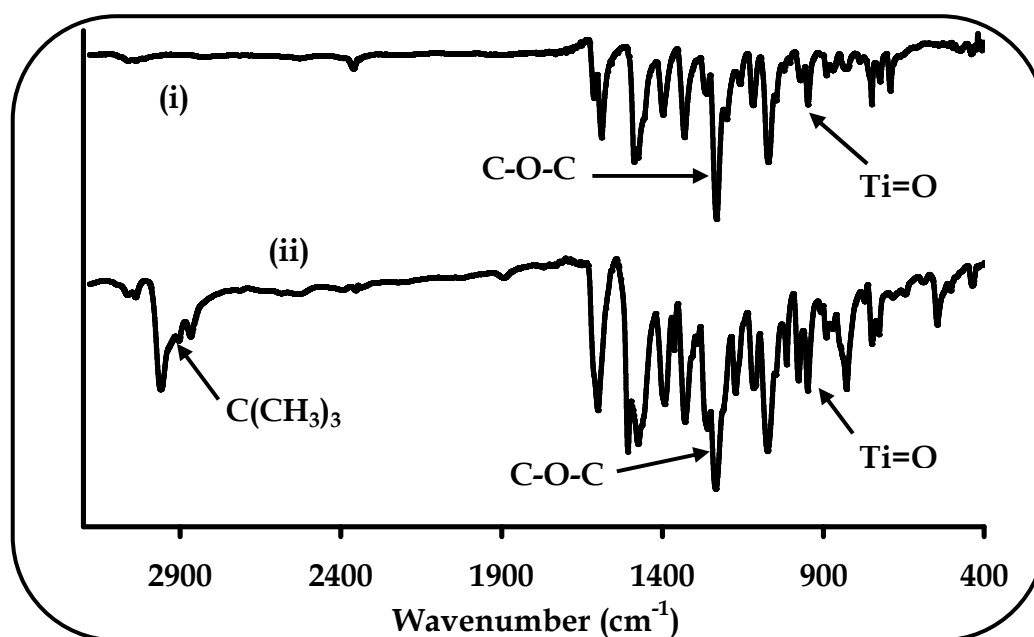


Figure 3.9: IR spectra of complexes (i) 38a and (ii) 37b.

Typical phthalocyanine skeletal vibrations were observed between 400 and 1100 cm^{-1} . The ethereal (C-O-C) and thiol (C-S-C) bands were observed at ~ 1200 and 690 cm^{-1} respectively. Bands at $\sim 3000\text{ cm}^{-1}$ were assigned to 4-*tert*-butyl groups for complexes 37b, 38b and 39b. Characteristic symmetric and asymmetric stretching vibrations of $-\text{NO}_2$ (in complex 40) were observed at 1328 and 1520 cm^{-1} respectively. The disappearance of the nitro stretch at 1328 cm^{-1} following reduction of 40 to 41 was observed and the appearance of the bending and stretching vibration of NH_2 was observed at 3358 cm^{-1} .

The complexes were found to be pure by $^1\text{H-NMR}$ with all the substituents and ring protons observed in their respective regions. The peripherally substituted phenoxy complex **38a** showed different behaviour from other tetra-substituted complexes in that the complex showed more resolved and split bands for the ring, Fig. 3.10. Three sets of resonances were observed between 7.69 ppm and 8.92 ppm each integrating for four protons, thus making a total of 12 protons expected for both peripheral and non-peripheral protons. The more deshielded ring protons between 8.66 and 8.92 ppm were reasonably well-resolved while the least deshielded ring protons at 8.37 – 8.56 ppm and 7.69 – 7.82 ppm resonated as multiplets. This splitting suggested that the two sets of the non-peripheral protons were in different environments.

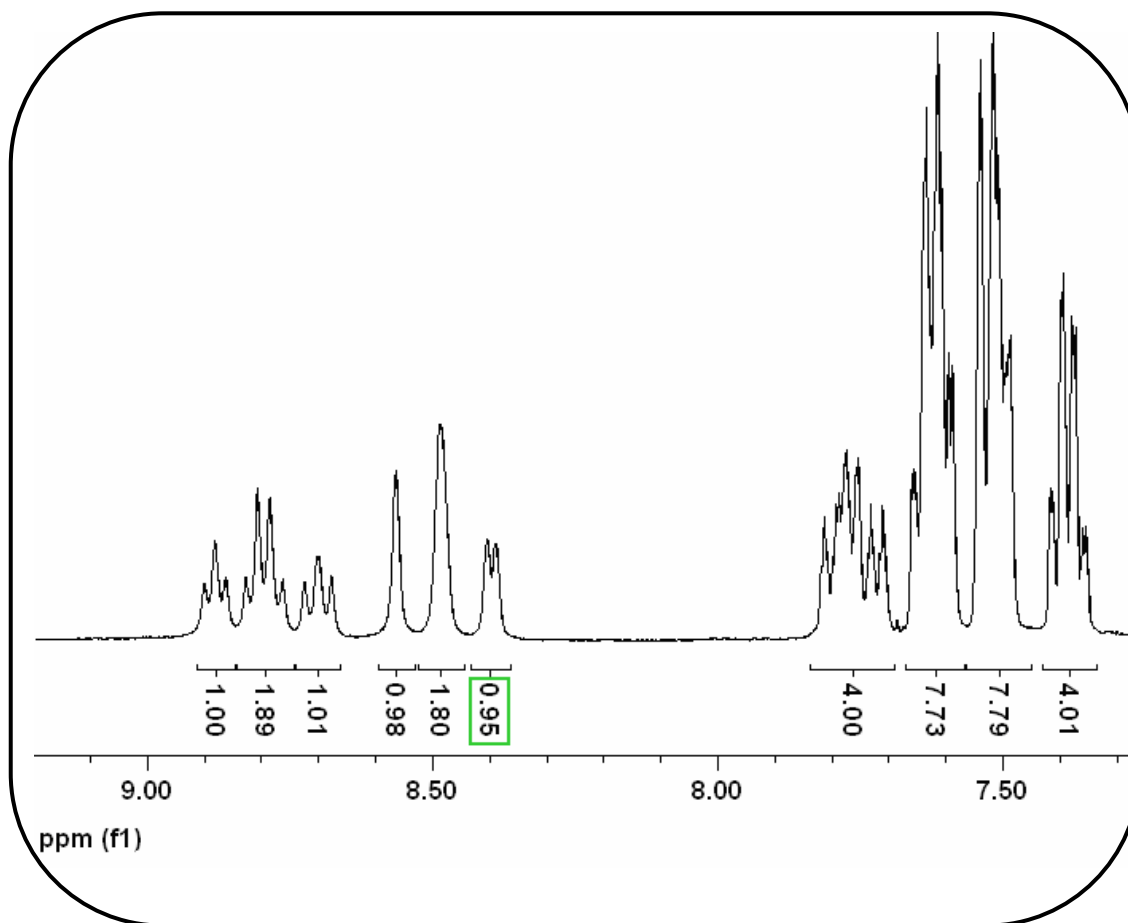


Figure 3.10: $^1\text{H-NMR}$ spectrum of complex **38a** in CDCl_3 .

The non-peripherally substituted phenoxy complex **37a** did not exhibit a similar splitting of bands. Instead the spectrum showed unresolved multiplets between 7.53 ppm and 9.03 ppm however these correctly corresponded to the expected number of protons. The differences in the $^1\text{H-NMR}$ spectra of the phenoxy complexes were most likely to be due to the presence of more isomers in complex **37a** than was the case with complex **38a**, which were probably collected as a single band during purification by chromatography. As is typical with tetra-substituted complexes, both complexes are expected to have positional isomers due to the presence of a single substituent on either two of the peripheral and non-peripheral positions [413,414]. Steric effects which are mostly expected in non-peripherally substituted complexes may play a role. Also lack of symmetry may have caused the split in the $^1\text{H-NMR}$ spectrum of complex **38a**. Moreover, the phenyl ring substituents which integrated for 20 protons were observed at 7.15 - 7.50 ppm and 7.34 - 7.66 ppm for complexes **37a** and **38a** respectively. Unresolved multiplets integrating for a total of 12 protons were observed for the 4-*tert*-butylphenoxy substituted complexes **37b** and **38b**. The ring, phenyl and methyl protons were respectively observed at 7.62 - 9.52 ppm, 7.18 - 7.57 ppm and 1.42 ppm for complex **37b**, whereas they were respectively observed at 8.34 - 8.96 ppm, 7.32 - 7.84 ppm and 1.52 ppm for complex **38b**.

Complexes **37c**, **37d**, **38c** and **38d** were found to exhibit Pc ring and substituent protons at 6.80 - 8.90 ppm, with methylene protons observed at ~ 5.15 ppm. The observed peaks for all the complexes were broad however differentiation between distinct protons of the benzyloxy-substituted complexes **37c** and **38c** was difficult as the observed protons were even more broad. It has been reported that the presence of isomers as well as phthalocyanine aggregation at high concentrations used

for NMR measurements lead to weak and broadened aromatic signals [107,415-417]. Integration of the peaks correctly corresponded to the expected number of protons for each complex, i.e. 40 protons for complexes **37c** and **38c**, and 56 protons for **37d** and **38d**.

The ^1H -NMR spectra of the thiol derivatised tetra-substituted complexes **37e**, **37f**, **38e** and **38f** showed substituent and ring protons between 6.80 – 9.20 ppm, with the methylene protons observed at 4.63 ppm and 4.40 ppm respectively for complexes **37f** and **38f** (see experimental section). The ^1H -NMR spectra of complexes **37e** and **38e** were almost identical and similarly for complexes **37f** and **38f**. However, the protons of the non-peripherally substituted complexes **37e** and **37f** were more deshielded than those of the peripherally substituted complexes **38e** and **38f**. This trend is typical of MPcs with substituents at the α positions and even more so for thiol substituted complexes, compared to the β substituted MPcs [415]. The protons of the phenyl substituents were also deshielded such that their proton signals overlapped with those of the Pc ring.

The ^1H -NMR spectra of complexes **39a** – **d** showed a singlet – as is expected for octa-substituted MPcs - due to the non-peripheral protons integrating for 8 protons between 8.70 and 8.90 ppm. For complexes **39a**, **39c** and **39d** unresolved substituent protons were observed between 7.00 and 7.80 ppm. This was however not the case with complex **39b** because well-resolved substituent protons were observed as doublets at 7.43 ppm (for the deshielded protons nearest the ether bond) and 7.22 ppm, Fig. 3.11. The presence of the bulky 4-*tert*-butyl may have caused the complex to be monomeric even at high concentrations used for NMR measurements. Additionally, 4-*tert*-butyl protons (complex **39b**) integrating for 72 and methylene protons (complex **39c**) integrating for 16 were respectively observed at 1.40 ppm and

5.20 ppm. The relative purity of the complexes was also confirmed since integration of the peaks correctly corresponded to the expected number of protons for each complex in this study.

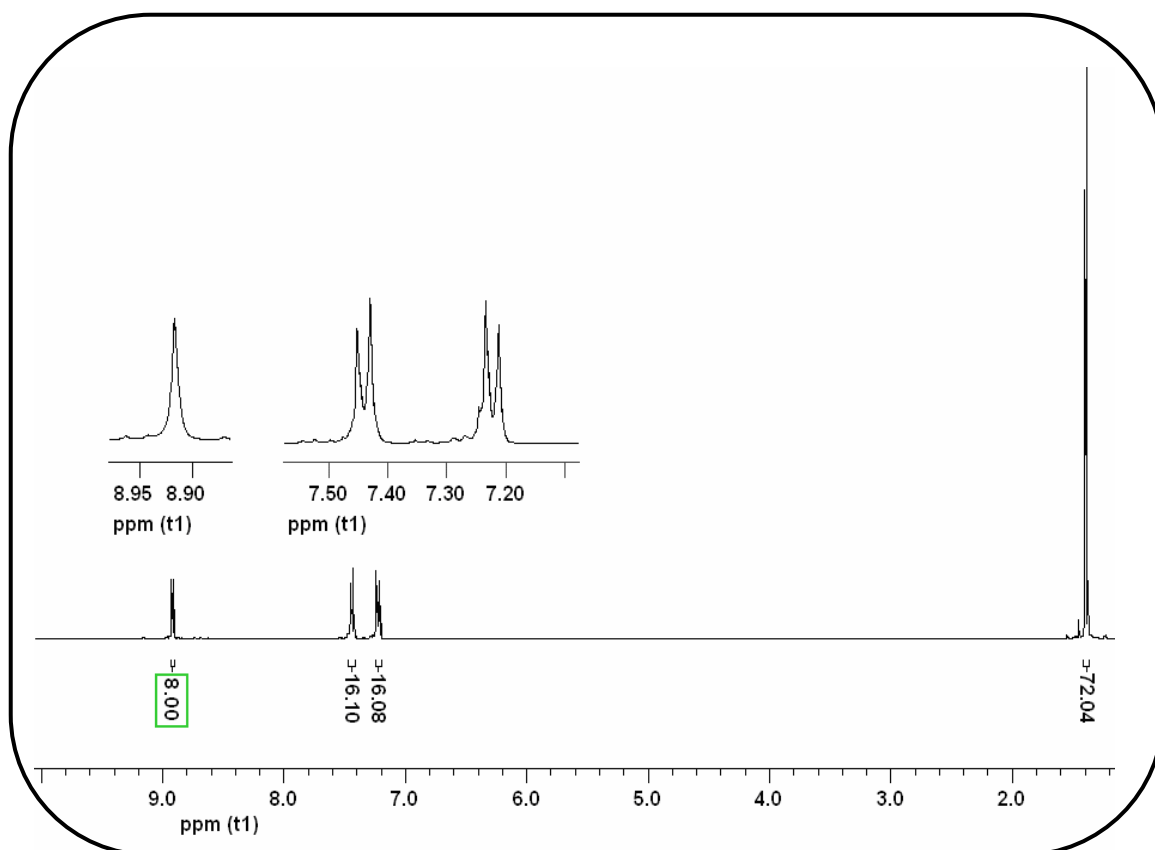


Figure 3.11: ¹H-NMR spectrum of complex 39b in CDCl₃.

The tetraaminophthalocyanine (**41**) was found to be pure by ¹H-NMR with all the substituents and ring protons corresponding to the expected number of protons. The ring protons were observed as multiplets at 8.24 – 9.21 ppm, 7.41 – 8.20 ppm and 6.45 – 7.39 ppm which integrated for five, four and three protons respectively. The multiplets were prevalent due to the presence of positional isomers. Hence a total of twelve protons was obtained as expected for a tetra-substituted phthalocyanine complex. The substituent (amino) protons integrating for eight protons were observed as a singlet at 3.25 ppm.

3.3.4 Ground state electronic absorption spectra

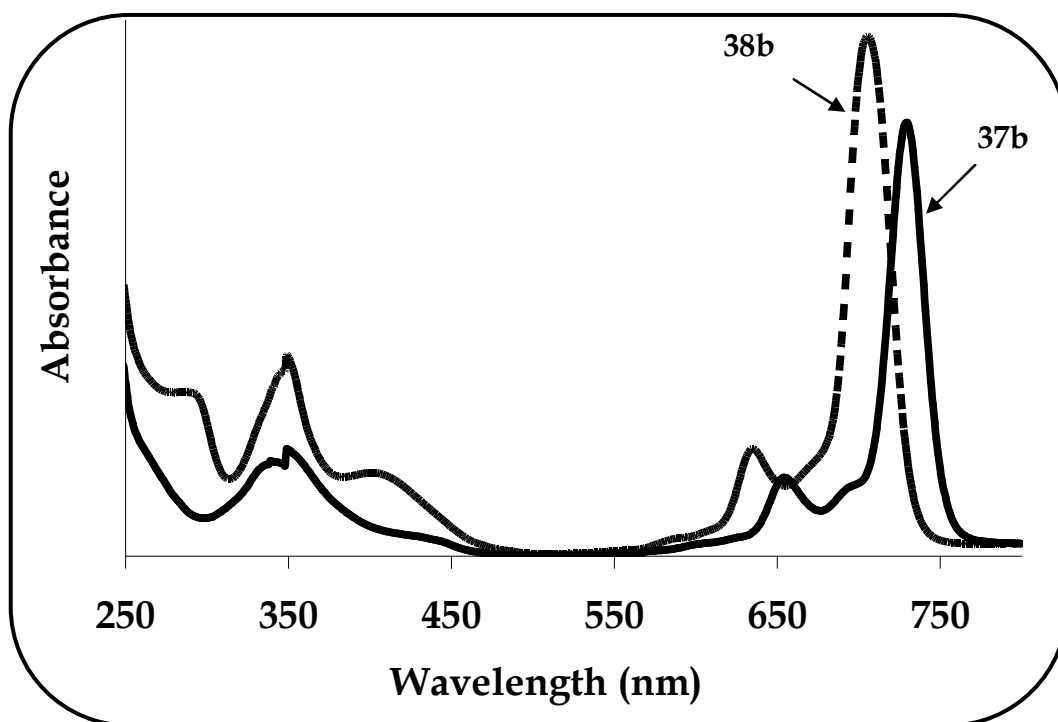
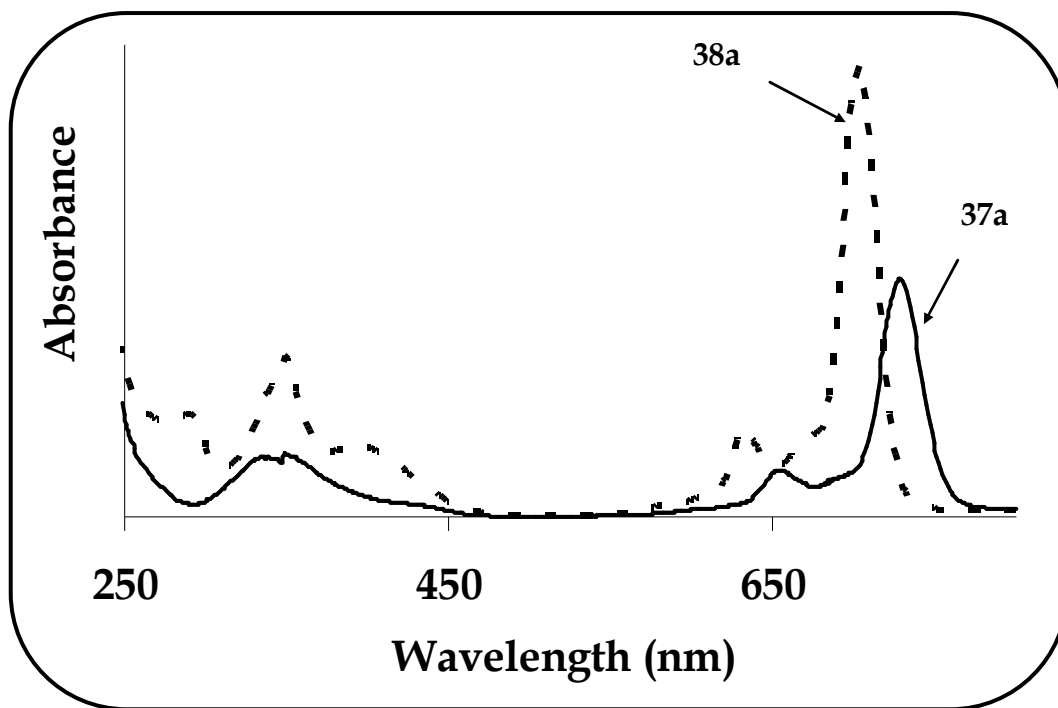
Generally, MPc complexes are insoluble in most organic solvents; however, introduction of substituents on the ring increases the solubility. All tetra-substituted complexes **37** and **38** exhibited excellent solubility in most organic solvents such as DCM, CHCl₃, 1-CNP, THF, toluene, DMSO, DMF, etc. The octa-substituted complexes however, showed better solubility in solvents of weak polarity, i.e. 1-CNP, DCM, CHCl₃ and THF, than in solvents of stronger polarity, e.g. DMSO and DMF (Table 3.6), in which they were sparingly soluble. This behaviour can possibly be related to the symmetric structure of these MPcs since high symmetry decreases the polarity of the ground-state molecule. Moreover, the octa-substituted phthalocyanines are usually less soluble than their corresponding tetra-substituted Pcs due to the formation of isomers and high dipole moments that occur in the latter which result from the unsymmetrical arrangement of the substituents at the periphery [110-112]. Complexes **40** and **41** were however highly soluble in polar solvents such as DMF and DMSO.

Table 3.6: Properties of solvents used to observe UV/Vis spectra of octa-substituted OTiPc complexes.

Solvent	Dipole moment	Dielectric constant
1-Chloronaphthalene (1-CNP)	1.55	5.00
Chloroform (CHCl₃)	1.90	4.81
Dichloromethane (DCM)	1.36	9.08
Tetrahydrofuran (THF)	1.69	7.52
Dimethylformamide (DMF)	37.9	38.2
Dimethylsulphoxide (DMSO)	39.6	47.0

The electronic absorption spectra of the aryloxy complexes (**37a – d** and **38a – d**) in CHCl_3 are shown in Fig. 3.12. Characteristic absorptions due to $\pi\text{-}\pi^*$ transitions in the Q-band region at ~ 700 nm and in the B-band region at ~ 350 nm were observed. The spectra show monomeric behaviour evidenced by a single (narrow) Q-band, typical of metallated MPc complexes [168]. Aggregation in MPc complexes is however typified by a broadened or split Q-band, with the high energy band being due to the aggregate and the low energy band due to the monomer. The Q-band maxima of the complexes are collated in Table 3.7. The Q-bands of the α -substituted complexes (**37a – d**) were red-shifted by ~ 26 nm when compared to the corresponding β -substituted complexes (**38 a – d**).

The observed spectral red-shift is typical of MPc with substituents at the α positions [191,418,419] and has been explained [420,421] to be due to linear combinations of atomic orbitals (LCAO) coefficients at the α (non-peripheral) positions of the HOMO being greater than those at the β (peripheral) positions. As a result, the HOMO level is destabilized more at the α position than it is at the β position. Essentially, the energy gap (ΔE) between the HOMO and LUMO becomes smaller, resulting in a 20 – 30 nm bathochromic shift. Thus substitution at the non-peripheral positions causes an effective shift of the energy of the orbital, such that a diminished HOMO-LUMO gap is obtained, hence a significant red spectral shift was observed.



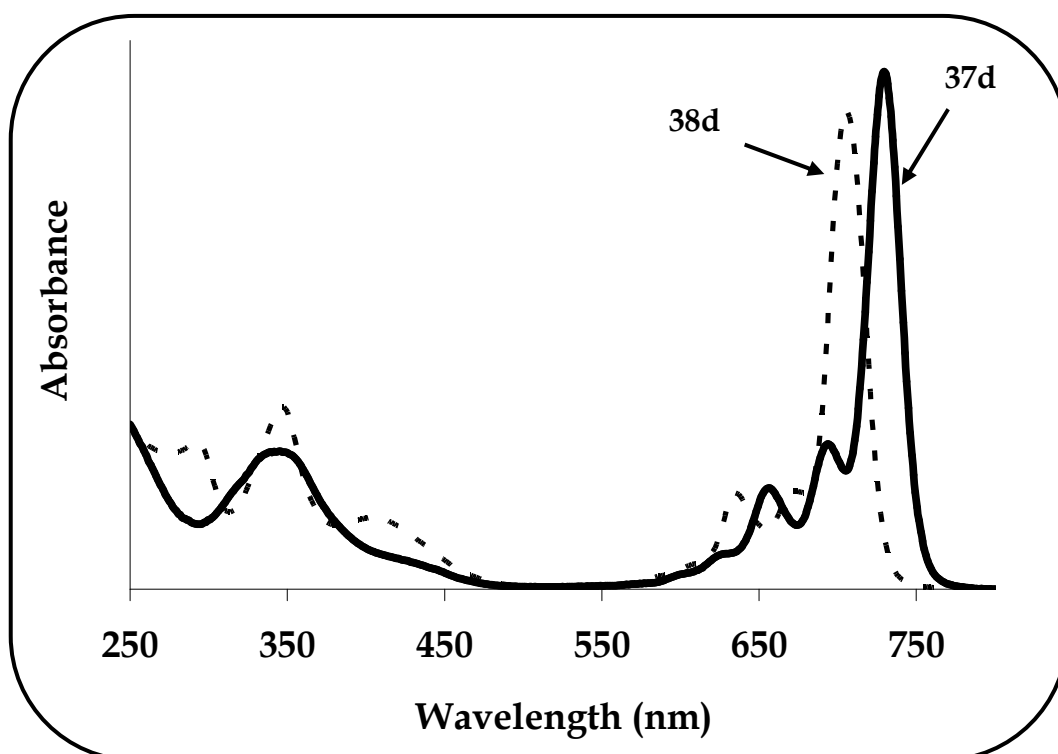
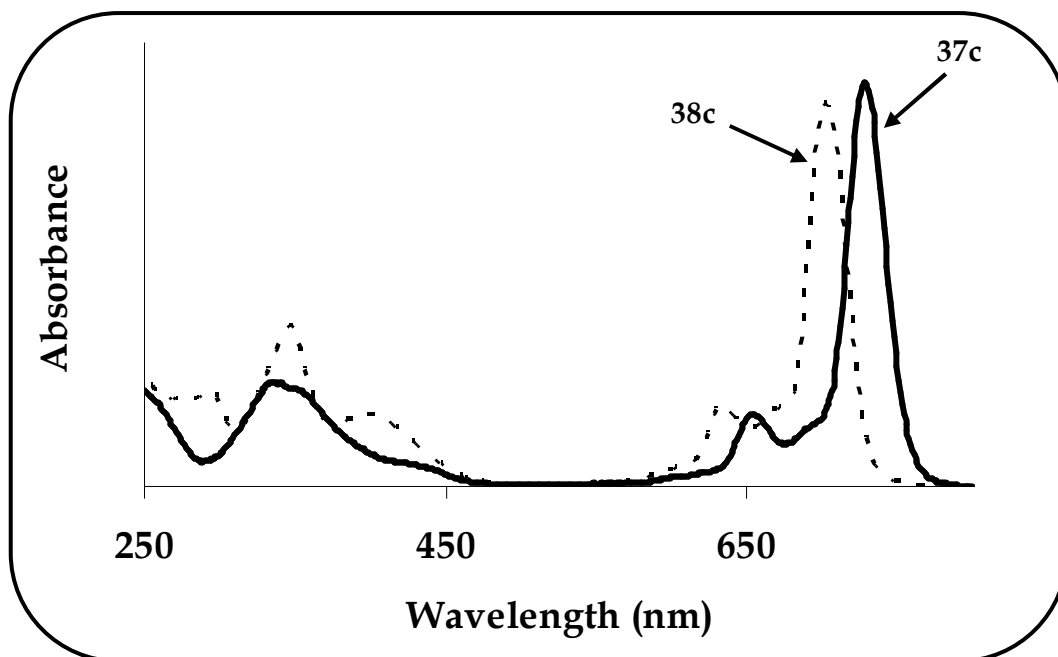


Figure 3.12: UV/Vis spectra of complexes 37a – d and 38a – d in CHCl_3 .
Concentration = 1×10^{-5} M.

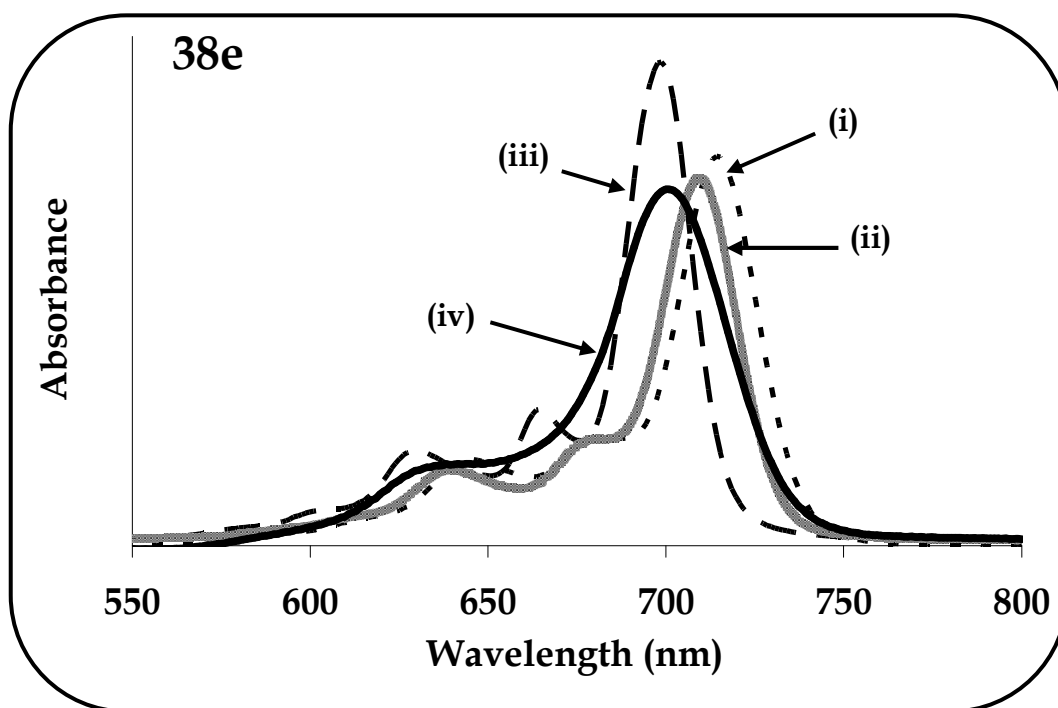
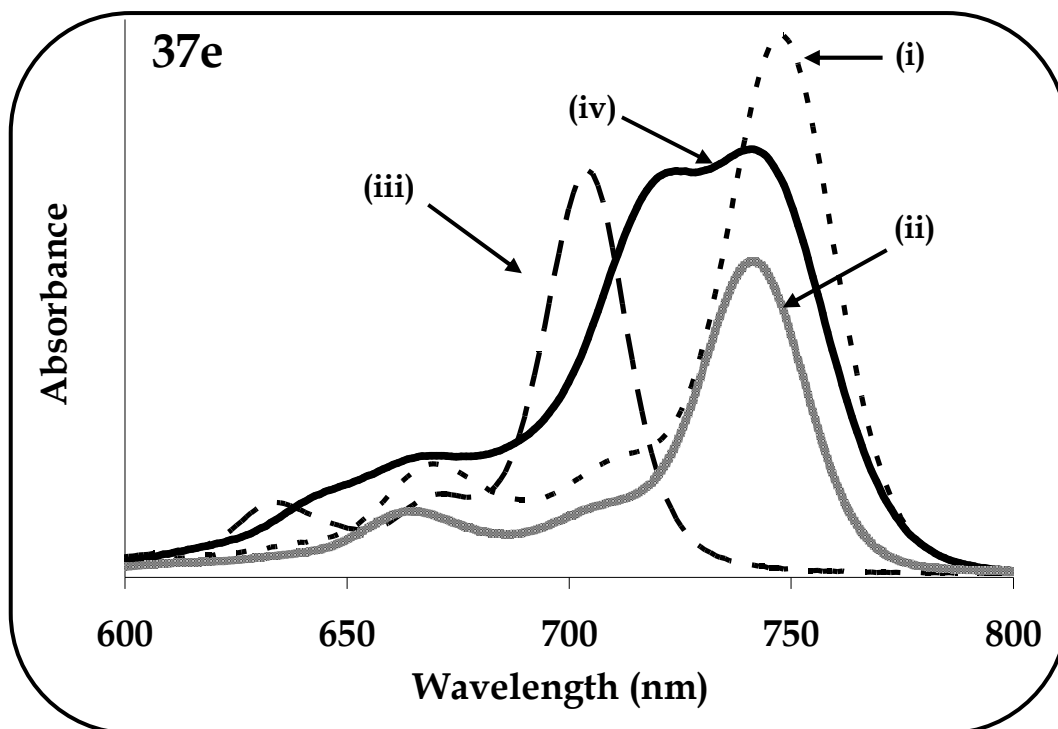
Table 3.7: Q-band spectral data of all the complexes (33-41) in various solvents.

Complex	Solvent	λ_Q / nm (log ϵ)	Complex	Solvent	λ_Q / nm (log ϵ)
33	CHCl ₃	692		THF	741
34	CHCl ₃	697		CHCl ₃	708
35	Methanol	687		DMSO	747 ^a , 705 ^b
	DMSO	694	38e	DCM	714 (5.06)
	PBS 7.4	690		THF	710
36	Methanol	688		CHCl ₃	699
	DMSO	696		DMSO	700
	PBS 7.4	691	38f	DCM	714 (5.19)
37a	CHCl ₃	728 (5.41)		THF	711
37b	CHCl ₃	730 (5.29)		CHCl ₃	700
38a	CHCl ₃	702 (5.21)		DMSO	708
38b	CHCl ₃	704 (5.40)	39a	CHCl ₃	705 (5.44)
37c	CHCl ₃	728 (5.38)		1-CNP	709 (5.08)
37d	CHCl ₃	730 (5.41)	39b	CHCl ₃	703 (5.19)
38c	CHCl ₃	703 (5.21)		1-CNP	710 (5.35)
38d	CHCl ₃	705 (5.24)	39c	CHCl ₃	706 (5.34)
37e	DCM	747 (5.36)		1-CNP	712 (5.38)
	THF	741	39d	CHCl ₃	738 (5.31)
	CHCl ₃	704		1-CNP	742 (5.29)
	DMSO	741 ^a , 721 ^b	40	DMF	705 (5.09)
37f	DCM	745 (5.10)	41	DMF	755 (5.24)

^a aggregated species, ^b monomeric species

Also, the spectra of the complexes exhibited typical B-bands which were broad due to the superimposition of the B₁ and B₂ bands [165]. A broad band between 400 and 450 nm, which is typical of substituted TiPcs [155] and is due to charge transfer from the electron-rich ring to the electron-poor metal, was observed. This charge transfer (CT) band was found to be weaker for the α -substituted complexes whereas a sharper CT band was observed for the corresponding β -substituted derivatives, Fig. 3.12. A rarely observed N-band arising from deeper π levels to LUMO transitions [422,423] was observed at \sim 300 nm, Fig. 3.12. Complexes with 4-*tert*-butylphenoxy and 4-(benzyloxy)phenoxy groups, i.e. **37b**, **37d**, **38b** and **38d**, were red shifted by 2 nm relative to the other complexes since the groups inductively donate protons to the ring. Moreover, insertion of the TiO²⁺ moiety contributed to the red spectral shift, compared to other transition metal phthalocyanines (e.g. CoPc), hence titanyl phthalocyanines are classified as near-infrared absorbing complexes as their Q-bands are generally found between 700 to 850 nm.

The UV/Vis spectra of the thiol derivatised complexes **37e**, **37f**, **38e** and **38f**, shown in Fig. 3.13, were recorded in several solvents as these complexes exhibited interesting properties. In DCM and THF, the spectra exhibited typical B-bands between 330 to 345 nm, and Q-bands in the near infrared between 710 to 750 nm, Table 3.7. Similar to the aryloxy complexes, these arylthio complexes showed charge transfer bands between 400 and 500 nm, as well as superimposed B-bands in the 350 nm region. All the bands were red-shifted relative to the O-substituted phthalocyanines, which is not surprising as sulphur is more electron-donating than oxygen.



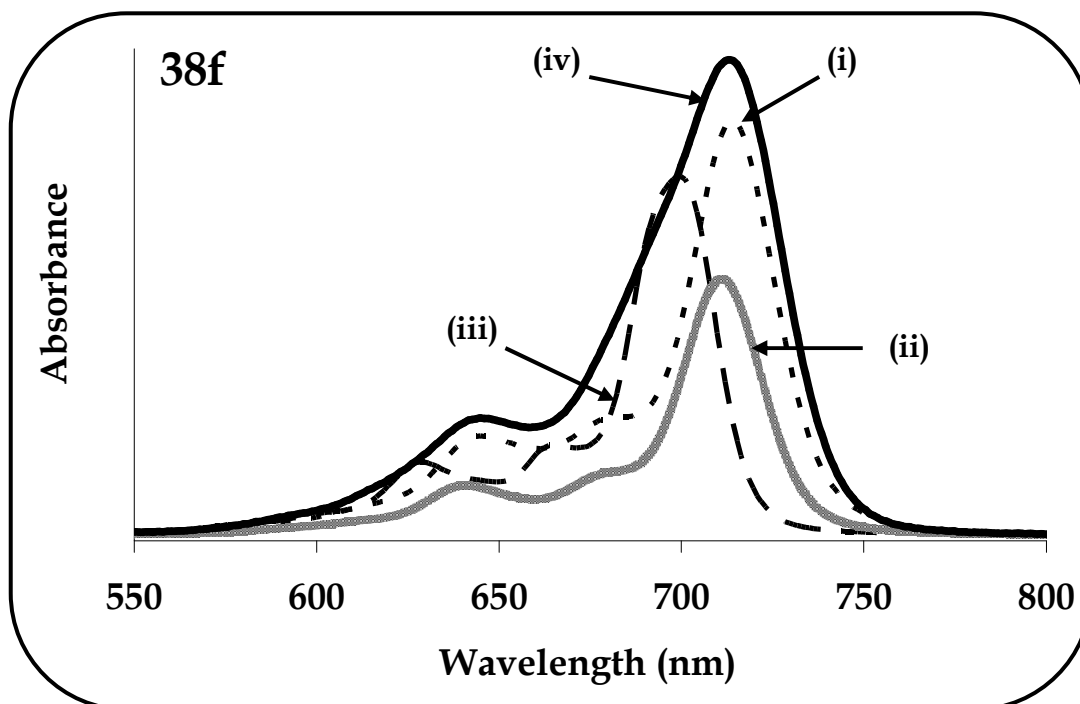
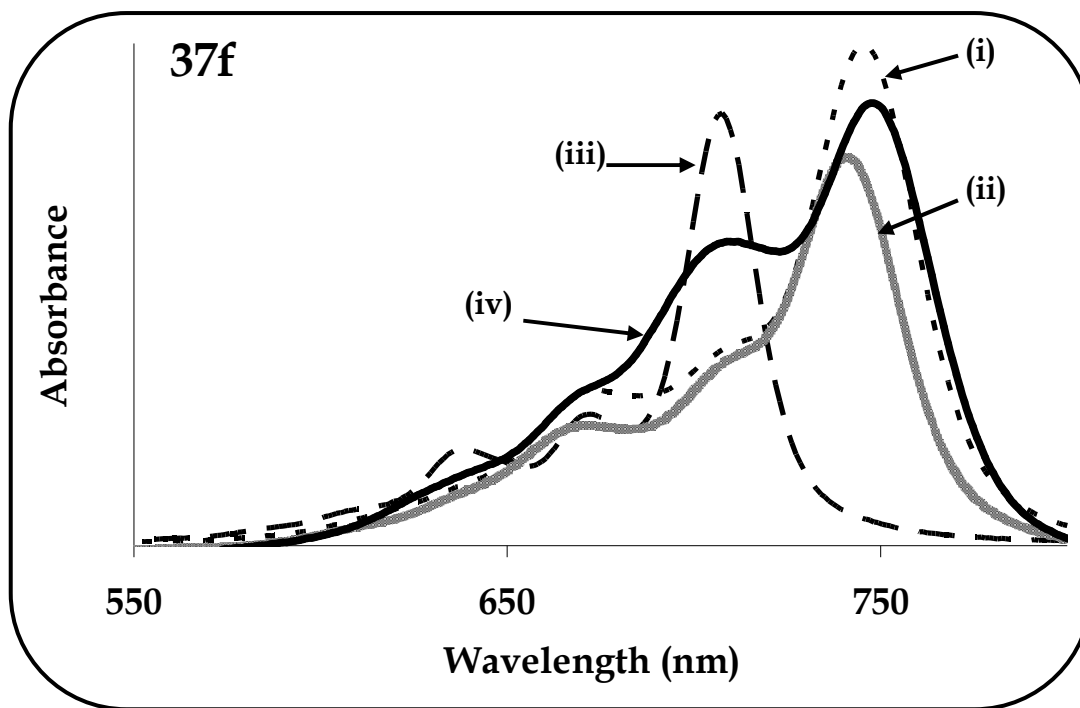


Figure 3.13: UV/Vis spectra of 37e, 37f, 38e and 38f in (i) DCM, (ii) THF, (iii) CHCl_3 and (iv) DMSO. Concentration = 1×10^{-5} M.

Substitution at the α positions (**37e** and **37f**) resulted in ~ 32 nm red shift of the Q-band when compared to the corresponding β -substituted complexes (**38e** and **38f**), Table 3.7. In general, significant bathochromic shifts into the near infrared region of the spectrum occur in the presence of electron-donating groups. As earlier mentioned, the effect is more pronounced when the electron-donating substituents are at the non-peripheral (α) position and less pronounced for most peripherally (β) substituted complexes. In CHCl_3 , the colour of the complexes changed from deep green (in DCM) to blue. The Q-bands were blue-shifted by ~ 40 nm (**37e** and **37f**) and by ~ 14 nm (**38e** and **38f**) in CHCl_3 relative to the spectra observed in DCM. It has been reported that a decrease in the polarity of non-coordinating solvents results in the blue-shifted Q-band positions [154], hence the spectra were blue shifted in the less polar CHCl_3 than was the case in DCM.

In DMSO, the non-peripherally substituted complexes (**37e** and **37f**) exhibited split Q-bands at 721 and 741 nm for **37e** and 705 and 747 nm for **37f**, Table 3.7. A slightly broadened single Q-band for the peripherally substituted complexes was observed, Fig. 3.13. The difference in the spectra at peripheral versus non-peripheral is not surprising since it is known that the effects of non-peripheral substitution on Pc Q-band position are larger than those at peripheral substitution [173]. Broadening of the Q-band and appearance of new peaks in the Q-band region is associated with aggregation in MPc complexes [424]. DMSO which normally prevents aggregation [425], is a strong coordinating solvent with a high donor number [426] and is able to coordinate to most central metals of porphyrins and phthalocyanines through either the sulphur or the oxygen atoms [404]. Thus aggregation should be more enhanced in the non-coordinating

solvents such as DCM than in DMSO. However, this was not the case in this work.

As expected, dilution tends to disaggregate neighbouring Pc rings. Dilution of DMSO solutions of complexes **37e** and **37f** (Fig. 3.14) to concentrations lower than 1×10^{-5} M showed more decrease in the low energy band (741 nm) relative to the high energy band (721 nm) suggesting that the former was due to aggregated species. Generally in MPc complexes, the peak due to aggregation is blue shifted with respect to the monomer. However a less common type of aggregation in solution (called the J-aggregation) results in a red-shifted peak [427]. Thus the observation of a decrease in the low energy peak on dilution suggested the presence of the J-aggregate. This suggested that the observed broadening or presence of extra peaks for complexes in DMSO was due to aggregation.

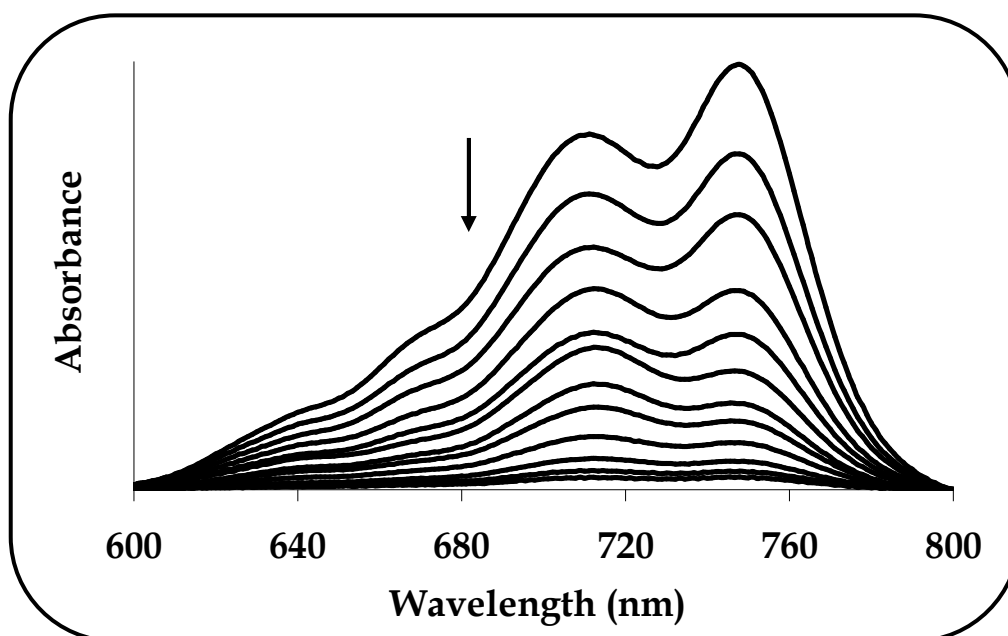


Figure 3.14: UV/Vis spectra of **37f** in DMSO upon decreasing the concentration. Starting concentration = 1.4×10^{-5} M.

The UV/Vis spectra of the ground state electronic absorptions of the octa-substituted complexes under study, in 1-CNP, were also typical of monomeric MPc complexes with characteristic Q-bands and B-bands due to π - π^* transitions, Fig. 3.15. The complexes with aryloxy groups, i.e. **39a** – **c** did not bring about significant Q-band shifts. Substitution by a thiol group however resulted in a significant shift of the Q-band of complex **39d** to deeper red relative to complexes **39a** – **c** which is not surprising as sulphur is more electron-donating than oxygen.

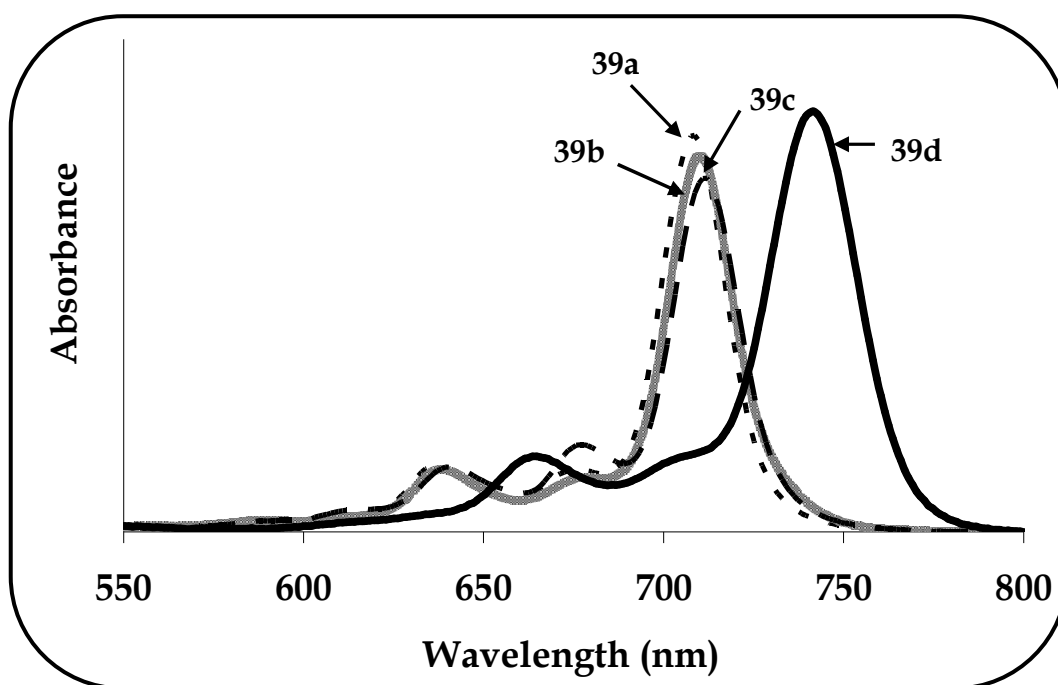


Figure 3.15: Ground state absorption spectra of complexes **39a** – **d** in 1-CNP. Concentration = $\sim 1 \times 10^{-5}$ M.

Figure 3.16 shows UV/Vis spectra typical of nitro and amino phthalocyanine complexes with the Q-bands observed at 705 nm and 755 nm for complexes **40** (Fig. 3.16(i)) and **41** (Fig. 3.16(ii)) respectively. The red-shift observed with complex **41** was as a result of the electron-donating ability of the amino groups while the electron-withdrawing nitro groups effectuate a blue-shift. The effect of substitution is even

more obvious in comparison with the unsubstituted OTiPc derivative (**33**) which exhibits a Q-band at 693 nm. Also the DMF solution of the amino complex was unusually reddish-brown, similar to that of the red-shifted manganese tetraaminophthalocyanine complex which exhibited a Q-band at 800 nm [428]. In addition, a broad band at ~ 450 nm due to ligand-to-metal charge-transfer was observed for complex **41** as opposed to complex **40** which did not exhibit this band. The reddish-brown DMF solution of complex **41** is as a result of the charge-transfer band observed at ~ 450 nm, since the Q-band which generally gives phthalocyanines their green colour, is now “transparent”. Furthermore, the Q-bands of both complexes were broadened, an indication that the complexes were aggregated due to the configurational interaction between phthalocyanine molecules.

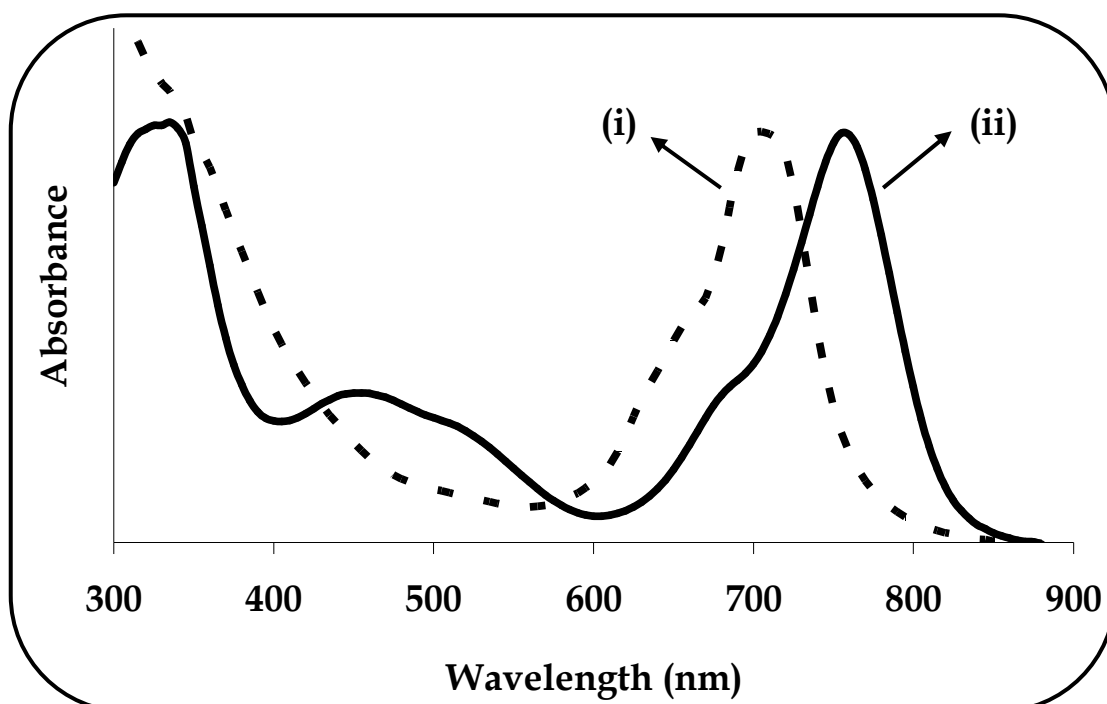


Figure 3.16: UV/Vis spectra of (i) OTiPc(NO₂)₄ (**40**) and (ii) OTiPc(NH₂)₄ (**41**) in DMF. Concentration $\sim 10^{-5}$ M.

3.4 Conclusion

Unsubstituted titanium (**33**) and tantalum (**34**) phthalocyanines were synthesised and sulphonated to obtain the first differently sulphonated complexes **35** and **36** respectively. The latter complexes formed ion-pairs with the cation acceptor, methyl viologen, with stronger interactions observed for complex **36**. Furthermore, soluble **37a – f**, **38a – f**, **39a – d**, nitro- and amino-derivatised oxotitanium complexes **40** and **41**, substituted in the 1,(4)-, 2,(3) or octa (peripheral) positions; were newly synthesised. The complexes are the first examples of aryloxy-, arylthio-, nitro- and amino-substituted oxotitanium phthalocyanine complexes. These complexes were characterised by spectroscopic methods and exhibited interesting properties. Also, the solubilities of these complexes in different solvents effectuate their possible use in various applications such as photocatalysis and electrochemistry. In addition, substitution with sulphur and amino groups, as well as the presence of the titanyl moiety resulted in larger bathochromic shifts. Therefore complexes that absorb in the near-IR range were obtained.

CHAPTER 4

Photochemical,

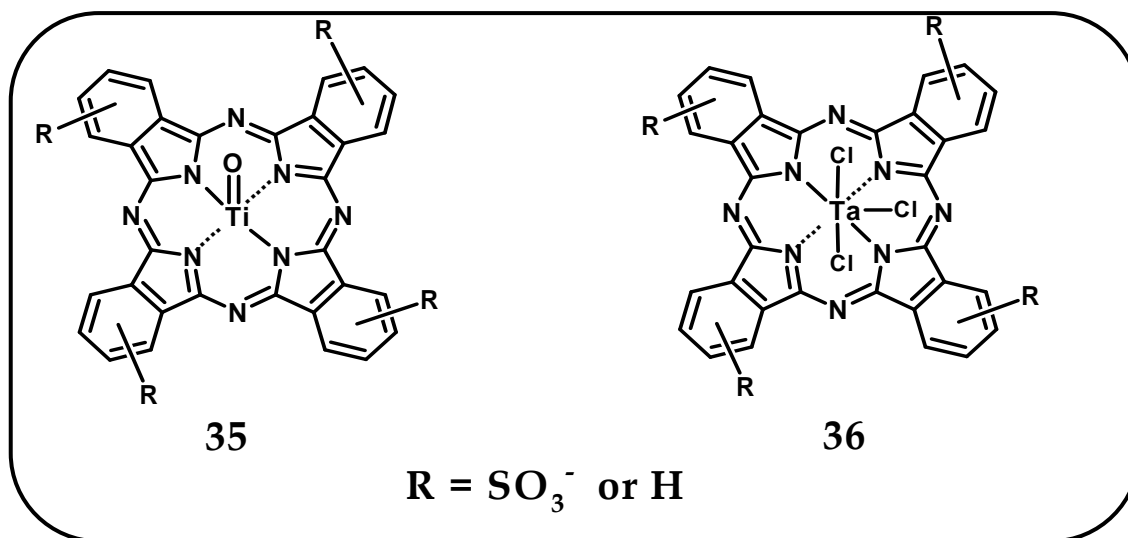
Photophysical

and

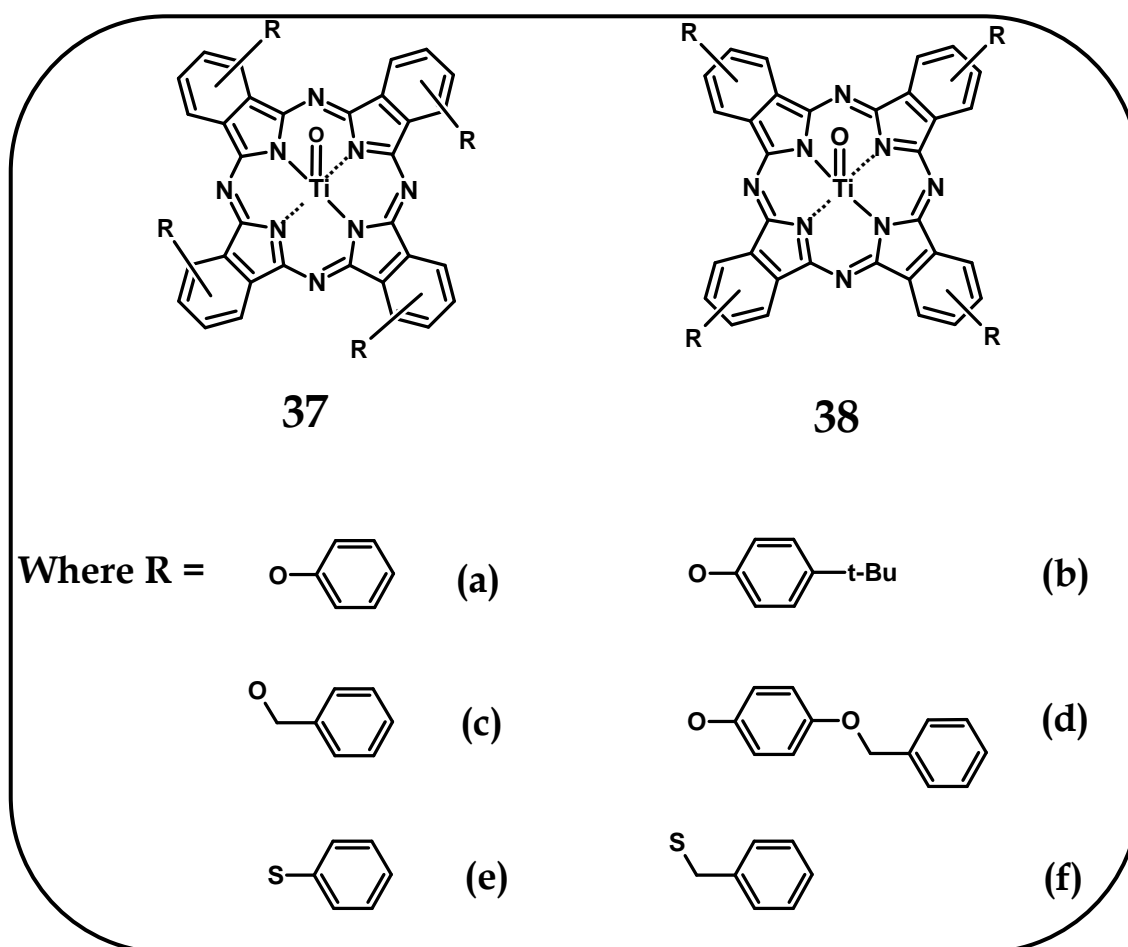
Photocatalytic

properties

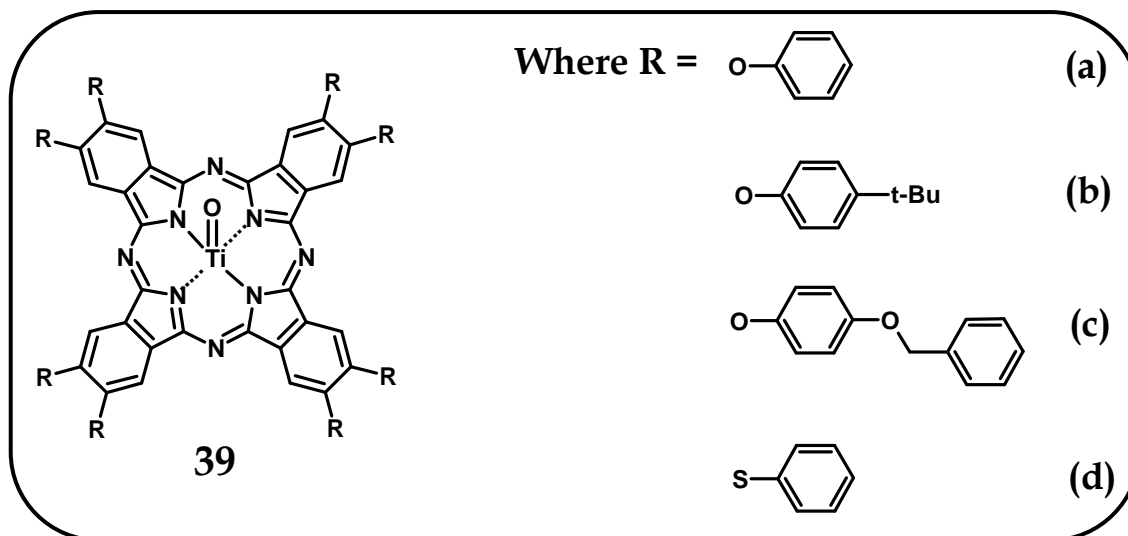
The structures of the MPCs employed are provided again for the convenience of the reader.



Structures of OTiPcS_n (35) and Cl₃TaPcS_n (36) used in this study



Tetra-substituted aryloxy and arylthio OTiPc complexes in this study



Octa-substituted OTiPc complexes in this study

This chapter deals with the photochemical and photophysical properties of the synthesised complexes. A selected number of OTiPcs are also investigated for their photocatalytic efficiency towards the transformation of 1-hexene to useful products.

4.1 Photochemical processes

4.1.1 Singlet oxygen

Singlet oxygen quantum yields are a measure of a photosensitiser's ability to generate singlet oxygen. Determination of singlet oxygen quantum yields, Φ_{Δ} , involved use of DPBF as a singlet oxygen quencher. The quantum yields for singlet oxygen, using the complexes under study, are presented in Table 4.1. Following irradiation of MPc with light at an appropriate wavelength, energy ($h\nu$) is absorbed and subsequently excitation from the singlet ground state to the singlet excited state to produce $^1\text{MPc}^*$ occurs followed by ISC to form $^3\text{MPc}^*$. A triplet-triplet energy transfer from $^3\text{MPc}^*$ to triplet oxygen, results in the formation of the energetically rich and chemically more reactive singlet oxygen ($^1\text{O}_2$). The generation of singlet oxygen by the OTiPc complexes was determined in DMSO for the tetra-substituted complexes **37a – f** and **38a – f** or in 1-CNP for the octa-substituted complexes **39a – d** in the presence of DPBF as chemical singlet oxygen quencher. 1-CNP is employed for the latter complexes since they are sparingly soluble in DMSO. Upon irradiation with light, the decay of DPBF was monitored spectrophotometrically at $\lambda = 416$ nm since the rate of singlet oxygen generation is directly proportional to the rate of DPBF bleaching. Subsequently, the Q-band intensity of each complex was not degraded during the Φ_{Δ} determinations, Fig. 4.1, since the intensity of light was low enough

not to affect the MPCs. Typical spectral changes observed during the photolysis of complex **37a** are shown in Fig. 4.1.

Table 4.1: DPBF (Φ_{DPBF}), singlet oxygen (Φ_{Δ}) and photobleaching (Φ_P) quantum yields of the complexes under study in DMSO.

Complex	Φ_{DPBF}	Φ_{Δ}	$\Phi_P (10^4)$
37a	0.51	0.52	6.2
37b	0.56	0.54	6.5
37c	0.53	0.50	6.7
37d	0.59	0.56	6.8
37e	0.30	0.28	7.5
37f	0.29	0.39	7.7
38a	0.60	0.65	3.2
38b	0.49	0.67	3.1
38c	0.55	0.64	4.0
38d	0.58	0.70	3.8
38e	0.49	0.77	5.5
38f	0.53	0.75	5.6
39a^a	0.53	0.32	28.1
39b^a	0.42	0.40	30.3
39c^a	0.47	0.38	31.9
39d^a	0.50	0.29	42.0

^a 1-CNP used as solvent

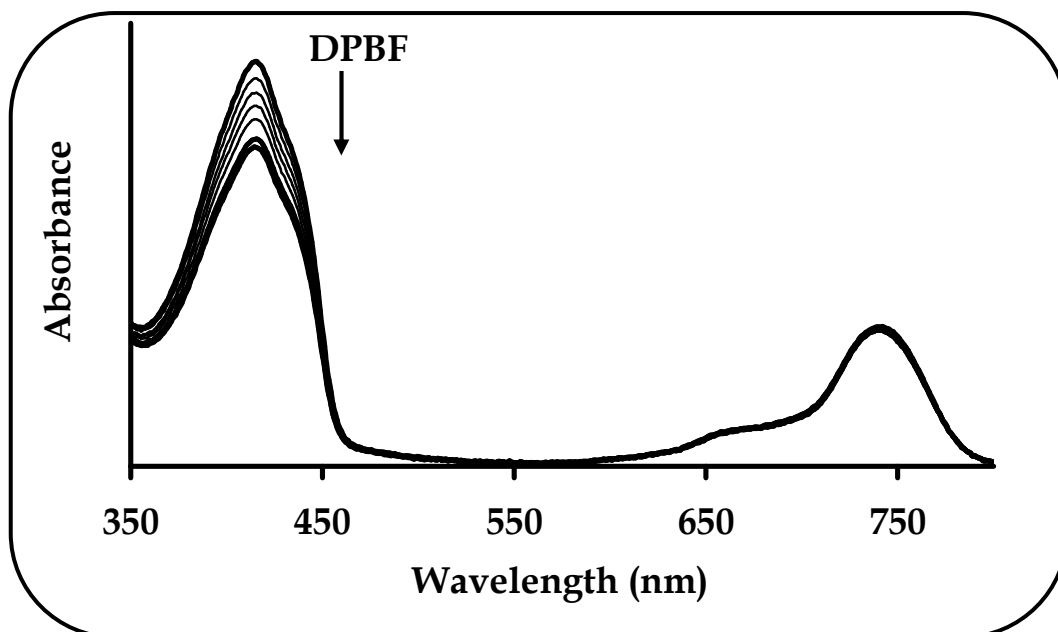


Figure 4.1: Spectral changes observed during irradiation of complex **37a** in the presence of DPBF, in DMSO, for singlet oxygen quantum yield determination. Starting $[DPBF] = 2.9 \times 10^{-5} \text{ M}$ and $[MPc] = 2.4 \times 10^{-6} \text{ M}$.

The singlet oxygen quantum yields were calculated by firstly determining the DPBF quantum yields (Eq. 1.5) which were further used in Eq. 4.1 (same as Eq. 1.7).

$$\frac{1}{\Phi_{DPBF}} = \frac{1}{\Phi_{\Delta}} + \frac{1}{\Phi_{\Delta}} \cdot \frac{k_d}{k_q} \cdot \frac{1}{[DPBF]} \quad (4.1)$$

The complexes exhibited relatively high singlet oxygen quantum yields, ranging from 0.28 to 0.77 in DMSO (Table 4.1). It can be seen that the quantum yields were high due to the presence of the electron donating groups. The Φ_{Δ} values for the peripherally tetra-substituted complexes (**38**) were slightly higher than those of the non-peripherally tetra-substituted derivatives (**37**). Additionally, the Φ_{Δ} values of the arylthio-substituted complexes at the peripheral positions (**38e** and **38f** with $\Phi_{\Delta} = 0.77$ and 0.75 respectively) were much larger than those of the non-peripherally substituted complexes (**37e** and **37f** with $\Phi_{\Delta} = 0.28$ and 0.39 respectively), Table 4.1. The high quantum yields of **38e** and **38f** were a reflection of the monomeric nature of

the complexes in DMSO. This was however not the case with the non-peripherally substituted arylthio complexes **37e** and **37f** which were earlier explained to be aggregated in DMSO. Aggregation lowers the Φ_{Δ} values through energy dissipation of the excited state; hence lower Φ_{Δ} values of complexes **37e** and **37f** were obtained. Moreover, the β -substituted arylthio complexes **38e** and **38f** exhibited the largest quantum yields due to the presence of the heavier sulphur atoms which may promote ISC to yield higher Φ_{Δ} values. Overall, the complexes exhibited singlet oxygen quantum yields that were comparable to those in literature [429].

For the octa-substituted complexes, the singlet oxygen quantum yields were determined in 1-CNP, since the complexes were sparingly soluble in DMSO. The observed Φ_{Δ} values were lower as a result of the formation of radicals following irradiation in 1-CNP, which are prevalent in chlorinated solvents. This is a disadvantage in that DPBF has the ability to react with both radicals and singlet oxygen, hence the lower Φ_{Δ} values.

4.1.2 Photobleaching

The degradation of the OTiPc complexes was studied in DMSO (or 1-CNP for complexes **39**) following photolysis in the Q-band region over time. The reduction in the Q-band intensity is indicative of the photobleaching process and can thus be monitored by UV/Vis spectroscopy. Typical spectral changes observed during clean photobleaching of the macrocycles without any transformation are shown in Fig. 4.2. Photobleaching studies were undertaken in order to determine the stability of the complexes in the presence of light. The photostabilities were also determined in order to determine the effect of the substituents on the stability of the complexes, which is

an important property in photocatalysis. These spectral changes were observed for all complexes as a result of the oxidative attack of the singlet oxygen generated by the complexes, Scheme 1.13.

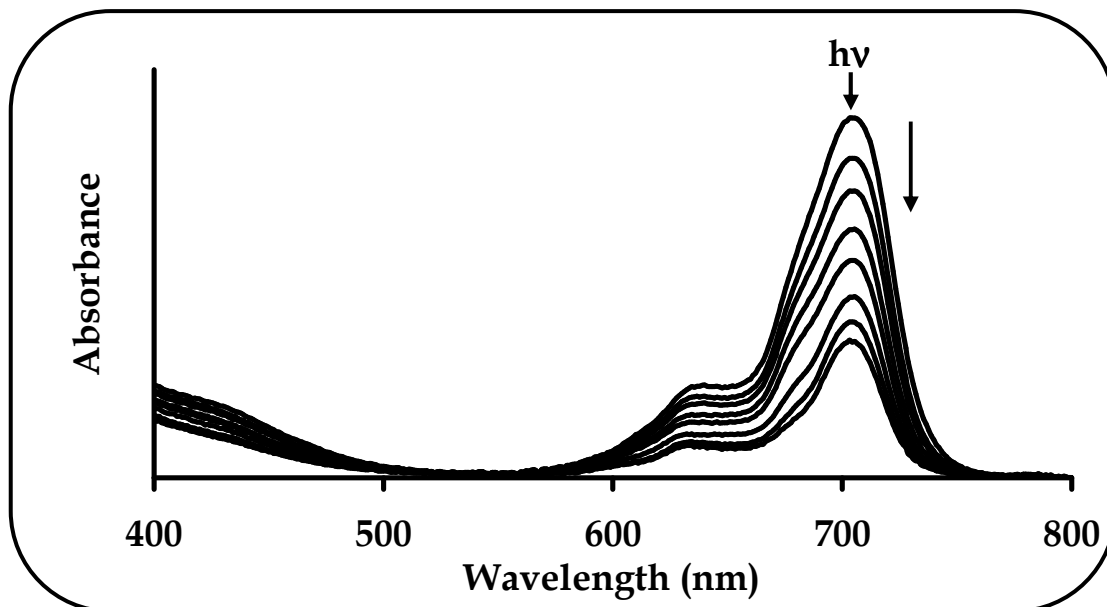


Figure 4.2: UV/Vis spectral changes of complex 38a in DMSO, following irradiation in the Q-band region. Starting [MPc] = 1.5×10^{-5} M.

The measure of the stability of the macrocycles is determined by the magnitude of the photobleaching quantum yield, Φ_p , which was determined by Eq. 1.8, given here as Eq. 4.2:

$$\Phi_p = \frac{(C_0 - C_t)V}{t \cdot I_{abs}} \quad (4.2)$$

The Φ_p values of the complexes are presented in Table 4.1 and were found to be of the order of 10^{-4} . Smaller Φ_p values correspond to high complex stability. Electron donating groups tend to accelerate the photobleaching process by making the macrocycles easier to oxidise. The arylthio complexes (**37e**, **37f**, **38e** and **38f**) were less stable than the corresponding aryloxy complexes (**37a**, **37c**, **38a** and **38c**) since

thiols are more electron-donating than oxygen containing groups. Additionally the non-peripherally substituted complexes **37a – f** were found to be less stable than the peripherally substituted derivatives because the latter have a more stabilising effect than the former.

The octa-substituted complexes **39a – d**; were however found to be even less stable, although this was expected because of the nature of the solvent, i.e. 1-CNP. The radicals formed from C-Cl bond cleavage accelerated the photobleaching rate and hence the low stability. Also, singlet oxygen has been reported to be long-lived in less polar solvents [430], and hence the probability of photobleaching in 1-CNP (dielectric constant = 5.00) would be high as opposed to DMSO (dielectric constant = 47.0), Table 3.6. There is a possibility that stabilisation in DMSO is effectuated by interaction of the S atom in DMSO with the nitrogen bridges of the Pc ring. Therefore a partial back-polarisation of π -electrons inside the macrocycle may result, thus strengthening the C-N bonds which link the benzopyrrole units of the ring. In DMSO, stabilisation is brought about by protection of these N-bridges from attack, since these are the weakest points of the Pc ring.

4.2 Photophysical processes

4.2.1 Fluorescence properties

The excitation and fluorescence spectra of complex **39a** obtained in 1-CNP, are typical of monomeric MPcs and are shown in Fig. 4.3. Those of the other complexes were obtained in DMSO. The excitation spectra of all the complexes (except complexes **37e** and **37f**) were similar to the absorption spectra and both were mirror images of their fluorescence spectra.

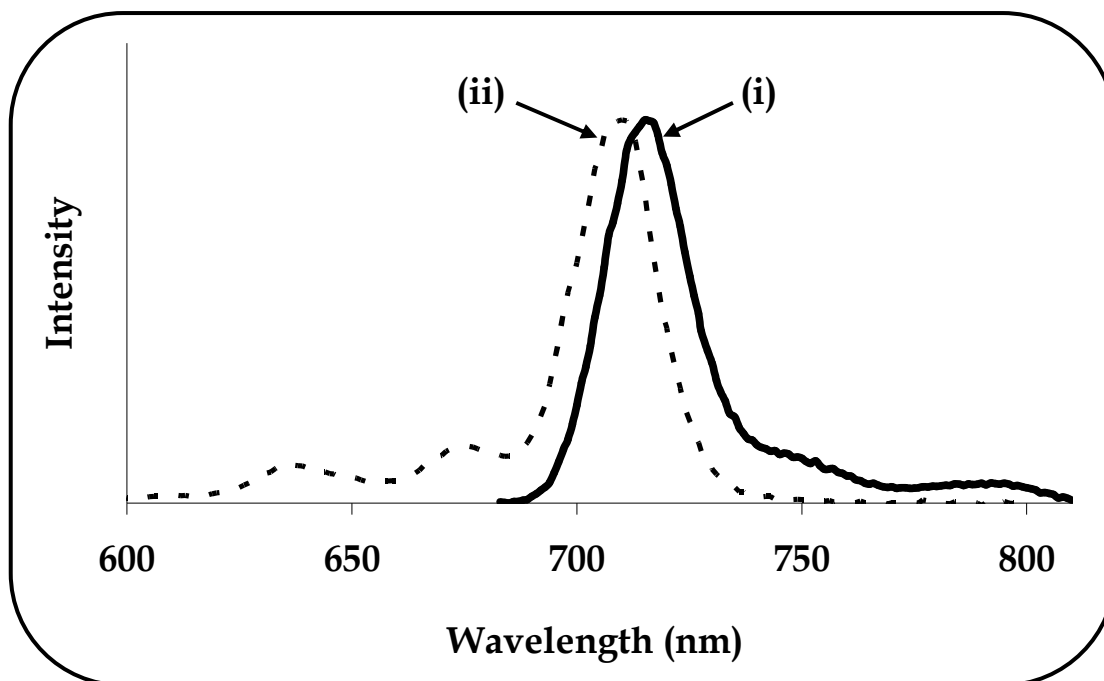


Figure 4.3: Normalised fluorescence emission (i) and excitation (ii) spectra of complex 39a in 1-CNP. $[MPC] = 1.0 \times 10^{-7} M$

Stokes shifts of less than 10 nm, typical of MPC complexes were observed, suggesting that the nuclear configurations of the ground and excited states were similar and not affected by excitation. The fluorescence quantum yields - determined from Eq. 4.3 (same as Eq. 1.11) - were within the range for MPC complexes [431] depending on their substituents (i.e. 0.03 to 0.42) and are listed in Table 4.2.

$$\Phi_F = \Phi_{F(std)} \frac{F \cdot A_{std} \cdot \eta^2}{F_{std} \cdot A \cdot \eta_{std}^2} \quad (4.3)$$

Table 4.2: Photophysical parameters, i.e. fluorescence (Φ_F) and triplet quantum yields (Φ_T) as well as fluorescence (τ_F) and triplet lifetimes (τ_T) of the complexes under study in DMSO, unless otherwise stated

Complexes^a	λ_Q^b /nm	λ_F^b /nm	λ_E^b /nm	Φ_F	τ_N /ns	τ_F /ns	Φ_T	τ_T /μs
35 (CH₃OH)	687	693	652,688	0.18	19.5	3.51	^c	^d
35	694	695	695	0.42	14.7	6.17	0.31	660
35 (PBS 7.4)	690	679	677	0.03	25.1	0.75	^c	^d
36 (CH₃OH)	688	678	674	0.22	17.3	3.81	^c	^d
36	696	688	680	0.18	26.2	4.72	0.62	280
36 (PBS 7.4)	691	680	679	0.15	19.4	2.91	^c	^d
37a	720	725	721	0.18	26.3	4.73	0.62	180
37b	722	728	722	0.19	25.7	4.88	0.59	200
37c	723	730	725	0.17	29.8	5.07	0.56	190
37d	726	733	729	0.16	27.1	4.34	0.58	190
37e	741^e,721^f	758,725	742,722	0.05	1.38	0.07	0.38	150
37f	747^e,705^f	758,720	750,706	0.07	1.42	0.10	0.50	150
38a	698	701	699	0.15	27.7	4.16	0.66	220
38b	700	706	702	0.18	28.2	5.08	0.70	250
38c	701	709	701	0.18	29.4	5.29	0.72	230
38d	703	711	706	0.17	26.8	4.56	0.75	210
38e	700	725	702	0.11	28.3	3.11	0.82	210
38f	708	726	710	0.14	25.7	3.60	0.70	200

Table 4.2 continued

Complexes ^a	λ_Q ^b /nm	λ_F ^b /nm	λ_E ^b /nm	Φ_F	τ_N /ns	τ_F /ns	Φ_T	τ_T / μ s
39a (1-CNP)	709	715,	710,	0.16	7.65	1.22	0.23	40
39b (1-CNP)	710	717	711	0.17	3.79	0.64	0.56	100
39c (1-CNP)	712	716	712	0.19	4.26	0.81	0.45	60
39d (1-CNP)	742	745	740	0.14	4.39	0.61	0.13	70

^a solvents in brackets, ^b λ_Q , λ_F , λ_E = ground state Q-band, fluorescence and excitation wavelengths; τ_N = natural lifetime, ^c not determined due to lack of standards, ^d not determined, ^e aggregated species, ^f monomeric species.

As was earlier stated, complexes **37e** and **37f** showed split Q bands in DMSO. Excitation for these complexes was performed at both Q band peaks. Although the excitation spectra of the other complexes were similar to their absorption spectra, those of complexes **37e** and **37f** were dependent on the wavelength of excitation. The excitation spectra of complex **37e** on excitation at the monomer peak (721 nm, trace i) and the peak due to the aggregate (741 nm, trace ii) are shown in Fig. 4.4. The excitation spectra at both wavelengths were different from the absorption spectra in that a single Q-band was observed instead of a split Q-band observed in absorption. This showed that two species with different excitation spectra existed in solution of **37e**. Similar behaviour was observed for **37f**. These observations suggested that there was some fluorescence from the J-aggregate. Aggregated MPc complexes are not known [269] to fluoresce since aggregation lowers the photoactivity of molecules through dissipation of energy by aggregates. Hence the observation of fluorescence from the peak due to the aggregate was surprising. Fluorescence spectra of **37e** and **37f** showed two bands (Fig. 4.4) consistent with the fact that both species fluoresce.

The proximity of the wavelength of each component of the Q-band absorption to the Q band maxima of the excitation spectra for **37e** and **37f** suggested that the molecules in the ground and excited states remained the same and thus were not affected by excitation. The low fluorescence quantum yields for complexes **37e** and **37f** suggested that either the substituents at the α position enhanced the intersystem crossing or there was quenching of the singlet state. The former would have resulted in high triplet quantum yields. However this was not the case, thus quenching by aggregation was expected for these complexes in DMSO.

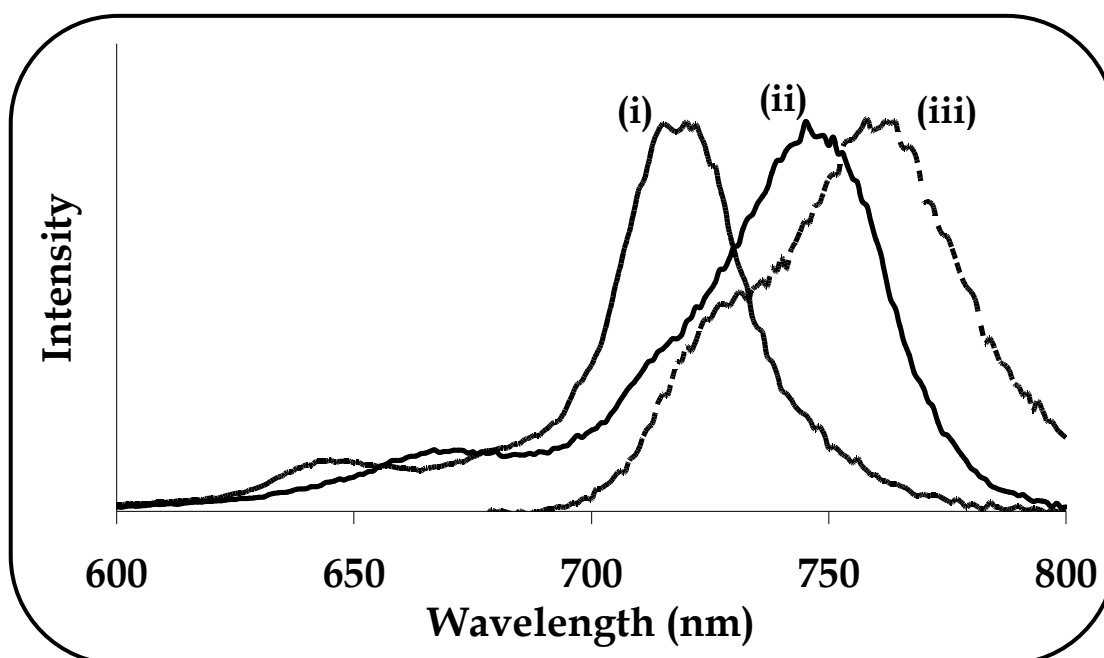


Figure 4.4: Normalised excitation spectra for 37e. (i) excitation from the 721 nm band (ii) excitation from the 741 nm band (iii) fluorescence spectrum of 37e (excitation at 685 nm) in DMSO. Concentration of complex $\sim 1.0 \times 10^{-7}$ M.

The excitation spectra of the sulphonated complexes **35** and **36** were performed in DMSO, methanol and PBS 7.4. In DMSO the absorption and excitation spectra were similar and were also mirror images of their emission spectra. In

methanol, the fluorescence spectrum of TiPcS_n was not a mirror image of the excitation spectrum, but was a mirror image of the absorption spectrum, Fig. 4.5. Excitation spectrum exhibited a somewhat split Q-band, and since monomerisation was expected in organic solvents, the observed splitting in excitation spectrum was probably as a result of changes in the molecule following excitation. The excitation spectrum suggested that there was aggregation following excitation as judged by the presence of the high energy band associated with aggregates. Another possibility of the difference in absorption and excitation spectra in methanol may be that the complex is solvated by a solvent-separated ion-pairs mechanism thus effectuating some structural changes to take place in the excited relative to the ground state [432]. The observation of a difference between the excitation and absorption spectra in methanol and not in DMSO suggests that methanol encourages solvent-separated ion-pairs of the excited state.

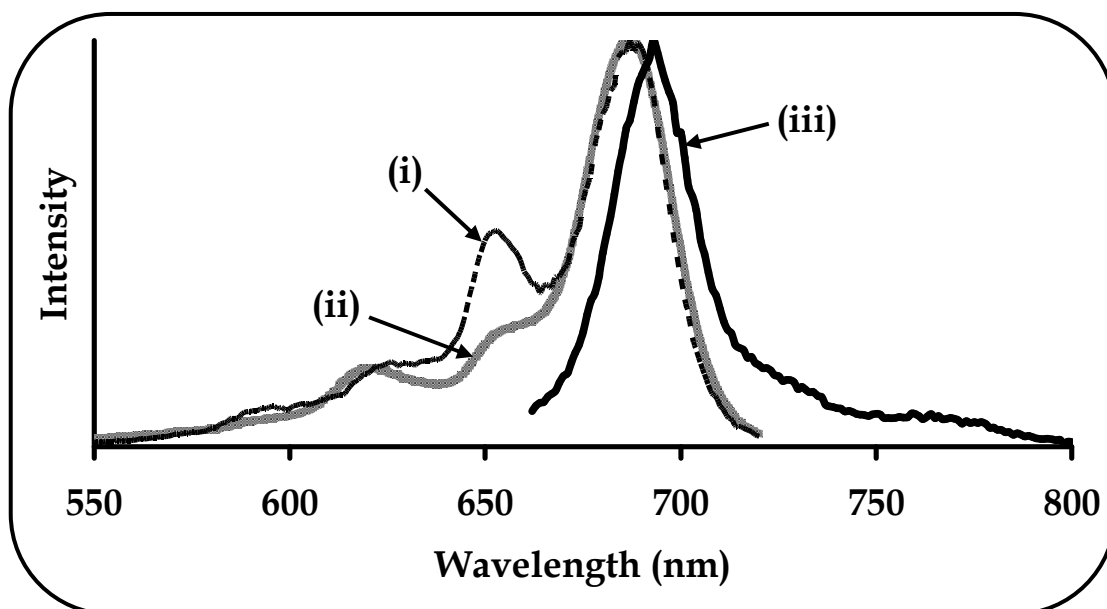


Figure 4.5: Normalised (i) excitation (652 and 688 nm), (ii) absorbance (687 nm) and (iii) emission (693 nm) spectra of TiPcS_n in methanol. Concentration of complex $\sim 1.0 \times 10^{-7}$ M.

A much narrower excitation spectrum was observed for TiPcS_n in PBS (Fig. 4.6) compared to its absorption spectrum and was a mirror image of the emission spectrum (not shown). The disappearance of the band that was associated with aggregated species around 630 nm suggested that it was only the monomer that fluoresced.

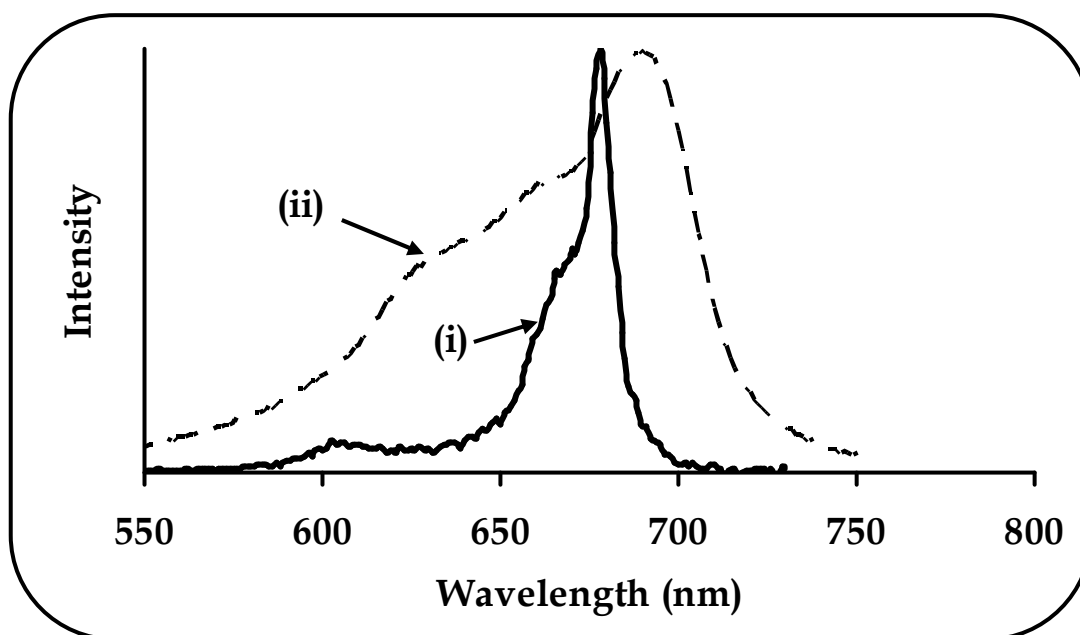


Figure 4.6: Normalised (i) excitation (677 nm), (ii) absorbance (690 nm) spectra of TiPcS_n in PBS 7.4. Concentration of complex $\sim 1.0 \times 10^{-7}$ M.

The absorption, excitation and emission spectra of TaPcS_n in methanol are shown in Fig. 4.7. The absorption and excitation spectra were different in that they had different Q band maxima, suggesting that the absorbing species was different from the emitting species. The excitation spectrum was the mirror image of the emission spectrum. What was very uncommon with this complex was the observation of a blue-shifted emission spectrum, i.e. emission: $\lambda_{\max} = 678$ nm; absorption: $\lambda_{\max} = 688$ nm, Table 4.2. A similar behaviour was observed in DMSO, where a blue-shift of 8 nm was observed, but the absorption and excitation spectra were similar and were mirror images of their emission spectrum. The occurrence of the observed blue-

shifted emission spectra with TaPcS_n was very surprising and could not be explained as most if not all phthalocyanine complexes comply with Stokes law. Even though multiple experiments were performed, the blue-shifted emission spectra were still observed. The occurrence of the blue-shifted emission spectra may be due to some components fluorescing, Fig. 4.7 (e.g. components absorbing at ~ 660 nm), probably more than other components of the complex. This observation may explain the narrowing of the Q-band in that some of the components of TaPcS_n readily undergo excitation when compared to other components of the complex, with emission occurring from these components hence agreement between excitation and emission spectra. The behaviour reported here for TaPcS_n was not observed for unsubstituted TaPc, showing this was a characteristic of the sulpho substituents and not the solvent since DMSO, methanol and PBS showed the same behaviour.

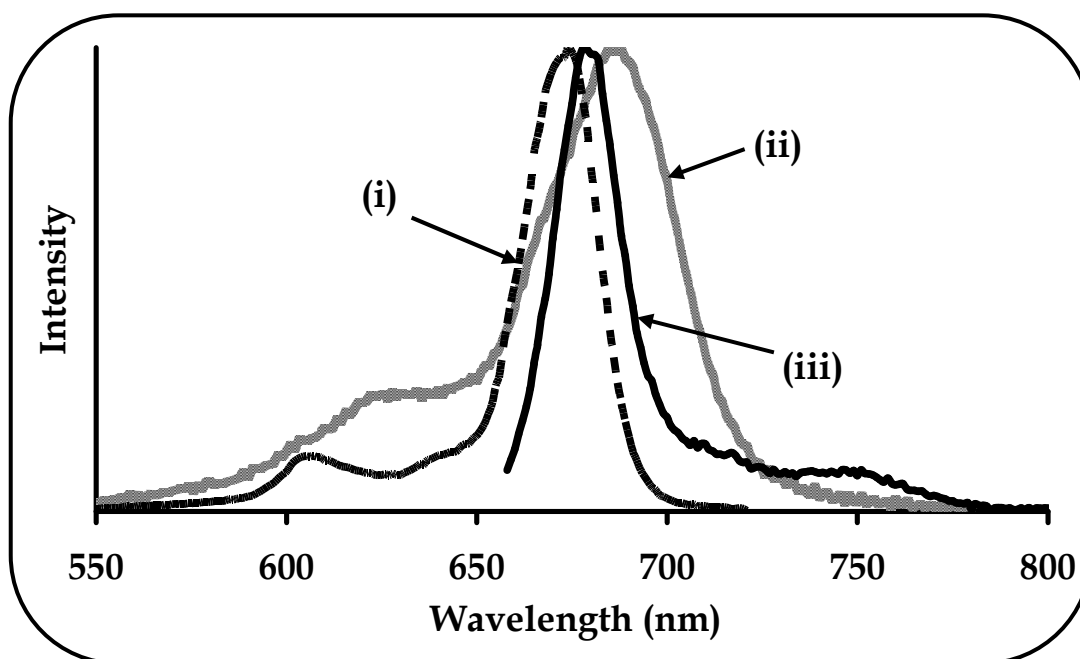


Figure 4.7: Normalised (i) excitation (674 nm), (ii) absorbance (688 nm) and (iii) emission (678 nm) spectra of TaPcS_n in methanol. Concentration of complex ~ 1.0×10^{-7} M.

The absorption and excitation of the TaPcS_n in PBS solution were also not similar and were not mirror images of the emission spectrum, Fig. 4.8. Since the addition of Triton X-100 did not show any presence of aggregated species in PBS, the observed excitation spectrum in PBS could be as a result of the components of the complex not fluorescing equally with one of the isomeric components fluorescing. Here, the emission spectrum was blue-shifted by 11 nm, again due to the difference in components fluorescing.

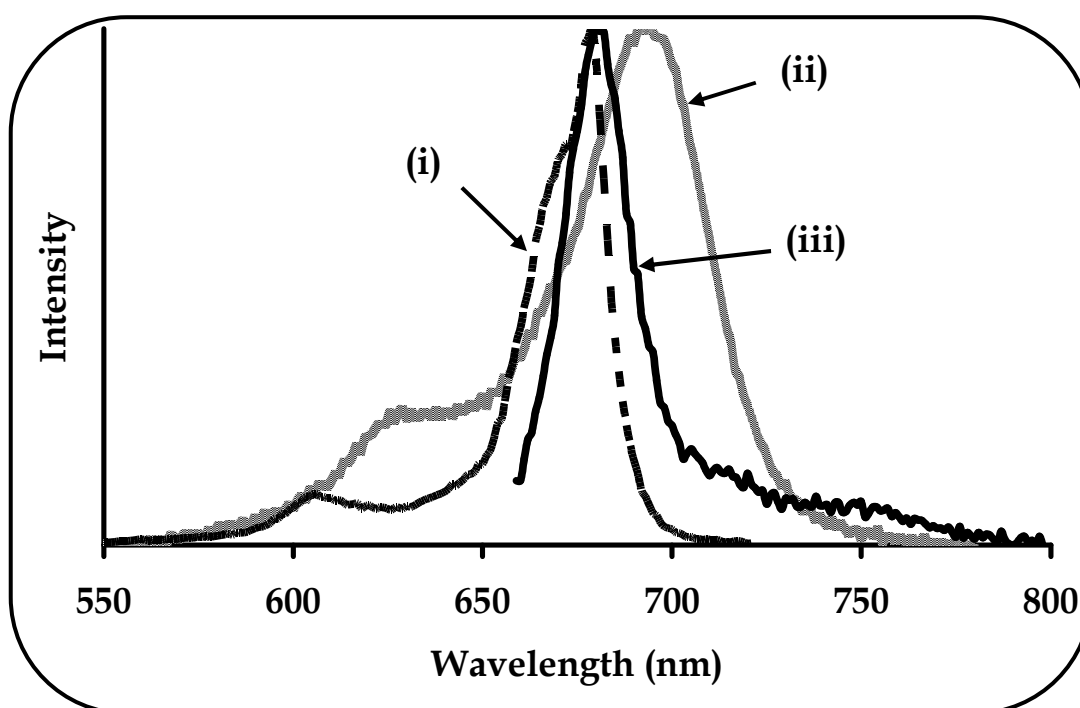


Figure 4.8: Normalised (i) excitation (ii) absorbance and (iii) emission spectra of TaPcS_n in PBS 7.4. Concentration of complex $\sim 1.0 \times 10^{-7}$ M.

Dissolving a phthalocyanine macrocycle in an aqueous environment strongly increases its dimer/monomer ratio, thus favouring aggregation. Generally, aggregation between neighbouring phthalocyanine molecules leads to fluorescence quenching and this was observed with TiPcS_n (**35**) in PBS 7.4, which had the lowest Φ_F value (i.e. $\Phi_F = 0.03$) compared to the values in organic solvents (i.e. $\Phi_F = 0.18$

and 0.42 in methanol and DMSO respectively). This was however not the case with TaPcS_n (**36**) in PBS 7.4 with $\Phi_F = 0.15$. As there was no evidence of aggregation in PBS 7.4 solution, the fluorescence quantum yield values of TaPcS_n were found to be comparable with those obtained in organic solvents in this work with $\Phi_F = 0.22$ and 0.18 in methanol and DMSO respectively, and also typical of MPcs [269]. Lower Φ_F values are expected in DMSO (compared to methanol for example) for the same complex due to enhanced intersystem crossing (heavy atom effect) of this solvent, Table 4.2. This was not the case for Φ_F of TiPcS_n (**35**). Comparing TaPcS_n (**36**) and TiPcS_n (**35**) in DMSO (or methanol), lower Φ_F is expected for the former due to the heavy atom effect of Ta. This was the case for DMSO and not methanol, Table 4.2. Values of PBS were affected by aggregation as stated above.

Fluorescence lifetimes, τ_F , were determined from Eq. 1.11, as the product of the quantum yields and the estimated radiative natural lifetimes, τ_N . The natural lifetimes were calculated from Eq. 1.12 or 1.13 on the basis of the absorption and fluorescence data. The calculated natural lifetimes were within the nanosecond time scale as is typical of MPc complexes. The coefficients of determination (r^2) were ~ 0.99 suggesting that the natural lifetime values obtained using both equations were a good measure of the calculated fluorescence lifetimes. The fluorescence lifetimes (τ_F) of the octa-substituted complexes increased in the order **39d** < **39b** < **39c** < **39a** possibly due to quenching by ring substituents with the thiol complex (**39d**) displaying the shortest lifetime and the phenoxy complex (**39a**) displaying the longest lifetime. The lifetimes of **37e** and **37f** were significantly lower most probably due to the aggregated nature of the complexes. Other complexes displayed lifetimes that were comparable to those in literature.

Fluorescence quenching

Fluorescence of MPcs is readily quenched by quenchers such as benzoquinone or hydroquinone. Quenching studies were performed on octa-substituted complexes in order to determine quenching rate constants, k_q . The fluorescence quenching of complexes **39a – d** was assessed by monitoring the decrease in the emission intensity of the complexes with increasing quencher concentration, *i.e.* [BQ], Fig. 4.9. Upon successive addition of BQ, the fluorescence intensities of the complexes decreased, due to the quenching of the excited state of the Pcs in the presence of BQ. The ratio of the emission intensity in the absence and presence of the quencher (Eq. 4.4 which is the same as Eq. 1.16),

$$\frac{F_0}{F} = 1 + K_{sv} [Q] \tag{4.4}$$

was found to depend linearly on the concentration of added quencher [BQ], *i.e.* the Stern-Volmer kinetics were obeyed, Fig. 4.10.

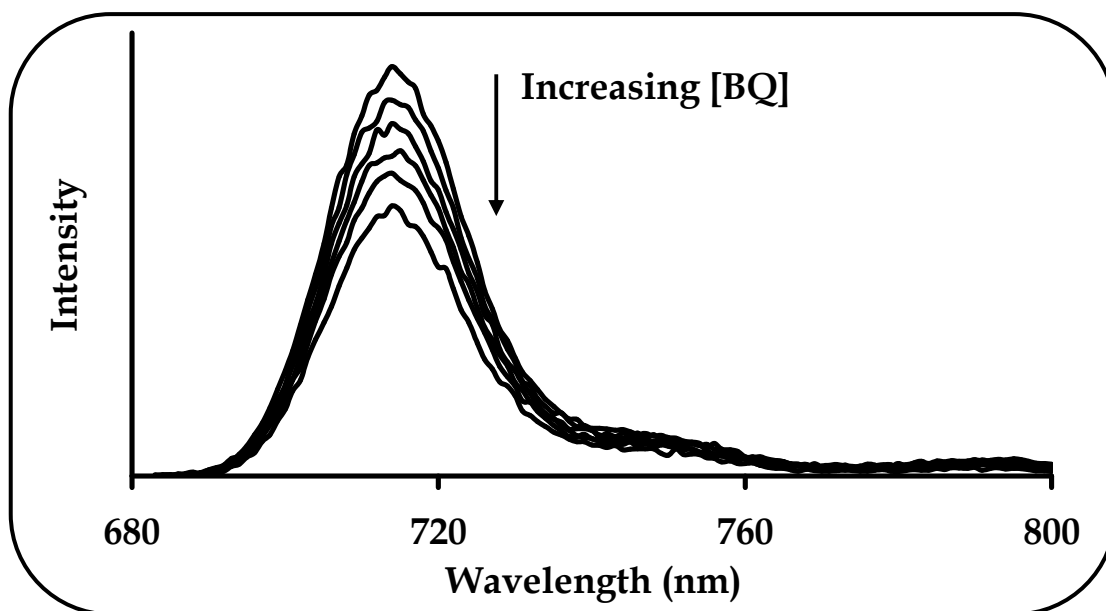


Figure 4.9: Fluorescence emission spectral changes of **39a** (1.0×10^{-6} M) on addition of increasing concentrations of BQ. [BQ] = 0.005, 0.010, 0.015, 0.020, 0.025 M.

The linear dependence suggested typical homogeneous dynamic quenching of the complexes by BQ. The corresponding Stern-Volmer quenching constants, K_{SV} , were found to range from 15 to 45 M^{-1} and from Eq. 1.15 ($K_{SV} = k_q \cdot \tau_F$), the bimolecular quenching rate constants, k_q , were determined. The bimolecular quenching rate constants were found to be close to the diffusion-controlled limits, $\sim 10^{10} M^{-1}s^{-1}$, Table 4.3.

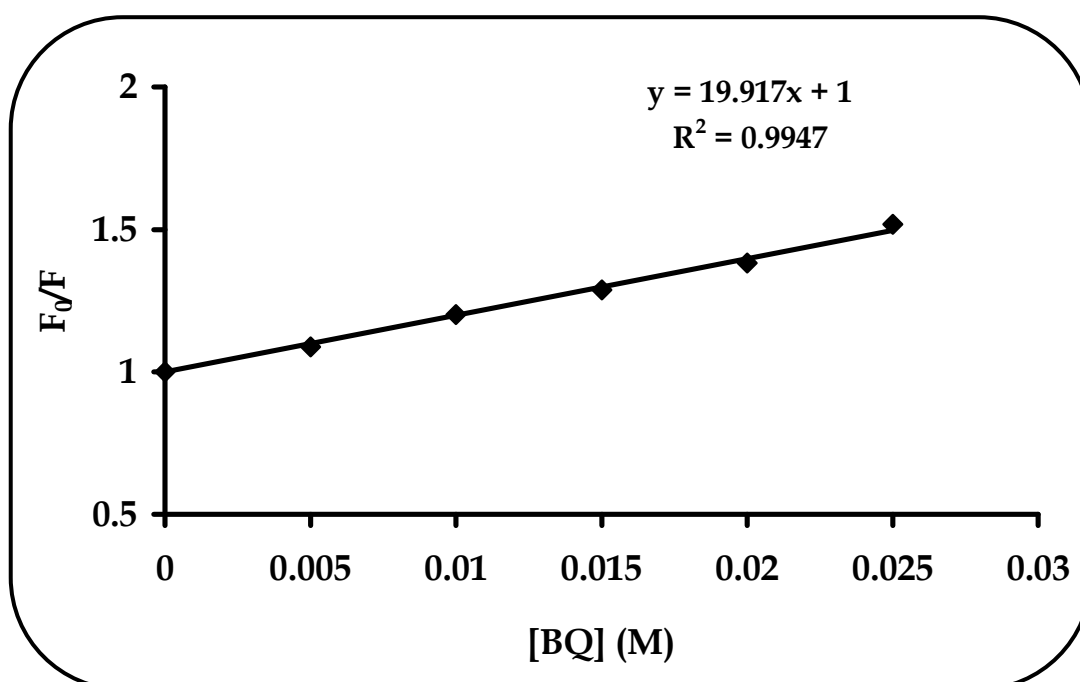


Figure 4.10: Stern-Volmer plot for fluorescence quenching of 39a ($1.0 \times 10^{-6} M$) by increasing concentrations of BQ. $[BQ] = 0.005, 0.010, 0.015, 0.020, 0.025 M$

Values near $10^{10} M^{-1}s^{-1}$, reflect the efficiency of the quencher, here BQ, which was observed for complexes **39**, more especially for the thiol-substituted complex **39d**. The values obtained were comparable to those observed with other phthalocyanines and quenchers [268]. Since the interactions of the excited states with BQ were diffusion-controlled, it thus follows that the chances of collision will be higher, if the number of molecules in the excited state is higher. In this study the diffusion-

controlled quenching was observed since practically each collision of the excited complexes should result in quenching, thus suggesting that BQ was an effective quencher.

Table 4.3: Fluorescence quenching data for complexes 39a – d in 1-CNP.

Complex	K_{SV} (M^{-1})	k_q ($M^{-1}s^{-1}$)
39a	19.9	1.63×10^{10}
39b	16.5	2.58×10^{10}
39c	14.9	1.84×10^{10}
39d	44.6	7.31×10^{10}
AlPcTS		3.20×10^{10} ^a

^a quenching by benzohydroquinone (BQH₂) [268]

The quenching of TiPcS_n (**35**) and TaPcS_n (**36**) fluorescence in the presence of MV²⁺ was also performed to determine the effect of quenching in ion-pairs. Addition of increasing MV²⁺ concentrations to TiPcS_n and TaPcS_n in methanol resulted in the progressive reduction of the fluorescence intensity, i.e. quenching of the fluorescence of the complexes was observed. Treatment of the emission suppression data by the standard Stern-Volmer analysis (Eq. 4.3), i.e. fluorescence intensity vs. the quencher concentration, resulted in plots with a downward curvature, Fig. 4.11. The downward curving SV plots indicated that the fluorescence quenching was not simply dynamic. Essentially this observation suggested that two types of fluorophores which were not equally accessible to the quencher existed in the system. Thus one type was accessible to the quencher while the other was inaccessible.

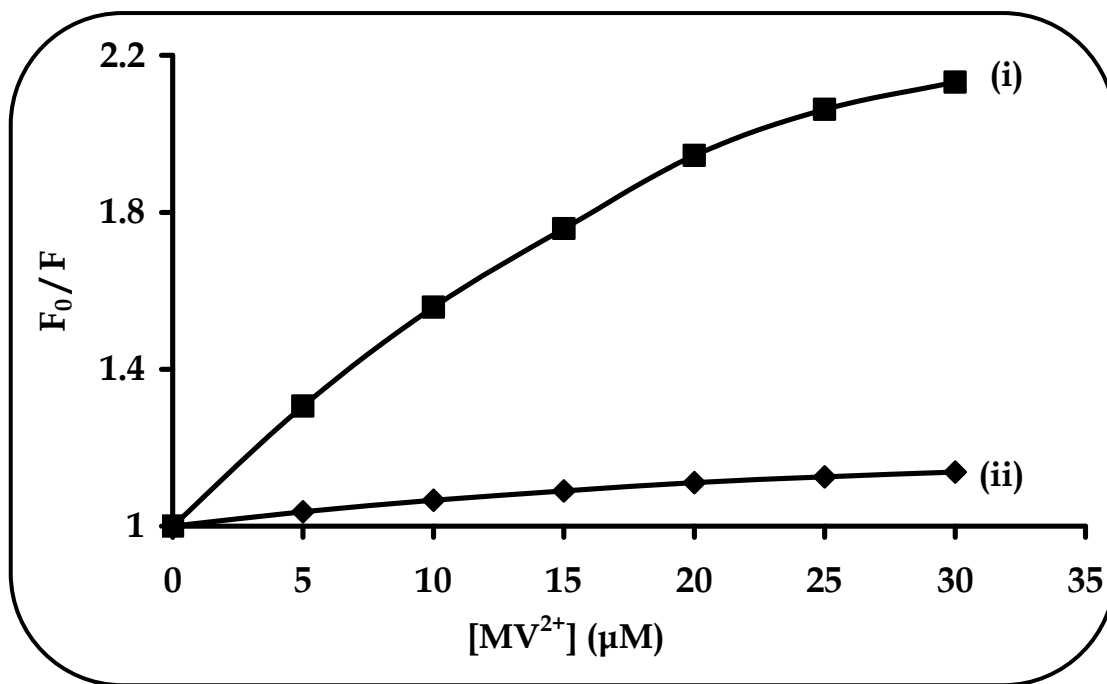


Figure 4.11: Stern-Volmer plots showing fluorescence quenching of (i) TiPcSn and (ii) TaPcSn in methanol as determined by fluorescence intensity as a function of $[MV^{2+}]$.

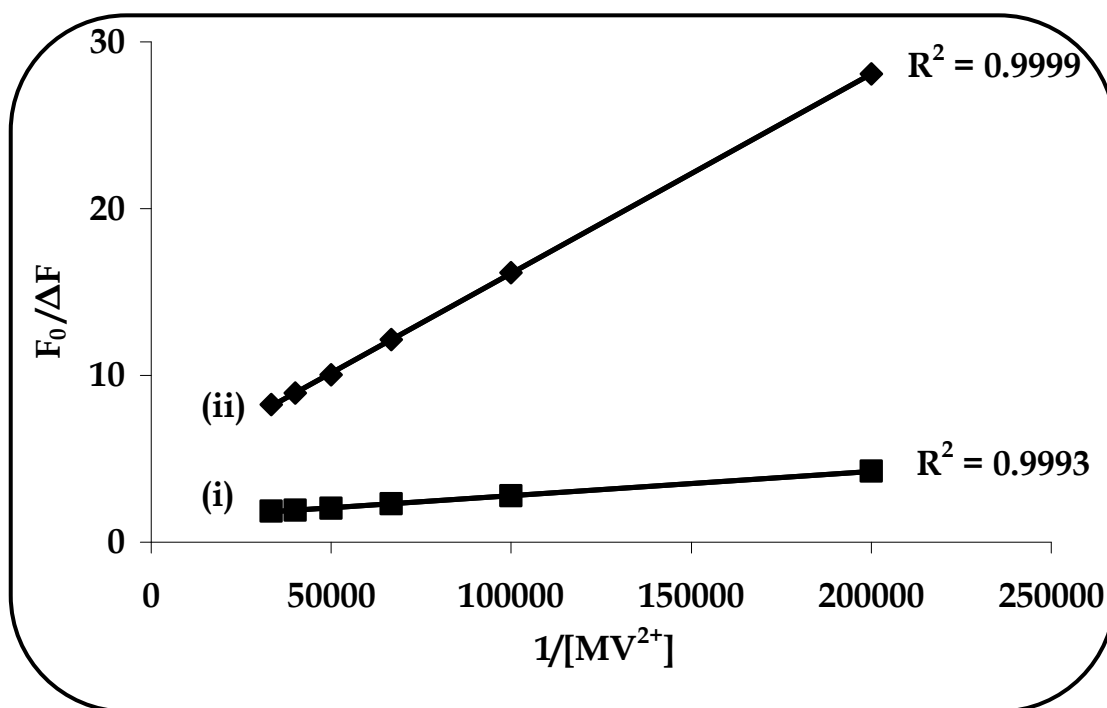


Figure 4.12: Modified Stern-Volmer plots showing quenching of (i) TiPcSn and (ii) TaPcSn in methanol as determined by fluorescence intensity as a function of $[MV^{2+}]$.

To determine the fractional accessibility of the fluorescing MPcS_n, to the quencher MV²⁺, the SV equation was thus modified [237,275] to Eq. 4.5 (same as Eq.1.18)

$$\frac{F_0}{\Delta F} = \frac{1}{f_a K_f [Q]} + \frac{1}{f_a} \quad (4.5)$$

Plots of $F_0/\Delta F$ vs. $1/[Q]$ were linear, with intercept f_a^{-1} and $(f_a K_f)^{-1}$ as slope, Fig. 4.12. From the intercepts, the data obtained suggested that 73.5 % and 23.9 % of the total fluorescence of TiPcS_n and TaPcS_n was accessible to the quencher (MV²⁺) respectively. The quenching constants, K_f , for TiPcS_n and TaPcS_n were calculated to be $9.3 \times 10^4 \text{ M}^{-1} \text{ s}^{-1}$ and $3.49 \times 10^4 \text{ M}^{-1} \text{ s}^{-1}$ respectively, Table 4.4.

Table 4.4: Quenching parameters of TiPcS_n (35) and TaPcS_n (36) in methanol in the absence and presence of MV²⁺

Complex	f_a^{-1}	AF (%) ^a	K_f (M ⁻¹ .s ⁻¹)
TiPcS _n	1.36	73.5	9.43×10^4
TaPcS _n	4.18	23.9	3.49×10^4
AlPcTS			2.00×10^{10} ^b

^a AF is the percentage Accessible Fluorescence to the quencher (MV²⁺), ^b [268]

The values obtained were small compared to reported [268] collisional quenching constants ($\sim 10^{10} \text{ M}^{-1} \text{ s}^{-1}$) thus suggesting that the fluorescence was not directly quenched by collision. The downward curving SV plots in Fig. 4.11 indicated that only fluorescence from the complexed MPcS_n is quenched and the unquenched fluorescence is as a result of uncomplexed MPcS_n. The fluorescence quenching constant (K_f) was much larger for TiPcS_n than it is for TaPcS_n because there were

more complexed ions, i.e. $(MV^{2+})-(TiPcS_n)_2$ and $(MV^{2+})_2-(TiPcS_n)$ than there were in the latter complex with methyl viologen, i.e. $(MV^{2+})-(TaPcS_n)_2$, see section 3.2, Fig. 3.7.

4.2.2 Triplet state properties

The triplet quantum yields and triplet lifetimes listed in Table 4.2 were determined by the laser flash photolysis system described in Chapter 2. A typical decay curve of **39b** (characteristic of all complexes) in 1-CNP is shown in Fig. 4.13. The insert shows a first order dependence of the triplet state, thus confirming that the decay was monoexponential and that the observed decay was only due to the depopulation of the triplet state and not quenching by triplet quenchers such as oxygen.

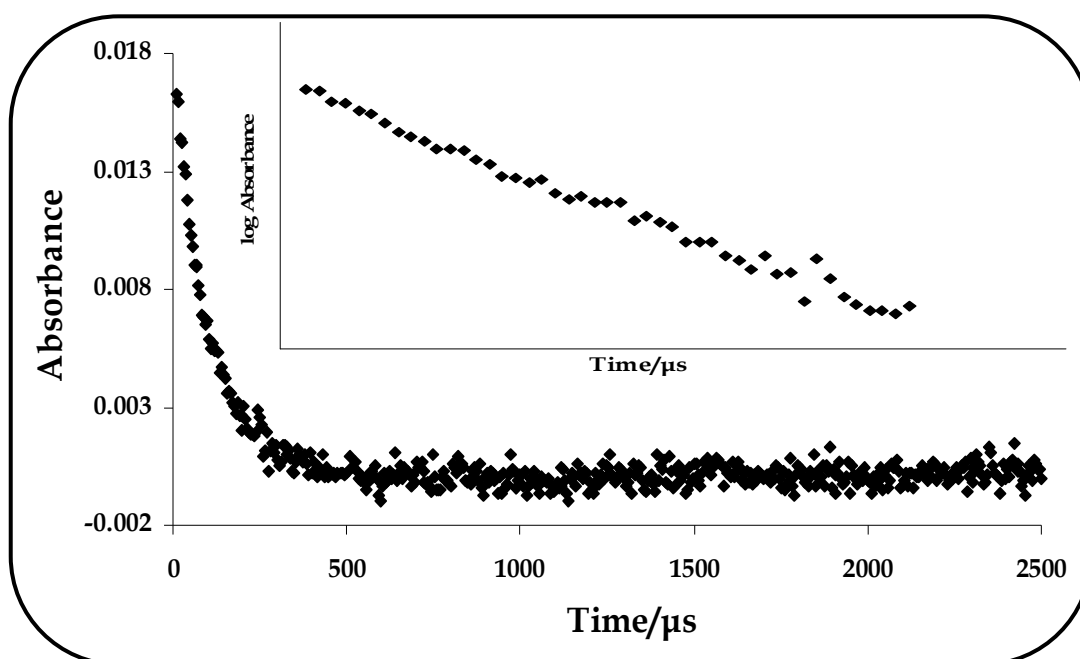


Figure 4.13: Triplet state decay curve of **39c** in 1-CNP. Inset shows the first order plot of the complex.

The tetra-substituted complexes **37a – f** and **38a – f**, gave relatively high triplet quantum yields, Φ_T , which were determined by the triplet absorption method, compared in general to the octa-substituted complexes **39**. The wavelengths of the triplet species where maximum absorptions took place were centred around 500 nm. The Φ_T values were dependent on the substitution position. Of all the complexes **35 – 38**, the sulphonated complex **35** (TiPcS_n) gave lower triplet yield and longest triplet lifetime in DMSO, Table 4.2. The non-peripherally substituted complexes (**37**) had lower quantum yields than the corresponding peripherally substituted derivatives (**38**), an indication that efficient intersystem crossing occurred with the latter complexes since deactivation by IC was minimal. The triplet quantum yields were complemented by the singlet oxygen quantum yields, Table 4.1 and 4.2, i.e. high Φ_Δ for complexes **38** compared to complexes **37**. Triplet lifetimes, τ_T , were determined by fitting the data to OriginPro 7.5 and were found to be relatively long-lived, except those of complexes **37e** and **37f** which were slightly shorter, probably affected by aggregation.

Of the octa-substituted, complexes **39b** and **39d** exhibited the highest and lowest triplet quantum yields respectively in 1-CNP, Table 4.2. The substantial decrease in the yield of **39d** may be due to the less efficient intersystem crossing as a result of loss through internal conversion. Complex **39a** had the shortest triplet lifetime while complex **39b** had the longest lifetime. The long lifetime for the latter could be due to its less aggregated nature because of the bulky *tert*-butyl substituents. The lifetimes obtained for all the octa-substituted complexes are unusually small when compared to values reported for phthalocyanines and to complexes **35 – 38** in DMSO, Table 4.2. This may be related to the transformation that took place in 1-

CNP following irradiation by the laser and white light than it was the case for complexes **35** – **38** in DMSO.

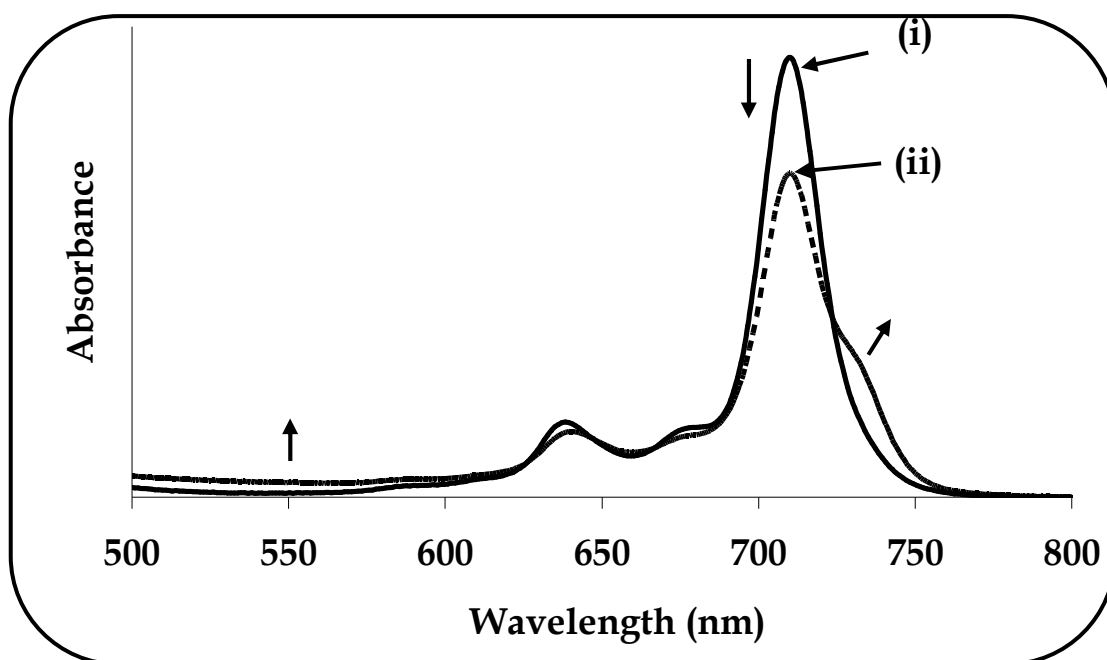
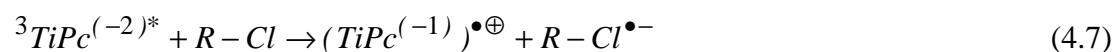


Figure 4.14: UV/Vis spectra obtained before (i) and after (ii) laser irradiation of **39b** in 1-CNP

Figure 4.14 shows a change in the spectrum of complex **39b** following laser irradiation in deaerated 1-CNP. Similar (but less prominent) changes were observed when white light was employed. The spectral changes showed a drastic decrease in the Q-band as well as an emergence of a broad shoulder in the longer wavelength side (~730 nm) coupled with an increase in intensity in the 500 nm region. These spectral changes were observed in 1-CNP but not in non-chlorinated solvents such as THF. However due to lack of appropriate standards in THF, and low solubility in DMSO, the laser-flash photolysis was studied in 1-CNP rather than the more commonly employed DMSO. Exposing the MPC in 1-CNP following white light or laser light irradiation to air or bubbling oxygen did not result in the regeneration of the Q-band, thus suggesting that the observed transformation was not due to the reduction product

of the complex, but most likely due to oxidation. Addition of a reductant (sodium borohydride) to the solution resulted in the increase in the Q-band intensity, and a decrease in the background in the 500 nm region, thus confirming the regeneration of the Pc following reduction. In phthalocyanine chemistry, a decrease in the Q-band intensity and an increase in the intensity in the 500 nm region imply a ring-based oxidation or reduction [338]. Thus irradiation of the complexes resulted in ring oxidation. Furthermore, photooxidation of MPc complexes in the presence of chlorinated solvents with the formation of a phthalocyanine cation radical has been documented [433,434]. The following mechanism was thus proposed for the photooxidation of complexes **39a – d** in the presence of 1-CNP (Eq. 4.6 and 4.7).



where R-Cl is 1-CNP and the axial ligand has been left out for clarity.

There was however no change in the intensity of the band at ~730 nm upon reduction with sodium borohydride, implying that this band was not due to an oxidation product. A similar band to the one observed in Fig. 4.14, termed the “X” band, has been observed before in substituted ZnPc complexes [435] and was attributed to the distortion of the Pc ring in substituted ZnPc complexes. It is also known that the presence of eight phenyl groups on the peripheral position of the phthalocyanine ring results in high distortion of the ring [436]. Thus, the presence of an extra band for complexes **39a – d** may suggest loss of symmetry following photolysis in these molecules due to the distortion of the MPc molecule.

4.3 Photocatalytic oxidation of 1-hexene

4.3.1 Photochemical properties

The comparative photocatalytic activities of aryloxy (**37a**, **37c**, **38a** and **38c**) and arylthio (**37e**, **37f**, **38e** and **38f**) tetra-substituted oxotitanium(IV) phthalocyanine complexes for the oxidation of 1-hexene were investigated. The complexes were selected because they bore similar substituents, however they differed in their ether (C-O-C) and thiol (C-S-C) bond linkages. The singlet oxygen quantum yields as well as the photostabilities of the complexes were determined with the methods described in the experimental section. The rates at which the complexes degraded were also determined. The photochemical parameters were discussed above in Table 4.1, but the photocatalysis experiments were performed in DCM, hence are presented in Table 4.5 for this solvent.

Table 4.5: Singlet oxygen quantum yields, photobleaching quantum yields and the rate constants of 37a, 37c, 38a, 38c, 37e, 37f, 38e and 38f in DCM.

Complex	Φ_{DPBF}	Φ_{Δ}	Φ_P	k (min ⁻¹)
37a	0.58	0.63	3.3×10^{-4}	4.2×10^{-2}
37c	0.54	0.61	3.5×10^{-4}	3.8×10^{-2}
37e	0.56	0.69	5.3×10^{-4}	3.2×10^{-1}
37f	0.51	0.64	5.0×10^{-4}	2.9×10^{-1}
38a	0.53	0.84	2.7×10^{-4}	3.1×10^{-2}
38c	0.54	0.73	2.2×10^{-4}	3.4×10^{-2}
38e	0.55	0.86	4.8×10^{-4}	2.7×10^{-1}
38f	0.50	0.77	4.5×10^{-4}	2.4×10^{-1}

The photocatalytic experiments were carried out in DCM because it was a suitable solvent in which the complexes were soluble, in the monomeric form. Solutions containing appropriate amounts of catalyst and substrate (1-hexene) were irradiated with light in the Q-band region of the respective catalyst and the reactions monitored with time using GC and UV/Vis. As earlier explained, irradiation of MPC with light at an appropriate wavelength results in the formation of the energetically rich and chemically more reactive singlet oxygen ($^1\text{O}_2$), which is responsible for many photooxidation reactions [437].

The singlet oxygen was determined as described before with DPBF as the singlet oxygen scavenger. The singlet oxygen quantum yields of the complexes in DCM were relatively high, ranging from 0.61 to 0.86, Table 4.5. The Φ_{Δ} values of the peripherally substituted complexes **38** were larger than those of the non-peripherally substituted complexes **37** considering the same substituents. This observation was similar to that in DMSO, Table 4.1. Additionally, Φ_{Δ} values of the arylthio-substituted complexes **37e**, **37f**, **38e** and **38f** were marginally larger than those of the aryloxy-substituted complexes **37a**, **37c**, **38a** and **38c**. This was the case in DMSO for **38e** and **38f** compared to **38a** and **38c**, but not for **37e** and **37f** compared to **37a** and **37c** due to aggregation of **37e** and **37f** in DMSO, Table 4.1. All the complexes exhibited excellent efficiencies in the singlet oxygen generation under the employed experimental conditions. Thus the large Φ_{Δ} values were sufficient for photooxidation reactions.

The photostabilities were determined in DCM in order to determine the effect of the substituents on the stability of the complexes. The photobleaching quantum yield (Φ_p) values of the complexes were found to range from 2.2×10^{-4} to

5.3×10^{-4} with the arylthio-substituted complexes (**e** and **f**) slightly less stable than the corresponding aryloxy-substituted complexes (**a** and **c**). The substituent electronic effects could explain the slight variation in the Φ_p values, i.e. the arylthio groups are more electron-donating than their corresponding aryloxy groups and thus tend to enhance the probability of the photobleaching process [226]. Furthermore, the non-peripherally substituted complexes (**37a**, **37c**, **37e** and **37f**) were slightly less stable than their peripherally substituted counterparts (**38a**, **38c**, **38e** and **38f**).

The photobleaching rate constants (k) of the complexes were calculated from Eq. 1.9 (Table 4.5) where smaller values of k correspond to a higher photostability. It is obvious that the aryloxy-substituted complexes (**a** and **c**) exhibited a higher photostability than the corresponding arylthio-substituted complexes (**e** and **f**). The observed trend is as a result of the more electron-donating arylthio groups slightly reducing the stabilities of the complexes as discussed above. A relation between the photostabilities and singlet oxygen quantum yields could exist. For example, the arylthio-substituted complexes generated higher yields of singlet oxygen than the aryloxy-substituted complexes, thus the probability of photobleaching was higher in the former than in the latter, since photobleaching is initiated by singlet oxygen. The dependence of the photocatalytic oxidation of 1-hexene towards the complex photostabilities is discussed below.

4.3.2 Photocatalysis

The photocatalytic activities of the various OTiPc complexes for the oxidation of 1-hexene in the presence of oxygen were investigated. The transformation of 1-hexene was found to yield 1,2-epoxyhexane as a major product, identified and verified by spiking of authentic samples from GC (Fig. 4.15) and GC-MS. In addition

the allylic oxidation product, i.e. 1-hexene-3-ol was obtained as a minor product.

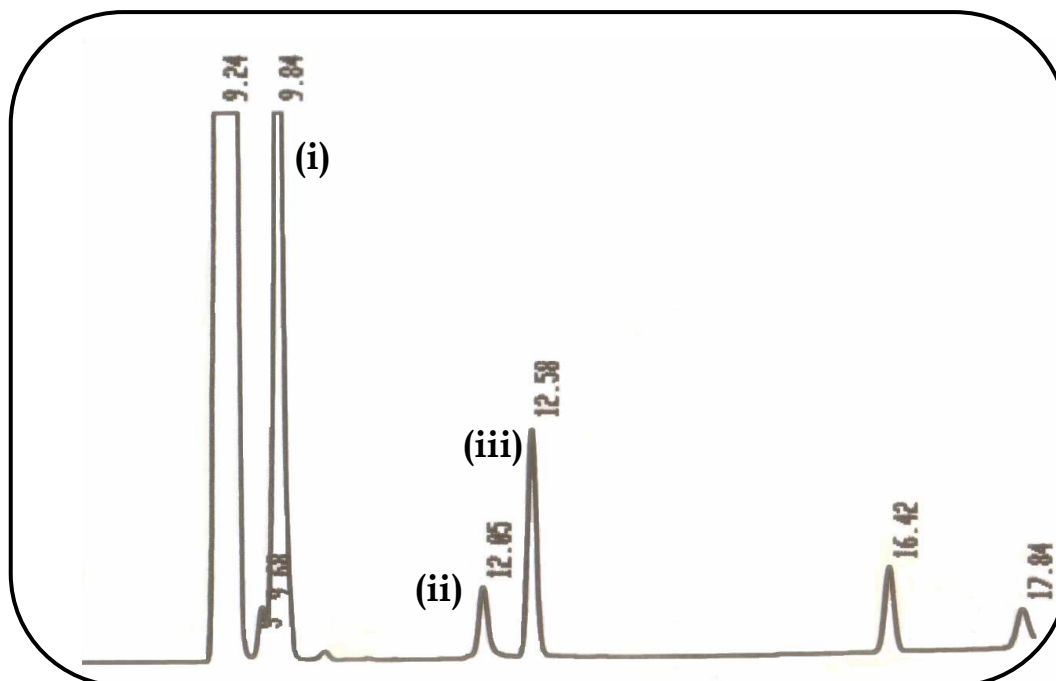


Figure 4.15: GC traces obtained during the photocatalysis of 1-hexene (i) in DCM yielding oxidation products: 1-hexene-3-ol (ii) and 1,2-epoxyhexane (iii).

The resultant 1-hexene conversions and 1,2-epoxyhexane selectivities are summarised in Table 4.6, obtained after 8 hours. The arylthio-substituted complexes (e and f) enhanced the catalytic activities compared to the corresponding aryloxy-substituted derivatives (a and c). Also, the peripherally substituted derivatives exhibited excellent catalytic activities compared to their corresponding non-peripherally substituted counterparts. A correlation between the observed photocatalytic trends and singlet oxygen quantum yields existed (Table 4.5 and 4.6), whereby complexes **38** > complexes **37** in Φ_{Δ} values. Furthermore, the phenoxy- and phenylthio substituted complexes **38a** and **38e** showed the highest conversions, Figs. 4.16 and 4.17 respectively, as well as epoxide selectivities (Table 4.6). The benzyloxy and benzylthio substituted complexes **37c** and **37f** however showed the

lowest activities and epoxide selectivities (Table 4.6). No oxidation product was observed in the absence of catalyst thus confirming the need to utilise OTiPcs as photocatalysts.

Table 4.6: Photocatalytic oxidation of 1-hexene by complexes 37a, 37c, 38a, 38c, 37e, 37f, 38e and 38f in DCM.

Complex	% Conversion⁽ⁱ⁾	% 1,2-Epoxyhexane selectivity⁽ⁱⁱ⁾
37a	12.97	76.4
37c	11.92	73.7
37e	13.66	78.0
37f	12.36	75.5
38a	17.56	87.1
38c	15.91	80.5
38e	18.02	90.8
38f	16.11	82.1

$$(i) \text{ \%conversion} = \frac{(1 - \text{hexene}_{\text{initial}}) - (1 - \text{hexene}_{\text{remaining}})}{(1 - \text{hexene}_{\text{initial}})} \times 100$$

$$(ii) \text{ \% selectivity} = \text{epoxide}_{\text{obtained}} / [(1 - \text{hexene}_{\text{initial}}) - (1 - \text{hexene}_{\text{final}})]$$

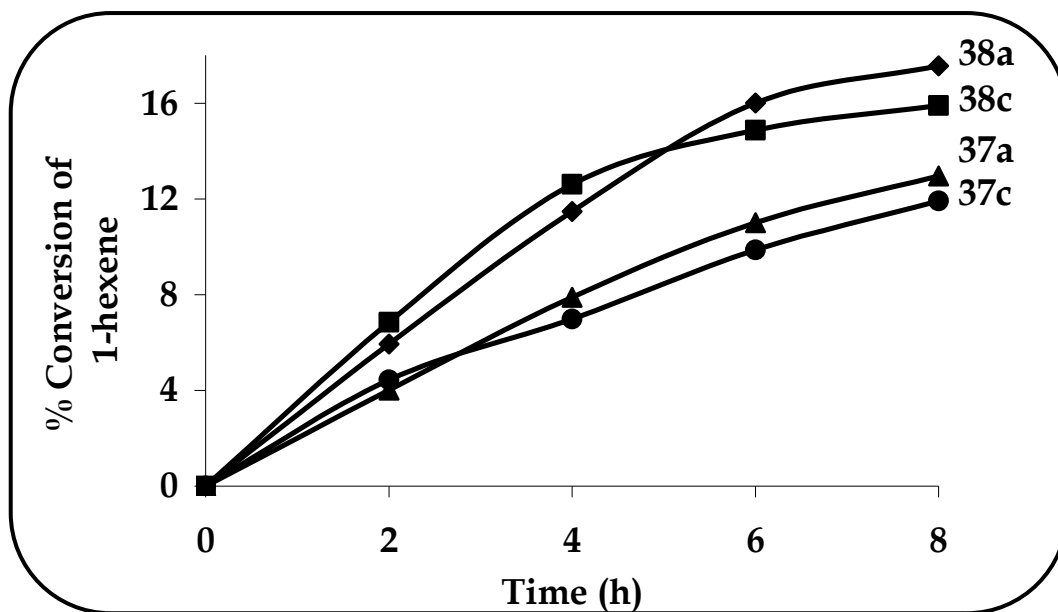


Figure 4.16: % Conversion plots of 1-hexene over time for the photocatalytic oxidation of 0.5 mmol 1-hexene in the presence of 1 μ mol aryloxy substituted oxotitanium(IV) phthalocyanines (37a, 37c, 38a and 38c) in DCM.

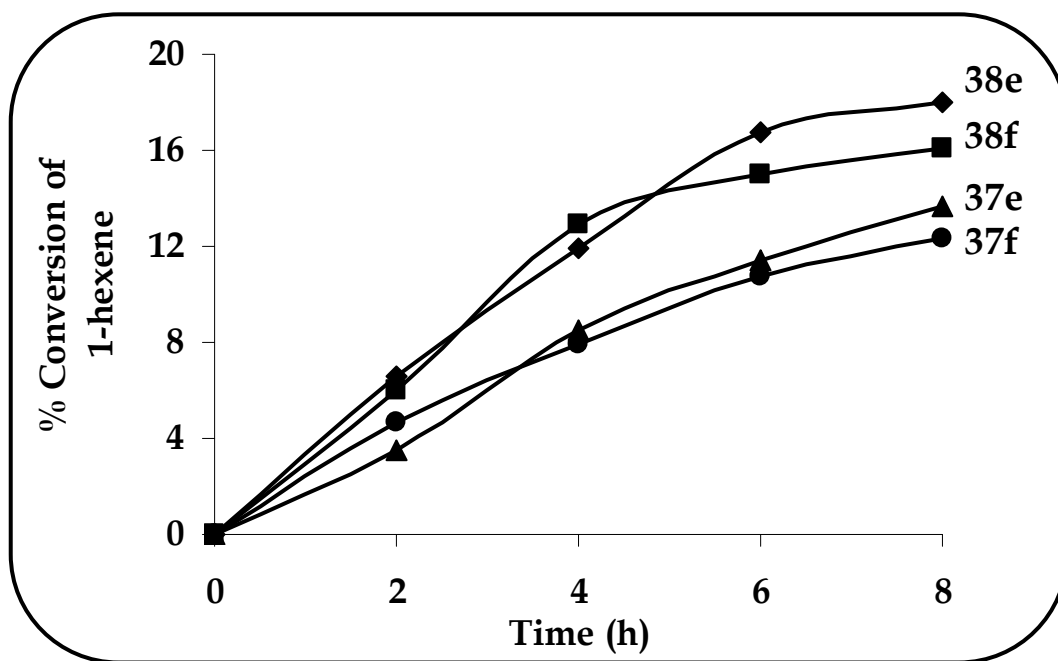


Figure 4.17: % Conversion plots of 1-hexene over time for the photocatalytic oxidation of 0.5 mmol 1-hexene in the presence of 1 μ mol arylthio substituted oxotitanium(IV) phthalocyanines (37e, 37f, 38e and 38f) in DCM.

The fate of the OTiPc complexes during the photocatalysis of 1-hexene was monitored by UV/Vis spectroscopy. The rate of photostability was found to be dependent on the light intensity as shown in Fig. 4.18. As mentioned in the experimental section, the optimum intensity of light used was 4.0×10^{16} photons. $\text{s}^{-1}.\text{cm}^{-2}$, which was high enough to effectuate the photocatalysis and low enough to avoid photodegradation of the catalyst. Overall, all the complexes exhibited excellent photocatalytic activities.

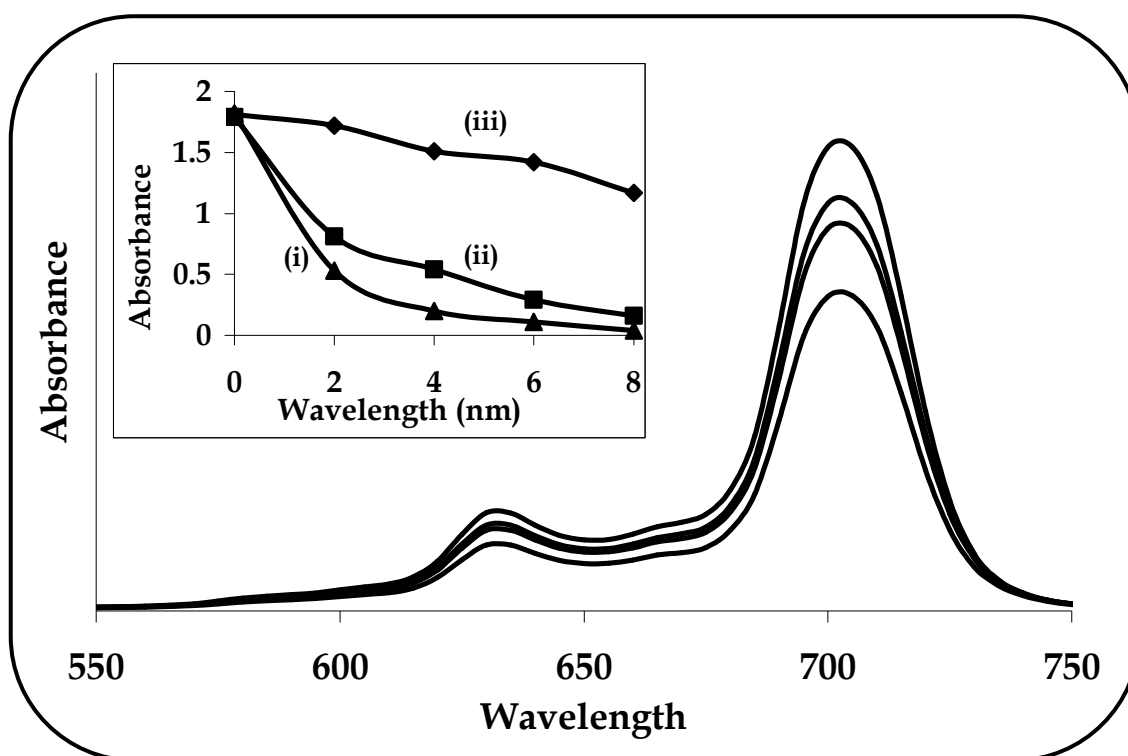


Figure 4.18: UV/Vis spectral changes of 38b observed with variation of light intensities: (i) 6.5×10^{16} (ii) 5.2×10^{16} and (iii) 4.0×10^{16} photons. $\text{s}^{-1}.\text{cm}^{-2}$ during the photocatalysis of 1-hexene.

A point to consider is the relationship between the photocatalytic activities and the catalyst photostability. A plot of 1-hexene conversion vs. catalyst photobleaching rate constant is shown in Fig. 4.19. The peripherally substituted complexes **38a**, **38c**, **38e** and **38f** showed higher activities than the corresponding non-peripherally

substituted complexes **37a**, **37c**, **37e** and **37f**, which showed moderate activities. However, complexes **38e** and **38f** were relatively unstable, while complexes **38a** and **38c** were more stable. It was obvious from the plot that the phenoxy and benzyloxy substituted complexes **38a** and **38c** were better catalysts as they combined good photocatalytic activity, singlet oxygen quantum yield and photostability.

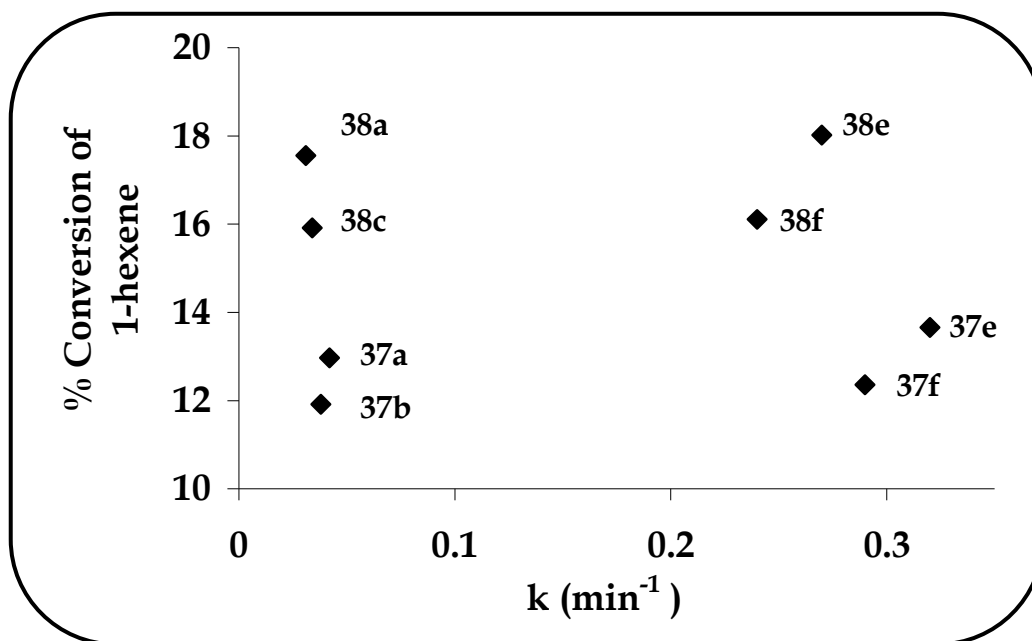


Figure 4.19: % Conversion of the photocatalytic oxidation of 1-hexene in relation to the photobleaching rate constants (k) of oxotitanium (IV) phthalocyanines in DCM.

It is important to note that the formation of the epoxide and the allylic product suggested that there were two possible types of active species, one of which was responsible for the production of the 1,2-epoxyhexane and the other for 1-hexen-3-ol [438]. Thus to determine the mechanisms involved in the production of the oxidation products, photocatalytic reactions were undertaken in the presence of DABCO (singlet oxygen quencher) and a radical quencher, 2,6-di-*tert*-butyl-4-methylphenol (BHT), Fig. 4.20 and 4.21 respectively. Addition of DABCO led to a pronounced decrease of 1,2-epoxyhexane formation, Fig. 4.20, while the amount of allylic alcohol

was not affected. This observation thus suggested that singlet oxygen was the sole active species in the production of the epoxide. Addition of BHT however deactivated the active species responsible for the formation of the allylic alcohol, thus suggesting that radicals in solution were the active species, Fig. 4.21. The formation of the epoxide in the presence of BHT was not affected. The presence of the radicals may also be facilitated by the solvent, DCM, as chlorinated solvents are known to form radicals during photolysis [226]. Thus both Type II (singlet oxygen) and Type I (radicals) mechanisms were involved in the photocatalytic oxidation of 1-hexene mediated by the OTiPc complexes, with the former favouring the formation of epoxide and the latter the allylic alcohol. The Type II mechanism was the dominant process since the selectivity of 1,2-epoxyhexane was over 70 %, Table 4.6 and Fig. 4.20.

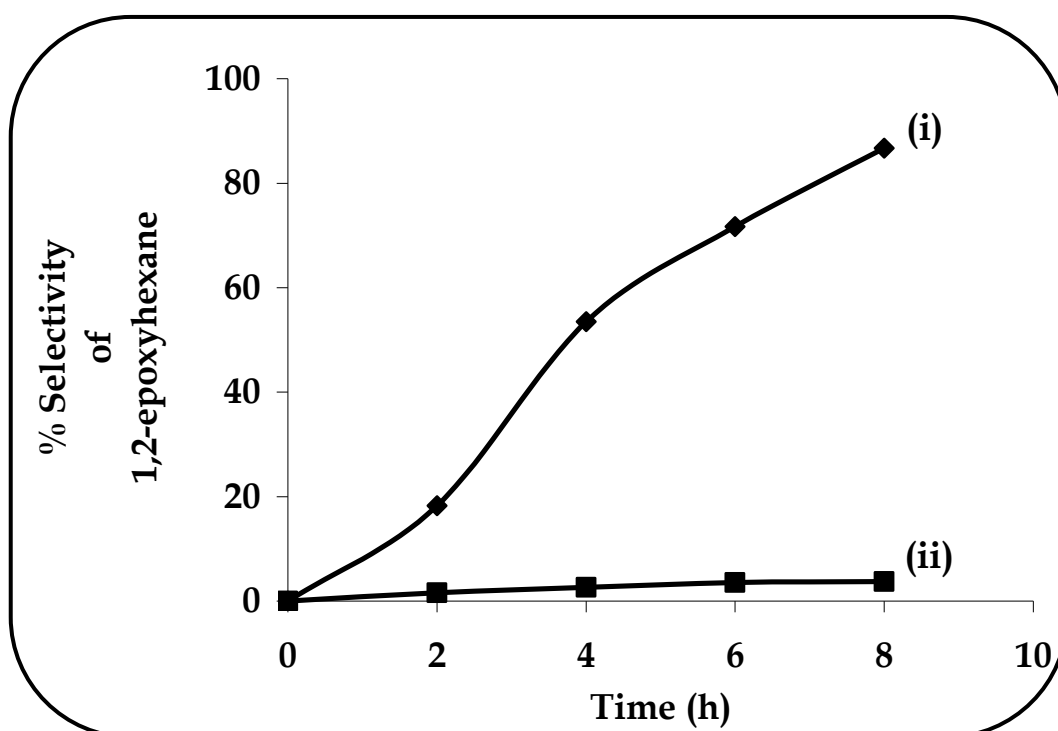


Figure 4.20: % Selectivity plots of 1,2-epoxyhexane in (i) absence and (ii) presence of DABCO over time during the photocatalysis of 1-hexene by 38a (1 μ mol) in DCM.

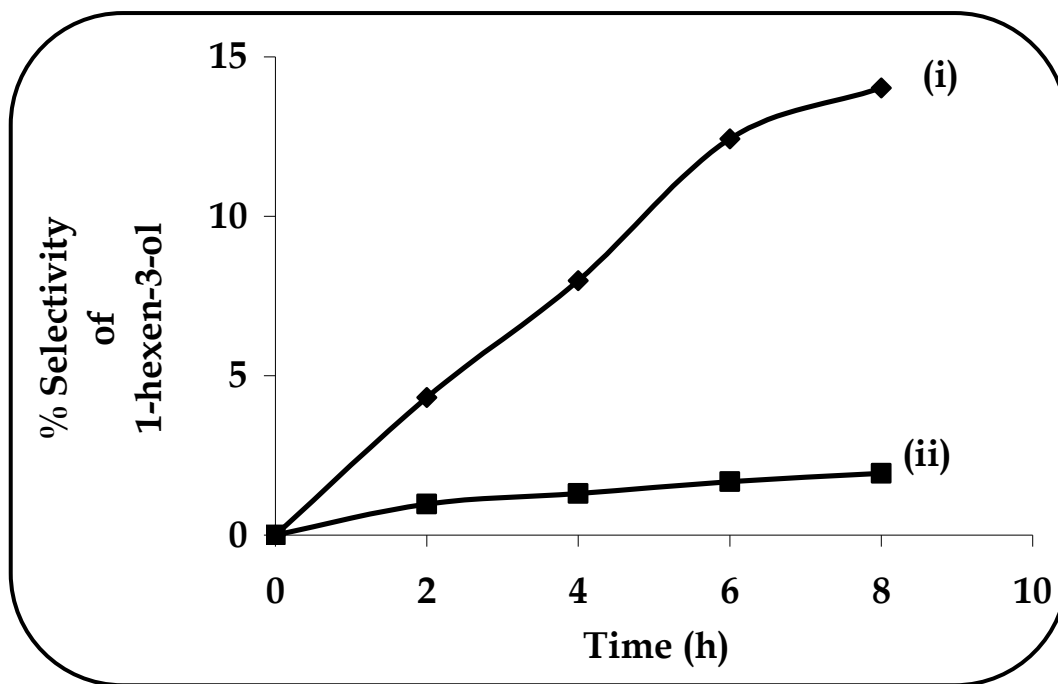
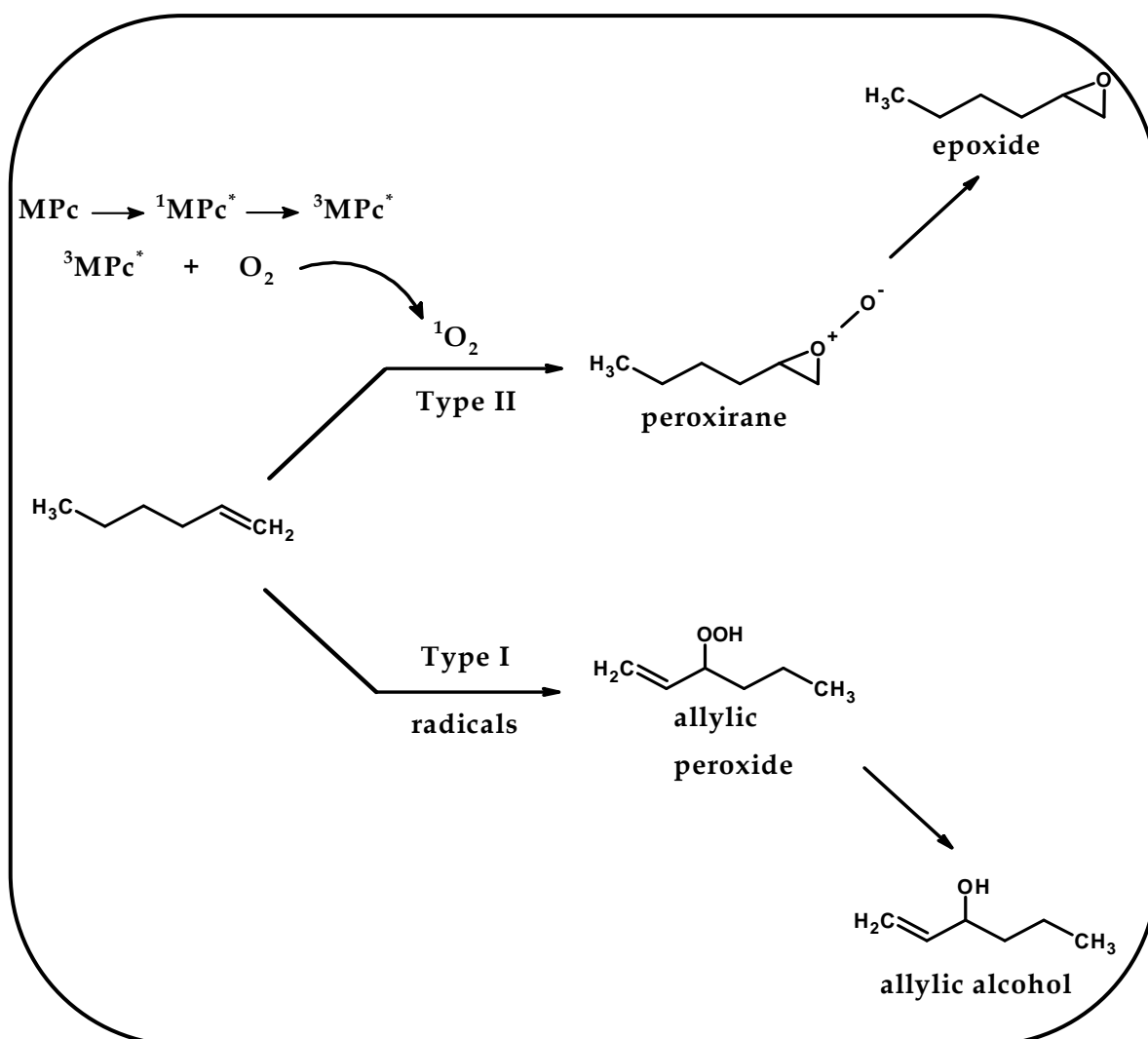


Figure 4.21: % Selectivity plots of 1-hexen-3-ol in (i) absence and (ii) presence of BHT over time during the photocatalysis of 1-hexene by 38a (1 μ mol) in DCM.

In light of this, epoxidation and allylic oxidations were two competing processes that typically took place due to attack at the 1-hexene double bond in the former and hydrogen abstraction in the latter. These processes often occur simultaneously [291]. Although the role of the metal complex as well as the mechanistic route was not clear, the mechanism shown in Scheme 4.1 was proposed. Following irradiation, the fate of 1-hexene was determined by either Type I or Type II mechanisms. As earlier mentioned the former implies radicals as oxidising agent, which form the hydroperoxide intermediate by hydrogen abstraction/hydroxylation, thus yielding the allylic alcohol, i.e. 1-hexen-3-ol as a minor product. Singlet oxygen in the Type II mechanism is the oxidising agent, which probably forms the diradical intermediate, i.e. peroxirane. The abstraction of the terminal oxygen results in the epoxide, i.e. 1,2-epoxyhexane, as the major product. The epoxidation selectivity over

hydroxylation might be due to the fact that the former tends to dominate with oxometallic complexes [291].



Scheme 4.1: Proposed mechanism for the formation of the photooxidation products

4.4 Conclusion

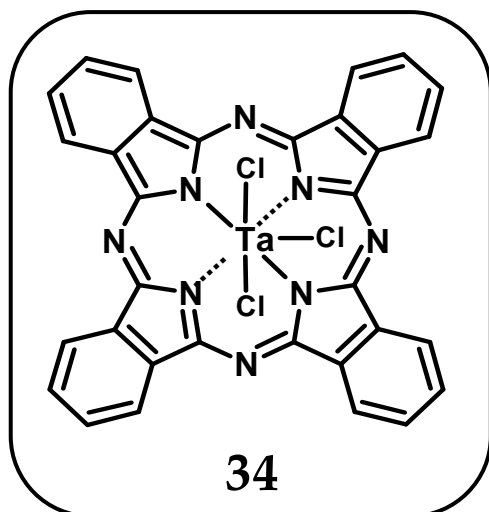
It was shown that in DMSO the complexes produced sufficient singlet oxygen and were relatively unstable – compared to MPcs in general with Φ_p values of $\sim 10^{-5}$ – due to increased photooxidation brought about by the electron-donating ability of the

substituents. The β -substituted arylthio complexes **38e** and **38f** exhibited the largest Φ_{Δ} values, while their α -substituted counterparts, i.e. complexes **37e** and **37f**, exhibited the lowest in DMSO. The Φ_{Δ} values for octa-substituted complexes were relatively low due to the radicals emanating from the chlorinated solvent, 1-CNP. Fluorescence lifetimes and quantum yields as well as triplet quantum yields were comparable to those in literature, while the photophysical parameters of complexes **37e** and **37f** were low due to aggregation. Selected complexes were found to photocatalyse 1-hexene by the Type I and Type II mechanisms to respectively produce an allylic alcohol (1-hexen-3-ol) and epoxide (1,2-epoxyhexane).

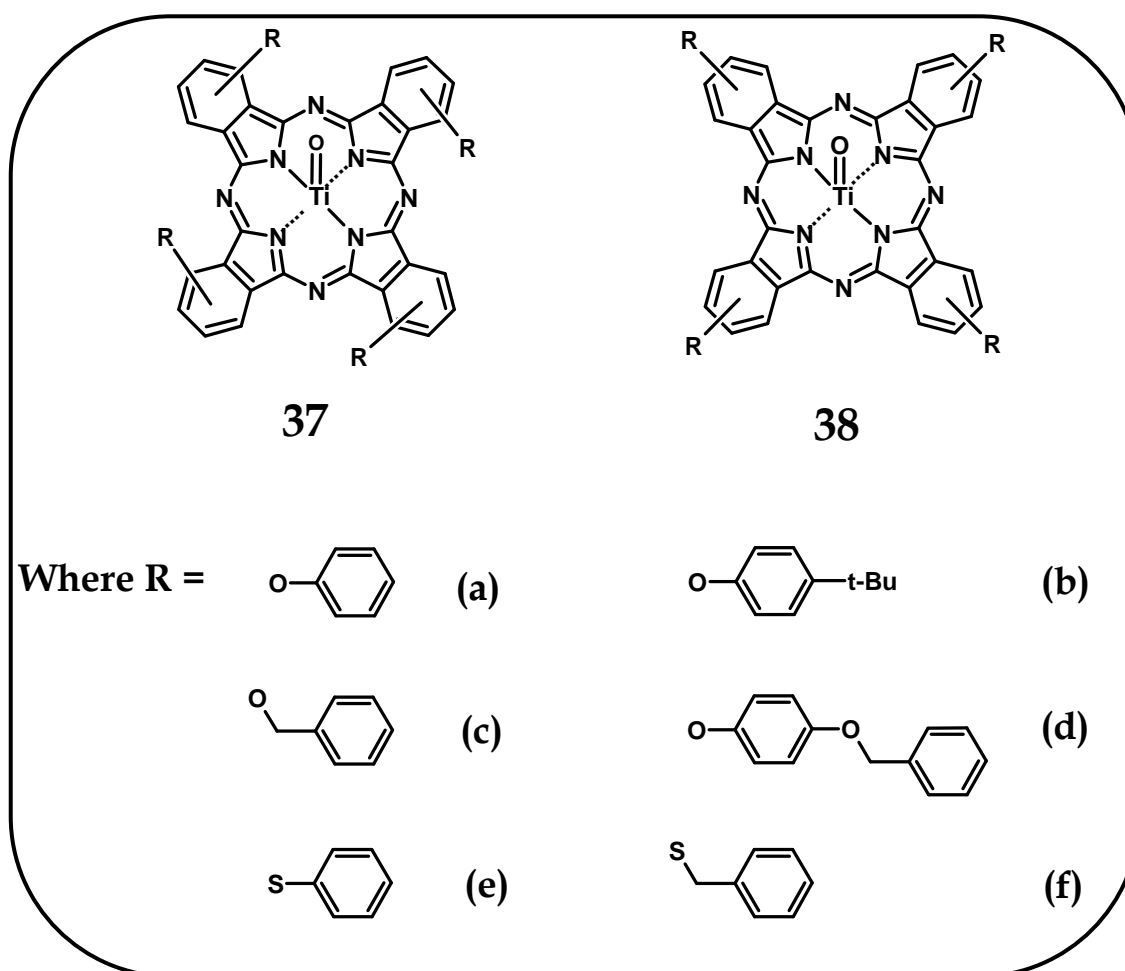
CHAPTER 5

Electrochemical characterisation

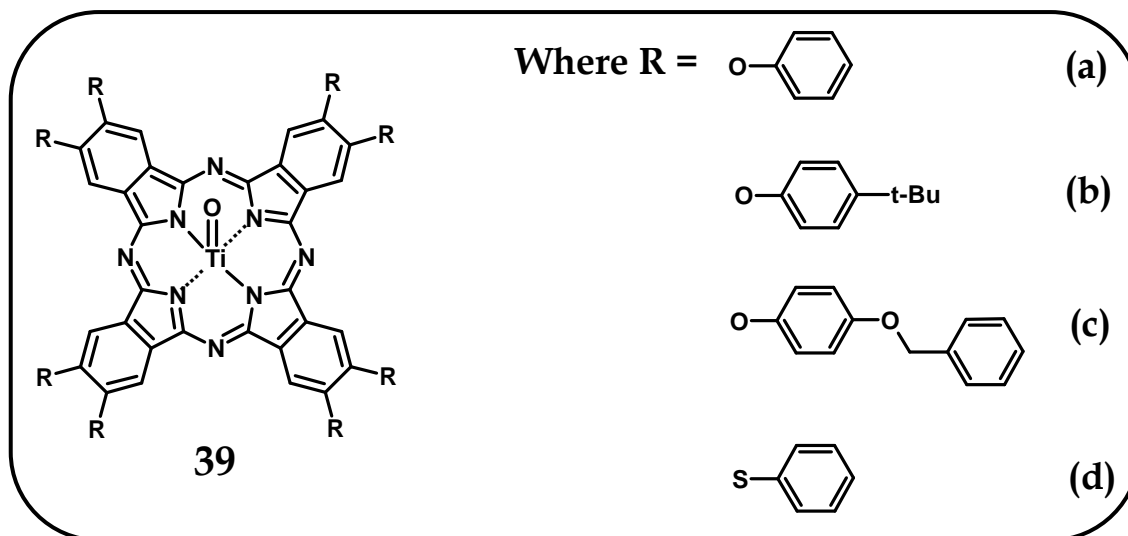
The structures of the MPcs employed are provided again for the convenience of the reader.



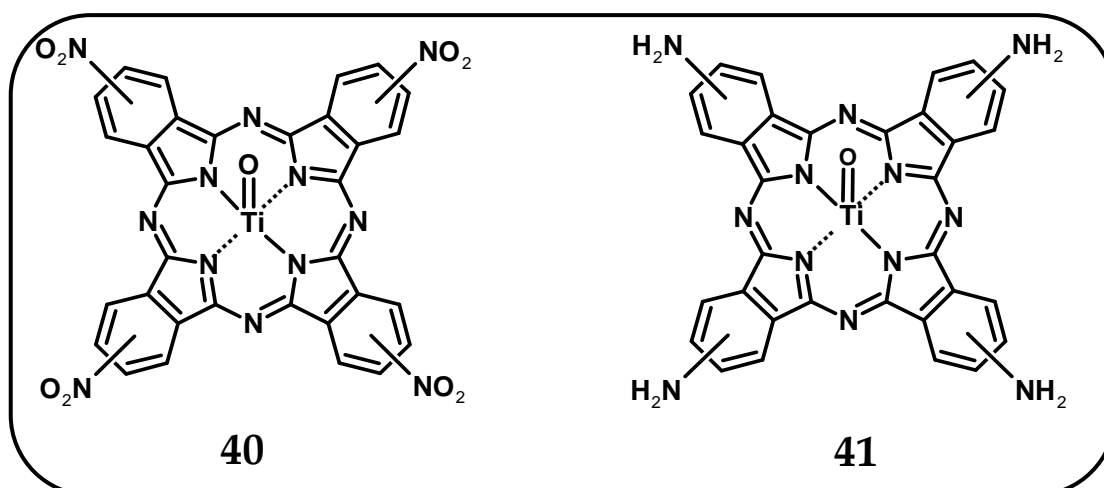
Cl₃TaPc (34) studied in this chapter.



Tetra-substituted aryloxy and arylthio OTiPc complexes used in this study.



Octa-substituted OTiPc complexes used in this study.



Tetra-substituted nitro (40) and amino (41) OTiPc complexes used in this study.

This chapter is based on the electrochemical characterisation of the complexes by methods such as cyclic voltammetry, square wave voltammetry, chronocoulometry and spectroelectrochemistry. The electrochemical properties exhibited by the complexes are discussed.

5.1 Tantalum phthalocyanine

The electrochemical properties of tantalum phthalocyanines are unknown and hence the following studies were undertaken.

Phthalocyanine oxidation and reduction usually occur in one-electron steps. Up to two one-electron ring oxidations may be observed and up to four one-electron ring reductions are possible which are at times difficult to observe due to electrolyte, solvent and electrode limits [341]. For MPCs containing electroactive central metals, additional oxidation or reduction processes may be observed, generally occurring between the first ring oxidation and the first ring reduction.

The cyclic and square wave voltammograms (insert) of Cl_3TaPc (**34**) in DMF containing 0.1 M TBABF₄ are shown in Fig. 5.1. Oxidation of complex **34** is expected to occur only on the ring, however, oxidation processes were not observed. The presence of the electropositive central metal (i.e. Ta⁺⁵) with a high oxidation state, causes charge migration from the ring to the central metal to occur. Therefore the ring in this complex is expected to be more difficult to oxidize such that oxidations occur at much higher positive potentials. Reduction of Cl_3TaPc may occur at the central metal (Ta⁺⁵) and/or at the ring. In Fig. 5.1, three reduction processes labelled **I** – **III** were observed at half-wave ($E_{1/2}$) potentials of -0.31, -0.48 and -0.94 V vs. Ag|AgCl respectively. The ratio of anodic to cathodic currents (I_{pa}/I_{pc}) was near unity for the couples. The cathodic to anodic peak separation (ΔE) was 90 mV for

couple **II** (peak separation for the ferrocium/ferrocene couple was also 90 mV), but for **I** and **III**, cathodic to anodic peak separations greater than 90 mV were observed suggesting quasi-reversibility and slow electron transfers. A look at relative CV currents for processes **I** and **II** compared to process **III** may suggest that the latter involved more electrons than each of the first two couples, Fig. 5.1.

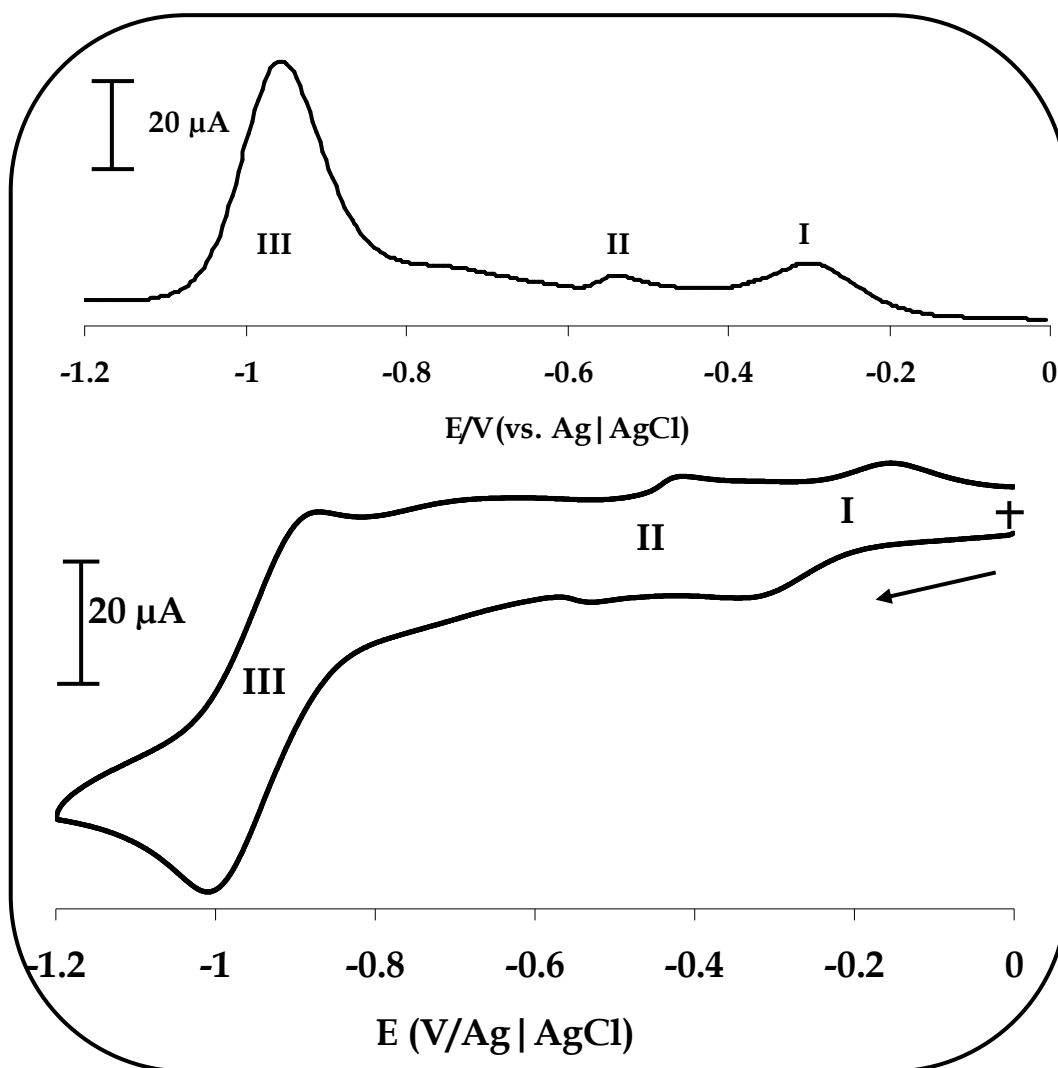


Figure 5.1: Cyclic and square wave voltammograms of 34 in DMF containing 0.1M TBABF₄. Scan rate 0.2 V.s⁻¹.

Multi-electron processes which occur in one step are not common in phthalocyanines. However, there have been reports of a $\text{Co}^{\text{III}}\text{Pc}$ being reduced to a $\text{Co}^{\text{I}}\text{Pc}$ in one step [341]. In related porphyrins, two-electron transfers in one step are known for distorted (non-planar) complexes [439]. Thus, it is possible that the distorted Cl_3TaPc will also exhibit a single step, multi-electron transfer process. The number of electrons (n) for couple **III** was calculated using Eq. 5.1 which applies to reversible processes [440],

$$n = \frac{I_p 4RT}{QFv} \quad (5.1)$$

where Q is the charge under a given voltammetric peak (either cathodic or anodic), v is the scan rate and R , F and T have their usual meaning. Even though couple **III** was not completely reversible, Eq. 5.1 was employed to give an approximate number of electrons transferred and this was found to be ~ 4 . The nature of redox processes occurring and the number of electrons transferred was confirmed using spectroelectrochemistry discussed below. Plots of cathodic current vs. the square root of scan rate ($v^{1/2}$) taken from 100 mVs^{-1} to 800 mVs^{-1} were linear, (or $I_c v^{1/2}$ vs. v was constant), thus suggesting a diffusion controlled process.

In order to further probe the redox mechanism of complex **34**, spectroelectrochemistry in an optically transparent thin layer electrochemical (OTTLE) cell was employed. Spectroelectrochemistry involves both electrochemistry and *in situ* UV/Vis spectroscopy to measure simultaneous electric, optical and structural changes observed in the electrochemical reactions. The spectral changes observed upon reduction of complex **34** at potentials of process **I** (i.e. -0.31 V vs. $\text{Ag}|\text{AgCl}$) in DMF containing 0.1 M TBABF_4 are shown in Fig. 5.2. The spectral changes in Fig. 5.2 showed a shift in the Q-band from 692 to 684 nm . A shift in the

Q-band without a lowering of intensity is typical of a redox process occurring on the central metal [168]. Thus process **I** was due to the reduction of the central metal (Ta^{+5}). Coulometry confirmed the number of electrons transferred to be 1.3 (~1) following reduction at potentials of process **I**, hence a one-electron reduction of $\text{Ta}^{\text{V}}\text{Pc}$ to $\text{Ta}^{\text{IV}}\text{Pc}$ was confirmed. Further reduction (starting with the last trace in Fig. 5.2) at potentials of process **II** (-0.48 V vs. Ag|AgCl) resulted in the spectral changes shown in Fig. 5.3. These spectral changes consisted of an increase in absorption between 550 and 650 nm, with peaks being observed at 620 and 655 nm.

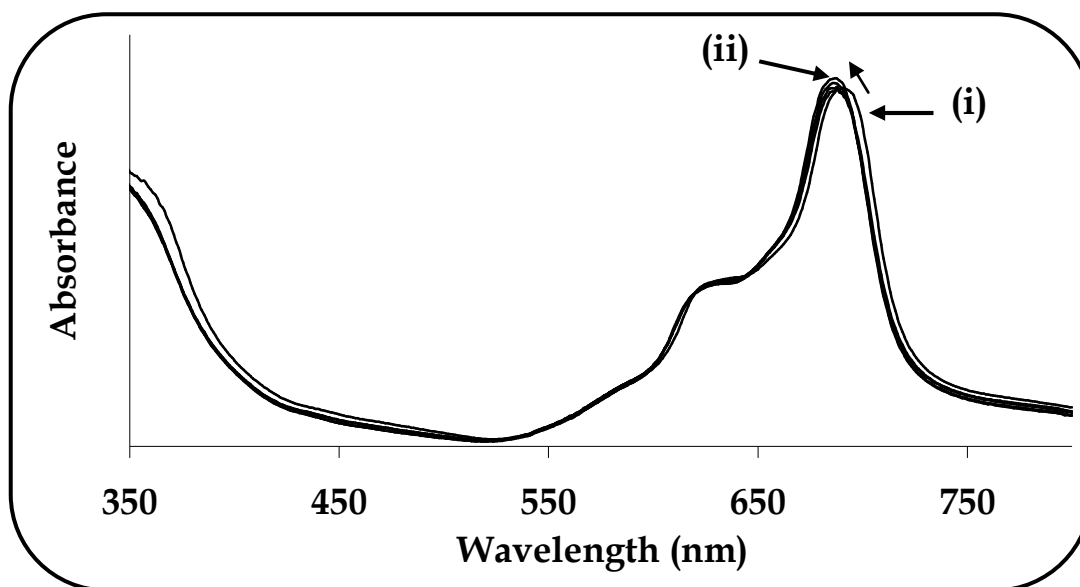


Figure 5.2: UV-Vis spectral changes observed during controlled potential reduction of **34** in DMF containing 0.1 M TBABF₄ at process **I** (-0.31 V) where (i) the first scan and (ii) the last scan.

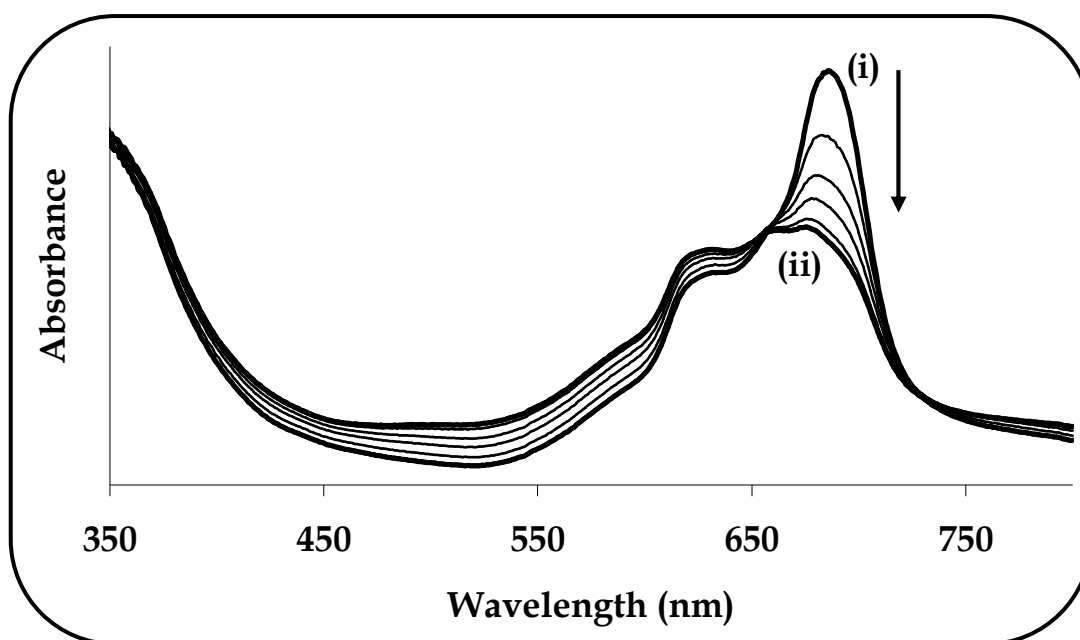


Figure 5.3: UV-Vis spectral changes observed during controlled potential reduction of 34 in DMF containing 0.1 M TBABF₄ at process II (-0.48 V). The first spectrum in (i) is the same as the last spectrum in Fig. 5.2, where (i) the first scan and (ii) the final scan.

Clear isosbestic points were observed at 725 and 657 nm thus confirming the involvement of only two species in solution. An increase of intensity in the 550 to 650 nm region is typical of ring-based processes in MPc complexes [338]. Thus the spectral changes shown in Fig. 5.3 were consistent with a one-electron process involving the reduction of the ring. Coulometry confirmed the number of electrons transferred to be near unity for reduction at potentials of process II and hence the formation of a Ta^{IV}Pc⁻³ species.

Further reduction at the potentials of process III (-0.98 V vs. Ag|AgCl) resulted in spectral changes shown in Fig. 5.4. These consisted of an increase in the peaks at 620 and 655 nm (associated with the Ta^{IV}Pc⁻³ species), without any shift in wavelength. The relative intensities of the peaks however changed with electrolysis time, with the low energy peak at 655 nm (Fig. 5.4(ii)) being more prominent than the

high energy peak at 620 nm, even though the two were about the same intensity at the start of the reaction (Fig. 5.4(i)). The increase in absorbance continued for over two hours, without any shifting in wavelength of the peaks. This is an unknown behaviour in MPc complexes. Further ring reduction to the $\text{Ta}^{\text{IV}}\text{Pc}^{-4}$ species would result in a broad peak around 500 nm, and the disappearance of the peaks at 620 and 655 nm due to the $\text{Ta}^{\text{IV}}\text{Pc}^{-3}$ species [338]. A broad band was formed in the 500 nm region in Fig. 5.4, which may imply the presence of a Pc^{-4} species. However, the increased absorbance in the bands in the visible region suggested simultaneous reduction of the central metal. At the end of the electrolysis, coulometry confirmed a 4 electron transfer in Fig. 5.4. It was not possible to unequivocally assign process III from this work. However, since it was proven that this couple was a four electron process, the spectral changes shown in Fig. 5.4 were tentatively assigned to further reduction of Ta and the ring.

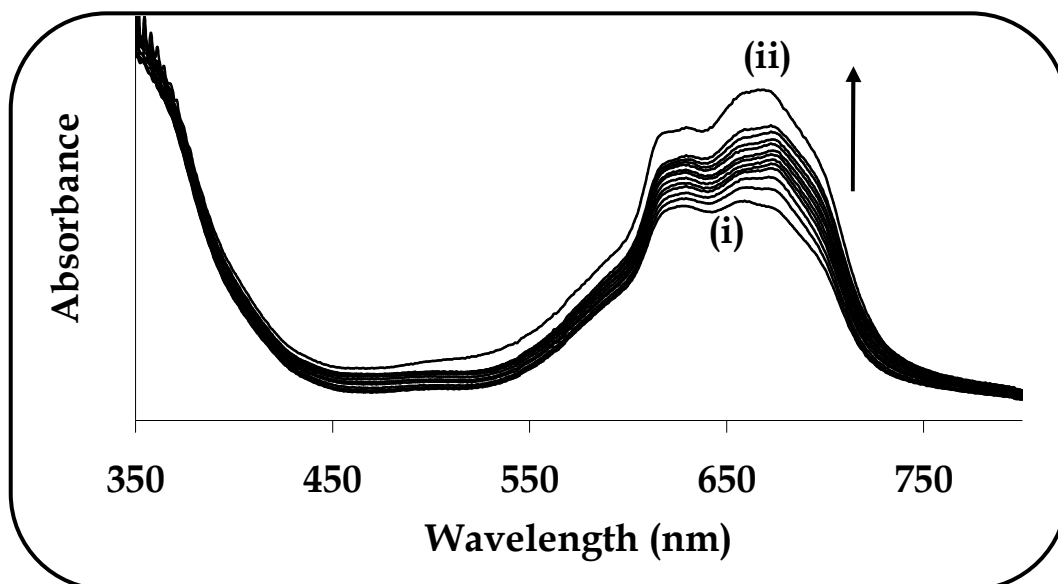
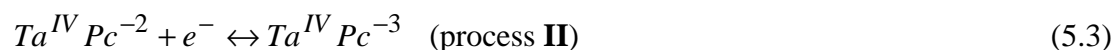
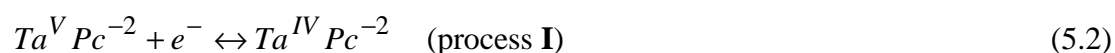


Figure 5.4: UV-Vis spectral changes observed during controlled potential reduction of 34 in DMF containing 0.1 M TBABF₄ at process III (-0.94 V). The first spectrum in (i) is the same as the last spectrum in Fig. 5.3, where (i) the first scan and (ii) the final scan.

Simultaneous two electron processes are very rare in phthalocyanines and simultaneous four electron processes are unknown. The occurrence of multi-electron transfer processes may be as a result of the non-planar nature of complex **34**, similar to non-planar porphyrins [439]. It is theoretically possible to reduce Ta^{IV} to Ta^I and to reduce the Pc ring by a further five electrons to form Pc⁻⁶ species. The spectral changes shown in Fig. 5.4, suggested ring reduction to Pc⁻⁴ and metal reduction, as discussed above.

Based on the above discussion, a mechanism was proposed for the electrochemical reduction of Cl₃TaPc (**34**) as follows, Eqs. 5.2 and 5.3, with axial chloride ligands left out:



Process **III** was tentatively assigned to:



Reduction of Cl₃TaPc (**34**) is expected to be accompanied by a stepwise loss of the Cl⁻ ligands. Equations 5.2 and 5.3 were proposed based on the spectroelectrochemical data which showed a one-electron reduction (at potentials of process **I**) at the metal and a one-electron reduction at the ring at potentials of process **II**. Equation 5.4 was tentatively proposed to account for the 4e⁻ transfer confirmed by spectroelectrochemistry.

5.2 Oxotitanium(IV) phthalocyanines

5.2.1 Phenoxy- and 4-*tert*-Butylphenoxy-substituted OTiPcs:

(37a, 37b, 38a, 38b)

Similar to TaPcs, detailed electrochemical studies of titanium phthalocyanine derivatives had not been reported. Figure 5.5 shows the cyclic voltammogram (CV) and square wave voltammogram (SWV, insert) performed in de-aerated DMF containing TBABF₄. Only one set of CV and SWV (for complex **37a**) is shown since all the complexes (**37a**, **37b**, **38a** and **38b**) had similar behaviour. The half-wave potentials ($E_{1/2}$) are listed in Table 5.1.

Three reversible reduction processes (labelled **I** – **III**), a poorly defined quasi-reversible oxidation process (labelled **IV**) and an irreversible oxidation peak (labelled **V**), were observed. For couples **I** – **III**, the cathodic to anodic peak currents (I_{pa}/I_{pc}) were near unity and anodic to cathodic peak separation (ΔE) ranged from 60 to 98 mV, thus suggesting reversible to quasi-reversible behaviour, ΔE of 90 mV was obtained for the ferrocene standard. A plot of the peak current (I_p) as a function of the square root of the scan rate ($v^{1/2}$) for all processes gave straight lines which are characteristic of a behaviour associated with a diffusion controlled process. Comparing the relative CV currents for processes **I** and **II** to those of process **III** may suggest that the former two couples involved more electrons than the latter. As stated above for Cl₃TaPc, multi-electron processes occurring in one step are not common. Stated above also is the fact that two-electron transfers in one step are known for distorted (non-planar) porphyrin complexes [441-443]. Therefore, it is possible that the complexes will show a single step multi-electron transfer process since titanyl phthalocyanine complexes have been reported to be distorted [33,36,444,445].

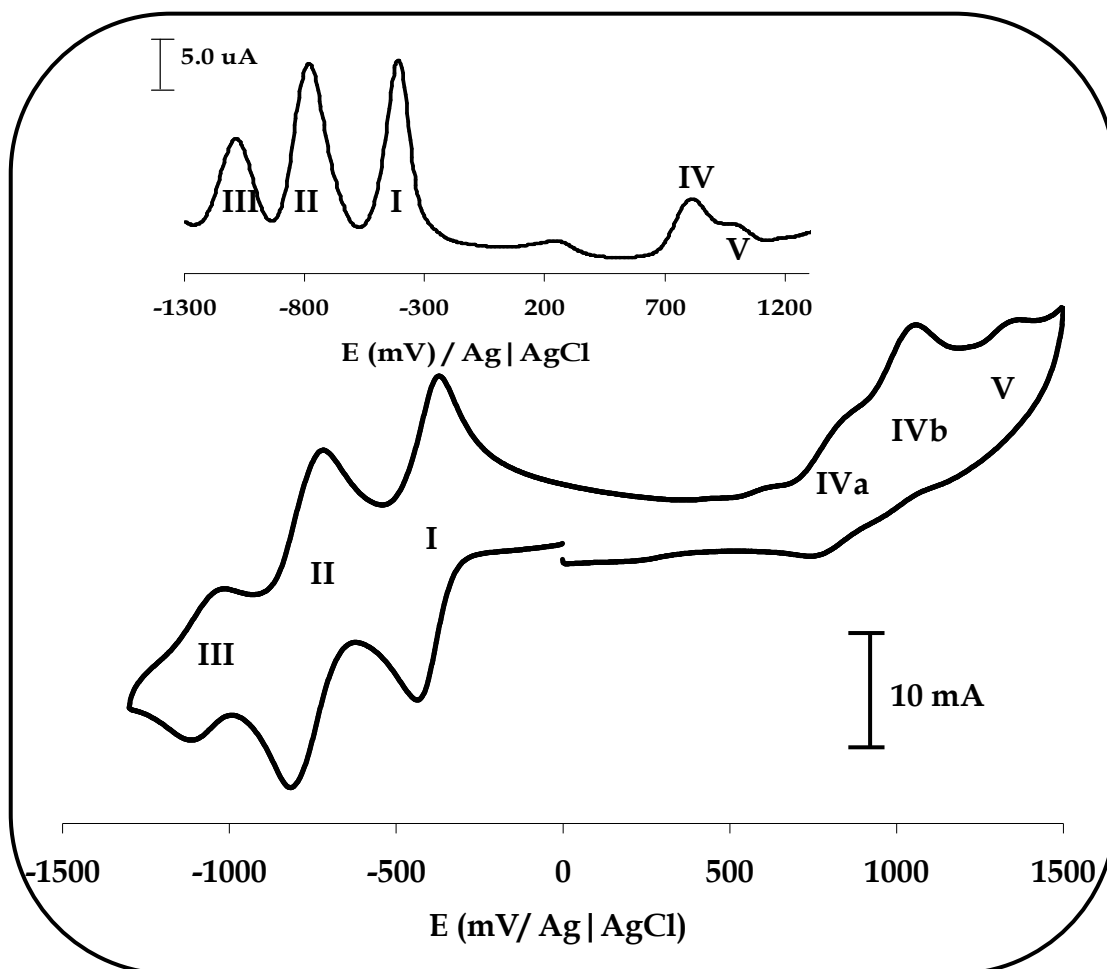


Figure 5.5: Cyclic and square wave (insert) voltammograms of **37a** in DMF containing 0.1 TBABF₄. Scan rate 0.1 Vs⁻¹.

The lack of symmetry of TiPc complexes thus resulted in electrochemical behaviour different from that of the corresponding ZnPc complexes such as the Zn complex of 2,(3)-tetra-*tert*-butylphenoxyphthalocyanine (ZnTBPPc), which showed two one-electron reductions and one one-electron oxidation [289], Table 5.1. MPc complexes are known to show one-electron redox processes [341], therefore the different behaviour exhibited by the TiPc complexes was due to their highly distorted nature, as was observed above for complex **34** (Cl₃TaPc).

Table 5.1: List of redox potentials for MPc complexes studied in this work.

Complex	Redox process [$E_{1/2}$ (V)]				
	I $\text{Ti}^{\text{IV}}\text{Pc}^{-2}/\text{Ti}^{\text{III}}\text{Pc}^{-2}$	II $\text{Ti}^{\text{III}}\text{Pc}^{-2}/\text{Ti}^{\text{II}}\text{Pc}^{-2}$	III $\text{Ti}^{\text{II}}\text{Pc}^{-2}/\text{Ti}^{\text{I}}\text{Pc}^{-3}$	IV $\text{Ti}^{\text{II}}\text{Pc}^{-3}/\text{Ti}^{\text{I}}\text{Pc}^{-4}$	Oxidations
33	-0.72	-0.98	-1.21		1.35
37a	-0.37 ^a	-0.78 ^b	-1.04 ^c	---	0.81, 0.99, 1.19
37b	-0.40 ^a	-0.77 ^b	-1.08 ^c	---	0.81, 1.00, 1.20
37c	-0.18	-0.58	-1.51	-1.76	---
37d	-0.14	-0.55	-1.42	-1.71	---
37e	-0.07	-0.46	-1.33	---	---
37f	-0.09	-0.40	-1.30	---	---
38a	-0.32 ^a	-0.74 ^b	-1.05 ^c	---	0.88, 0.99, 1.19
38b	-0.37 ^a	-0.78 ^b	-1.01 ^c	---	0.82, 1.01, 1.40
38c	-0.17	-0.59	-1.48	-1.74	---
38d	-0.14	-0.52	-1.40	-1.70	---
38e	-0.07	-0.37	-1.20	---	---
38f	-0.09	-0.42	-1.28	---	---
39a	-0.10	-0.47	-1.32	---	---
39b	-0.08	-0.42	-1.33	---	---
39c	-0.09	-0.41	-1.26	---	---
39d	-0.05	-0.37	-1.22	---	---
41	-0.42	-0.80	---	---	0.75, 0.98
ZnTBPPc ^d		-0.84	-1.32		0.70

^a Two electron reduction assigned to $\text{Ti}^{\text{IV}}\text{Pc}^{-2}/\text{Ti}^{\text{II}}\text{Pc}^{-2}$, ^b Two electron reduction assigned to $\text{Ti}^{\text{III}}\text{Pc}^{-2}/\text{Ti}^{\text{I}}\text{Pc}^{-3}$, ^c One electron reduction, assigned to $\text{Ti}^{\text{II}}\text{Pc}^{-3}/\text{Ti}^{\text{I}}\text{Pc}^{-4}$

^d TBPPc = *tert*-butylphenoxy phthalocyanine. Data from [289].

In order to identify ring-based redox processes in Fig. 5.5 and Table 5.1, the peak potentials were compared to those of the corresponding zinc derivative containing the same ring substituents. All processes are ring-based in ZnPc complexes since the central Zn metal is electroinactive [341]. In Table 5.1, the peak potentials of ZnTBPPc (as an example) reported before [289], have been included. The first ring reduction in this complex was observed at -0.84 V vs. Ag|AgCl in DMF, a value in the range of process **II**, and the first oxidation at 0.70 V, which is less positive than process **IV** of complexes **37b** and **38b**, containing the same substituents, i.e. 4-*tert*-butylphenoxy groups. These observations showed that in ZnTBPPc, oxidation was easier and reduction more difficult compared to the corresponding complexes **37b** and **38b**. This observation was due to the electropositive nature of the Ti^{+4} which makes oxidation more difficult and reduction easier.

Analysis of the closely spaced couples (**IVa** and **IVb**) observed for the oxidation process, suggested that they may have resulted from aggregation of the complexes. It has been well documented [341] that the closeness of the peaks generally results from aggregation of the electroactive species due to the concentrations employed for voltammetric studies. UV/Vis data of the complexes recorded at these concentrations ($\sim 10^{-4}$ M) showed broadening of spectra. The effect was further supported by the disappearance of the couple labelled **IVa** on dilution of the solution, showing that this process was due to the aggregated species. Processes **I** – **IV** were easily seen on the SWV and a small peak was observed on the SWV at ~ 200 mV, but not on CV and thus could not be assigned. Reduction in TiPc complexes is expected to occur at the central metal and at the ring, while oxidation is expected to occur only at the ring. Comparing the phenoxy substituted **37a** (non-peripheral) and **38a** (peripheral), shows that the latter was marginally more easily

reduced (for couples **I** and **II**) and more difficult to oxidize (process **IV**). The trend for the 4-*tert*-butylphenoxy substituted complexes **37b** and **38b** was not clear. Aromatic ring substituents function as electron donors hence are expected to enhance oxidation. Complexes **37b** and **38b** containing the 4-*tert*-butylphenoxy substituents should oxidise easily, hence the observation of oxidation peaks. Similarly, complexes **37a** and **38a** containing phenoxy substituents also showed oxidation peaks, due to the electron donating behaviour of the phenoxy group. Compared to the unsubstituted TiPc (**33**), complexes **37a**, **37b**, **38a** and **38b** were easily oxidised and easily reduced, Table 5.1.

To obtain a more accurate measurement of the redox equivalency, the three reduction processes were studied by chronocoulometry. Plots of Q (charge) vs. $t^{1/2}$ (time) from Eq. 5.5 (same as Eq. 1.24)

$$Q = \frac{2nFACD^{1/2}t^{1/2}}{\pi^{1/2}} \quad (5.5)$$

showed linear behaviour for processes **I** – **III**, Fig. 5.6.

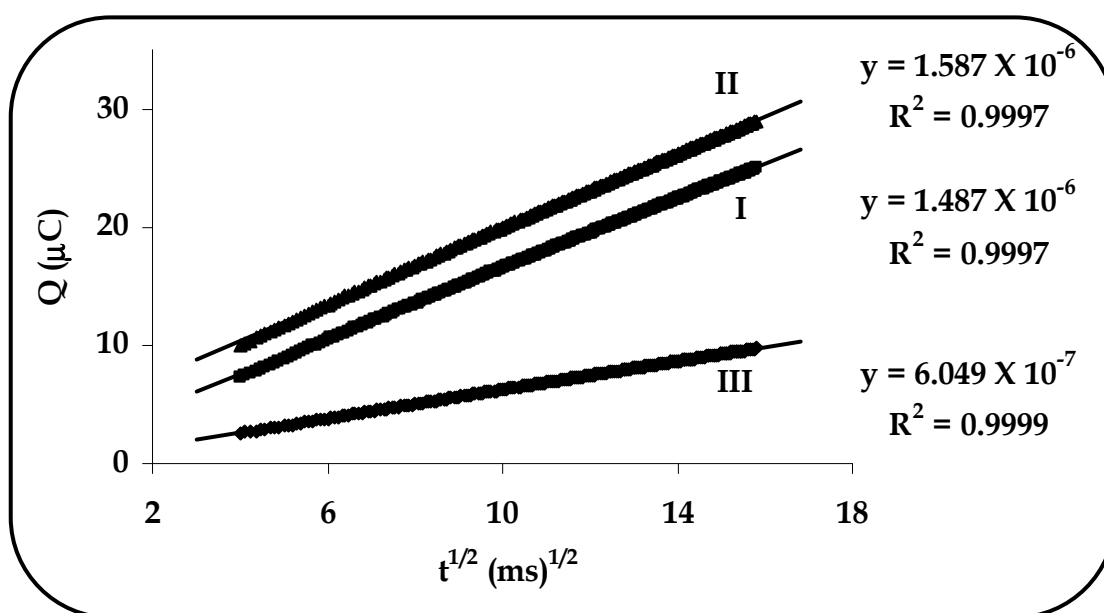


Figure 5.6: Anson plots for complex **37a** showing process **I** – **III**.

The linear responses were also obtained for these complexes. Slopes with a 2:2:1 ratio were obtained and were consistent with the involvement of two electrons for **I** and **II**, and one electron for **III**. The 2:2:1 ratio was determined in the following manner: For processes **I – III**, the potential was swept from 0 to -0.40 V, 0 to -0.80V and 0 to -1.05 V vs. Ag|AgCl respectively. From the Anson plots in Fig. 5.6, the slopes for processes **I – III** were respectively found to be 1.487×10^{-6} , 1.587×10^{-6} and 6.049×10^{-7} .

The ratios were found using Eqs. 5.6 – 5.8, i.e.

$$\text{process I} = \frac{1.487 \times 10^{-6}}{1.487 \times 10^{-6}} = 1.0 \quad (5.6)$$

$$\text{process II} = \frac{1.587 \times 10^{-6}}{1.487 \times 10^{-6}} = 1.1 \quad (5.7)$$

$$\text{process III} = \frac{6.049 \times 10^{-7}}{1.487 \times 10^{-6}} = 0.4 \quad (5.8)$$

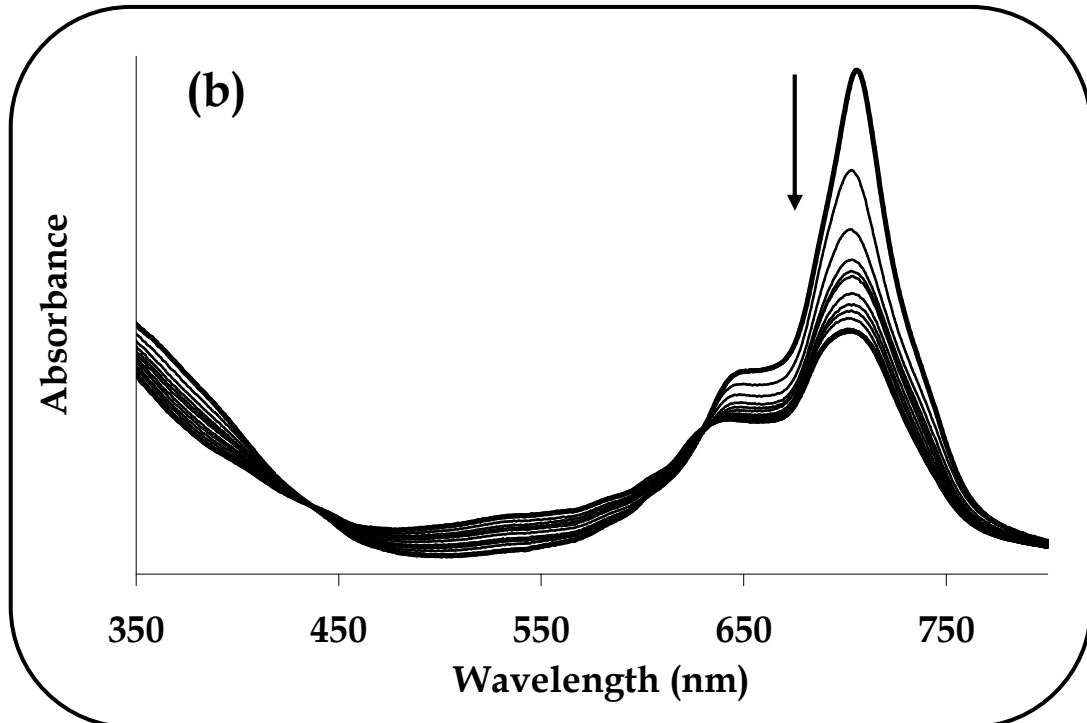
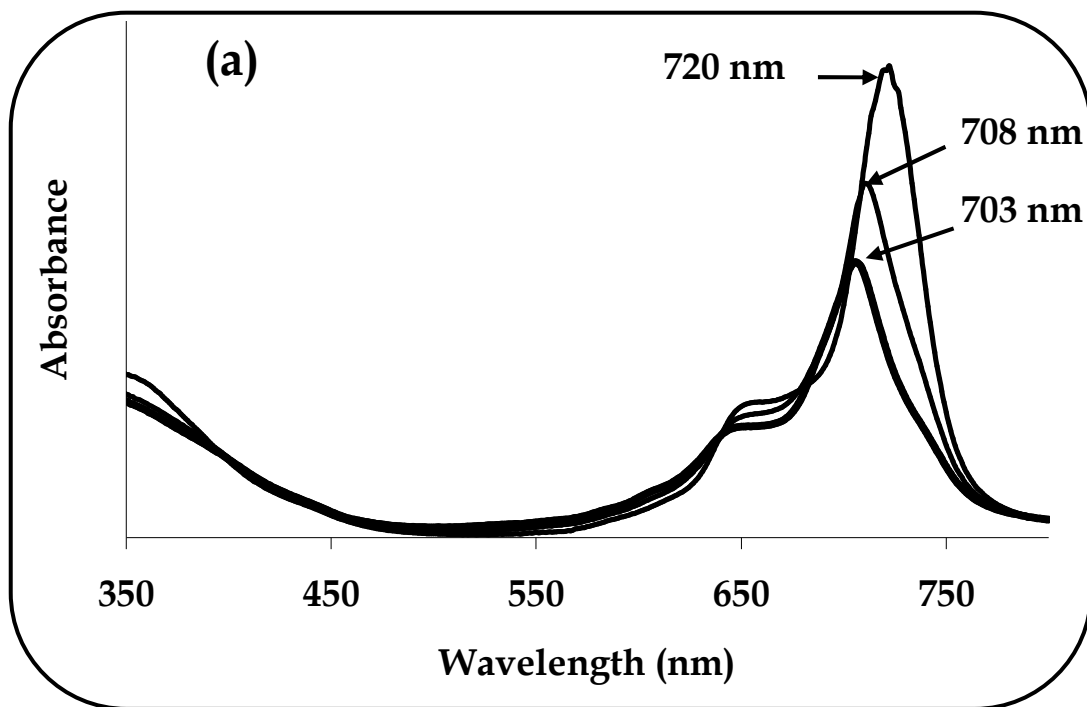
And therefore:

$$\begin{aligned} \mathbf{I} &: \mathbf{II} : \mathbf{III} \\ 1.0 &: 1.1 : 0.4 \quad (\times 2) \\ 2.0 &: 2.2 : 0.8 \end{aligned}$$

Spectroelectrochemistry was employed to further provide information on the nature of the redox processes observed in Fig. 5.5. As was the case with cyclic voltammetry all the complexes showed similar spectroelectrochemical behaviour, and complex **37a** was employed as an example, Figs. 5.7 and 5.8. Reduction at potentials of process **I**, resulted in the spectral changes shown in Fig. 5.7a, which consisted of a fast shift of the Q-band from 722 nm, first to 710 nm and then to 703 nm. These changes occurred within seconds. Coulometry ($Q = nFVC$) confirmed the number of electrons to be 1.93 (~2), hence confirming a two electron reduction. The step-wise

nature of the visible spectral changes confirmed the step-wise one-electron transfers, hence process **I** in Fig. 5.5 indicated an overlap of two one-electron transfers. The observed spectral changes were typical of reduction at the central metal which consists of shifting in the Q-band [168]. Thus the spectral changes in Fig. 5.7a were consistent with metal reduction from $\text{Ti}^{\text{IV}}\text{Pc}$ to $\text{Ti}^{\text{II}}\text{Pc}$ species. Further reduction at potentials of couple **II** resulted in the spectral changes observed in Fig. 5.7b and 5.7c. The figures have been separated for clarity. The first part of the changes in Fig. 5.7b, consisted of a decrease in intensity of the Q-band at 703 nm, and an increase in intensity in the 500–650 nm region. These spectral changes were typical of ring-based processes in MPc complexes [338], and suggested the formation of $\text{Ti}^{\text{II}}\text{Pc}^{-3}$.

Continuation of the reduction at processes of couple **II**, resulted in spectral changes shown in Fig. 5.7c. These changes consisted of a further increase in intensities of the peaks in the 500 – 650 nm region, a shifting of the 703 nm band to 713 nm and the increase of the peak at 638 nm. These spectral changes suggested continuation of ring reduction accompanied by metal reduction as judged by the shift in the Q-band. However, the final spectrum in Fig. 5.7c essentially showed a split Q-band, which could be a result of decrease in symmetry (such as demetallation). Demetallation was ruled out since re-oxidation of the complex at this stage, resulted in the regeneration (>65%) of the starting spectrum. Thus the spectral changes were due to simultaneous reduction of the ring and further reduction of the central metal to form the $\text{Ti}^{\text{I}}\text{Pc}^{-3}$, accompanied by a decrease in the symmetry of the molecule, hence the split Q-band. The number of electrons was calculated to be two at this stage, hence confirming the simultaneous reduction of the ring and metal to $\text{Ti}^{\text{I}}\text{Pc}^{-3}$. Again the observed step-wise nature of the spectra suggested that one-electron transfers overlapped in the CVs.



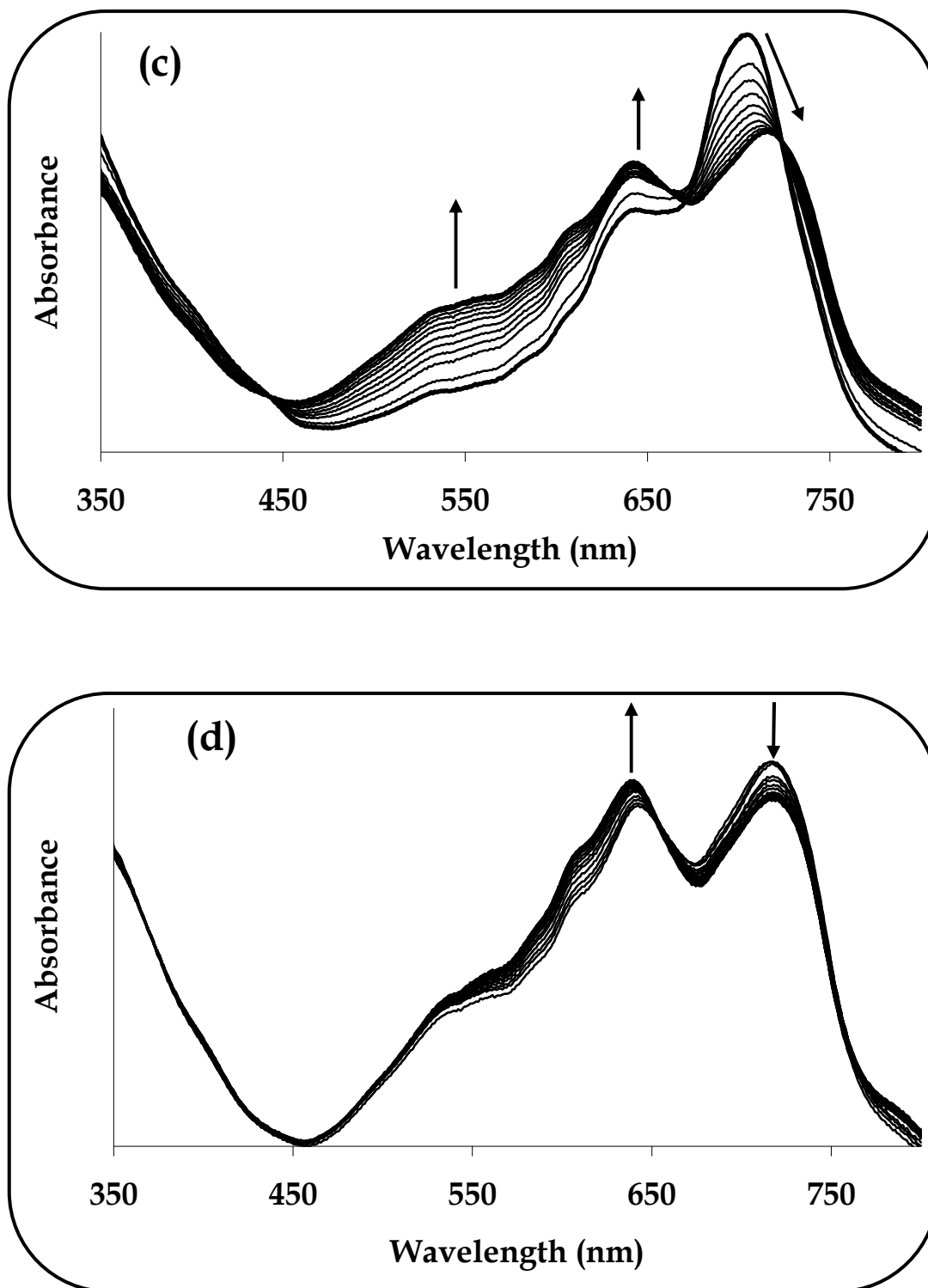


Figure 5.7: UV/Vis spectral changes observed during controlled potential reduction of 37a in DMF containing 0.1 M TBABF₄. Applied potential at: (a) couple I, (-0.50 V); (b) couple II (-0.80 V); (c) continuation of couple II (-0.80 V) and (d) couple III (-1.2 V). The first scan in (b) is the same as the last scan in (a). The first scan in (c) is the same as the last scan in (b) and the first scan in (d) is the same as the last scan in (c).

Continuation of the reduction at potentials of couple **III** resulted in spectral changes shown in Fig. 5.7d. These consisted of the decrease in the peak at 713 nm and an increase in the peak at 638 nm, without any shift. The total number of electrons obtained at the end of electrolysis (from couple **I** to **III**) was 5, as confirmed by coulometry. This suggested that the last stage of reduction involved one electron. The only possibility is further reduction of the ring and the formation of the $\text{Ti}^{\text{I}}\text{Pc}^{-4}$ species. However, reduction to Pc^{-4} species is expected to show a new broad band near 500 nm and the decrease in the peaks due the Pc^{-3} species. These changes were not clear in Fig. 5.7d.

Reduction of the central Ti^{I} metal would result in demetallation. However, the reoxidation of the final species even at this stage could still regenerate spectra. Thus process **III** was tentatively assigned to the formation of the $\text{Ti}^{\text{I}}\text{Pc}^{-4}$ species. Oxidation at potentials of process **IV** and **V** resulted in spectral changes shown in Fig. 5.8 (shown for complex **37a**). The changes showed clear decomposition as evidenced by the decrease in the Q-band with no new bands being formed. These observations confirmed the CV behaviour shown in Fig. 5.5, which showed oxidation of these TiPc molecules to exhibit irreversible to quasi-reversible behaviour.

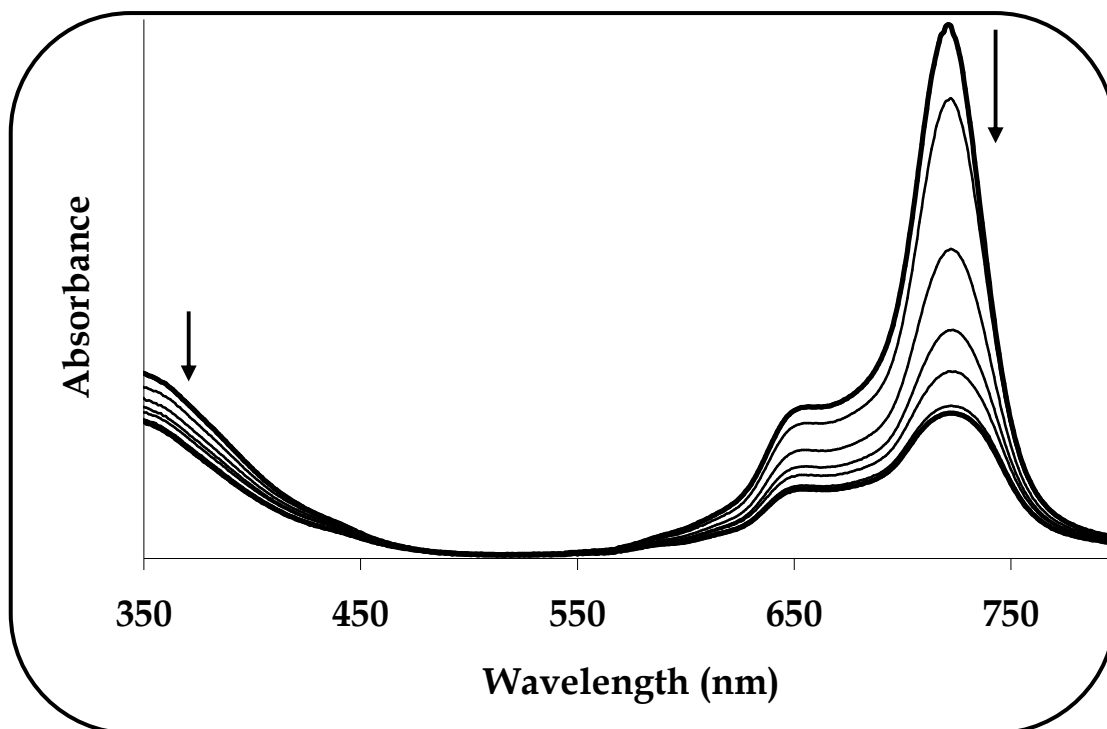
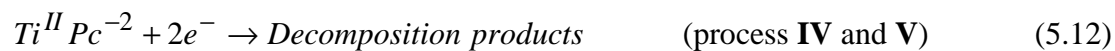
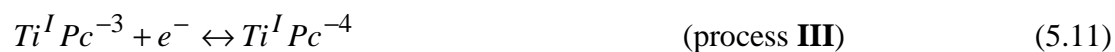


Figure 5.8: UV/Vis spectral changes observed during controlled potential oxidation of 37a in DMF containing 0.1 M TBABF₄. Applied potential for 1.10V.

Based on the cyclic voltammetry, square wave voltammetry, chronocoulometry and spectroelectrochemistry discussed above, the following mechanism may be proposed for the reduction, Eqs. 5.8 – 5.10 and oxidation, Eq. 5.11 of the TiPc complexes:



5.2.2 Benzyloxy- and 4-(benzyloxy)phenoxy tetra- and octa-substituted OTiPcs: (37c, 37d, 38c, 38d, 39a – d)

The need to study the electrochemical properties of OTiPcs in literature cannot be expressed enough as it is under-developed or has not been reported. As was the case with these abovementioned complexes, the electrochemical characterisation of the complexes under study was undertaken. The solution electrochemical characterisation of benzyloxy and 4-(benzyloxy)phenoxy tetra-substituted complexes (37c, 37d, 38c and 38d) as well as the octa-substituted (39a – d) complexes was studied and compared to that of phenoxy and 4-*tert*-butylphenoxy tetra-substituted complexes discussed in 5.2.1, Table 5.1. The reason to further study a wide range of OTiPcs is that the complexes exhibited different electrochemical behaviour.

The cyclic voltammogram (CV) and square wave voltammogram (OSWV) of complexes 37c, 37d, 38c, 38d and 39a – d were also performed in deaerated DMF containing TBABF₄ as electrolyte, Figs. 5.9 and 5.10. For complexes 37c, 37d, 38c and 38d, only one set of the CV and OSWV are shown since the complexes displayed similar electrochemical behaviour, Fig. 5.9. Similarly for complexes 39a – d, the CV and OSWV of 39b are shown as representative of the rest of the complexes, Fig. 5.10. The half-wave potentials ($E_{1/2}$) of the couples are listed in Table 5.1. The CV and OSWV of complexes 37c, 37d, 38c and 38d exhibited four reduction processes labelled I – IV while complexes 39a – d exhibited three couples labelled I – III. The anodic to cathodic peak separation (ΔE) of couples I – III at 0.1 Vs⁻¹ ranged from 60 to 70 mV for all complexes, thus suggesting that couples I – III were reversible. The ΔE of process IV was ~60 mV for complexes 37c, 37d, 38c and 38d; however, the current for the forward (cathodic) peak was much more enhanced than the current of

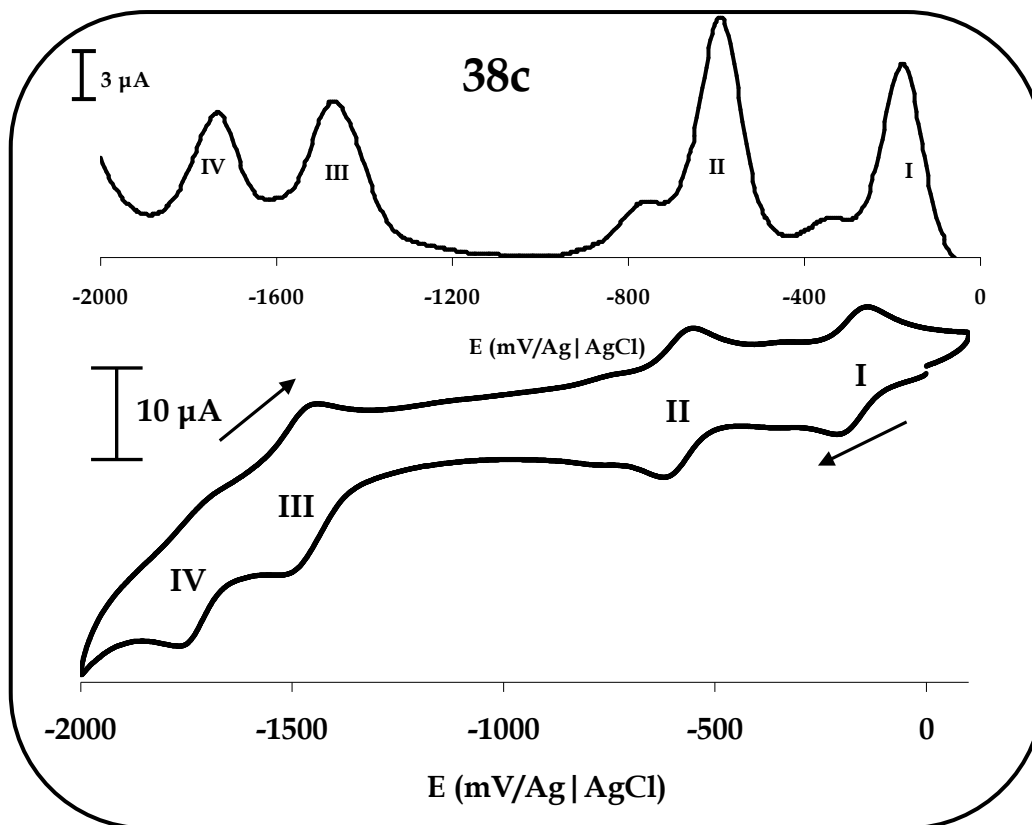


Figure 5.9: CV and SWV (insert) of 38c in DMF containing 0.1M TBABF₄.

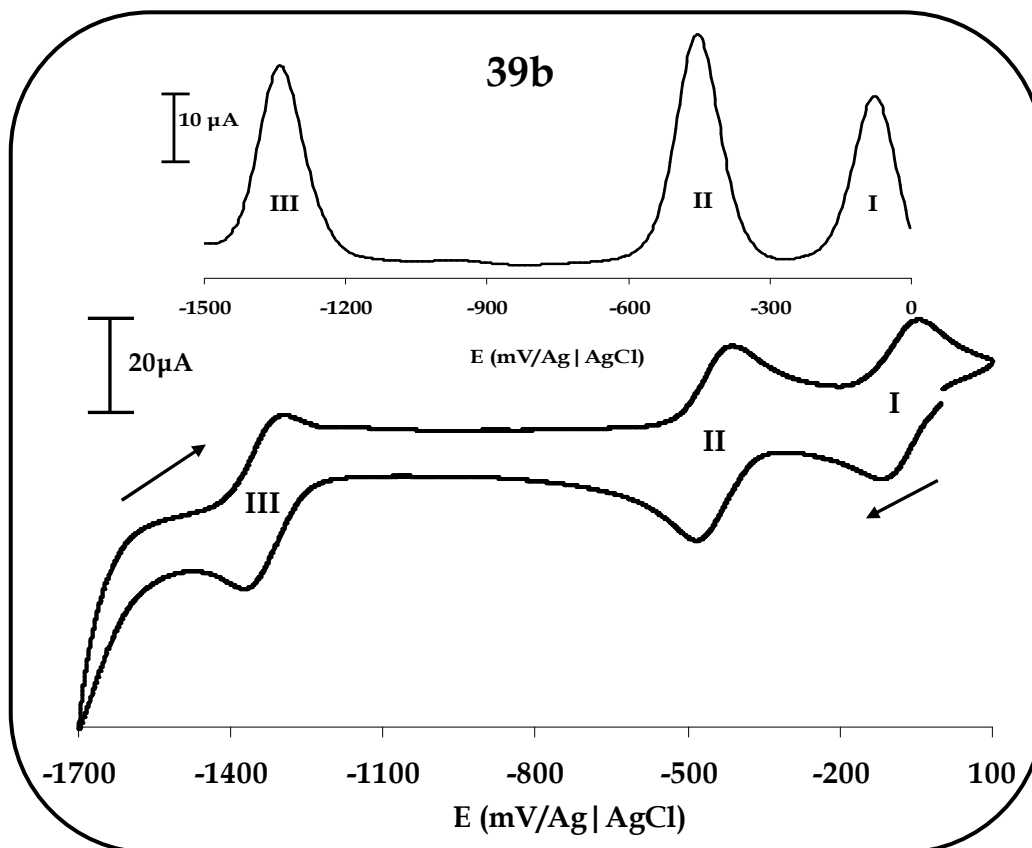


Figure 5.10: CV and SWV (insert) of 39b in DMF containing 0.1M TBABF₄. Scan rate 0.1 V.s⁻¹.

the return (anodic) peak, thus suggesting quasi-reversible behaviour. The cathodic to anodic peak current ratio (I_{pc}/I_{pa}) were near unity for couples **I** – **III**. Linear plots of I_p as a function of the square root of the scan rate ($v^{1/2}$) were obtained, thus suggesting diffusion control. The nature of the couples and the number of electrons transferred were confirmed by spectroelectrochemistry below. The $E_{1/2}$ values of the complexes (Table 5.1) show that the benzyloxy appended complexes (**37c** and **38c**) were marginally more difficult to reduce than the respective 4-(benzyloxy)phenoxy appended complexes (**37d** and **38d**). Table 5.1 also shows that the benzyloxy and 4-(benzyloxy)phenoxy appended complexes (**37c**, **37d**, **38c** and **38d**) were much easier to reduce (1st and 2nd reduction) than the phenoxy and 4-*tert*-butylphenoxy substituted complexes (**37a**, **37b**, **38a** and **38b**). The 4-*tert*-butylphenoxy substituted complexes (**37b** and **38b**) contain strong electron donating ligands making reduction more difficult. Complexes **39a** – **d** were even easier to reduce (1st and 2nd reduction) than the rest of the complexes. However, the 3rd reduction did not follow the same trend for all the complexes. Of the octa-substituted complexes, **39b** is expected to be more difficult to reduce than **39a** and **39c** due to the electron-donating nature of the 4-*tert*-butylphenoxy substituents, as was the case for the corresponding tetra-substituted complexes (**37b** and **38b**) compared to **37a**, **37c**, **37d**, **38a**, **38c** and **38d**). However, the three octa-substituted complexes (**39a** – **c**) have about the same first reduction potentials. It is not clear at the moment why the 4-*tert*-butylphenoxy substituents did not shift the reduction potential to more negative values for the octa-substituted derivatives. Similarly, the octa-substituted thiol derivative (**39d**) was expected to be more difficult to reduce than complexes (**39a** – **c**) due to the even more electron-donating nature of the thiol groups. The first reduction for **39d** was observed in the same range as that of complexes **39a** – **c**.

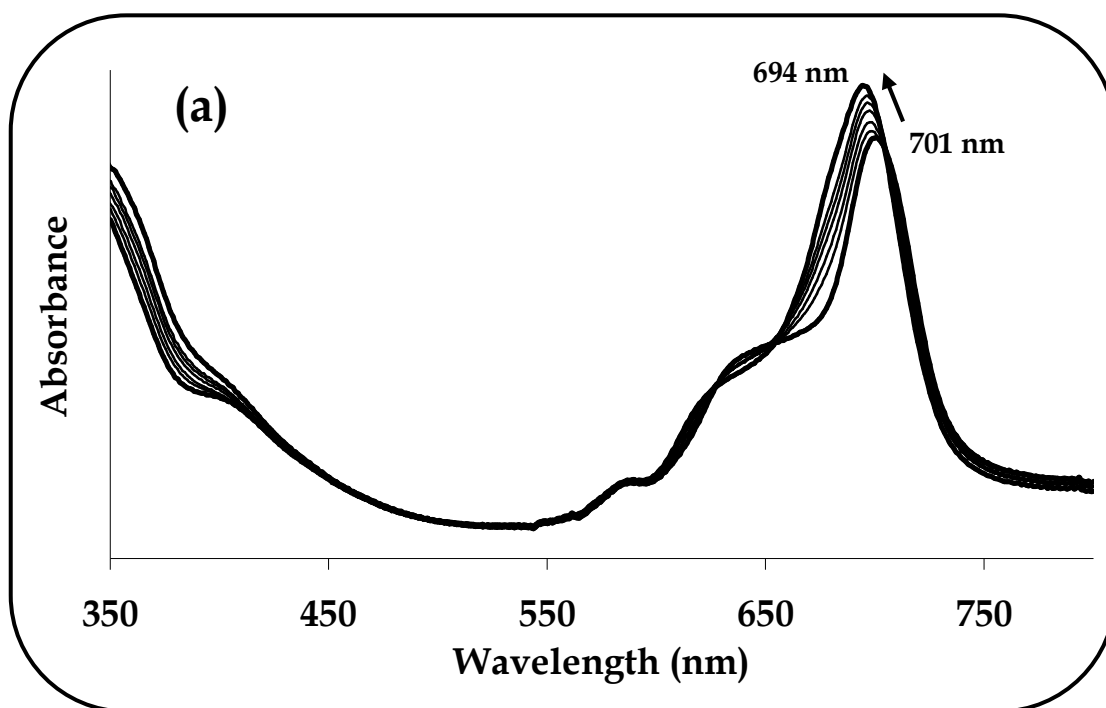
First reductions for **37c**, **37d**, **38c**, **38d** and **39a – d** were shifted to less negative potentials compared to **33**, **37a**, **37b**, **38a** and **38b**; implying that the first oxidations were also shifted to more positive values, hence the latter were outside the usable range of the solvent-electrolyte-electrode system employed in this work. Within the potential window of 0 – 1.50V, no oxidation peaks were observed for complexes **37c**, **37d**, **38c**, **38d** and **39a – d**, but oxidation was observed for complexes **33**, **37a**, **37b**, **38a** and **38b**. Also looking at the unsubstituted TiPc (**33**) in Table 5.1, oxidation was not easier. This suggested that substituents do affect the redox properties of TiPcs. For complexes **37a**, **37b**, **38a** and **38b** described in 5.2.1, an overlap of voltammograms whereby 2 one-electron reductions resulted in one couple were observed, Table 5.1. For the rest of the complexes it was further proved below that they were one-electron processes without overlapping of currents.

Oxidation of complexes **39a** and **39b** was expected, due to the electron donating nature of the phenoxy and 4-*tert*-butylphenoxy substituents as was the case with **37a**, **37b**, **38a** and **38b**, but no oxidation peaks were observed for the former complexes within the potential window employed. This might imply differences in the electrochemical behaviour of octa- vs. tetra-substituted derivatives. For example, the octa-substituted derivatives are easier to reduce compared to the rest of the complexes implying that the redox processes are shifted to more positive values.

For a more accurate measurement of the redox equivalency of couples **I – IV** for complexes **37c**, **37d**, **38c** and **38d**, chronocoulometry was employed. For the complexes, plots of Q versus $t^{1/2}$ (not shown) yielded linear responses with slopes in a 1:1:1:1 ratio, for potential steps encompassing processes **I – IV**. Similarly for complexes **39a – d**, a 1:1:1 ratio for the slopes for processes **I – III** was obtained. The observation suggested that a one-electron transfer process was involved in each

redox step. For complexes **37a**, **37b**, **38a** and **38b**, however, the ratio was 2:2:1 for the CV couples of the 1st, 2nd and 3rd reductions respectively.

To obtain further information on the nature of the redox processes observed in Figs. 5.9 and 5.10, spectroelectrochemistry was employed. The tetra-substituted complexes **37c**, **37d**, **38c** and **38d** showed similar spectroelectrochemical behaviour; hence complex **38c** was employed as an example. Complex **39b** was used as a representative of the octa-substituted derivatives. Reduction at potentials of couple **I**, resulted in the spectral changes shown in Fig. 5.11a (**38c**) and 5.11b (**39b**), which consisted of a shift of the Q-band from 701 to 694 nm for complex **38c** and from 698 to 693 nm for complex **39b**. The observed spectral changes were typical of a metal-based reduction in MPcs. A one-electron transfer was confirmed by coulometry ($Q=nFVC$), therefore suggesting a metal reduction from $Ti^{IV}Pc$ to $Ti^{III}Pc$ species.



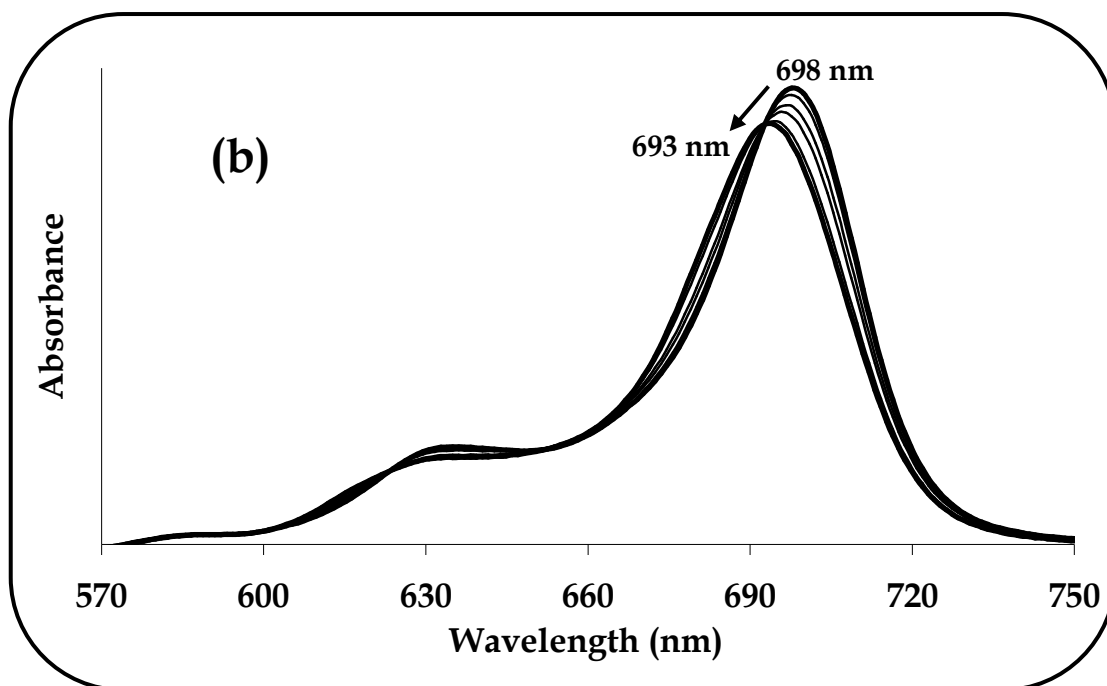


Figure 5.11: UV/Vis spectral changes observed during controlled potential reduction of (a) **38c** at an applied potential of couple I (-0.14 V) and (b) **39b** at an applied potential of couple I (-0.08 V) in DMF containing 0.1 M TBABF₄.

Further reduction at potentials of couple **II** resulted in the spectral changes observed in Fig. 5.12a (**38c**) and 5.12b (**39b**). At the potentials of couple **II**, the Q-band shifted from 694 to 687 nm for **38c**, thus suggesting another metal-based reduction. Coulometry confirmed a one-electron transfer thus suggesting that Ti^{III}Pc was reduced to Ti^{II}Pc. For **39b**, a shift from 693 to 687 nm occurred. Thus, both processes shown in Figs. 5.11 and 5.12 involved reduction at the central metal as judged by the shift in Q-band positions without significant loss in intensity [168]. The spectral changes occurred with clear isosbestic points showing that only two species were involved in each transformation. Reduction at the central metal is expected to result in the loss of the oxygen atom, resulting in irreversibility, however the CV showed reversibility and the original spectra in Fig. 5.11, could be regenerated ($>75\%$) by applying 0 V following reduction.

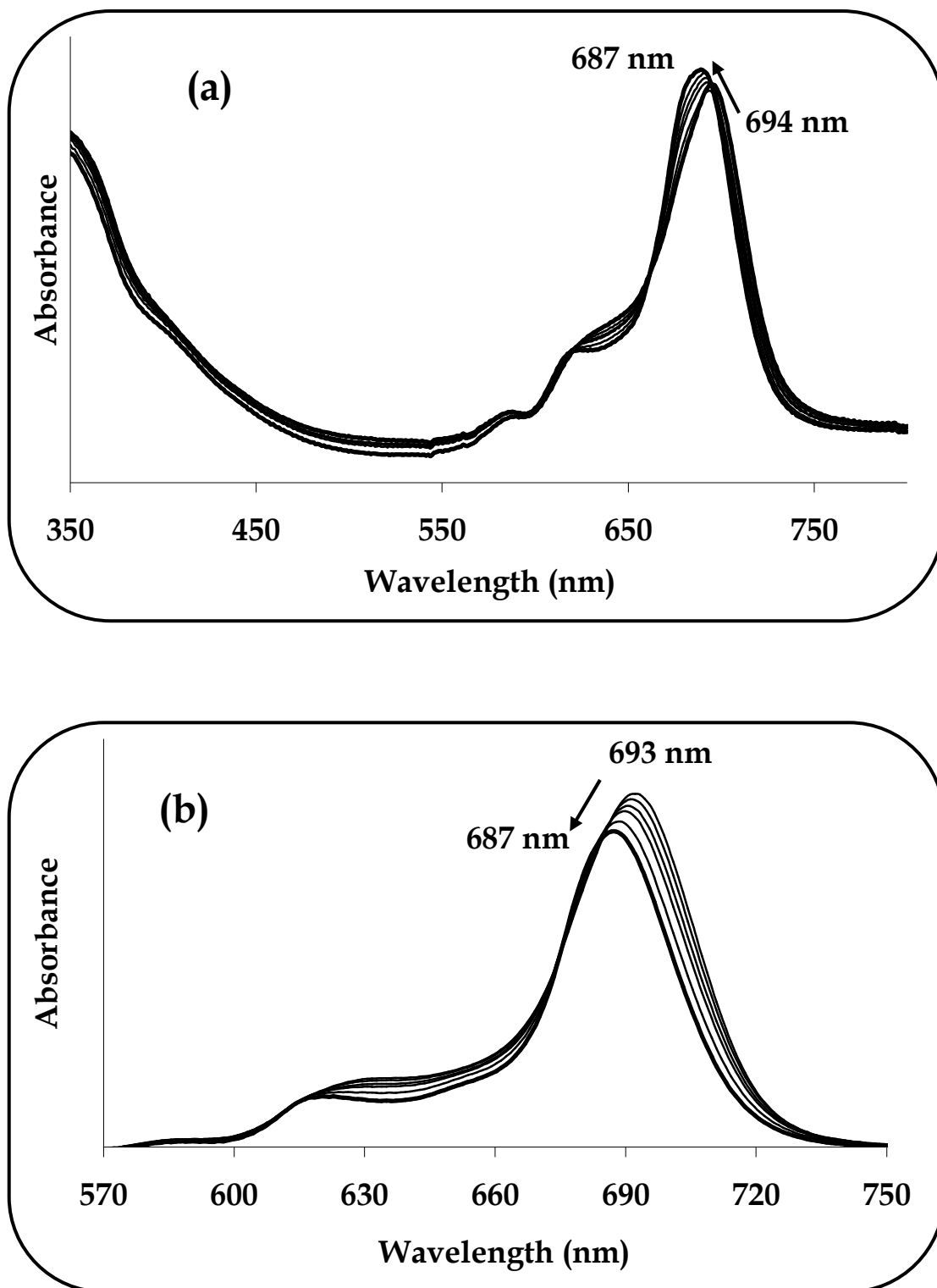


Figure 5.12: UV/Vis spectral changes observed during controlled potential reduction of (a) 38c at an applied potential of couple II (-0.6 V) and (b) 39b at an applied potential of couple II (-0.4 V) in DMF containing 0.1M TBABF₄. The first scans in (a) and (b) are the same as the last scans in Fig. 5.11(a) and (b), respectively.

Spectral changes observed during the reduction of complexes **37c**, **37d**, **38c** and **38d** to give $\text{Ti}^{\text{III}}\text{Pc}$ followed by $\text{Ti}^{\text{II}}\text{Pc}$ were in agreement with the reported reduction of **37a**, **37b**, **38a** and **38b** in that distinct spectral changes were observed for each species ($\text{Ti}^{\text{III}}\text{Pc}$ and $\text{Ti}^{\text{II}}\text{Pc}$), Table 5.1, even though the CV of the latter complexes showed only one couple for both processes. Therefore an overlap of one-electron reductions was observed for **37a**, **37b**, **38a** and **38b**, but was separated for **37c**, **37d**, **38c** and **38d** and complexes **39a – d**. Pc ring substitutions are expected to modify the redox potentials of the central metal. It seemed for the tetra-substituted phenoxy and tetra-substituted 4-*tert*-butylphenoxy TiPc complexes; the first reduction was shifted to more negative potential values to an extent that it overlapped with the second reduction. However, for the octa-substituted derivatives containing the same ring substituents, the overlap of reduction potentials was not evident. Isomers could also play a role on the reduction potentials of the complexes. Tetra-substituted complexes have isomers while the octa-substituted derivatives do not. From Table 5.1, it seemed that the easily reduced complexes (**37c**, **37d**, **38c** and **38d**, **39a – d**) are the ones that did not exhibit overlap of redox processes, as opposed to complexes **37a**, **37b**, **38a** and **38b**. An even further reduction at potentials of couple **III** resulted in spectral changes observed in Fig. 5.13a and 5.13b, which consisted of a decrease in the Q-band maxima accompanied by an increase in intensity in the 500 – 600 nm region. The spectral changes observed were typical of ring-based processes in MPcs, therefore, suggesting formation of $\text{Ti}^{\text{II}}\text{Pc}^{-3}$ [338].

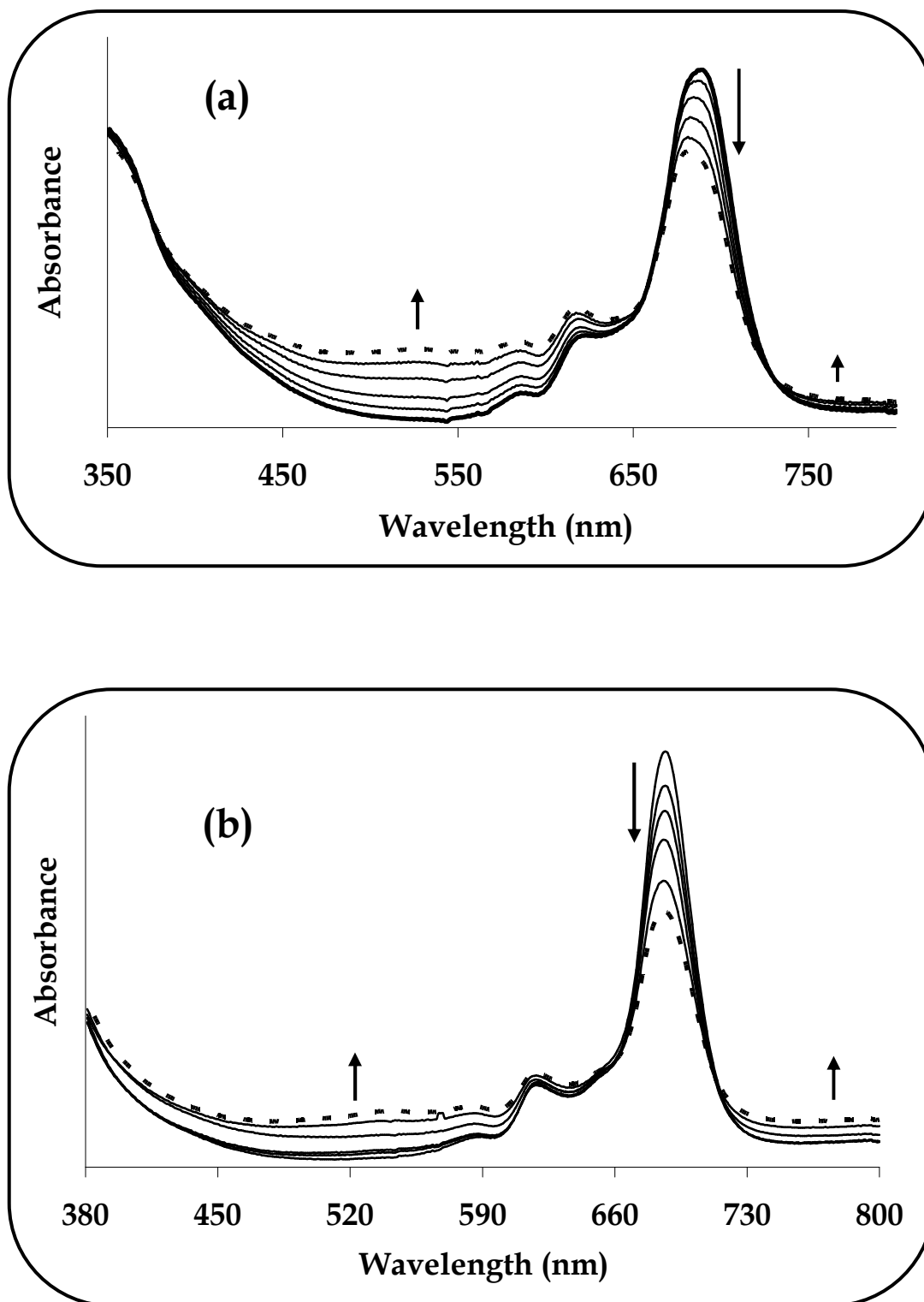


Figure 5.13: UV/Vis spectral changes observed during controlled potential reduction of (a) 38c at an applied potential of couple III (-1.4 V) and (b) 39b at an applied potential of couple III (-1.3 V) in DMF containing 0.1M TBABF₄. The first scans in (a) and (b) are the same as the last scans in Fig. 5.12(a) and (b), respectively.

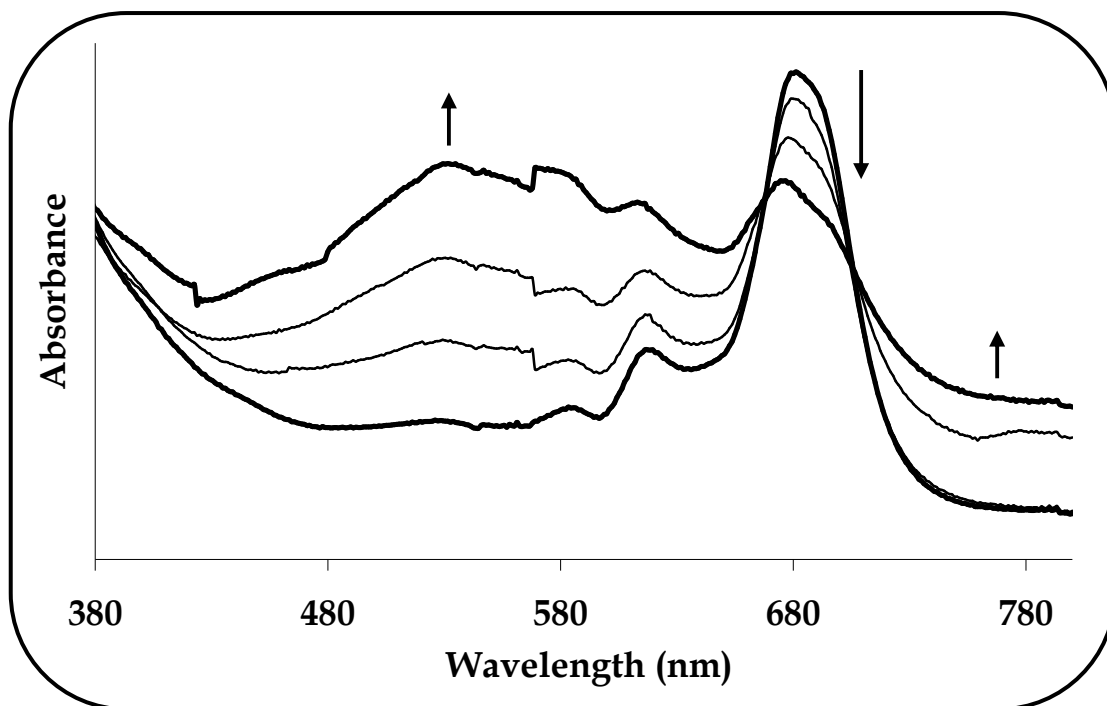


Figure 5.14: UV/Vis spectral changes observed during controlled potential reduction of **38c** at an applied potential of couple **IV** (-1.71 V) in DMF containing 0.1M TBABF₄. The first scan in Fig. 5.14 is the same as the last scan in Fig. 5.13(a).

Further reduction at potentials of couple **IV** for complex **38c** resulted in the spectral changes observed in Fig. 5.14. The Q-band maxima further decreased while there was an emergence of a broad peak at ~ 500 nm. This was typical [338] of a reduction of Pc^{-3} to Pc^{-4} , thus suggesting that $\text{Ti}^{\text{II}}\text{Pc}^{-3}$ was further reduced to $\text{Ti}^{\text{II}}\text{Pc}^{-4}$ for **38c**. Coulometry also confirmed a one-electron transfer for couples **III** and **IV**. Up to four Pc ring reductions are possible however limitations due to electrolyte, solvent and electrode can impose difficulty in observing at times, the last two ring reductions.

It was interesting to note that for complexes **37a**, **37b**, **38a** and **38b**, reduction to the $\text{Ti}^{\text{I}}\text{Pc}^{-4}$ species was observed, but in the case of **37c**, **37d**, **38c** and **38d**, reduction to the $\text{Ti}^{\text{II}}\text{Pc}^{-4}$ was observed without going through the $\text{Ti}^{\text{I}}\text{Pc}$ species. Based on the discussed electrochemical techniques, i.e. CV, SWV, chronocoulometry and

spectroelectrochemistry; the following mechanism for the reduction [Eqs. (5.13)–(5.16)] of the newly synthesised tetra-substituted (**37c**, **37d**, **38c**, **38d**) and octa-substituted (**39a – d**) TiPc complexes was proposed:



and for complexes **37c**, **37d**, **38c** and **38d**



5.2.3 Phenylthio- and benzylthio-substituted OTiPcs:

(**37e**, **37f**, **38e**, **38f**)

Thiol-substituted titanium phthalocyanines are unknown and hence their solution electrochemistry data is unknown. Similar to the complexes discussed above, the cyclic voltammograms of the four thiol-derivatised complexes **37e**, **37f**, **38e** and **38f**, were performed in deaerated DMF containing TBABF₄ as electrolyte. Only one set of cyclic voltammogram (CV) and square wave voltammogram (SWV) is shown since the complexes shared similar structural features and thus displayed similar electrochemical behaviour. The half-wave potentials ($E_{1/2}$) for all complexes are summarised in Table 5.1.

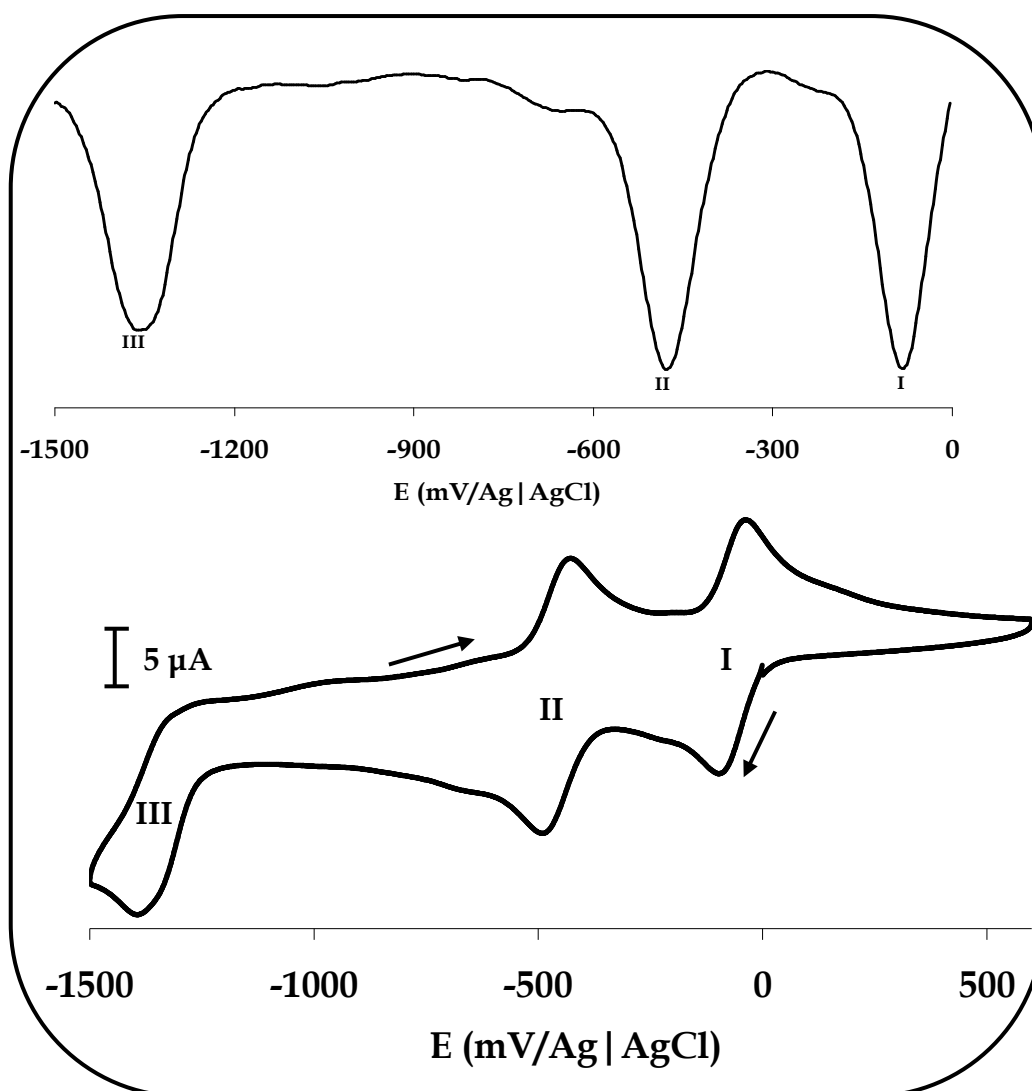
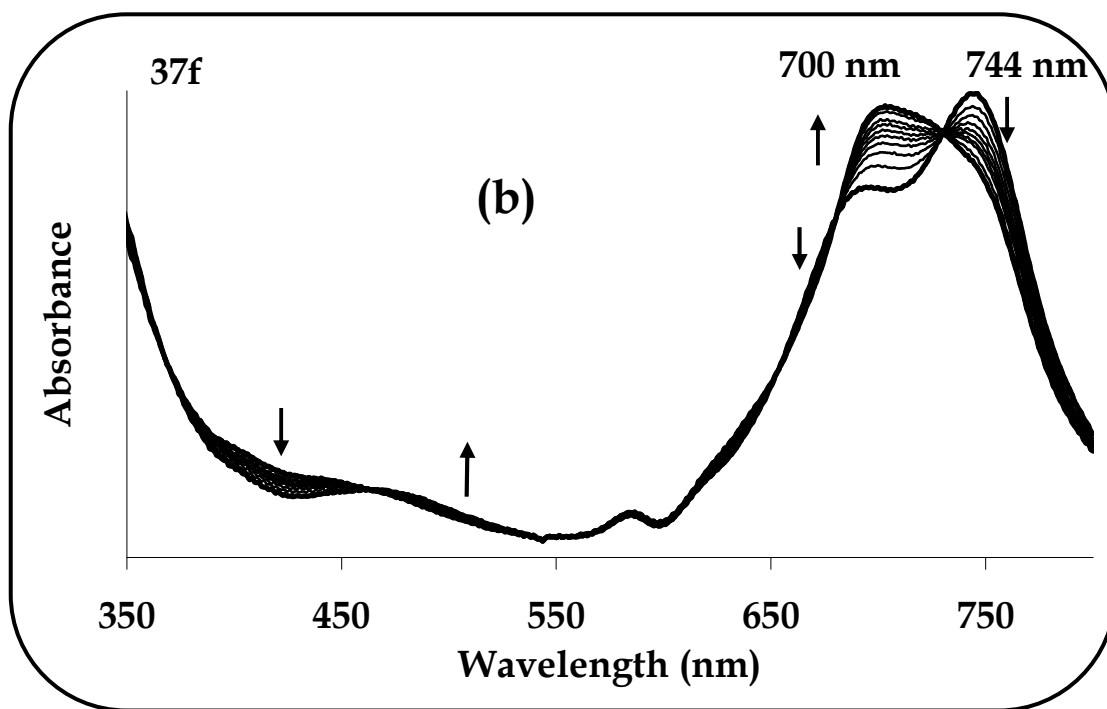
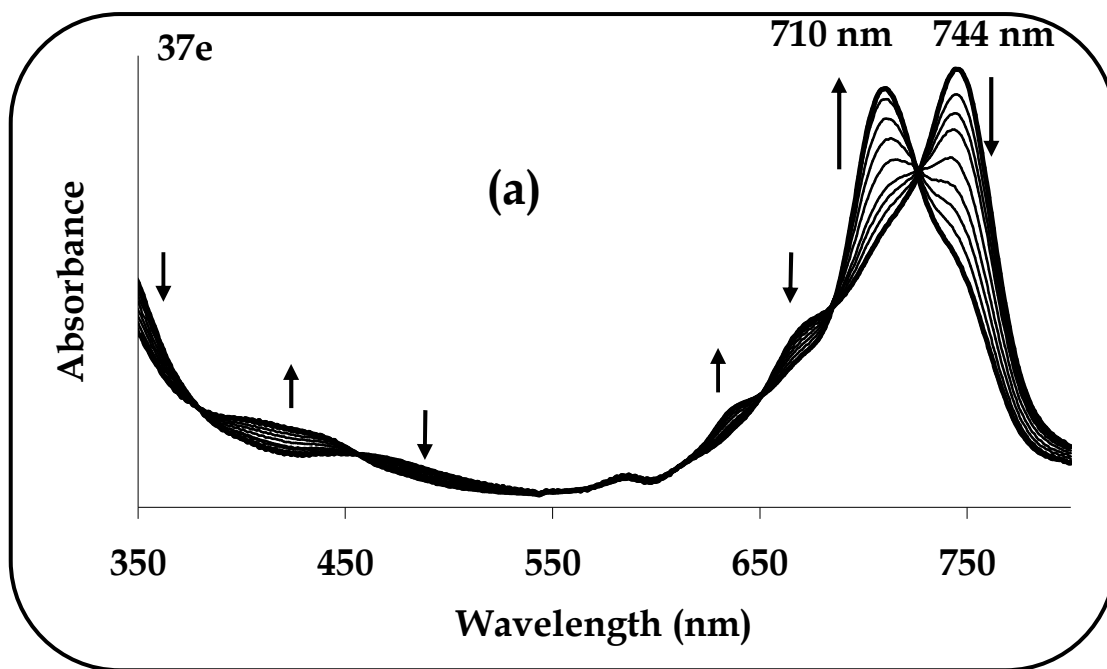


Figure 5.15: Cyclic and square wave (inset) voltammograms of **37e** in DMF containing 0.1 M TBABF₄. Scan rate 0.1 V s⁻¹.

Fig. 5.15 shows the CV and SWV of complex **37e** exhibiting three reduction processes labelled **I** ($E_{1/2} = -0.07$ V vs. Ag|AgCl), **II** ($E_{1/2} = -0.46$ V vs. Ag|AgCl) and **III** ($E_{1/2} = -1.33$ V vs. Ag|AgCl), Table 5.1. Reduction processes (**I** and **II**) displayed reversible behaviour with the anodic to cathodic peak separation (ΔE) of 62 and 60 for processes **I** and **II**, respectively at 0.1 Vs⁻¹. For couple **III**, ΔE was 56 mV but the current for the forward (cathodic) peak was more enhanced compared to the return (anodic) peak, suggesting quasi-reversible behaviour. For couples **I** and **II**, the cathodic to anodic peak current ratio (I_{pc}/I_{pa}) was near unity. The peak potentials did

not change with increasing scan rates for all the redox couples. For all redox couples, plots of peak current (I_p) vs. the square root of scan rate ($v^{1/2}$) were linear, thus suggesting diffusion control at the electrode surface. The relative CV currents of processes **I** – **III** were almost identical, thus suggesting that the couples involved the same number of electrons. The nature of the couples as well as the number of electrons transferred was confirmed by spectroelectrochemistry below.

Using a narrower scan window (600 to 800 mV) did not change the shape of the cyclic voltammograms. The $E_{1/2}$ values of the complexes (Table 5.1) did not show a clear trend when comparing peripherally and non-peripherally substituted complexes. Complexes containing the phenylthio substituent (**37e** and **38e**) showed marginally lower reduction potentials for the first reduction, compared to **37f** and **38f**. The complexes also showed similar reduction potentials to the octa-substituted complexes **39a** – **d**, Table 5.1. There were no peaks for the oxidation of the TiPc complexes within the potential range of 0 V to 1.4 V, confirming the difficulty in oxidizing these complexes due to the highly electropositive central titanium metal, in a similar manner to complexes **37c**, **37d**, **38c**, **38d** and **39a** – **d**. Further experiments such as chronocoulometry and spectroelectrochemistry were performed in order to accurately assign processes **I** – **III**. For potential steps encompassing processes **I** – **III**, plots of Q vs. $t^{1/2}$ (not shown) yielded linear responses with slopes in a 1:1:1 ratio for all the complexes. The observation suggested that a one electron transfer process was involved in each redox step. To identify the nature of the redox processes observed in Fig. 5.15, spectroelectrochemistry was employed.



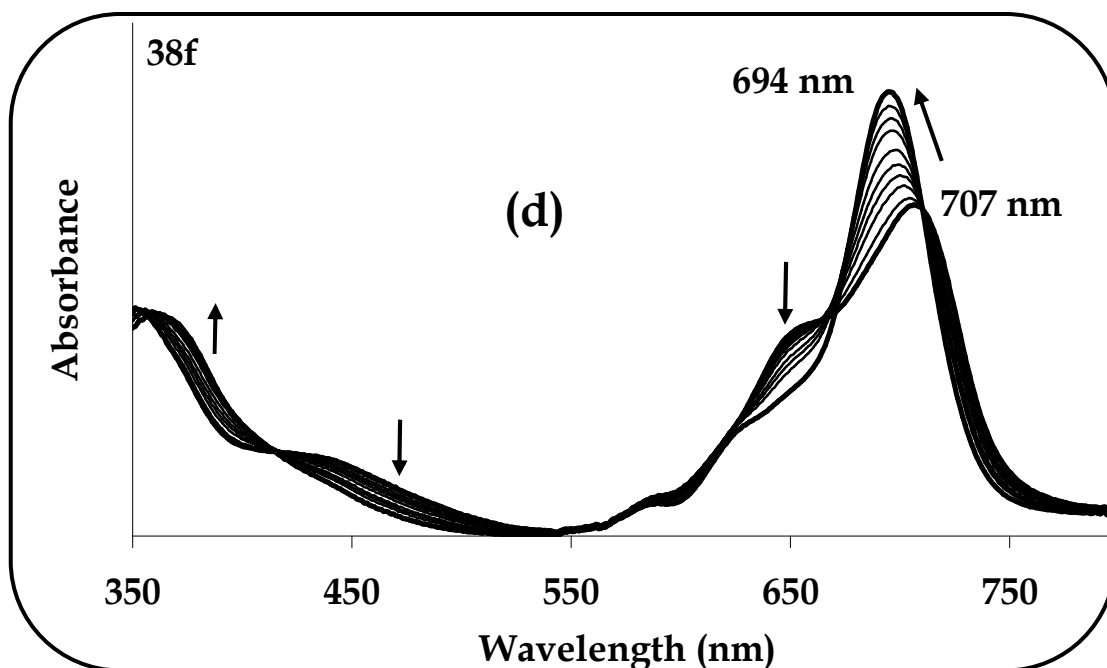
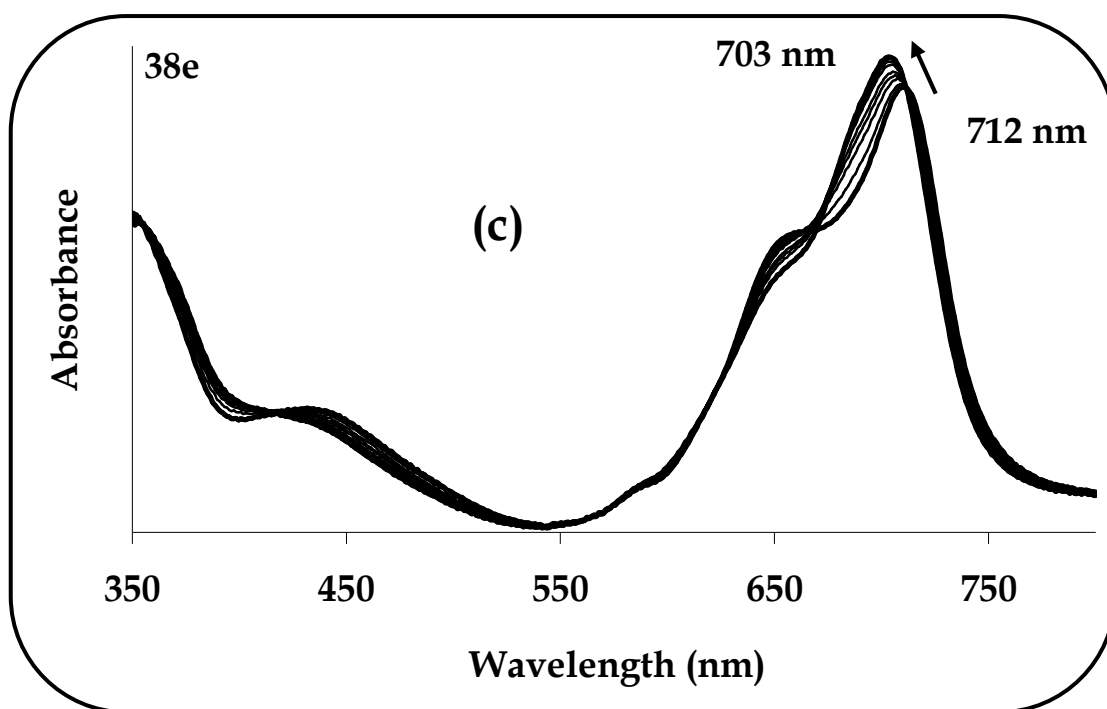
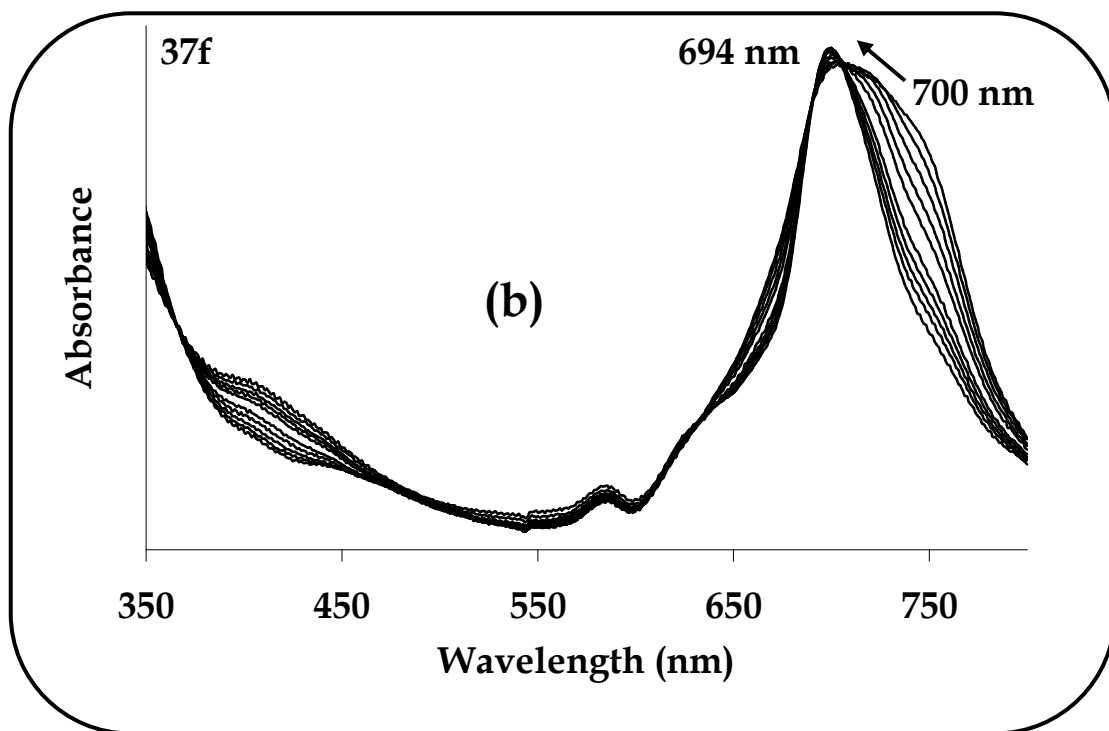
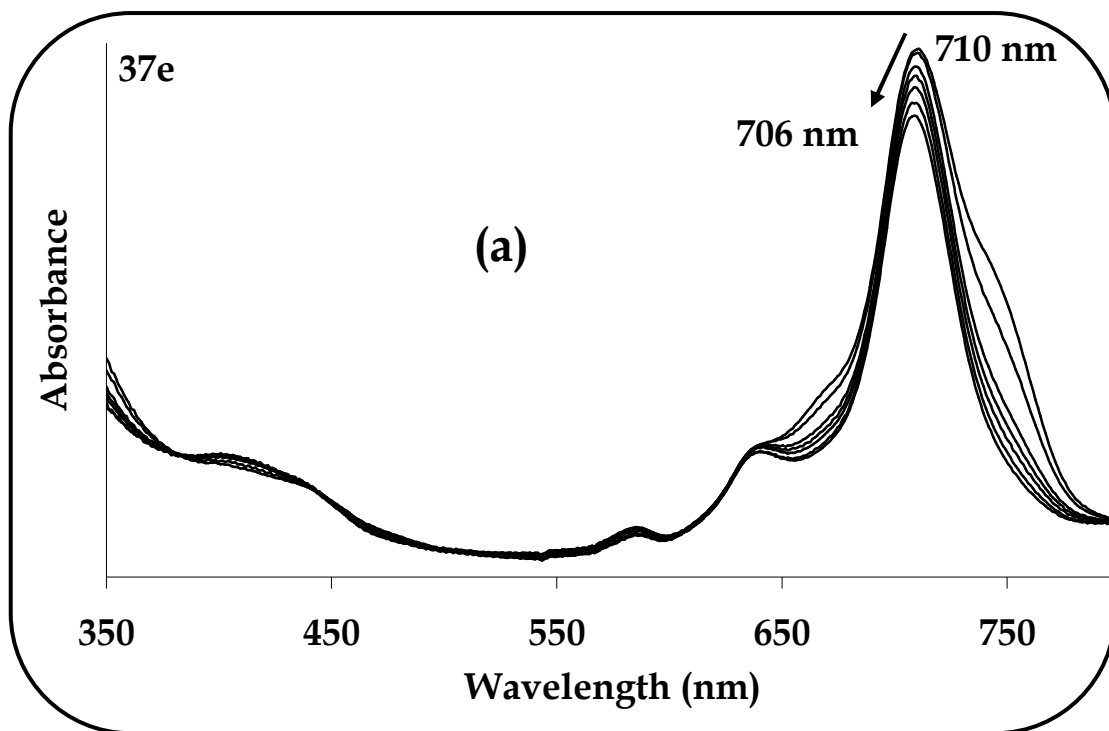


Figure 5.16: UV-visible spectral changes observed during controlled potential reduction of (a) 37e (b) 37f (c) 38e and (d) 38f in DMF containing 0.1 M TBABF₄. Applied potential just above couple I (-0.13 V).

The starting spectra in Fig. 5.16a - d (obtained in DMF) were broadened - an indication of aggregated species - due to high concentrations employed in the OTTLE cell studies. Fig. 5.16a - d show spectral changes observed when a controlled potential reduction of complexes **37e**, **37f**, **38e** and **38f** was respectively carried out at the potentials of process **I** of each complex. Reduction at process **I** resulted in the shift of the Q-bands with isosbestic points clearly showing the change from 744 nm to 710 nm (**37e**, Fig. 5.16a), 744 nm to 700 nm (**37f**, Fig. 5.16b), 712 nm to 703 nm (**38e**, Fig. 5.16c) and 707 nm to 694 nm (**38f**, Fig. 5.16d). These spectral changes were typical of a metal-based reduction in MPcs [168]. Coulometry ($Q = nFVC$) confirmed a one electron transfer ($n \sim 1$), therefore suggesting metal reduction from $Ti^{IV}Pc$ to $Ti^{III}Pc$ species. Further reduction at potentials of process **II**, resulted in the spectral changes observed in Fig. 5.17a - d for **37e**, **37f**, **38e** and **38f** respectively. The Q-band maxima shifted from 710 nm to 706 nm (**37e**, Fig. 5.17a), 700 nm to 694 nm (**37f**, Fig. 5.17b), 703 nm to 692 nm (**38e**, Fig. 5.17c) and 694 nm to 687 nm (**38f**, Fig. 5.17d); thus suggesting a metal-based reduction of couple **II**. A one electron transfer process was confirmed by coulometry therefore suggesting reduction of $Ti^{III}Pc$ to $Ti^{II}Pc$ species. Also, the observed spectral changes showed that upon reduction, the aggregated complexes gradually disaggregated, as judged by the narrowing of the absorption spectra.



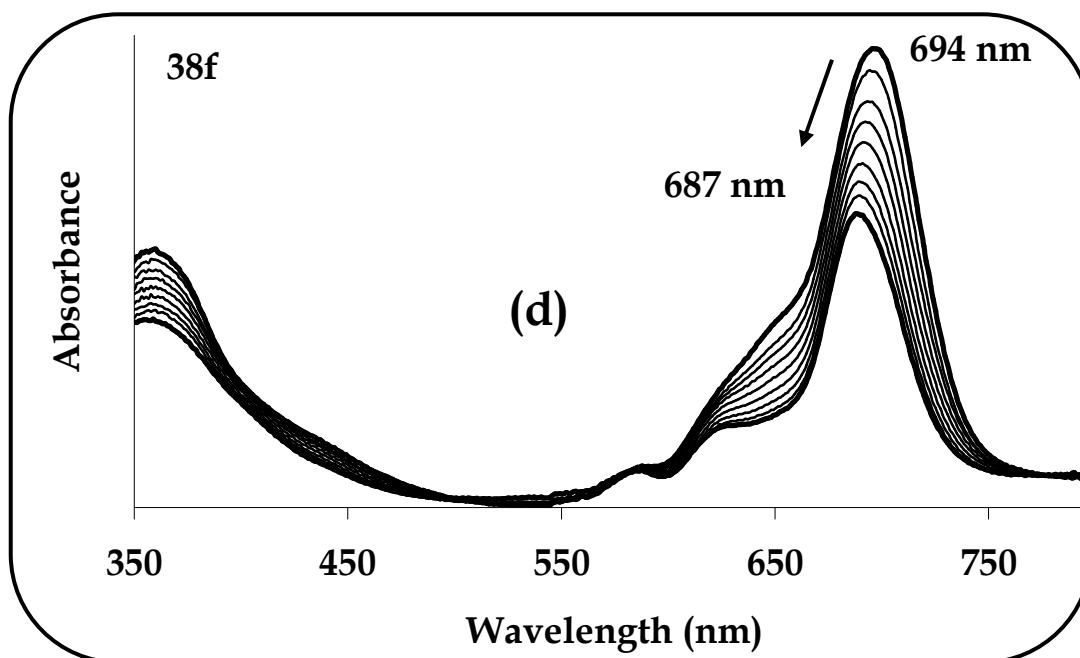
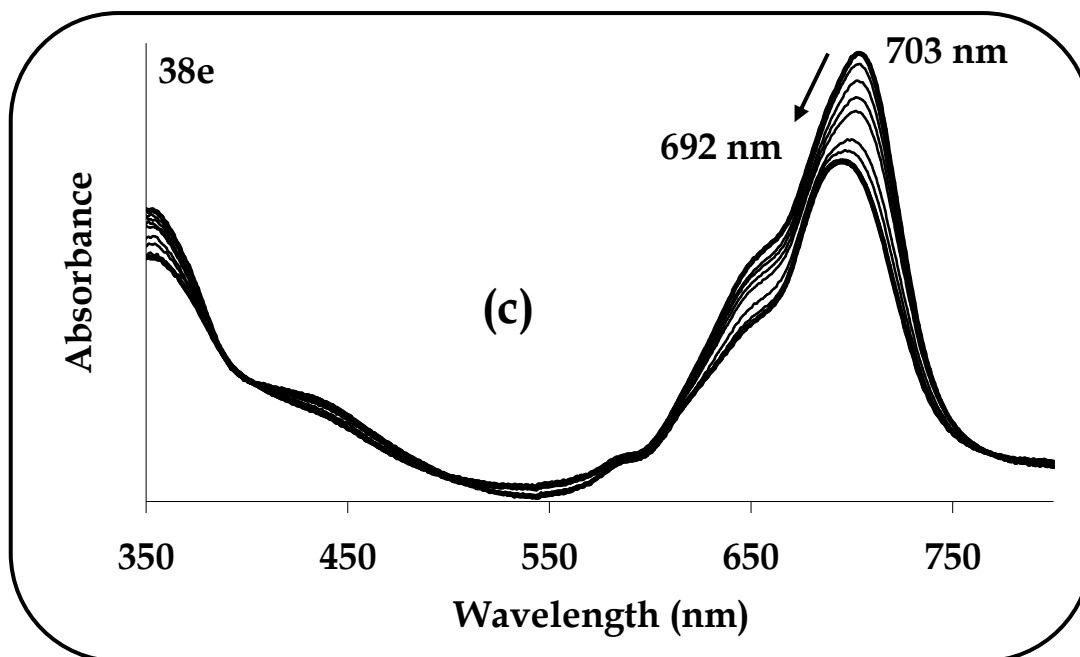
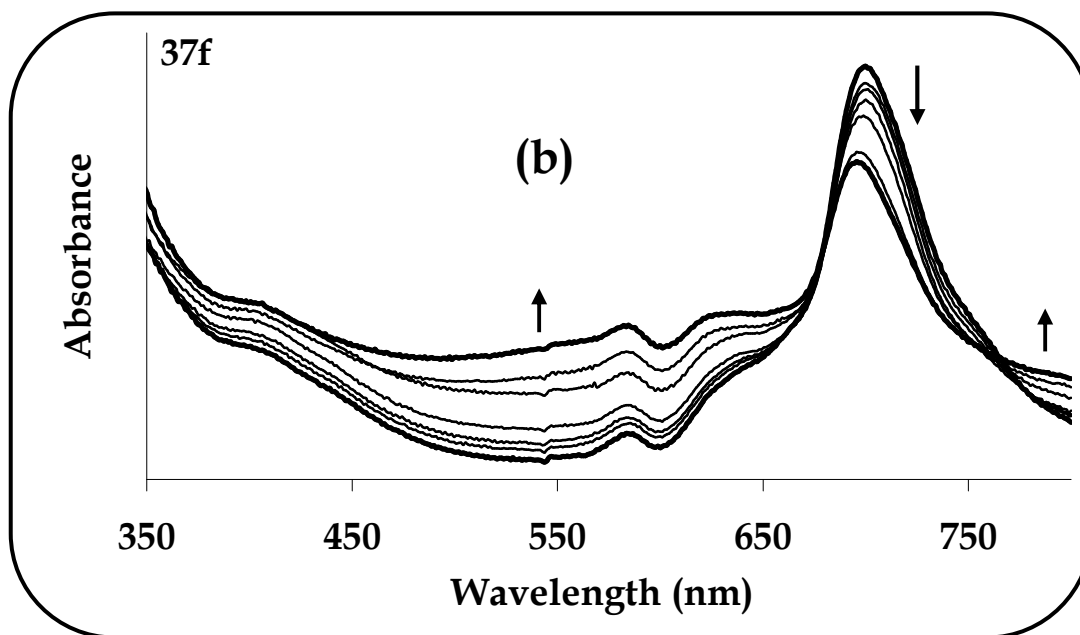
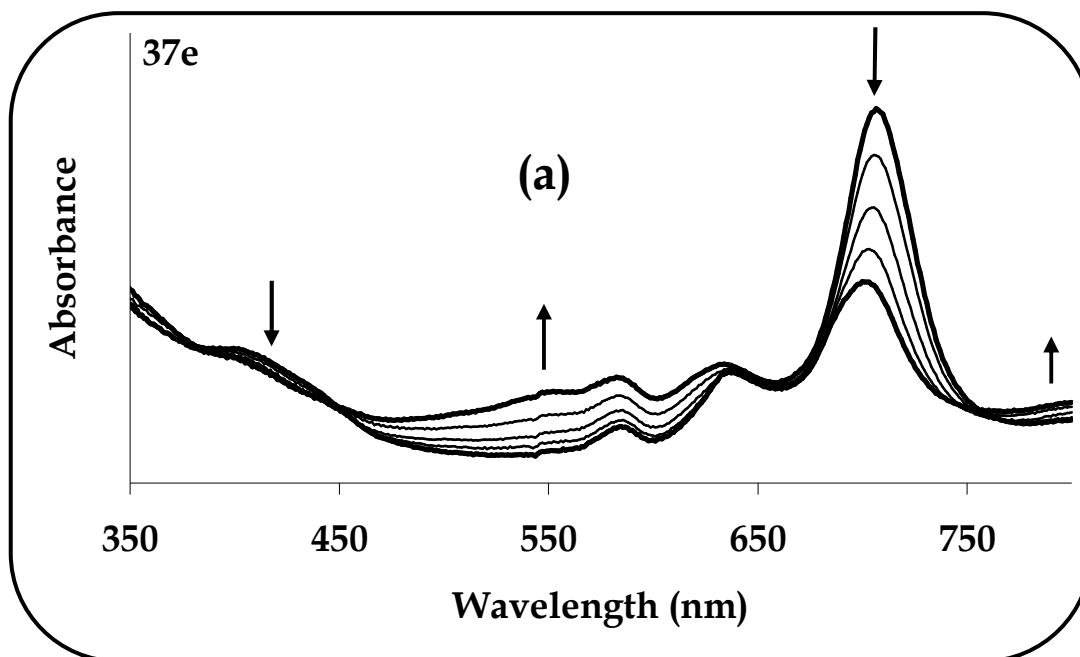


Figure 5.17: UV/Vis spectral changes observed during controlled potential reduction of (a) 37e (b) 37f (c) 38e and (d) 38f in DMF containing 0.1 M TBABF₄. Applied potential at couple II (−0.60 V). The first scans in (a) 37e (b) 37f (c) 38e and (d) 38f are the same as the last scans in Fig. 5.16 (a) 37e (b) 37f (c) 38e and (d) 38f, respectively.

Further reduction at potentials of process **III** resulted in spectral changes observed in Fig. 5.18a – d for **37e**, **37f**, **38e** and **38f** respectively, which consisted of a decrease in the Q-band maxima accompanied by an increase in intensity in the 500–600 nm region. The spectral changes observed were typical of ring-based processes in MPcs [338], thus suggesting formation of $\text{Ti}^{\text{II}}\text{Pc}^{-3}$.



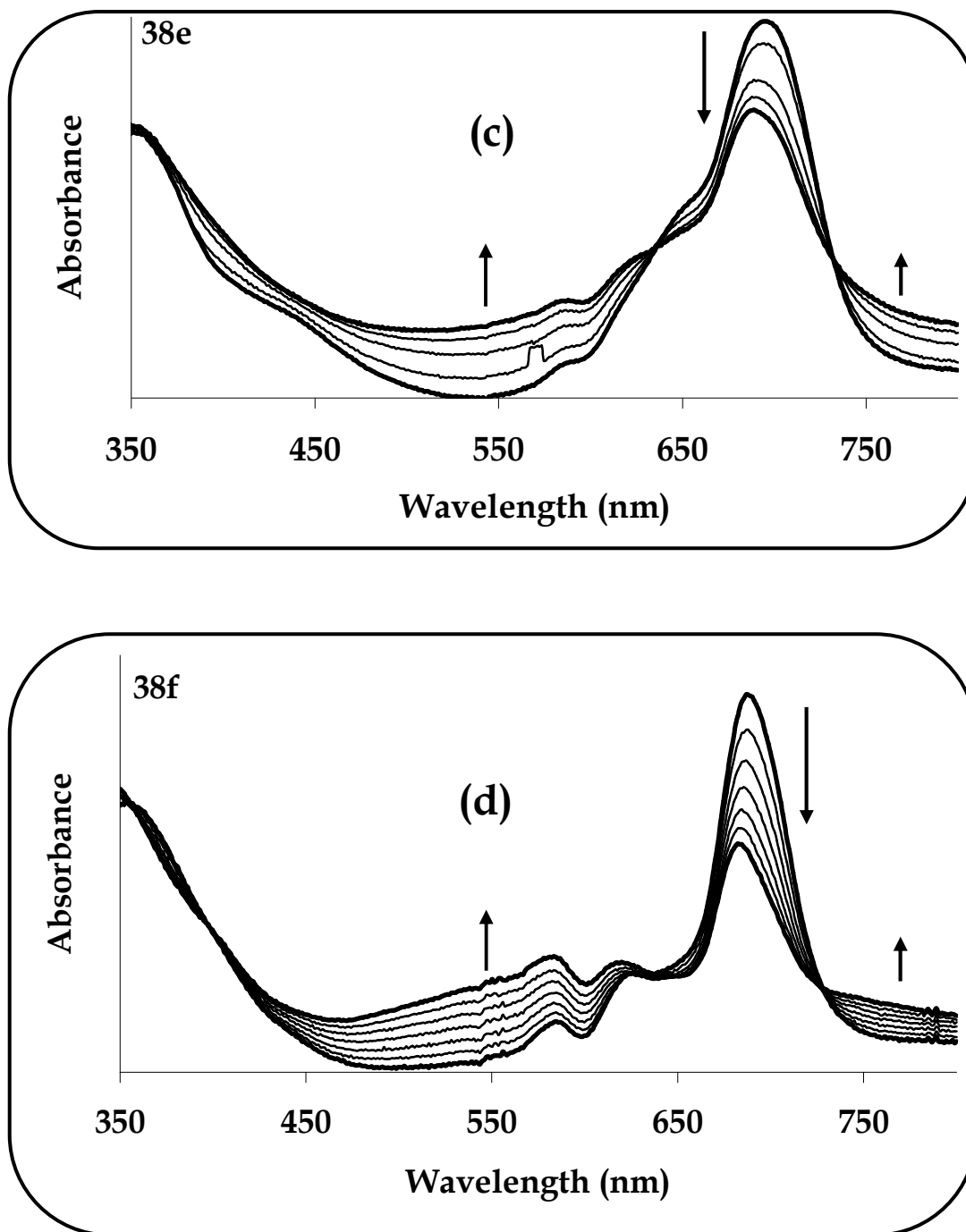


Fig. 5.18: UV/Vis spectral changes observed during controlled potential reduction of (a) 37e (b) 37f (c) 38e and (d) 38f in DMF containing 0.1 M TBABF₄. Applied potential at couple III (-1.35 V). The first scans in (a) 37e (b) 37f (c) 38e and (d) 38f are the same as the last scans in Fig. 5.17 (a) 37e (b) 37f (c) 38e and (d) 38f, respectively.

About 75% of the starting spectra were regenerated when potential was applied at rest potential, *i.e.* 0 V, suggesting reversibility of the complexes. Based on the discussed electrochemical techniques, *i.e.* CV, SWV, chronocoulometry and spectroelectrochemistry, the following mechanism for the reduction of the TiPc complexes is proposed:



5.2.4 Tetraamino oxotitanium(IV) phthalocyanine: (41)

Similar to the discussed OTiPcs, the electrochemical properties of TiPc(NH₂)₄ (**41**) are unknown, thus the electrochemical characterisation of the complex was also undertaken. The electrochemical behaviour of **41** was similarly investigated in deaerated DMF containing 0.1 M TBABF₄ as a supporting electrolyte. The cyclic and square wave (insert) voltammograms of the complex are shown in Fig. 5.19. The complex exhibited two reduction processes (labelled **I** and **II**) as well as two oxidation processes (labelled **III** and **IV**). The four processes were observed at half-wave potentials, $E_{1/2} = -0.42$ V (**I**), $E_{1/2} = -0.80$ V (**II**), $E_{1/2} = 0.75$ V (**III**) and $E_{1/2} = 0.98$ V (**IV**) vs. Ag|AgCl, Table 5.1. The anodic to cathodic peak separations (ΔE) of the processes ranged from 0.1 V to 0.18 V, suggesting the quasi-reversible nature and sluggish electron transfer of the processes. For all redox processes, plots of peak current (I_p) as a function of the square root of scan rate ($v^{1/2}$) were linear, an indication that the redox processes were diffusion controlled.

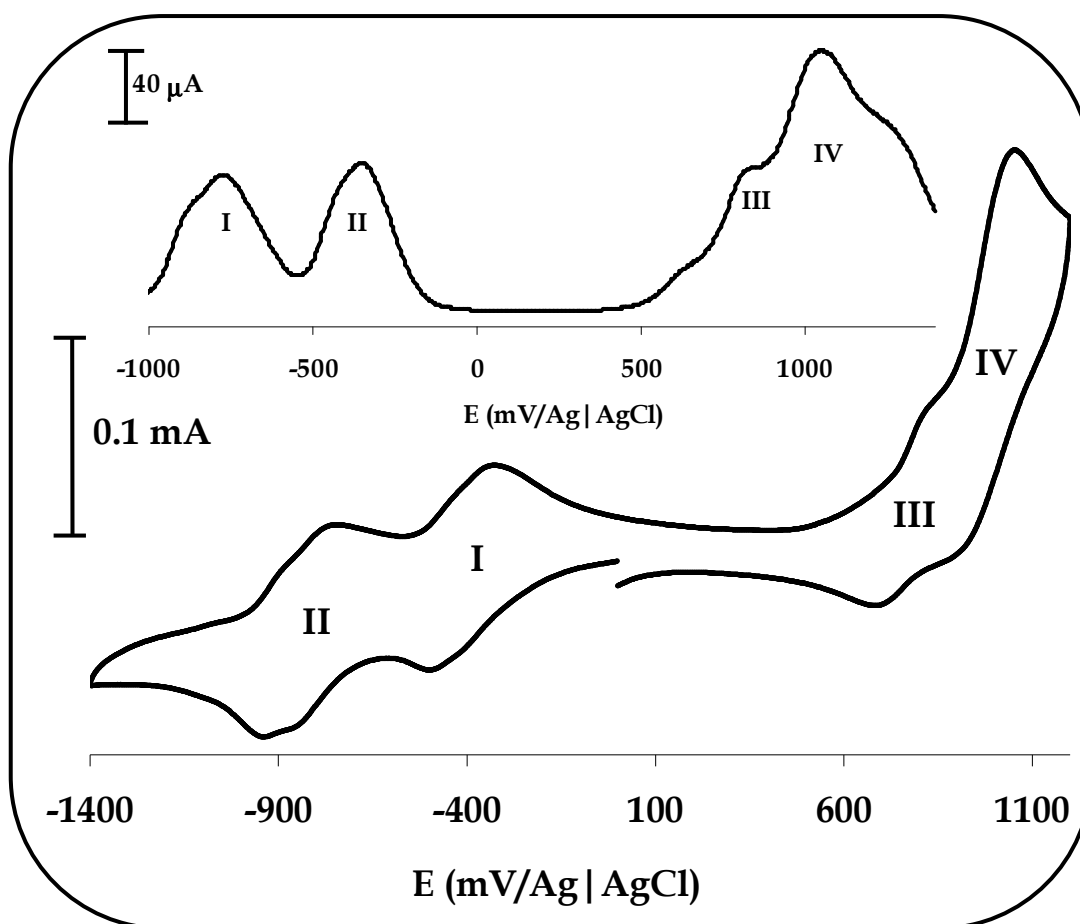


Figure 5.19: Cyclic and square wave (inset) voltammograms of complex **41** in DMF containing 0.1 M TBABF₄. Scan rate 0.1 Vs⁻¹.

Looking at the relative CV currents of processes **I** – **III** and comparing them to that of process **IV**, suggested that the latter involved a multi-electron transfer. Chronocoulometry was employed to determine an accurate measurement of the redox equivalency occurring at the four processes. The latter peak was in the range for amino group oxidation, whose potential tends to vary with the nature of the central metal, being observed at 0.63 V, 0.93 V, 1.15 V and 1.40 V for Cr [355], Mn [356], Co [341] and Fe [447] tetraaminophthalocyanines respectively. A closer look at process **II** shows two peaks, typical of aggregation in MPc complexes [341]. Linear plots of Q vs. $t^{1/2}$ (not shown) were obtained, with slopes in a 1:1:1 (reduction processes **I** – **II**). The ratios were consistent with the involvement of one electron

transfer for processes **I** – **III**. Processes **I** and **II** were assigned to the reduction of the metal, i.e. $\text{Ti}^{\text{IV}}\text{Pc}$ to $\text{Ti}^{\text{III}}\text{Pc}$ (**I**) and $\text{Ti}^{\text{III}}\text{Pc}$ to $\text{Ti}^{\text{II}}\text{Pc}$ (**II**) in comparison with the electrochemistry of the complexes discussed above, see Table 5.1. The oxidation process **III** was assigned to the oxidation of the ring, i.e. $\text{Ti}^{\text{IV}}\text{Pc}^{-2}$ to $\text{Ti}^{\text{IV}}\text{Pc}^{-1}$ (**III**). Complex **41** was marginally more difficult to reduce and easier to oxidise than complexes **37a** – **f**, even more so for complexes **38a** – **f** and **39a** – **d**, due to the electron donating ability of the amino groups, Table 5.1. However, the complex was much easier to reduce than the unsubstituted TiPc (**33**). Compared to the substituted complexes **37a** – **f**, **38a** – **f** and **39a** – **d**; the effect of amino substitution caused a potential shift to more negative values while oxidation potentials were shifted to less positive potentials.

5.3 Conclusion

The OTiPcs exhibited differences in electrochemical behaviour, hence the studies of this wide range of complexes. The easily oxidised complexes **37a**, **37b**, **38a** and **38b** exhibited overlap of redox processes as opposed to the easily reduced complexes **37c**, **37d**, **38c**, **38d** and **39a** – **d** which did not exhibit multi-electron transfers. Complexes **37b**, **38b** and **39b** with 4-*tert*-butylphenoxy as substituent exhibited a peculiar behaviour in that the tetra-substituted derivatives were easily oxidised while the octa-substituted derivative was easily reduced. For all complexes, the first two reductions were proved to be of metal character with that of complex **41** being marginally more difficult to reduce than the other complexes due to the electron-donating amino groups.

CHAPTER 6

Electrocatalytic properties

This chapter describes the electrocatalytic properties of OTiPc towards the oxidation of nitrite. The glassy carbon electrode is modified with these complexes either by the drop-dry or electropolymerisation methods. The catalytic efficiencies and kinetic parameters of these complexes are discussed.

6.1 Aryloxy tetra-substituted oxotitanium(IV) phthalocyanines:

(37a – d and 38a – d)

The tetra-substituted aryloxy complexes (**37a – d** and **38a – d**) were adsorbed onto the GCE by the drop-dry method since these complexes were not polymerisable. The main challenge of lowering overpotentials and increasing oxidation currents remains in the electrocatalytic oxidation of nitrite. A decrease in overpotential with a subsequent increase in catalytic current, are two important factors that determine the catalytic effect of various complexes at an electrode surface. In this study the electrooxidation of nitrite at a glassy carbon electrode modified by the drop-dry method was investigated. The drop-dry method was performed as described in the experimental section, using the aryloxy tetra-substituted OTiPc complexes, **37a – d** and **38a – d**. The cyclic voltammograms of the OTiPc complexes adsorbed onto the GCE were obtained in pH 7.4 phosphate buffer solution by scanning between -0.75 V and 1.00 V vs. Ag|AgCl. As an example, the CV of complex **38c** which exhibited an ill-defined peak (labelled process **I**) at 0.35 V vs. Ag|AgCl, is shown in Fig. 6.1. Since no metal oxidation of the complexes was expected, the peak was assigned to a ring-based oxidation process due to $\text{Ti}^{\text{IV}}\text{Pc}^{-2}/\text{Ti}^{\text{IV}}\text{Pc}^{-1}$. The assignment was compared to the solution electrochemistry of the complex described in chapter 5, however peaks were shifted to more negative potentials in the aqueous medium compared to the organic medium (DMF) used in chapter 5.

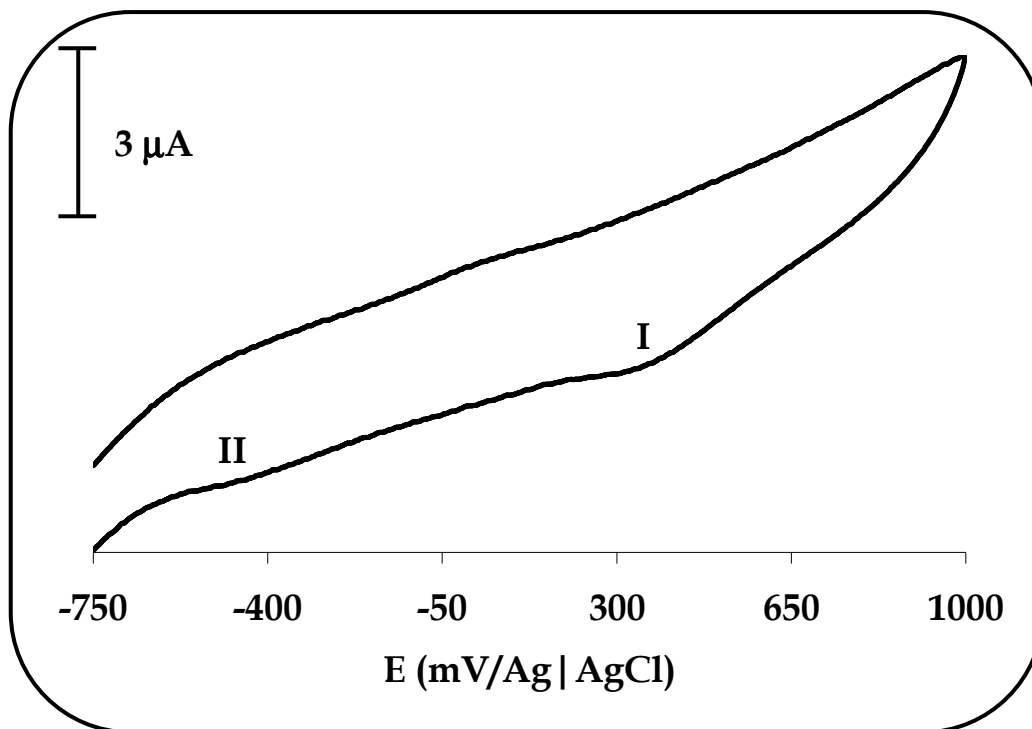


Figure 6.1: Cyclic voltammograms of 38c adsorbed on GCE in phosphate buffer solution, pH 7.4. Scan rate 0.1 Vs^{-1} .

For complexes **37a–d**, **38a**, **38b** and **38d**, process **I** was similarly observed at 0.30, 0.32, 0.31, 0.33, 0.29, 0.30 and 0.38 V vs. Ag|AgCl respectively. It was clear that adsorption as well as the nature of the solvent, allowed a shift to more negative potentials such that oxidation peaks which were not observed in the organic medium, e.g. for complexes **37c**, **37d**, **38c** and **38d**, were now observed under the conditions of Fig. 6.1, i.e. through adsorption in phosphate buffer solution (pH 7.4). For all complexes, the ring based process **I** was irreversible. The irreversible behaviour was not unusual as it has been reported for CoPcs [70]. At most, assignment of such peaks to specific redox processes may appear difficult. Fig. 6.1 also shows the first reduction potential due to $\text{Ti}^{\text{IV}}\text{Pc}/\text{Ti}^{\text{III}}\text{Pc}$ (process **II**) occurring at $\sim -0.45 \text{ V}$ vs. Ag|AgCl in comparison to -0.17 V , a potential which was observed in solution for

38c. Again, adsorbed species normally exhibit different potential values compared to those obtained in solution. The surface concentrations of the complexes adsorbed on the electrode were estimated from the slope of linear plots of I_p vs. v (not shown), based on Eq. 6.1 (which is the same as Eq. 1.32), [357]:

$$I_p = \frac{n^2 F^2 \Gamma_{MPC} A v}{4RT} \quad (6.1)$$

The surface concentrations were found to be of monolayer thickness, i.e. $\sim 10^{-10}$ mol.cm⁻² (Table 6.1), therefore suggesting a flat orientation on the electrode surface.

For the electrocatalytic oxidation of nitrite, a known amount of NaNO₂ was dissolved in phosphate buffer solution of pH 7.4 to generate the nitrite ion. At this pH, nitrite disproportionation to NO is insignificant, therefore the reaction catalysed was that of the oxidation of nitrite. The effect of adding 1 mM nitrite on the response of the GCE modified by adsorption of the OTiPc complexes is shown in Figs. 6.2 and 6.3. The activity of the OTiPcs bearing different substituents was explored and as examples, the peripherally substituted complexes **38a**, **38c** and **38d** are illustrated in Fig. 6.2, while the non-peripherally substituted complexes **37a** and **37d** are illustrated in Fig. 6.3. As can be seen, the electrode modified with the complexes showed better responses than the bare electrode. This observation implied that the complexes held properties which could catalyse nitrite oxidation, since a high current response towards nitrite oxidation was achieved compared to the bare electrode. The response observed at the modified electrode is as a result of nitrite diffusion towards the electrode surface, along with the anodic sweep of potential, thus reducing the oxidised TiPc⁻¹ to TiPc⁻² (as will be determined later by a mechanism). Simultaneous oxidation of the regenerated TiPc⁻² occurs several times in one scan, thus resulting in the enhancement of the catalytic current. The cathodic current at the modified

electrode is for the same reason not observed in the presence of nitrite since the oxidised TiPc, i.e. TiPc^{-1} is consumed during a chemical step.

Table 6.1: Peak potentials (E_p) obtained during the electrooxidation of nitrite (1 mM) at a modified GCE with 37a – d, 38 a – d, *poly-37e*, *poly-37f*, *poly-38e*, *poly-38f* and *poly-41* in phosphate buffer solution (pH 7.4).

Method of modification	Complex	Γ_{MPc} (mol.cm ⁻²)	E_p (V)
Drop-dry	37a	1.5×10^{-10}	0.77
	37b	1.8×10^{-10}	0.75
	37c	2.7×10^{-10}	0.74
	37d	1.9×10^{-10}	0.70
	38a	2.0×10^{-10}	0.77
	38b	1.4×10^{-10}	0.77
	38c	2.5×10^{-10}	0.64
	38d	2.7×10^{-10}	0.62
Electropolymerisation	<i>poly-37e</i>	2.2×10^{-10}	0.64
	<i>poly-37f</i>	2.5×10^{-10}	0.67
	<i>poly-38e</i>	2.7×10^{-10}	0.59
	<i>poly-38f</i>	3.6×10^{-10}	0.67
	<i>poly-41</i>	3.3×10^{-9}	0.67

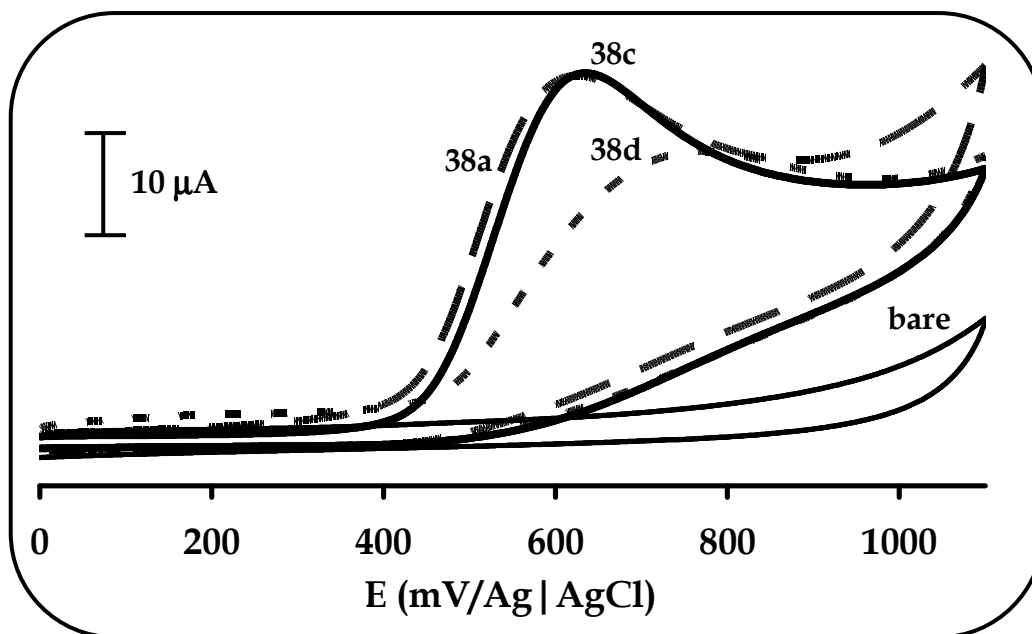


Figure 6.2: Cyclic voltammograms of bare GCE, 38a, 38c and 38d for 1 mM nitrite oxidation in phosphate buffer solution, pH 7.4. Scan rate 0.1 Vs^{-1} .

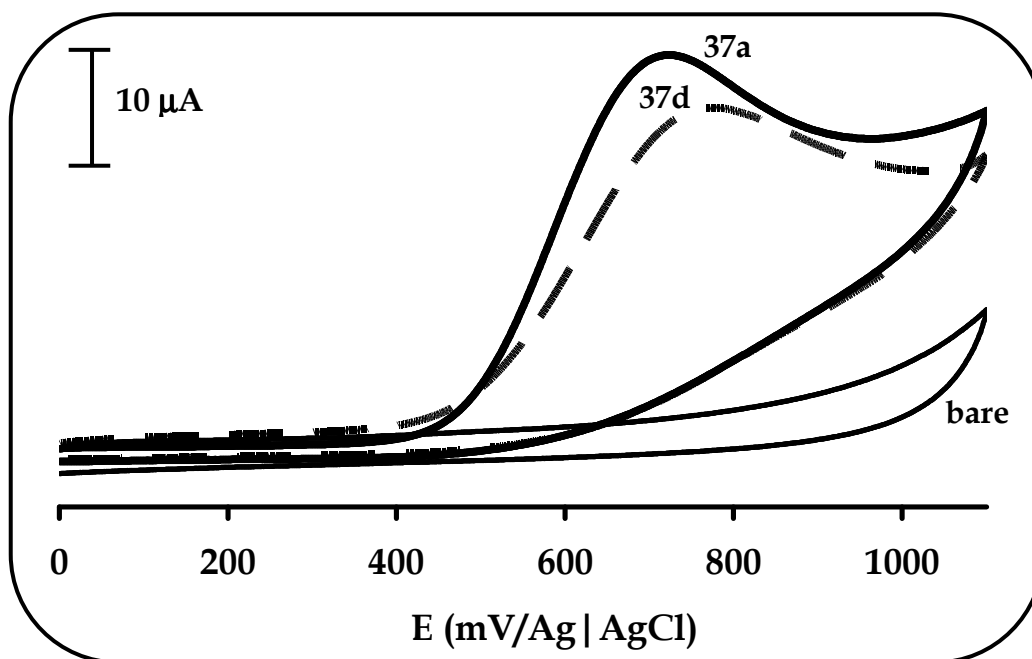


Figure 6.3: Cyclic voltammograms of bare GCE, 37a and 37d for 1 mM nitrite oxidation in phosphate buffer solution, pH 7.4. Scan rate 0.1 Vs^{-1} .

Based on the position of the catalytic peak potential, the order of increasing catalytic activity was found to be: **38d** > **38c** > **37d** > **37c** > **37b** > **38a** ~ **38b** ~ **37a**, Table 6.1. From this trend, it was obvious that complex **38d** exhibited the best response in terms of reduction of overpotential, i.e. 0.62 V, followed by **38c** with catalytic peak potential observed at 0.64 V. Complexes **37a**, **38a** and **38b** exhibited the lowest catalytic activities, i.e. 0.77 V, although these were comparable to those in literature [355]. Overall, the overpotential of nitrite oxidation at the bare electrode was lowered by the complexes, illustrating the better catalytic activity of the modified electrodes.

The modified electrodes were investigated at various scan rates for a fixed nitrite concentration, obtained by analyses of their cyclic voltammograms. Peak currents, I_p were found to be proportional to the square root of scan rate ($v^{1/2}$) (not shown), an indication that the nitrite electrooxidation is under diffusion control. Additionally, kinetic irreversibility was confirmed by the peak potential, E_p , shifting with log of scan rate, Fig. 6.4 [70]. Moreover, a typical shape that is indicative of a catalytic process, i.e. EC', as a result of a plot of sweep-rate normalised current density ($I_p v^{-1/2}$) versus the scan rate was obtained, Fig. 6.5 [70]. This type of process is catalytic since following the electrochemical oxidation step (E), the oxidised complex regenerates the starting complex via a chemical reaction step (C).

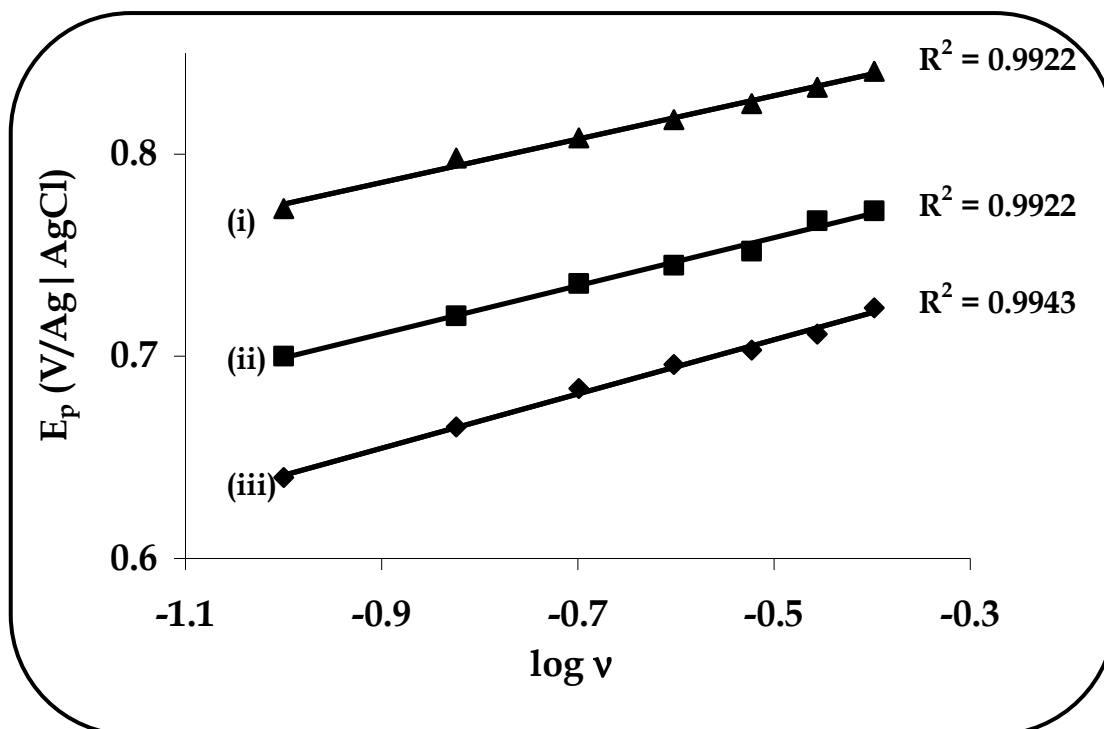


Figure 6.4: Plot of E_p vs. $\log v$ for the electrocatalytic oxidation of 1 mM nitrite solution in phosphate buffer, pH 7.4 on: (i) 37a, (ii) 37d, and (iv) 38b.

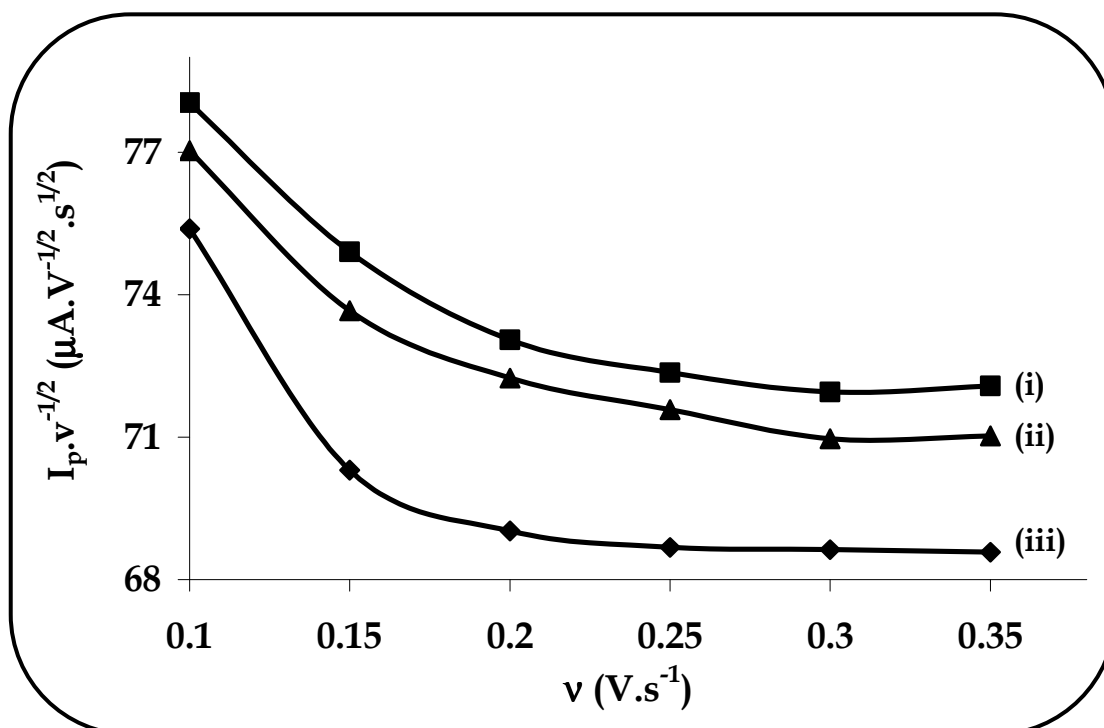


Figure 6.5: Plot of $I_p v^{-1/2}$ vs. v for the electrocatalytic oxidation of 1 mM nitrite solution in phosphate buffer, pH 7.4 on 38a, (ii) 37b, and (iii) 38b.

Table 6.2: Kinetic parameters for 1 mM nitrite detection on 37a – d, 38a – d, poly-37e, poly-37f, poly-38e, poly-38f and poly-41 in phosphate buffer solution (pH 7.4).

	Complex	E_p (V)	$(1-\alpha)n_a$	α	b (mV)	k ($\text{cm}\cdot\text{s}^{-1}$)	n
Drop- dry	37a	0.77	0.25	0.75	212	0.0106	1.8
	37b	0.75	0.32	0.68	167	0.0107	1.6
	37c	0.74	0.36	0.64	184	0.0110	1.8
	37d	0.70	0.42	0.58	128	0.0109	1.7
	38a	0.77	0.25	0.75	217	0.0130	1.7
	38b	0.77	0.39	0.61	138	0.0124	1.7
	38c	0.64	0.29	0.71	188	0.0143	2.2
	38d	0.62	0.33	0.67	164	0.0132	1.9
Electropolymerisation	poly-37e	0.64	0.37	0.63	160	0.0114	1.6
	poly-37f	0.69	0.31	0.69	191	0.0108	1.7
	poly-38e	0.59	0.33	0.67	179	0.0118	2.2
	poly-38f	0.67	0.36	0.64	164	0.0108	1.6
	poly-41	0.67	0.1	0.90	294	0.0620	2.4

For this totally irreversible diffusion-controlled system, Eq. 6.2 was used to obtain additional information. According to Eq. 6.2, the Tafel slope b (values shown in Table 6.2), is defined by: $b = 2.3RT / (1-\alpha)n_a F$ and the anodic peak potential is represented by [337],

$$E_p = \frac{2.3RT}{2(1-\alpha)n_a F} \log v + K \quad (6.2)$$

where α is the transfer coefficient, n_a is the number of electrons involved in the rate determining step, v is the scan rate, K is a constant (intercept) and the remaining symbols have their usual meaning. Values of $(1-\alpha)n_a$ for the complexes were calculated and related with the Tafel slope, b , where $b/2 = m$ (or $b = 2 \times m$) where m is the slope of the E_p vs. $\log v$ plot.

Tafel slopes ranging from 138 – 217 mV/decade were obtained, Table 6.2. The values suggested that the first one-electron transfer is the rate limiting step for the electrocatalytic oxidation of nitrite. Tafel slopes much greater (> 240 mV/decade) than the normal 30-120 mV/decade are known [447-449] and have been related either to chemical reactions coupled to electrochemical steps [70] or to substrate-catalyst interactions in a reaction intermediate [447-449]. The Tafel slopes obtained in this work deviated from the normal value of 120 mV/decade, but were less than the values (≥ 280 mV) reported in literature [70] for substrate-catalyst interaction, hence suggesting a weaker substrate-catalyst interaction in the reaction intermediate. The Tafel values reported in this work could also reflect chemical reactions coupled with electrochemical steps [70]. The magnitude of the values is however related to substrate-catalyst interactions where substrate binding to the catalyst during the interaction as the reaction step is moderate to strong. Therefore, the obtained Tafel slopes may be rationalised as moderate to strong binding of nitrite to the OTiPc catalysts at the electrode surface since they were larger than 120 mV/decade. The values of the transfer coefficient α were relatively high, ranging from 0.58 - 0.75, Table 6.2. Transfer coefficients of approximately 0.5 indicate that there is an equal probability that the reaction activated transition state can form either products or reactants. The values obtained for these complexes suggested that product formation was favoured since the values were above 0.5, more so for the phenoxy-substituted

complexes **37a** and **38a** which exhibited high α values of 0.75, Table 6.2. Complex **37d** moderately favoured product formation with $\alpha = 0.58$.

Furthermore, the electrode kinetics were evaluated by determining the heterogeneous electron transfer coefficient, k , obtained from Eq. 6.3 [337]:

$$K = E^{o'} + \frac{RT}{(1-\alpha)n_a F} \times \left[0.78 + \frac{2.3}{2} \log \left(\frac{(1-\alpha)n_a FD}{k^2 RT} \right) \right] \quad (6.3)$$

where $E^{o'}$ is the formal potential, D is the diffusion coefficient of nitrite ($2.1 \times 10^{-5} \text{ cm}^2 \cdot \text{s}^{-1}$), [71,450], and the remaining symbols are as they were described above. The heterogeneous rate constant, k , is a kinetic facility of a redox process which when large, defines a system that is able to reach equilibrium in a short time scale, but for a small k value, the system will be sluggish. For complexes **37a – d** and **38a – d**, values ranging from $0.0106 - 0.0143 \text{ cm} \cdot \text{s}^{-1}$ (Table 6.2) were obtained, thus suggesting that the electron transfer in the rate determining step is faster for complex **38c** ($0.0143 \text{ cm} \cdot \text{s}^{-1}$) and slowest for complex **37a** ($0.0106 \text{ cm} \cdot \text{s}^{-1}$). The electron transfer was also found to be faster for the peripherally substituted complexes compared to their corresponding non-peripherally substituted derivatives. The rate constant at the bare electrode was found to be $2.6 \times 10^{-9} \text{ cm} \cdot \text{s}^{-1}$, which is orders of magnitude smaller than those observed at the modified electrodes. The heterogeneous rate constant therefore explains the large feature of the catalytic oxidation of nitrite at the modified than at the unmodified electrode. It was clear that the modified electrodes significantly promoted the reaction.

For totally irreversible diffusion-controlled electrode processes, the total number of electrons (n) involved in the electrocatalytic oxidation of nitrite was calculated, from Eq. 6.4, i.e.:

$$I_p = 2.99 \times 10^5 n [(1-\alpha)n_a]^{1/2} A C_o D^{1/2} v^{1/2} \quad (6.4)$$

where A is the area of the electrode in cm^2 (for glassy carbon 0.071 cm^2), C_o is the concentration of the electroactive reactant in $\text{mol}\cdot\text{cm}^{-3}$ and the remaining symbols are as they were described above. For all the complexes, the total number of electrons transferred was found to be ~ 2 , Table 6.2. This suggested that two electrons were involved in the nitrite oxidation, resulting in the most likely product, namely nitrate (NO_3^-).

The chronoamperometric behaviour of the electrooxidation of nitrite with modified electrodes was also studied using the double potential-step technique. Using the Cottrell equation (Eq. 6.5), a plot of the net current I_{net} versus $t^{-1/2}$ was obtained, Fig. 6.6, i.e.:

$$I = nFD^{1/2}AC\pi^{-1/2}t^{-1/2} \quad (6.5)$$

where the symbols are as described above. In the presence and absence of nitrite, I_{net} was obtained by subtracting the background current, point-to-point from the current observed for the modified electrodes. Figure 6.6 showed that the linearity of the plot was maintained at short time periods however, the plot deviated from linearity at longer times. From the slope of the plot, the number of electrons transferred for the electrooxidation of nitrite was further confirmed to be ~ 2 . Also, by extrapolation to the origin, transient currents of $\sim 4.0 \mu\text{A}$ that are largely associated with the catalytic oxidation of nitrite by the modified electrodes were observed. Under the same experimental conditions, only a small residual current was observed for a bare electrode which was complimentary to its CV in Fig. 6.2 and 6.3, thus confirming the electrooxidation of nitrite.

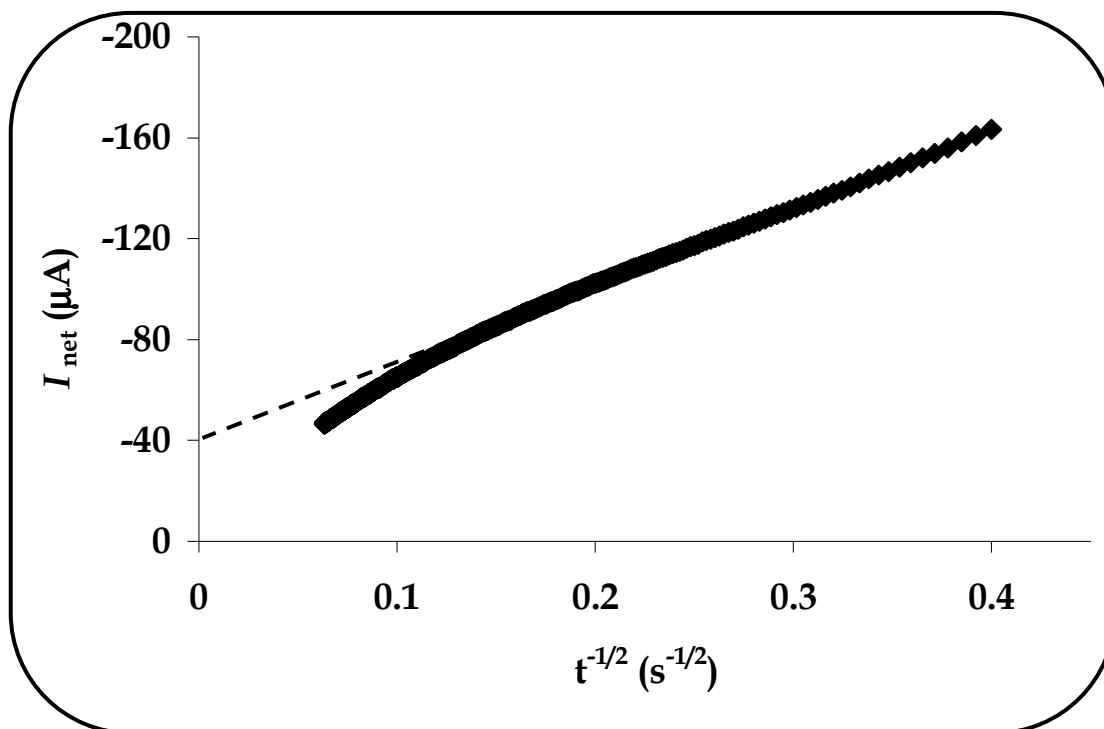


Figure 6.6: Plot of I_{net} vs. $t^{-1/2}$ for GCE modified with 38a for the electrocatalytic oxidation of 1 mM nitrite solution in phosphate buffer, pH 7.4. Scan rate 0.1 Vs^{-1} .

The electrooxidation of nitrite seems to be mediated by the ring based process, i.e. $\text{Ti}^{\text{IV}}\text{Pc}^{-2}/\text{Ti}^{\text{III}}\text{Pc}^{-1}$, since the catalytic peak potentials were in the range of this process. Further understanding of the mechanism involved in the electrooxidation of nitrite was probed by spectroscopic studies, where changes in absorption spectra were monitored on addition of nitrite to solutions of the complexes in DMSO, Fig. 6.7. The spectral changes shown in Fig. 6.7 consisted of a shift of the Q-band from 700 nm to 695 nm, followed by an increase in intensity. Changes in the Q-band without decrease in intensity are associated with either axial ligand exchange or metal-based reduction/oxidation processes. Metal reduction is expected in TiPcs as discussed before. Spectral changes observed on metal reduction of the complexes have been discussed in chapter 5 and consist of much larger shifts, e.g. 701 nm to 690 nm for

complex **38b** than were observed in Fig. 6.7. Thus Fig. 6.7 confirmed the loss of the axial oxygen ligand in the complexes and its replacement with the nitrite ion.

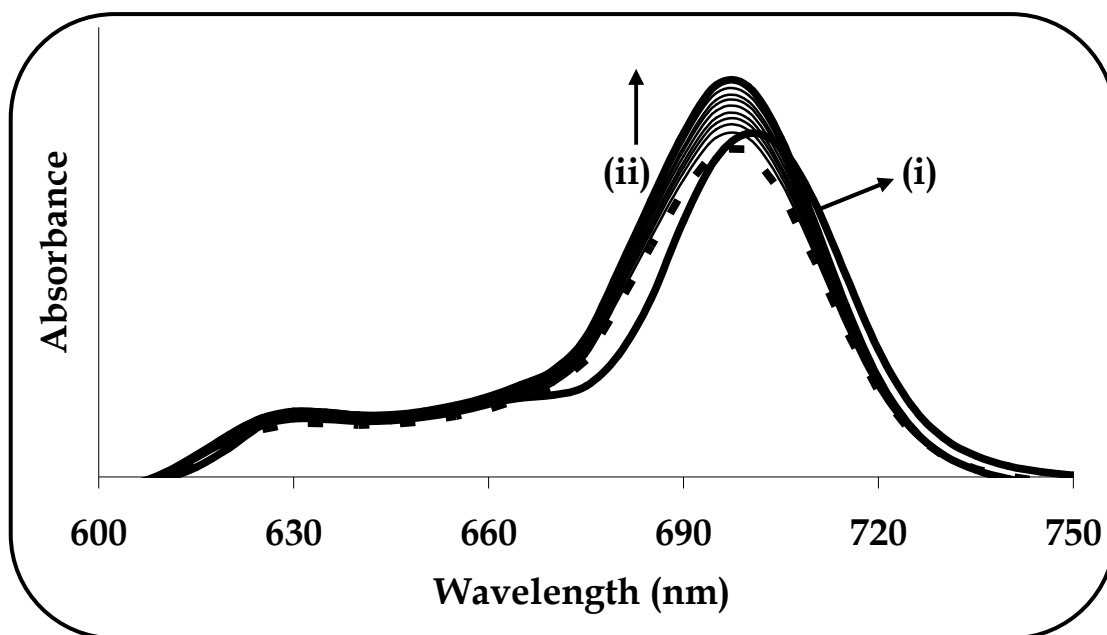
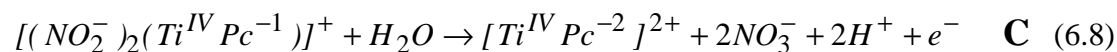
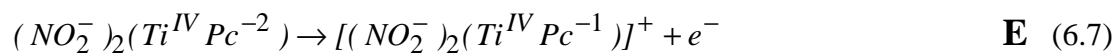
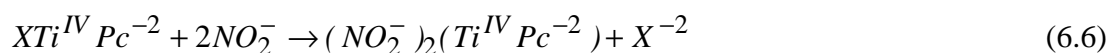


Figure 6.7: UV-Vis spectral changes observed on addition of nitrite to **38b** in DMSO, where (i) is **38b** in absence of nitrite with $\lambda_{\text{max}} = 700 \text{ nm}$ and (ii) in the presence of nitrite.

In light of this and based on the discussion above, a mechanism was proposed for the electrocatalytic oxidation of nitrite, i.e.:



where X = axial ligand

The proposed mechanism may be explained by the following: according to the spectrum observed immediately following addition of nitrite, the 5 nm blue-shift suggested coordination or binding of nitrite to $\text{Ti}^{\text{IV}}\text{Pc}^{-2}$ in Eq. 6.6 as predicted by the

Tafel slopes, i.e. substrate-catalyst binding took place. The rate-determining step in Eq. 6.7 accounts for the oxidation of $\text{Ti}^{\text{IV}}\text{Pc}^{-2}$ to $\text{Ti}^{\text{IV}}\text{Pc}^{-1}$. Since no metal oxidation was expected, the observed catalytic activity was most likely mediated by the phthalocyanine ligand. Thus the $\text{Ti}^{\text{IV}}\text{Pc}^{-2}/\text{Ti}^{\text{IV}}\text{Pc}^{-1}$ was responsible in mediating the electrocatalytic oxidation of nitrite which took place within the range where oxidation to $\text{Ti}^{\text{IV}}\text{Pc}^{-1}$ occurred, i.e. nitrite oxidation began at ~ 0.4 which involved the oxidised ring observed at ~ 0.3 . The $\text{Ti}^{\text{IV}}\text{Pc}^{-2}$ is regenerated and nitrate is the end product of nitrite oxidation as was confirmed by the number of electrons transferred during the catalysis (Eq. 6.8). A feature with the EC' mechanism is that before any reaction with nitrite can take place, the phthalocyanine complexes must be in an oxidised state as was the case with $\text{Ti}^{\text{IV}}\text{Pc}^{-2}$ being oxidised to $\text{Ti}^{\text{IV}}\text{Pc}^{-1}$ (Eq. 6.7). Thus before nitrite oxidation can be observed, the electrode potential must be sufficiently near the redox potential of the $\text{Ti}^{\text{IV}}\text{Pc}^{-2}/\text{Ti}^{\text{IV}}\text{Pc}^{-1}$ couple to generate at least a small concentration of $\text{Ti}^{\text{IV}}\text{Pc}^{-1}$.

6.2 Arylthio tetra-substituted oxotitanium(IV) phthalocyanines:

(37e, 37f, 38e and 38f)

Electropolymerisation of the arylthio tetra-substituted OTiPcs (**37e**, **37f**, **38e** and **38f**) was employed since these complexes were easily electropolymerisable on the GCE surface compared to the aryloxy-substituted complexes which were adsorbed by the drop-dry method. In this study the electrooxidation of nitrite at a glassy carbon electrode modified by electropolymerisation was investigated. The electropolymerisation of the OTiPc complexes onto the GCE was best performed by repetitive scan of cyclic voltammetry. Continuous potential cycling from 0.10 V to -0.90 V vs. Ag|AgCl at 0.1 Vs^{-1} in DCM containing 0.1 M TBABF₄, resulted in the

deposition of an electroactive polymer on the electrode surface and this procedure was the same for each OTiPc complex.

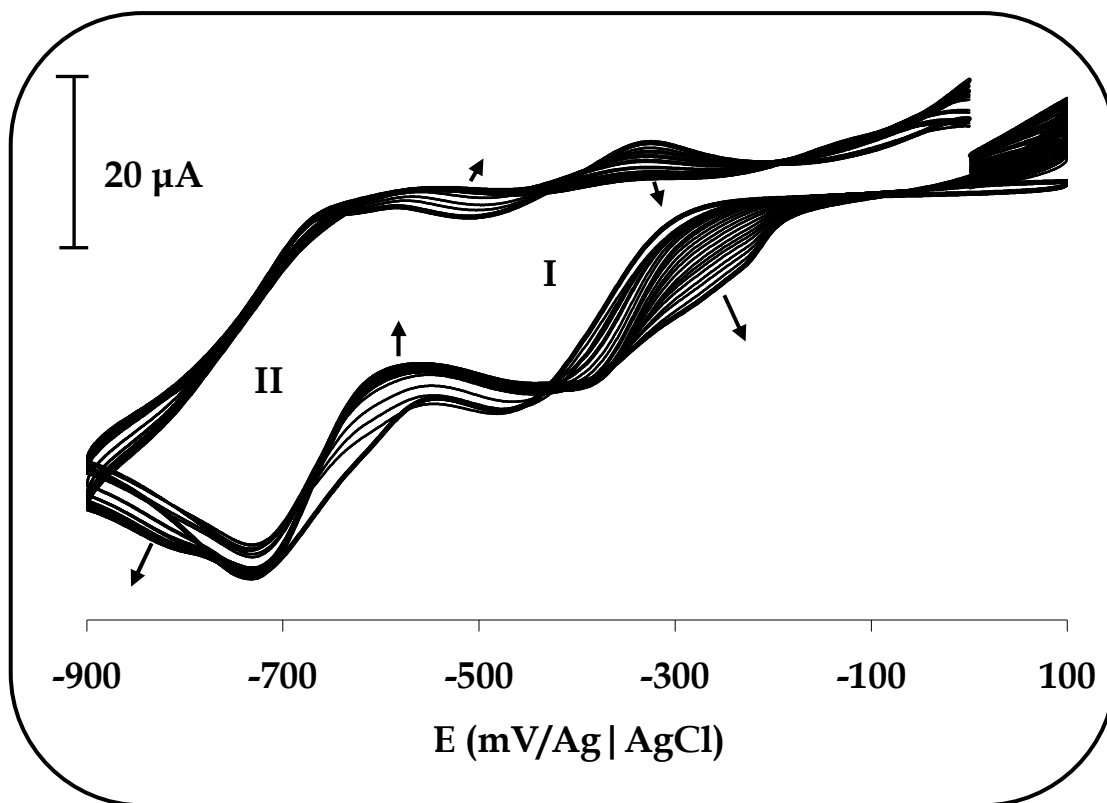


Figure 6.8: Evolution of cyclic voltammograms of **38f** (1 mM) in DCM containing 0.1 M TBABF₄ during cathodic repetitive cycling on a glassy carbon electrode (GCE). Scan rate = 0.1 Vs⁻¹.

The CVs were recorded in the range of the processes encompassing the two metal reductions, i.e. $\text{Ti}^{\text{IV}}/\text{Ti}^{\text{III}}$ and $\text{Ti}^{\text{III}}/\text{Ti}^{\text{II}}$. The evolution of the cyclic voltammograms during the cathodic electropolymerisation of **38f** (1 mM) in DCM solution – representative of the rest – is shown in Fig. 6.8. DCM was employed for electropolymerisation of these complexes due to its ease of evaporation and it is known [451] to form better polymers for phthalocyanine complexes substituted with bulky groups, than in DMF. The voltammogram showed a pair of redox peaks that were associated with $\text{Ti}^{\text{IV}}/\text{Ti}^{\text{III}}$ (process I) and $\text{Ti}^{\text{III}}/\text{Ti}^{\text{II}}$ (process II), as was previously established in chapter 5, with $E_{1/2} = -0.46$ V and -0.72 V vs. Ag|AgCl respectively.

The half wave potentials obtained in DCM were different from those observed in DMF (Table 5.1) where $E_{1/2} = -0.09$ V and -0.42 V vs. Ag|AgCl for $\text{Ti}^{\text{IV}}/\text{Ti}^{\text{III}}$ (process I) and $\text{Ti}^{\text{III}}/\text{Ti}^{\text{II}}$ (process II) respectively.

With increase in scan number, irreversibility as well as a general progressive shift to less negative potentials of the $\text{Ti}^{\text{IV}}/\text{Ti}^{\text{III}}$ couple to -0.39 V was observed. Peak shifts are an indication that the surface of the electrode is changing due to deposition, hence film growth. The shift was accompanied by a decrease in the anodic peak current resulting in the irreversibility of the process. Additionally, an emergence of a broad peak which successively increased with scan number was observed around -0.28 V vs. Ag|AgCl. The presence of new peaks is indicative of polymer formation.

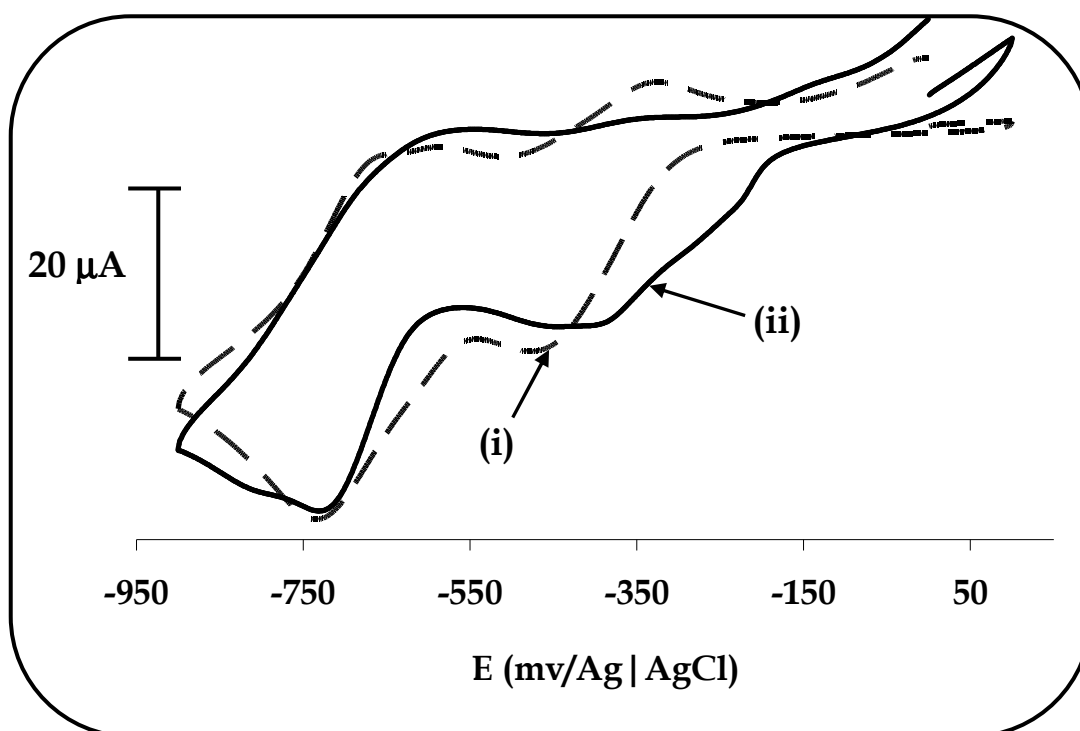


Fig. 6.9: Cyclic voltammograms 38f (1 mM) at GCE in DCM containing 0.1 M TBABF₄ showing (i) first and (ii) last scans.

For comparative purposes as well as to control the film thickness, hence the surface density, 50 electropolymerisation scans were performed with each complex now represented as *poly-37e*, *poly-37f*, *poly-38e* and *poly-38f*. The Pc molecular structure (with or without substituents), the central metal, electrode material and the deposition rate are conditions that tend to determine the mode of growth of Pc films [446]. It was obvious that after 50 scans, the first scan was different from the last scan (Fig. 6.9), further confirmation that the complexes were electropolymerised on the GCE surface. Hence electropolymerisation is typified by an increase in peak currents, peak shifts and formation of new peaks as the number of scans increases. Rinsing the electrode in DCM removed unadsorbed OTiPc and a layer of green substance was found to be deposited on the electrode. The OTiPc-modified electrode was then transferred to a fresh phosphate buffer solution (pH 7.4) and characterising it by CV confirmed the adsorption of an electroactive film, Fig 6.10. The couples associated with the metal reductions were observed at -0.63 V for Ti^{IV}/Ti^{III} and -0.87 V for Ti^{III}/Ti^{II} and were shifted to more negative potentials (compared to Fig. 6.8) as they were in a different medium.

To further confirm deposition onto the electrode, a linear plot of current (I_p) vs. scan rate (v), typical of a surface reaction of adsorbed species was obtained, Fig. 6.10 (inset). The polymer surface coverage of the MPcs on the electrode was estimated from Eq. 6.9 (same as Eq. 1.33) by integrating the peak area under the Ti^{III}/Ti^{II} couple, i.e.

$$\Gamma_{MPc} = \frac{Q}{nFA} \quad (6.9)$$

The Γ values were found to be of the order of $1 \times 10^{-10} \text{ mol cm}^{-2}$, thus indicating monolayer coverage as illustrated in Table 6.1. Equation 6.1 could also be employed to determine the surface coverage of the adsorbed MPcs.

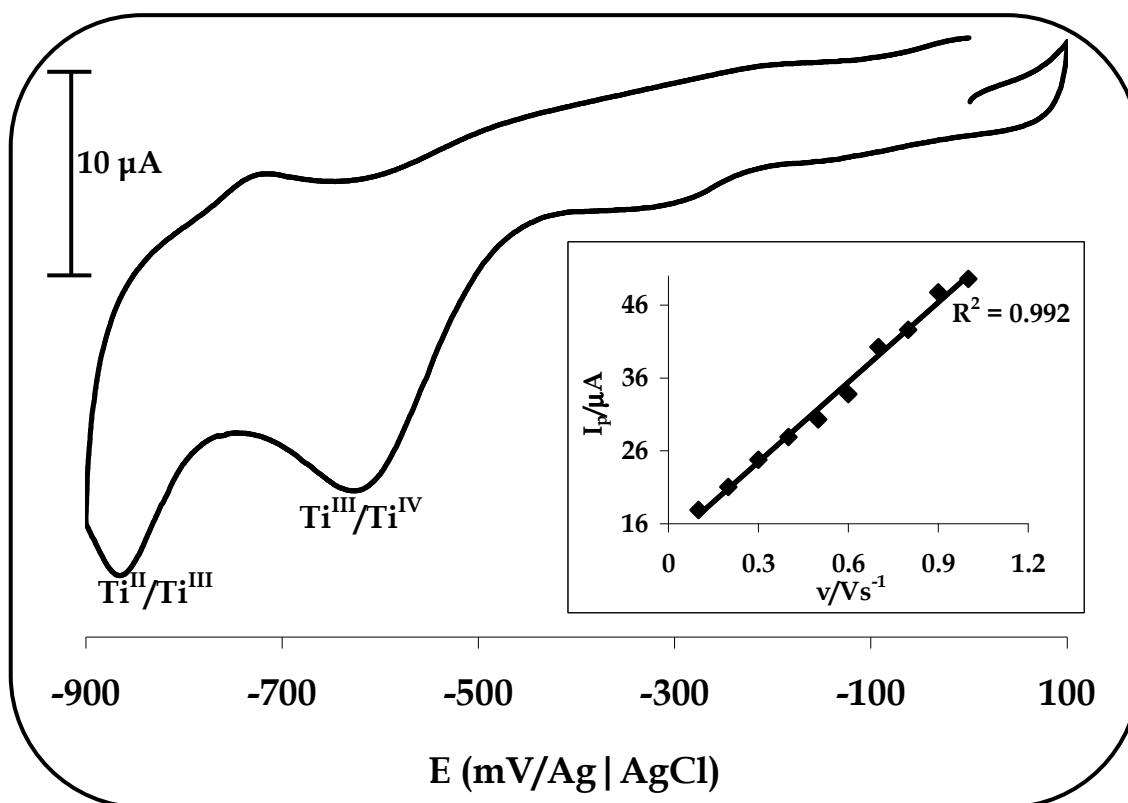


Figure 6.10: Cyclic voltammetry of modified GCE with complex 38f phosphate buffer solution, pH 7.4. Inset = Plot of current versus scan rate. Scan rate 0.1 Vs⁻¹.

Varying the potential window - such that wider cathodic and anodic ranges are utilised - was not promising and CVs shown in Fig 6.8 were not obtained. However, scanning the electrode potential in the cathodic region alone and in the anodic region alone resulted in the electropolymerisation of the complexes as shown in Fig. 6.8 and Fig. 6.11 respectively. Anodic electropolymerisation was obtained by cycling a solution of the OTiPc complexes in DCM from 0.20 V to 1.60 V vs. Ag|AgCl, Fig. 6.11. Two peaks associated with Pc ring oxidation or the sulphur substituents at ~1.2

V and ~ 1.5 V vs. Ag|AgCl were observed. The Pc ring oxidation peaks were expected at high potentials due to the high electronegativity of the titanyl ion bond to the Pc ring. Complexes **37e**, **37f**, **38e** and **38f** exhibited oxidation peaks in DCM (Fig. 6.11) but not in DMF (Table 5.1), showing that they are more easily oxidised in DCM and more difficult to reduce as was observed above. In DMF these complexes were found to be easier to reduce and difficult to oxidise (Table 5.1). Electropolymerisation of the complexes onto the electrode was probably facilitated through π - π interactions between the phenyl substituents and the GCE and radical polymerisation from sulphur groups, as was the case with amino groups in MPc complexes [355]. In the case of the sulphur containing MPc complexes, S-S bonds would form, giving disulphides. In this work, the modified GCE by cathodic electropolymerisation (Figs. 6.8 and 6.10) was used to determine the efficiency of the electrode as an electrocatalyst towards the oxidation of nitrite in aqueous solutions.

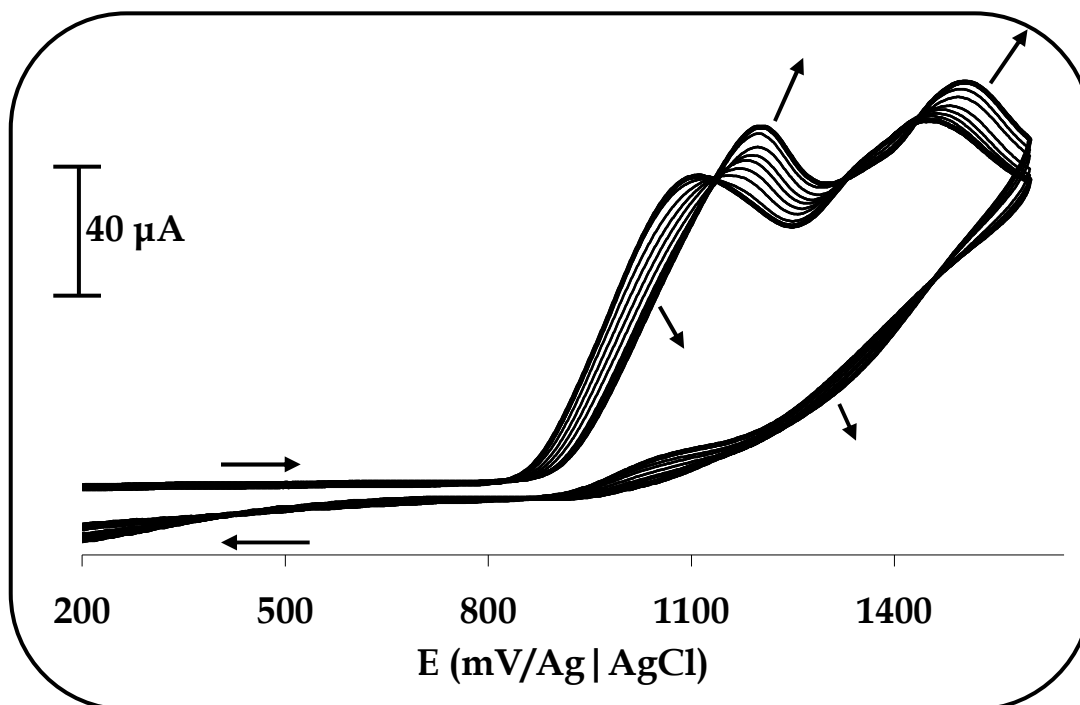


Figure 6.11: Anodic electrodeposition of **38f** (1 mM) in DCM containing 0.1 M TBABF₄. Scan rate 0.1 Vs⁻¹.

Fig. 6.12 shows CVs of 1 mM nitrite on a bare electrode and on the electropolymerised film in pH 7.4 phosphate buffer solution. As mentioned earlier the catalysed reaction is that of nitrite since its disproportionation to NO is insignificant. At the bare electrode, only a weak and broad anodic peak at ~ 0.80 V was observed, Fig. 6.12. At the modified electrode however, an anodic oxidation peak current for *poly-38e*, *poly-37e*, *poly-38f* and *poly-37f* was respectively observed at 0.59 V, 0.64 V, 0.67 V and 0.69 V, Fig. 6.12. It was obvious that the best responses were obtained with the modified electrodes, i.e. a negative shift of the peak potentials (lowering of overpotential) and an increase of the current densities were observed. Furthermore, the bare electrode exhibited a more positive response, thus clearly confirming the catalytic effect of the polymerised complexes.

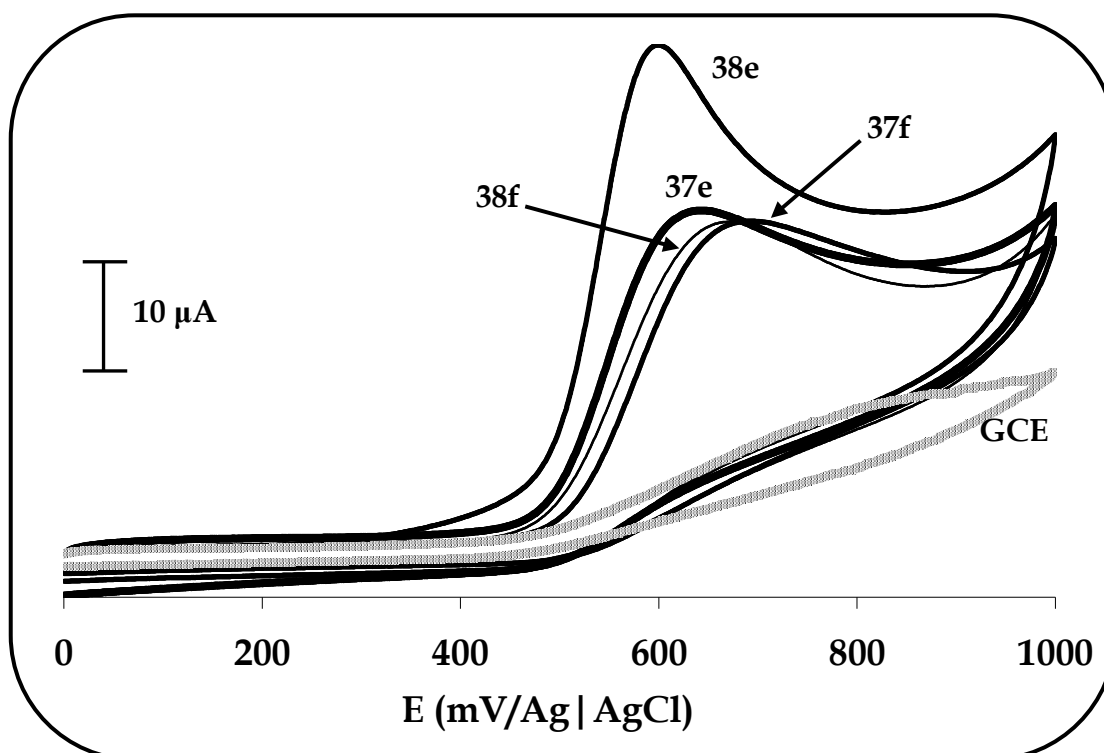


Figure 6.12: Cyclic voltammograms of unmodified GCE, *poly-37e*, *poly-37f*, *poly-38e* and *poly-38f*, for 1 mM nitrite oxidation in phosphate buffer solution, pH 7.4. Scan rate 0.1 Vs^{-1} .

Of the four complexes, *poly-38e* displayed the best catalytic activity in terms of the extensive lowering of the overpotential, i.e. 0.59 V. To the best of the author's knowledge and compared to adsorbed aryloxy complexes above, i.e. **37a – d** and **38a – d**, this was the lowest reduction in nitrite overpotential ever observed for any MPc modified electrode. Nitrite overpotentials have been lowered to potentials mostly in the 0.70 V region. The shift to negative potentials and an increase in current density could be of importance in applications of sensors. Also, the phenylthio substituted derivatives (**37e** and **38e**) showed better catalysis than the corresponding benzylthio derivatives (**37f** and **38f**) in that the former shifted the oxidation of nitrite more to less positive potentials than the latter.

The modified electrodes were investigated for stability and reproducibility by repetitively scanning (10 scans) 1 mM nitrite in phosphate buffer solution (pH 7.4), Fig. 6.13 and 6.14. About 24 – 40 % decrease in catalytic peak current was observed after the 1st scan, an indication that there was some passivation on the electrode surface probably due to moderate coordination of the nitrite oxidation product(s) to the TiPc catalysts. Thereafter, the peak currents stabilized showing no significant differences between the subsequent scans and hence high resistance to passivation. Potential windows larger than the 1.0 V used in Fig. 6.12 resulted in increased passivation of the electrode; hence the analyses were limited to 1.0 V. Interestingly, the initial catalytic peak current (i.e. 1st scan) was simply obtained upon renewal of the electrode by rinsing in buffer solution.

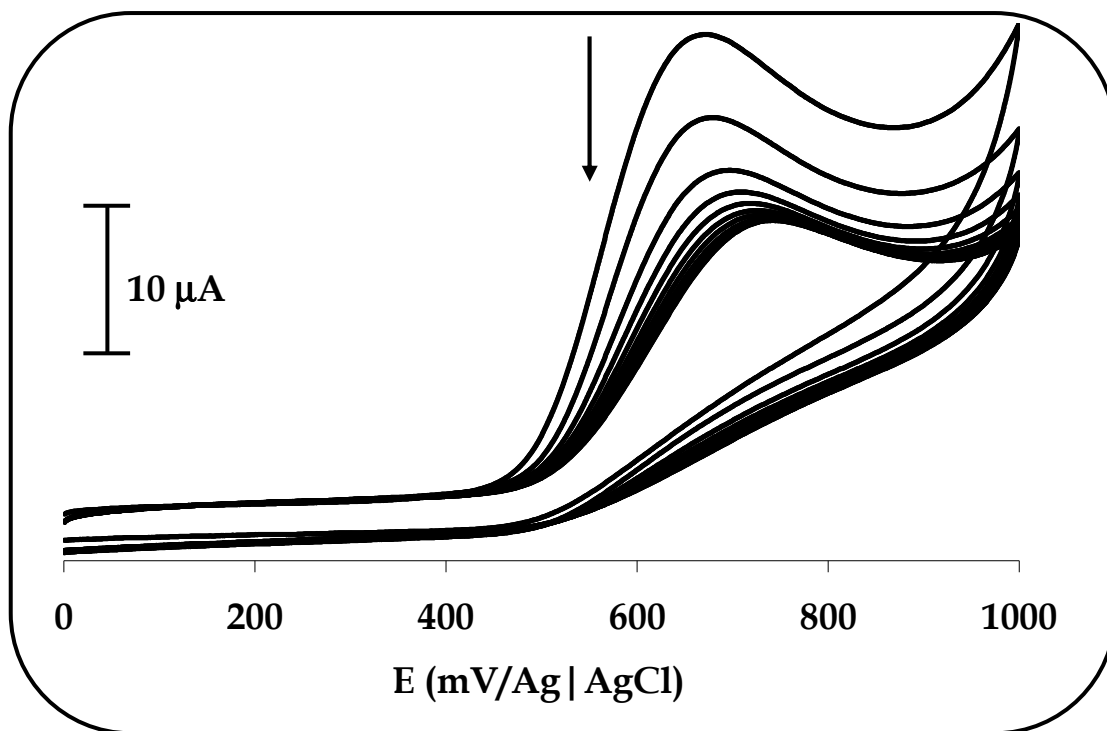


Figure 6.13: Repetitive cyclic voltammogram of 1 mM nitrite at a 38f modified GCE in phosphate buffer, pH 7.4. Scan rate 0.1 Vs^{-1} .

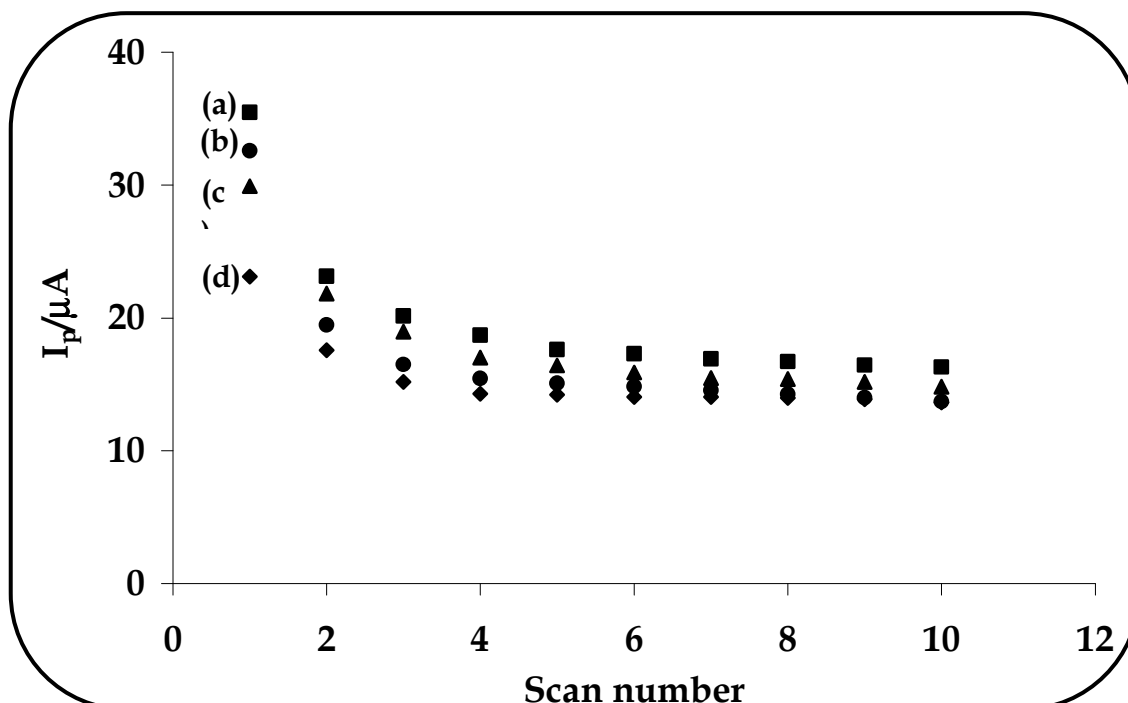


Figure 6.14: Plots of variation of peak currents with scan number for the voltammetric response of 1 mM nitrite in phosphate buffer solution, pH 7.4 on (a) *poly-38e*, (b) *poly-37e*, (c) *poly-38f* and (d) *poly-37f*.

Analyses of cyclic voltammograms at various scan rates for a fixed nitrite concentration were obtained. Firstly, a linear relationship between the peak current (I_p) and square root of scan rate ($v^{1/2}$) was obtained (Fig. 6.15), thus indicating a diffusion-controlled nitrite electrocatalytic oxidation. Secondly, a plot of sweep-rate normalised current density ($I_p v^{-1/2}$) vs. the sweep rate (Fig. 6.16), exhibited a typical shape indicative of a catalytic process. Lastly, for all the complexes, Fig. 6.17 showed that the peak potentials increased with scan rate ($\log v$), thus indicating the chemical irreversibility of the nitrite electrocatalytic oxidation process.

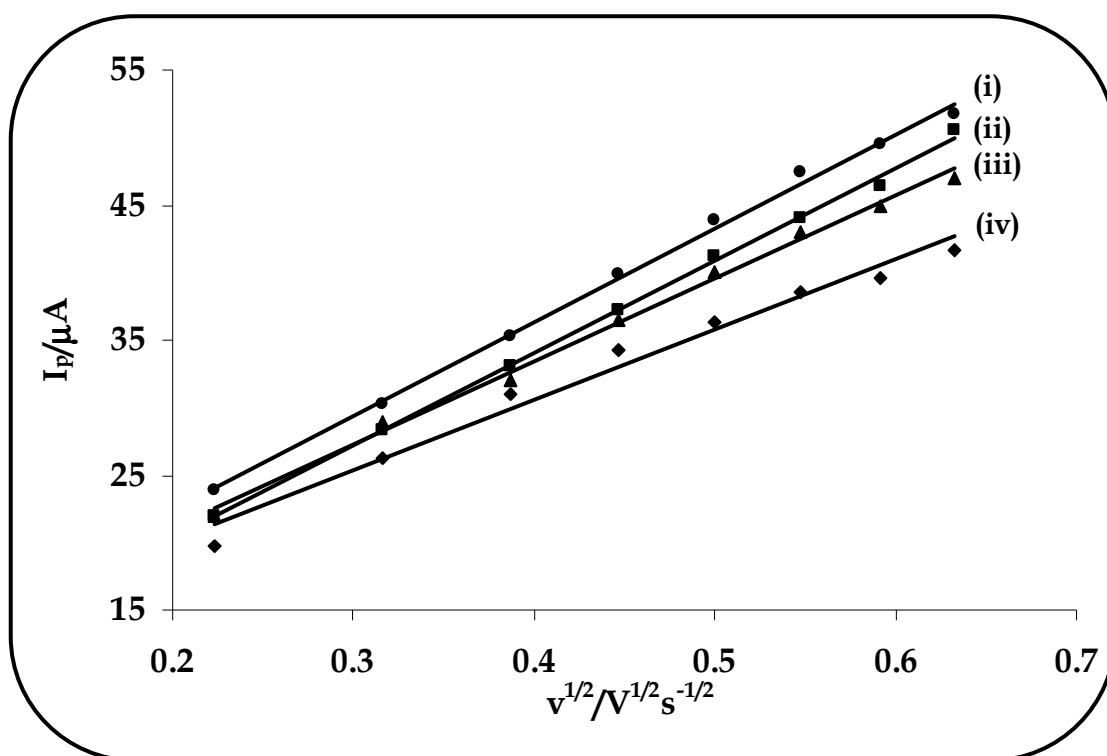


Figure 6.15: Plot of I_p vs. $v^{1/2}$ for the electrocatalytic oxidation of 1 mM nitrite solution in phosphate buffer, pH 7.4 on: (i) *poly-38e*, (ii) *poly-37e*, (iii) *poly-38f* and (iv) *poly-37f*.

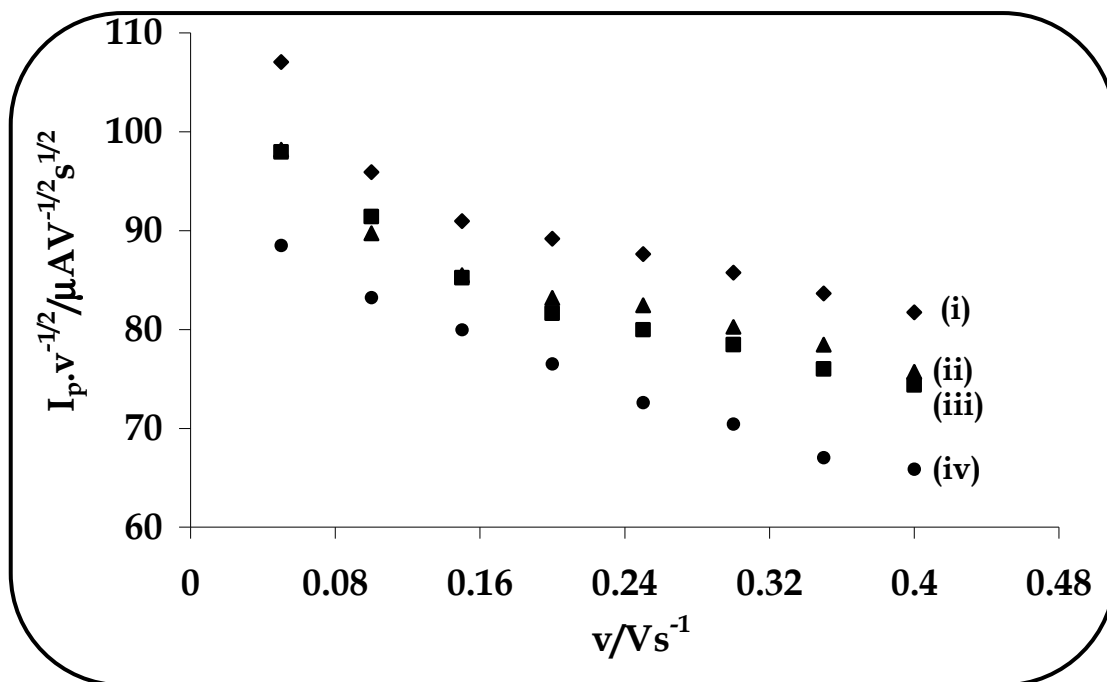


Figure 6.16: Plot of $I_p v^{-1/2}$ vs. v for the electrocatalytic oxidation of 1 mM nitrite solution in phosphate buffer, pH 7.4 on: (i) *poly-38e*, (ii) *poly-37e*, (iii) *poly-38f* and (iv) *poly-37f*.

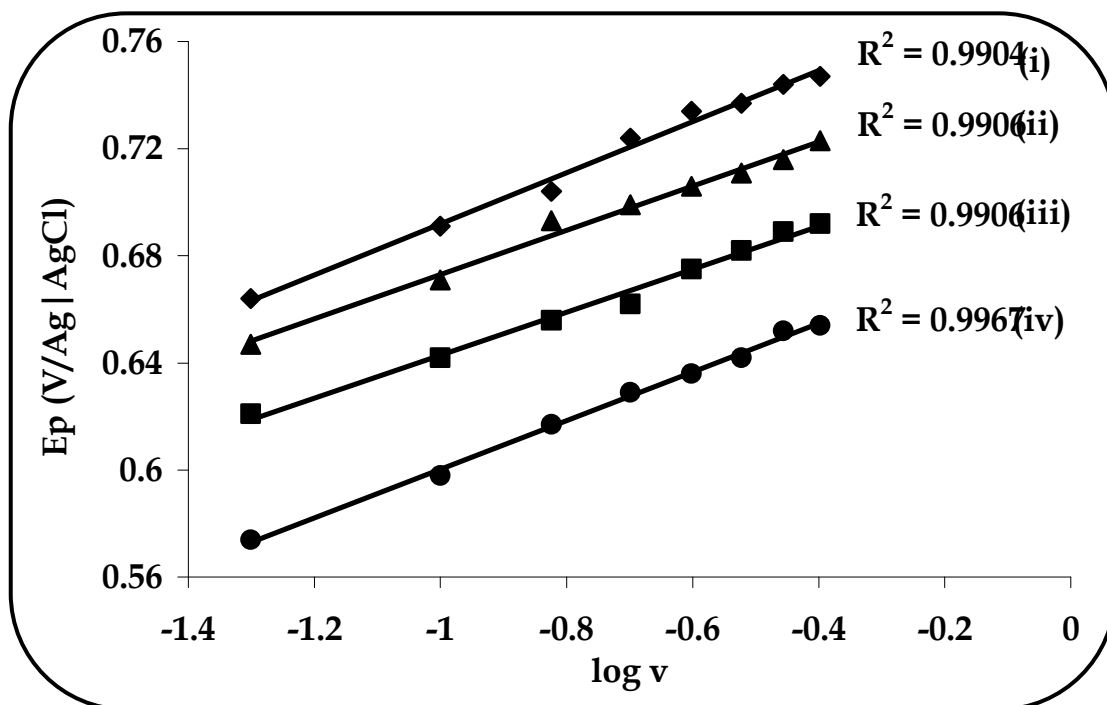


Figure 6.17: Plot of E_p vs. $\log v$ for the electrocatalytic oxidation of 1 mM nitrite solution in phosphate buffer, pH 7.4 on: (i) *poly-37f*, (ii) *poly-38f*, (iii) *poly-37e* and (iv) *poly-38e*.

Figure 6.18 shows a linear relation of the peak current against the concentration of nitrite ions for the range 0.4 – 3.5 mM, i.e. the anodic oxidation peak of nitrite is proportional to the nitrite concentration. At concentrations higher than 3.5 mM, linearity is lost, thus the electrode is useful for analyses at nitrite concentrations less than 3.5 mM. The linear part of Fig. 6.18 indicates that the concentration of nitrite in solution can be determined through possible use of I_p as an analytical parameter. Additional information was obtained for a totally irreversible diffusion-controlled system. The anodic peak potential can be represented by Eq. 6.2. In accordance with Eq. 6.2, values of $(1-\alpha)n_a$ (obtained from Fig. 6.17) ranging from 0.31 – 0.37 (Table 6.2) for the complexes were calculated and related with the Tafel slope ($b = 2.3RT / (1-\alpha)n_a F$).

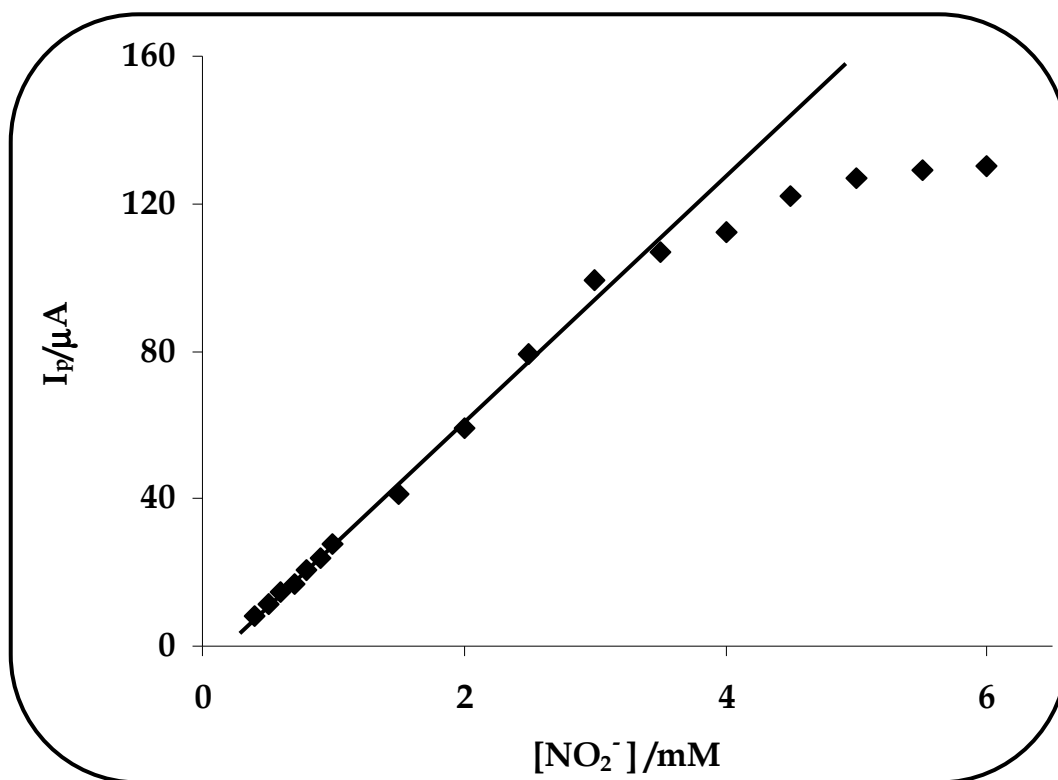


Figure 6.18: Plot of variation of peak current (I_p) vs. nitrite concentration ($[\text{NO}_2^-]$) for *poly-38f* in phosphate buffer, pH 7.4 on. Scan rate 0.1 Vs^{-1} .

Values ranging from 160–191 mV/decade for **37e**, **37f**, **38e** and **38f** (Table 6.2) were obtained for Tafel slopes, thus suggesting that the first one-electron transfer was the rate limiting step for the electrocatalysis as was the case for adsorbed complexes **37a – d** and **38a - d**. The large Tafel slopes are more likely to involve chemical reactions that are coupled with electrochemical steps since as will be discussed below, a chemical reaction between nitrite and the catalyst was observed. As was the case with **37a – d** and **38a – d**, the values of the transfer coefficient α were relatively high, ranging from 0.63 - 0.69, thus suggesting product formation. Generally, when one electron is involved in the rate-determining step, (i.e. $n_a=1$) α is equal to 0.5 for Tafel slopes of 120 mV/decade. Values of α listed in Table 6.1 were close to 0.5, hence confirming that one electron was involved in the rate determining step.

Furthermore, the heterogeneous electron transfer coefficient, k , was obtained from Eq. 6.3. Using $D = 2.1 \times 10^{-5} \text{ cm}^2 \cdot \text{s}^{-1}$ for nitrite ion, the values of the constant k , **37e**, **37f**, **38e** and **38f** were obtained and they ranged from 0.0108 - 0.0118 $\text{cm} \cdot \text{s}^{-1}$ (Table 6.2). These were comparable to those of the aryloxy complexes. The transfer of the electron involved in the rate determining step, was found to be faster for *poly-38e* (0.0118 $\text{cm} \cdot \text{s}^{-1}$), followed by *poly-37e* (0.0114 $\text{cm} \cdot \text{s}^{-1}$), and slowest for *poly-37f* and *poly-38f* (0.0108 $\text{cm} \cdot \text{s}^{-1}$ for both).

Comparing all the complexes, i.e. **37a – f** and **38a – f**, it was clear that complexes **37a – d**, **38e** and **38f** had lower rate constants compared to **38a – d**. The electron transfer from the nitrite to the catalytic active center in the Pc, is facilitated by the MPc-nitrite adducts, thus completing the oxidation cycle. Therefore the lower rate constants in **37a – d**, **38e** and **38f** may suggest that the bond between the adduct of MPc and nitrite is weaker such that electron transfer from the substrate to the

catalyst center becomes difficult. Ultimately, the total number of electrons (n) involved in the electrocatalytic oxidation of nitrite was evaluated according to Eq. 6.4, as stated above, which is valid for totally irreversible diffusion-controlled electrode processes. The number of electrons transferred was found to be ~ 2 for all the complexes (Table 6.2), thus suggesting that two electrons were involved in the oxidation mechanism of nitrite ($-NO_2$), with nitrate ($-NO_3$) as the most likely product of the reaction.

The interaction between nitrite and the OTiPc complexes (**37e**, **37f**, **38e** and **38f**) was investigated in solution using UV-Vis spectroscopy. Fig. 6.19 shows the spectrum of complex **38e** before (Fig. 6.19a) and after addition of nitrite (Fig. 6.19b) in DMSO. Addition of nitrite to the complex solution resulted in the Q-band shift from 713 nm to 705 nm. The observed shift could either be due to the reduction of the central metal (Ti^{IV}) in complex **38e** or to ligand exchange of the axial oxygen for nitrite, as was observed for **37a – d** and **38a – d** above. In section 5.2.3, the reduction of Ti^{IV} (712 nm) to Ti^{III} (703 nm) determined during the controlled potential reduction of complex **38e** was observed. Therefore the peak at 705 nm was due to $Ti^{III}Pc$ species. The spectral changes in Fig 6.19 were thus due to the metal being reduced to $Ti^{III}Pc$. The reduction occurred instantly on addition of nitrite.

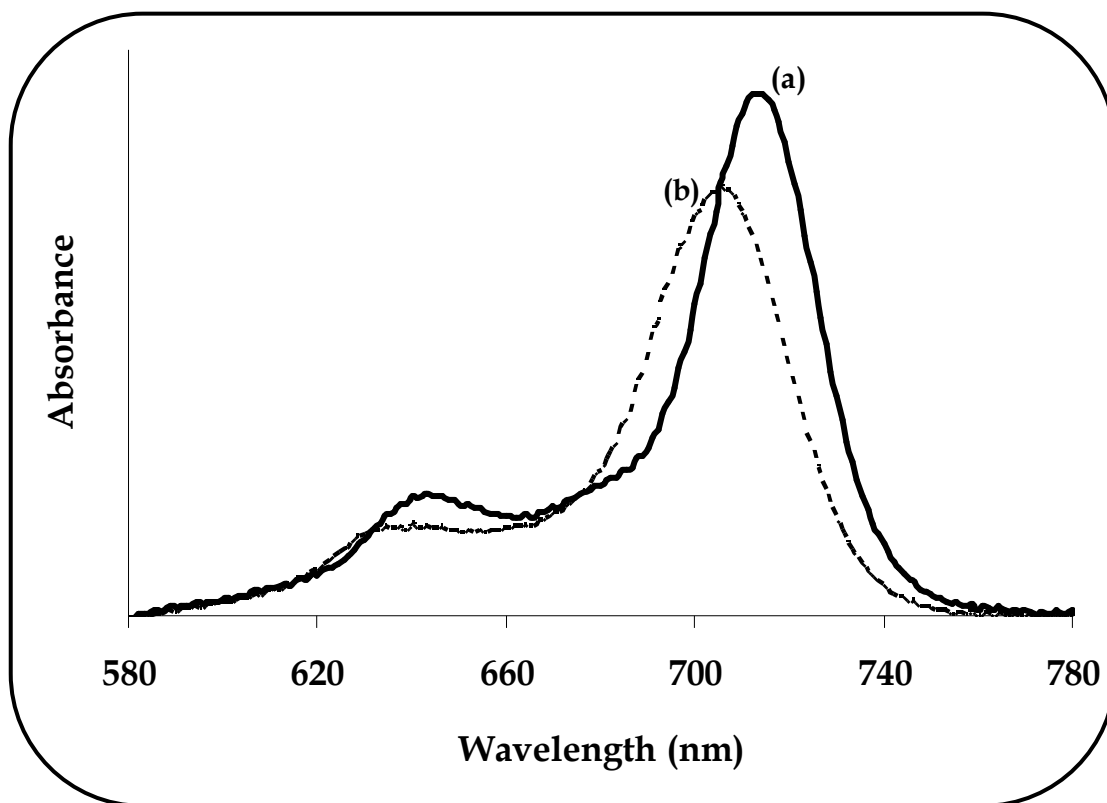


Figure 6.19: UV-Vis spectral changes observed on addition of nitrite to 38e in DMSO, where spectrum of (a) 38e ($\text{OTi}^{\text{IV}}\text{Pc}$) in absence of nitrite with $\lambda_{\text{max}} = 713$ nm and (b) in the presence of nitrite resulting in formation of $\text{Ti}^{\text{III}}\text{Pc}$ with $\lambda_{\text{max}} = 705$ nm.

To understand and ultimately propose the mechanism of nitrite oxidation catalysed by the *poly*-thiol-modified electrodes, several factors are considered. Nitrite is an ambident ion which contains more than one type of lone pairs that are able to potentially coordinate to a metal atom. The three types of possible structural isomers are shown in Fig. 6.20, whereby coordination may occur via nitrogen or oxygen atom, formally called nitro and nitrito complexes respectively. Coordination must first take place before reduction of Ti^{IV} by nitrite occurs.

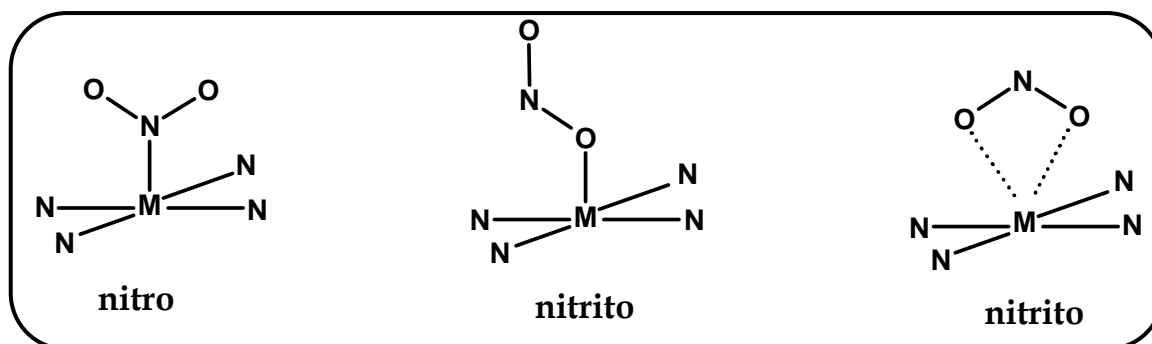


Figure 6.20: Schematic diagram illustrating the three limiting coordination modes of the nitrite ligand.

Table 5.1 showed that the arylthio-substituted complexes **37e**, **37f**, **38e** and **38f** were easier to reduce than the aryloxy-substituted complexes **37a – d** and **38a – d**. The latter complexes were not reduced by nitrite, but only effectuated axial ligand exchange, instead of reduction observed for the former complexes in Fig. 6.19. Since nitrite oxidation occurred in the range for ring oxidation for complexes **37e**, **37f**, **38e** and **38f**, a mechanism similar to that proposed for **37a – d** and **38a – d** is proposed. However, oxidation of the central metal to Ti^{IV} would occur first or $\text{Ti}^{\text{III}}\text{Pc}^{-1}$ species could be involved. The nature of the mechanism is not clear at this stage.

6.3 Amino tetra-substituted oxotitanium(IV) phthalocyanine

The electropolymerisation of complex **41** on GCE in DMF containing TBABF_4 was accomplished by repeatedly cycling the applied potential between 1.20 V and -0.70 V vs. $\text{Ag}|\text{AgCl}$. A series of consecutive CVs (20 scans) for the coating of GCE with complex **41** at a constant scan rate of 0.1 Vs^{-1} is illustrated in Fig. 6.21. Upon electropolymerisation, the peak associated with the first metal reduction at $\sim 0.40 \text{ V}$ gradually increased in current intensity and broadened. The broadening is due to the presence of more than one peak or due to the monomer and polymer. The peaks due to the first ring oxidation disappeared while that associated with amino

group shifted to more positive potentials and the latter peak became more irreversible. The shift to positive potentials with increase in scan number is an indication that the electrical resistance of the film is increased and an overpotential would be required to overcome this resistance. The observed anodic peak at ~ 1.18 V narrowed and exhibited quasi-reversible to irreversible behaviour as the electropolymerisation proceeded due to the slow charge transfer incurred within the polymeric film.

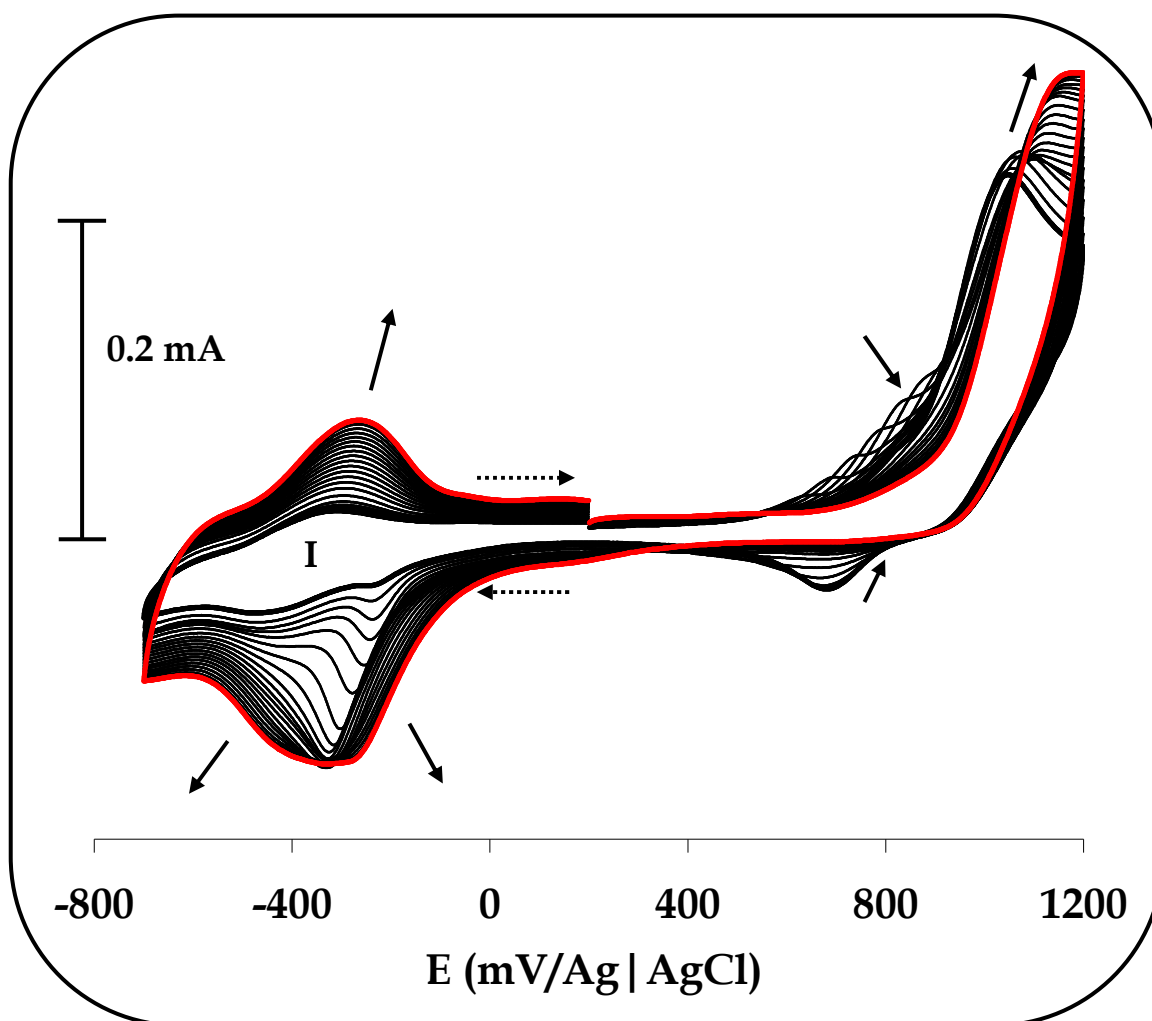
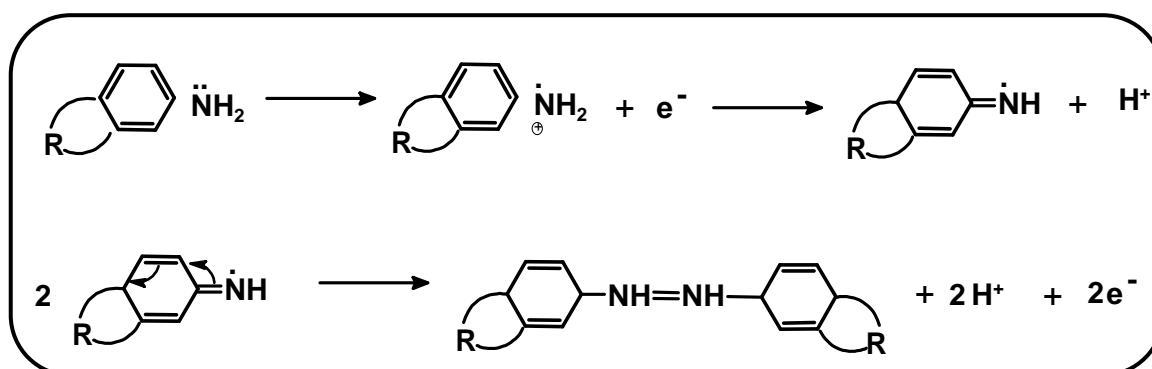


Figure 6.21: Evolution of CVs during the electropolymerisation of complex 41 on GCE in DMF containing 0.1 M TBABF₄ at a potential range of -0.70 to 1.20 V vs. Ag/AgCl. Scan rate 0.1 Vs⁻¹.

The initial step in the polymerisation of the complex occurs via the oxidised amino group, resulting in the deposition of an electroactive polymer on the electrode surface. The simplified electropolymerisation process is illustrated in Scheme 6.1. The redox-active polymer film formed on the electrode surface is now represented as *poly-41*. Also, variation of the number of electropolymerising scans controls the polymer thickness [452].



Scheme 6.1: Initial sequence of the electropolymerisation process which is sustained by repeating this initial sequence via the NH_2 groups remaining on the **R** residue. **R** represents the rest of the tetraaminophthalocyanine.

A plot of anodic peak current of the quasi-reversible couple (labelled **I**) as a function of electropolymerisation scan number (10, 20, 30, 40 and 50) was linear, showing that the relative conductivity of the polymer increases (at least up to 50 scans), Fig. 6.22. Thus when the film was thin (10 scans), the current response was low due to the film possessing few catalytically active sites, as opposed to a thicker film (50 scans).

The *poly-41*-modified electrode was removed from solution subsequent to the coating and rinsed with DMF and then water. On close examination of the surface of the modified electrode, a green colour which became darker as the film thickened was observed. The modified electrode was further characterised by cyclic voltammetry,

which confirmed the deposition of an electroactive film, when immersed in fresh phosphate buffer (pH 7.4) solution, Fig. 6.23.

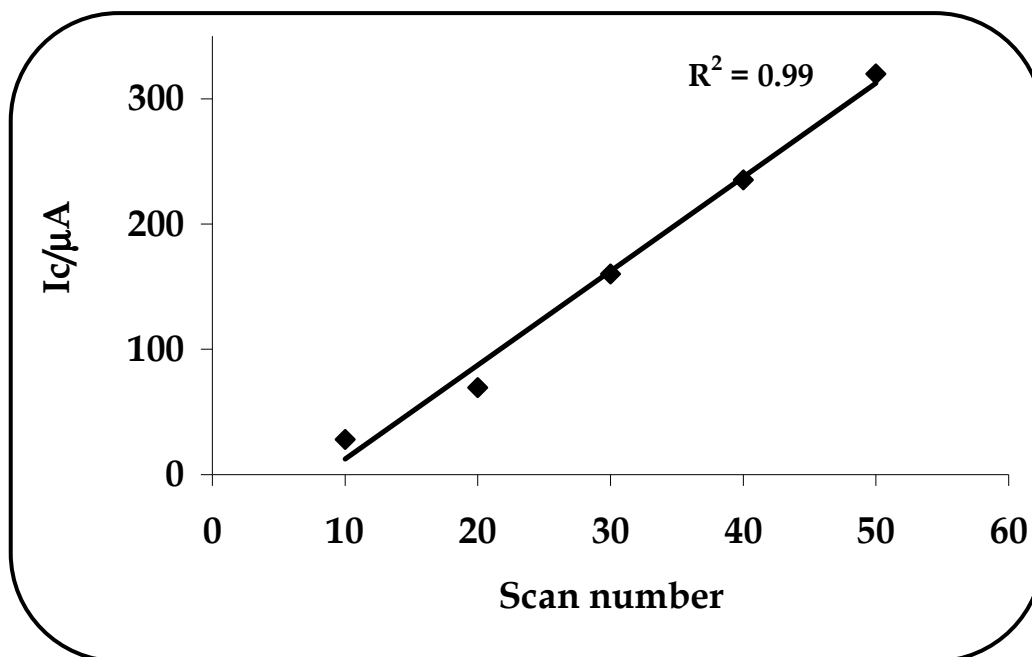


Figure 6.22: Redox activity of polymer in terms of cathodic current, I_{pc} , as a function of the electropolymerisation scan number of complex 41 in DMF containing 0.1 M TBABF₄. Scan rate 0.1 Vs⁻¹.

The redox processes observed in Fig. 6.21 were observed in Fig. 6.23, with the feature associated with the first metal reduction observed at more negative potentials, i.e. -0.61 V and the processes associated with the ring (labelled **II**) and amino oxidations at ~0.1 V and 0.72 V respectively. The amino oxidation was observed as an irreversible peak. The shift to negative potentials in Fig. 6.23 (compared to Fig. 6.21) is not unusual and is brought about by the difference in media, i.e. organic (Fig. 6.21) vs. aqueous (Fig. 6.23). The surface concentration (Γ) was estimated according to the following Langmuir isotherm equation (Eq. 6.1) was determined to be

$3.33 \times 10^{-9} \text{ mol.cm}^{-2}$, which was slightly higher than an average monolayer coverage of $\sim 10^{-10} \text{ mol.cm}^{-2}$ and thus indicates multilayer adsorption [453,454].

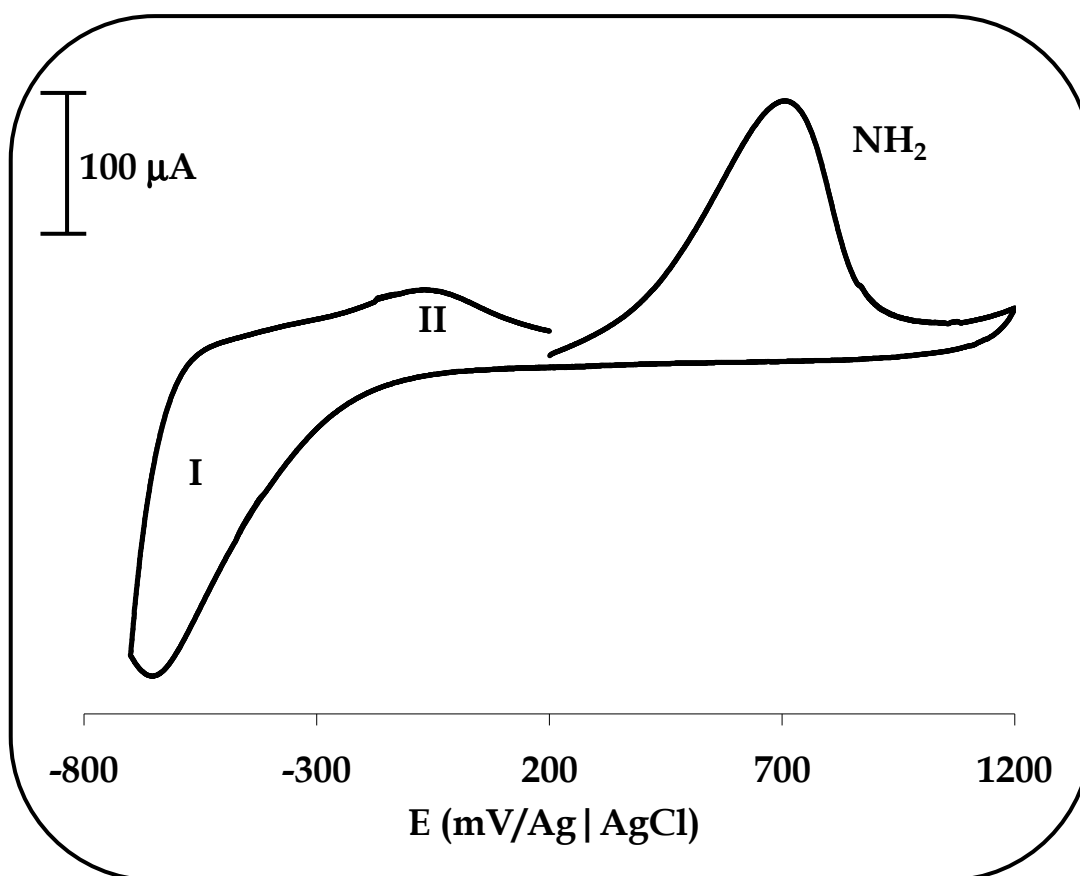


Figure 6.23: Cyclic voltammetry of *poly-41*-modified GCE in phosphate buffer solution (pH 7.4). Scan rate 0.1 Vs^{-1} .

A linear plot (not shown) of current (I_p) vs. scan rate (up to 0.1 Vs^{-1}) for process **I** in Fig. 6.23, that is typical of a surface reaction of adsorbed species, further confirmed the deposition onto the electrode. At scan rates higher than 0.1 Vs^{-1} , the separation between peak potentials (ΔE_p) for process **I** increased with increase in scan rates, i.e. the peaks become more asymmetrical and appear irreversible. Thus the electron exchange process between the GCE and complex **41** was retarded, indicating the limitation that arises from the charge transfer kinetics. Kinetic data of electron transfer between the complex **41** and the GCE surface was obtained from the

parameters of the peak separation in process **I** described by Laviron [455]. Laviron derived general expressions for the linear potential sweep voltammetric response for the case of surface-confined electroactive species. By measuring the variations of the anodic and cathodic peak potentials (E_p) with the logarithm of scan rates, it is possible to determine the apparent charge transfer rate constant (k) as well as the transfer coefficient (α) for electron transfer between the GCE and complex **41**. The following expressions are for $\Delta E_p > 200/n$ mV commonly obtained at very high scan rates,

$$E_{pc} = E_c^o - (RT / \alpha nF) \ln(RTk_c / \alpha nFv_c) \quad (6.10)$$

$$E_{pa} = E_a^o - (RT / (1 - \alpha)nF) \ln(RTk_a / (1 - \alpha)nFv_a) \quad (6.11)$$

where v_c and v_a respectively denote critical cathodic and anodic scan rates obtained from the extrapolation of the linear portion of the E_p vs. $\log v$ plots, to the formal cathodic (E_c^o) and anodic (E_a^o) potentials observed at slow scan rates. From the E_p vs. $\log v$ plots, the slopes of the linear portions are $-2.3RT/\alpha nF$ and $2.3RT/(1 - \alpha)nF$ for the cathodic and anodic branches respectively. The charge transfer rate constants k_c and k_a are respectively given by $\alpha nFv_c/RT$ and $(1 - \alpha)nFv_a/RT$.

Figure 6.24 shows the typical plots of the peak potentials as a function of the log of scan rates for the *poly-41* film in phosphate buffer of pH 7.4. As can be seen, the E_p values were proportional to the log of scan rate for high scan rates. Kinetic parameters, k_c , k_a and α were extracted from the linear parts of the plots. The evaluated values for the charge transfer rate constants, k_c and k_a , were 5.33 s^{-1} and

4.96 s⁻¹ respectively and the transfer coefficients α and $(1-\alpha)$ were 0.12 and 0.10 respectively. The values of the rate constants justified the slow establishment of equilibrium, and were similar and comparable to those of other surface-confined species. The transfer coefficients however were low and deviated from 0.5 considerably due to defect of the orientation of the complex **41** molecules on the electrode surface [456,457]. Kinetic parameters for complexes **37e**, **37f**, **38e** and **38f** could not be compared since irreversibility of the film was observed with increase in scan rate, whereas for complex **41** reversibility of process **I** was maintained with increase in scan rate, allowing the use of Eq. 6.10 and 6.11.

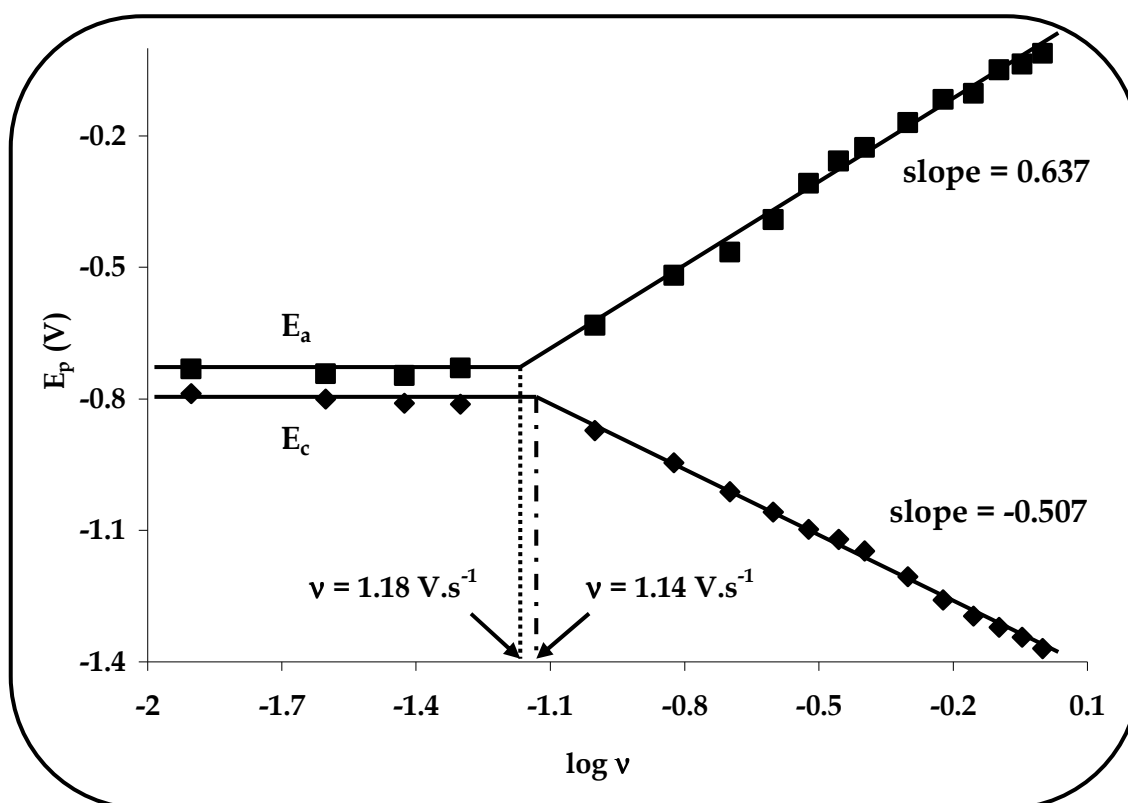


Figure 6.24: Variation of the cathodic (E_{pc}) and anodic (E_{pa}) peak potentials with the log of scan rate for *poly-41* in phosphate buffer (pH 7.4).

The main aim of this work was to develop a modified electrode that is capable of the electrocatalytic oxidation of nitrite. The potential of the *poly-41*-modified

electrode to electrocatalyse nitrite was tested against that of the bare electrode. Cyclic voltammetric responses were obtained in the presence of 1 mM nitrite in pH 7.4 phosphate buffer solution, Fig. 6.25. As already stated, the disproportionation of nitrite to NO was insignificant at this pH, thus the observed responses were as a result of the oxidation of nitrite. A weak response at ~ 0.80 V was obtained at the bare electrode, Fig. 6.25(i), while an enhancement of the anodic peak current with a very strong electrocatalytic effect was observed, Fig. 6.25(ii), as has already been observed for complexes **37a – f** and **38a – f** above.

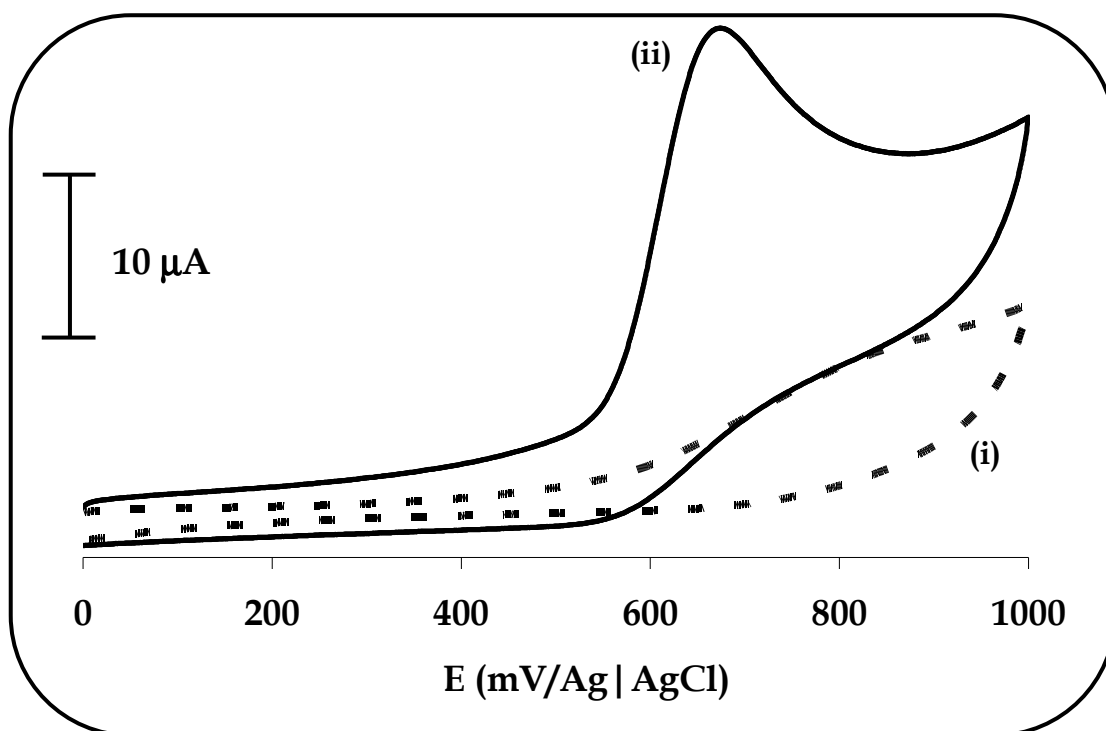


Figure 6.25: Cyclic voltammograms of electrooxidation of 1 mM nitrite at (i) the bare GCE and (ii) *poly-41*-modified electrode in phosphate buffer (pH 7.4). Scan rate 0.1 Vs^{-1} .

Additionally, the peak current was observed at less positive potentials than that observed with the bare electrode. Therefore, consistent with the strong electrocatalytic effect, a decrease in the overpotential of ~ 150 mV was achieved, i.e. $E_p = 0.67$ V. It can be envisaged that the *poly-41* exhibited a catalytic response,

however it performed worse than *poly-38e* (0.59 V), 38d (0.62 V), *poly-37e* (0.64 V) and **38c** (0.64 V). The stability and reproducibility of the modified electrode was examined by potential recycling in the phosphate buffer. A 23 % rapid current decrease was observed after the first scan, Fig. 6.26, thereafter the current remained almost constant for a number of scans, exhibiting high resistance to passivation. The current decrease may be owed to passivation by nitrite oxidation product(s).

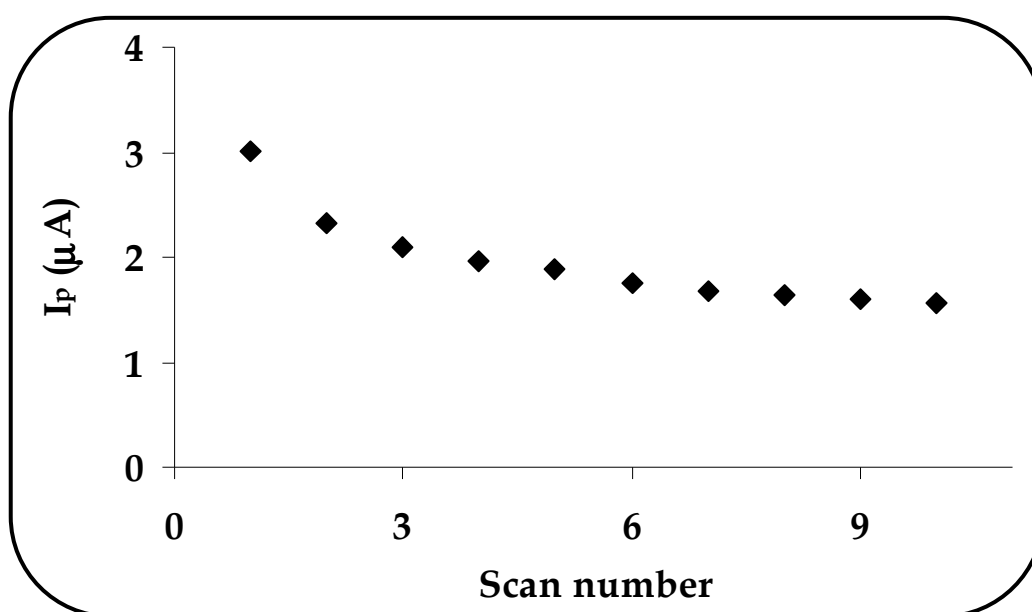
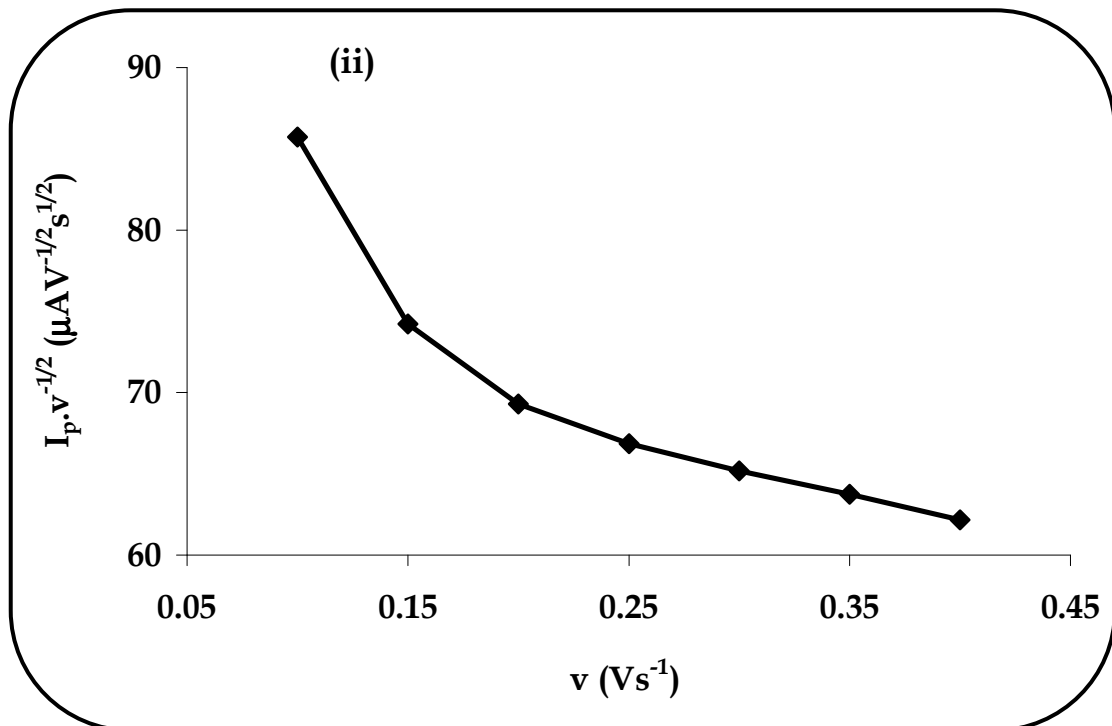
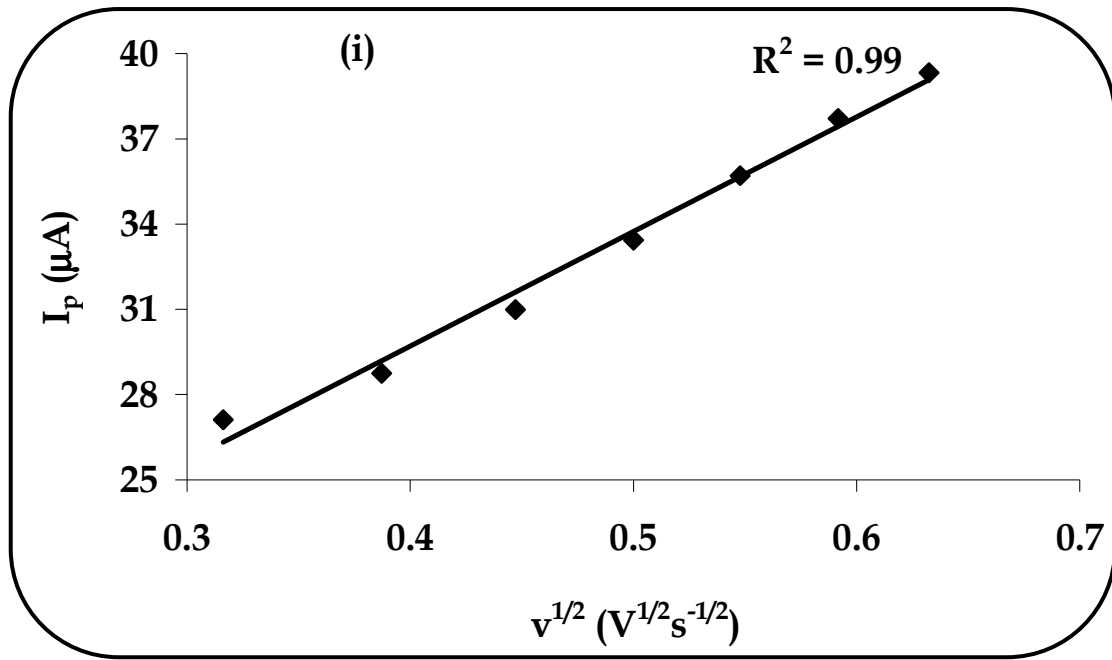


Figure 6.26: Plot of variation of peak currents with scan number for the voltammetric response of 1 mM nitrite in phosphate buffer solution (pH 7.4) on *poly-41*. Scan rate 0.1 Vs^{-1} .



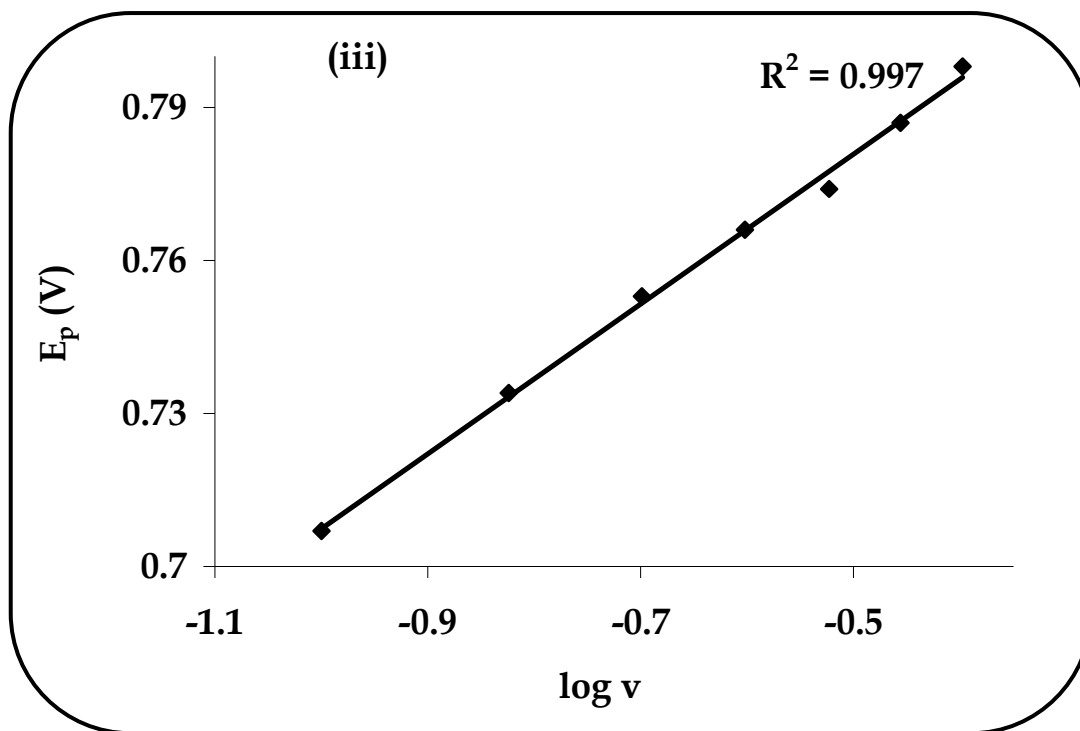


Figure 6.27: (i) Plot of I_p vs. $v^{1/2}$ for the electrocatalytic oxidation of 1 mM nitrite solution in phosphate buffer (pH 7.4) on *poly-41*. (ii) Plot of $I_p v^{-1/2}$ vs. v for the electrocatalytic oxidation of 1 mM nitrite solution in phosphate buffer (pH 7.4) on *poly-41*. (iii) Plot of E_p vs. $\log v$ for the electrocatalytic oxidation of 1 mM nitrite solution in phosphate buffer (pH 7.4) on *poly-41*.

For a fixed nitrite concentration, i.e. 1 mM, analyses of cyclic voltammograms at various scan rates were obtained, Fig. 6.27. A linear relation between the peak current (I_p) and square root of scan rate ($v^{1/2}$) was obtained, an indication of a diffusion-controlled nitrite electrooxidation, Fig. 6.27(i). A typical EC' curve, indicative of a catalytic process was obtained for a sweep-rate normalised current density ($I_p v^{-1/2}$) vs. the scan rate, Fig. 6.27(ii). Also, a plot of the peak potentials increased with log scan rate thus indicating the chemical irreversibility of the electrooxidation process.

Kinetic parameters for the electrocatalytic oxidation of nitrite were further obtained, Table 6.2. For a totally irreversible system, the anodic peak potential was

given by Eq. 6.2. A Tafel slope ($b = 2.3RT / (1 - \alpha)n_a F$) of 294 mV/decade was determined and related to $(1 - \alpha)n_a$ which was calculated to be 0.10. The Tafel slope suggested substrate-catalyst interactions confirmed by UV/Vis spectroscopic studies (not shown) and that a first one-electron transfer is the rate-determining step for the electrocatalytic oxidation of nitrite. The transfer coefficient $\alpha = 0.90$ was high, an indication that the reaction equilibrium favoured product formation, i.e. nitrate, much more than for complexes **37a – f** and **38a – f**, Table 6.2. The value was much higher than the other discussed complexes, an indication that electrocatalysis by complex **41** ensures product formation. The heterogeneous electron transfer coefficient, k , at the modified electrode, was obtained from Eq. 6.3. The obtained rate constant, $k = 0.0620 \text{ cm.s}^{-1}$ was found to be ~ 6 times larger than those of other tetra-substituted titanium phthalocyanine complexes discussed, an indication that the acceleration of the rate of electron transfer at the surface of the *poly-41* is faster and more efficient than that of the latter complexes. The total number of electrons (n) transferred in the electrocatalytic oxidation of nitrite was calculated from Eq. 6.4. A total of 2.4 (~ 2) electrons were obtained, therefore suggesting that the nitrite oxidation results in nitrate (NO_3^-) as the most likely product, Table 6.2.

The electrode reaction of the catalytic oxidation of nitrite at the surface of *poly-41*-modified electrode was also investigated by double-potential step chronoamperometry. Measurements for *poly-41*-modified electrode were done in the absence and presence of nitrite. The catalytic rate constant, k , was evaluated for the chemical reaction between nitrite and the surface-bound *poly-41* according to the method of Galus [458]. At intermediate times (5.5 – 8.75 s in this work), the catalytic

current, I_{cat} , is dominated by the rate of electrocatalysed oxidation of nitrite. Thus the rate constant can be estimated from the following Eq. 6.12

$$\frac{I_{cat}}{I_l} = \pi^{1/2} \gamma^{1/2} = (\pi k C_o t)^{1/2} \quad (6.12)$$

where I_l is the limited current in the absence of nitrite, $\gamma = k C_o t$ (C_o is the concentration of nitrite) is the argument of an error function and t is the elapsed time.

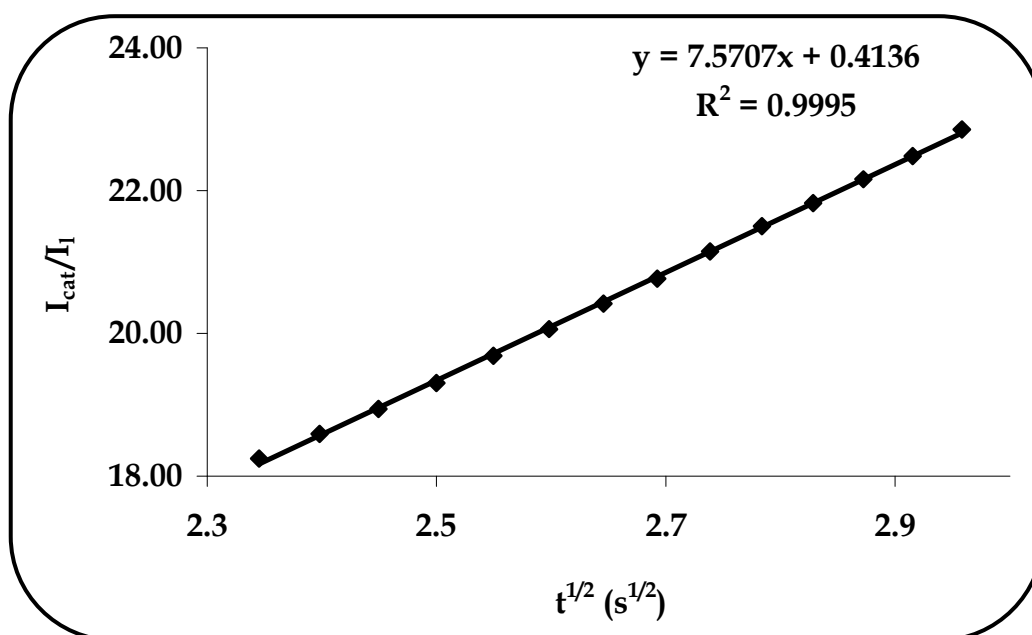
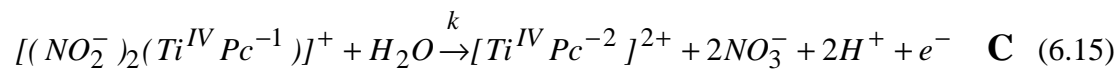
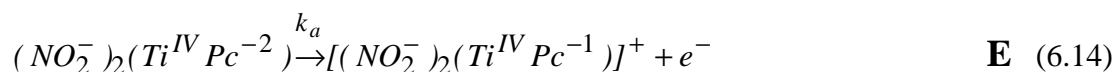
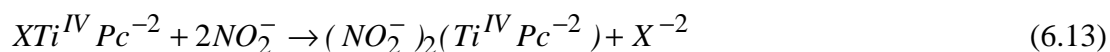


Figure 6.28: Plot of I_{cat}/I_l derived from chronoamperometric data for 1 mM nitrite in phosphate buffer (pH 7.4) solution on *poly-41*.

From the slope of I_{cat}/I_l vs. $t^{1/2}$ in Fig. 6.28, the value of k was found to be 0.0603 $\text{cm}\cdot\text{s}^{-1}$ which was in good agreement from that obtained in cyclic voltammetry, i.e. 0.0620 $\text{cm}\cdot\text{s}^{-1}$. Since the catalytic peak potential is in the stability range of the ring based process, the nitrite oxidation is thus mediated by $\text{Ti}^{\text{IV}}\text{Pc}^{-2}/\text{Ti}^{\text{IV}}\text{Pc}^{-1}$. Based on the data discussed above, the oxidation of nitrite was believed to occur as was described in Eq. 6.6 – 6.8, represented here again as Eq. 6.13 – 6.15.



where X = axial ligand.

Therefore the end product is nitrate as was confirmed by the number of electrons transferred during the catalysis.

6.4 Conclusion

The electrocatalytic oxidation of nitrite was facilitated by the aryloxy-, arylthio and amino-substituted OTiPcs through the phthalocyanine ring as the active catalytic center. Nitrate was confirmed as the product of oxidation. Although the lowering in the nitrite oxidation overpotential was observed for all complexes, modification by electropolymerisation was found to be better in terms of stability and reproducibility. The arylthio-substituted complexes underwent chemical reactions, i.e. metal reduction in the presence of nitrite. The same cannot be said for the aryloxy and amino-substituted complexes which were instead coordinated to nitrite. Complex **41** facilitated the transfer of electrons six times faster than the other complexes. Overall, complex **41** exhibited better performance in terms of rate of oxidation, but complex **38e**, gave the largest lowering of overpotential.

CHAPTER 7

Conclusions

And

Future perspectives

7.1 GENERAL CONCLUSIONS

In conclusion, this work reports on the synthesis of a new family of oxotitanium phthalocyanines which were substituted with aryloxy, arylthio and amino groups at the peripheral or non-peripheral positions. The majority of the complexes were tetra-substituted while others were octa-substituted. The differently sulphonated tantalum and titanium phthalocyanines which were found to be disulphonated by HPLC, were obtained from the sulphonation of the unsubstituted derivatives. The complexes were fully characterised by spectroscopic methods as well as methods of mass spectroscopy and elemental analysis which confirmed the purity of the complexes. Significant solubility increase was observed and remarkable solution properties such as UV/Vis were exhibited. Substitution with arylthio and amino groups resulted in the red-shift of the Q-band, which was more obvious for substituents at the non-peripheral position. The sulphonated complexes exhibited different properties in DMSO, methanol and PBS 7.4 solution, with the titanium derivative highly aggregated in PBS. The tantalum derived showed broadened Q band in DMSO, methanol and aqueous solvents. However, in aqueous solutions, addition of Triton X-100 had no effect on the spectra. Ionic interactions between the cationic methylviologen and the anionic sulphonated complexes were followed by spectroscopic methods. Evidence of the interaction of the studied MPcS_n complexes with MV^{2+} was obtained, where two heterotrimers in the $\text{TiPcS}_n / \text{MV}^{2+}$ and one heterotrimer in the $\text{TaPcS}_n / \text{MV}^{2+}$ systems were obtained by spectrophotometric titrations. The complexation served as potential supramolecular assemblies for electron transfer. The complexation was found to be stronger for the TaPc derivative than it was for TiPc. The synthesised complexes were further studied for their photophysicochemical and electrochemical properties.

Sufficient singlet oxygen in air-saturated solutions was generated by the complexes. Substitution at the peripheral positions, and more especially with arylthio groups seemed to enhance the singlet oxygen quantum yield as opposed to those at the non-peripheral positions. The arylthio-substituted complexes (**37e** and **37f**) at the non-peripheral position generated the lowest yields due to the J-type aggregation in DMSO. Moreover, the peripherally substituted complexes were found to be slightly more stable than the non-peripherally substituted counterparts, at the same time the arylthio-substituted MPcs were found to be slightly less stable than the corresponding derivatives. The use of chloronaphthalene as solvent for singlet oxygen quantum yield determination of octa-substituted derivatives, proved to lower the yields due to the radical-attack of the MPcs. OTiPc fluorescence quantum yields and triplet yields were found to be comparable to those in literature except for complexes **37e** and **37f** due to quenching by aggregation. The triplet lifetimes of the octa-substituted derivatives however varied due to other processes, i.e. phototransformation of the complexes taking place. Fluorescence lifetimes which may otherwise be impossible to obtain due to equipment limitations, were determined by quenching experiments. Correspondingly, the quenching efficiency of BQ was presented through fluorescence-quenching experiments which were found to be diffusion-controlled. Quenching of the photoexcited singlet state of the water-soluble complexes by methylviologen was also investigated. Depending on the combination of the MPc with the quencher, the fluorescence properties of the TiPcS_n and TaPcS_n complexes were explored, and the fluorescence of TiPcS_n heavily quenched (~ 73 %) by MV²⁺ compared to the fluorescence of TaPcS_n (~ 24 %) due to complexation.

Aryloxy and arylthio tetrasubstituted complexes were selected for the photocatalytic transformation of 1-hexene. The complexes were found to catalyse the

photooxidation of 1-hexene by two competing Type I and Type II mechanisms. The photooxidation products were found to be 1-hexen-3-ol as minor product as well as 1,2-epoxyhexane as the major product in good selectivities (75.5 – 87.1 %). The reaction products were dependent on the nature and position of the substituents with the peripherally substituted complexes being better catalysts than the corresponding non-peripherally substituted counterparts. These in turn governed the generation of singlet oxygen quantum yields which were also found to be directly related to the photostability of each complex. Moreover, the arylthio substituted complexes better performed than the aryloxy complexes. Overall the phenoxy substituted complex **38a** was found to be the best catalyst in terms of singlet oxygen quantum yield, photostability and activity. Use of molecular oxygen as being attractive in these photocatalytic processes for economic reasons was demonstrated.

The complexes were investigated for their electrochemical properties. Electrochemistry and spectroelectrochemistry of tantalum phthalocyanine were reported and confirmed that the reduction occurred at the central metal followed by the ring. Spectroelectrochemistry confirmed two one electron process, followed by a simultaneous four electron process. A multielectron transfer in a single step is a unique behavior which is not common in phthalocyanines and was explained in terms of the nonplanar nature of the complex. For complexes **37a**, **37b**, **38a** and **38b**, the first two reductions consisted of two electron reduction steps, and the last reduction is a one electron step confirmed by spectroelectrochemistry to be a confirmed 2 electron and 1 electron reductions respectively. For complexes **37c – f**, **38c – f**, **39a – c** and **41**, reduction processes were found to involve one electron transfers, thus further emphasising the role that the substituents have towards properties of these MPcs. For

all complexes, the first two reductions were metal-based followed by ring-based processes.

The aryloxy-substituted complexes were adsorbed while the arylthio and amino-substituted complexes were electropolymerised. The overpotential of nitrite oxidation was lowered to values as low as 0.59 V which are much lower than the reported values of ~0.80 V. The catalytic peak currents were also enhanced compared to the bare electrode. Kinetic parameters were elucidated, where a one-electron transfer was the limiting chemical step. The total number of electrons transferred for the nitrite electrocatalytic oxidation was ~2, thus suggesting that the final product is nitrate. Again the effect of substituents could not be ignored as the complexes displayed unique electrocatalytic properties. The modified electrodes thus offer an effective route in the fabrication of nitrite electrochemical sensors.

7.2 Future perspectives

The synthesis of substituted tantalum phthalocyanines could be attempted since these complexes have not been exploited and may exhibit interesting properties that may be useful in many applications. The synthesis of titanium phthalocyanines can further be exploited, e.g. axial substitution or octa-substitution at the non-peripheral positions. The TiPcs can also be investigated as catalysts for the selective formation of epoxides (> 90 %) in the presence of an oxidant such as oxygen and a reducing agent, e.g. benzaldehyde. Furthermore, the TiPcs may be investigated as electrocatalysts of various analytes, including the reduction of oxygen and nitrate since the complexes exhibit a number of redox processes, i.e. first two metal reductions as well as ring-based reductions.

REFERENCES

1. A. von Braun, J. Tscherniac, *Ber. Deut. Chem. Ges.*, **40** (1907) 2709
2. H. de Diesbach, E. von der Weid, *Helv. Chim. Acta*, **10** (1927) 886
3. A.G. Dandridge, H.A.E. Drescher, J. Thomas, *Dyes British Patent*, **322** (1929) 169
4. R.P. Linstead, *J. Chem. Soc.*, (1934) 1016
5. G.T. Byrne, R.P. Linstead, A.R. Lowe, *J. Chem. Soc.*, (1934) 1017
6. R.P. Linstead, A.R. Lowe, *J. Chem. Soc.*, (1934) 1022
7. C.E. Dent, R.P. Linstead, *J. Chem. Soc.*, (1934) 1027
8. R.P. Linstead, A.R. Lowe, *J. Chem. Soc.*, (1934) 1031
9. C.E. Dent, R.P. Linstead, *J. Chem. Soc.*, (1934) 1033
10. J.M. Robertson, *J. Chem. Soc.*, (1935) 615
11. J.M. Robertson, *J. Chem. Soc.*, (1936) 1195
12. J.M. Robertson, I. Woodward, *J. Chem. Soc.*, (1937) 219
13. L.E. Webb, E.B. Fleischer, *J. Chem. Phys.*, **43** (1965) 3100
14. M.S. Fischer, D.H. Templeton, A. Zalkin, M. Calvin, *J. Am. Chem. Soc.*, **97** (1975) 2676
15. G.P. Moss, *Pure Appl. Chem.*, **59** (1987) 779
16. G. Dufour, C. Poncey, F. Rochet, H. Roulet, S. Iacobucci, M. Sacchi, F. Yubero, N. Motta, M.N. Piancastelli, A. Sgarlata, M. de Crescenzi, *J. Electron Spectrosc.*, **76** (1995) 219
17. C.J. Brown, *J. Chem. Soc. A*, (1968) 2488
18. R.P. Linstead, F.T. Weiss, *J. Chem. Soc.*, (1950) 2981
19. K. Ukei, *Acta Cryst. B*, **B29** (1973) 2290
20. Y. Iyechika, K. Yakushi, I. Ikemoto, H. Kuroda, *Acta Cryst. B*, **38** (1982) 766
21. P.N. Day, Z.Q. Wang, R. Pachter, *J. Mol. Struct. (Theochem)*, **455** (1998) 33

22. R. Kubiak, J. Janczak, *J. Alloy Compd.*, **189** (1992) 107
23. M.K. Friedel, B.F. Hoskins, R.L. Martin, S.A. Mason, *J. Chem. Soc., Chem. Commun.*, (1970) 400
24. Y. Zhang, X. Zhang, Z. Liu, H. Xu, J. Jiang, *Vib. Spectrosc.*, **40** (2006) 289
25. P.A. Barrett, C.E. Dent, R.P. Linstead, *J. Chem. Soc.*, (1936) 1719
26. K.A. Martin, M.J. Stillman, *Inorg. Chem.*, **19** (1980) 2473
27. V.P. Kulinic, G.P. Shaposhnikov, *Russ. J. Gen. Chem.*, **73** (2003) 794
28. R.F. Ziolo, M. Extine, *Inorg. Chem.*, **20** (1981) 2709
29. R.F. Ziolo, W.H.H. Günther, J.J. Troup, *J. Am. Chem. Soc.*, **103** (1981) 4629
30. G. Guyon, A. Pondaven, P. Guenot, M. L'Her, *Inorg. Chem.*, **33** (1994) 4787
31. J. Jiang, R.C.W. Liu, T.C.W. Mak, T.W.D. Chan, D.K.P. Ng, *Polyhedron*, **16** (1997) 515
32. N.B. McKeown, I. Chambrier, M.J. Cook, *J. Chem. Soc. Perkin Trans. I*, (1990) 1169
33. V. Goedken, G. Dessy, C. Ercolani, V. Fares, L. Gastaldi, *Inorg. Chem.*, **24** (1985) 991
34. L. Cellucci, C. Ercolani, P.J. Lukes, A. Chiesi-Villa, C. Rizzoli, *J. Porphyrins Phthalocyanines*, **2** (1998) 9
35. F. Gingl, J. Strähle, *Z. Naturforsch B*, **43** (1988) 445
36. W. Hiller, J. Strähle, W. Kobel, M. Hanack, *Z. Kristallogr.*, **159** (1982) 173
37. X. Wang, Y. Chen, H. Liu, J. Jiang, *Thin Solid Films*, **496** (2005) 619
38. J. Zang, F. Lu, H. Huang, J. Wang, H. Yu, J. Jiang, D. Yan, Z. Wang, *Synthetic Met.*, **148** (2005) 123
39. N. Koike, H. Uekusa, Y. Ohashi, C. Harnode, F. Kitamura, T. Ohsaka, K. Tokuda, *Inorg. Chem.*, **35** (1996) 5798

40. A. DeCian, M. Moussavi, J. Fischer, R. Weiss, *Inorg. Chem.*, **24** (1985) 3162
41. S. Zhou, X. Jin, W. Hu, Y. Liu, S. Liu, *Solid State Commun.*, **112** (1999) 269
42. D.M. Pai, B.E. Springett, *Rev. Mod. Phys.*, **65** (1993) 163
43. Z. Bao, *Adv. Mater.*, **12** (2000) 227
44. C.W.M. Yuen, S.K.A. Ku, P.S.R. Choi, C.W. Kan, *Text. Res. J.*, **75** (2005) 319
45. K.Y. Law, *Chem. Rev.*, **93** (1993) 449
46. T. Enokida, R.J. Hirohashi, T. Nakamura, *J. Imag. Sci.*, **34** (1990) 234
47. P. Gregory, R.W. Kenyon, *United States Patent*, (1994), 5296023
48. C. Schlebusch, J. Morenzin, B. Kessler, W. Eberhardt, *Carbon*, **37** (1999) 717
49. H. Seis, *Angew. Chem.*, **98** (1986) 1061
50. M. Soncin, A. Busetti, R. Biolo, G. Jori, G. Kwag, Y. Li, M.E. Kenney, M.A.J. Rodgers, *J. Photochem. Photobiol. B*, **42** (1998) 202
51. R. Bonnett, *Chemical Aspects of Photodynamic Therapy*, Gordon and Breach Science, Amsterdam, (2000)
52. T.J. Dougherty, *Oncology*, **3** (1989) 67
53. B.W. Henderson, T.J. Dougherty, *Photochem. Photobiol.*, **55** (1992) 145
54. R. Bonnett, *Chem. Soc. Rev.*, **24** (1995) 19
55. J.S. Shirk, R.G.S. Pong, F.J. Bartoli, A.W. Snow, *Appl. Phys. Lett.*, **63** (1993) 1880
56. J.W. Perry, K. Mansour, I.Y.S. Lee, X.L. Wu, P.V. Bedworth, C.T. Chen, D. Ng, S.R. Marder, P. Miles, T. Wada, M. Tian, H. Sasabe, *Science*, **273** (1996) 1533
57. O.L. Kaliya, E.A. Luk'yanets, G.N. Vorozhtsov, *J. Porphyrins Phthalocyanines*, **3** (1999) 592
58. A. Sorokin, B.J. Meunier, *J. Chem. Soc., Chem. Commun.*, (1994) 1799

59. T. Ichinohe, H. Miyasaka, A. Isoday, M. Kimura, K. Hanabusa, H. Shirai, *React. Funct. Polym.*, **43** (2000) 63
60. J.H. Zagal, *Coord. Chem. Rev.*, **119** (1992) 89
61. M.N. Golovin, P. Seymour, K. Jayara, Y. Fu, A.B.P. Lever, *Inorg. Chem.*, **29** (1990) 1719
62. J.H. Zagal, G.I. Cárdenas-Jirón, *J. Electroanal. Chem.*, **489** (2000) 96
63. A. El Hourch, S. Belcadi, P. Moisy, P. Crouigneau, J.-M. Léger, C. Lany, *J. Electroanal. Chem.*, **339** (1992) 1
64. Y.H. Tse, P. Janda, A.B.P. Lever, *Anal. Chem.*, **66** (1994) 384
65. M.A. Gulppi, M.A. Paez, J.A. Costamagna, G. Cárdenas-Jirón, F. Bedioui, J.H. Zagal, *J. Electroanal. Chem.*, **580** (2005) 50
66. B.A. Retamal, M.E. Vaschetto, J.H. Zagal, *J. Electroanal. Chem.*, **431** (1997) 1
67. Z. JiuJun, T. Yu-Hong, W.J. Pietro, A.B.P. Lever, *J. Electroanal. Chem.*, **406** (1996) 203
68. J.H. Zagal, *J. Electroanal. Chem.*, **109** (1980) 389
69. J.H. Zagal, E. Muñoz, S. Ureta-Zañartu, *Electrochim. Acta.*, **27** (1982) 1373
70. C.A. Caro, F. Bedioui, J.H. Zagal, *Electrochim. Acta.*, **47** (2002) 1489
71. M.H. Pournaghi-Azar, H. Dastango, *J. Electroanal. Chem.*, **567** (2004) 211
72. C.A. Caro, F. Bedioui, M.A. Páez, G.I. Cárdenas-Jirón, J.H. Zagal, *J. Electrochem. Soc.*, **151** (2004) E32
73. H. Hopff, P. Gallegra, *Helv. Chim. Acta*, **51** (1968) 253
74. M. Hanack, J. Mertz, G. Pawlowski, *Chem. Ber.*, **115** (1982) 2836
75. G.P. Ellis, T.M. Romney-Alexander, *Chem. Rev.*, **87** (1987) 779
76. C. Couture, A.J. Paine, *Can. J. Chem.*, **63** (1985) 111
77. P. Gregory, *J. Porphyrins Phthalocyanines*, **4** (2000) 432

78. M.D. Maree, T. Nyokong, *J. Porphyrins Phthalocyanines*, **5** (2001) 555
79. M. Hanack, M. Lang, *Adv. Mat.*, **6** (1994) 819
80. M.J. Cook, A.J. Dunn, S.D. Howe, A.J. Thomson, K.J. Harrison, *J. Chem. Soc., Perkin Trans. 1*, (1988) 2453
81. F. Baumann, B. Bienert, G. Rösch, H. Vollmann, W. Wolf, *Angew. Chem.*, **68** (1956) 133
82. M. Brewis, G.J. Clarkson, P. Humberstone, S. Makhseed, N.B. McKeown, *Chem. Eur. J.*, **4** (1998) 1633
83. S.A. Mikhalenko, V.M. Derkacheva, E.A. Luk'yanets, *J. Gen. Chem. USSR*, **51** (1981) 1405
84. J.A. Thompson, K. Murata, D.C. Miller, J.L. Stanton, W.E. Broderick, B.M. Hoffmann, J.A. Ibers, *Inorg. Chem.*, **53** (1983) 2339
85. I. Gürol, V. Ahsen, Ö. Bekaroglu, *J. Chem. Soc., Dalton Trans.*, (1994) 497
86. A. Tomoda, S. Saito, S. Ogawa, S. Shiraishi, *Chem. Lett.*, (1980) 1277
87. H. Tomoda, S. Saito, S. Shiraishi, *Chem. Lett.*, (1983) 313
88. D. Wöhrle, G. Schnupfheil, G. Knothe, *Dyes Pigments*, **18** (1992) 91
89. A.W. Snow, J.R. Griffith, N.P. Marullo, *Macromolecules*, **17** (1984) 1614
90. A.W. Snow, N.L. Jarvis, *J. Am. Chem. Soc.*, **106** (1984) 4706
91. R.D. George, A.W. Snow, *Chem. Mater.*, **6** (1994) 1587
92. C.J. Walsh, B.K. Mandal, *Chem. Mater.*, **12** (2000) 287
93. C.-H. Lee, D.K.P. Ng, *Tetrahedron Lett.*, **43** (2002) 4211
94. M.A. Robinson, S.I. Trotz, T.J. Hurley, *Inorg. Chem.*, **6** (1967) 392
95. T.J. Hurley, M.A. Robinson, S.I. Trotz, *Inorg. Chem.*, **6** (1967) 389
96. C.H. Yang, C.-T. Chang, *J. Chem. Soc., Dalton Trans.*, (1982) 2539

97. P.J. Brach, S.J. Grammatica, O.A. Ossanna, L. Weinberger, *J. Heterocycl. Chem.*, **7** (1970) 1403
98. S.A. Mikhalenko, E.A. Luk'yanets, *J. Gen. Chem. USSR*, **39** (1969) 2081
99. A. Shaabani, *J. Chem. Res.*, (1998) 672
100. A. Kempa, J. Dobrowolski, *Can. J. Chem.*, **66** (1988) 2553
101. M.K. Lowery, A.J. Starshak, J.N. Esposito, P.C. Krueger, M.E. Kenney, *Inorg. Chem.*, **4** (1965) 128
102. M. Hanack, P. Vermehren, *Inorg. Chem.*, **29** (1990) 134
103. M. Hronec, J. Sitek, *React. Kinet. Cat. Lett.*, **21** (1982) 351
104. R.P. Linstead, F.T. Weiss, *J. Chem. Soc.*, (1950) 2975
105. A.R. Monahan, J.A. Brado, A.F. DeLuca, *J. Phys. Chem.*, **76** (1972) 446
106. G. Schmid, M. Sommerauer, M. Hanack, *Angew. Chem., Int. Ed. Engl.*, **32** (1993) 1422
107. M. Sommerauer, C. Rager, M. Hanack, *J. Am. Chem. Soc.*, **118** (1996) 10085
108. C.C. Leznoff, M. Hu, C.R. McArthur, Y. Qin, J.E. van Lier, *Can. J. Chem.*, **72** (1994) 1990
109. G. Schmid, M. Sommerauer, M. Geyer, M. Hanack, in *Phthalocyanines: Properties and Applications*, C.C. Leznoff, A.B.P. Lever (Eds), VCH, New York, **Vol. 4** (1996) 1
110. A. Beck, K.-M. Mangold, M. Hanack, *Chem. Ber.*, **124** (1991) 2315
111. W. Eberhardt, M. Hanack, *Synthesis*, (1995) 95
112. C.C. Leznoff, S.M. Marcuccio, S. Greenberg, A.B.P. Lever, K.B. Tomer, *Can. J. Chem.*, **63** (1985) 623
113. F. Henari, A. Davey, W. Blau, P. Haisch, M. Hanack, *J. Porphyrins Phthalocyanines*, **3** (1999) 331

114. E. Orti, J.L. Bredas, C. Clarisse, *J. Chem. Phys.*, **92** (1990) 1228
115. L.F. Levy, H. Stephen, *J. Chem. Soc.*, (1931) 79
116. J.G. Young, W. Onyebuagu, *J. Org. Chem.*, **55** (1990) 2155
117. V.M. Vlasov, *Russ. Chem. Rev.*, **72** (2003) 681
118. N. Kornblum, L. Cheng, R.C. Kerber, M.M. Kestner, B.N. Newton, H.W. Pinnick, R.G. Smith, P.A. Wade, *J. Org. Chem.*, **41** (1976) 1560
119. D. Mauleon, R. Granados, C. Minguillon, *J. Org. Chem.*, **48** (1983) 3105
120. J.R. Beck, *J. Org. Chem.*, **37** (1972) 3224
121. J.D. Loudon, N. Shulman, *J. Chem. Soc.*, (1941) 772
122. D.S. Terekhov, K.J.M. Nolan, C.R. McArthur, C.C. Leznoff, *J. Org. Chem.*, **61** (1996) 3034
123. D. Wöhrle, M. Eskes, K. Shigehara, A. Yamada, *Synthesis*, (1993) 194
124. R.F. Heck, *Acc. Chem. Res.*, (1979) 146
125. J.K. Stille, *Angew. Chem. Int. Ed. Engl.*, **25** (1986) 508
126. N. Miyaura, A. Suzuki, *Chem. Rev.*, **95** (1995) 2457
127. C.F. van Nostrum, S.J. Picken, A.-J. Schouten, R.J.M. Nolte, *J. Am. Chem. Soc.*, **117** (1995) 9957
128. G.J. Clarkson, N.B. McKeown, K.E. Treacher, *J. Chem. Soc., Perkin Trans. 1*, (1995) 1817
129. J.H. Weber, D.H. Busch, *Inorg. Chem.*, **4** (1965) 469
130. S.V. Kudrevich, M.G. Galpern, J.E. van Lier, *Synthesis*, (1993) 779
131. R.W. Boyle, J.E. van Lier, *Synlett*, (1993) 351
132. A.G. Dandridge, H.A.E. Drescher, J. Thomas, *Scottish Dyes Ltd.*, (1929) GB322169
133. A. Riley, *ICI Ltd.*, (1937), GB476243

134. M. Ambroz, A. Beeby, A.J. MacRobert, M.S.C. Simpson, R.K. Svensen, D. Phillips, *J. Photochem. Photobiol. B: Biol.*, **9** (1991) 87
135. H. Ali, R. Langlois, J.R. Wagner, N. Brasseur, B. Paquette, J.E. van Lier, *Photochem. Photobiol.*, **47** (1988) 713
136. R.W. Boyle, D. Dolphin, *Photochem. Photobiol.*, **64** (1996) 469
137. N. Brasseur, H. Alic, R. Langlois, J.R. Wagner, J. Rousseau, J.E. van Lier, *Photochem. Photobiol.*, **45** (1987) 581
138. N. Brasseur, H. Ali, R. Langlois, J.E. van Lier, *Photochem. Photobiol.*, **47** (1988) 705
139. R. Edrei, V. Gottfried, J.E. van Lier, S. Kimel, *J. Porphyrins Phthalocyanines*, **2** (1998) 191
140. P.C. Martin, M. Gouterman, B.V. Pepich, G.E. Renzoni, D.C. Schindele, *Inorg. Chem.*, **30** (1991) 3305
141. J. Moan, K. Berg, J.C. Bommer, A. Western, *Photochem. Photobiol.*, **56** (1992) 171
142. R.P. Linstead, E.G. Noble, J.M. Wright, *J. Chem. Soc.*, (1937) 911
143. M. Yokete, F. Shibamiya, *J. Chem. Soc., Jpn. Ind. Chem. Sect.*, **62** (1959) 224
144. K. Sakamoto, F. Shibamiya, *J. Jpn. Soc. Colour Mater.*, **59** (1986) 517
145. T.D. Smith, H. Livorness, H. Taylor, J.R. Pilbrow, G.R. Sinclair, *J. Chem. Soc., Dalton Trans.*, (1983) 139
146. R. Taube, *Z. Chem.*, **3** (1963) 194
147. J. Yao, H. Yonehara, C. Pac, *Bull. Chem. Soc. Jpn.*, **68** (1995) 1001
148. B.P. Block, E.G. Meloni, *Inorg. Chem.*, **4** (1965) 111
149. A.S. Akopov, N.Y. Borovkov, *J. Gen. Chem. (USSR)*, **56** (1986) 931
150. N. Kobayahsi, A. Muranaka, *J. Chem. Soc., Chem. Commun.*, (2000) 1855

151. Y. Arslanoğlu, E. Hamaryudan, *Dyes Pigments*, **68** (2006) 1
152. Y. Arslanoğlu, A.M. Sevim, E. Hamaryudan, A. Gül, *Dyes Pigments*, **68** (2006) 119
153. W.-F. Law, K.M. Lui, D.K.P. Ng, *J. Mater. Chem.*, **7** (1997) 2063
154. W.-F. Law, R.C.W. Lui, J. Jiang, D.K.P. Ng, *Inorg. Chim. Acta*, **256** (1997) 147
155. P. Haisch, G. Winter, M. Hanack, L. Lüer, H.-J. Egelhaaf, D. Oelkrug, *Adv. Mater.*, **9** (1997) 316
156. M. Barthel, D. Dini, S. Vagin, M. Hanack, *Eur. J. Org. Chem.*, (2002) 3756
157. M. Barthel, M. Hanack, *J. Porphyrins Phthalocyanines*, **4** (2000) 635
158. N. Kobayashi, A. Muranaka, K. Ishii, *Inorg. Chem.*, **39** (2000) 2257
159. C.G. Claessens, A. Gouloumis, M. Barthel, Y. Chen, G. Martin, F. Agulló-López, I. Ledoux-Rak, J. Zyss, M. Hanack, T. Torres, *J. Porphyrins Phthalocyanines*, **7** (2003) 291
160. J. Mizuguchi, G. Rihs, H.R. Karfunkel, *J. Phys. Chem.*, **99** (1995) 16217
161. J. Zyss, I. Ledoux, *Chem. Rev.*, **94** (1994) 77
162. C.J. Liu, S.Y. Wang, J.C. Hsieh, Y.H. Ju, *Sens. Actuators B: Chem.*, **65** (2000) 371
163. M. Brinkmann, J.-C. Wittmann, M. Barthel, M. Hanack, C. Chaumont, *Chem. Mater.*, **14** (2002) 904
164. Y.A. Buslaev, A.A. Kuznetsova, L.F. Goryachova, *Inorg. Mater. (USSR)*, **3** (1967) 1488
165. J. Mark, M.J. Stillman, *J. Am. Chem. Soc.*, **116** (1994) 1292
166. L.K. Lee, N.H. Sabelli, P.R. LeBreton, *J. Phys. Chem.*, **86** (1982) 3926
167. P.D. Hale, W.J. Pietro, M.A. Ratner, D.E. Ellis, T.J. Marks, *J. Am. Chem. Soc.*, **109** (1987) 5943

168. M.J. Stillman, T. Nyokong, in *Phthalocyanines: Properties and Applications*, C.C. Leznoff, A.B.P. Lever (Eds), VCH, New York, **Vol. 1** (1989) 133
169. M. Gouterman, *J. Mol. Spectrosc.*, **6** (1961) 138
170. M. Gouterman, G.H. Wagniere, L.C. Snyder, *J. Mol. Spectrosc.*, **11** (1963) 108
171. A.B.P. Lever, S.R. Pickens, P.C. Minor, S. Licoccia, B.S. Ramaswamy, K. Magnell, *J. Am. Chem. Soc.*, **103** (1981) 6800
172. T. Fukuda, S. Homma, N. Kobayashi, *Chem. Eur. J.*, **11** (2005) 5205
173. N. Kobayashi, H. Ogata, N. Nonaka, E.A. Luk'yanets, *Chem. Eur. J.*, **9** (2003) 5123
174. N. Kobayashi, A.B.P. Lever, *J. Am. Chem. Soc.*, **109** (1987) 7433
175. A.R. Monahan, J.A. Brado, A.F. DeLuca, *J. Phys. Chem.*, **76** (1972) 1994
176. Z.A. Schelly, R.D. Farina, E.M. Eyring, *J. Phys. Chem.*, **74** (1970) 617
177. Z.A. Schelly, D.J. Harward, P. Hemmes, E.M. Eyring, *J. Phys. Chem.*, **74** (1970) 3040
178. A.R. Kane, J.F. Sullivan, D.H. Kenny, M.E. Kenney, *Inorg. Chem.*, **9** (1970) 1445
179. W.E. Ford, B.D. Rihter, M.E. Kenney, M.A.J. Rodgers, *Photochem. Photobiol.*, **50** (1989) 277
180. M. Kasha, *Radiat. Res.*, **20** (1960) 55
181. Z. Gasyna, N. Kobayashi, M.J. Stillman, *J. Chem. Soc., Dalton Trans.*, (1989) 2397
182. E.S. Emerson, M.A. Conlin, A.E. Rosenoff, K.S. Norland, H. Rodriguez, D. Chin, G.R. Bird, *J. Phys. Chem.*, **71** (1967) 2396
183. E. Coates, *J. Soc. Dyers. Col.*, **85** (1969) 355
184. N.B. McKeown, *J. Mater. Chem.*, **10** (2000) 1979

185. J.M. Kroon, H.M. Koehorst, M. van Dijk, G.M. Sanders, E.J.R. Sudhölter, *J. Mater. Chem.*, **7** (1997) 615
186. M.J. Cook, *Chem. Rec.*, **2** (2002) 225
187. M.J. Cook, *J. Mater. Chem.*, **6** (1996) 677
188. S. Vagin, M. Hanack, *Eur. J. Org. Chem.*, (2003) 2661
189. J.V. Bakboord, M.J. Cook, E. Hamuryudan, *J. Porphyrins Phthalocyanines*, **4** (2000) 510
190. R.D. George, A.W. Snow, J.S. Shirk, W.R. Barger, *J. Porphyrins Phthalocyanines*, **2** (1998) 1
191. M.J. Cook, J. McMurdo, D.A. Miles, R.H. Poynter, *J. Mater. Chem.*, **4** (1994) 1205
192. R.A. Marcus, *Rev. Mod. Phys.*, **65** (1993) 599
193. J.F. Lipskier, T.-H. Tran-Thi, *Inorg. Chem.*, **32** (1993) 722
194. A. Harriman, G. Porter, M.-C. Richoux, *J. Chem. Soc., Faraday Trans. 2*, **76** (1980) 1618
195. C.L. Bard, A.T. Kuhn, *Chem. Soc. Rev.*, **10** (1981) 49
196. J.R. Darwent, P. Douglas, A. Harriman, G. Porter, M.-C. Richoux, *Coord. Chem. Rev.*, **44** (1982) 83
197. I. Okura, *Coord. Chem. Rev.*, **68** (1985) 83
198. M. Kaneko, H. Ueno, S. Masuda, K. Suzuki, H. Okimi, M. Hoshino, L. Lapok, D. Wöhrle, *J. Porphyrins Phthalocyanines*, **9** (2005) 667
199. S.L. Lugunov, M.A. Rodgers, *J. Phys. Chem.*, **96** (1992) 8697
200. S. Radzki, S. Gaspard, C. Giannotti, *J. Chem. Res. M.*, (1986) 360
201. T.-H. Tran-Thi, *Coord. Chem. Rev.*, **160** (1997) 53
202. S. Argitas, R.-M. Ion, O. Bekaroglu, *Mater. Sci. Eng. C*, **7** (2000) 105

203. E.A. Kapp, S. Daya, C.G. Whitley, *Biochem. Biophys. Res. Commun.*, **167** (1990) 1383
204. P. Suppan, *Chemistry and Light*, Royal Society, Cambridge, **1st ed.** (1994)
205. D.R. Arnold, N.C. Baird, J.R. Bolton, J.C.D. Brand, P.W.M. Jacobs, P. de Mayo, W.R. Ware, *Photochemistry: An Introduction*, Academic Press, New York, 1974
206. X.-F. Zhang, H.-J. Xu, *J. Photochem. Photobiol. B: Biol.*, **24** (1994) 109
207. E.A. Lissi, M.V. Encinas, E. Lemp, M.A. Rubio, *Chem. Rev.*, **93** (1993) 699
208. M. Prein, W. Adam, *Angew. Chem.*, **108** (1996) 519
209. M. Prein, W. Adam, *Angew. Chem. Int. Ed. Engl.*, **35** (1996) 495
210. K. Inoue, T. Matsuura, I. Saito, *Bull. Chem. Soc. Japan*, **55** (1982) 2959
211. R. Livingston, K.E. Owens, *J. Am. Chem. Soc.*, **78** (1956) 3304
212. R.S. Mullikan, *Phys. Rev.*, **32** (1928) 186
213. R.S. Mullikan, *Rev. Mod. Phys.*, **4** (1932) 1
214. S.J. Arnold, M. Kubo, E.A. Ogryzlo, *Adv. Chem. Ser.*, **77** (1968) 133
215. P.B. Merkel, D.R. Kearns, *J. Am. Chem. Soc.*, **94** (1972) 1029
216. S. Yamaguchi, Y. Sasaki, *J. Photochem. Photobiol. A: Chem.*, **142** (2001) 47
217. P. Tau, A.O. Ogunsipe, S. Maree, M.D. Maree, T. Nyokong, *J. Porphyrins Phthalocyanines*, **7** (2003) 439
218. I. Seotsanyana-Mokhosi, T. Nyokong, *J. Porphyrins Phthalocyanines*, **6** (2004) 1214
219. P.B. Merkel, D.R. Kearns, *J. Am. Chem. Soc.*, **97** (1975) 462
220. X. Zhang, H. Xu, *J. Chem. Soc., Faraday Trans.*, **89** (1993) 3847
221. H. Li, T.F. Guarr, *J. Chem. Soc., Chem. Commun.*, (1989) 833

222. W. Spiller, H. Kliesch, D. Wöhrle, S. Hackbarth, B. Röder, G. Schnurpfeil, *J. Porphyrins Phthalocyanines*, **2** (1998) 145
223. J.W. Verhoeven, *Pure Appl. Chem.*, **68** (1996) 2223
224. R. Bonnett, B.D. Djelal, P.A. Hamilton, G. Martinez, F. Wierrani, *J. Photochem. Photobiol. B: Biol.*, **53** (1999) 136
225. M.J. Cook, I. Chambrier, S.J. Cracknell, D.A. Mayes, D.A. Russel, *Photochem. Photobiol.*, **62** (1995) 542
226. A.K. Sobbi, D. Wöhrle, D. Schlettwein, *J. Chem. Soc., Perkin Trans. 2*, (1993) 481
227. G. Schnurpfeil, A.D. Sobbi, W. Spiller, H. Kliesch, D. Wöhrle, *J. Porphyrins Phthalocyanines*, **2** (1998) 145
228. R. Bonnett, G. Martinez, *J. Porphyrins Phthalocyanines*, **4** (2000) 544
229. R. Slota, G. Dyrda, *Inorg. Chem.*, **42** (2003) 5743
230. J.D. Spikes, *Photochem. Photobiol.*, **55** (1992) 797
231. G. Schnurpfeil, A.K. Sobbi, U. Michelsen, D. Wöhrle, *Proc. SPIE.*, **3191** (1997) 299
232. M.D. Maree, N. Kuznetsova, T. Nyokong, *J. Photochem. Photobiol. A: Chem.*, **140** (2001) 117
233. S. Maree, T. Nyokong, *J. Porphyrins Phthalocyanines*, **5** (2001) 782
234. T.S. Mang, *Photochem. Photobiol.*, **45** (1987) 501
235. D. Wröbel, A. Boguta, R.M. Ion, *Int. J. Photoenergy*, **2** (2000) 87
236. I. Rosenthal, *Photochem. Photobiol.*, **53** (1991) 870
237. J.R. Lakowicz, *Principles of Fluorescence Spectroscopy*, Kluwer Academic/Plenum Publishers, New York, (1999)
238. J.R. Lakowicz, *Anal. Biochem.*, **298** (2001) 1

239. R. Pandey, *J. Porphyrins. Phthalocyanines*, **4** (2000) 368
240. A.T.R. Williams, S.A. Winfield, J.N. Miller, *Analyst*, **108** (1983) 1067
241. P. Jacques, A.M. Braun, *Helv. Chim. Acta*, **64** (1981) 1800
242. A.G. Montalban, H.G. Meunier, R.B Ostler, A.G.M. Barrett, B.M. Hoffman, G. Rumbles, *J. Phys. Chem. A*, **103** (1999) 4352
243. S. Dhimi, A.J. de Mello, G. Rumbles, S.M. Bishop, D. Phillips, A. Beeby, *Photochem. Photobiol.*, **61** (1995) 341
244. D.R. Lide, *CRC handbook of chemistry and physics*, Boca Raton, CRC Press, Florida, **84th ed.** 2003
245. D.A. Fernandez, J. Awruch, L. Dicelio, *Photochem. Photobiol.*, **63** (1996) 784
246. A. Ferencz, D. Neher, M. Schulze, G. Wegner, L. Viaene, F.C. de Schryver, *Chem. Phys. Lett.*, **245** (1995) 23
247. C. Farren, S. Fitzgerald, A. Beeby, M.R. Bryce, *Chem. Commun.*, **6** (2002) 572
248. S. Fitzgerald, C. Farren, C.F. Stanley, A. Beeby, M.R. Bryce, *Photochem. Photobiol. Sci.*, **1** (2002) 581
249. A.P. de Silva, H.Q.N. Gunaratne, T. Gunnlaugsson, A.J.M. Huxley, C.P. McCoy, J.T. Rademacher, T.E. Rice, *Chem. Rev.*, **97** (1997) 1515
250. T. Minami, M. Kawahigashi, Y. Sakai, K. Shimamoto, S. Hirayama, *J. Lumin.*, **35** (1986) 347
251. G. Valduga, E. Reddi, G. Jori, R. Cubeddu, P. Taroni, G. Valentini, *J. Photochem. Photobiol. B: Biol.*, **16** (1992) 331
252. A. Gilbert, J. Baggot, *Essentials of Molecular Photochemistry*, Blackwell Scientific Publications, Oxford, (1991) 98
253. C. Oncioiu, A. Nicolae, M. Hillebrand, *Seria Chemie*, **1** (2002) 111

254. M.A.M.J. van Zandvoort, D. Wróbel, P. Letting, G. van Ginkel, Y.K. Levine, *Photochem. Photobiol.*, **62** (1995) 279
255. D. Wróbel, A. Boguta, *J. Photochem. Photobiol. A: Chem.*, **150** (2002) 67
256. D. Wróbel, J. Lukasiewicz, H. Manikowski, *Dyes Pigments*, **58** (2003) 7
257. H. Du, R.-C. Fuh, J. Li, L.A. Corkan, J.S. Lindsey, *Photochem. Photobiol.*, **68** (1998) 141
258. S.J. Strickler, R.A. Berg, *J. Chem. Phys.*, **37** (1962) 814
259. S. Maree, D. Phillips, T. Nyokong, *J. Porphyrins Phthalocyanines*, **6** (2002) 17
260. M.D. Maree, T. Nyokong, K. Suhling, D. Phillips, *J. Porphyrins Phthalocyanines*, **6** (2002) 373
261. M. Kropf, E. Joselevich, H. Durr, I. Willner, *J. Am. Chem. Soc.*, **118** (1996) 655
262. B.L. Wheeler, G. Nagasubramanian, A.J. Bard, L.A. Schechtman, D.R. Dininny, M.E. Kenney, *J. Am. Chem. Soc.*, **106** (1984) 7404
263. W. Freyer, H. Stiel, M. Hild, K. Teuchner, D. Leupold, *Photochem. Photobiol.*, **66** (1997) 596
264. W. Freyer, S. Mueller, K. Teuchner, *J. Photochem. Photobiol. A: Chem.*, **163** (2004) 231
265. C.A.T. Laia, S.M.B. Costa, D. Phillips, A.W. Parker, *Photochem. Photobiol. Sci.*, **2** (2003) 555
266. E.K. Yeow, S.E. Braslavsky, *Phys. Chem. Chem. Phys.*, **4** (2002) 239
267. A. Ogunsipe, T. Nyokong, *J. Porphyrins Phthalocyanines*, **9** (2005) 121
268. J.R. Darwent, I. McCubbin, D. Phillips, *J. Chem. Soc., Faraday Trans. 2*, **78** (1982) 347
269. A. Ogunsipe, T. Nyokong, *J. Photochem. Photobiol. A: Chem.*, **173** (2005) 211
270. J. Zakrzewski, C. Giannotti, *Inorg. Chim. Acta*, **232** (1995) 63

271. J. Delaire, C. Giannotti, J. Zakrzewski, *J. Photochem. Photobiol. A: Chem.*, **112** (1998) 205
272. J. Zakrzewski, C. Giannotti, *Coord. Chem. Rev.*, **140** (1995) 169
273. J.R. Darwent, *J. Chem. Soc., Chem. Commun.*, (1980) 805
274. C. Wang, M.R. Bryce, A.S. Batsanov, C.F. Stanley, A. Beeby, J.A.K. Howard, *J. Chem. Soc., Perkin Trans. 2*, (1997) 1671
275. S.S. Lehrer, *Biochemistry*, **10** (1971) 3254
276. C. Schweitzer, R. Schmidt, *Chem. Rev.*, **103** (2003) 1685
277. R.V. Bensasson, C.R. Goldsmith, E.J. Land, T.G. Truscott, *Photochem. Photobiol.*, **28** (1978) 277
278. T.-H. Tran Thi, C. Desforge, C. Thiec, S. Gaspard., *J. Phys. Chem.*, **93** (1989) 1226
279. R.A. Keller, S.G. Hadley, *J. Chem. Phys.*, **42** (1965) 2382
280. M.C. Spaeth, W.R. Sooy, *J. Chem. Phys.*, **48** (1968) 2315
281. J. McVie, R.S. Sinclair, T.G. Truscott, *J. Chem. Soc., Faraday Trans. 1*, **74** (1978) 1870
282. M.G. Lagori, L.E. Dicelio, E.S. Román, *J. Photochem. Photobiol. A: Chem.*, **72** (1993) 153
283. L. Lüer, H.-J. Egelhaaf, D. Oelkrug, G. Winter, M. Hanack, A. Weber, H. Bertagnolli, *Synth. Met.*, **138** (2003) 305
284. G. Winter, H. Heckmann, P. Haisch, W. Eberhardt, M. Hanack, L. Lüer, H.-J. Egelhaaf, D. Oelkrug, *J. Am. Chem. Soc.*, **120** (1998) 11663
285. Z.D. Popovic, M.I. Khan, S.J. Atherton, A.-M. Hor, J.L. Goodman, *J. Phys. Chem. B*, **102** (1998) 657
286. Y. Chen, M.E. El-Khouly, M. Sasaki, Y. Araki, O. Ito, *Org. Lett.*, **7** (2005) 1613

287. D. Gust, T.A. Moore, *Topics Curr. Chem.*, **159** (1991) 103
288. A. Ogunsipe, J.-Y. Chen, T. Nyokong, *New. J. Chem.*, **28** (2004) 822
289. P. Matlaba, T. Nyokong, *Polyhedron*, **21** (2002) 2463
290. S.R. Cicco, M. Latronica, P. Mastrorilli, G.P. Suranna, C.F. Nobile, *J. Mol. Catal. A: Chem.*, **165** (2001) 135
291. R.A. Sheldon, *J. Mol. Catal. A: Chem.*, **117** (1997) 1
292. T. Shiragami, J. Matsumoto, H. Inoue, M. Yasuda, *J. Photochem. Photobiol. C: Photochem. Rev.*, **6** (2005) 227
293. E.M.K. Mansour, P. Maillard, P. Krausz, S. Gaspard, C. Giannotti, *J. Mol. Catal. A: Chem.*, **41** (1987) 361
294. P.E. Esser, B. Drießen-Hölscher, W. Keim, *J. Mol. Catal. A: Chem.*, **140** (1999) 13
295. M. Brink, O. Wennerström, *J. Photochem. Photobiol. A: Chem.*, **143** (2001) 201
296. L. Cermenati, C. Richter, A. Albini, *Chem. Commun.*, (1998) 805
297. O. Legrin, E. Oliveros, A.M. Braun, *Chem. Rev.*, **93** (1993) 671
298. D. Wöhrle, O. Suvorova, R. Gerdes, O. Bartels, Ł. Łapok, N. Baziakina, S. Makarov, A. Słodek, *J. Porphyrins Phthalocyanines*, **8** (2004) 1020
299. G. Schneider, D. Wöhrle, W. Spiller, J. Stark, G. Schulz-Ekloff, *Photochem. Photobiol.*, **60** (1994) 333
300. R. Gerdes, O. Bartels, G. Schneider, D. Wöhrle, G. Schulz-Ekloff, *Intern. J. Photoenergy*, **1** (1999) 41
301. A. Maldotti, R. Amadelli, C. Bartocci, V. Carassiti, E. Polo, G. Varani, *Coord. Chem. Rev.*, **125** (1993) 143

302. L. Weber, G. Haufe, D. Rehorek, H. Hennig, *J. Chem. Soc., Chem. Commun.*, (1991) 502
303. L. Weber, J. Behling, G. Haufe, H. Hennig, *J. Am. Chem. Soc.*, **116** (1994) 2400
304. H. Hennig, J. Behling, R. Meusiger, L. Weber, *Chem. Ber.*, **128** (1995) 229
305. S. Mosseri, P. Neta, P. Hambright, D.Y. Sabry, A. Harriman, *J. Chem. Soc., Dalton Trans.*, (1988) 2705
306. Y. Matsuda, S. Sakamoto, H. Koshima, Y. Murakami, *J. Am. Chem. Soc.*, **107** (1985) 6415
307. Y. Matsuda, H. Koshima, K. Nakamura, Y. Murakami, *Chem. Lett.*, (1988) 625
308. L. Weber, G. Haufe, D. Rehorek, H. Hennig, *J. Mol. Catal.*, **60** (1990) 267
309. H.J. Ledon, M. Bonnet, D. Galland, *J. Am. Chem. Soc.*, **103** (1981) 6209
310. C.J. Boreham, J.-M. Latour, J.-C. Marchon, *Inorg. Chim. Acta*, **45** (1980) L69
311. L.M. González, A.L. Villa de P, C. Montes de C, A. Sorokin, *Tetrahedron Lett.*, **47** (2006) 6465
312. T. Ohno, K. Nakabeya, M. Matsumura, *J. Catal.*, **176** (1998) 76
313. T. Akasaka, M. Haranaka, W. Ando, *J. Am. Chem. Soc.*, **113** (1991) 9898
314. M. Masteri-Farahani, F. Farzaneh, M. Ghandi, *J. Mol. Catal. A: Chem.*, **248** (2006) 53
315. Y. Sun, Z. Xi, G. Cao, *J. Mol. Catal. A: Chem.*, **166** (2001) 219
316. Z. Xi, H. Wang, Y. Sun, N. Zhou, G. Cao, M. Li, *J. Mol. Catal. A: Chem.*, **168** (2001) 299
317. M. L'Her, A. Pondaven, *The Porphyrin Handbook*, Eds: K.M. Kadish, K.M. Smith, R. Guilard, Academic Press, California, **Vol. 16** (2003) 117
318. D.W. Clack, N.S. Hush, *J. Am. Chem. Soc.*, **87** (1965) 4238
319. T. Nyokong, *S. Afr. J. Chem.*, **48** (1995) 23

320. A.B.P. Lever, J.P. Wilshire, *Inorg. Chem.*, **17** (1978) 1145
321. M.-S. Liao, J.D. Watts, M.-J. Huang, S.M. Gorun, T. Kar, S. Scheiner, *J. Chem. Theory Comput.*, **1** (2005) 1201
322. A. Giraudeau, F.R. Fan, A.J. Bard, *J. Am. Chem. Soc.*, **102** (1980) 5137
323. A.B.P. Lever, P.C. Minor, J.P. Wilshire, *Inorg. Chem.*, **20** (1981) 2550
324. A.B.P. Lever, *Adv. Inorg. Radiochem.*, **7** (1965) 28
325. Ö. Bekaroglu, *Appl. Organomet. Chem.*, **10** (1996) 605
326. A.B.P. Lever, P.C. Minor, *Inorg. Chem.*, **20** (1981) 4015
327. N.L. Weinberg, *Proc. Electrochem. Soc.*, **84-5** (1984) 463
328. J. Jörissen, *Encyclopedia of Electrochemistry*, Ed.: H.J. Schäfer, Wiley-VCH, Weinheim, **Vol. 8** (2004) 25
329. C.M.A. Brett, A.M.O. Brett, *Electrochemistry: Principles, Methods and Applications*, Oxford University Press Inc. Publishers, USA, (1993)
330. J.G. Osteryoung, R.A. Osteryoung, *Anal. Chem.*, **57** (1985) 101A
331. P.T. Kissinger, W.R. Heineman, *Laboratory Techniques in Electroanalytical Chemistry*, Marcel Dekker Inc., New York, 1984
332. W.R. Heineman, *J. Chem. Ed.*, **60** (1983) 305
333. W.R. Heineman, *Anal. Chem.*, **50** (1978) 390A
334. T.P. DeAngelis, W.R. Heineman, *J. Chem. Ed.*, **53** (1976) 595
335. J.Y. Gui, G.W. Hance, T. Kuwana, *J. Electroanal. Chem.*, **309** (1991) 73
336. R. Murray, W.R. Heineman, G.W. O'Dom, *Anal. Chem.*, **39** (1967) 1666
337. A.J. Bard, L.R. Faulkner, *Electrochemical Methods, Fundamentals and Applications*, John Wiley and Sons, New York, (1996)
338. M.J. Stillman, in: *Phthalocyanines: Properties and Applications*, C.C. Leznoff, A.B.P. Lever (Eds), VCH Publishers, New York, **Vol. 3** (1993) Ch. 5

339. J. Silver, P. Lukes, P. Hey, M.T. Ahmet, *J. Mater. Chem.*, **1** (1991) 881
340. A. Koca, A.R. Özkaya, Y. Arslanoğlu, E. Hamuryudan, *Electrochim. Acta*, (2006) in press
341. A.B.P. Lever, E.R. Milaeva, G. Speier, in: *Phthalocyanines: Properties and Applications*, C.C. Leznoff, A.B.P. Lever (Eds), VCH Publishers, New York, **Vol. 3** (1993)
342. J. Wang, in *Analytical Electrochemistry*, VCH Publishers, New York, **1st ed** (1994)
343. J. Zagal, M. Paez, C. Fierro, *Proc. Electrochem. Soc.*, **87** (1987) 198
344. P. Vasuvedan, N. Poughat, A.K. Shuklat, *Appl. Organomet. Chem.*, (1996) 951
345. S. Maree, T. Nyokong, *J. Electroanal. Chem.*, **492** (2000) 120
346. N. Diab, J. Oni, A. Schulte, I. Radtke, A. Blöchl, W. Schuhmann, *Talanta*, **61** (2003) 43
347. A.M. Saleh, A.O. Abu-Hilal, R.D. Gould, *Curr. App. Phys.*, **3** (2003) 345
348. M. Siswana, K.I. Ozoemena, T. Nyokong, *Talanta*, **69** (2006) 1136
349. K.I. Ozoemena, T. Nyokong, *Electrochim. Acta*, **51** (2006) 2669
350. K.I. Ozoemena, P. Westbroek, T. Nyokong, *Electrochem. Commun.*, **3** (2001) 529
351. S. Mho, B. Ortiz, S.-M. Park, *J. Electrochem. Soc.*, **142** (1995) 1436
352. J. Obirai, T. Nyokong, *Electrochim. Acta*, **50** (2005) 5427
353. N. Grootboom, T. Nyokong, *Anal. Chim. Acta*, **50** (2005) 5427
354. B.O. Agboola, K.I. Ozoemena, T. Nyokong, *Electrochim. Acta*, **51** (2006) 6470
355. J. Obirai, T. Nyokong, *J. Electroanal. Chem.*, **573** (2004) 77
356. J. Obirai, T. Nyokong, *Electrochim. Acta*, **49** (2004) 1417
357. D. Martel, N. Sojic, A. Kuhn, *J. Chem. Educ.*, **79** (2002) 349

358. R.A. Durst, A.J. Bäumner, R.W. Murray, R.P. Buck, C.P. Andrieux, *Pure Appl. Chem.*, **69** (1997) 1317
359. E.M. Genies, G. Bidan, A.F. Diaz, *J. Electroanal. Chem.*, **149** (1983) 101
360. A. Deronzier, J.C. Moutet, *Acc. Chem. Res.*, **22** (1989) 249
361. D. Curran, J. Grimshaw, S.D. Perera, *Chem. Soc. Rev.*, **20** (1991) 391
362. J. Roncali, **92** (1992) 711
363. H. Randriamahazaka, V. Noël, C. Chevrot, *J. Electroanal. Chem.*, **472** (1999) 103
364. J. Roncali, *Chem. Rev.*, **92** (1992) 711
365. R. John, G.G. Wallace, *J. Electroanal. Chem.*, **306** (1991) 157
366. S.J. Higgins, *Chem. Soc. Rev.*, **26** (1997) 247
367. T. Nyokong, in *N₄-Macrocyclic Metal Complexes*, (Eds): J.H. Zagal, F. Bedioui, J.-P. Dodelet, Springer, New York, (2006) 315
368. S.S. Mirvish, *Cancer Lett.*, **93** (1995) 17
369. I.A. Wolf, A.E. Wasserman, *Science*, **177** (1972) 15
370. C.I. Walters, *Oncology*, **37** (1980) 289
371. I.G. Casella, A.M. Salvi, *Electroanalysis*, **9** (1997) 596
372. W. Frenzel, J. Schulz-Brussel, B. Zinvirt, *Talanta*, **64** (2004) 278
373. S. Arias-Negrete, L.A. Jimenez-Romero, M.O. Solis-Martinez, J. Ramiirez-Emiliano, E.E. Avila, P. Cuella-Mata, *Anal. Biochem.*, **328** (2004) 14
374. D.C. Siu, A. Henshall, *J. Chromatogr. A*, **804** (1998) 157
375. M.I.H. Helaleh, T. Korenaga, *J. Chromatogr. B*, **744** (2000) 433
376. S. Wang, Y. Yin, X. Lin, *Electrochem. Commun.*, **6** (2004) 259
377. H. Winnischofer, S.S. Lima, K. Araki, H.E. Toma, *Anal. Chim. Acta*, **480** (2003)

378. L. Jiang, R. Wang, X. Li, L. Jiang, G. Lu, *Electrochem. Commun.*, **7** (2005) 597
379. K. Horita, G.F. Wang, M. Satake, *Analyst*, **122** (1997) 1569
380. M. Badea, A. Amine, G. Pallesche, D. Moscone, G. Volpe, A. Curulli, *J. Electroanal. Chem.*, **509** (2001) 66
381. N. Sparatu, T.N. Rao, D.A. Tryk, A. Fujishima, *J. Electrochem. Soc.*, **148** (2001) E112
382. S.M. Silva, C.R. Alves, S.A.S. Machado, L.H. Mazo, L.A. Avaca, *Electroanal.*, **8** (1996) 1055
383. A.Y. Chamsi, A.G. Fogg, *Analyst*, **113** (1988) 1723
384. X. Xing, D.A. Scherson, *Anal. Chem.*, **60** (1988) 1723
385. M.C. Granger, J.S. Xu, J.W. Strojek, G.M. Swain, *Anal. Chim. Acta*, **397** (1999) 145
386. J.E. Newbry, M.P.I. de Haddad, *Analyst*, **110** (1985) 81
387. J.N. Barisci, G.G. Wallace, *Anal. Lett.*, **24** (1991) 2059
388. J.Z. Li, X.Y. Pang, R.Q. Yu, *Anal. Chim. Acta.*, **297** (1994) 437
389. N. Chebotareva, T. Nyokong, *J. Appl. Electrochem.*, **27** (1997) 975
390. M. Thamae, T. Nyokong, *J. Electroanal. Chem.*, **470** (1999) 126
391. J.N. Younathan, K.S. Wood, T.J. Meyer, *Inorg. Chem.*, **31** (1992) 3280
392. F. Bedioui, S. Trevin, V. Albin, M.G. Gomez-Villegas, J. Devynck, , *Anal. Chim. Acta*, **341** (1997) 177
393. A. Schultz, *J. Electroanal. Chem.*, **237** (1984) 163
394. L.M. Moretto, P. Ugo, M. Zanata, P. Guerriero, C.R. Martin, *Anal. Chem.*, **70** (1998) 2163
395. R. Lin, M. Bayachou, J. Greaves, P.J. Farmer, *J. Am. Chem. Soc.*, **119** (1997) 12689

396. N. Chebotareva, T. Nyokong, *J. Coord. Chem.*, **46** (1999) 433
397. D. Mimica, J.H. Zagal, F. Bedioui, *J. Electroanal. Chem.*, **497** (2001) 106
398. Z.-H. Wen, T.-F. Kang, *Talanta*, **62** (2004) 351
399. W.J.R. Santos, A.L. Sousa, R.C.S. Luz, F.S. Damos, L.T. Kubota, A.A. Tanaka, S.M.C.N. Tanaka, *Talanta*, **70** (2006) 588
400. J. Bendig, D. Kreysig, R. Schoeneich, *Z. Chem.*, **19** (1979) 151
401. M. Krejčík, M. Daněk, F. Hartl, *J. Electroanal. Chem.*, **317** (1991) 179
402. R.D. George, A.W. Snow, *J. Heterocyclic Chem.*, **32** (1995) 495
403. B.H. Nicolet, J.A. Bender, *Org. Synth., Coll.*, **1** (1941) 410
404. A.G. Gürek, O. Bekaroğlu, *J. Chem. Soc., Dalton Trans.*, (1994) 1419
405. K. Bergesen, L. Haugland, M.J. Cook, G.C. Bryant, *J. Porphyrins Phthalocyanines*, **4** (2000) 665
406. B. Agboola, K.I. Ozoemena and T. Nyokong, *J. Mol. Cat. A: Chem.*, **248** (2006) 84
407. I. McCubbin, D. Phillips, *J. Photochem.*, **34** (1986) 187
408. B. Agboola, K.I. Ozoemena, T. Nyokong, *J. Mol. Cat. A: Chem.*, **227** (2005) 209
409. T.M. Keller, T.R. Price, J.R. Griffith, *Synthesis*, (1980) 613
410. W.O. Siegel, *J. Heterocycl. Chem.*, **18** (1981) 1613
411. D. Wöhrle, G. Knothe, *Synth. Commun.*, **19** (1989) 3231
412. B.N. Achar, G.M. Fohlen, J.A. Parker, J. Keshavayya, *Polyhedron*, **6** (1987) 1463
413. F. Giuntini, D. Nistri, G. Chiti, L. Fantetti, G. Jori, G. Roncucci, *Tetrahedron Lett.*, **44** (2003) 515

414. B. Görlach, M. Dachtler, T. Glaser, K. Albert, M. Hanack, *Chem. Eur. J.*, **7** (2001) 2459
415. S. Gaspard, P. Maillard, *Tetrahedron*, **43** (1987) 1083
416. S.M. Marcuccio, P.I. Svirskaya, S. Greenberg, A.B.P. Lever, C.C. Leznoff, K.B. Tomer, *Can. J. Chem.*, **63** (1985) 3057
417. I. Seotsanyana-Mokhosi, J-Y. Chen, T. Nyokong, *J. Porphyrins Phthalocyanines*, **9** (2005) 316
418. G. Cheng, X. Peng, G. Hao, V.O. Kennedy, I.N. Ivanov, K. Knappenberger, J.J. Hill, M.A.J. Rodgers, M.E. Kenney, *J. Phys. Chem.: A*, **107** (2003) 3503
419. M. Aoudia, G. Cheng, V.O. Kennedy, M.E. Denney, M.A.J. Rodgers, *J. Am. Chem. Soc.*, **119** (1997) 6029
420. A.B. Anderson, T.L. Gorden, M.E. Kenney, *J. Am. Chem. Soc.*, **107** (1985) 192
421. M. Konami, M. Hatano, A. Tajiri, *Chem. Phys. Lett.*, **166** (1990) 605
422. E.A. Ough, T. Nyokong, K.A.M. Creber, M.J. Stillman, *Inorg. Chem.*, **27** (1988) 2724
423. T. Nyokong, Z. Gasyna, M.J. Stillman, *Inorg. Chem.*, **26** (1986) 1087
424. M. Hanack, T. Schneider, M. Barthe, J.S. Shirk, R.S. Flom, R.G.S. Pong, *Coord. Chem. Rev.*, **219-221** (2001) 235
425. D. Wrobel, I. Hanyz, R. Bartowiak, R.M. Ion, *J. Fluoresc.*, **8** (1998) 191
426. T.H. Tran-Thi, H. Palacin, B. Clergeot, *Chem. Phys. Lett.*, **157** (1989) 92
427. K. Adachi, H. Watarai, *J. Mat. Chem.* **15** (2005) 4701
428. J. Zhu, Y. Shen, F. Gu, J. Tao, J. Zhang, *Mater. Lett.*, (2006) in press
429. G. Kostenich, T. Babushkina, A. Lavi, Y. Langzam, Z. Malik, A. Orestein, B. Ehrenberg, *J. Porphyrins Phthalocyanines*, **2** (1998) 382

430. K. Kasuga, T. Miyazako, T. Sugimori, M. Handa, *Synthesis and reactivity in inorganic metal-organic chemistry*, **33** (2003) 403
431. J.H. Brannon, D. Magde, *J. Am. Chem. Soc.*, **102** (1980) 62
432. A.S. Tokilov, K.S. Dzhulibekov, Z.A. Krasnaya, *Izvestiya Akad. Nauk. Seriya Khim.*, (1993) 69
433. T. Nyokong, *Polyhedron*, **13** (1994) 215
434. K. Kasuga, H. Morimoto, M. Ando, *Inorg. Chem.*, **25** (1986) 2478
435. K. Kasuga, N. Matura, K. Inoue, M. Handa, T. Sugimori, K. Isa, M. Nakata, *Chem. Lett.*, **31** (2002) 352
436. N. Kobayashi, T. Fukuda, K. Ueno, H. Ogino, *J. Am. Chem. Soc.*, **123** (2001) 10740
437. D. Wöhrle, O. Suvorova, R. Gerdes, O. Bartels, L. Lapok, N. Baziakina, S. Makarov, A. Slodek, *J. Porphyrins Phthalocyanines*, **8** (2004) 1020
438. Y. Tsuda, S. Matsui, K. Takahashi, *J. Mol. Catal.*, **148** (1999) 183
439. J.A. Hodge, M.G. Hill, H.B. Gray, *Inorg. Chem.*, **34** (1995) 809
440. S. Zecevic, B. Simic-Glavaski, E. Yeager, A.B.P. Lever, P.C. Minor, *J. Electroanal. Chem.*, **196** (1985) 339
441. J.A. Hodge, H.B. Gray, *Inorg. Chem.*, **34** (1995) 812
442. B. Tulythan, W.E. Geiger, *J. Am. Chem. Soc.*, **107** (1985) 5960
443. A.W. Bott, *Current Separations*, **2** (1997) 61
444. P.N. Dwyer, L. Puppe, J.W. Buchler, W.R. Scheidt, *Inorg. Chem.*, **14** (1975) 1782
445. R. Guillard, J. Latour, C. Lecomte, J. Marchon, J. Protas, D. Ripoll, *Inorg. Chem.*, **17** (1978) 1228

446. T.F. Guarr, in: *Handbook of Organic Conductive Molecules and Polymers*, (Ed) H.S. Nalwa, Wiley, Chichester, **Vol. 4** (1997)
447. B. Werneckers, F. Beck, *Electrochim. Acta*, **30** (1985) 1491
448. M.E.G. Lyons, C.A. Fitzgerald, M.R. Smyth, *Analyst*, **119** (1994) 855
449. J.-M. Zen, A. Senthil Kumar, M.-R. Chang, *Electrochim. Acta*, **45** (2000) 1691
450. A.P. Abbott, A. Bettley, D.J. Schiffrin, *J. Electroanal. Chem.*, **347** (1993) 153
451. J. Obirai, N.P. Rodrigues, F. Bedioui, T. Nyokong, *J. Porphyrins Phthalocyanines*, **7** (2003) 508
452. S. Griveau, J. Pavez, J.H. Zagal, F. Bedioui, *J. Electroanal. Chem.*, **497** (2001) 75
453. S. Dong, B. Liu, J. Liu, N. Kobayashi, *J. Porphyrins Phthalocyanines*, **1** (1997) 333
454. N. Kobayashi, Y. Nishiyama, *J. Electroanal. Chem.*, **181** (1984) 107
455. E. Laviron, *J. Electroanal. Chem.*, **101** (1979) 19
456. H.-G. Hong, T.E. Mallouk, *Langmuir*, **7** (1991) 2362
457. R.F. Lane, A.T. Hubbard, *J. Phys. Chem.*, **77** (1973) 1401
458. Z. Galus, *Fundamentals of Electrochemical Analysis*, Ellis Horwood Press, New York, (1976) 313